PETROGENETIC EVOLUTION OF HIGHER HIMALAYAN LEUCOGRANITES IN THE SIKKIM REGION

A Thesis Submitted

To

Sikkim University

In Partial Fulfilment of the Requirement for the

Degree of Doctor of Philosophy

By

Tanya Srivastava

Department of Geology

School of Physical Sciences

March 2023

DECLARATION

I declare that the Ph.D. research work entitled **"Petrogenetic Evolution of Higher Himalayan Leucogranites in the Sikkim Region"** was carried out by me for the partial fulfillment of the requirements for the degree of **Doctor of Philosophy (Geology)** at Sikkim University. The work has been done under the guidance of Dr. Nishchal Wanjari, Assistant Professor, Sikkim University, Department of Geology. This thesis does not contain any material that infringes copyright. I also declare that the subject matter of this thesis is originally based on the field investigation done in Sikkim and published work cited through references. This is being submitted to the Department of Geology, Sikkim University for the completion of the degree of Doctor of Philosophy in Geology.

Tanya Srivastava

Dated: 11.03.2023

Tanya Srivastava

Place: Gangtok

Department of Geology
Sikkim University
Gangtok, Sikkim

ACKNOWLEDGMENTS

Above all, I would like to thank **Shri Kashi Vishwanath** for his countless acts of grace that have helped me to get through this. This research work would not have been possible without his blessings. In the process of completing my Ph.D., many people have provided me with incredible support and assistance.

I would like to express my sincere gratitude to my research supervisor **Dr. Nishchal Wanjari**, Assistant Professor Department of Geology, Sikkim University for his supervision, valuable guidance, and suggestions that benefited this research. He has always motivated me to do better in the field of research.

I would like to extend my sincere gratitude and appreciation to **Professor Nigel Harris** Emeritus Professor at Open University (UK) for extending all the help in suggesting various research articles, and new ideas which have immensely helped the research. The encouragement and wishes have always inspired me to strive for excellence. I will always be grateful for your kindness and valuable mentorship in the field of research. I would like to express my appreciation to **Dr. Catherine Mottram**, Senior Lecturer, at the University of Portsmouth for her valuable ideas, support, and encouragement. Whatever you have taught during all the online sessions has immensely helped me. You have always been kind and patient with me and thank you for sparing your valuable time.

I am grateful to the **Department of Science and Technology (DST)** for awarding me the **INSPIRE** fellowship **(IF160729)** which has immensely helped me to carry out the research. Besides this, I would like to thank the **Head of the Department, of Geology, at Banaras Hindu University, and the Director of the National Centre for Earth Science Studies (NCESS), Thiruvananthapuram, Kerala** for allowing to me carry out the analysis.

I would like to thank the **Head of the Department (Geology), Sikkim University Prof. Anil Kumar Misra the rest of the faculty members, lab assistants, and fellow members** of the Department of Geology, Sikkim University for their encouragement, and **Mr. Bhanu Manger and Mr. Abhishek Rai** for their help in the laboratory work.

I would like to appreciate **Martina Krekula** for helping me with tourmaline samples her continuous assistance was of great help.

Lastly, I would like to thank my parents **Vinita Srivastava, and Nirmalendra Srivastava,** my **younger brother Neelesh Srivastava and** my **dearest friends** who have supported me throughout my research and in life, with patience, kindness, and unconditional love. This would have not been possible without you all. Thank you for being my source of inspiration and enthusiasm throughout my Ph.D. years.

Tanya Srivastava

6 माइल, सामदुर, तादोंग - 737102
गंगटोक, सिक्किम, भारत
फोन-03592-251212, 251415, 251656
टेलीफैक्स - 251067
वेबसाइट - www.cus.ac.in

6th Mile, Samdur, Tadong-737102
Gangtok, Sikkim, India
Ph. 03592-251212, 251415, 251656
Telefax : 251067
Website : www.cus.ac.in

सिक्किम विश्वविद्यालय
SIKKIM UNIVERSITY

(भारत के संसद के अधिनियम द्वारा वर्ष 2007 में स्थापित और नैक (एनएएसी) द्वारा वर्ष 2015 में प्रत्यायित केंद्रीय विश्वविद्यालय)
(A central university established by an Act of Parliament of India in 2007 and accredited by NAAC in 2015)

Date: 6/3/2023

CERTIFICATE

This is to certify that the thesis work entitled **"Petrogenetic Evolution of Higher Himalayan Leucogranites in the Sikkim Region"** has been carried out by **Ms. Tanya Srivastava** for the fulfillment of the award of the degree of **Doctor of Philosophy (Geology)**. This work is original and has not been submitted in part or full, for any other degree or diploma in any University/Institution. Wherever required contributions of others, and their efforts are indicated clearly, with due reference to the literature, and acknowledgment of collaborative research and discussions.

Anil Kr Mishra 6/3/2023

(Anil Kumar Misra)

Head
Professor
Department of Geology
Sikkim University

6/3/2023

(Nishchal Wanjari)

Supervisor
Assistant Professor
Department of Geology
Sikkim University

LIST OF TABLES

LIST OF FIGURES

Figure 3.2. Photomicrographs of tourmaline leucogranites (a-c) tourmaline leucogranite with the typical mineral assemblage of K-feldspar, muscovite, quartz, and plagioclase (d) Perthitic texture (e) Tourmaline grains surrounded by quartz and K-feldspar (f) muscovite grains embedded in tourmaline leucogranites.

Figure 3.3. (a-f) Photomicrographs of tourmaline pegmatite of different samples from North Sikkim.

Figure 4.1. (a-i) Harker variation plot of North Sikkim leucogranites.

Figure 4.2. FeOt /MgO versus SiO_2 diagram after Miyashiro (1974).

Figure 4.3. The K_2O vs SiO_2 diagram after Peccerillo and Taylor (1976).

Figure 4.4. The molar Na_2O – Al_2O_3 – K_2O ternary plot Shand (1943).

Figure 4.5. AFM diagram after Irvine and Baragar (1971).

Figure 4.6. (a) Na_2O+K_2O-CaO (wt.%) vs SiO_2 for the samples of North Sikkim leucogranites Frost et al. (2001). (b) FeO/(FeO+MgO) vs SiO_2 (wt.%) after Frost et al. (2001) indicating peraluminous nature of the Leucogranites. (c) R_1vs. R_2 Tectonic Discrimination diagram of North Sikkim Leucogranites after Batchelor and Bowden (1985).

Figure 4.7. Ternary diagram of Al_2O_3/ (TFeO + MgO) vs. 3CaO vs. 5(K_2O/Na_2O) (after Laurent et al. (2014). A range of melt compositions (tonalites, metasediments, low- and high-K mafic rocks) was determined by the major-element compositions of partial melts in experiments.

Figure 4.8. (a) A/NK versus A/CNK diagram (Shand 1943) (b) K_2O+Na_2O versus SiO_2 diagram (Middlemost 1994) 1.Foidolite 2.Foid Syenite 3.Foid monzosyenite 4.Foidmonzo-gabbro5.Foid gabbro 6.Peridot gabbro7.Syenite 8.Monzonite

9.Monzodiorite 10.Monzogabbro 11.Gabbro 12.Quartz monzonite 13.Granite 14.Quartzolite 15.Granodiorite 16.Diorite 17.Gabbroic diorite (c) Normative (An-Ab-Or) classification diagram of North Sikkim leucogranites (O'Connor 1965) (d) Composition of melt produced by H_2O fluxed melting and dehydration melting (Patiño Douce and Harris 1998).

Figure 4.9. (a) log(Y+Nb) vs. log Rb (b) log Y vs. log Nb (c) log Ta+Yb vs. log Rb (d) log Yb vs log Ta trace-element based geotectonic classification of granitoids by Pearce et al. (1984) WPG, within-plate granite; VAG, volcanic-arc granite; ORG, orogenic granite; syn-COLG, syn-collisional granite.

Figure 4.10. Rb/30-Hf-Ta×3 ternary diagram showing that most of the sample's plot within the syn-collisional and post-collisional field (Harris, 1986).

Figure 4.11. (a, c) Chondrite normalized REE pattern for the two-mica leucogranites and tourmaline leucogranites respectively; (b, d) Primitive mantle-normalized trace element diagram for the two mica leucogranites. The normalizing values are taken from Sun and McDonough (1989).

Figure 4.12. (a) Geochemical classification diagram $Al_2O_3/(FeO_t + MgO + TiO_2)$ versus (Al_2O_3 + FeOt + MgO +TiO_2) Patiño Douce (1999) (b) CaO/ (TFeO+MgO + TiO_2) versus CaO + TFeO+MgO + TiO_2 diagram from Patino and Douce (1999).

Figure 4.13. (a) Rb/Ba versus Rb/Sr diagram modified from Sylvester (1998); (b) Al_2O_3/TiO_2 versus CaO/Na_2O diagram.

Figure 4.14. (a) Ce/Pb vs Ce (ppm); (b) Nb/U vs Nb (ppm) from Guo and Wilson (2012).

Figure 4.15. (a) Molar A/CNK vs. A/NK plot for tourmaline pegmatites (Shand,1947) b) Na_2O+K_2O versus SiO_2 (wt.%) diagram (Middlemost 1994) area 12 &13 represents quartz monzonite and granite. Green represents Type 1 and Blue represents Type 2.

Figure 4.16. In triangular $CaO-Al_2O_3-Na_2O-K_2O-Fe_2O_{3T}$ + MgO diagram, samples plot in mainly S-type field and on border with I-type field Chappell and White (1992).

Figure 4.17. (a) Chondrite normalized REE pattern for tourmaline leucogranite (b) Primitive mantle normalized trace element diagram for tourmaline leucogranites. The normalizing values are taken from Sun and McDonough (1989).

Figure 4.18. The trace element Zr vs TiO_2 diagram indicate mainly S-type granitic source for both the pegmatites after, Watson and Harrison (1983).

Figure 5.1. Classification of the principal groups of the tourmalines from Sikkim leucogranites and pegmatites Henry et al. (2011).

Figure 5.2. Ca-Fe-Mg ternary diagram after Henry and Guidotti (1985). These fields are: (l) Li-rich granitoid pegmatites and aplites These fields are: (l) Li-rich granitoid pegmatites and aplites; (2) Li-poor granitoids and associated pegmatites and aplites; (3) Ca-rich metapelites, metapsammites, and calc-silicate rocks.

Figure 5.3. (a) The ternary diagram $2Li^{+} - Mg^{2+} - Fe^{2+}$ for Y-site occupancy of alkali-group tourmalines indicates that all of the analyzed samples are schorl (b) The plot of Mg/ (Fe + Mg) vs. X-site vacancy/(Na + X-site vacancy) of tourmaline grains (Henry and Dutrow (2012).

ABBREVIATIONS

ITSZ	Indo Tsangpo Suture Zone
THS	Tethyan Himalayan Sequences
STDS	South Tibetan Detachment Systems
HHCS	Higher Himalayan Crystalline Sequences
LHS	Lesser Himalayan Sequences
MCT	Main Central Thrust
MBT	Main Boundary Thrust
MFT	Main Frontal Thrust
FTB	Fold Thrust Belt
XRF	X-ray Fluorescence
LA-ICPMS	Laser ablation-Inductively Coupled Plasma Mass Spectrometry
EPMA	Electron Probe Micro Analyzer
HREE	Heavy rare earth element
LILE	Large Ion Lithophile Element
REE	Rare earth element
MSWD	Mean Square Weighted Deviates
HFSE	High Field Strength Elements
LREE	Light Rare Earth Elements

6 माइल, सामदुर, तादोंग - 737102
गंगटोक, सिक्किम, भारत
फोन-03592-251212, 251415, 251656
टेलीफैक्स - 251067
वेबसाइट - www.cus.ac.in

6th Mile, Samdur, Tadong-737102
Gangtok, Sikkim, India
Ph. 03592-251212, 251415, 251656
Telefax : 251067
Website : www.cus.ac.in

सिक्किम विश्वविद्यालय
SIKKIM UNIVERSITY

(भारत के संसद के अधिनियम द्वारा वर्ष 2007 में स्थापित और नैक (एनएएसी) द्वारा वर्ष 2015 में प्रत्यायित केंद्रीय विश्वविद्यालय)
(A central university established by an Act of Parliament of India in 2007 and accredited by NAAC in 2015)

Date: 9/03/2023

PLAGIARISM CHECK CERTIFICATE

This is to certify that the plagiarism check has been carried out for the following Ph.D. thesis with the help of **OURIGINAL SOFTWARE (earlier URKUND)** and the result is **3%** which is within the permissible limit (below 10% tolerance rate) as per the norms of Sikkim University.

"Petrogenetic Evolution of Higher Himalayan Leucogranites in the Sikkim Region"

submitted by **Ms. Tanya Srivastava** under the supervision of **Dr. Nishchal Wanjari, Assistant Professor, Department of Geology, School of Physical Sciences, Sikkim University.**

Tanya Srivastava
9/3/2023

Tanya Srivastava
Signature of the Scholar

9/3/2023

Dr. Nishchal Wanjari
Countersigned by Supervisor

9.3.2023

Vetted by Librarian

पुस्तकालयाध्यक्ष
Librarian
केन्द्रीय पुस्तकालय Central Library
सिक्किम विश्वविद्यालय
Sikkim University

PREFACE

The Himalayan orogeny resulted due to the collision of the Indian and Eurasian plates. Various researchers have studied the Himalayan leucogranites from the western to eastern Himalayas. With the advancement in the U-Pb dating of zircons and monazite, granite crystallization and emplacement ages records have poured in, which has also fascinated various researchers in the Himalayan region.

This doctoral thesis focuses on the integrated geochemical, geochronological, and mineral chemistry studies of leucogranites and pegmatites occurring in the Sikkim Himalayas using whole rock geochemistry- major oxide elements rare earth elements (REEs) along with zircon and monazite U-Pb geochronological studies and boron isotopic studies to unravel the tectonic-magmatic and petrogenetic evolution. The doctoral thesis has been organized into ten chapters. They are summarised as follows: the first chapter discusses the introduction and leucogranites in the Himalayas. This chapter also introduces the objectives of the thesis and analytical techniques used for generating the geochemical, geochronological, and mineral chemistry data (XRF, LA-ICPMS, and EPMA). The second chapter deals with the regional geology of Sikkim with a detailed explanation of each litho-tectonic unit in the Sikkim Himalayas and comprehensive field observations. The third chapter elucidates the detailed petrography of two-mica leucogranite, tourmaline leucogranite, and pegmatites from the Sikkim Himalayas. The fourth chapter deals with the whole rock geochemistry (major, trace, and rare earth elements) of two-mica leucogranites, tourmaline leucogranite, and pegmatite samples. The fifth chapter addresses the mineral chemistry of tourmaline, biotite, muscovite, K-feldspar, and plagioclase from leucogranites and pegmatites from

the Sikkim Himalayas. The sixth chapter discusses the zircon U-Pb geochronological data and trace elements from zircons of two-mica leucogranite (ZY-LG-2) samples from Higher Himalayan Sequences, Sikkim.

The seventh chapter addresses the monazite U-Pb geochronological data and trace element data from the monazite of two mica leucogranite samples (ZY-LG-2) and tourmaline leucogranite sample (ZY-LGT-1). The eighth chapter discusses the Sr-Nd whole-rock isotope geochemistry which will elucidate the potential source for the generation of leucogranites. The ninth chapter deals with the boron isotopic composition from pegmatites, in Sikkim Himalayas, and the tenth chapter deals with the correlation of Sikkim leucogranites with leucogranites in the Eastern Himalayas. The eleventh chapter titled discussion, model, and conclusions present the summary and crucial findings of the research area.

CHAPTER 1

INTRODUCTION

1.1 Geology and Formation of the Himalayas

The Himalayas are the youngest, tectonically active mountain belts, and are the classic example of an orogenic system created by continent-continent collision (Yin, 2006). The collision also resulted in the uplift of the Tibetan plateau, the evolution of the Himalayas would have been different if the Tibetan plateau had not formed, which is thought to have greatly impelled both the tectonics and climate of the region (Hodges, 2000). The Himalayan range stretches over 2500 km from the south of the Indus valley beyond Nanga Parbat in the west to Namcha Barwa in the east (Singh, 2020; Valdiya, 1984). In the west, the ranges are 350 km wide, whereas in the east they are 150 km wide (Roy & Purohit 2018). Himalaya's evolution is closely related to the Andaman-Nicobar-Indonesia island arc in the southeast as well as the Makran Range-Oman Trench in the southwest (Valdiya, 1984). The paleomagnetic studies alluded that approximately 2600 ± 900 km of convergence took place between India and Eurasia in nearly three episodes of subduction of continental crust, intracontinental thrusting and internal deformation, and lateral extrusion (Patriat and Achache, 1984). The collision and northward convergence of the Indian plate produced main intracrustal faults accommodating approximately 580 to 900 km this crustal related shortening was observed in the different parts of the Himalayan fold-thrust belt (FTB) (DeCelles et al., 2002; Srivastava and Mitra, 1994). At mid-crustal level (15–20 km), leucogranites and metamorphism were produced by crustal shortening, and the metamorphic and granitic rocks were exhumed along the Main Central Thrust (MCT) as Higher Himalayan Crystallines (HHCS) (Thakur,1984).

With the breakup of Gondwanaland approximately 165 Ma ago, the Indian lithospheric crust began its northward migration along with other components of the Eastern Gondwana (Roy & Purohit 2018). The subduction of the Indian oceanic plate under the

Tibet block and subsequent ophiolite emplacement has resulted in the disappearance of the Tethys oceanic lithosphere along the Indo Tsangpo Suture Zone (ITSZ), and Tethys ocean closure is primarily restricted to the Kohistan Arc and the Indus- Tsangpo suture Zone (Ahmad et al., 1998; Singh and Jain, 2003). The Himalayan orogen (Fig. 1.1) from north to south is separated from four roughly parallel tectonic units defined by Indo Tsangpo suture in the north and south by Main Frontal thrust (MFT) (Godin et al., 2001; Le Fort, 1975; Yin, 2006). The four tectonostratigraphic units in the Himalayan orogen from north to south are (Yin, 2006) i) Tethyan Himalayan Sequence (THS) consisting of sequences of sedimentary rocks alternating with volcanics of Proterozoic to Eocene in age is defined by South Tibetan Detachment System (STDS) in the south and Indus Tsangpo suture in the north ii) HHCS, also known as Greater Himalayas consisting of high-grade metamorphic rocks of Paleoproterozoic to Ordovician in age lies between STDS and MCT iii) Lesser Himalayan Sequence (LHS) consisting of low-grade meta-sedimentary-volcanic rocks of Proterozoic-Cambrian in age separated by MCT to the north and Main Boundary Thrust (MBT) in the south (Richards et al., 2005) iv) Neogene Siwalik Formation consists of sediments of molasse type, restricted by MBT in the north and MFT in the south (Guillot et al., 1994; Yin, 2006).

1.2 Magmatism in Himalayas and Granitoids

In the Himalayas, distinct episodes of magmatism are known which are classified based on their age and tectonic emplacement: Proterozoic granites, Early Palaeozoic or Late Pan-African granites, Trans-Himalayan plutonic complex, and collision-related leucogranites with ages (2200-1800 Ma), (550-450 Ma),(103-40 Ma), (25-9 Ma) respectively (Guo and Wilson, 2012; Islam et al., 2005; Jain et al., 2012; Singh and Jain, 2003)

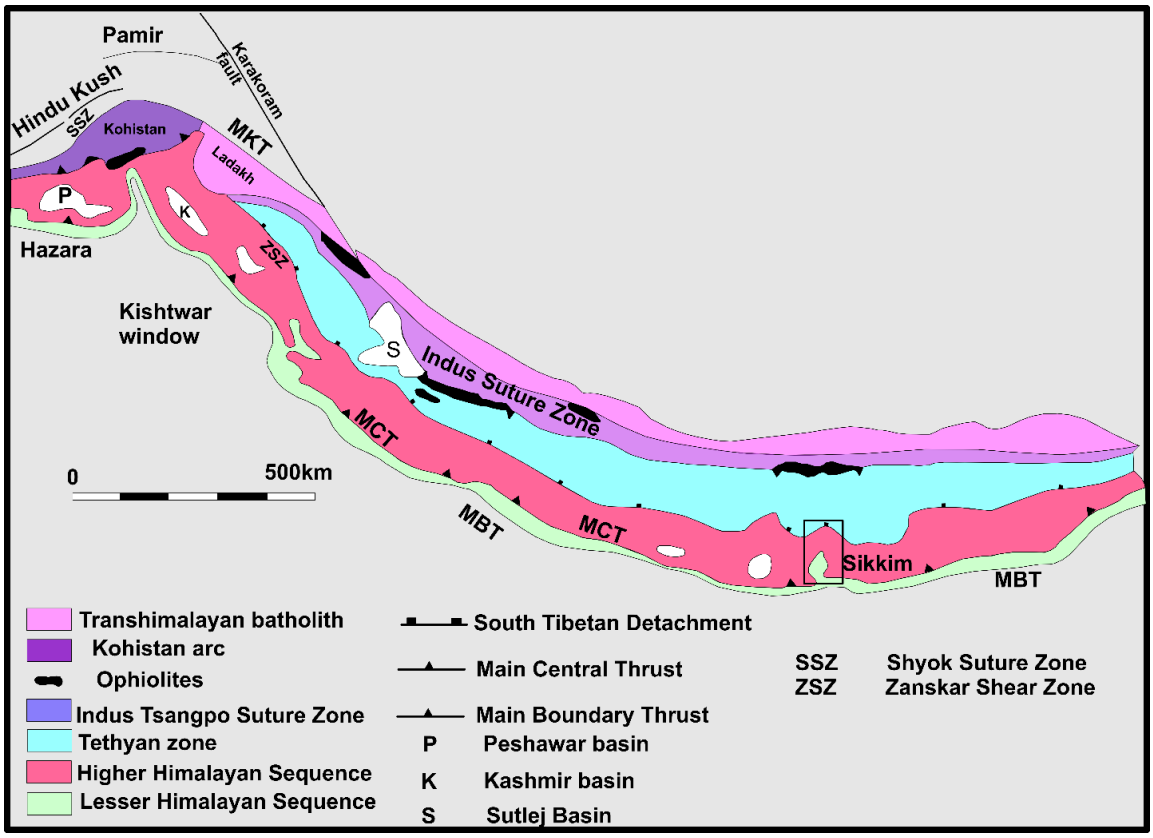

Figure 1.1. Geologic Map of the Himalayas showing major faults and major structural units modified after Searle (2015).

The early Proterozoic granites range from (2200-1800 Ma) in the Himalayas (Islam et al., 2005). The Proterozoic granites in the north-west Himalayas are Iskere (1852 Ma; Zeitler et al., 1989) Wangtu (1866 Ma; Singh et al., 1994), Ulleri augen gneiss in Central Nepal (1800-1880 Ma Célérier et al., 2009; 1780 Ma; Kohn et al., 2010), Lingtse augen gneiss in Eastern Himalayas Sikkim (1837-1854 Ma; Mottram et al., 2014a), Pegmatite are emplaced in Daling phyllite (~1854-1862 Ma; Acharyya et al., 2017), Orthogneiss Daling Formation (1896 Ma; McQuarrie et al., 2013). These Paleoproterozoic magmatic records indicate the assembly and accretion of the Columbia supercontinent (Kohn et al., 2010; Martin, 2017), and understanding the configuration of Columbia

depends critically on the Paleoproterozoic reconstruction of the Indian plate, particularly its northern margin (Phukon et al., 2018).

Rogers and Santosh (2002) and Zhao et al. (2004) contemplated that the Indian plate was adjacent to East Antarctica and North America, and East Antarctica and North China Craton respectively, whereas (Hou et al., 2008) deduced that it was located between North China craton and North America with a subduction zone in the north The models representing the reconstruction of the supercontinent Columbia is depicted in (Fig 1. 2).

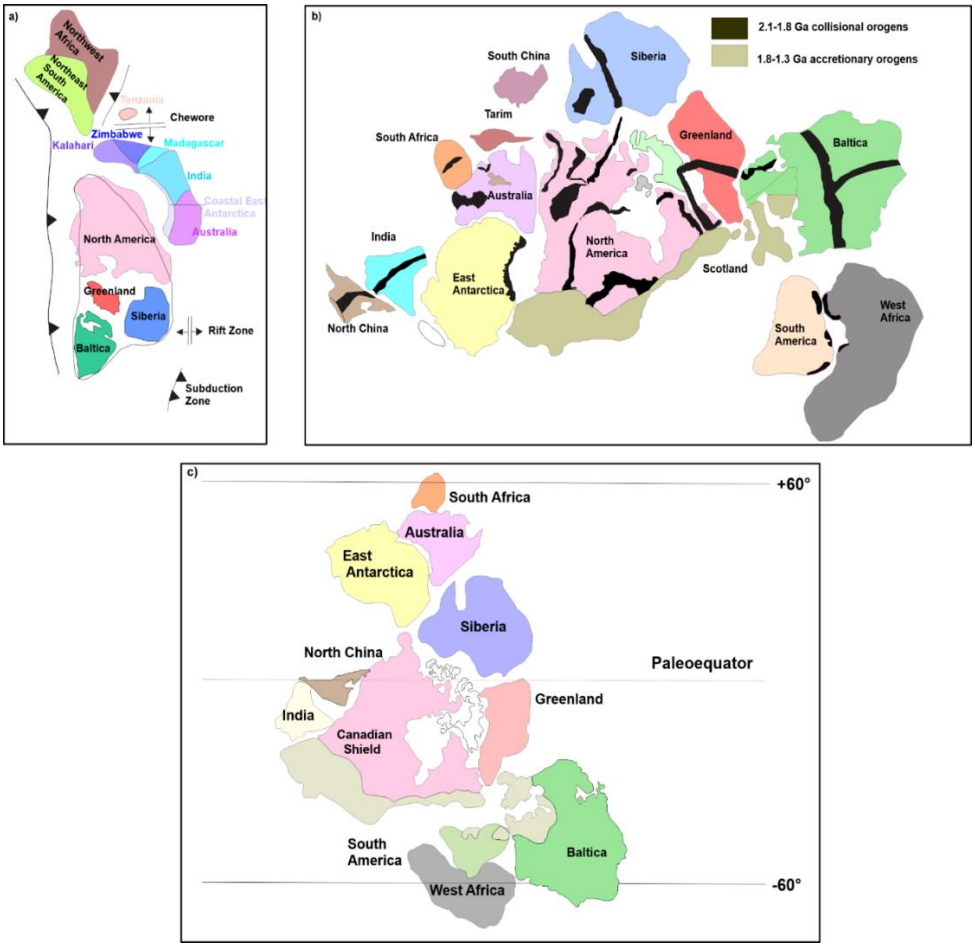

Figure 1.2. Models depicting the reconstruction of supercontinent Columbia a) Model of Rogers and Santosh (2002) b) Model of Zhao et al. (2004) c) Model of Hou et al. (2008).

The Neoproterozoic ages 1200-900 Ma (809-855Ma; Wang et al., 2017), Chaur, western Himalaya (823 Ma; Singh et al., 2002; 929 Ma; Singh et al., 2020), Jutogh granitic gneiss, western Himalaya (861 Ma; Singh et al., 2020); Bhutan granitic gneiss (~825 Ma; Richards et al., 2006), Hapoli granitic gneiss, Arunachal Himalaya (~878-825 Ma; Yin et al., 2010a); Peshawar granitic gneiss (~816 Ma; Ahmad et al., 2013). These magmatic ages have been related to the presence of superplume and breakup of the Rodinia supercontinent (Li et al., 2008; Wang et al., 2017), and also subduction and collision during Grenvillian orogeny and formation of the Rodinia supercontinent (Singh et al., 2020).

During the early Pan-African event, the southern tip of India collided with the Congo and the northwest margin with Azania and northern Madagascar (Singh, 2020). The early Paleozoic granites range from (550-450 Ma). The Cambrian- Ordovician orogeny is also termed Bhimphedian Orogeny (Cawood et al., 2007; Myrow et al., 2016; Palin et al., 2018) or Kurgiah orogeny (Srikantia, 1981) and in the wake of Gondwana assembly, the orogeny is linked to Andean-type orogenic activity along the northern margin of the Indian continent (Cawood et al., 2007). To comprehend the final assembly of the Gondwana supercontinent and initial subduction along the boundary of the peri-Gondwana assembly, early Paleozoic magmatism in the Tibetan Himalayan orogen has been considered crucial (Cawood et al., 2007; Gehrels et al., 2006; Zhu et al., 2011). However apart from Andean-type Paleozoic magmatism is attributed to lithospheric thickening and delamination (Li et al., 2015; Zhao et al., 2016). The Carboniferous (349 Ma) age of the studied leucogranites is comparable to several late Paleozoic magmatic rocks found along the Paleo-Tethys margin of Gondwana. In the eastern part of the Lhasa terrane, coeval magmatic rocks have been reported from the Gyaca (367–345 Ma; Ji et al., 2012), Zhengga (366–353 Ma; Wu et al., 2013) and Nang (371–

341 Ma; Dong et al., 2014). Studies have also described many late Devonian-early Carboniferous (381–331 Ma) magmatic rocks in the Qiangtang and Longmu Co-Shuanghu suture zone lying north of the Lhasa terrane (Dan et al., 2019; Liu et al., 2018; Zhai et al., 2018). This early Carboniferous magmatism can be linked to the separation of the Lhasa terrane from Gondwana which led to the opening of the Sumdo Paleo-Tethys Ocean.

The subducting Indian Plate is responsible for the Trans-Himalayan plutons, also known as the Ladakh, Kohistan, and Karakoram batholiths and Gangdese magmatic belt (Singh and Jain, 2003 and references therein). The Ladakh plutonic complex has multiple intrusions ranging from 103 to 20 Ma (Wu et al., 2007). There are several assemblages of low-grade metamorphosed sedimentary rocks of the Palaeozoic-Mesozoic Era found in the Trans-Himalayan and Lhasa Karakoram blocks that form the southern margin of the Eurasian plates (Henderson et al., 2011).

The signature of early Cretaceous magmatism is also seen as 144 Ma age in the studied 2mg have and 101 Ma age of sillimanite bearing gneiss have been reported across the whole Tethyan Himalaya. These ages are similar to the age of the Rajmahal–Bengal–Sylhet Traps (118–117 Ma) (Ghatak and Basu, 2011), Comei–Bunbury Large Igneous Province of southeastern Tibet and SW Australia and are also reported across Australia, India, Antarctica, and the nascent Indian Ocean (Whittaker et al., 2016) The separation of the Tethyan Himalaya from the Indian craton is suggested to have occurred during ongoing Early Cretaceous extension related to the Kerguelen mantle plume that resulted in the breakup of eastern Gondwana (Chen et al., 2021, 2018; Ma et al., 2017; Singh et al., 2021). During the Oligocene-Miocene period, leucogranite magmatism persisted for ca. 19 Ma (Wu et al., 2020)**.** The granites in the Himalayas were mostly emplaced from Oligocene to Miocene (Weinberg, 2016; Wu et al., 2020), while in the

Tethyan Himalayas, a few of them are interpreted to be the product of an amphibolitic source of Eocene age (Aikman et al., 2008; Hou et al., 2012; Zeng et al., 2011). The Miocene-Oligocene leucogranites distributed in the HHS include Gangotri, Shivling, Manaslu, Nyalam, Annapurna, Gyirong, Shisha Pangma, Rongbuk, Everest-Makalu, Dinggye, Gaowu, Khula Kangri, Masang Kang, Leo Pargil granites (Cottle et al., 2015b; Guo and Wilson, 2012; Lederer et al., 2013; Searle et al., 2003). The U (Th)-Pb ages from the zircons and monazite from HHCS are reported by various researchers, 25-9 Ma (Guo and Wilson, 2012), 35-16 Ma (Streule et al., 2010), 32-17 Ma (Searle et al., 2003), 37-20 Ma (Kohn and Corrie, 2011) 30-15 Ma (Larson et al., 2011), 39-13 Ma (Cottle et al., 2009). Cenozoic leucogranites from the Himalayas are typically linked to the partial melting of metasedimentary rocks are typically linked to the partial melting of metasedimentary rocks at low temperatures of 770 °C (Gao et al., 2021).

1.3 Granite and Pegmatite Classifications

1.3.1 Granite Classification

The Granitoid or granitic rocks are essentially composed of quartz and feldspar and can be classified based on mineralogy, petrographic features, isotopic characteristics, and geochemistry of major and trace elements. Though granites have uncomplicated mineralogy they possess different modal compositions, genesis, tectonic environments, and types of emplacements (Barbarin, 1990, 1999; Bonin et al., 2020). Two types of mechanisms result in the formation of granitoid, i.e., either through differentiation of basaltic magma which leads to the formation of new continental crust, or partial melting of metasedimentary and meta-igneous rocks (Moyen et al., 2017). Previously various geologists have given different classification schemes: (Streckeisen, 1976) classified granitoids based on nomenclature based on the relative proportion of quartz, alkali

feldspar, and plagioclase. In the Lachlan fold belt of east Australia, two types of granitoids were identified i.e. I type, which is metaluminous to weakly peraluminous resulting from igneous sources whereas S type granitoids, strongly peraluminous having higher silica content in comparison to the former type, derived from anatexis of sedimentary protoliths. Further again based on Na_2O content, Molecular Al_2O_3/ (Na_2O+K_2O+CaO), normative corundum, and variation diagrams differences between both were mentioned (Chappell and White, 1974; Chappell and White., 2001). M-type derived from the mantle (White & Chappell, 1983) and A-type granitoids having high potassic, high FeO/ (FeO +MgO), and was considered anorogenic. (Loiselle &Wones, 1979) however, later studies by (Eby, 1990; Whalen, 1987) suggest that it may be related to continental extension (Eby,1992) further dividing them into A1 and A2 categories occurring within post-collisional settings. **(**Pearce et al., 1984). In the present study, to differentiate between the tectonic environment, geochemical analysis of the samples was done, and four tectonic discrimination diagrams: collisional granites, within-plate granites, and volcanic arc granite were specified based on plots of Nb vs., Ta vs., Rb vs. (Y+Nb), and Rb vs. (Y+Ta) (Pearce et al., 1984).

Ishihara (1977), differentiated granites into the magnetite series which is mostly oxidized and other into the ilmenite series which is reduced**,** but this is applicable mostly for arc granites and less feasible for other tectonic environments. According to Frost et al. (2001) classification includes Fe number, Modified Alkali Lime Index (MALI), and Alumina Saturation Index (ASI). Based on the Fe number granitoids are divided into Ferron and magnesian, In MALI the granitoids are divided as alkali, calcic, calc-alkalic, and calcic-alkali. Based on Alumina Saturation Index (ASI) the granites can be classified as Peraluminous, Metaluminous, and Peralkaline (Shand, 1947, Frost et al., 2001, 2008). ASI= [Al/Ca-1.67P +Na+K] molecular granitoids are divided into

peraluminous if ASI>1.0, in metaluminous ASI<1.0, Na + K< Al, peralkaline ASI<1.0, Na+K>Al. The peraluminous, calc-alkaline, and (tholeiitic, peralkaline, and alkaline granitoids) are crustal, mixed, and mantle origin respectively (Barbarin, 1990, 1999). In the continental crust, variation in granites from dike to batholith, in terms of emplacement and textural, mineralogical, and geochemical aspects as well form a crucial component (Wu et al., 2017). In comparison to the lower continental crust, the upper continental crust is enriched in highly incompatible minerals than lower crust (Rudnick and Gao, 2003). There are two models given to describe the origin of granitic rocks i.e., firstly by the crustal melting model which includes the production of granitic melts by partial melting of the lower crust, and secondly by the fractionation of the basaltic magma in which the main cause is the melting of the mantle (Moyen et al., 2021).

1.3.2 Pegmatite classification

Due to their similar mineral assemblage and bulk composition, granitic pegmatites also known as pegmatites are sometimes thought to be derivatives of granitic melt and they may or may not have a relation to parental granite (Černý, 1991; London, 2018) and other processes, such as anatexis, can contribute to pegmatite production besides fractional crystallization (Dill, 2015). From a scientific standpoint, the study of pegmatite petrogenesis is essential because they represent a significant magmatic event and also helps to establish the source and conditions of the melting. These studies also have economic significance because the conclusions can be used to help locate rare metal ore deposits (Lv et al., 2021).

The granitic pegmatites are classified into five divisions based on geological setup (Černý and Ercit, 2005)

(i) Abyssal (high grade, high to low pressure)

(ii) Muscovite (high pressure, low temperature)

(iii) Muscovite rare element (moderate to high T and P)

(iv) Rare element (low temperature and pressure)

(v) Miarolitic (shallow level)

Secondly, the division is based on the petrogenetic approach into three families

(i) NYF type accumulates Nb, Y, and F (besides Be, REE, Sc, Ti, Zr, Th, and U), and are fractionated from sub-aluminous to metaluminous A and I type granites.

(ii) LCT with the prominent accumulation of Li, Cs, and Ta (besides Rb, Be, Sn, B, P, and F) originate from S-type granites and less commonly from I-type granites.

(iii) NYF+LCT (mixed).

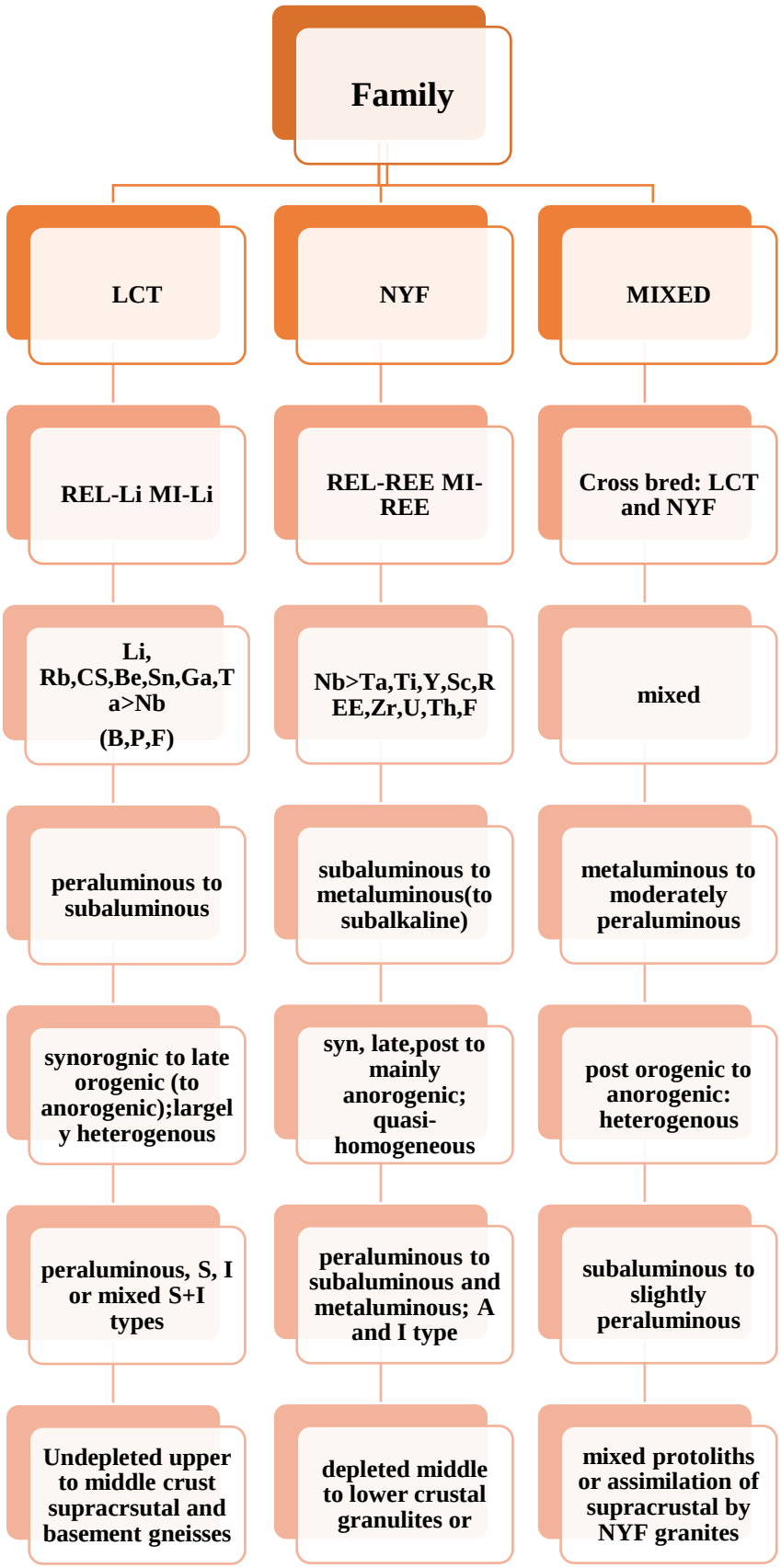

Table 1: The Family system of Petrogenetic classification of Granitic Pegmatites of Plutonic derivation (Černý and Ercit, 2005).

1.4 Tectonic Models

Numerous explanations have been put forward to explain the exhumation of the HHS (Fig. 1.3 a-e) including gravity-driven collapse (Colchen et al.1986), wedge extrusion (Burchfiel et al., 1992; Grujic et al., 1996) tectonic wedging (Yin, 2006), and, channel flow (Beaumont et al., 2001; Godin et al., 2006; Grujic, 2006; Grujic et al., 2002; Harris, 2007; Jamieson et al., 2006; Nelson et al., 1996) and another one is critical taper (Kohn, 2008). Among these models, the channel flow model and critical taper seem to be more popular.

Gravity-driven collapse - This model suggests that the STDS activity, that slides northward resulting from the gravitational instability caused by thickened crust in the orogenic belts. The sliding may result due to a decrease in crustal strength and compressive stress (Searle, 2010; Zhang et al., 2020).

Wedge extrusion - The HHS extruded southward as a northward tapering wedge by combining thrust along MCT at its base and extension along STDS at the top of the unit as a wedge deformed by non-coaxial general flow, a rigid wedge or a ductile wedge undergoing simple shear (Grujic et al., 1996; Hodges et al., 1992; Vannay and Grasemann, 2001).

Tectonic Wedging /duplexing - This model suggests that the northward movement of the THS along the STDS may not be caused by north-south extension but by the reverse thrust of the hanging wall of MCT (Webb et al., 2011).

Critical Taper - The Himalayas are modeled as a Coulomb wedge in a critical taper wedge undergoing shortening and extension when the wedge is thinned and over thickened respectively (Davis et al., 1983; Kohn, 2008).

Channel Flow - According to the classical channel flow model for the Higher Himalayas, the entire HHS is bounded by MCT, and the movement of MCT was synchronous with normal shear-sense motion on the STDS (Burchfiel et al., 1992; Grujic et al., 1996; Searle and Rex, 1989). This further led to the advancement of channel flow, according to (Beaumont et al., 2001; Godin et al., 2006; Harris, 2007; Jamieson et al., 2006), a low viscosity partially molten mid-crustal channel tunneled southward from beneath Tibet's thickened crust towards the Himalayas, caused by a lithostatic pressure gradient.

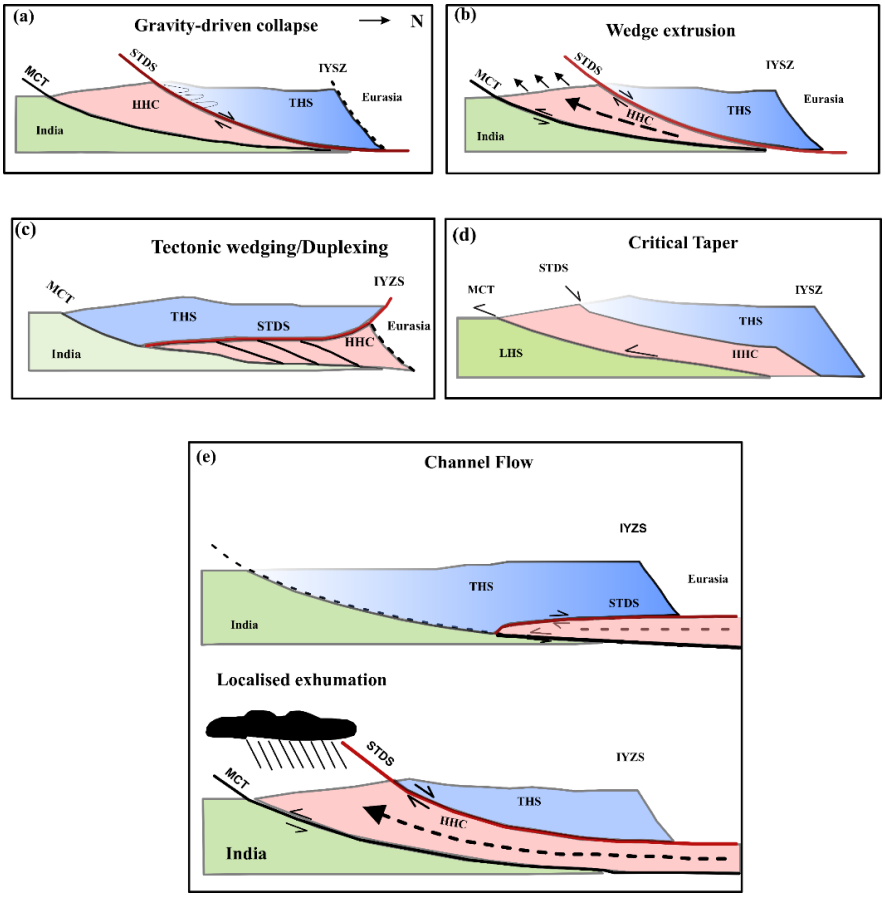

Figure 1.3. Schematic representation of tectonic models for the exhumation of HHC rocks between Main Central Thrust (MCT) and South Tibetan Detachment System (STDS) (Webb, 2013 and references therein) a) Gravity driven collapse b) Wedge extrusion c) Tectonic wedging/Duplexing e) Channel flow (HHC: Higher Himalayan Crystallines; THS: Tethyan Himalayan Sequence; HHS: Higher Himalayan Sequence; LHS: Lesser Himalayan Sequence; IYSZ: Indus Yarlung Suture Zone).

1.5 Leucogranite significance and Evolution in the Himalayas

Himalayan leucogranites serve as a time capsule for the tectonic development of the Himalayan orogen and an insight into its deep dynamic processes (Fan et al., 2021). Leucogranites are important for understanding plateau uplift, melting within continental collisional belts, and crustal thickening (Zhang et al., 2012). In collisional orogens like the Himalayas, Variscan, Hercynides, and Caledonides, leucogranites are common (Barbarin, 1999; Harris et al., 1995; Hopkinson et al., 2017). The leucogranites are perceived as peraluminous, nearly having a eutectic composition, crustal melting products, evolved in collisional orogen usually contains quartz, feldspar, plagioclase, and mafic minerals (< 5 volume percent), the silica and alumina content are high and consists of garnet, tourmaline, and muscovite (Brown, 2007; Harrison et al., 1999; Inger and Harris, 1993; Le Fort et al., 1987; Ma et al., 2017b; Nabelek, 2019; Wu et al., 2015; Zhang et al., 2020). In the Himalayas, andalusite-bearing leucogranite has been reported by various researchers (Castelli and Lombardo, 1988; Visonà and Lombardo, 2002) it shows textures indicating that andalusite is in an early crystallization phase. The majority of leucogranites have been defined as crustal melts (Chappell and White, 2001; Hopkinson et al., 2017) that are derived from the partial melting of metasediments, while some have suggested that it may have been derived from a mantle component (Healy et al., 2004). The granitoids in the Himalayas range from Proterozoic to Recent and are divided into two types: pre-collision and syn-collisional to post-collisional which occur in the form of granites and gneisses in pre-collisional and leucocratic type in the other (Singh and Jain, 2003). The evolution of the Himalayas and Tibet is the result of a collision between India and Eurasia (Hodges, 2000). The Himalayan leucogranites, Cenozoic in age are confined into two sub-parallel

belts: The northern belt intrudes into the Tethyan Himalayan sequence composed of clastic and carbonate rocks are known as Tethyan Himalayan leucogranites, whereas the southern belt referred as Higher Himalayan leucogranites intrude into high-grade metasedimentary rocks (Wang et al., 2017).The Himalayan leucogranites are important in understanding, studying, and interpreting metamorphism, anatexis, evolutionary models, and deformation after collisional activity (Yang et al., 2005) and tectonic evolution and melting behavior can be understood by the timing of emplacement and geochemistry of the leucogranites (Guo and Wilson, 2012; King et al., 2011; Zhang et al., 2014).

1.6 Literature Review

Earlier workers (Gansser, 1964; Le Fort, 1975; Valdiya, 1984) have provided standard reviews of the Himalayas and its formations over the years which have been continuously updated since then. Similarly, various studies have been done on numerous granitoids in the Himalayas to decipher the dates ranging from Precambrian to Early Palaeozoic in age. As stated above four episodes of magmatic activity have been reported in the Himalayas which has assisted to categorize the Himalayas granites into four groups based on age and their tectonic location i.e., Proterozoic granites, Early Palaeozoic granites, intrusive phases of the Ladakh plutonic complex and Tertiary leucogranites. As this research work focuses on Tertiary leucogranites from Sikkim Himalayas, as they are of utmost importance due to their association with collisional events and activity around the STDS. In the Himalayas various researchers have provided studies on the source, petrogenesis, and petrogenetic model, however, these remain controversial. Le Fort et al. (1987) explain the investigation of two mica-leucogranites from the Manaslu pluton in which major elements showed homogeneity whereas trace elements were variable, although the melting was homogeneous. (Guillot

and Le Fort (1995), discussed the bimodal origin of leucogranites where the generation of leucogranites from two different sources i.e., two mica leucogranites from the metagreywacke origin, water-saturated condition and the tourmaline leucogranites, water absent conditions. Patiño Douce and Harris (1998) observed in their study that dehydration melts at 750-800˚C whereas H_2O flux melting occurs at a temperature less than 750˚C. The melting of muscovite is more rapid than the biotite schist whereas the slope of dehydration melting for the latter is more than the earlier one. Nabelek and Liu (2004) explained that the collision leucogranites are derived from pelitic sources and further elucidated in the paper that shear heating deals with partial melting to deformation and metamorphism which leads to the generation of leucogranites.

Guo and Wilson (2012), described leucogranites are derived from both the Lesser Himalayas (20%) and Higher Himalayas Sequence (80%) based on the Sr-Nd isotope. The northward underthrusting resulted in the metasomatisation of Higher Himalayan Sequences by the dehydration fluid derived from the LH sequence. Singh (2013), reported on the origin and emplacement of leucogranites from Arunachal Pradesh. The High Field Strength Elements (HFSE), depletion indicates that the granite is generated by partial melting of the crust. The geothermobarometric calculation validates that melt was generated in the middle crust at approximately 20 km of depth. Liu et al. (2014) unveiled leucogranitic magmatism through U-Th-Pb dating of zircon, monazite, and xenotime. The granites of age 44-28 Ma according to major elements and isotopes showed that these were not derived from metasedimentary rocks of HHS whereas in the granite showing 8 Ma age, it is major and trace element composition indicate origin from muscovite or biotite dehydration melting. Liu et al. (2016). explained laser ablation technique has been used to constrain the age of Kampa leucogranites by using a set of U-(Th)-Pb zircon, monazite, and xenotime. According to this study, it is

suggested that Kampa leucogranites were crystallized between ~26-24 Ma and monazite data shows the tetrad effect and leucogranites are highly fractionated. Weinberg (2016), compared the conditions of anatexis in the Greater Himalayan Sequences in the Himalayas. Along with nature, duration, and timing the study of ages of zircon and monazite ages of anatectic rock range between 25 to 15 Ma for prolonged crustal melting. Along the Himalayan range, fault movement associated with internal strain distribution took place at different times and durations according to the STDS. Hopkinson et al. (2017), expounded on the significance of geochemistry in understanding crustal evolution. In recent studies, it has been mentioned that even S-type granite has both the compositions of crustal and upper mantle sources which indicate evidence of crustal growth. However, in this study, isotopic signatures from zircons reveal that leucogranites were solely derived from crustal sediments and do not have mantle inputs. This study states that crustal growth is not a result of syn-orogenic melting during collision activity.

Gou et al. (2019), illustrated that the Himalayan Leucogranites provide inputs about partial melting, tectonic and magmatic history. The leucogranites from Paiku are enriched in LREE and LILE. The study results that garnet and tourmaline leucogranites are formed due to muscovite dehydration and cordierite leucogranites are the product of biotite dehydration melting. The data obtained from the LA-ICPMS technique for zircons indicate a low degree of partial melting. Nabelek (2019), elucidated the thermal model for the generation of leucogranites and the role of flux melting, vapor absent melting role in the generation of leucogranites which involves the peritectic breakdown of muscovite. The difference between muscovite dehydration melting and biotite is explained as the former has a narrower range of temperature and occurs at lower temperature and producing wet melts and a wide variety of textures can be seen. Zhang

et al. (2020), explain the activity and effect of the South Tibetan Detachment system on leucogranites. The youngest syn-kinematic cut by STDS, syn-kinematic sheared and post kinematic which is cut across the STDS gives the age ~18 Ma, ~24-25Ma, ~17.4Ma and affects the age of Cuonadong, Lhozhag, Xiaozhan Leucogranites respectively. In the eastern Himalayas, the Kuju leucogranites are affected by north-south trending rifts (NSTR) with an age of ~ 16 Ma. Cao et al. (2022) reviewed the geochemistry, geochronology, genesis, and rare metal mineralization of Himalayan leucogranites.

In Sikkim Himalayas, researchers have tried to explain the age constraints on metamorphism. The protracted melting and high-temperature history documented by zircon and monazite ranges from ~31 to 17 Ma (Rubatto et al., 2013), U-Th-Pb monazite ages from rocks below the MCT indicate that prograde metamorphism ranges from ~21-18 Ma (Mottram et al., 2015), Sm-Nd garnet ages of migmatites spans from 23-16 Ma (Harris et al., 2004). Sorcar et al. (2014), discussed migmatite melting, in which isothermal decompression is followed by isobaric cooling. Two stages of the cooling have been discussed along with the triggering of the decompression explained by the reduction in density due to the generation of the melt.

Catlos et al.(2004), have dated the deformed leucogranites from north Sikkim which yielded zircon and monazite U-Th-Pb ages ranging from 17-15 Ma which evoked that from 17-15, Ma deformation activity along the STDS took place. Kellett et al.(2013), explained that the activity along the STDS north of Sikkim is 24-13 Ma.

1.7 Research Gap

- In the Sikkim region, earlier there was a lack of a detailed set of petrographical, geochemical, geochronological, and mineral chemistry data on Higher Himalayan leucogranites.
- A lack of detailed sampling and data has precluded constraints on the petrogenesis and source of leucogranites in the Sikkim region.
- This region had no detailed explanation for the petrogenetic evolution of leucogranites.

1.8 Objectives

To address the research gaps in the previous section, this thesis aims to address five primary objectives to study the petrogenetic evolution of the Higher Himalayan in Sikkim.

Objective 1: To reveal the characteristics and origin of Higher Himalayan Leucogranites in Sikkim.

Objective 2: To generate geochronological, geochemical, and mineral chemistry data from the Higher Himalayan Leucogranites of Sikkim.

Objective 3: To constrain source characteristics and chronological evolution of Higher Himalayan Leucogranites.

Objective 4: Isotopic analysis of whole rock samples and accessory minerals in Higher Himalayan Leucogranites

Objective 5: Correlation of Higher Himalayan Leucogranites from Sikkim region with Leucogranites from other region in Himalayas.

1.9 Methodology

1.9.1 Sample Preparation Procedure:

a) Powdering of samples for Geochemical Analysis

The samples of leucogranites and associated rocks were chipped to reduce grain size with the help of a geological hammer and were washed to remove any dirt or contamination and were air dried.

Next, the jaw crusher was used for breaking the samples into smaller fragments. The chipped samples were reduced to mesh size ~40 mesh - ~80 mesh. The samples were collected in a polybag. After running each sample, the crusher was cleaned with acetone to avoid any sort of contamination in the next sample (Fig.1.4).

Figure 1.4. Jaw crusher machine for the reduction of sample size.

b) Tema mill Procedure

Post crushing by jaw crusher the samples were fed to a Tema Mill. In Tema, mill samples are grounded by horizontal vibrations and friction in a rounded disc-shaped apparatus. To make the sample homogenized the apparatus used for grinding contains 2-3 metal rings made up of chrome steel with a heavy metal disc at the centre. The samples are placed in between these metal rings. During the operation, the metal disc collides with the rings, and the sample is crushed to a fine powder. After the completion of each cycle round the container should be cleaned properly. The conditioning can also be done before processing each sample to remove the memory effect of the previous sample by running a small amount of sample each time (Fig. 1.5).

Figure 1.5 Tema mill used for grinding the samples.

1.9.2. X-Ray Fluorescence

X-Ray Fluorescence is a powerful analytical method used for the elemental analysis of geological materials. It is widely used for whole rock analysis of major, minor, and trace element content of the rocks from ppm to wt.% level in pellet or bead form.

a) Principle:

The basic principle involved in XRF is, X-rays produced by a source irradiate a sample, the x-rays can either be scattered or absorbed, when the X-rays are absorbed, the atoms become ionized as a result the electron from the inner shell gets ejected if the primary X-ray had sufficient energy and an electron from higher energy shell falls into the position being vacated by inner electron and emits X-rays of characteristic wavelength. As a result, we can measure the elemental composition of the sample by the X-rays with a discrete set of energies. The emitted radiation is of lower energy than the incident X-rays and this process of emission of X-rays is called X-ray Fluorescence and it is counted in kcps (Kilo Count Per seconds). The working theory is based on the activation of the sample atoms by high-energy X-rays followed by the emission of distinctive photons with a given energy, correlated to the atomic number Z of each element (Moseley's law). The concentration is calculated by using a set of standards by the calibration curve. It is of two types: Energy Dispersive X-Ray fluorescence (EDX) and Wavelength Dispersive X-Ray Fluorescence (WDX). In comparison to EDX, WDX has much better energy resolution.

Figure 1.6. Wavelength Dispersive X-Ray Fluorescence Spectrometer (WD-XRF Bruker model S4 Pioneer) facility for determining whole-rock major oxide at NCESS, Kerala.

b) Pellet and Bead Preparation

The Tema mill is used to powder the samples into 1-2 gm of each sample powder (200 mesh), which is then placed in circular aluminium cups to prepare pellets (Fig.1.7). Since the powder is difficult to bind, it can be pelletized by mixing it with a binder; in this case, boric acid (H_3BO_3) was used; the sample should be placed above the binder as shown in (Fig. 1.7). The samples were then placed over the binder in (Fig. 1.7), and pellets were formed by pressing it under INSMART pellet pressure. (Fig.1.7).

Figure 1.7 Pellet preparation for determination of major oxides.

c) Analytical Details:

The major element oxides were measured using WD-XRF (Bruker S-4 Pioneer) at NCESS, Thiruvananthapuram. The international rock standards used for calibrations are Basalt, Hawaiian Volcanic Observatory (BHVO-2), and JG-2. (Japanese Granite) at National Centre for Earth Science Studies (NCESS).

Reference materials

The USGS Geochemical Reference Materials provides geochemical reference materials to be used by earth scientists all over the world. Most of the reference materials used are from silicate rock collected from the United States and Hawaii. A variety of

analytical techniques and testing in various laboratories have been done to determine the composition of these materials.

1.9.3 Laser ablation-Multi Collector-Inductively Coupled Plasma Mass Spectrometry (LA-ICP-MS)

A potent instrument for the high-precision assessment of the isotopic ratios of numerous elements in geological samples is Laser Ablation coupled to Multi-Collector Inductively Coupled Plasma Mass Spectrometry (LA-ICPMS). This technique is widely used in the field of geology, archaeology, and environmental science.

a) Principle:

Laser ablation inductively coupled plasma mass spectrometry (LA-ICP-MS) has a number of advantages due to its simplicity and sensitivity and is considered one of the most versatile methods in solid materials analysis. The advantages of LA-ICPMS include minimal sample preparation, high-resolution output, and low contamination whereas isobaric interference, severe matrix effect, and complex isotopic fractionation/mass behavior are its major disadvantages (Zhang et al.2020). Some of the isotopes which are measured by LA-ICP-MS are Li, B, C, Mg, Si, Ca, etc. whereas the radiogenic isotopes include Sm-Nd, Rb-Sr, Lu-Hf, etc. This method allows laser spot size <10 μm with accurate determination of elements at ppm level.

b) Heavy mineral separation and magnetic separation

Procedure:

i) Sieving: The samples were sieved after reducing the size in Disc Mil l between 40 mesh- 50 mesh size (ASTM). Firstly, the samples were washed with water to remove clay-sized particles and dirt. Secondly, the samples were kept in a laboratory oven for drying between 80°-90°C.

ii) Density separation: It is one of the common methods used in separation based on different specific gravities. If minerals of different densities are mixed and put in heavy liquid, the minerals lighter than liquid will float and heavier grains will settle down. The minerals like quartz and feldspars that have low specific gravity are known as light minerals or lights. The minerals like zircon (4.85g/cc), monazite (5.15g/cc), apatite (3.19g/cc), garnet (3.5-4.3g/cc), etc. having density more than that of heavy liquid are known as heavy minerals or heavies. The heavy liquid used for separation is Bromoform, with a density of 2.89 g/cc, and a Di-iodomethane density of 3.3 g/cc. synthesized by Merck Life Pvt Ltd and Central Drug Pvt Ltd.

The separation was done in a separatory funnel with a stopped clock. Firstly, the heavy liquid was placed in the funnel, and the sample was added, then again liquid was added, and after stirring it was left for some time to permit heavy minerals to be separated from lighter minerals. (Fig. 1.8).

After separation heavy minerals were transferred on Whatman filter paper and the heavy liquid was allowed to drain through the funnel. The heavy mineral on filter paper was washed with deionized water and acetone and was kept for drying.

Figure 1.8. Heavy Mineral Separation using separating funnel used for separating heavy and light minerals.

iii) Magnetic separation (Frantz Isodynamic Separator)

The minerals in a separator are separated depending on the magnetic susceptibility and work according to the response of individual grains to the electromagnetic field versus gravity. It has a chute between the poles of an electromagnet. It works in two directions forward and sideways which controls the speed of movement of grains and separation of minerals through susceptibility respectively. In Frantz Isodynamic Separator the minerals were separated into magnetic and non-magnetic minerals by adjusting the angle (20°-5°) and current (0-1.5 ampere) (Fig. 1.9).

Figure 1.9. Frantz Isodynamic Separator used for separating magnetic and non-magnetic minerals.

1.9.4 Analytical methods for whole rock, Mineral chemistry U-Pb Geochronology, and boron isotopes

a) Whole rock analysis for leucogranites

Major and trace elements found in whole-rock samples were examined by Bureau Veritas in Canning Vale, Australia, and the National Centre for Earth Science Studies (NCESS). By using X-ray fluorescence, the major element oxides were identified (XRF). The precision for measurements is more than 1%, and the accuracy for the reference standards is better than 0.5% for SiO_2 and 3% for other main oxides. Using Laser Inductively Coupled Plasma Mass Spectrometry, the trace elements, including REE, were identified (LA-ICPMS). The measurements were performed with precision and accuracy better than 5% using a New Wave EXCIMER 193nm UV Laser connected to an Agilent 7900 ICP-MS (Srivastava et al., 2022).

At the National Centre for Earth Science Studies (NCESS), the main oxides from the leucogranites of the Thangu region (eight samples) were examined using wavelength-dispersive (WD)- X-ray fluorescence (XRF) (Bruker S-4 Pioneer) (Boraiaha et al., 2020). Nineteen samples of leucogranites from Yumesamdong, Yumthang, and surrounding areas were examined using glass beads made with 66:34 flux and 4% lithium nitrate. The results were obtained using a Panalytical MagiX FAST XRF spectrometer at Bureau Veritas Minerals in Canning Vale, Australia. Greater than 1% analytical precision was achieved. SARM-6, OREAS 45e, OREAS 45d, OREAS 45e, and European Certified Reference Material (Euro Norm 782-1) are among the numerous standards that are employed. Laser Inductively Coupled Plasma Mass Spectrometry (LA-ICPMS) was utilized to analyze the fused bead produced at Bureau

Veritas, Canning Vale, Australia, to determine the trace elements, including Rare Earth Elements (REEs), in leucogranites.

b) Whole rock analysis for pegmatites

At Bureau Veritas Minerals in Canning Vale, Australia, the major and trace elements from the examined pegmatites, including REEs, were analyzed. Glass beads were made using 66:34 flux and 4% lithium nitrate for the major oxides (SiO_2, Al_2O_3, MnO, MgO, Fe_2O_3T, CaO, Na_2O, K_2O, TiO_2, and P_2O_5), and Panalytical MagiX FAST X-ray Fluorescence spectrometer was used for the analysis. The analytical precision was better than 1% Using a New Wave EXCIMER 193 nm UV Laser coupled to an Agilent 7900 ICPMS, trace elements, including REEs, were measured on the same glass beads with precision and accuracy better than 5%. Chinese Certificate Reference Material (NCS DC 86,308 Zirconium Ore), Canadian Certified Reference Material (Canmet RTS-1), European Certified Reference Material (EURONORM-CRM) European Certified Reference Material (Euro Norm 782-1), and other certified reference materials are among the numerous standards that are used.

c) Mineral chemistry analytical details

A detailed petrographic study was conducted, and the representative polished sections of two-mica leucogranites, tourmaline leucogranites, and tourmaline leucogranite with characteristic mineral assemblage were marked for defining the mineral chemistry of the representative samples using an Electron Probe Micro-analyzer CAMECA SX-5 SA at Department of Geology, BHU, Varanasi, India and at National Centre for Earth Science Studies, Thiruvananthapuram, Kerala. The thin sections were further carbon-coated to make them conductive at the laboratory for quantitative analysis. Natural silicate mineral and andradite as internal standard was used to verify the positions of

crystals (SP1-TAP, SP2-LiF, SP3-LPET, SP4-LTAP, and SP5-PET). After repeated analysis, it was found that the error on major element concentrations is <1% whereas the error on trace elements varied between 3-5%.

Different natural and synthetic standards were used for calibration. The following X-ray lines were used for oxide analysis: Al-*Kα*, Mg-*Kα*, Ba-*Lα*, Cl-*Kα*, P-*Kα*, K-*Kα*, Ca-*Kα*, Ti-*Kα*, Cr-*Kα*, Cu-*Kα*, Mn-*Kα*, Si-*Kα*, Na-*Kα*, Fe-*Kα* and F-*Kα*. Natural mineral standards: fluorite, albite, halite, periclase, peridote, corundum, wollastonite, apatite, pyrite, orthoclase, rutile, chromite, rhodonite, hematite, and barite; pure metal standard: Ni and synthetic glass standard YAG supplied by CAMECA-AMETEK were used for routine calibration, X-ray elemental mapping, and quantification.

The operating conditions were 15 kV acceleration voltage, 10nA beam current, and 1µm beam diameter. The software SX-results and SxSAB version 6.1 were used for the acquisitions, calibrations, and quantifications. The ideal coating thickness is 20nm done under a vacuum evaporator.

d) Analytical methods for LA-ICPMS U-Pb dating of zircons (ZY-LG-2)

At CODES Analytical Laboratories at the University of Tasmania, the sample was crushed, and non-magnetic heavy minerals were separated using magnetic and gravity separation methods. Selected crystals were mounted on double-sided adhesive tape after extensive mineral and magnetic separation, and epoxy glue was then applied on top of the zircons in a 2.5 cm diameter mould. Following a 12-hour drying period, the epoxy mount was polished with fresh sandpaper and a polishing lap. The samples were then cleaned in an ultrasonic bath with distilled water. Mounts were desiccated overnight in a vacuum to remove moisture from the air Thompson et al. (2018).

The analyses in this study were carried out using a Coherent Compex Pro 110 Ar-F excimer laser with a 193nm wavelength and a 20ns pulse width on an ASI RESOLution S-155 ablation system. An Agilent 7900 quadrupole ICP-MS was connected to the laser system. In Thompson et al. (2018) further analytical conditions are presented. The CODES Analytical Laboratory at the University of Tasmania is where all of the equipment is kept. For each study of the zircons, a blank gas measurement of 30 seconds was followed by an additional 30 seconds of analysis time when the laser was turned on. A laser beam with a diameter between 20 and 30 microns, a firing frequency of 5 Hz, and an energy density of less than 2 J/cm2 was used to analyze zircons.

The procedure that was extensively described by Thompson et al. (2018) and Halpin et al. (2014) served as the foundation for the data reduction used for U-Pb dating. Each analysis has chosen a subset of the data for quantification that most closely resembles a concordant composition. Using data from analyses of the 91500 zircon and Wiedenbeck et al. (1995) values, the downhole fractionation, instrument drift, and mass bias correction factors for Pb/U ratios were computed using analyses of the NIST610 glass and Baker et al. (2004) Pb isotopic values, the instrument drift and mass bias correction factors for the 207Pb/206Pb ratio (ages) were computed.

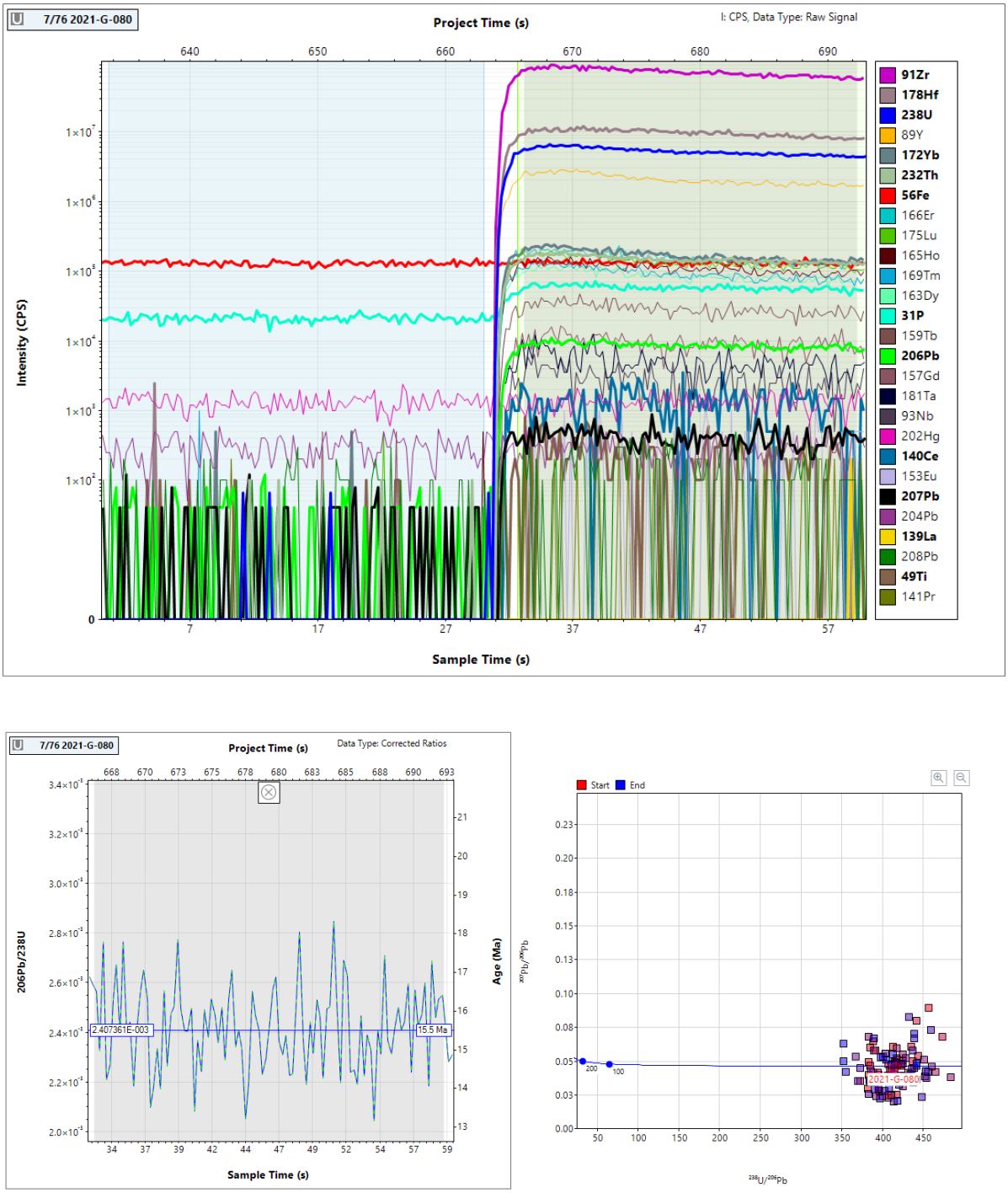

Figure 1.10. A representative example of a time-resolved signal from LA-ICPMS analysis of zircon for sample ZY-LG-2. The sections of the time-resolved signal used for calculating background values (left) and signal values (right) are shown on the top graph. Lower graphs show this same analysis on Concordia (right) as well as the time-resolved plot of the age through the analysis (left).

The secondary standard corrections based on the compositions of glasses BCR-2G and GSD-1G (GeoReM preferred values; http://georem.mpch-mainz.gwdg.de/) are used to calibrate trace element abundances in zircon on the NIST610 glass. All detected cations were normalized to the Zr site total of a stoichiometric zircon to do the quantification using 91Zr as the internal standard element. At the start, end, and every 60 minutes throughout the analytical session, duplicates of the 91500 zircon, NIST610, BCR-2G, and GSD-1G glasses were analyzed. The Temora zircon (Black et al., 2003) and Plesovice zircon (Sláma et al., 2008) analyses, which were analyzed throughout the analytical session and regarded as unknowns, were used to test the calibration of the U-Pb ages.

e) Analytical methods for LA-ICPMS U-Pb monazite dating (ZY-LG-2) and (ZY-LGT-1)

At CODES Analytical Laboratories at the University of Tasmania, samples were crushed and non-magnetic heavy minerals were separated using magnetic and gravity separation methods. After thorough mineral and magnetic separation, the monazites then adhered to double-sided adhesive tape, and epoxy glue was poured into a 2.5 cm diameter mould. After the epoxy mount had been allowed to dry for 12 hours, it was cleaned using clean sandpaper and a polishing cloth. The samples were then cleaned in an ultrasonic bath with distilled water. Mounts were left in a vacuum desiccator overnight to get rid of ambient moisture Thompson et al. (2018).To get rid of any surface contamination, all monazite analyses undergo a pre-ablation of five laser shots. The laser-ablated particles were transported out of the chamber by a 0.35 liter/minute flow of He carrier gas, where they were combined with Ar gas and brought to the

plasma torch. Every isotope was tested every 0.202 seconds and included ^{31}P, ^{89}Y, ^{139}La, ^{140}Ce, ^{141}Pr, ^{146}Nd, ^{147}Sm, ^{153}Eu, ^{157}Gd, ^{159}Tb, ^{163}Dy, ^{166}Er, ^{169}Tm, ^{172}Yb, ^{175}Lu, ^{202}Hg, ^{206}Pb, ^{207}Pb, ^{208}Pb, ^{232}Th, ^{235}U, and ^{238}U.The approach that was utilized for data reduction for U-Pb dating is described in full by Thompson et al. (2018) and Halpin et al. (2014) subset of the data that most closely resembles a concordant composition has been chosen for quantification for each investigation. Utilizing investigations of the 14971 monazites, an UTAS internal reference material whose age was established via isotope dilution MC-ICPMS at the University of Melbourne, the downhole fractionation, instrument drift, and mass bias correction factors for Pb/U ratios were derived (Mass et al., 2018 unpublished). The $^{207}Pb/^{206}Pb$ ratio (ages) instrument drift and mass bias correction factors were determined using studies of the NIST610 glass isotopic values of lead Baker et al. (2004).

f) Analytical methods for boron isotopic composition

The Thermo Scientific NEPTUNE Plus Multi-Collector Inductively Coupled Mass Spectrometry (MC-ICPMS) was used for the measurements of the boron isotopes, which were bracketed by Standard Reference Materials (SRMs) from ALS Scandinavia AB in Lulea, Sweden. The samples Y-TG-1, Y-TP-3, Y-TP-1, and TP-1 were made using the KCO_3 fusion technique, then boron was separated using the ion exchange technique. The analytical procedure for matrix separation and sample preparation has been taken directly from Tonarini et al. (1997). The boron delta values are computed using the NIST SRM 951 formula, and the standard deviation is computed using data from two successive independent observations. NIST SRM 951 was the reference standard used in the analysis, and the calculated $^{11}B/^{10}B$ ratio is 4.043623.

CHAPTER 2
SIKKIM HIMALAYAS

2.1 Geology

Based on structural, geological outlines, geochronological, geothermobarometric, and petrological aspects the Sikkim Himalayas have been discussed by various researchers (Bhattacharyya et al., 2015a; Bhattacharyya and Mitra, 2011; Catlos et al., 2004; Dasgupta et al., 2004; Faak et al., 2012; Harris et al., 2004; Kellett et al., 2014a; Mottram et al., 2015, 2014b, 2014a; Mukul, 2010; Parui and Bhattacharyya, 2018; Rubatto et al., 2013; Searle and Szulc, 2005; Sorcar et al., 2014). The (Fig. 2.1), shows the location of the study area which lies in the Higher Himalayan Sequence (HHS) of Sikkim in the eastern Himalayas. The Tethyan Sedimentary Sequences (TSS) comprising of carbonate and clastic rocks ranging from Devonian-Jurassic is separated from GHS by STDS (Kellett et al., 2014a). The STDS comprises two detachments: the upper brittle-ductile normal fault and the lower mylonitised ductile shear zone (Carosi et al., 1998; Kellett et al., 2019; Zhang et al., 2020**;** Burchfield et al., 1992; Kellett et al., 2019). The HHS is formed by the upper amphibolite–granulite facies Kanchenjunga–Darjeeling gneiss, which is bordered by the MCT zone below and the STDS above, and the GHS is composed of calc-silicates and leucogranites, migmatites, mica schist, sillimanite kyanite bearing gneiss and biotite gneiss (Bhattacharyya et al., 2015a; GSI, 2012; Kellett et al., 2014a). The MCT is defined as the ductile thrust or shear zone that separates GHS from LHS (Le Fort, 1975), however, due to different criteria used to define the thrust, different methodologies and approaches and changes in the thrust over the length of the Himalaya, the MCT is one of the most contentious structures in the Himalayas (Kellett et al., 2014a; Mottram et al., 2014a; Searle et al., 2008).

The MCT's deformation zone is known as the Main Central Thrust Zone (MCTZ) and is recognized as high strain zone of distributed deformation based on structural analysis

and the inverted Barrovian sequence is essentially contained within the MCTZ over the entire length of the Himalayas (Dasgupta et al., 2004). The inverted Barrovian sequences are made up of an assemblage of pelitic schists with schistosity and mineral lineations, as well as an assemblage of Barrovian sequence index minerals (Mottram et al., 2014b). The LHS is divided into two levels based on structural position, the structurally higher level, bordered by the MCT above and the Pelling thrust (PT) below, is made up of the amphibolite facies, Paro, and Lingste gneiss and the PT above and the MBT below define the structurally lower level (Bhattacharyya et al., 2015a; Bhattacharyya and Mitra, 2009) divided into Daling group consisting of pelites, wackes and psammites, Buxa formation consisting of carbonate rocks, Gondwana Group of Carboniferous-Permian age consisting sandstone and coal seams (Bhattacharyya et al., 2015a; Bhattacharyya and Mitra, 2009; Dasgupta et al., 2004).

The Himalayan leucogranites are confined into two sub-parallel belts from north to south: The northern belt intrudes into the Tethyan Himalayan sequence composed of clastic and carbonate rocks and in the core of gneiss domes are known as Tethyan Himalayan leucogranites (THL), whereas the southern belt referred as Higher Himalayan leucogranites (HHL) intrude into high-grade metasedimentary rocks (Guo and Wilson, 2012; King et al., 2011; Wang et al., 2017), and the emplacement of Himalayan leucogranites took place in the Oligocene to Miocene (Wu et al., 2020).

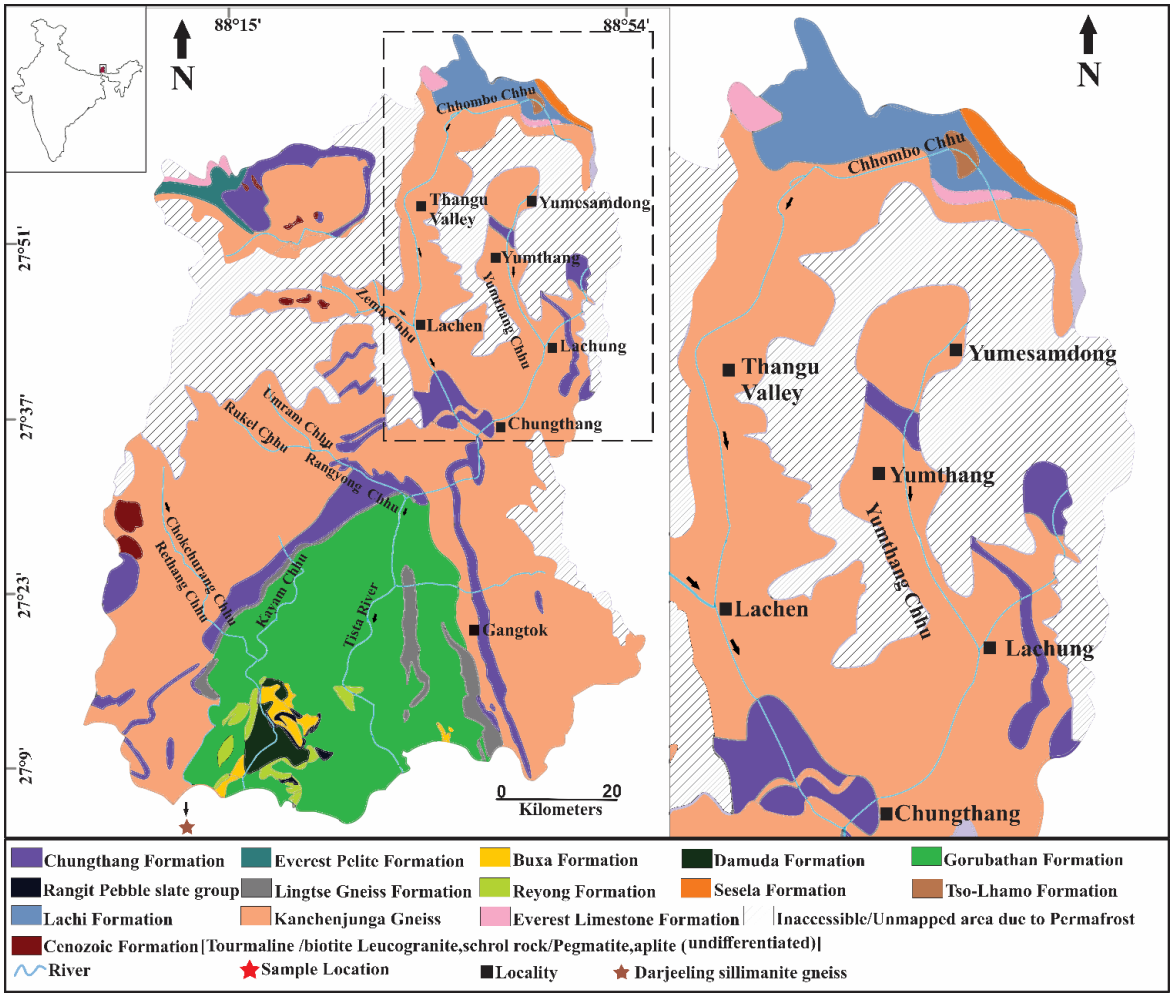

Figure 2.1. Regional geological Map of Sikkim and the study area with leucogranites sampling locations. Map modified after (Sivakumar and Ghosh 2017).

2.1.1. Tethyan Himalayan Sequences

The Tethyan belt constitutes a thick pile of fossiliferous Cambrian to Eocene sedimentary rocks that lie along the north-dipping normal faults of the STDS and the HHC form its footwall (Dasgupta et al., 2004; Kellett et al., 2014a).

i) Everest Pelite Formation

The Everest Pelite Formation is exposed in the north-western part of Sikkim and overlies the lime silicate rocks of the Chungthang Formation and quartz-biotite schist forms the base (GSI, 2012). A succession of quartzites and phyllitic-quartzites follows the basal horizon and at the base, these rocks are affected by granitization as well as deformation and fracture (Raina and Bhattacharya, 1965). Dark phyllites become more noticeable near the top of this formation. The minerals in these low-grade metamorphic phyllites include quartz, sericite, and chlorite together with a small amount of graphitic material.

ii) Everest Limestone Formation

The name for this formation was initially used by (Wager, 1939), to refer to a distinctive arenaceous limestone deposit that was found outcropping along the summit of Mount Everest and was traced eastward to Sikkim. A thick litho-assemblage made up of argillaceous brown limestone, cherty and flaky quartzite, mainly corrugated ferruginous sandstone, and limestone and distinctive arenaceous limestone in ascending sequence (Raina and Bhattacharya, 1965).

iii) Lachi Formation

In the north-eastern part of Sikkim, the Lachi formation is visible, and the Tethyan series starts with a basal conglomerate. A series of shale and quartzite, as well as some

pebble beds, identify this formation. Based on the fossil evidence Wager (1939), assesses the Permo-Carboniferous age of the Lachi Formation. The Lachi Formation is characterized by quartzite, shale, and crinoidal limestone at its base (Raina and Bhattacharya, 1965).

iv) Chho Lhamo (Tso Lhamo) Formation

An ammonite-bearing horizon made up of sandstone, shale, and limestone that was exposed on the eastern side of the Lachi ridge was given the name the "Chho Lhamo" by Auden (1935). The Chho Lhamo Formation is characterized by sandstone, limestone, and shale overlying the basal zone. The tectonic deformation of the entire formation led to faulted contact between the limestone and subordinate shale. Additionally, there is a faulted contact between this formation and the underlying Lachi Formation (GSI, 2012).

v) Sesela Formation

The Sesela Formation is made up of well-rounded, ball and disk-shaped pebbles made up of tilloids, sandstone, shale, limestone, quartzite, and granite that are encased in a matrix of sand the rocks feature alternating layers of pebbles, fine and medium-grained sand, and variegated clay (GSI, 2012). This formation has Pleistocene age and fluvioglacial signatures can be seen on the rocks and were deposited in a shallow depression.

2.1.2. Higher Himalayan Sequences

The HHS commonly referred to as consists of rocks that are predominantly of pelitic composition with sporadic quartzites, orthogneisses, leucogranites, calc-silicate rocks, and metabasites (Dasgupta et al., 2004; Neogi et al., 1998)**.** The HHS in the hanging wall is separated from LHS in the footwall by MCT (Kellett et al., 2014b)**.** The HHS is

characterized by εNd (0) signature of -15 to 20 indicative of younger source regions intruded by granites by ca. 830 Ma (Kellett et al., 2014b)**.** It has been observed that the migmatites in the HHC of Sikkim reached peak P-T conditions of ~750-800°C, 8-12 kbar (Ganguly et al., 2000; Rubatto et al., 2013; Sorcar et al., 2014), followed by steep isothermal decompression to 3-5 kbar, followed by cooling to 600°C (Sorcar et al., 2014). The metamorphic stages within a complex tectonic setting are related to U-Pb ages in the Sikkim migmatites and in HHC monazite and zircon growth zones show a prolonged melting and high-temperature history between 31 -17 Ma (Rubatto et al., 2013).

i) Kanchenjunga gneiss

In the Darjeeling-Sikkim Himalaya, the MCT sheet is made of the highest-grade metamorphic rock of the GHS, the Kanchenjunga gneiss (Bhattacharyya et al., 2015b). The northern region of Sikkim and the area to the west of the Tethyan sequence have good exposure to Kanchenjunga/Darjeeling gneiss. These gneisses are made of quartz, feldspar, and biotite. They can be divided into three types: i) banded gneisses/migmatites streaky gneiss, ii) augen bearing biotite gneiss with or without garnet, kyanite sillimanite, iii)sillimanite granite gneisses (GSI, 2012).

ii) Chungthang Formation

The Chungthang Formation in North Sikkim mainly consists of quartzites, calc-silicate, graphitic schist, biotite schist, and amphibolite (Raina and Bhattacharya, 1962). In the districts of East Sikkim and West Sikkim, the rocks from this formation are also exposed. It has been noted that the quartzites occasionally contain chlorites.

2.1.3 Lesser Himalayan Sequence

In Sikkim, the Lesser Himalayan Sequence (LHS) is composed of three clastic metasedimentary units: the Daling, Buxa, Gondwana, and sub-Himalayan groups (including the Siwaliks) (Mottram et al., 2014a). The LHS is a Paleoproterozoic sequence with εNd(0) signature of -20 to-25 intruded by granite of ca 1.8 Ga (Kellett et al., 2014b).

i) Daling Group: The Daling group is primarily comprised of greywacke, tuffaceous-wacke, greenish phyllite, quartzite, garnet mica schist, mica schist, metapelite with minor mafic dyke and sill, and is intruded by Lingtse granites/gneiss of early Proterozoic age (Acharyya et al., 2017; Mottram et al., 2014a; Saha, 2013). The Daling group is divided into Gorubathan, Reyong, and Buxa formation (Acharyya, 1989; Chakrabarti, 2016; Ray, 1976). The Gorubathan consists of green phyllite, quartzites, and metabasics slate and the Reyong formation consist of variegated quartzites and slates (Matin and Mukul, 2010). The Buxa Formation is composed of dolomitic limestone intercalated with phyllite or slate, chert, and fine-grained quartzite (Saha, 2013). The Gondwana group belonging to the Carboniferous to Permian age is divided based on lithostratigraphic units into Rangit pebble slate of Permian age consisting of diamictite of sand or pebble slates, conglomerate, phyllite and is overlain by Damuda group consisting of sandstone, carbonaceous sediments with coal (Acharyya and Ray, 1977; Acharyya et al., 2017; Dasgupta et al., 2004) In Darjeeling-Sikkim Himalaya dating of crystalline, detrital zircon, which clusters with the peak at c.1800-1900 Ma, has been used to constrain the age of Daling Group (Mottram et al., 2014a).

ii) Gondwana Supergroup

The Gondwana Group consists of two lithostratigraphic units Rangit pebble slate overlain by Damuda Formation. The Rangit pebble slate is associated with diamictite-bearing sandstone or pebbly slates of early Permian age and coal and carbonaceous sediments of the Damuda formation contain fossils of Glossopteris of Permian age (Acharyya and Ray, 1977; Acharyya et al., 2017). The new stratigraphic which consists of diamictite dominant marine mudstone facies is recognized as the Phongla formation equivalent to Rangit Pebble Slate (Ray and Neogi, 2011).

iii) Lingtse Granite Gneiss

The Lingtse Granite Gneiss is an orthogneiss, coarse to medium-grained, generally found as intrusive in the Daling group. The occurrence of a stretched lineation is the most distinctive aspect of the Lingtse granite. Additionally, some research (Dasgupta et al., 2004; Mottram et al., 2014a; Neogi et al., 1998) have used the peculiar Paleoproterozoic Lingtse gneiss, which is strongly sheared along the MCT zone the Sikkim Himalaya, as a characterizing lithology for identifying the MCT position. The Rb-Sr ages from the Lingtse gneiss yielded the age of ca. 1075-2034 Ma (Paul et al., 1996, 1982). The U-Pb geochronology of the zircon age of these rocks is (1834± 37 Ma and 1853±19 Ma) (Mottram et al., 2014a). Based on U-Pb SHRIMP analyses of zircon grains from the MCT sheet, two age groups for $^{206}Pb/^{238}U$ are identified, ca.2575 and ca.943 Ma, and from the PT, 1835±13 Ma (Bhattacharyya et al., 2015b).

2.1.4 Main Central Thrust

The MCT is a major structural feature of the Himalayas that accommodated a significant amount of the convergence between India and Asia (Mottram et al., 2014a;

Schelling and Arita, 1991). The MCT divides the Higher Himalayan Sequence (HHS), in the hanging wall, from the Lesser Himalayan Sequence (LHS), in the footwall and due to the diffuse nature of the deformation, it is often unclear exactly where the MCT runs along the entire orogen (Kellett et al., 2014a)**.** The inverted Barrovian sequences are well-documented and are associated with MCT in the Himalayas (Mottram et al., 2015).

2.1.5 South Tibetan Detachment

The STDS is a series of low-angle normal sense structures that separate high-grade metamorphic rocks of the HHS from low-grade metamorphic to sedimentary rocks of the Tethyan sedimentary sequence (TSS) (Kellett et al., 2014a).

2.2 Sample localities and Description

A total of 52 samples were collected rocks including pegmatites, calc-silicates, gneisses, leucogranites (two mica and tourmaline leucogranites), and migmatites, etc. Out of these 27 samples of leucogranites were collected for geochemical and geochronological studies. The localities of the collected samples of leucogranites and associated rocks are mentioned below. The details of the samples and locations of the studied leucogranites are mentioned in (Appendix A 1.1).

Chungthang: This place is a convergence point for the two of the studied areas i.e., Lachen and Lachung which are present at the western traverse and eastern traverse respectively. constitutes of quartzite, biotite schist, pegmatites and calc silicates.

Thangu-In Thangu area consists of leucogranites, pegmatites, and gneiss. In this area, leucogranites are present in the form of sills. The presence of garnet in the pegmatitic samples can also be seen. The leucogranites sills intrude in the high-grade metamorphic gneisses.

Gurudongmar area: This region lies at the southernmost end of the Tibetan Plateau. This region consists of leucogranites, gneisses and migmatites rocks. The presence of moraine is there between the lake and mountain peak indicating glacial erosion.

Bhimnala falls: The eastern traverse from the Chungthang area goes toward the Lachung area. This area of Lachung has the calc-silicate, migmatites, and leucogranites bodies The exposure of HHS rocks can be clearly seen in this area.

Yumesamdong: The samples of leucogranites were collected from this area and its adjoining areas.

Near Yumthang: In this area, the leucogranites and pegmatites samples were collected. The contact between leucogranites, gneiss, and pegmatite was seen. In the region, clear contact between gneiss and leucogranites was seen. The pegmatite samples for boron isotopic studies were collected from this area.

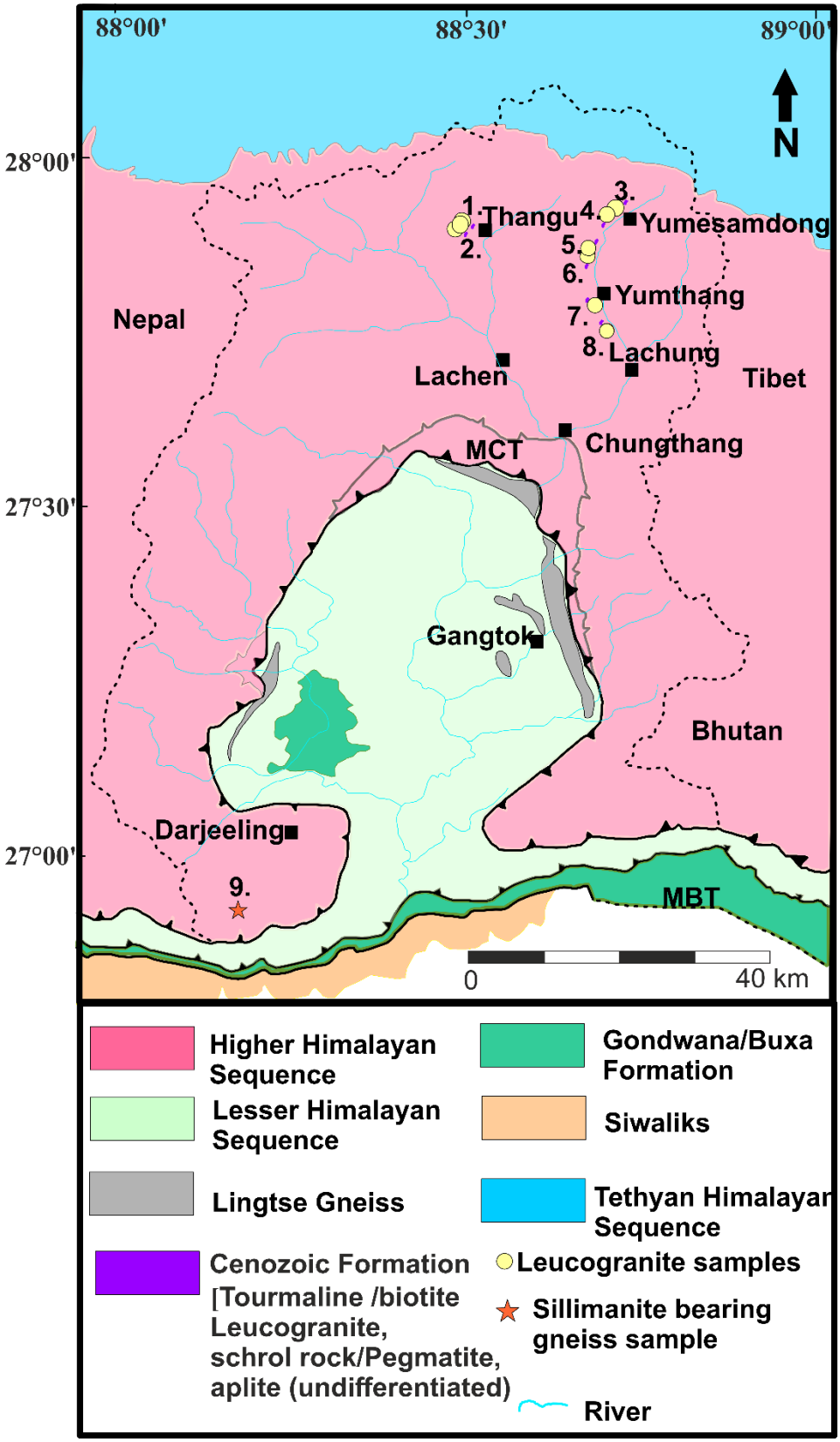

Figure 2.2. Geological map of Sikkim and Darjeeling Himalayas showing the distribution of leucogranites and sillimanite bearing gneiss [Modified after Kellet et al. (2014), Mottram et al. (2014a)].

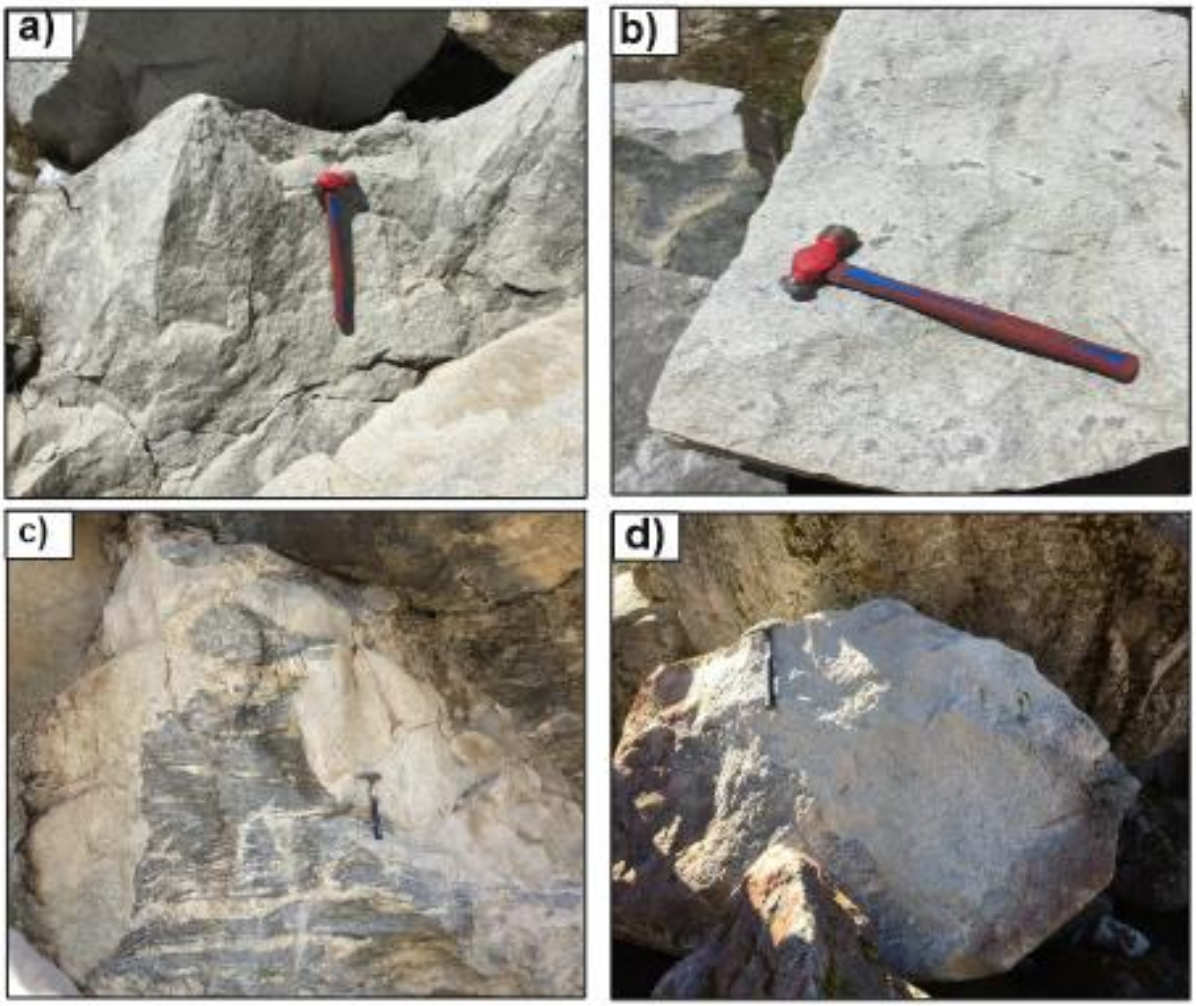

Figure 2.3. (a-d) Leucogranite outcrop in the Higher Himalayan Sequences, North Sikkim from the adjoining areas of Thangu and Yumthang.

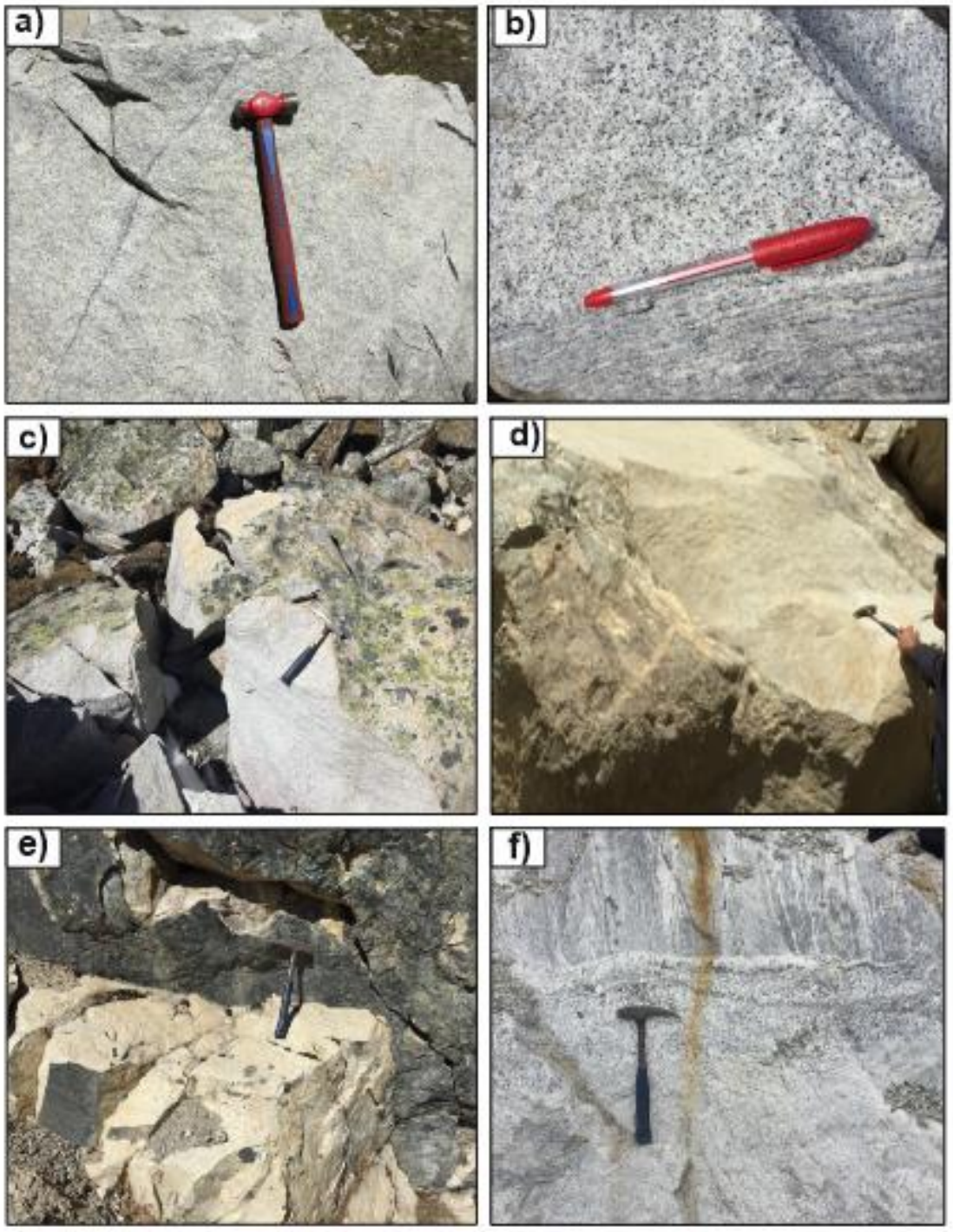

Figure 2.4. (a) Two-mica leucogranite from Thangu area (b) contact between leucogranite and granitic gneiss (c) Two-mica leucogranite from Yumesamdong area (d) Intrusion of leucogranite in the Higher Himalayan Crystallines (e) Tourmaline leucogranite outcrop (f) granitic gneiss in contact with leucogranite.

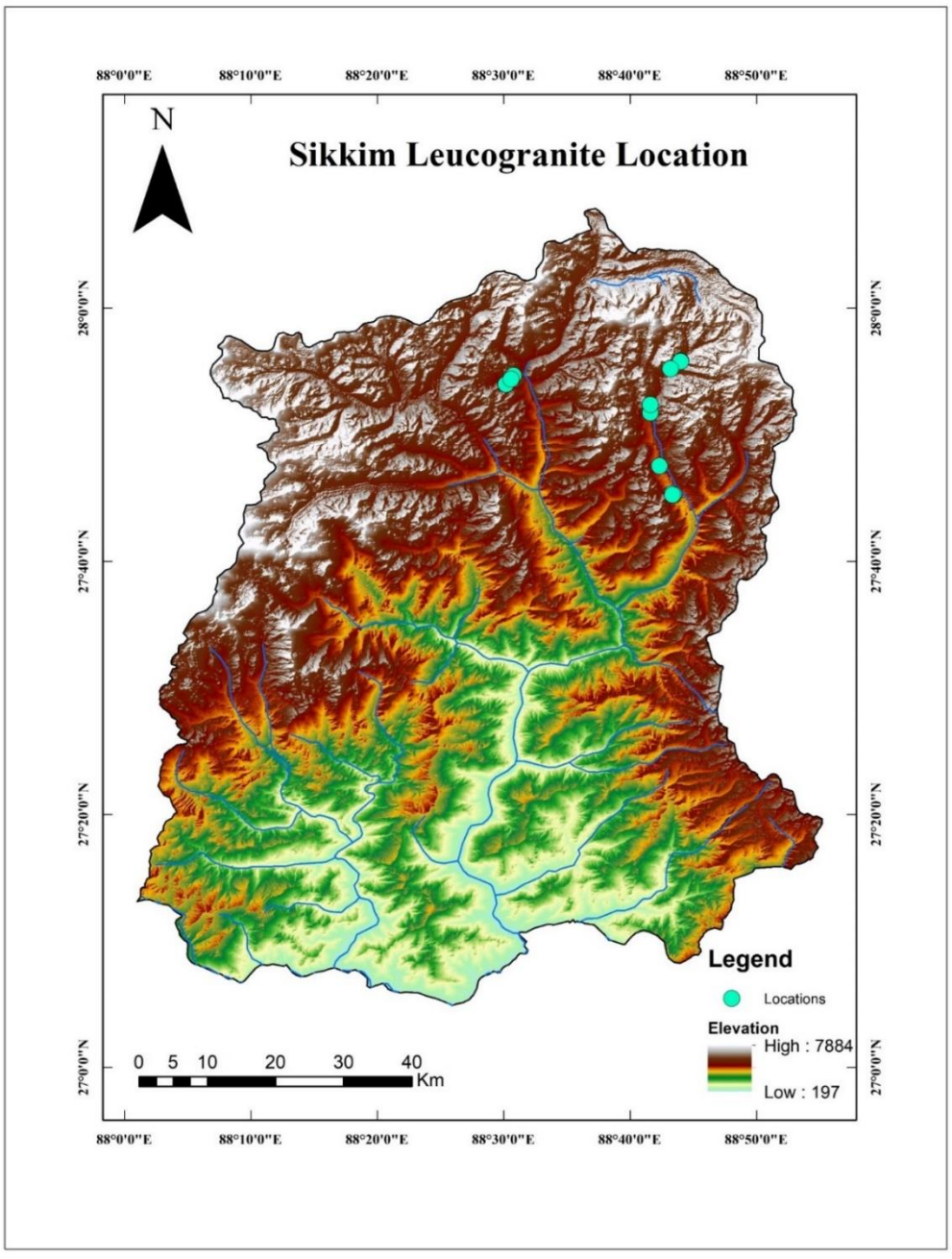

Figure.2.5 Sikkim map showing leucogranites samples on Digital Elevation Map (DEM), ASTER Data source: USGS.

CHAPTER 3

PETROGRAPHY

In the Himalayas, there are various types of leucogranites reported two -mica leucogranite and tourmaline leucogranite (Chen et al., 2017; Chen et al., 2021; Gou et al., 2019, 2016; Guillot and Le Fort, 1995; Guo and Wilson, 2012; Harris et al., 1995; He et al., 2021, 2020; Hopkinson et al., 2017; Yang et al., 2015) garnet leucogranite (Gou et al., 2019; He et al., 2021, 2020; Hopkinson et al., 2017), cordierite bearing leucogranite (Gou et al., 2019). In Sikkim, two categories of leucogranites found in the HHS are the two-mica leucogranite (2mg), and the tourmaline leucogranite (Tg).

3.1. Two-mica Leucogranite

The 2mg is composed of euhedral quartz and plagioclase, K-feldspar grains are subhedral to anhedral, biotite grains are subhedral to anhedral, muscovite grains are subhedral to anhedral and some samples might consist of tourmaline laths varying few centimeters in size. The quartz dominance is (~35%), K-feldspar (~25 %), plagioclase (~25 %), biotite (~10%), muscovite (~3%), and tourmaline (if present ~2%), in the 2mg. The biotite grains show pleochroism and range from 10-15mm in length and it includes zircons which might show pleochroic halos due to alpha particles radiated by radioactive elements in the inclusions. The muscovite grains are colorless and defined by high relief and one set of cleavage under plane-polarized light (PPL). In 2mg, muscovite occurs in association with biotite and shows first-order birefringence color under cross-polar light (XPL) (Fig 3.1a). In a few samples, tourmaline grains are also present which are coarse to medium-grained (Fig 3.1b). The plagioclase grains exhibit zoning which indicates the compositional variations (Fig 3.1c) carlsbad twinning can be observed (Fig 3.1d). Apart from the major minerals the accessory phases which have been identified in the two-mica leucogranite samples are zircon and monazite. The zircon grains are present as abundantly as inclusion in biotite and pleochroic haloes can be observed (Fig 3.1e). Zircon is euhedral, colorless, and has high relief whereas

monazite grains are non-pleochroic and also occur as inclusion in these leucogranites. The perthitic texture represents the intergrowth of K-feldspar and sodic plagioclase due to sub-solidus exsolution (Fig. 3.1 f).

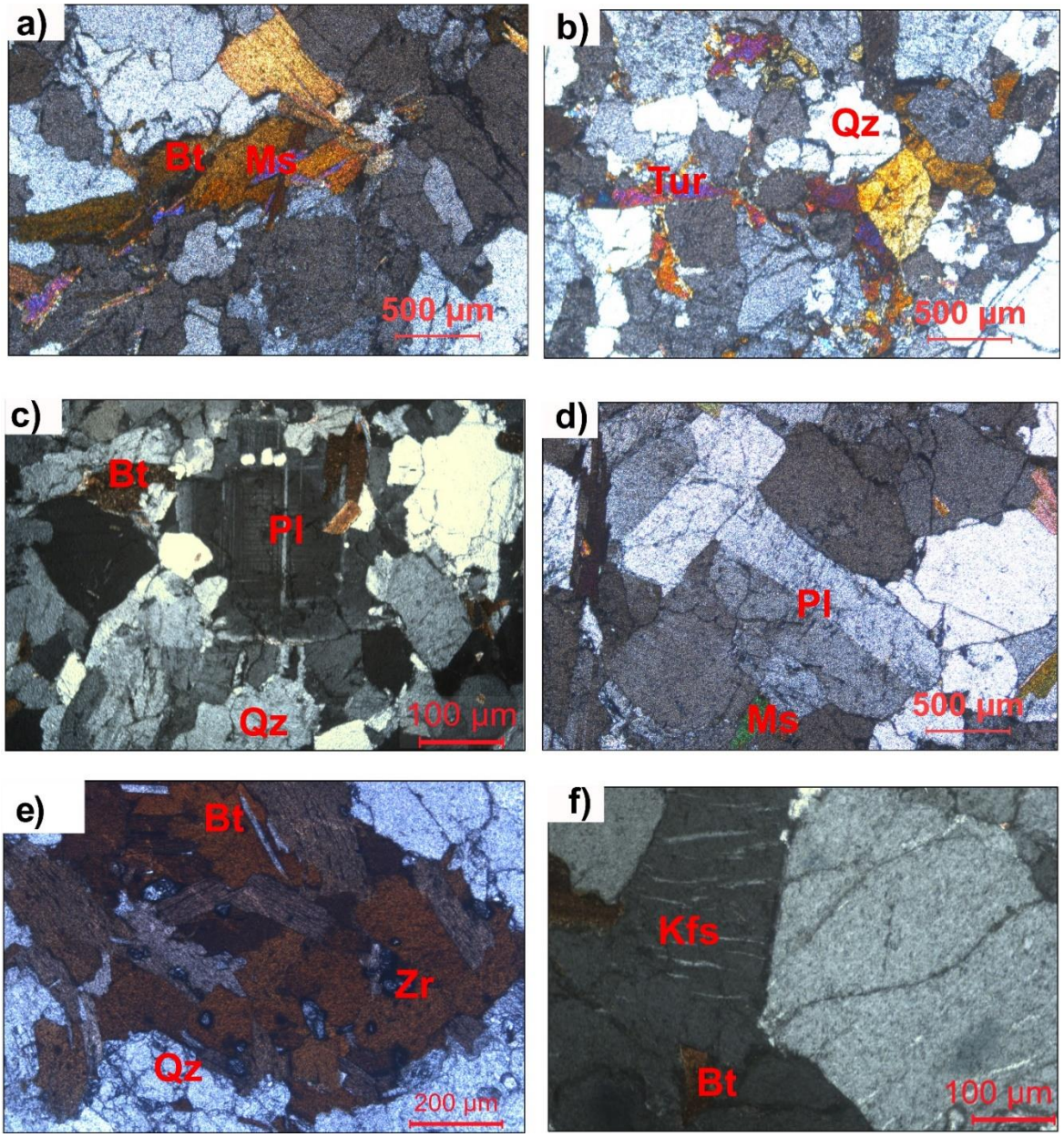

Figure 3.1. Photomicrographs of two-mica leucogranite from North Sikkim (a) presence of biotite and muscovite grains (b) Tourmaline grains surrounded by quartz (c) Zoning in plagioclase (d) Carlsbad twinning (e) presence of zircon grains in biotite as well as pleochroic haloes (f) perthitic texture in two-mica leucogranite.

3.2 Tourmaline Leucogranite

The Tg is composed of quartz and plagioclase, K-feldspar, muscovite, and tourmaline. With a quartz content of (35 %), K-feldspar (20 %), plagioclase (25 %), tourmaline (15 %), and muscovite (5 %), Tg has minimal or no biotite with zircon, monazite, and apatite as accessory phases. The tourmaline grains are present in the form of specs that vary from a few cm in the tourmaline leucogranite. In thin section tourmaline show pleochroism which may vary from green, to blue and yellow. The zircons and monazite are present in the accessory phases; however, monazite is in abundance in comparison to the zircons and the former is non-pleochroic. The major constituents of the tourmaline leucogranites can be observed in (Fig 3.2 a-f).

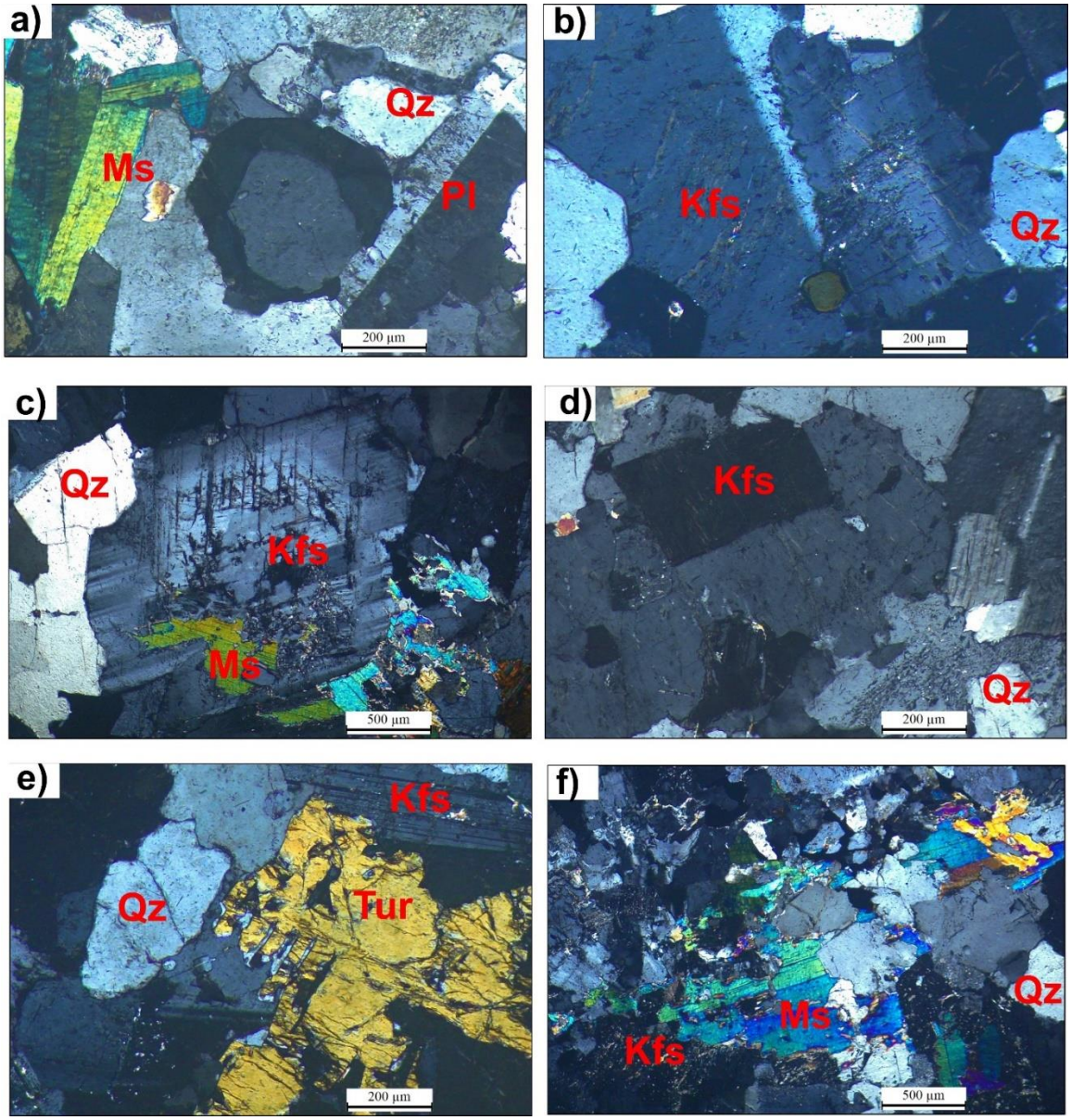

Figure 3.2. Photomicrographs of tourmaline leucogranites (a-c) tourmaline leucogranite with a typical mineral assemblage of K-feldspar, muscovite, quartz, and plagioclase (d) Perthitic texture (e) Tourmaline grains surrounded by quartz and K-feldspar (f) muscovite grains embedded in tourmaline leucogranites.

3.3 Pegmatites

The pegmatites in the study area are coarse-grained and are intruded into HHCS with sharp contacts with minimal to no chilled margins. Tourmaline (schorl) dominates the pegmatites, along with quartz, feldspar, and muscovite. The tourmaline crystals are columnar and form a radial pattern and are nearly less than 4 cm. The predominant phases in thin sections are quartz, K-feldspar, muscovite, and tourmaline, while zircon is an accessory phase. The muscovite grains are euhedral in shape, the quartz grains are anhedral, and K-feldspar exhibits subhedral to anhedral grains. The section demonstrates the euhedral to subhedral highly pleochroic tourmaline grains, which are mostly coupled with quartz and K-feldspar and show apparent microfractures in a few sections (Fig 3.3 a-f).

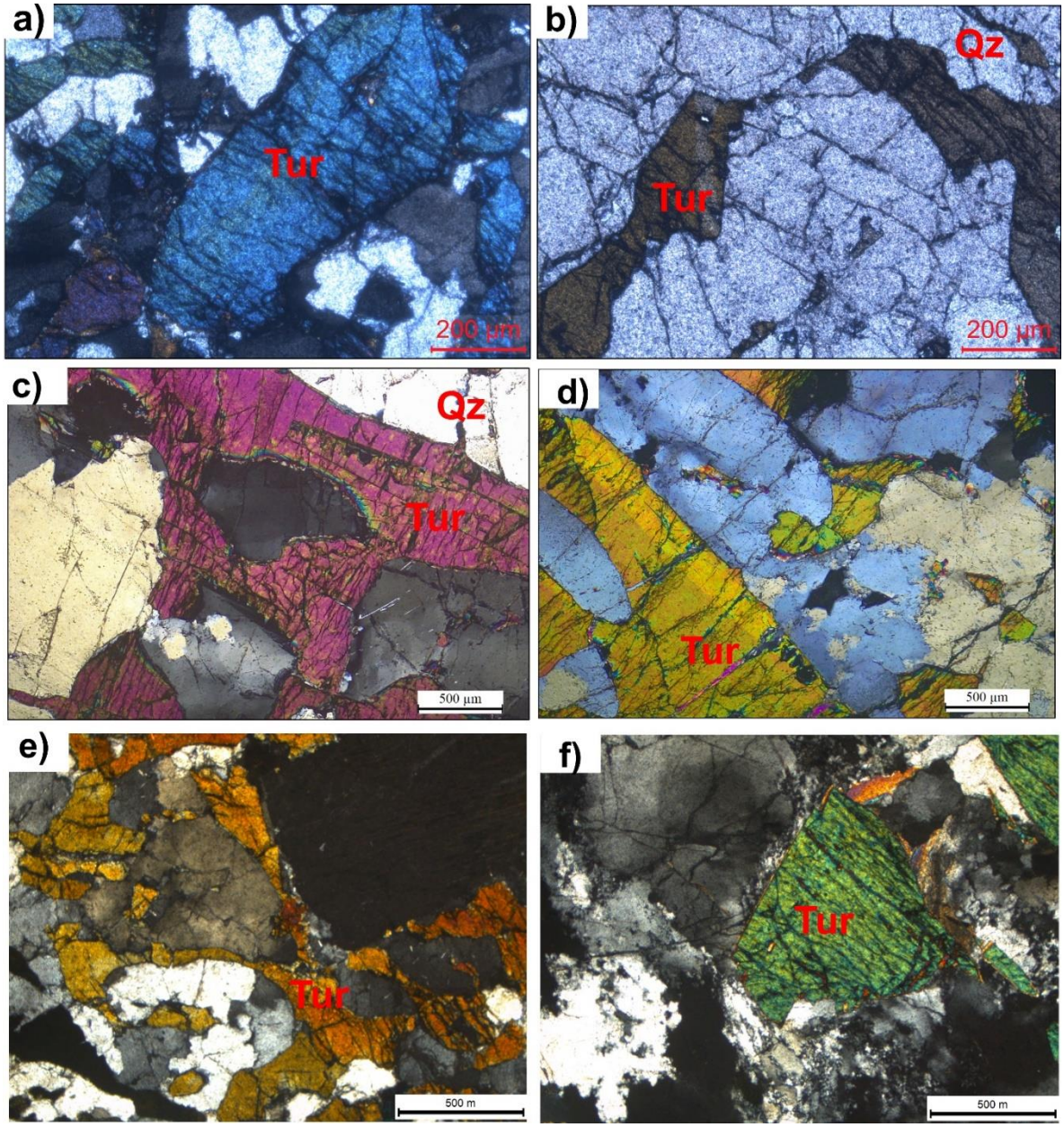

Figure 3.3 (a-f) Photomicrographs of tourmaline pegmatite of different samples from North Sikkim.

CHAPTER 4

MAJOR AND TRACE ELEMENT

GEOCHEMISTRY

4.1 Introduction

The purpose of this chapter is to provide a comprehensive overview of the major and trace element geochemistry of two types of leucogranites from North Sikkim to understand the magmatic history of this Himalayan terrain. The major, trace, and rare earth element (REE) geochemistry are potential tools for determining how igneous rocks were formed and their tectonic environment. This includes the major, trace, and rare earth data of 27 leucogranites from North Sikkim given in (Appendix A 1.2). Based on major element geochemistry and trace element geochemistry the differences have been obtained in the 2mg and Tg. These two leucogranites have been characterized by different symbols and colors.

4.2 Major element Geochemistry

In 2mg SiO_2 shows a variation between (70.91-74.61 wt.%), Al_2O_3 (13.69-15.82 wt.%), CaO (0.58-1.67 wt.%), TiO_2 (0.12-0.29 wt.%), MgO varies from (0.21-0.74 wt.%), P_2O_5 (0.06-0.15 wt.%), the values for K_2O/Na_2O (1.08-2.42). For Tg SiO_2 varies between (74.38-74.9 wt.%), Al_2O_3 (13.78-14.80 wt.%), CaO (0.45-1.13 wt.%), TiO_2 (0.06-0.09 wt.%), MgO varies from (0.13-0.20 wt.%), P_2O_5 (0.15-0.17 wt.%), the values for K_2O/Na_2O ranges from (1.13-2.31).

4.2.1 Harker variation diagram

In this variation diagram, the concentration of oxide is plotted against the SiO_2 for the igneous rock suite. Since SiO_2 shows a wide range of values (from 45% in ultramafic rocks to > 70% in acidic rocks), it is an appropriate choice for graphing with the concentrations of other elements and oxides. In (Fig. 4.1 a) Al_2O_3 vs SiO_2, the Al_2O_3 contents decrease steadily as SiO_2 increases. The Al_2O_3 content is higher for most of the 2mg in comparison to that of Tg. In (Fig 4.1 b) TiO_2 vs SiO_2, the TiO_2 contents

decrease SiO_2 increases. The TiO_2 content of 2mg is higher in comparison to Tg. In (Fig. 4.1c) MnO vs SiO_2 the MnO content remains more or less constant as SiO_2 increases. The value of MnO is constant for both 2mg and Tg. In (Fig.4.1 d) Fe_2O_3 vs SiO_2, Fe_2O_3 contents decrease steadily as SiO_2 increases. The plot is lower for Tg, whereas it is almost constant content for 2mg. In (Fig. 4.1e) CaO vs SiO_2, the plot shows negative variation. The CaO content is higher for 2mg in comparison to Tg. In (Fig. 4.1f) MgO vs SiO_2, MgO content decreases steadily as SiO_2 increases. MgO content is higher for 2mg with respect to Tg. In (Fig. 4.1 g) Na_2O vs SiO_2, content increases steadily as SiO_2 increases, however, for a few samples in 2mg, it decreases with an increase in Na_2O. In (Fig. 4.1 h) K_2O vs SiO_2, K_2O content is constant with the increase in SiO_2. In (Fig 4.1 i) P_2O_5 vs SiO_2, the P_2O_5 content increases with an increase in SiO_2.

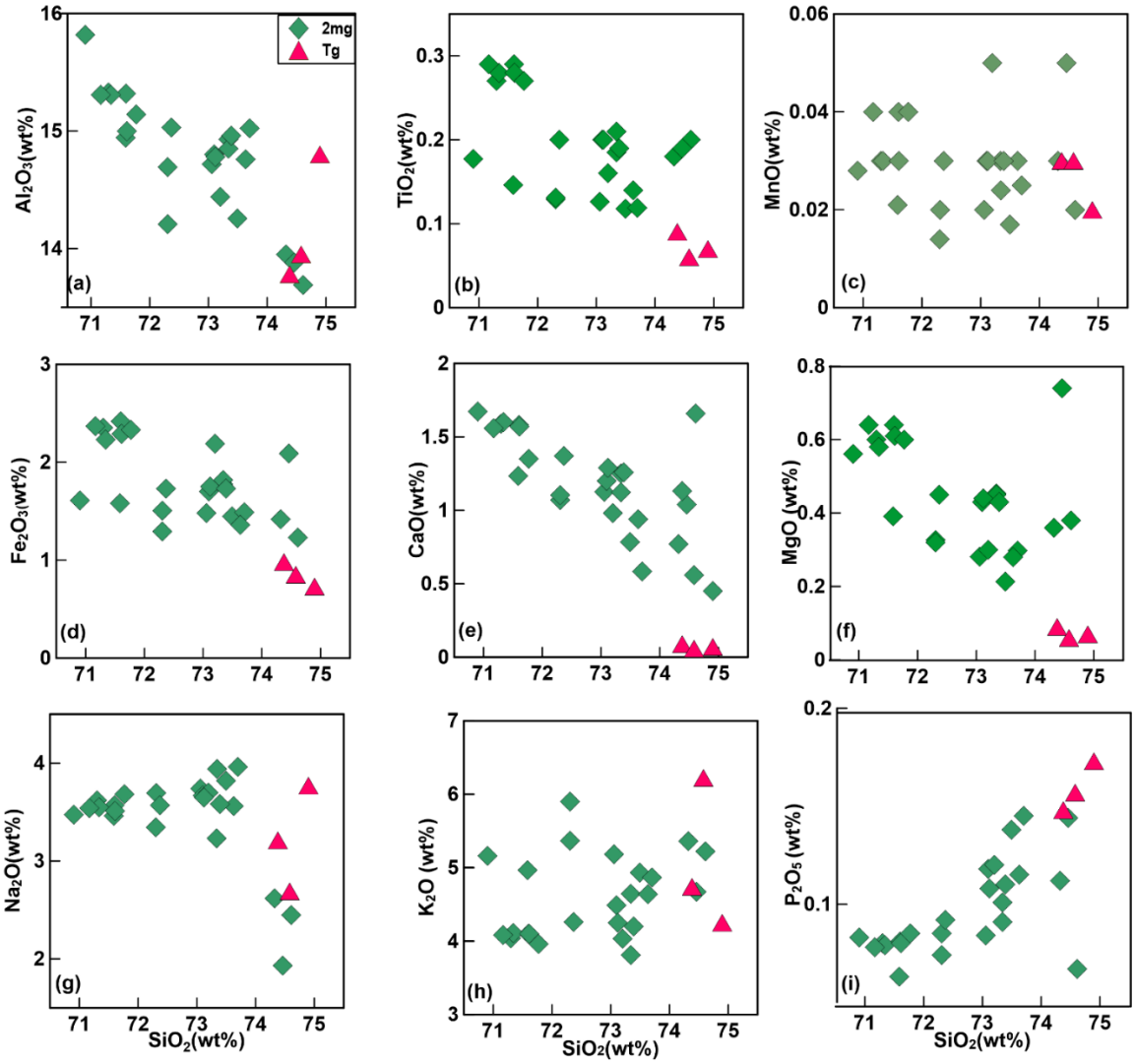

Figure 4.1 (a-i) Harker variation plot of North Sikkim leucogranites.

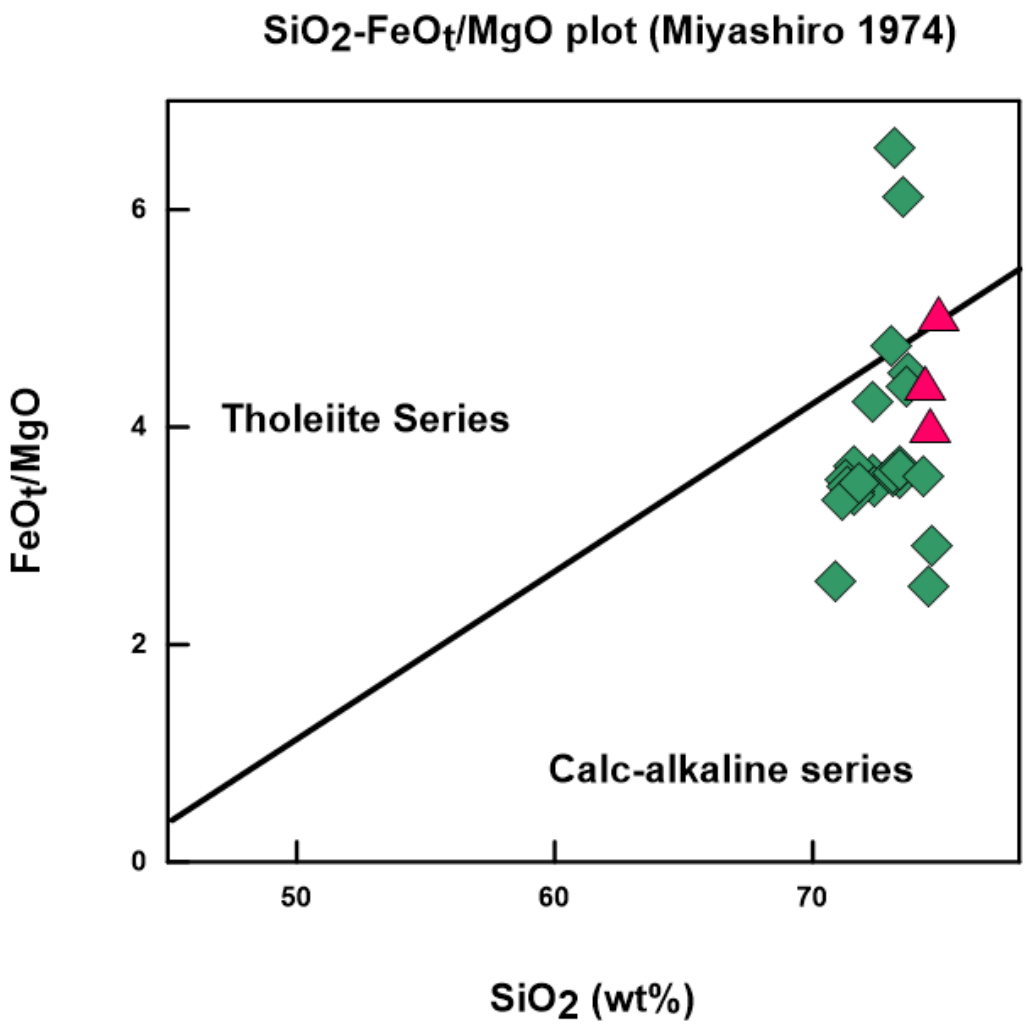

Figure 4.2. FeOt /MgO versus SiO_2 diagram after Miyashiro (1974).

In FeO_t /MgO versus SiO_2 diagram (after Miyashiro, 1974), (Fig. 4.2) the rocks series which shows increasing FeO_t /MgO ratios with increasing SiO_2 is grouped into tholeiitic and vice-versa for calc-alkaline series. In North Sikkim, the samples from 2mg and Tg belong to the calc-alkaline series.

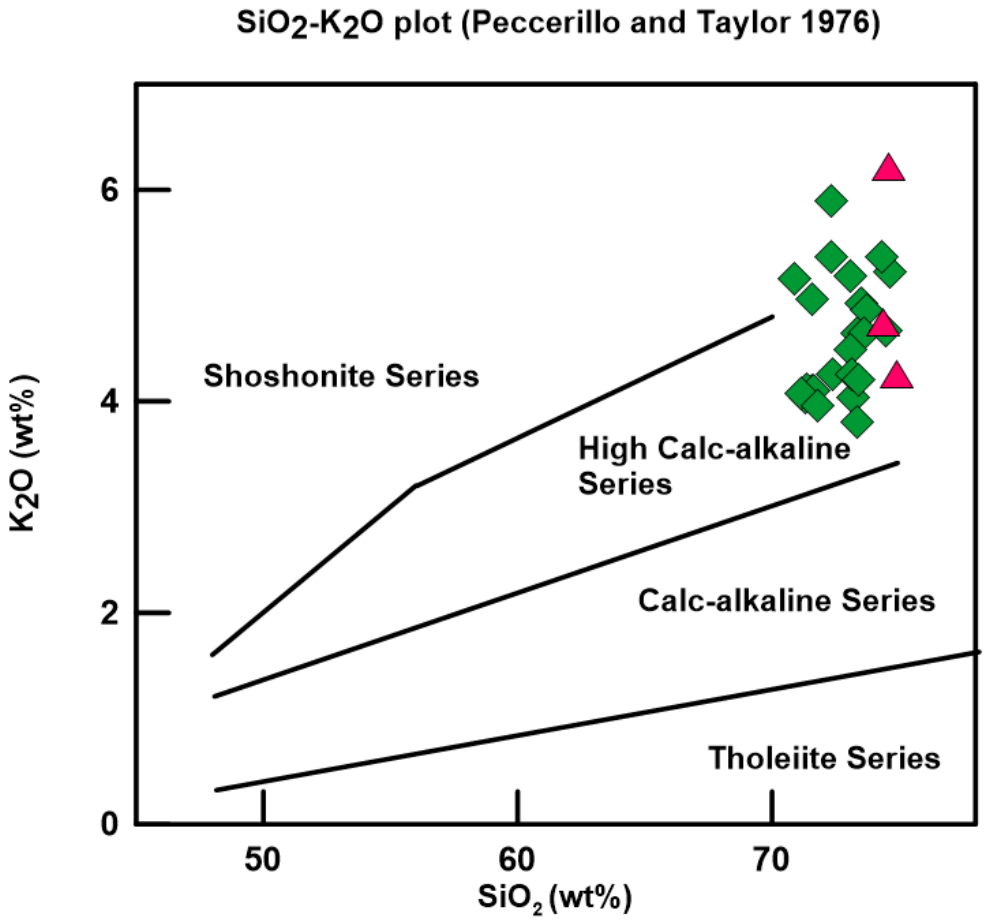

Figure 4.3. The K_2O vs SiO_2 diagram after Peccerillo and Taylor (1976).

In K_2O versus SiO_2 diagram Peccerillo and Taylor (1976) (Fig. 4.3), distinguish between tholeiitic and calc-alkaline igneous rocks. In North Sikkim, most of the samples from 2mg and Tg belong to the high calc-alkaline series.

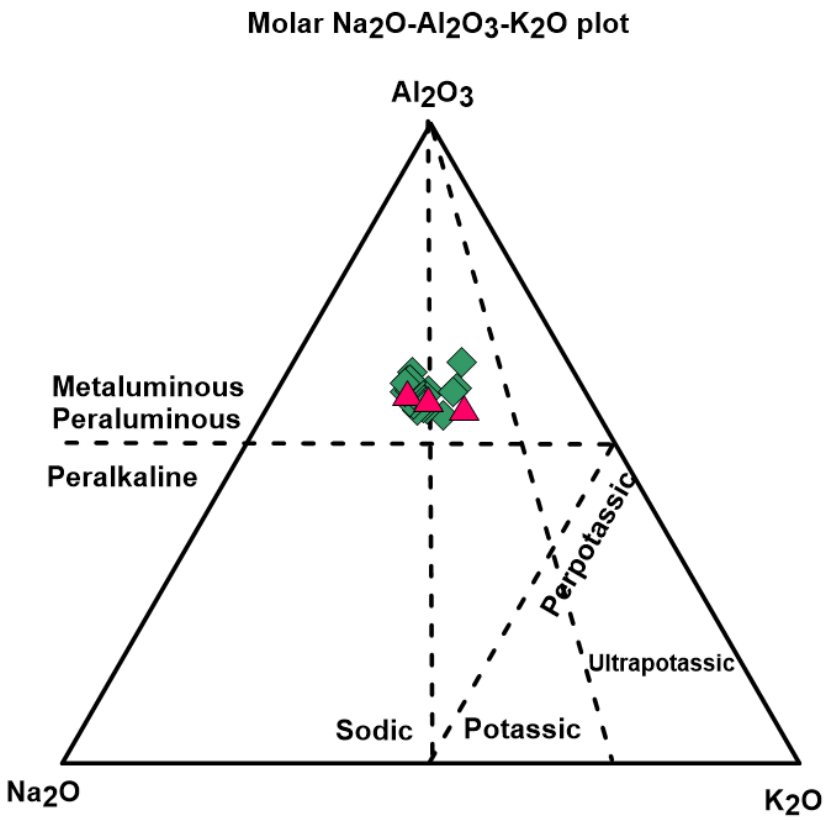

Figure 4.4. The molar Na_2O – Al_2O_3 – K_2O ternary plot Shand (1943)

In (Fig. 4.4), the plot differentiates meta-/peraluminous from peralkaline rocks as well as potassic, sodic, and ultrapotassic suites. The North Sikkim leucogranites plot under a peraluminous field for the samples of 2mg and Tg.

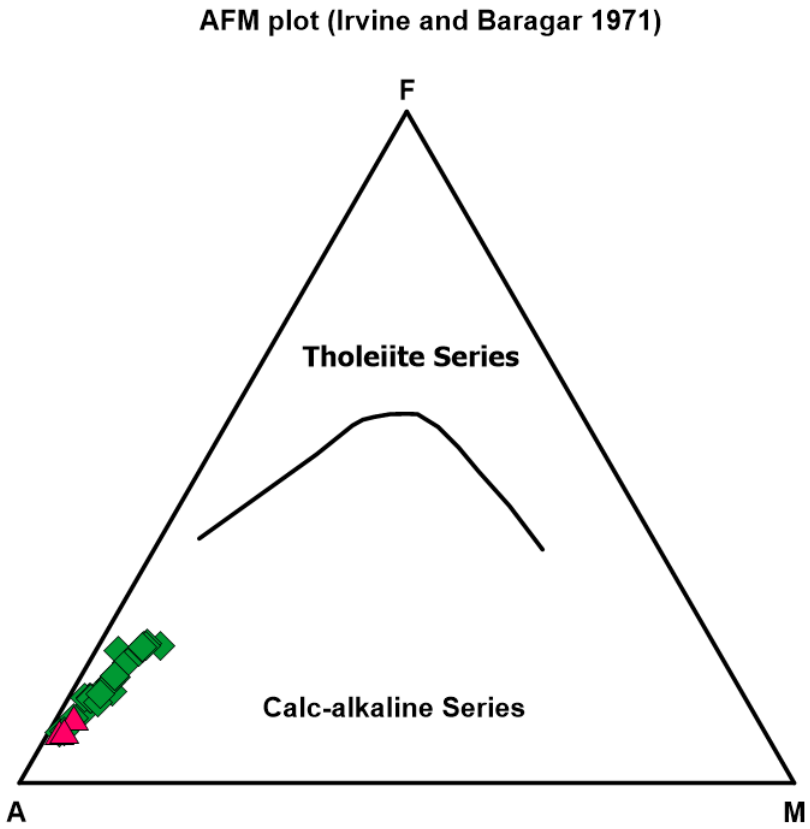

Figure 4.5. AFM diagram after Irvine and Baragar (1971).

The (Fig.4.5), shows a ternary plot of the concentrations of Na_2O + K_2O (alkalis; A), FeO (F), and MgO (M) in an igneous rock after being recalculated to a sum of 100%. In addition, the figure illustrates the difference between two commonly observed trends: Fe-enrichment indicates differentiation of a tholeiitic magma and, "a straight-line trend" representative of calc-alkalic magma differentiation. Thus, different types of igneous rocks can be analyzed using this diagram. As shown in the AFM plot (Irvine and Baragar 1971), the samples of 2mg and Tg show the calc-alkaline trend.

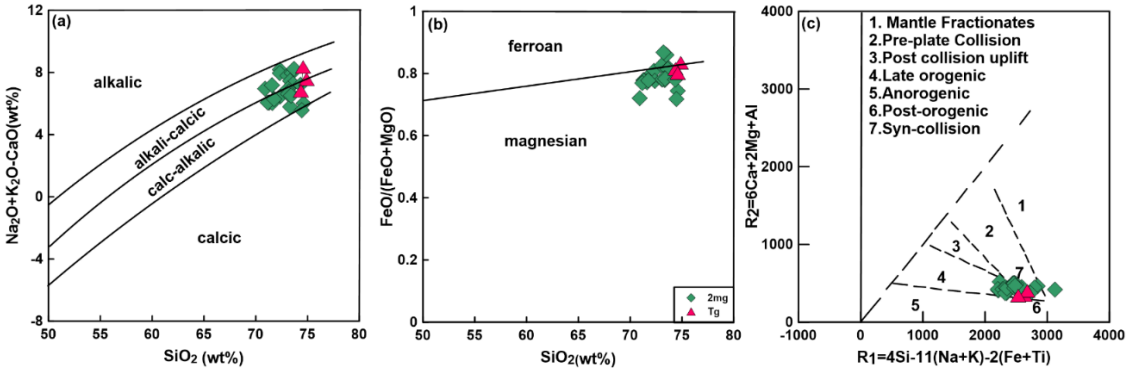

Figure 4.6. (a) Na_2O+K_2O-CaO (wt.%) vs SiO_2 for the samples of North Sikkim leucogranites Frost et al. (2001). (b) FeO/(FeO+MgO) vs SiO_2 (wt.%) after Frost et al. (2001) indicating peraluminous nature of the leucogranites. (c) R_1 vs R_2 Tectonic Discrimination diagram of North Sikkim leucogranites after Batchelor and Bowden (1985).

In SiO_2 vs. Na_2O+K_2O-CaO the studied samples of 2mg and Tg range from calc-alkaline to alkali-calcic (Fig. 4.6 a) In $FeO_t/(FeO+MgO)$ vs SiO_2 plot the samples lie on the borderline of ferroan and magnesian trend, the sample falling under the ferroan category show Fe enrichment (Fig. 4.6 b). In R_1 vs R_2 Tectonic Discrimination diagram, after Batchelor and Bowden (1985), the samples plot in the syn-collision zone, indicating S-type affinity (Fig. 4.6 c).

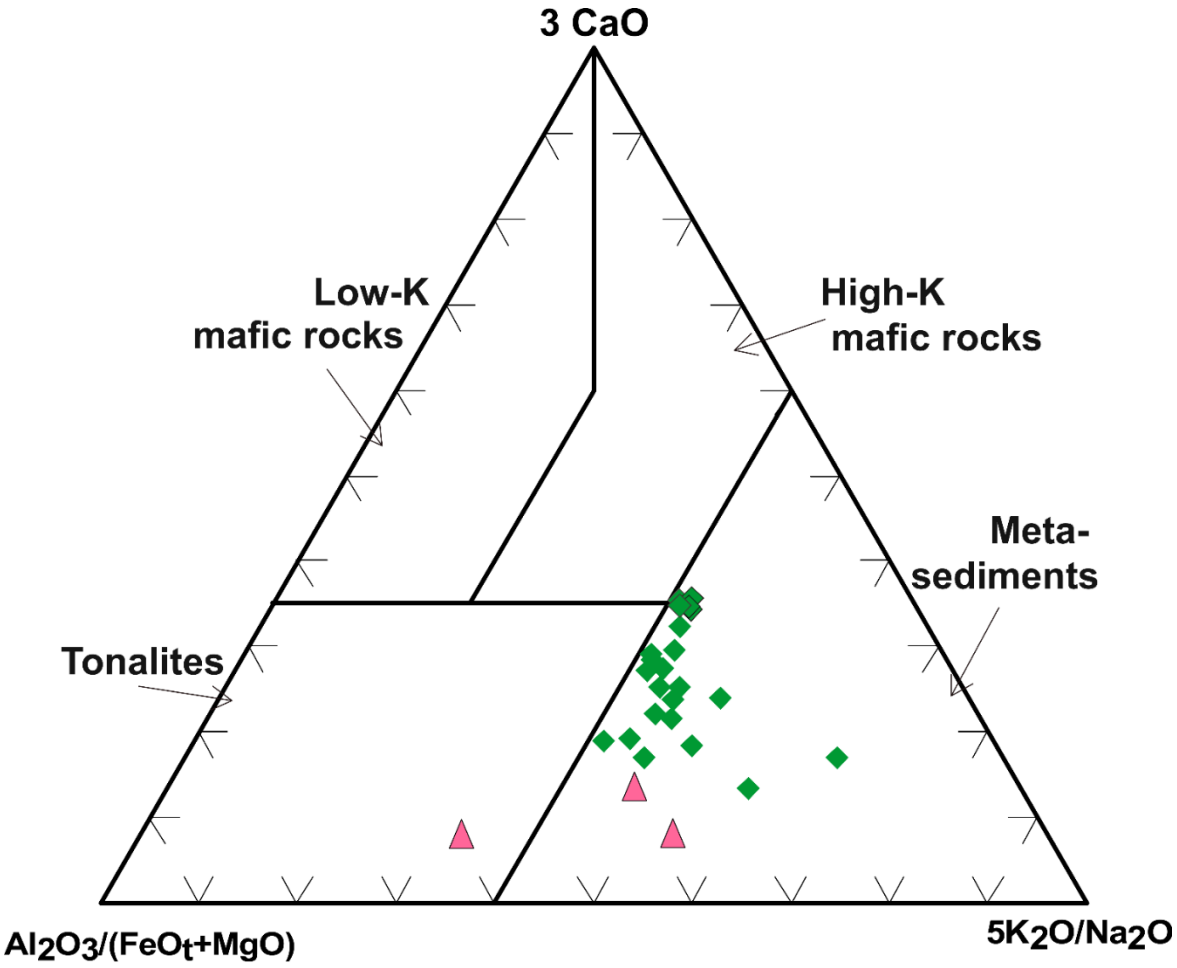

Figure 4.7. Ternary diagram of Al_2O_3/ (FeO_t + MgO) vs. 3CaO vs. 5(K_2O/Na_2O) (after Laurent et al. (2014). A range of melt compositions (tonalites, metasediments, low- and high-K mafic rocks) was determined by the major-element compositions of partial melts in experiments.

In (Fig. 4.7), The major element compositions of the leucogranite sample from 2mg and Tg fall close to the field of partial melts from metasediments.

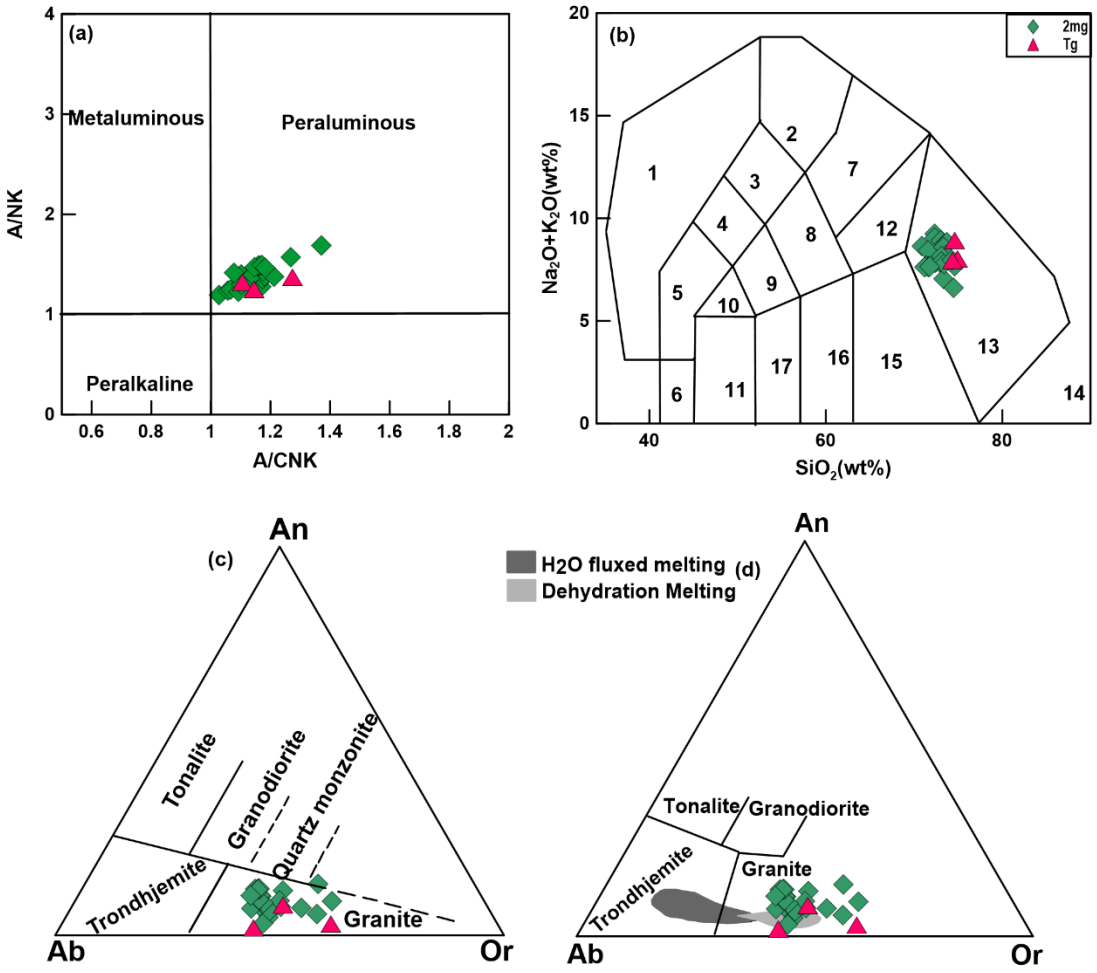

Figure 4.8. (a) A/NK versus A/CNK diagram (Shand 1943) (b) K_2O+Na_2O versus SiO_2 diagram Middlemost (1994) 1.Foidolite 2.Foid Syenite 3.Foid monzosyenite 4.Foidmonzo-gabbro5.Foid gabbro 6.Peridot gabbro7.Syenite 8.Monzonite 9.Monzodiorite 10.Monzogabbro 11.Gabbro 12.Quartz monzonite 13.Granite 14.Quartzolite 15.Granodiorite 16.Diorite 17.Gabbroic diorite (c) Normative (An-Ab-Or) classification diagram of North Sikkim leucogranites O'Connor (1965) (d) Composition of melt produced by H_2O fluxed melting and dehydration melting Patiño Douce and Harris (1998).

In this plot (Fig. 4.8 a), samples lie under a peraluminous (A/CNK>1.0) field for both the samples of the 2mg and Tg. In (Fig. 4.8 b) K_2O+Na_2O versus SiO_2 diagram the plots lie under the granitic field. Based on the normative classification diagram (An-Ab-Or),

of North Sikkim leucogranites (Fig.4.8 c), 2mg and Tg are classified as granitic. In (Fig. 4.8 d), all the samples fall under the category of dehydration melting.

4.3 Trace and REE Geochemistry

In contrast to major elements in igneous systems, trace elements tend to occur in low quantities (>0.1 wt.%) but provide valuable geological information due to their large variations. The composition of the source and the prevalent crystal-melt equilibria at the time of the rock genesis determine the concentration of REE in a given rock. The trace element variations show that both the leucogranites are enriched in Large-ion lithophile (LILE) and depleted in High Field strength elements (HFSE). The value of the Rb ranges from (176-327 ppm), Ba ranges from (295-1190 ppm), Sr values range from (86-277 ppm), Zr content ranges (60.5-158 ppm) from (U values range from (4.4-28.7 ppm), Th ranges (8.89-25 ppm), Hf ranges from (2.29-4.98 ppm), whereas in case of Tg, U contents ranges (14.9-18.9 ppm), Th (4.38-7.6 ppm), Hf (1.26 -1.68 ppm), Zr (25-39.5 ppm), Rb (258-301 ppm), Ba (65-342 ppm), Sr (23.7-79.6 ppm). In the REE plots the 2mg leucogranites are enriched in LREEs [ΣLREE= 72.57-203.52 ppm and show depletion in HREEs [(ΣHREE = 8.42-18.2 ppm)]. The Eu anomaly ranges from 0.48–0.75 whereas for Tg Eu anomalies range from 0.20–0.57.

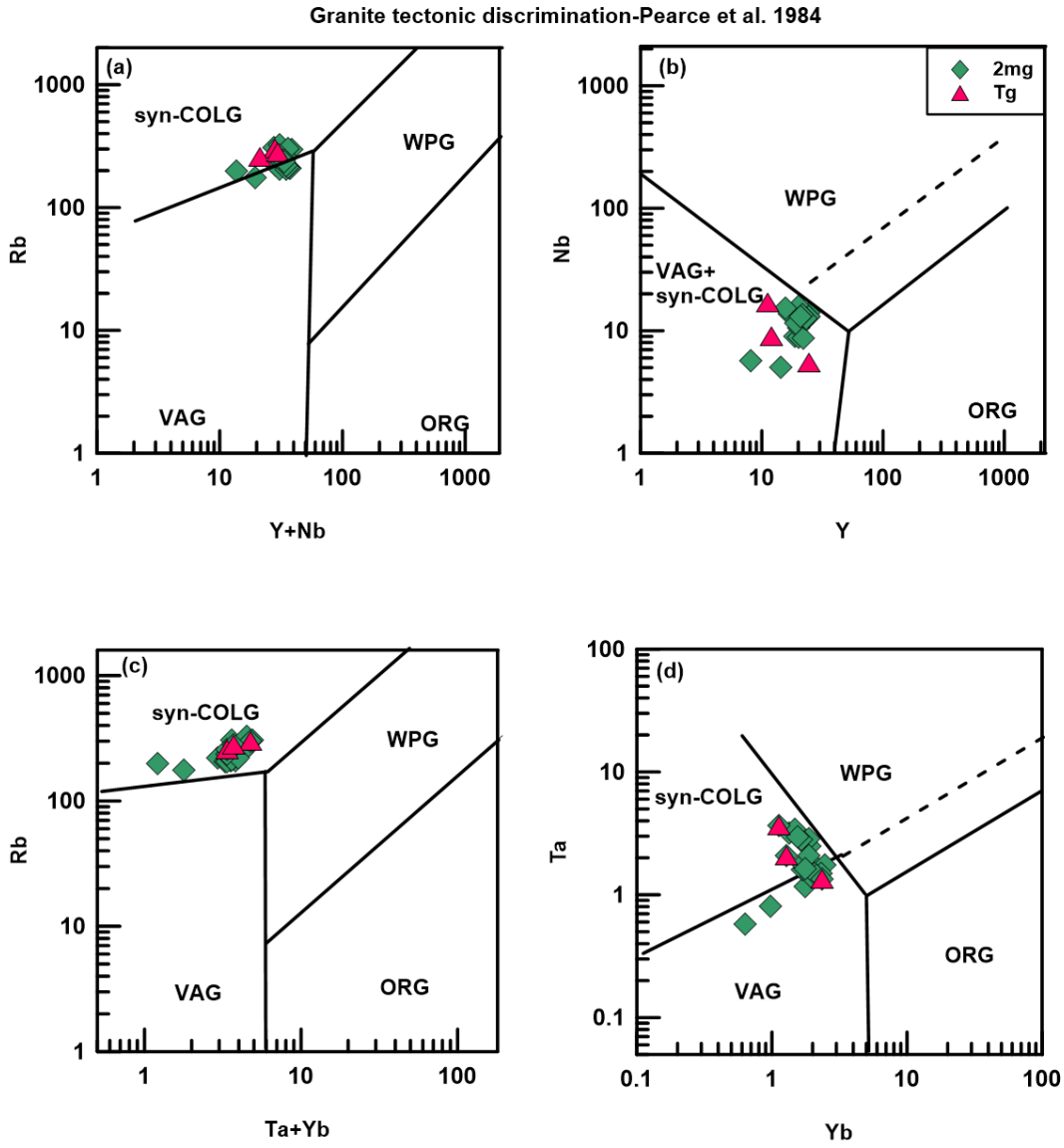

Figure 4.9. (a) log(Y+Nb) vs. log Rb (b) log Y vs. log Nb (c) log Ta+Yb vs. log Rb (d)log Yb vs log Ta trace-element based geotectonic classification of granitoids by Pearce et al. (1984) WPG, within-plate granite; VAG, volcanic-arc granite; ORG, orogenic granite; syn-COLG, syn-collisional granite.

In this plot log (Y+Nb) vs. log Rb (Fig. 4.9 a), the North Sikkim leucogranite lies under the syn COLG zone. In log Y vs. log Nb (Fig. 4.9 b), both types of leucogranites are mostly concentrated along VAG +syn-COLG fields. Similarly, in plot log Ta+Yb vs. log Rb (Fig. 4.9 c), all the samples lie in the syn-COLG field, whereas for the plot log Yb vs. log Ta (Fig. 4.9 d), most of the samples plot under syn-COLG whereas two samples are plotted within VAG field.

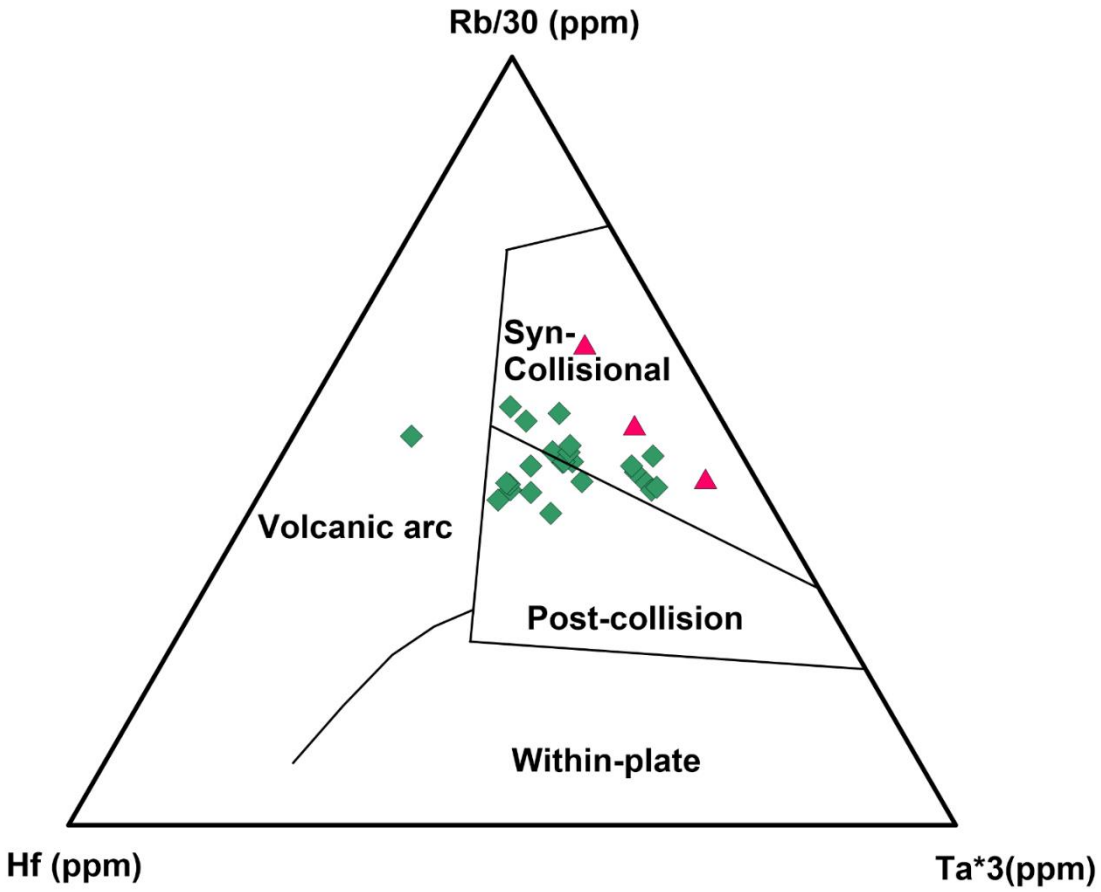

Figure 4.10. Rb/30-Hf-Ta×3 ternary diagram showing that most of the samples plot within the syn-collisional and post-collisional field (Harris, 1986).

In (Fig. 4.10), almost all the samples plot within the syn-collisional and post-collisional field.

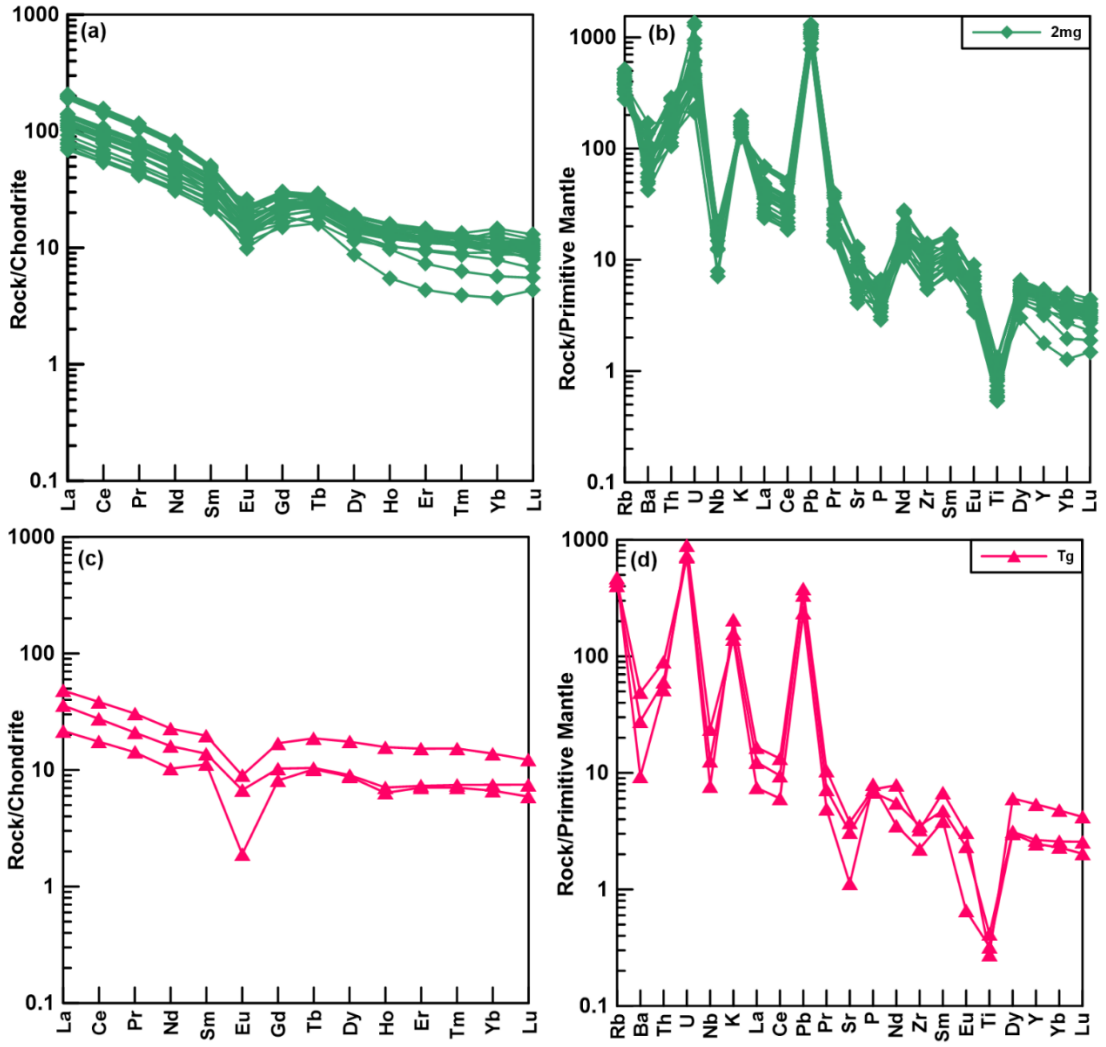

Figure 4.11 (a, c) Chondrite normalized REE pattern for the two-mica leucogranites and tourmaline leucogranites respectively; Fig (b, d) Primitive mantle-normalized trace element diagram for the two mica leucogranites. The normalizing values are taken from Sun and McDonough (1989).

The Chondrite normalized REE depletion in HREE and enrichment in LREE can be explained by the retention of feldspar in the source which suggests crustal melt origin (Fig. 4.11 a, c). According to the primitive mantle normalized spider diagrams all the studied leucogranites from North Sikkim are depleted in high-field strength elements and enriched in low-field strength elements (Rb, U, K, Pb, and Th) and depleted in high-field strength elements (Nb, Ta, Ba, and Ti), (Fig. 4.11 b, d). The enrichment and depletion of the elements are listed below:

Enrichment P- fractionation or retention of apatite.

Depletion of Sr- fractionation or K-feldspar.

Depletion of Ba- fractionation or retention of plagioclase.

Depletion of Nb and Ti- fractionation or retention of biotite.

4.4 Source of leucogranites

The studied North Sikkim leucogranites consists of high SiO_2 contents (>70% wt.%), Al_2O_3 (13.69-15.8 wt.%), and A/CNK values (1.11-1.27), indicating felsic and strongly peraluminous nature. The Ce/Pb (0.24-1.03) ratios and Nb/U (0.37-2.19), ratios in the studied leucogranites are similar to Upper Continental Crust (UCC; Taylor and McLennan, 1985), and Bulk Continental Crust (BCC; (Rudnick and Fountain, 1995) suggesting crustal melts as a probable source (Fig. 4.14 a-b). These traits are identical to those found in other Miocene Himalayan leucogranites which are indicative of their crustal origin (Guo and Wilson, 2012; Le Fort et al., 1987; Liu et al., 2014; Schärer et al., 1986; Xie et al., 2018). In the Al_2O_3 + FeO + MgO + TiO_2 versus Al_2O_3/ (FeO + MgO + TiO_2) and CaO/ (FeO + MgO +TiO_2) versus (CaO + FeO + MgO + TiO_2) diagram (Fig. 4.12 a-b), the 2mg fall in the graywacke field indicating their formation by partial melting of plagioclase rich metasedimentary rock. On the other hand, Tg falls in the pelitic derived field suggesting plagioclase poor nature of their source.Plagioclase and muscovite control the Rb-Ba-Sr budget in S-type granites as Sr and Ba are compatible in former while Rb is compatible with muscovite (Sylvester, 1998). Higher Rb/Sr (Rb/Sr>2) ratios, are suggestive of fluid absent muscovite melting while lower (Rb/Sr <2) ratios in fluid fluxed melting have been attributed to involvement of biotite (Gou et al., 2016; Visonà and Lombardo, 2002; Inger and Harris, 1993). Sylvester (1998), suggested that granites derived from graywacke and pelites vary in their Rb/Sr

ratio wherein graywacke-derived granites have lower Rb/Sr as compared to the ones derived from pelite. The studied 2mg from north Sikkim plot dominantly fall in clay-poor source with some samples falling in clay-rich region owing to their higher Rb/Sr (0.77-3.77) ratio (Fig. 4.13 a). On the other hand, the studied Tg from north Sikkim have higher Rb/Sr (3.54-12.70) ratio and fall in the clay rich region (Fig. 4.13 a). This suggests that the studied 2mg are dominantly derived from graywacke which Tg have been sourced from pelitic source. In Al_2O_3/TiO_2 versus CaO/Na_2O diagram (Fig. 4.13 b) most of the 2mg ranges from clay poor sources and the Tg samples lies under clay rich sources.

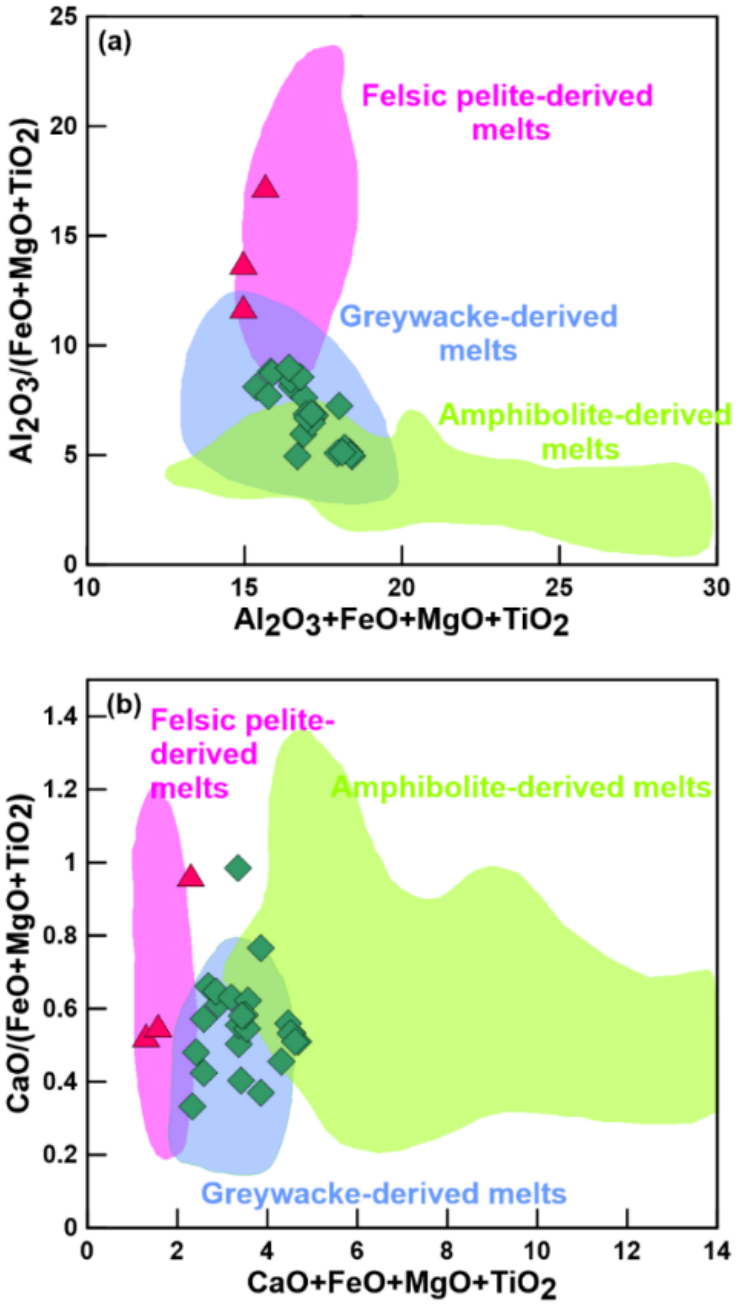

Figure 4.12 (a)Geochemical classification diagram Al_2O_3/ (FeOt + MgO + TiO_2) versus (Al_2O_3 + FeO t + MgO +TiO_2) (Patiño Douce 1999)(b) CaO/ (TFeO+MgO + TiO_2) versus CaO + TFeO+MgO + TiO_2 diagram from Patino and Douce (1999).

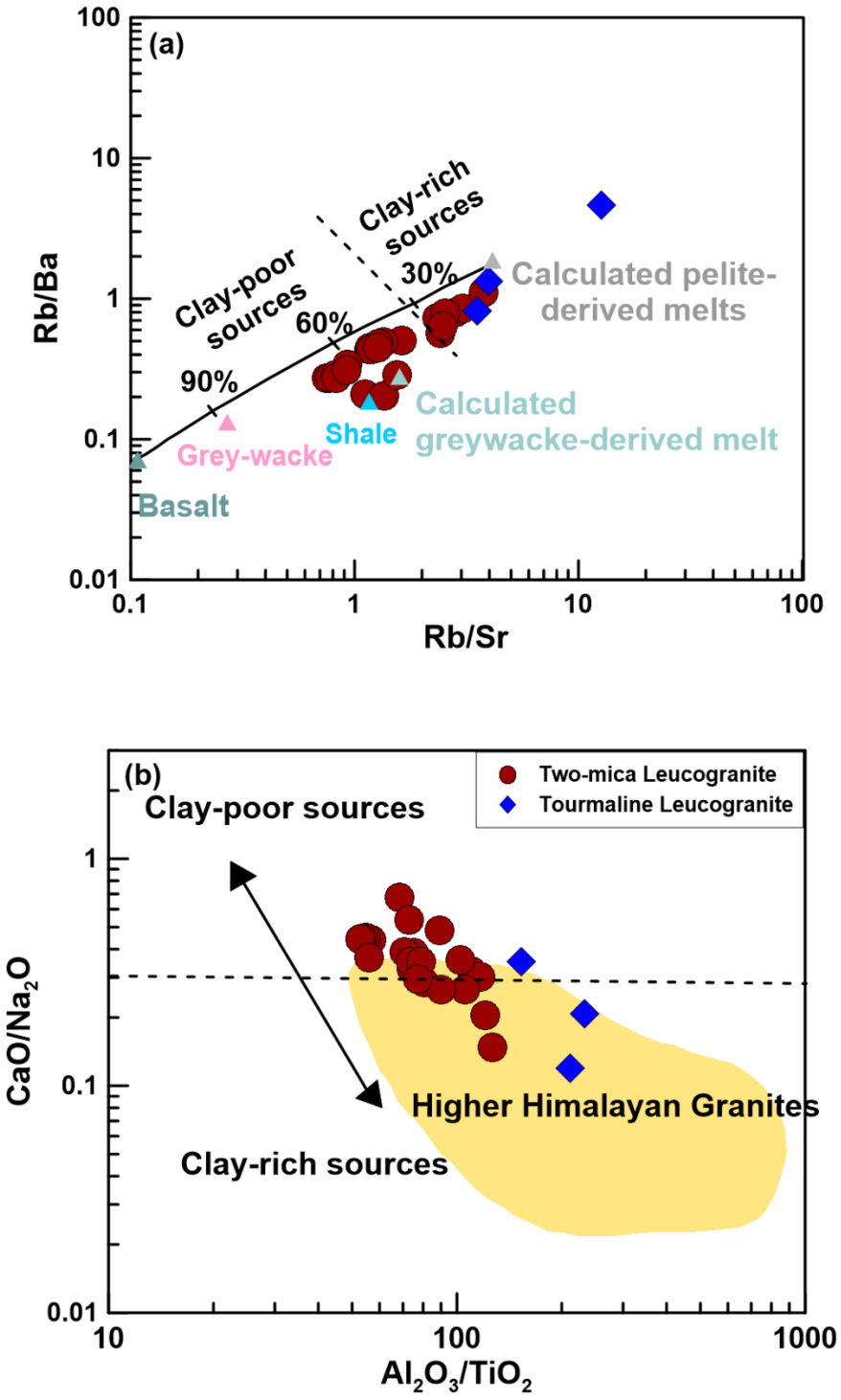

Figure 4.13 (a) Rb/Ba versus Rb/Sr diagram modified from Sylvester (1998); (b) Al_2O_3/TiO_2 versus CaO/Na_2O diagram;

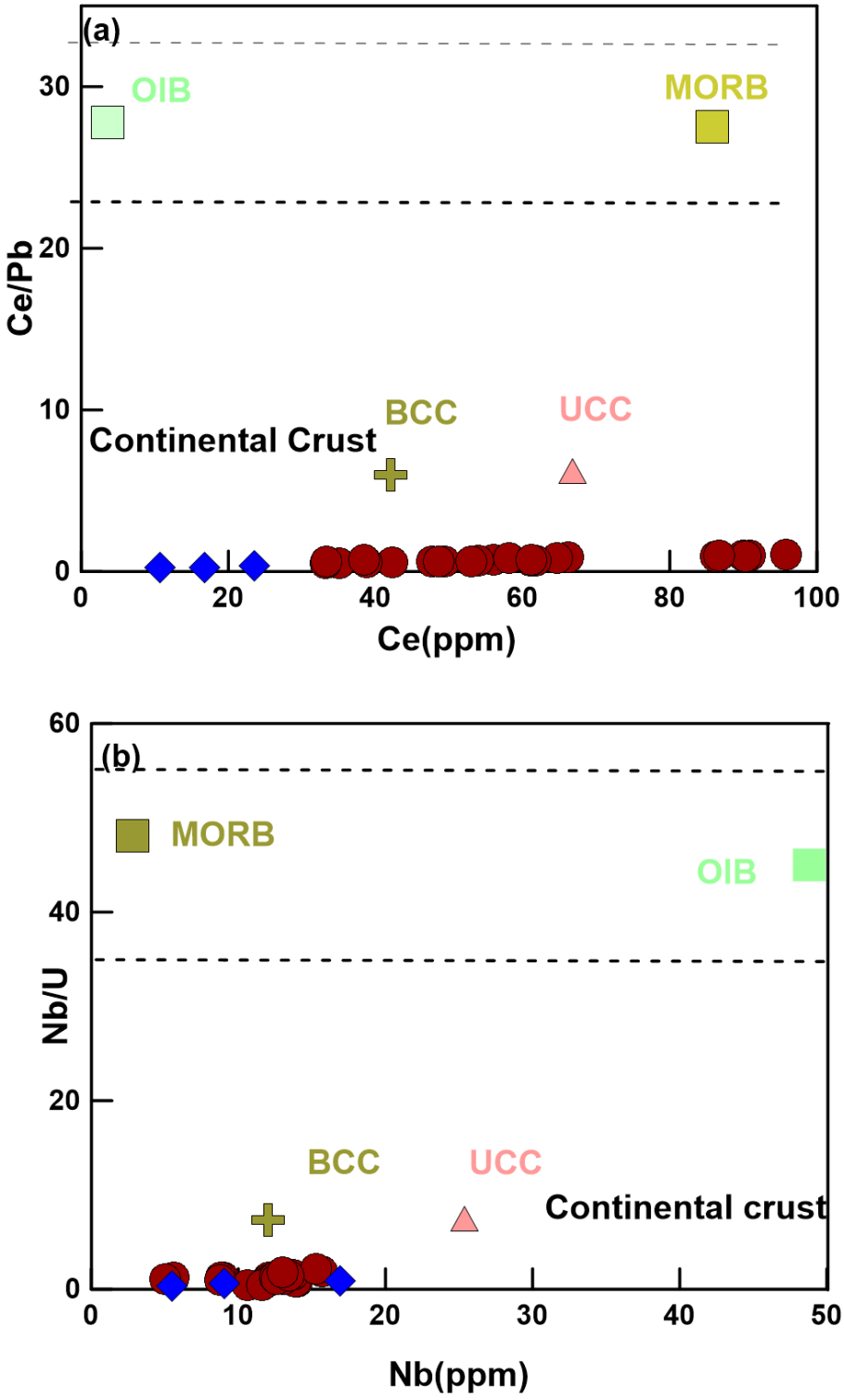

Figure 4.14. (a) Ce/Pb vs Ce (ppm); (b) Nb/U vs Nb (ppm) from Guo and Wilson (2012)

4.5 Pegmatite Geochemistry

4.5.1 Major oxide Geochemistry

In tourmaline pegmatite SiO2 is ranging from (67.83-75.35 wt.%), high Al2O3 varies from (14.58-17.51 wt.%), low amount of CaO ranges from (0.39-1.92 wt.%) TiO_2 ranges from (0.08-0.37 wt.%), Fe_2O_3 ranges from (1.25-3.36 wt.%), and K_2O ranges from (4.6-6.12 wt.%). In the molar A/CNK vs A/NK plot (Fig. 4.15 a), all the samples plot under peraluminous. In the plot Na_2O+K_2O vs SiO_2 studied samples plotted in quartz monzonite and granite fields (Fig.4.15 b).

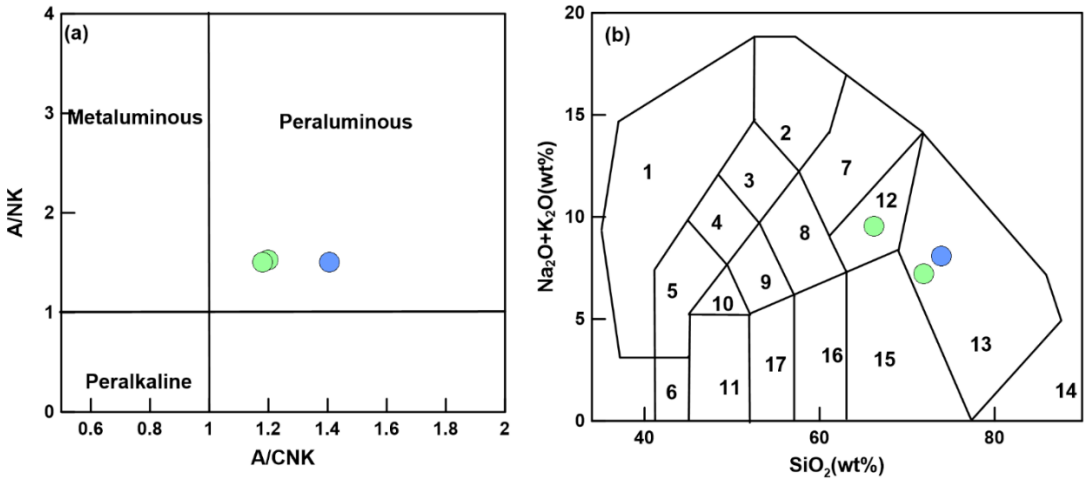

Figure 4.15. (a) Molar A/CNK vs. A/NK plot for tourmaline pegmatites Shand, (1947) (b) Na_2O+K_2O versus SiO_2 (wt.%) diagram Middlemost, (1994) area 12 &13 represents quartz monzonite and granite. Green represents Type 1 and Blue represents Type 2.

In the triangular plot, the $CaO-Al_2O_3-Na_2O-K_2O-Fe_2O_{3T}$-MgO diagram after Chappell and White (1992), indicates that the pegmatites belong to S-type (Fig.4.16).

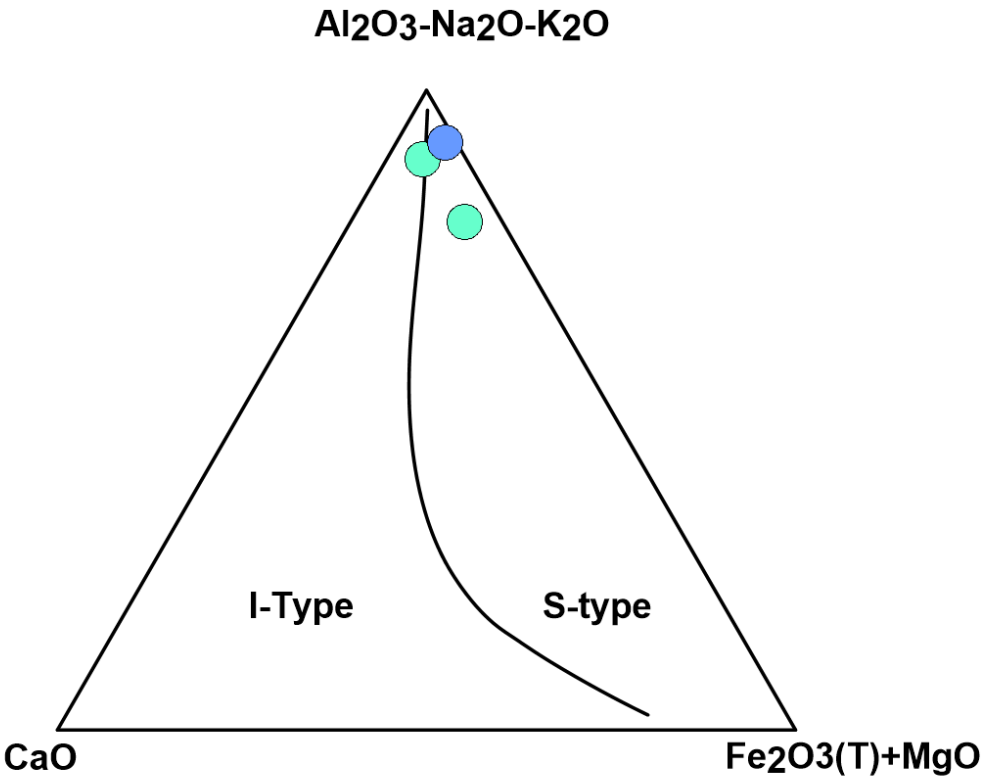

Figure 4.16. In triangular $CaO-Al_2O_3-Na_2O-K_2O-Fe_2O_{3T}$ + MgO diagram, samples plot in mainly S-type field and on border with I-type field Chappell and White (1992).

4.5.2 Trace element and REE Geochemistry

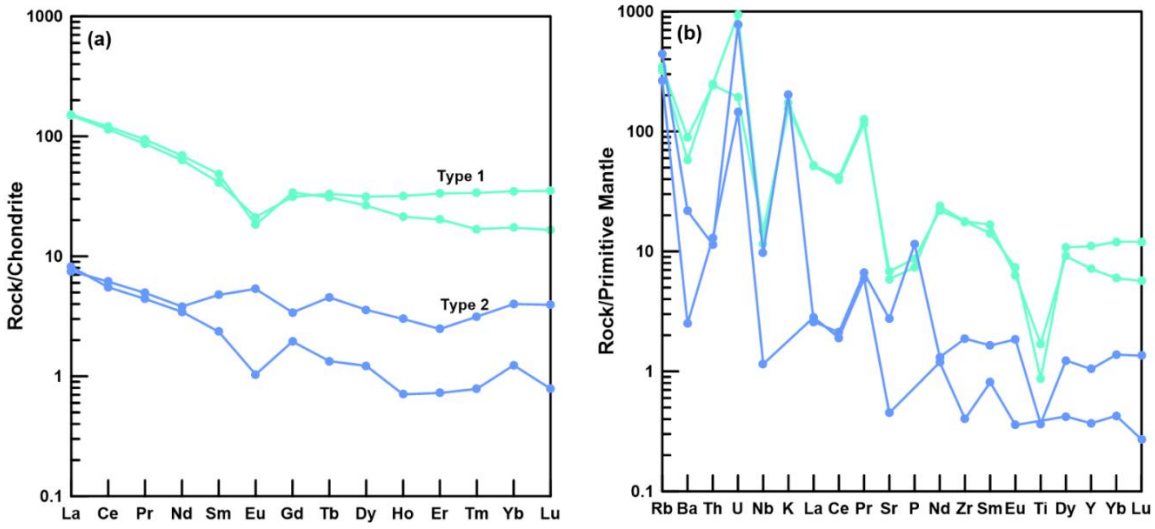

Figure 4.17. (a) Chondrite normalized REE pattern for tourmaline leucogranite (b) Primitive mantle normalized trace element diagram for tourmaline leucogranites. The normalizing values are taken from Sun and McDonough (1989).

The chondrite normalized REE pattern for tourmaline pegmatite is divided into two types. Type 1 is enriched in LREE and depleted in HREE with negative Eu anomaly with ratios ranging from 0.45-0.59, in comparison to former Type 2 is less enriched with Eu anomaly ranging from 0.48-1.33 (Fig. 4.17 a). In the primitive mantle normalized trace element plot (Fig.4.17 b), depleted in Sr, Ba whereas enriched in Rb and U. In (Fig.4.18) the trace element Zr vs TiO_2 indicate mainly S-type granitic source for the pegmatites.

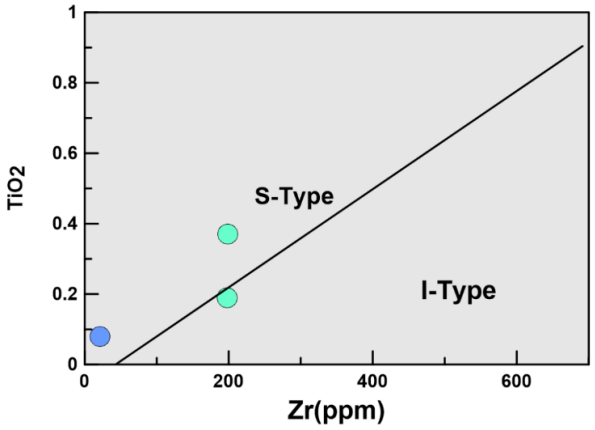

Figure.4.18. Zr vs TiO_2 diagram Watson and Harrison (1983).

CHAPTER 5
MINERAL CHEMISTRY

5.1 Introduction

This chapter focuses on the mineral chemistry of 2mg, Tg, and tourmaline pegmatite. Understanding the physiochemical conditions under which a mineral is formed requires using a chemical study of that mineral. The results have been used to interpret and discuss the variations of the minerals present in the leucogranites and pegmatites from the North Sikkim Himalayas.

5.2 Tourmaline

Tourmaline structural formulas were determined according to Henry and Dutrow (1996), by normalizing to 15 cations pfu (per formula unit) in the tetrahedral and octahedral sites (T + Z + Y), based on the general formula $XY_3Z_6T_6O_{18}(BO_3)_3V_3W$, where X = Na, Ca, K, vacancy; Y = Fe, Mg, Mn, Ti, Al. The data on the mineral chemistry is given in Appendix B 1.1.

In the case of 2mg, tourmaline is composed of SiO_2 (34.22-36.61wt.%), FeO varies for 2mg (1.23-17.45 wt.%), MgO (0.86-6 wt.%), Na_2O for 2mg ranges from (0.19 to 1.92 wt.%), TiO_2 (bdl-0.73 wt.%). For Tg SiO_2 (32.80-36.37 wt.%), FeO varies for 2mg (8.26-12.38 wt.%), MgO (1.76-4.07 wt.%), Na_2O for Tg ranges from (1.25 - 2.07 wt.%), TiO_2 (bdl-0.73 wt.%). Pegmatites show variations (33.85-35.64 wt.%), (34.57-33.95 wt.%), (8.30-11.25 wt.%), (2.13-3.98 wt.%), (1.46-1.93 wt.%), and (0.25-1.03 wt.%) for SiO_2, Al_2O_3, FeO, MgO, Na_2O and TiO_2 respectively.

The tourmaline analyses obtained in this study for 2mg, Tg, and pegmatites fall in the alkali group in the nomenclature of Henry et al. (2011), with low Ca contents and show a wide variation in the vacancies content (Fig. 5.1). In Ca-Fe-Mg plot most of the samples plot under Li-poor granitoids, pegmatites and aplite field (Fig. 5.2). In the ternary diagram $2Li^{+} - Mg^{2+} - Fe^{2+}$ for Y-site occupancy of alkali-group tourmalines

indicates that most of the tourmalines are classified as schorls (Fig. 5.3 a). In the plot of Mg/ (Fe + Mg) vs. X-site vacancy/(Na + X-site vacancy) of tourmaline mostly grouped as “schorl” (“oxy-schorl’’) (Fig. 5.3 b).

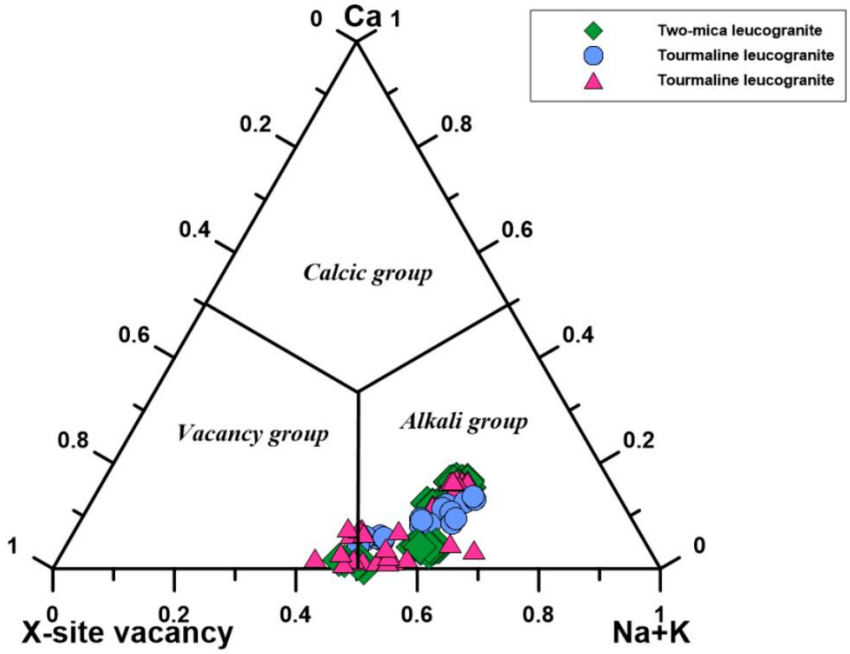

Figure 5.1. Classification of the principal groups of the tourmalines from Sikkim leucogranites and pegmatites Henry et al. (2011).

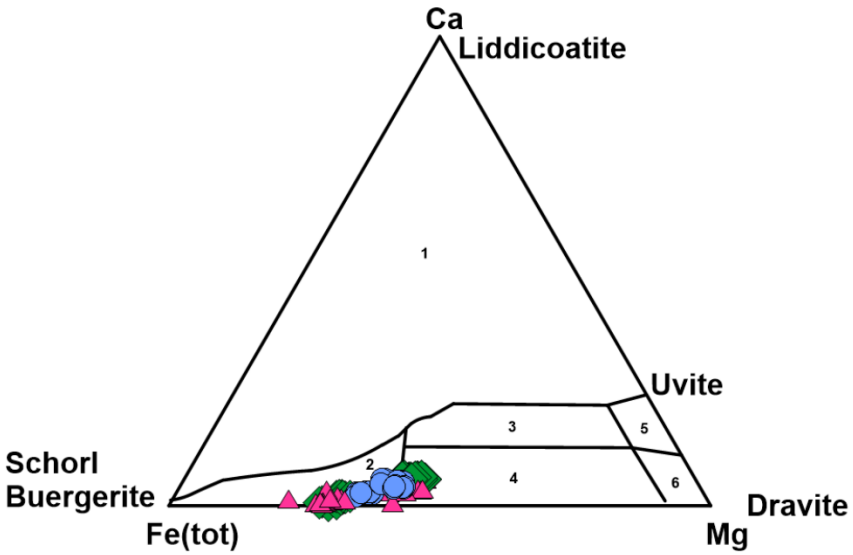

Figure 5.2. Ca-Fe-Mg ternary diagram after Henry and Guidotti (1985). These fields are: (l) Li-rich granitoid pegmatites and aplites These fields are: (l) Li-rich granitoid pegmatites and aplites; (2) Li-poor granitoids and associated pegmatites and aplites; (3) Ca-rich metapelites, metapsammites, and calc-silicate rocks.

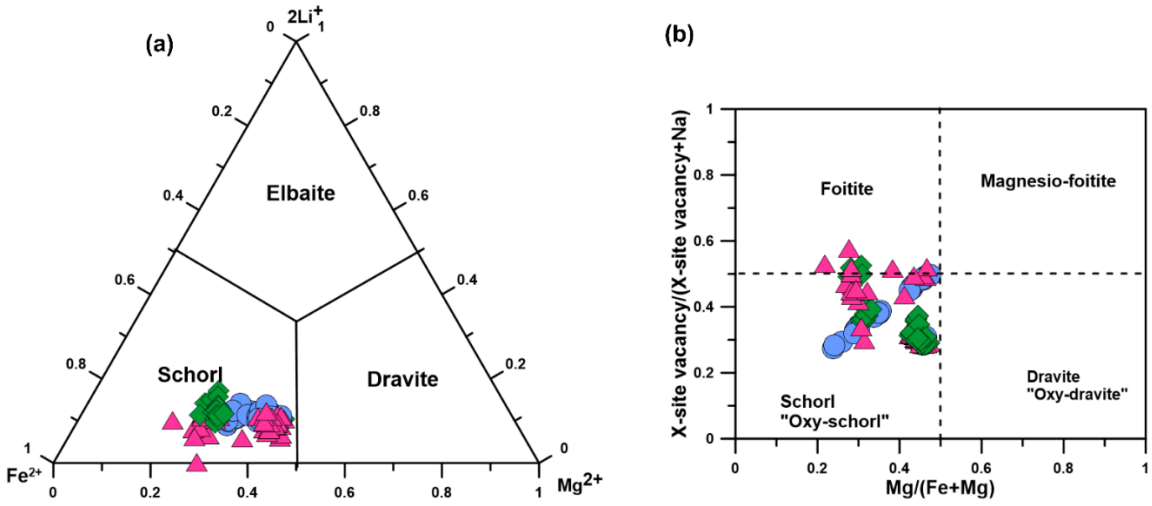

Figure 5.3. (a) The ternary diagram $2Li^{+}-Mg^{2+}-Fe^{2+}$ for Y-site occupancy of alkali-group tourmalines (b) The plot of Mg/ (Fe + Mg) vs. X-site vacancy/(Na + X-site vacancy) of tourmaline grains Henry and Dutrow (2012).

5.3 Biotite

Biotite is a mica group of sheet silicate with the following chemical formula:

$X_2Y_6Z_8O_{20}$ (F, OH)$_4$, where,

X= K, Na, and Ca,

Z= Si and Al^{iv},

Y= Al^{vi}, Mg, Fe, Mn, Cr, and Ti,

A detailed analysis of biotite has been carried out in terms of oxides. Representative chemical analyses and structural formulae of biotite are presented in Appendix B 1.2.

In the studied and analyzed 2mg samples for biotite, the sum of the cations for the 'Z' site is 8.00, whereas the sum of the 'Y' site varies from 5.143-5.682 and X varies from 1.524-1.956. In the case of Tg, 'Y' site values range from 5.380-5.595, and 'X'site varies from 1.260-1.865. For pegmatite 'Y' site and X-site value range from 5.316-6.432 and 0.111-1.920 respectively. The mineral formula has been calculated based on 22 oxygen atoms.

The SiO_2 of 2mg varies from 31.34 - 36.90 wt.%. biotite with the significant amount of TiO_2 ranging from 1.65-3.27 wt.%. The Al_2O_3 ranges from 17.47-23.01 wt.%, Cr_2O_3 varies from 0-0.41wt.%, FeO ranges from 14.68-22.78 wt.%, MgO varies from 3.52-7.05 wt.% while it has depleted Na_2O ranging from 0.05-0.52 wt.% and K_2O ranging from 7.22-9.51 wt.%. The biotite composition is quite and all the data set cluster in a peraluminous field (Fig 5.4 a-d) in the discrimination diagrams of Abdel-Rahman (1994). The biotite composition in the triangular plot after Nachit et al. (2005) suggests that biotite plot under primary biotite which might suggest that the biotite was formed at the high temperature and pressure (Fig 5.5). In the triangular variation plot Mg vs.

(Fe^{2+} +Mn) vs. (Fe^{3+} +Al ^{vi} +Ti) for biotites, after Foster (1960), the biotites fall under Fe-rich biotite (Fig. 5.6).

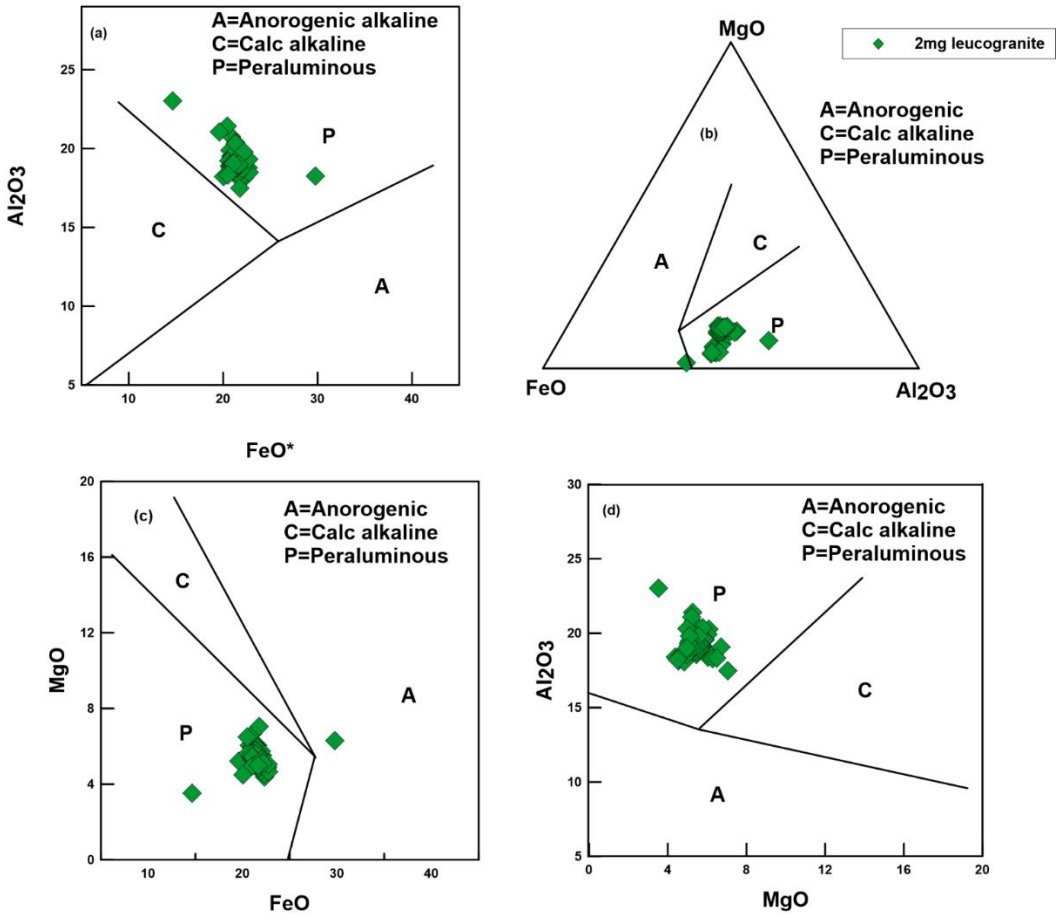

Figure 5.4. (a) Bivariate Al_2O_3 vs FeO * plot for biotite (b) Tectonic setting discrimination diagram based on FeO-MgO-Al_2O_3 contents (c) Bivariate MgO vs FeO plot for biotite (d) Magmatic source classification diagram Al_2O_3 vs MgO. Fields are taken from Abdel Rahman (1994).

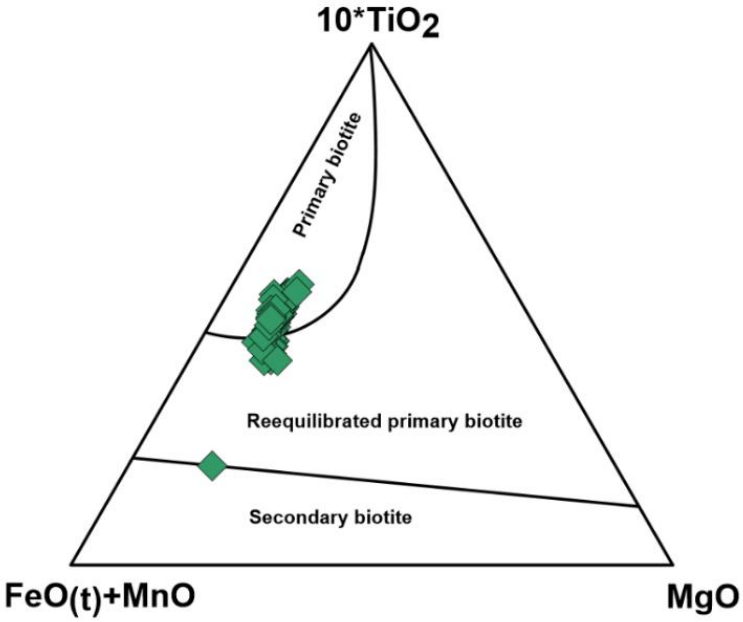

Figure 5.5. (FeO_T+MnO)-(10*TiO_2)-MgO (wt.%) diagram. Field after Nachit et al. (2005).

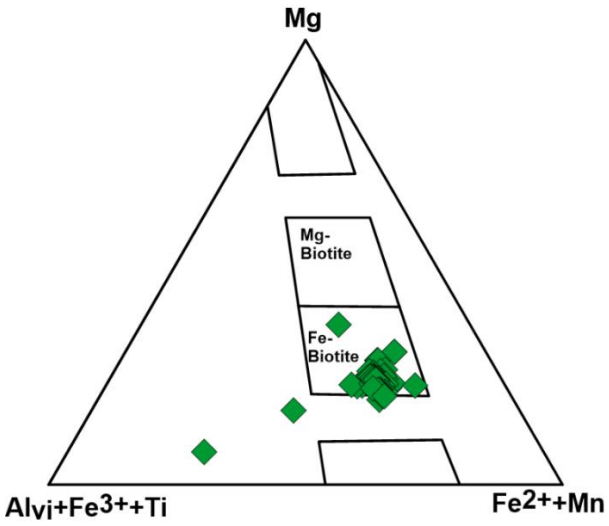

Figure 5.6. Variations in Mg vs. (Fe^{2+}+Mn)vs. (Fe^{3+}+Al^{vi}+Ti) in biotite, diagram after Foster (1960).

5.4 Muscovite

The muscovite from the two-mica leucogranite, tourmaline leucogranite, and pegmatites have been analyzed and data has been represented in (Appendix B 1.3). The general chemical formula of muscovite is $X_2Y_4Z_8O_{20}$ (F, $OH)_4$ where,

Z= Si and Al^{iv}

Y=$Al^{vi,}$ Mn, Mg, Fe, Cr, Ti

X=K, Na, and Ca

The SiO_2 in 2 mg ranges in composition from 43.99 to 46.47wt.%, FeO ranges from 0.36-4.39wt.%, and Al_2O_3 varies from 33.37 to 35.41 weight percent. The TiO_2, MnO, and MgO have bdl-0.58 wt.%, bdl-0.03 wt.%, and 0.16-1.00 wt.% ranges, respectively. In contrast, K_2O values range from 8.80 to 10.27 wt.% while Na_2O contents are low (0.63-1.76 wt.%). The SiO_2 values for Tg and pegmatites range from 44.78 to 45.57 wt.% and 45.03 to 45.99 weight percent, respectively.

TiO_2, FeO, MnO, MgO, Na_2O, and K_2O values for Tg ranges from 0.24 to 0.63 wt.%, 1.32 to 2.69 wt.%, bdl-0.07wt.%, 0.31 to 0.57 wt.%, 0.11-0.94 wt.% , and 8.52 to 10.23 wt.%. For pegmatite the values range from 0.027-0.24 wt.%, 0.75-1.32 wt.%, 0.00-0.059 wt.%, 0.16-0.37 wt.%,0.48-0.75 wt.% for TiO_2, FeO, MnO, MgO, Na_2O and K_2O respectively. In the triangular plot of muscovite crystal with chemistry compositional fields after Miller et al. (1981), most of the samples plots under primary muscovite field (Fig 5.7).

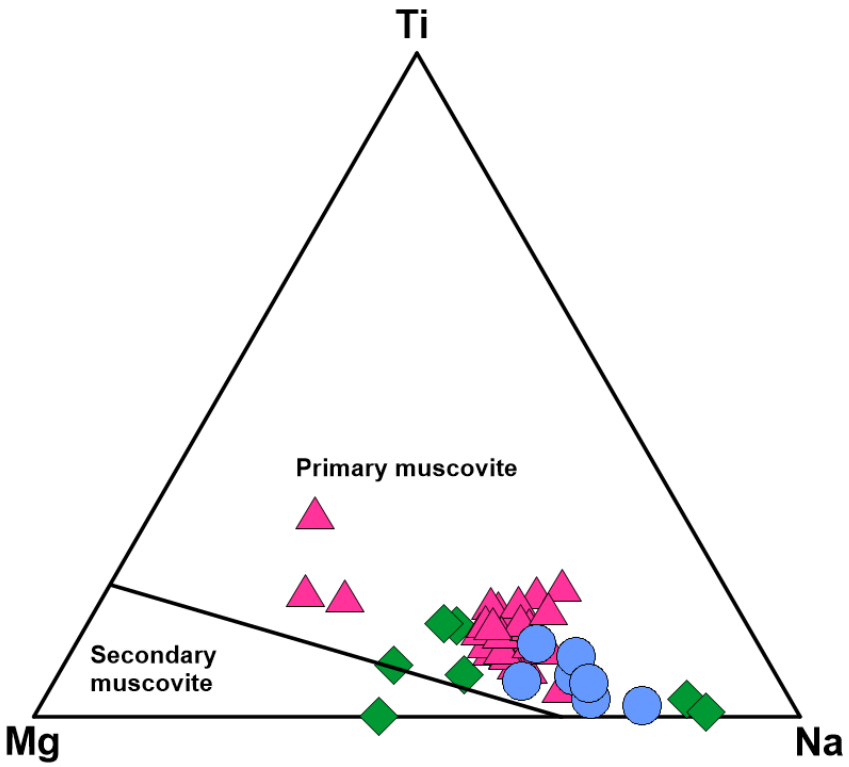

Figure 5.7. Muscovite crystal chemistry compositional fields after Miller et al. (1981).

5.5 Feldspar

The feldspar from two-mica leucogranite, tourmaline leucogranite, and pegmatite have been analyzed in their oxide form. The two- types of feldspar have been observed in these leucogranites and pegmatite from Sikkim Himalayas. The plagioclase and alkali feldspars data are presented in Appendix B 1.4. The feldspars belong to the tectosilicates minerals with chemical composition as AB_4O_8, where

A=Ca, Na, K,

B= Si and Al

The appendix shows the mineral chemistry of alkali feldspars for pegmatites, Tg, and 2mg. SiO_2 concentration for 2 mg of K-feldspar ranges from 59.62 to 69.07wt.%, whereas values for TiO_2, Al_2O_3, FeO, Na_2O, and K_2O are respectively bdl-0.0169 weight percent, 18.03 to 19.98 weight percent, bdl-0.16 weight percent, 0.47 to 3.84 weight percent, and 9.22 to 14.29 weight percent. For Tg and pegmatite, respectively, the weight percentages range from 64.05 to 64.87 and from 62.15 to 64.88. Tg is characterized by bdl-0.01 wt.% TiO_2, 18.15-19.33 wt.% Al_2O_3, bdl-0.09 wt.% FeO, 0.80-2.34 wt.% Na_2O wt.%, and 12.03-13.56 wt.% K_2O, while pegmatites have bdl-0.02 wt.% for TiO_2, 19.03-19.4 wt.% for Al_2O_3, bdl-0.04 wt.% for FeO, 1.19-1.90 wt.% for Na_2O, 12.02-13.96 wt.% for K_2O.

The K-feldspar in 2mg, Tg, and pegmatite are primarily orthoclase, however, one sample of 2mg plots under sanidine and anorthoclase with an Or content ranging between 61.26 and 95.27 wt.% percent (Fig.5.8). The anorthite content of the alkali feldspar is negligible, while the albite content ranges from 4.73 to 38.74 wt.%. Ab varies between (Ab 8.32-21.34 wt.%) and (Ab12.13-19.36 wt.%) for Tg and pegmatite

anorthite, respectively. Both (Or 78.66-91.68 wt.%) and (Or 80.64-87.87 wt.%) are Or contents for Tg.

Appendix B 1.4 shows the mineral chemistry of plagioclase feldspars in 2mg, Tg, and pegmatites. Plagioclase has varied SiO_2 content, with values for 2mg, Tg, and pegmatite ranging from 55.15 to 73.86 wt.%, 61.52-66.84 percent, and 65.91 to 66.92 weight percent, respectively (Fig 5.8). For 2 mg, the TiO_2, Al_2O_3, FeO, Na_2O, and K_2O ranges are 0.01 to 0.06 weight percent, 15.17 to 25.18, 6.55 to 9.83, and 0.09 to 0.30, respectively and for Tg varies bdl-0.01 wt.%, 19.06-21.93 wt.%, bdl-0.08 wt.%,10.04-10.25 wt.%,0.11-0.20 wt.% for TiO_2, Al_2O_3, FeO, Na_2O and K_2O respectively, whilst for pegmatites, the TiO_2, Al_2O_3, FeO, Na_2O, and K_2O values range from bdl-0.01 wt.%, 21.80-22.13 wt.%, bdl-0.04 wt.%, 9.04-9.07 wt.%, 0.37-0.38 wt.%. The anorthite content for plagioclase ranges from $An_{3.60}$-$An_{33.90}$, $An_{0.60-1.75}$, and $An_{8.04-8.16}$ for 2mg, Tg, and pegmatite respectively. The albite content varies from $Ab_{65.22-95.80}$, $Ab_{97.31-98.63}$, $Ab_{89.46-89.50}$, and orthoclase value ranges from $Or_{0.60-1.77}$, $Or_{0.71-1.28}$, $Or_{2.38-2.47}$ for 2mg, Tg and pegmatite respectively.

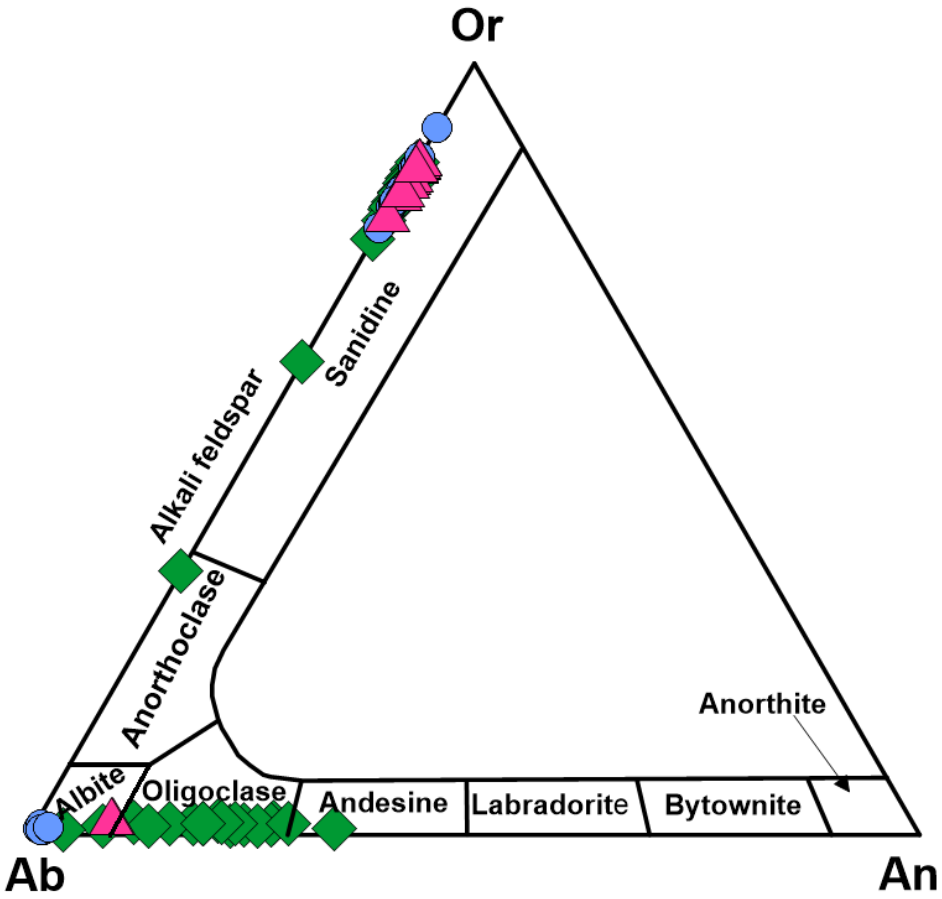

Figure 5.8 Mineral composition of feldspar plotted on the Or-Ab-An diagram Deer et al.(1992).

CHAPTER 6

U-Pb ZIRCON GEOCHRONOLOGY AND TRACE ELEMENTS

6.1 Introduction

Zircon is a widely occurring mineral with the chemical formula $ZrSiO_4$, a tetrahedral crystal system, and is the most robust accessory mineral present in igneous and metamorphic rocks (Corfu, 2003; Hoskin and Schaltegger, 2003). Zircon may incorporate U and Th into its crystal lattice, and trace element diffusion occurs slowly within its structure which makes it a leading U-Pb geochronometer (Cherniak and Watson, 2003; Watson and Harrison, 1983). Using cathodoluminescence (CL) and Back-scattered electron (BSE) imaging one can reveal multiple growth stages (Corfu, 2003; Schärer et al., 1986). In addition to providing insight into past environments and thermal histories, these features preserve isotopic and geochemical information (Harley et al., 2007). Due to its resistance to post-crystallization also, zircon is frequently employed in U-Pb dating (Hoskin and Schaltegger, 2003; Pettke et al., 2005).

The classification scheme for zircon typological populations is based on their morphology (Pupin, 1980). The topical studies have shown that the temperature is the main factor influencing the incorporation of Ti into zircon, and this information is utilized to determine the magma temperature at the time of crystallization (Claiborne et al., 2010). Ferry and Watson (2007) however, asserted that the Ti-in zircon thermometer also showed pressure dependence. Zircon trace element geochemistry sheds light on geochronology, petrological research, provenance, mineralization, terrestrial differentiation, and crystallization temperature (Watson and Harrison, 2005). Zircon investigations are also crucial in determining the origin of the igneous rock and revealing the genesis of the host rock (Claiborne et al., 2010).

The crystallization of temperature of magmatic zircons is higher than hydrothermal zircons having crystallization (>600ºC) and (<500ºC) respectively (Geisler et al., 2003;

Pelleter et al., 2007) and the concentration of trace elements is higher in hydrothermal zircons than magmatic zircons (Hoskin, 2005). The presence and ratios of these trace elements may help distinguish zircons from rocks of different origins since the behavior of the rare earth elements Y, Th, U, Nb, and Ta can be significantly influenced by zircons (Heaman et al., 1990). Zircons crystallized from crustal-derived magma contain higher trace element concentration than zircons from mantle-derived magma and have positive Ce anomaly and Eu deficient REE patterns (Lei et al., 2013). Zircon trace element geochemistry has been used to examine the composition of parental melts or the origin of zircon crystals, and zircon REE patterns can be utilized to track concurrent paragenesis (Heaman et al., 1990; Hoskin and Ireland, 2000). Zircon inheritance is found in granitoids, mafic rocks, MORB basalts, gabbros, and carbonatites, and zircons from granite provide information about the melting conditions (Bea et al., 2020; Miller et al., 2003).

Table 2.1: Zircon data from the Himalayas

	Leucogranite Body	Age (Ma)	Mineral used for Dating	Method used	Data sources
1	Annapurna	22.1± 0.1	Zircon	U-Pb	Hodges et al. (1996)
	Everest-Makalu	23.8± 01	Zircon	U-Pb	Searle and Godin (2003)
2		23.2± 0.1	Zircon	U-Pb	
	Kuday	27.5± 0.5	Zircon	U-Pb	King et al. (2011); Lee and Whitehouse, (2007); Zhang et al. (2004)
		28.1± 0.4	Zircon	U-Pb	
		27.5± 1.0	Zircon	U-Pb	
		14.5± 0.9	Zircon	U-Pb	
3		16.2± 0.4	Zircon	U-Pb	
	Kouwu (Lijun, Gomdre)	14.4± 0.1	Zircon	U-Pb	King et al. (2011); Lee and Whitehouse (2007); Zhang et al. (2004)
		25.4± 6.0	Zircon	U-Pb	
4		14.2± 0.2	Zircon	U-Pb	
5	Malashan-Cuobu	19.3± 3.9	Zircon	U-Pb/SHRIMP	Kawakami et al. (2007)

6	Malari Leucogranites	19± 0.5	Zircon	U-Pb/LA-ICPMS	Sachan et al. (2010)
7	Kampa Dome	23	Zircon	U-Pb	Lin et al.(2020)
8	Gurla Mandhata	11-12 Ma	Zircon	U-Pb/LA-ICPMS	Cheng et al., (2020)
	Yadong	20.0 Ma	Zircon	U-Pb	Gou et al. (2016) Liu et al. (2013)
9		21.0-11.7 Ma	Zircon	U-Pb	
10	Paiku	23.6-16.1 Ma	Zircon	U-Pb	Gou et al.(2019)
11	Lhozag	18 Ma	Zircon	U-Pb	Huang et al. (2017)
12		15 Ma	Zircon	U-Pb	
13	Cuonadong	21.5-20.7	Zircon	U-Pb/SHRIMP	Chen et al. (2021)
14	Mango Gusar Granite	37+0.8 Ma	Zircon	U-Pb	Rex et al. (1998)
15	MMT Dyke, Skardu Road near Sassi	13-6 Ma	Zircon	U-Pb	Schneider et al. (2001)
16	Rupal Leucogranite sheet (Lotbo Meadow)	4.3-1.8 Ma	Zircon	U-Pb	Schneider et al. (2001)
17	Sikkim leucogranite	~15-19 Ma	Zircon	U-Pb	This study

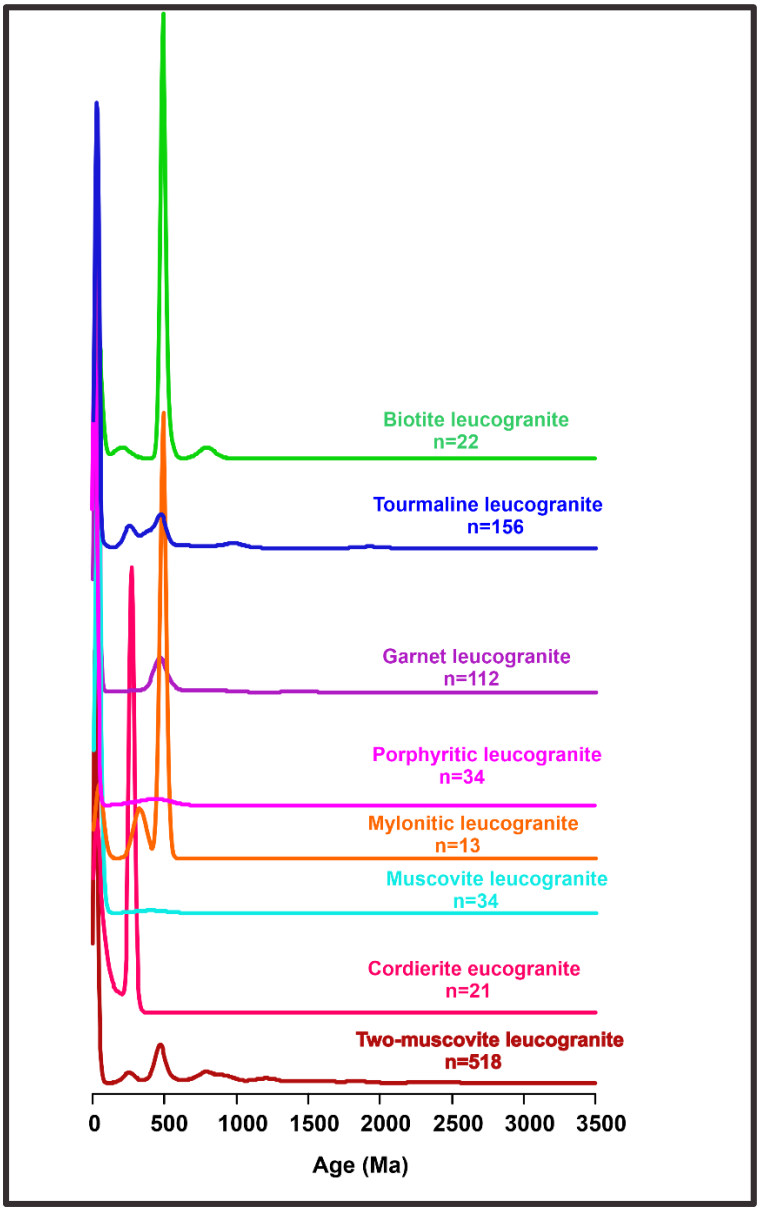

Figure 6.1. Summary of zircon age spectra of Himalayan leucogranites of previous work Data sources: Fan et al. (2021); Gao et al. (2017, 2013, 2021); Hopkinson et al. (2017); Huang et al. (2017); Ji et al. (2022); Lin et al. (2020); Liu et al. (2017, 2016); Streule et al. (2010); Xu et al. (2021).

6.2 Results

6.2.1 Zircons from two-mica leucogranites

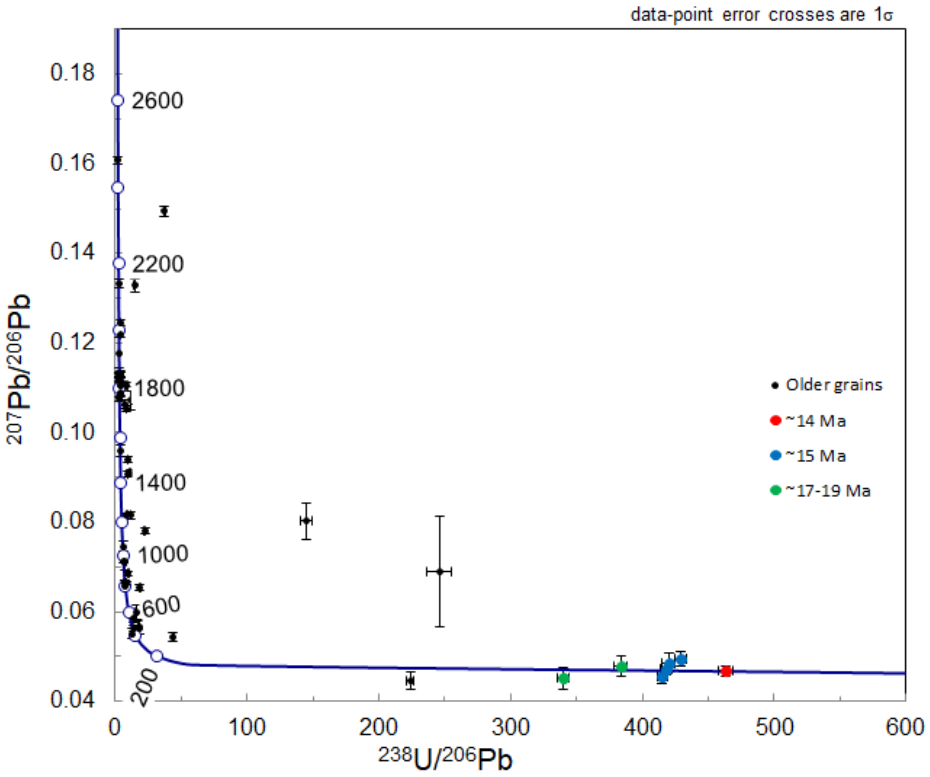

Figure 6.2. The Concordia plot for zircon from two-mica leucogranite (ZY-LG-2) showing the mean $^{206}Pb/^{238}U$ age. Analyses in red were used for age calculation.

In this sample more than 60 zircon grains were examined. The sample contains a relatively high percentage of inherited zircons (Fig.6.2). The seven youngest grains range in Miocene age from 14 to 19 Ma. The youngest grain is 13.9 Ma. However, the sample may be younger given the age distribution of the zircon samples analyzed. Most Miocene zircons are concordant and show no signs of common Pb or Pb loss, whereas all earlier zircons have obvious signs of Pb loss, and some contain considerable levels of common Pb. The following zircons are older: Oligocene (2), Eocene (1), Cretaceous/Jurassic border (2), Carboniferous (2), Devonian (1), Silurian (1),

Ordovician (2), Cambrian (1), Neoproterozoic (12), Mesoproterozoic (7), and Paleoproterozoic (24).

The 2mg zircons (ZY-LG-2) range in size from 50 μm to 150 μm and are euhedral to subhedral. The concordia ages for the ZY-LG-2 are 1718 ± 16 Ma (n=2, MSWD=0.58); 953 ± 28 (n=1); 775 ± 17 (n=2, MSWD = 3.2); 444 ± 7 (n=2, MSWD=1.4); 18.9 ± 0.6 (n=1) and of 15.29 ± 0.20 Ma (MSWD =1.3; n=3.), 16.78 ± 0.47, 18.91 ± 0.55 (MSWD=0.56; n=1), 145 ± 3.7, 349 ± 12 Ma (MSWD=1.16; n=2), 444 ± 6.9 Ma (MSWD=1.4; n=2) 481±11, 710 ± 14, 775 ± 17 Ma (MSWD=3.2; n=2), 808 ± 16, 918 ± 15, 953 ± 23, 1718 ± 16 (MSWD=0.58; n=2) and 1823 ± 31 . A few of the Concordia ages are represented in (Fig 6.1-6.2).

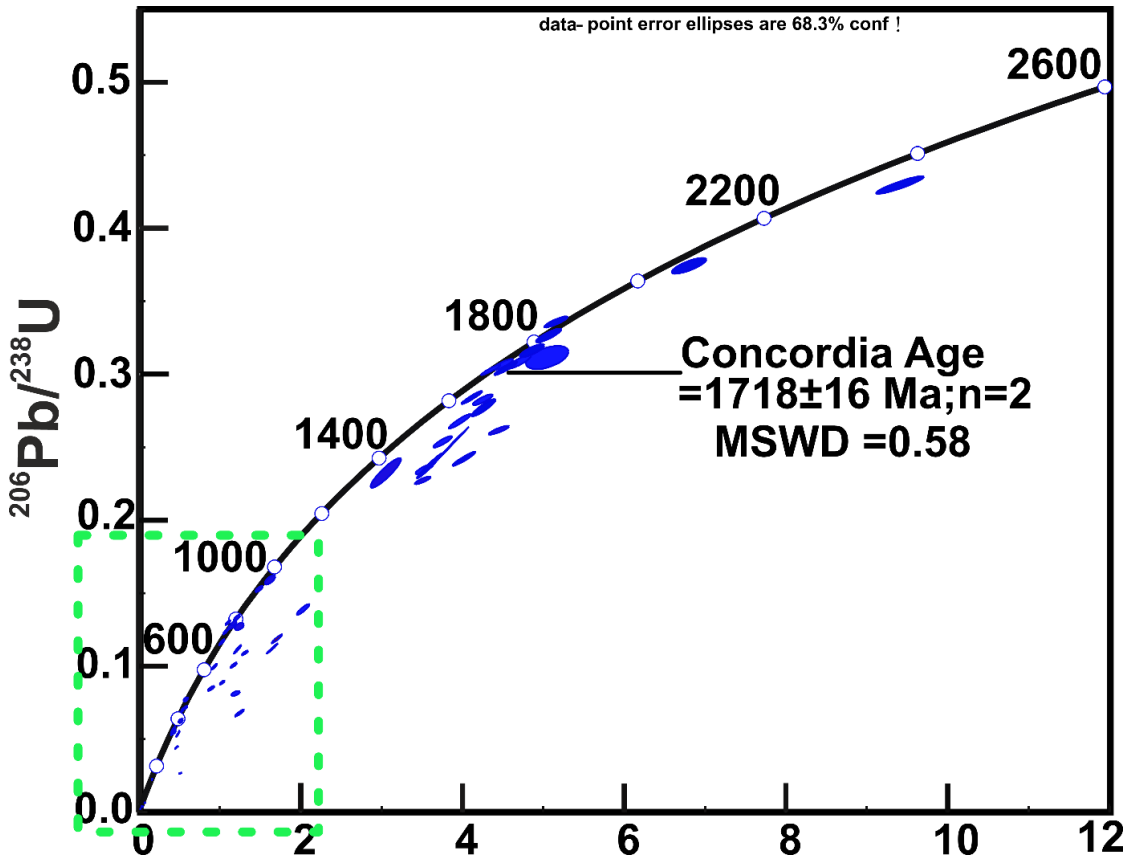

Figure 6.3. Zircon U–Pb Concordia diagrams for two-mica leucogranite ZY-LG-2.

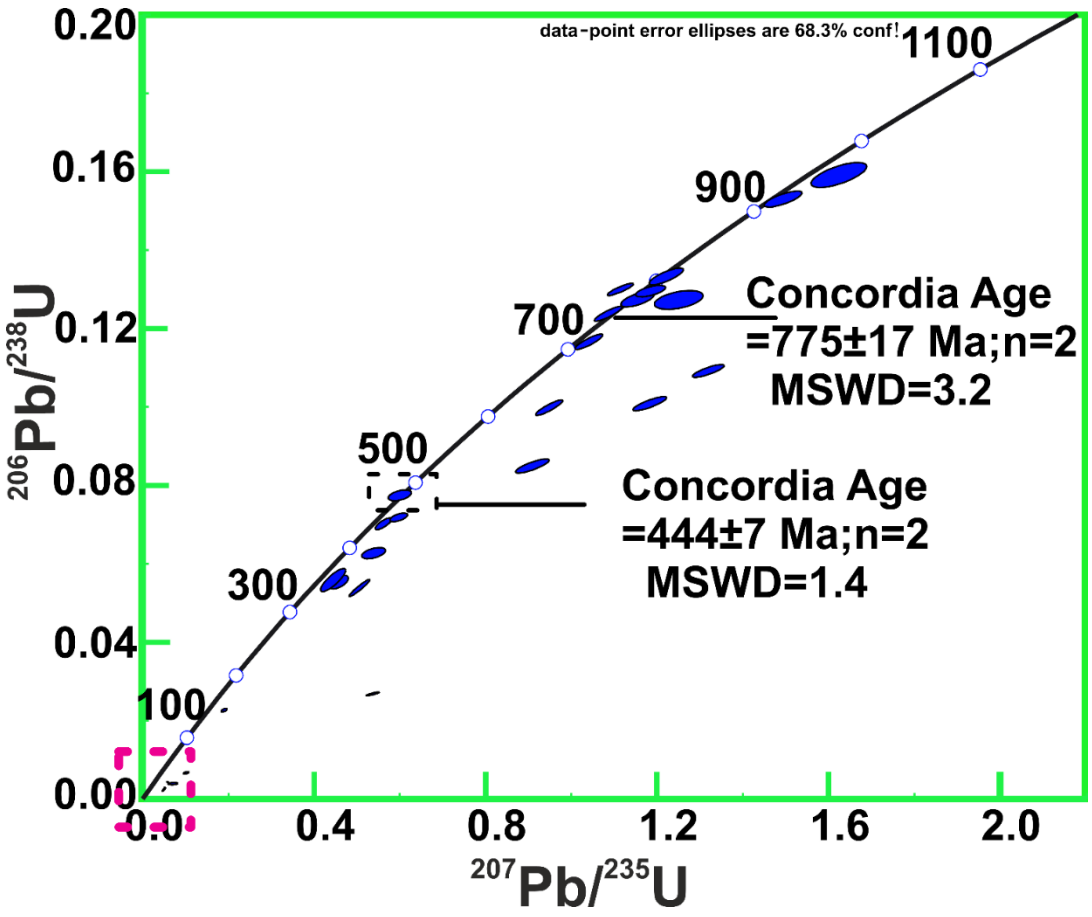

Figure 6.4. Zircon U–Pb Concordia diagrams for two-mica leucogranite ZY-LG-2 upto 1000 Ma.

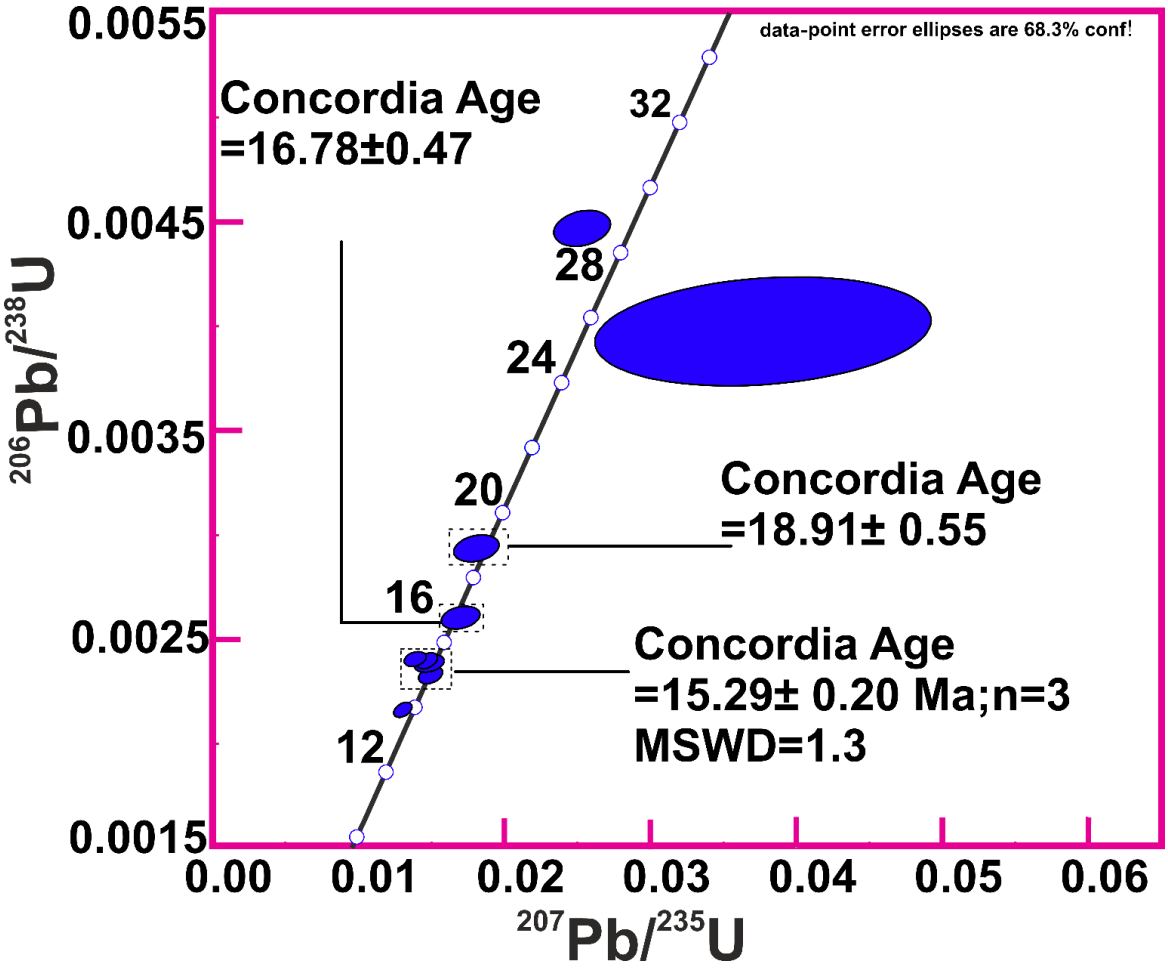

Figure 6.5. Zircon U–Pb Concordia diagrams for two-mica leucogranite ZY-LG-2 for younger ages.

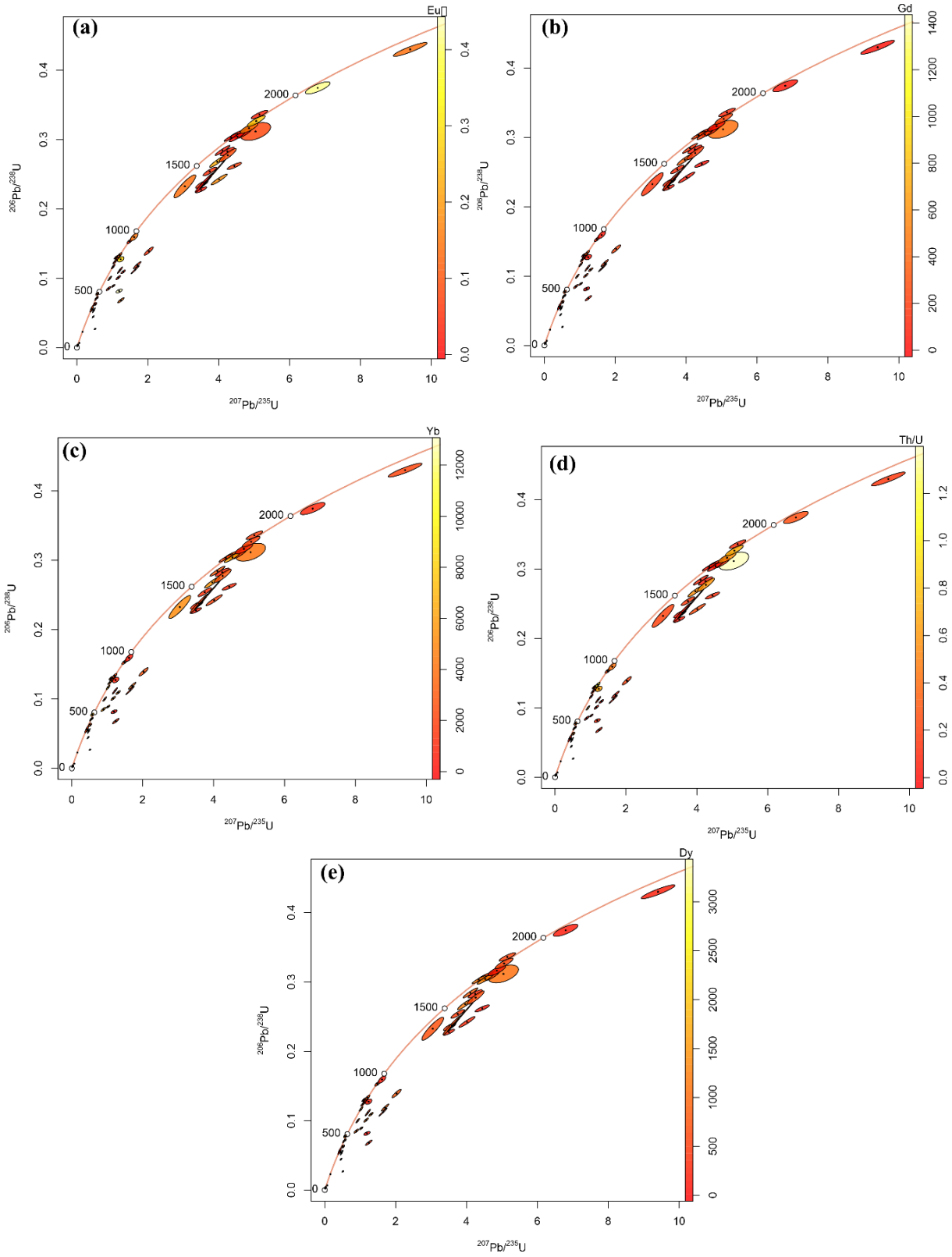

Figure 6.6. Concordia diagrams based on the variations in trace elements (a) Eu* (b) Gd (c) Yb (d) Th/U (e) Dy.

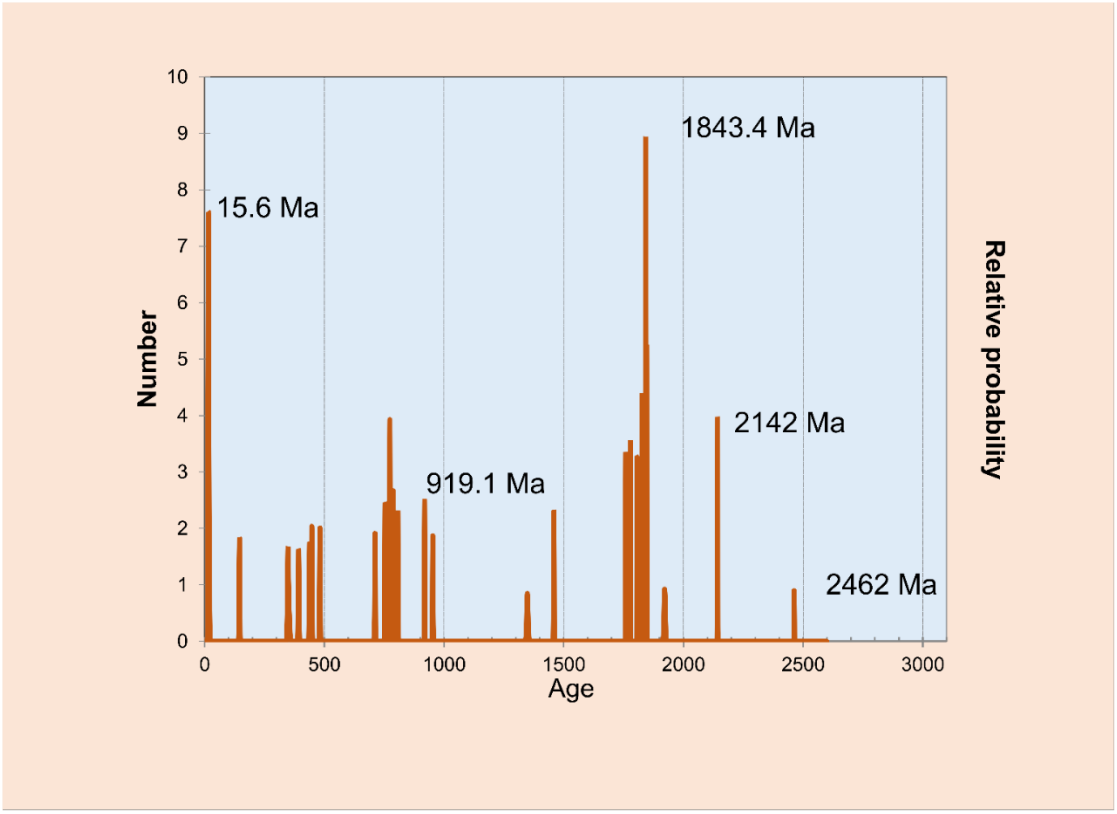

Figure 6.7. Relative probability plot of two-mica leucogranite (ZY-LG-2).

The cut-off for concordance was > 95%, and the Probability Density Plot (PDP) displays dominant peaks at around 15.6 Ma, 919.1 Ma, 1843.4 Ma, 2142 Ma, and 2462 Ma.

6.2.2 Rare Earth Elements variations in Zircons

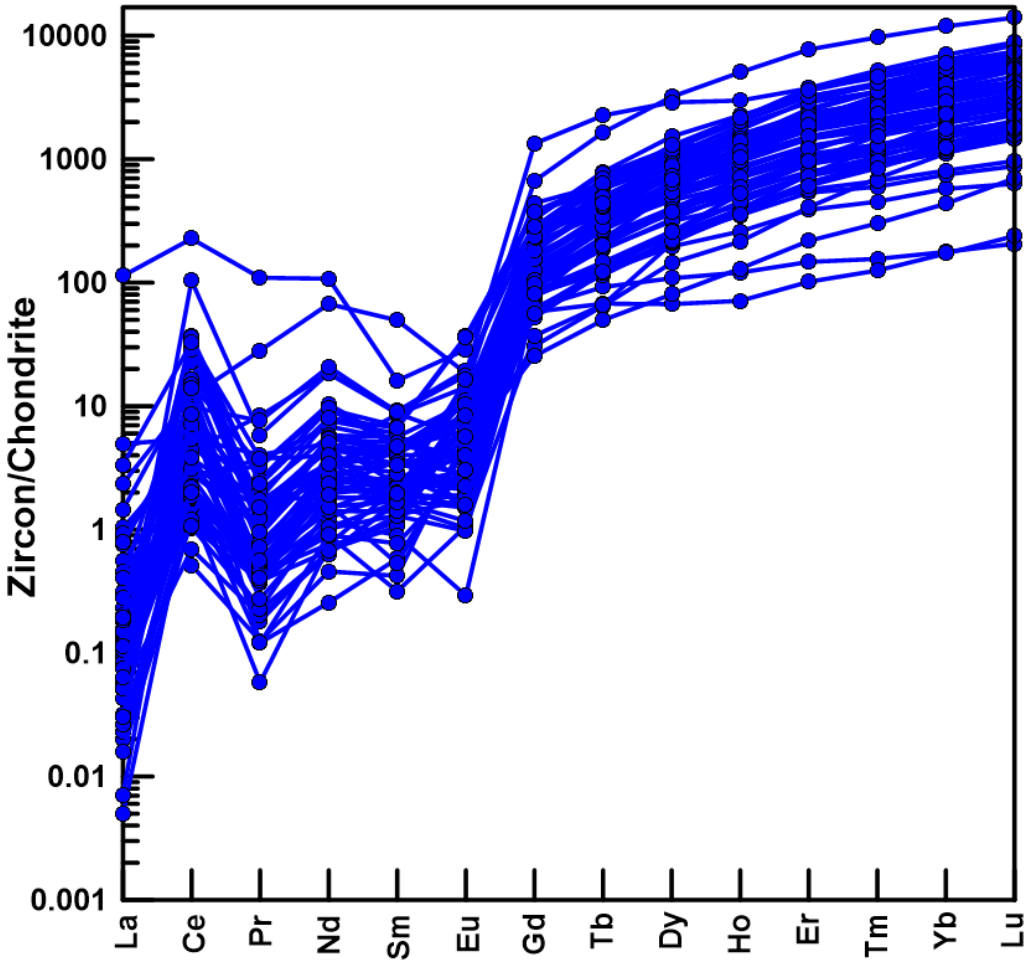

Figure 6.8. Chondrite normalized REE patterns for the zircons (ZY-LG-2). Normalized values for chondrite are from McDonough and Sun (1995).

The chondrite-normalized REE patterns (Fig.6.8) of zircons from 2mg have typical heavy REE enriched patterns with marked negative Eu (Eu/Eu* = 0.01–0.43) and positive Ce (Ce/Ce* of 1.22–142) anomalies. The U contents range from 141 to 8268 ppm, Th contents from 19.5 to 1274 ppm, Hf contents range from 9075 to 19762 ppm, and Th/U ratios range from 0.01 to 1.34. The examined zircons exhibit oscillatory zoning with rims that are rich in U and Th but have low Th/U ratios that have been used to infer anatexis events (Hoskin and Schaltegger, 2003; Liu et al., 2014).

CHAPTER 7

U-Pb MONAZITE GEOCHRONOLOGY AND TRACE ELEMENTS

In this chapter, monazite occurrence in the Himalayas, trace-element composition, analytical methods, and geochronological data is discussed. While zircon tends to contain inherited cores, monazite is resistant to Pb loss during the formation of leucogranite at low temperatures Since monazite contains a low quantity of common Pb and has an extremely low diffusion rate at high temperatures, it has attracted considerable attention as a geochronometer. This chapter also discusses the variation between the two-mica leucogranite and tourmaline leucogranite.

7.1 Introduction

In peraluminous granite, monazite PO4 (LREE, Y, Th, Ca, Si) occurs as an accessory phase and in meta-psammites with a low Ca content and low diffusion rate of Pb at high temperatures and negligible common Pb concentration of monazite makes it an ideal geochronological tool (Schulz, 2021). The stability varies with pressure, temperature, bulk rock chemistry, and interacting fluid chemistry (Schulz, 2021) and it is also used as an isotopic tracer for crustal growth for Sm-Nd (Goudie et al., 2014). The dissolution of zircon and monazite controls the abundances of Zr and LREE in granitic melts (Montel, 1993; E. B. Watson and Harrison, 1983). Numerous studies have used monazite U-Th-Pb geochronology to date granites in the Himalayas. (Copeland et al., 1988; Deniel et al., 1987; Harrison et al., 1999; King et al., 2011; Lederer et al., 2013; Zhang et al., 2004 and references therein).

The monazite U-(Th)-Pb dating suggests that partial melting of the HHC ranges from the late Eocene and Miocene (Yang et al., 2019). Compared to U, monazite prefers Th, ^{230}Th decays into ^{206}Pb after being an intermediate in the ^{238}U decay series. Since monazite incorporates ^{230}Th to a higher extent than ^{238}U, it typically contains excess ^{206}Pb as a result (Cottle et al., 2009). Recently geochronological studies focus on monazite because it is common in metasedimentary rocks and has low initial Pb

contents, high U and Th contents, and high Pb retentive values (Kohn et al., 2005). During early melting, minerals that are Th and Y enriched, such as monazite are typically separated from peraluminous magmas (Chappell and White, 1992; Zhang et al., 2019). Pb loss and protracted crystallization are all thought to be contributing factors to the complexity of accessory phase U-Pb geochronology (Cottle et al., 2019). In contrast to zircon, igneous monazite is restricted to low-Ca silicic rocks, while zircon is abundant throughout silicic rocks (Itano et al., 2020), and the monazite solubility is also influenced by its crystal size and content of water in the melt (Rapp and Watson, 1986).

Table 3.1: Monazite ages of the Himalayan leucogranites

	Leucogranite Body	Age (Ma)	Mineral used for Dating	Method used	Data sources
1	Gangotri	22.4±0.5	Monazite	U-Pb	Harrison et al. (1997)
	Shivling	23	Monazite	U-Pb	Harrison et al. (1997); Searle and Godin (2003)
2		21.9± 0.5	Monazite	U-Pb	
3	Manaslu	22.9	Monazite	U-Pb	Deniel et al.(1987); Harrison et al.(1997), (1999), (1995);Coleman and Parrish (1995)
		19.3	Monazite	U-Pb	
		22.4±0.5	Monazite	U-Pb	
		19±1	Monazite	U-Pb	
		25	Monazite	U-Pb	
		18.1	Monazite	U-Pb	
		25.7	Monazite	U-Pb	
		24.9	Monazite	U-Pb	
		13-21.4	Monazite	U-Pb	
4	Gyirong	16.1	Monazite	U-Pb	Liao et al. (2003)
5	Shisha Pangma	20.2±0.2	Monazite	U-Pb	Searle et al. (1997)
		17.3±0.2	Monazite	U-Pb	
6	Nyalam	16.8±0.6	Monazite	U-Pb	Schärer et al.(1986); Yang et al. (2019)
		16.9	Monazite	U-Pb	
		17	Monazite	U-Pb	
		21.4	Monazite	U-Pb	
		20.6	Monazite	U-Pb	
7	Rongbuk	20.3	Monazite	U-Pb	Harrison et al. (1995); Murphy and Harrison (1999); Searle and Godin, (2003)
		22	Monazite	U-Pb	
		16.8±0.8	Monazite	U-Pb/SIMS	
		16.4±0.6	Monazite	U-Pb/SIMS	
		16.2±0.8	Monazite	U-Pb	
8	Everest-Makalu	20.5	Monazite	U-Pb	Schärer et al.(1986), (1984); Searle and Godin (2003), Harrison et al. (1994)
		21.3±	Monazite	U-Pb	
		21.9± 0.2	Monazite	U-Pb/TIMS	
		24±0.4	Monazite	U-Pb/TIMS	
		23±1	Monazite	U-Pb	
9	Dinggye	15	Monazite	U-Pb	Liu et al. (1990)

10	Gaowu	22.9±0.17	Monazite	U-Pb	Wu et al. (1998)
11	Wagye La	11.9	Monazite	U-Pb	Wu et al. (1998)
12	Masang Kang-Paro	13	Monazite	U-Pb	Searle and Godin (2003)
		14	Monazite	U-Pb	
		23	Monazite	U-Pb	
		24	Monazite	U-Pb	
13	Khula Kangri	12.5±0.5	Monazite	U-Pb	Edwards and Harrison (1997)
14	Kouwu (Lijun, Gomdre)	14.4±0.1	Monazite	U-Pb	Zhang et al. (2004)
		14.5±0.1	Monazite	U-Pb	
15	Majia	9.8	Monazite	U-Pb	Scharer et al. (1986); Liu et al.(1990)
		9.2	Monazite	U-Pb	
		9.5	Monazite	U-Pb	
16	Malashan-Cuobu	18.6	Monazite	U-Pb	Aoya et al. (2005)
		17.8	Monazite	U-Pb	
17	Dolpu-Mugu Zanskar	17.6±0.3	Monazite	U-Pb	Harrison et al. (1999)
18	Zanskar	20	Monazite	U-Pb	Dèzes et al. (1999); Noble and Searle (1995)
		20.8±0.3	Monazite	U-Pb	
		19.5	Monazite	U-Pb	
		21.4	Monazite	U-Pb	
19	Kampa Dome	23.5	Monazite	U-Pb/LA-ICPMS	Lin et al. (2020)
20	Cuonadong	21.2-19.7	Monazite	U-Pb/LA-ICPMS	Chen et al., 2021
21	Yadong	22.9	Monazite	U-Pb/SHRIMP	Wu et al. (1998)
22	Dudh Kosi	21.8±0.05	Monazite	U-Pb/TIMS	Viskupic et al. (2005)
23		21.33±0.03	Monazite	U-Pb/TIMS	
24	Dzakaa Chu	20.4±0.6	Monazite	U-Pb/LA-ICPMS	Cottle et al. (2007)
		16.7±0.3	Monazite	U-Pb/ LA-ICPMS	
25	Kangshung glacier	20.8±0.8	Monazite	U-Pb/LA-ICPMS	Cottle et al. (2009)
		16.7±0.4	Monazite	U-Pb/LA-ICPMS	
26	Thongmon	15.2±0.2	Monazite	U-Pb/LA-ICPMS	Cottle et al. (2009)
		12.6±0.2	Monazite	U-Pb/LA-ICPMS	
27	Chichi granite	22-16	Monazite	Th-Pb ion-microprobe	
28	Safat Leucogranite	26	Monazite	U-Pb	
29	Dassu Gneisses	6.8±0.2	Monazite	U-Pb	Schneider et al. (1999)

30	Jutial, Karakoram-Nanga Parbat	10-5.3	Monazite	Th-Pb	Noble and Searle (1995)
31	Rupal leucogranite sheet (Tap Meadow)	1.98±0.19	Monazite	Th-Pb	Smith et al. (1992)
32	Sikkim	14.24 to15.44	Monazite	U-Pb/LA-ICPMS	Schneider et al. (1997)
		13.51 to 14.63	Monazite	U-Pb/LA-ICPMS	

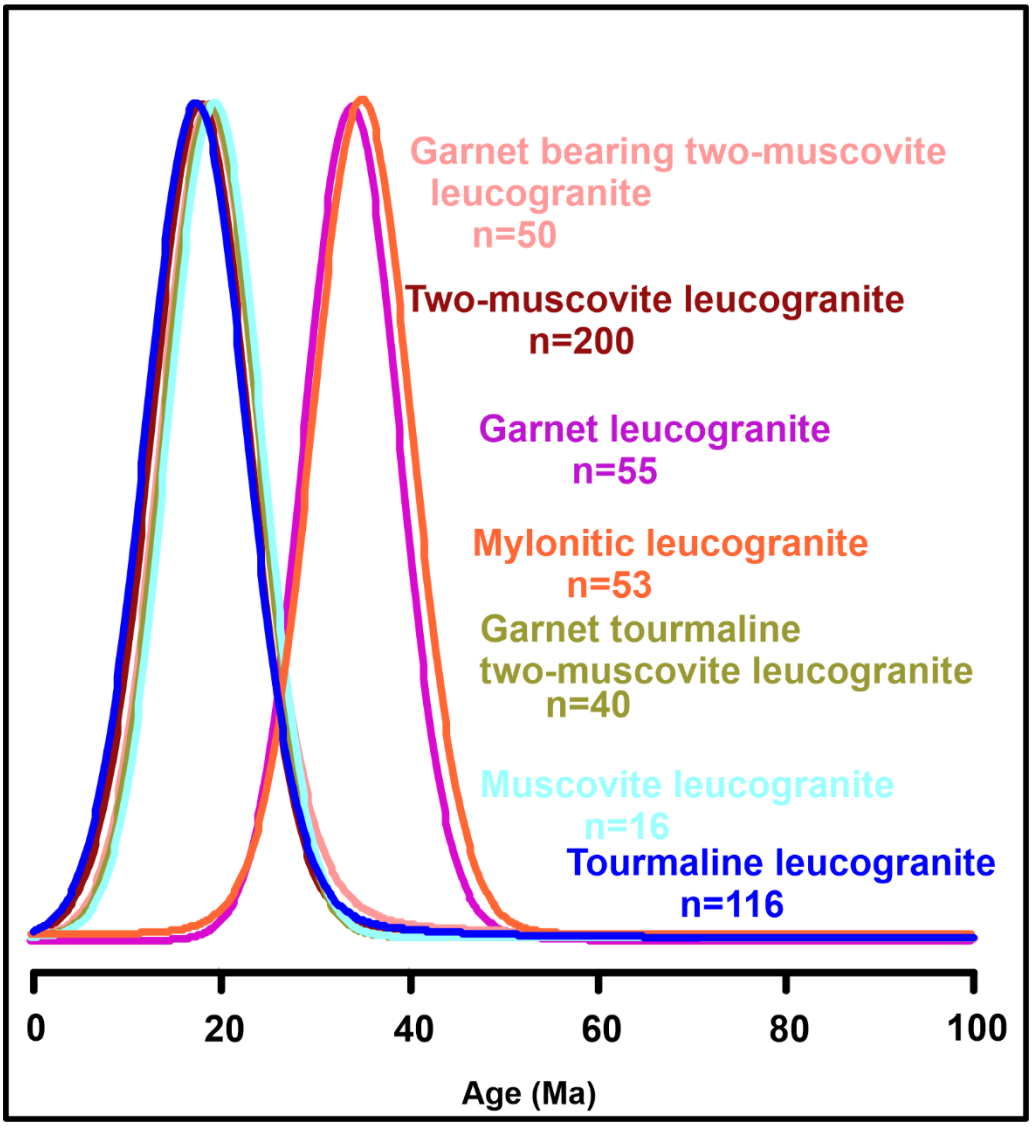

Figure 7.1. Summary of monazite age spectra of Himalayan leucogranites of previous work Data sources: Cottle et al. (2015); Lin et al. (2020); Liu et al. (2017, 2016); Streule et al. (2010); Wu et al. (1998); Xie et al. (2020); Yang et al. (2019).

7.2 Results

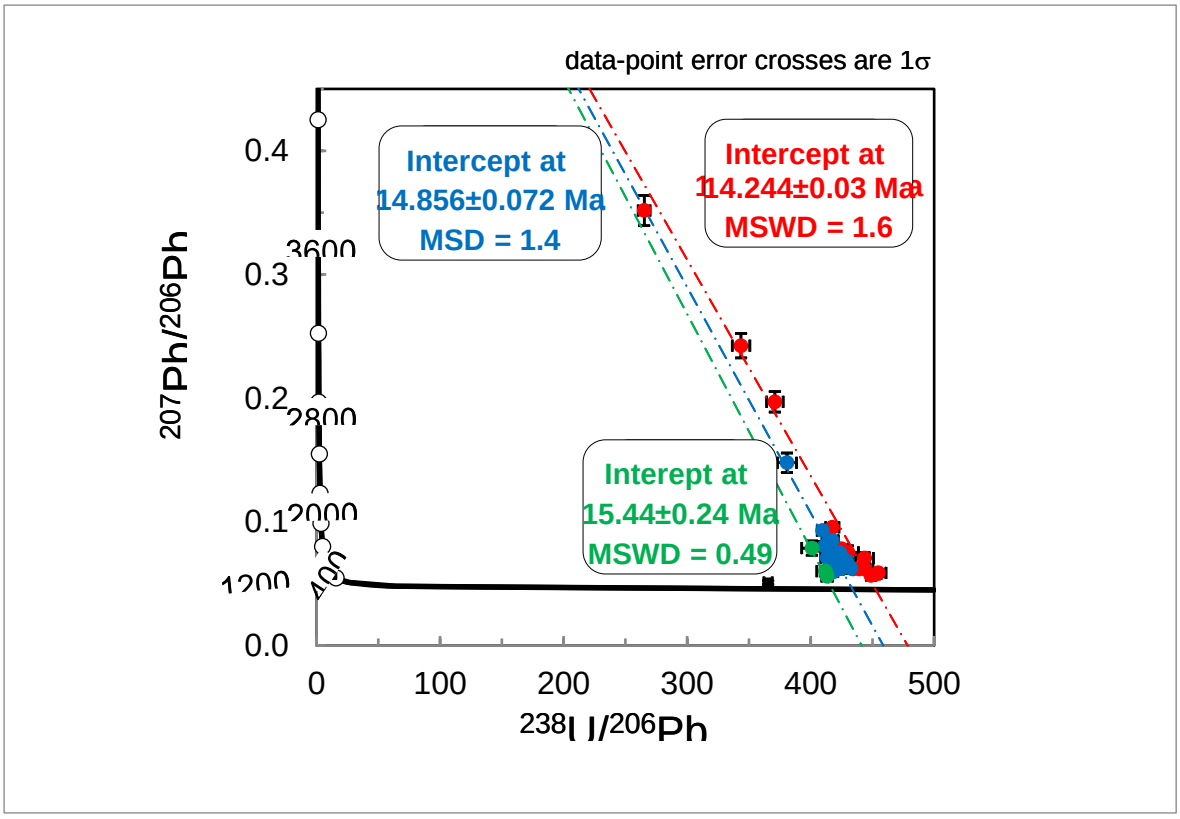

Figure 7.2. Terra-Wasserberg plot of monazite data two-mica leucogranite (ZY-LG-2).

In 2mg, the monazite grains yielded $^{206}Pb/^{238}U$ intercept dates of 14.24 ± 0.03, 14.85 ± 0.072, and 15.44 ± 0.24 Ma.

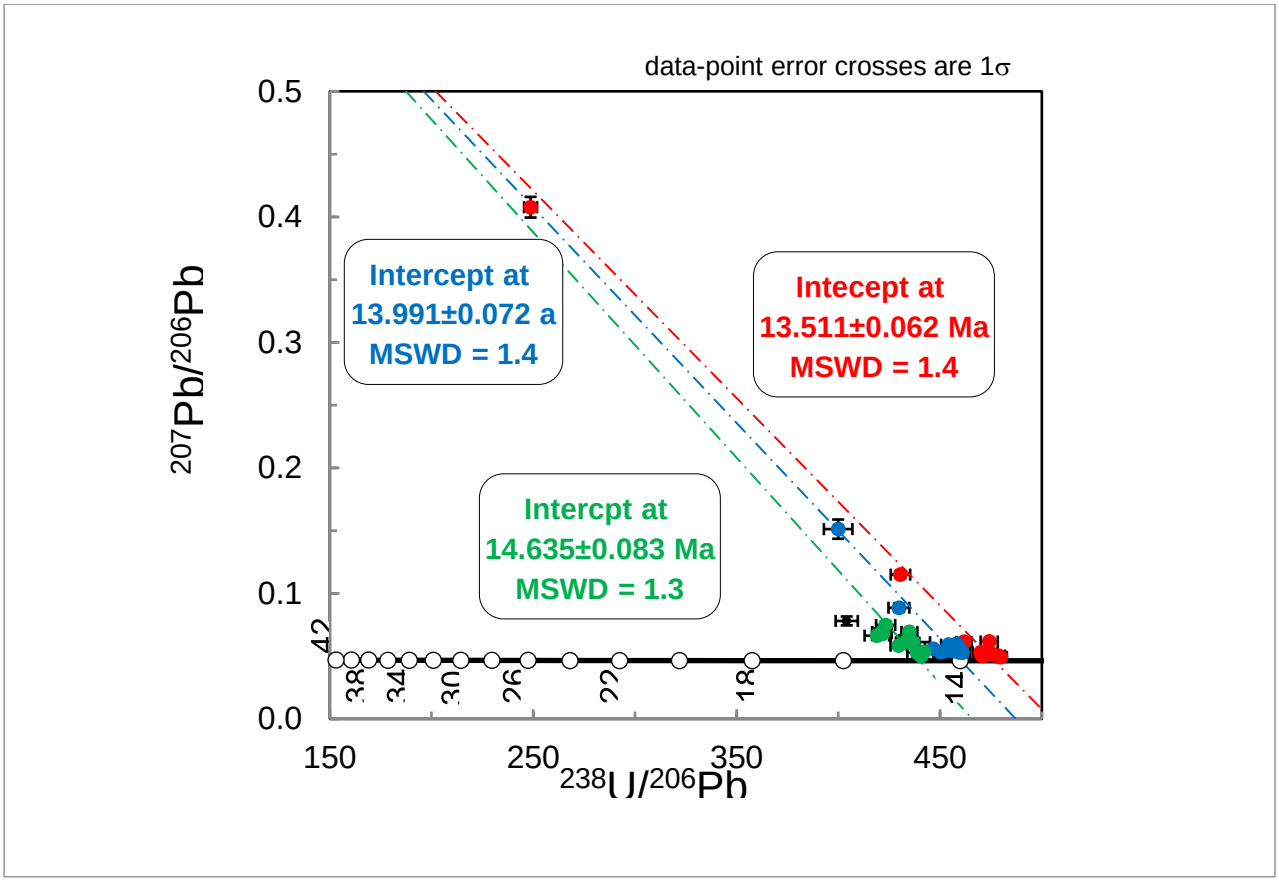

Figure 7.3. Terra-Wasserberg plot of monazite data tourmaline leucogranite (ZY-LGT-1).

In Tg the monazite grains yielded $^{206}Pb/^{238}U$ intercept dates of 13.51 ±0.062, 13.99 ±0.072, and 14.63 ± 0.083Ma.

7.2.1 REE variations of monazite in leucogranites

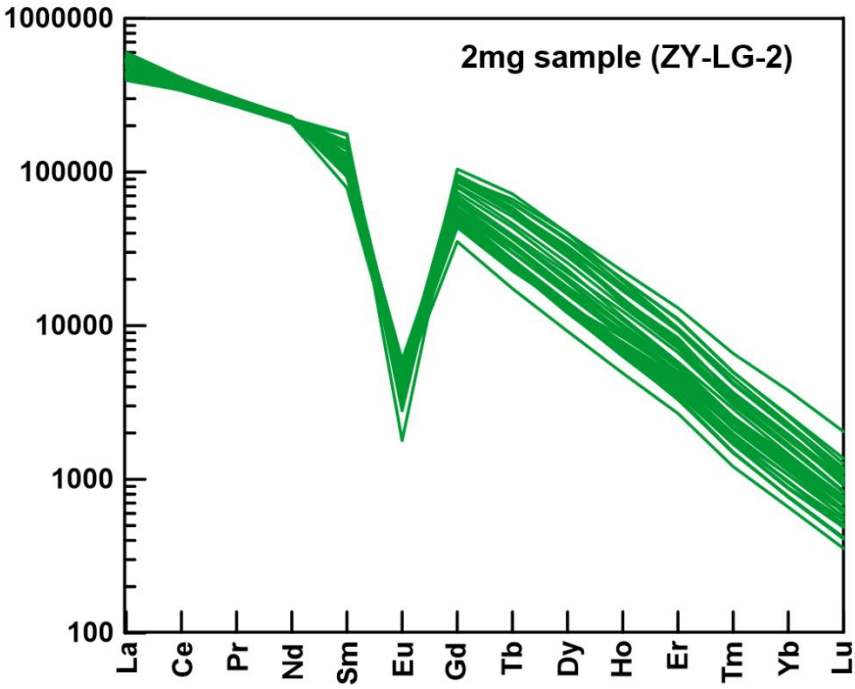

Figure 7.4. Monazite REE variations for a sample of two-mica leucogranite (ZY-LG-2). The chondrite values are normalized after Sun and McDonough (1995).

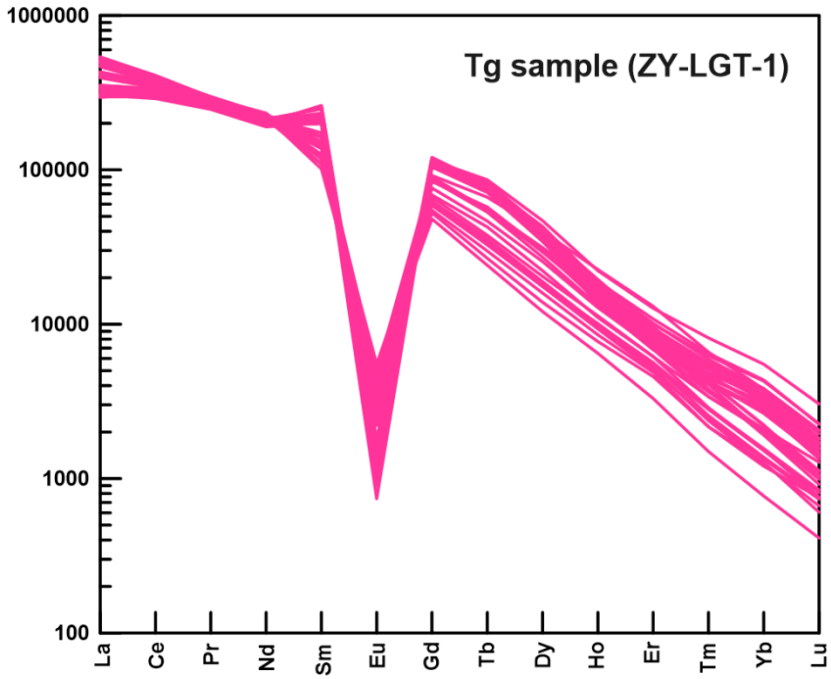

Figure 7.5. Monazite REE variations for sample of tourmaline leucogranite (ZY-LGT- 1). The chondrite values are normalized after Sun and McDonough (1995).

The LREEs are substantially enriched in monazites for 2mg and Tg relative to heavy rare earth elements HREEs, with marked negative Eu anomalies (Eu/Eu* of 0.01- 0.08), and (Eu/Eu* of 0.01- 0.05), respectively (Fig. 7.4-7.5) and little variation between the different aged areas of the grains. The co-crystallization of monazite and feldspar during melt crystallization, in which Eu preferentially divides into feldspar, is thought to be the cause of the negative Eu anomaly. Tg has a wide range of thorium levels compared to 2mg, but relatively little uranium. The changes in oxygen fugacity-induced changes in Eu valence have a major impact on the monazite Eu anomaly (Holder et al., 2020).

CHAPTER 8

Sr-Nd WHOLE ROCK ISOTOPE GEOCHEMISTRY

This chapter discusses the whole-rock Sr-Nd geochemistry of leucogranites, pegmatites and gneisses of North Sikkim. The data is presented for 14 North leucogranite samples out of which 10 are leucogranite and 4 are HHS gneisses samples. The isotopic data would help to elucidate the potential source of melting for the generation of leucogranites in North Sikkim.

8.1 Introduction

The lithophile element strontium is concentrated in the silicate portion of the Earth and is widely utilized in geoscientific applications. Strontium is a highly enriched element in melts in the mantle system. The extensive feldspar mineral involvement in crustal melts can result in its depletion in the crustal derived melts (Nebel, 2013). Neodymium is also one of the lithophile light rare earth elements, and during igneous processes, Nd is dispersed into phases of minerals. Nd distribution is largely determined by the composition of magmas derived from the mantle, while in more differentiated magmas derived from the crust or mixed origin, the distribution is determined both by the source and the behaviour of minerals.

Nd isotopic composition within the continental crust is a potent tool for determining the sources of granitic rocks and aids in determining the input of crustal recycled and little differentiated material to the granite (Chappell and White, 1992).

8.1.1 Nd systematics

i.) The model age estimates the length of time that has passed since a sample separated from its mantle source (Rollinson, 1993). The age of "crustal formation" is estimated using neodymium model age on the premise of a model mantle source composition. The most frequent applications of this technique are to determine the provenance ages

of clastic sedimentary rocks or to date the ages of crustal terranes within Precambrian orogenic belts (Dickin, 2013). Model ages are very important in Sm-Nd isotopic systems, since they can be determined from a single pair of parent-daughter isotopic ratios. Depleted Mantle (DM) and CHUR (Chondritic Uniform Reservoir) are two widely referred to models of initial mantle reservoirs.

ii) T-CHUR model ages

During the formation of the Earth, the CHUR model assumes that the primitive mantle had the same isotopic composition as the typical chondritic meteorite, which in this case is 4.6 Ga. This model makes the assumption that the Earth's early mantle, which is thought to have formed around 4.6 Ga, has the same isotopic composition as the average chondritic meteorite, where λ is the decay constant for ^{147}Sm to ^{144}Nd, having value of 6.54 X 10^{-12} yr^{-1}, the CHUR values for $(^{143}Nd/^{144}Nd)_{today}$ and $(^{147}Sm/^{144}Nd)_{today}$ are 0.512638 and 0.1966 respectively. The CHUR model ages determined by equation 1, are given Appendix D.

$$T_{CHUR} = \frac{1}{\lambda}\ln\left[\frac{(^{143}Nd/^{144}Nd)_{rock,today} - (^{143}Nd/^{144}Nd)_{CHUR,today}}{(^{147}Sm/^{144}Nd)_{rock,today} - (^{147}Sm/^{144}Nd)_{CHUR,today}} + 1\right] \quad \text{..... (1)}$$

iii)T-depleted mantle (DM) model ages

TDM is the model age calculated with reference to the depleted Mantle reservoir, it sheds light on how the mantle evolves with time. Due to the fact that the ^{143}Nd/^{144}Nd ratio of the mantle has changed since the development of the continental crust, presently has a higher ^{147}Sm/^{144}Nd ratio than CHUR. As a result, TDM ages are often older than T-CHUR ages (Rollinson, 1993).

$$T_{DM} = \frac{1}{\lambda}\ln\left[\frac{(^{143}Nd/^{144}Nd)_{rock,today} - (^{143}Nd/^{144}Nd)_{DM,today}}{(^{147}Sm/^{144}Nd)_{rock,today} - (^{147}Sm/^{144}Nd)_{DM,today}} + 1\right] \quad \textbf{.....(2)}$$

The values for Depleted Mantle used for $(^{143}Nd/^{144}Nd)_{DM,\,today}$ and $(^{147}Sm/^{144}Nd)_{DM,\,today}$ are 0.51315 and 0.2137 respectively (Jahn et al., 1988). The T_{DM} model ages determined by equation 2, for leucogranites and granitic gneiss are given in Appendix D.

iv) Epsilon Nd ε_{Nd} (Epsilon Nd) is a measure of the difference in 143Nd/144Nd ratios, expressed in parts per 104, between the sample suite and CHUR at a given time. Negative values of Nd indicate that, on average over the history of the earth, Sm/Nd ratios of rock or its precursors had been lower than chondritic ratios, indicating that they originated from enriched mantles or crustal sources whilst positive value of ε_{Nd} implies magma derived from a source with a greater Sm/Nd than CHUR, i.e., a depleted mantle source region (Rollinson,1993).

$$\varepsilon_{Nd} = \left[\frac{(^{143}Nd/^{144}Nd)_{Rock,today}}{(^{143}Nd/^{144}Nd)_{CHUR,today}} - 1\right] \times 10^4 \quad \textbf{.....(3)}$$

v) Two-stage Nd model ages

Nd model ages are also calculated using the two-stage model of Liew & Hofmann (1988). This two stage model is based on possibility of secondary Sm/Nd fractionation after the initial or first fractionation, that occurred during mantle melting. In the given equation 4, the indexes DM, CC, SA refer to Depleted Mantle, average crustal reservoir and the sample, respectively. T = two-stage Nd model age, t = crystallization age of the sample, 0 refers to the present day. I refers to $^{143}Nd/^{144}Nd$ and R refers to $^{147}Sm/^{144}Nd$ ratios.

$$T = \frac{1}{\lambda} ln \left[\frac{I^0_{SA} - (e^{\lambda t} - 1)(R^0_{SA} - R^0_{CC}) - I^0_{DM}}{(R^0_{CC} - R^0_{DM})} + 1 \right] \text{.....(4)}$$

For estimation of two stage model ages following parameter from Liew and Hofmann, (1988) were used

$$I^0_{DM} = \left[\frac{^{143}Nd}{^{144}Nd} \right]^0_{DM} = 0.513151$$

$$R^0_{DM} = \left[\frac{^{143}Sm}{^{147}Nd} \right]^0_{DM} = 0.219$$

$$R^0_{CC} = \left[\frac{^{143}Sm}{^{147}Nd} \right]^0_{CC} = 0.12$$

Two stage ages for the samples are given in Appendix D.

8.1.2 Sr Isotope Systematics

Model Age (Sr) T_{Sr}

The equation for the Sr model ages is given by equation 4,

$$T_{Sr} = \frac{1}{\lambda} \ln \left[\frac{(^{87}Sr/^{86}Sr)_{rock,today} - (^{87}Sr/^{86}Sr)_{Bulk-Earth,today}}{(^{87}Rb/^{86}Sr)_{rock,today} - (^{87}Rb/^{86}Sr)_{Bulk-Earth,today}} + 1 \right] \quad \textbf{……..(5)}$$

When combined with $^{144}Nd/^{143}Nd$ ratios, the $^{87}Sr/^{86}Sr$ ratios are particularly helpful in determining the source characteristics. However, in older crustal rocks, $^{87}Sr/^{86}Sr$ ratios are vulnerable to changes as a result of later metasomatic events, which result in an increase in Rb/Sr ratios in the rocks and ambiguous $^{87}Sr/^{86}Sr$ ratios (Rollinson, 1993). This is one of the key causes of the estimations for the current $^{87}Sr/^{86}Sr$ values being variable. The Bulk Earth $^{87}Sr/^{86}Sr$ ratio used in this study, is 0.7047 (Taylor and McLennan, 1985). $^{87}Sr/^{86}Sr$ ratios along with the Rb and Sr concentrations (in ppm) and the $^{87}Rb/^{86}Rb$ ratios along with the T_{Sr}, values for leucogranite and gneiss are given in Appendix D.

8.2 Results

The model ages (T_{CHUR} and T_{DM}) calculated for leucogranites and granitic gneisses are summarized in Appendix D. The granitic gneisses have the youngest model ages as it has T_{DM} and T_{CHUR} 1837.47 and 1270.52 respectively. The Tg samples have oldest T_{DM} and T_{CHUR} ages of 4275.11 and 4121.63 respectively. In case of 2mg the oldest T_{DM} and T_{CHUR} ages of 3382.95 and 2984.87 respectively. The evolution of $^{143}Nd/^{144}Nd$ over time compared with the CHUR and DM is depicted in (Fig.8.1).

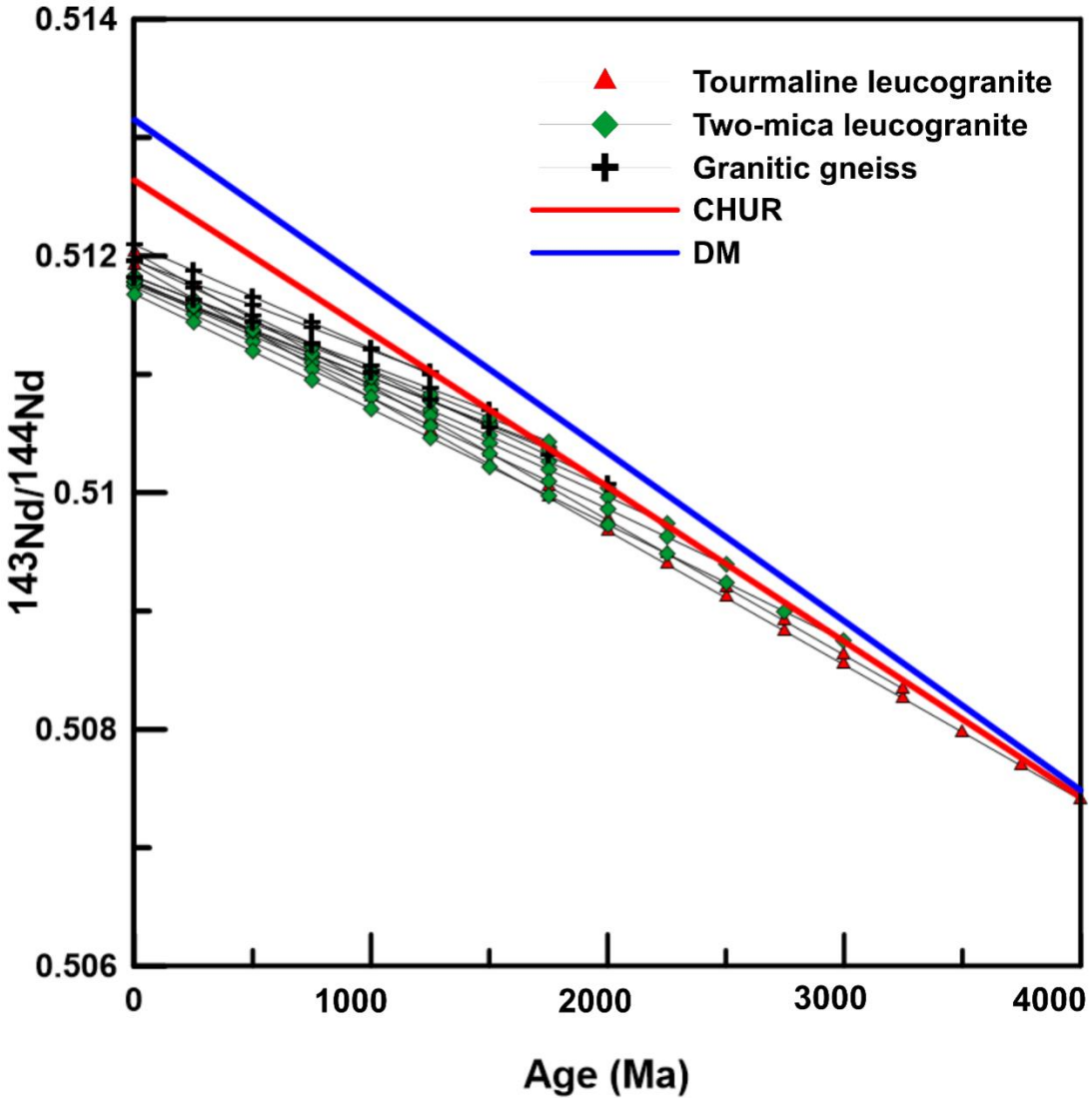

Figure 8.1 The evolution of $^{143}Nd/^{144}Nd$ over time for leucogranites and gneiss compared with the CHUR and DM.

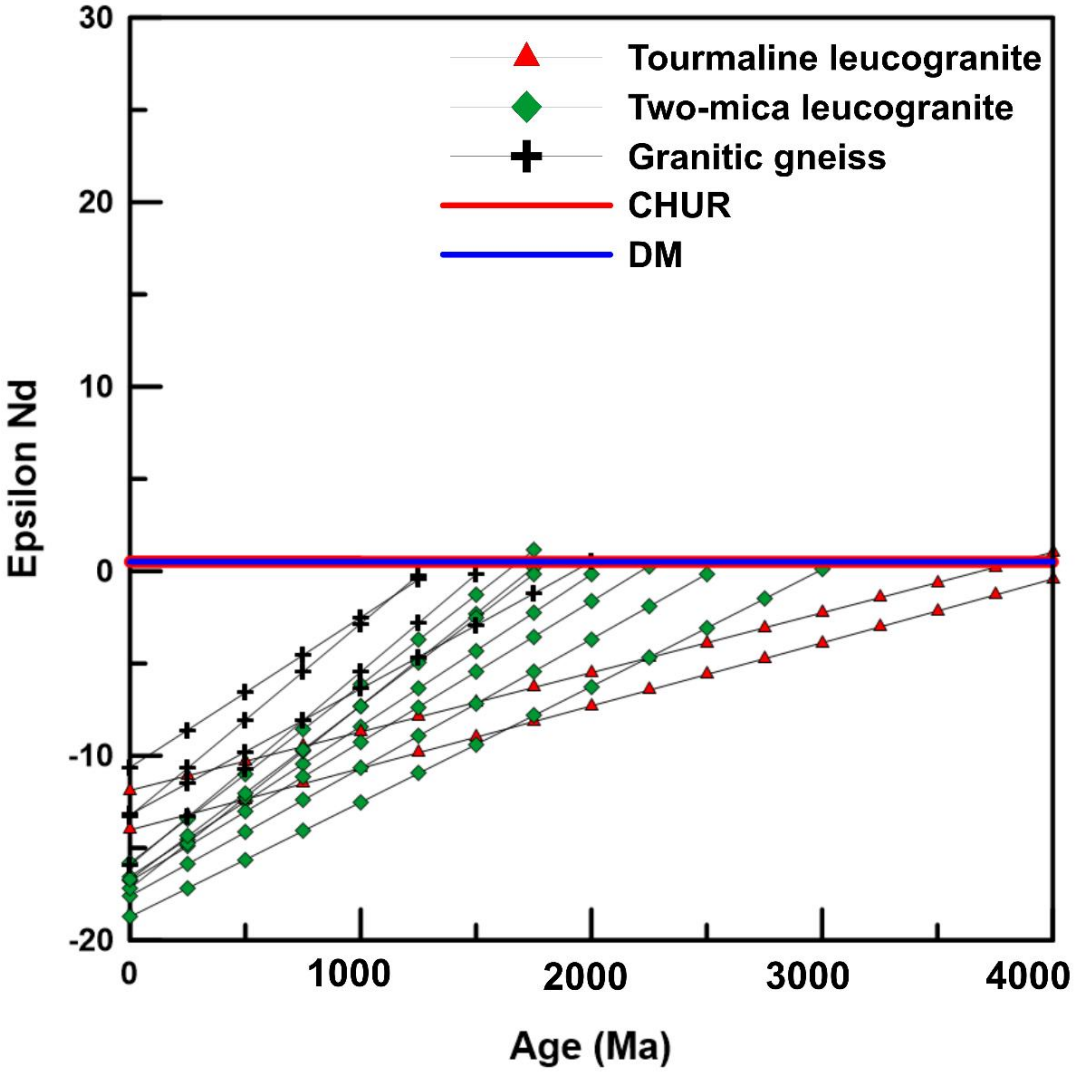

Figure 8.2 ε_{Nd} versus time growth curves for leucogranites and gneiss.

The present day ε_{Nd} (Epsilon Nd) values for leucogranites and gneiss is calculated using the equation (3). The 2mg has ε_{Nd} value ranging from -14.25 to -16.88, for Tg it ranges from -10.71 to -14.85 and for granitic gneiss from -9.58 to -14.36. The growth curve is depicted in (Fig.8.2).

The Sr-Nd isotopic compositions of 14 whole rock samples were measured yielding $^{87}Sr/^{86}$ Sr ratios ranging from 0.765379-0.777262 for Tg, 0.781782-0.813604 for 2mg and 0.746813-0.801866 for granitic gneisses. The measured $^{143}Nd/^{144}Nd$ ratios ranges from, 0.511678-0.511827 for 2mg, 0.511789-0.512029 for Tg, 0.511821-0.512903 for gneiss samples. The calculated $(^{87}Sr/^{86}Sr)_i$ ratios and εNd (t) values at t=15 Ma range

from 0.746229-0.811845 and -18.63 to -10.51 respectively. The Tg samples and the granite gneiss samples all fall within the HHS field, indicating that the HHS pelitic rocks are the source of these samples (Fig. 8.3). The evolution of the 2mg samples towards somewhat lower neodymium ratios and higher radiogenic Sr isotope ratios points to either a source in the HHC's metagreywacke rocks or, alternatively, indicates minor melt inputs from anatexis of the Lesser Himalayan formations. The whole-rock Sr–Nd isotopic compositions of the leucogranite and gneiss samples analyzed during this study are given in Appendix D.

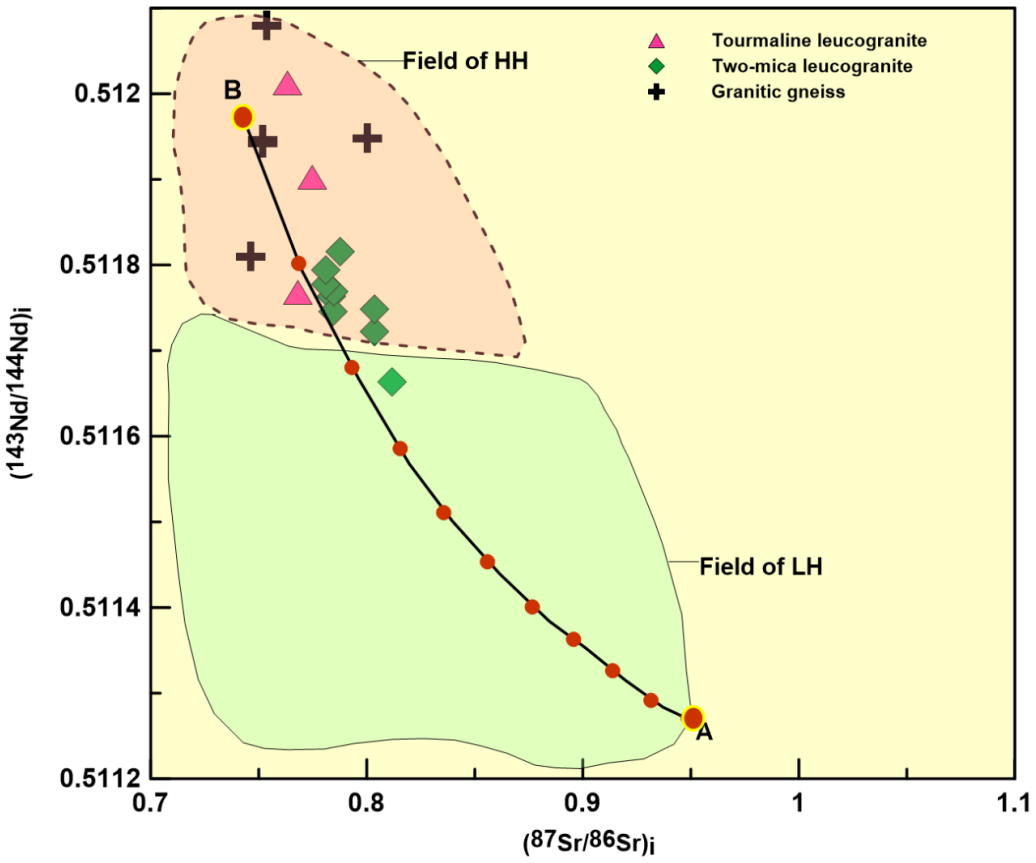

Figure 8.3 ($^{143}Nd/^{144}Nd)_i$ vs ($^{87}Sr/^{86}Sr)_i$ plot. HHS and LHS fields and the melting curve between A (fluid derived from pelitic slates), B (biotite gneiss) is from Guo and Wilson (2012) and references therein.

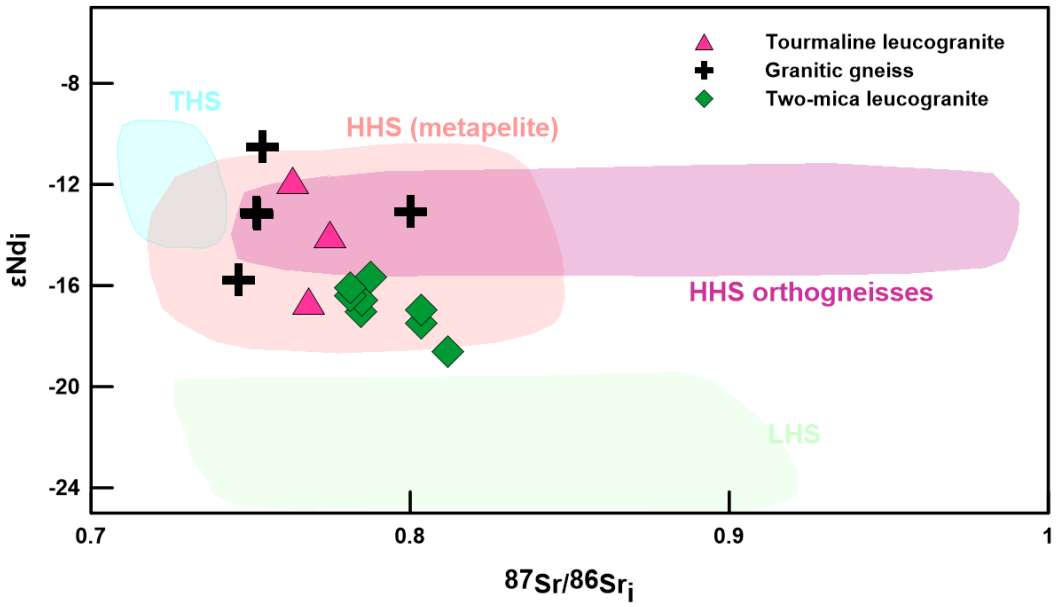

Figure 8.4 Plot of ε_{Ndi} and $^{87}Sr/^{86}Sr$ ratios for leucogranites and gneisses from North Sikkim, THS, HHS(metapelite) and HHS (orthogneiss) and LHS Fields from (Hopkinson, 2016 and references therein).

The $^{87}Sr/^{86}Sr_i$ and εNd_i for the analysed leucogranites and gneisses are plotted in (Fig. 8.4). Most of the samples plot in the HHS (metapelite) field. Out of all the samples one sample of two mica leucogranite having highest $^{87}Sr/^{86}Sr_i$ and lowest εNd_i is plots between HHS and LHS field.

CHAPTER 9

BORON ISOTOPES

This chapter discusses the boron isotopic composition of tourmaline pegmatites from North Sikkim. and focuses on the analytical methods and research work involving boron isotopes and also attempts to explain the source of the host rock with the help of boron isotopes.

9.1. Introduction

Boron is a crustal element and its average abundance in the continental crust is higher than in the mantle (Trumbull and Slack, 2018). In igneous and metamorphic systems boron occur in trace quantities, it is an incompatible element i.e., present in the melt phase during crystal fractionation, and due to this reason, it is enriched in rocks formed due to felsic magmas i.e., granites, pegmatites. The S-type granite and pegmatites are produced as late or post-tectonic products by partial melting. The studies of boron isotope have been used as a powerful tool to study geochemical cycling in the lithosphere (Nakano and Nakamura, 2001), metasomatic processes (Marschall et al., 2006), the study of ore deposits (Xavier et al., 2008), fluid-rock interaction (Konrad-Schmolke and Halama, 2014). Boron isotopic composition of granites was frequently utilized to identify the source feature since it appears that B isotopic fractionation between source rock and melt is negligible during partial melting (Kasemann et al., 2000; Trumbull and Slack, 2018).

The most common mineral studied in the case of boron isotopic studies is tourmaline. Tourmaline a cyclosilicate mineral is the most prevalent sink for boron and the concentration of boron in weight percentage in tourmaline is higher in comparison to white mica and feldspar (London and Morgan, 2012). The tourmaline present in peraluminous volcanic and plutonic rocks, if they are derived from metasedimentary rocks, contains considerable modal amounts of tourmaline (Hinsberg et al., 2011).

There are two types of boron isotopes ^{11}B and ^{10}B which are nearly 80% and 20% respectively. The boron isotopic composition is generally delta ^{11}B (Aggarwal and Palmer, 1995).The standard used is NIST SRM-951 (atom%: ^{11}B = 80.173;^{10}B = 19.827)(Catanzaro, 1970).The formula of tourmaline XY_3Z_6 $[T_6O_{18}][BO_3]_3V_3W$, where ions at each site are X=Na^+, K^+, $Ca^{2+,}$ and vacancy; Y=Li^+, $Fe^{2+,}$ Mg^{2+}, Mn^{2+}, Fe^{3+}, Al^{3+}, andCr^{3+}; Z=Mg^{2+}, $Al^{3+,}$ and Fe^{3+}; T=Al^{3+}, $B^{3+,}$ and Si^{4+}; B=B; V +W=O^{2-}, OH^- and F^- (Henry et al., 2011). Tourmaline occurs in diverse settings ranging from hydrothermal, sedimentary, magmatic, and metamorphic environments (Dutrow and Henry, 2018; Slack, 1996; van Hinsberg et al., 2011).

Hawthorne and Henry (1999) classified tourmaline based on chemical composition. The X-site constitutes Na^+, K^+, and Ca^{2+}. The compositional variation was represented by a triangular diagram for X-site constitutes three principal groups. (1) Alkali tourmalines where Na+K is dominant (2) Calcic tourmalines where Ca is dominant (3) X-site-vacant tourmalines where D is dominant. In the Y site major constitutes Li+, Fe^{2+}, Mg^{2+}, Mn^{2+}, Fe^{3+}, Al^{3+}, andCr^{3+}.The Z site contains Mg^{2+}, $Al^{3+,}$ and Fe^{3+}.

9.2 Boron isotopes in the Himalayan granites and pegmatites

A typical borosilicate mineral found in crustal rocks is tourmaline (Yang and Jiang, 2012). As tourmaline crystallizes late in magmatic evolution and is abundant in leucogranites (Henry and Dutrow, 2018) it can be used as a tracer of the source rocks and their genesis in the Himalayas (Van Hinsberg et al., 2011).

Recently various researchers have published boron isotope data for tourmaline in pegmatites and peraluminous granites in the Himalayas (Jiang and Palmer, 1998; Maner and London, 2017; Srivastava et al., 2022; Trumbull et al., 2013;). Numerous

Himalayan leucogranites are B-rich and present an ideal chance to study the B-isotope compositions of tourmaline and muscovite, which have significant boron concentrations (Hu et al., 2018). The boron isotopes can be used to detect the leucogranite source and the detrital tourmaline could be used as a provenance tracer (Guo et al., 2021).

9.3 Boron isotopic composition of tourmaline from North Sikkim

The $\delta^{11}B$ values of the studied pegmatitic tourmalines from North Sikkim ranges from − 13.83 ±0.37 ‰ to − 12.78 ± 0.84 ‰ listed in Table 5.1 and the histogram is represented in (Fig 9.1). These isotope values are within the range for tourmalines from granites and pegmatites as well as the typical 11B value of the continental crust, which is close to 10 ± 3 ‰. The detailed description about the boron composition is described in (Srivastava et al., 2022).

Sample Number	δ ^{11}B, ‰	2SD, ‰	^{11}B/^{10}B ratios
Y-TG-1	-12.78	0.84	3.9919
Y-TG-1, r.2	-12.55	0.91	3.9929
Y-TP-3	-12.86	0.84	3.9916
Y-TP-1	-13.03	0.41	3.9909
Y-TP-1, r.2	-12.59	0.44	3.9927
TP-1	-13.83	0.37	3.9877
TP-1, r.2	-14.13	0.40	3.9865

Table 4.1: Boron isotope analyses of Tourmaline bearing Pegmatites near Yumthang Valley, North Sikkim (Srivastava et al., 2022)**.**

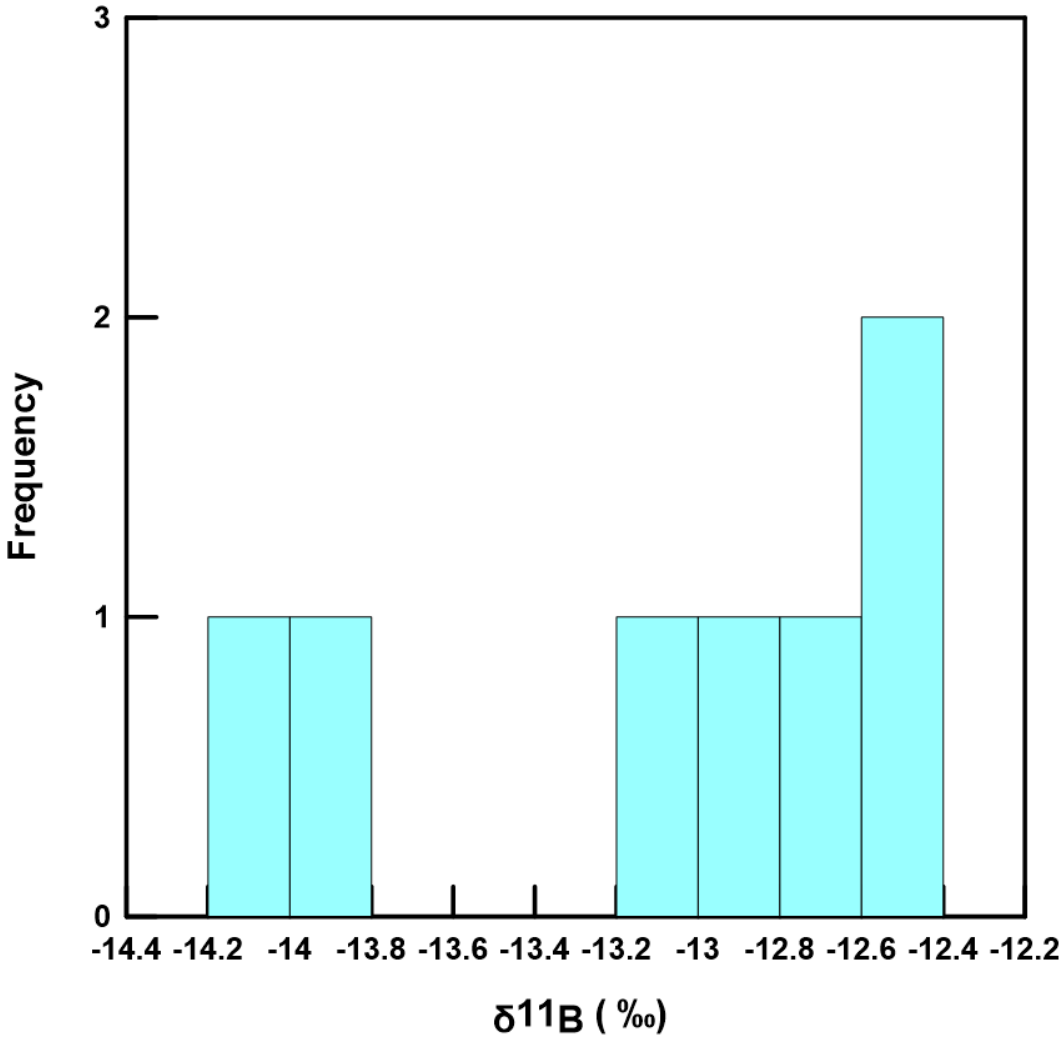

Figure 9.1. Histogram of δ ^{11}B, ‰ in studied pegmatite tourmaline.

CHAPTER 10

CORRELATION OF SIKKIM LEUCOGRANITES WITH EASTERN HIMALAYAN LEUCOGRANITES

In the eastern Himalayan region, the studied leucogranites are from the areas of Sikkim, Bhutan, and Arunachal Pradesh. This chapter focuses on the correlation between the geochemical characteristics of the Sikkim leucogranites from the other leucogranites in the Eastern Himalayan Region. The three leucogranites data from different regions of Bhutan, Garhwal, and Arunachal Pradesh region have been taken from published sources. The major oxide and trace element data variation has been compared with the leucogranites in North Sikkim.

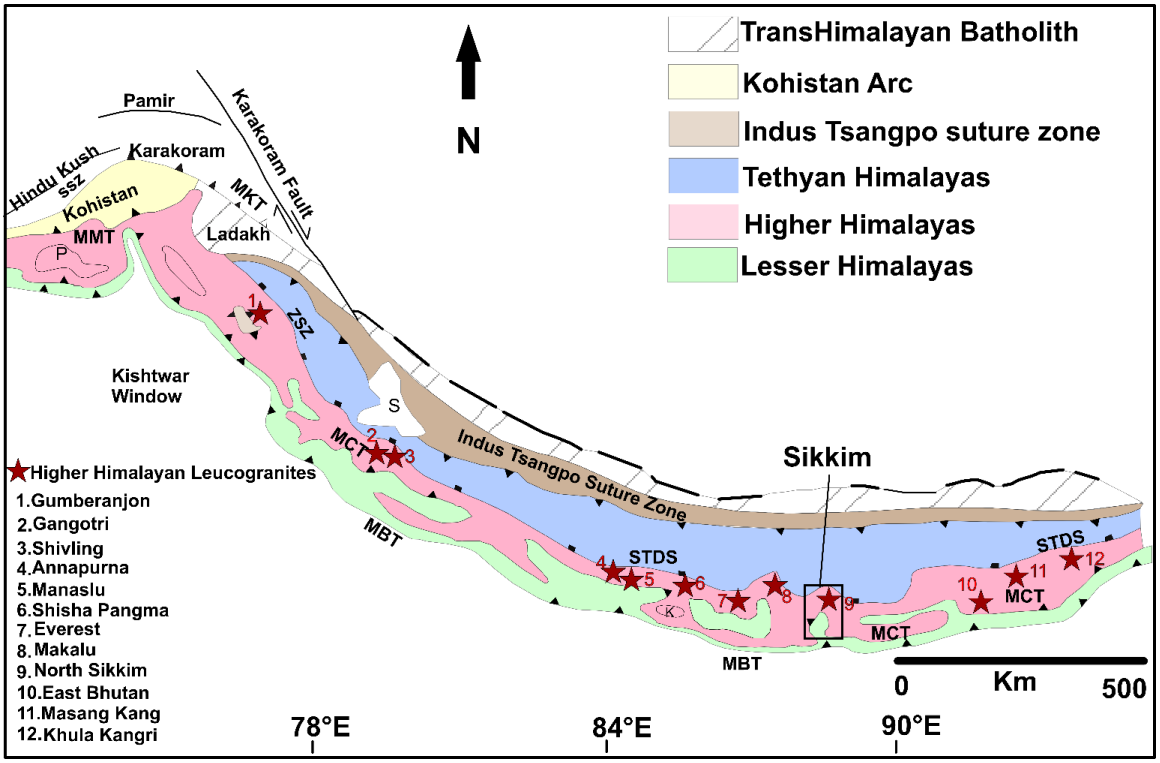

Figure 10.1. Himalayan Map showing Higher Himalayan Leucogranites in the footwall of the South Tibetan Detachment modified after Searle and Godin (2003).

10.1 Bhutan Himalayas

Bhutan is a country located in the Eastern Himalayan region surrounded by Arunachal Pradesh in the east and Sikkim in the west. In Bhutan, leucogranites are present in the upper part of the Higher Himalayan Sequence in the form of dykes and sills (Gansser, 1993) sheets or the form of the pluton. The data has been taken from Castelli and Lombardo (1988) of the Gophu La and western Lunana leucogranites and the geochemical data has been compared with the Sikkim leucogranites. In a research paper by Castelli and Lombardo (1988), both the leucogranites have muscovite which is phengitic in nature, biotite and minor tourmaline are also present, and are fine to medium-grained.

The Gophu La leucogranites are more homogeneous in comparison to western Lunana leucogranites. The modal variation for plagioclase varies from (29.6 to 38.9), quartz (28.4 to 31.8), and K-Feldspar (19.0 to 23.4). In the QAP field, the samples are present between the lines of monzogranite and granodiorite. The Gophu La granite has high values of SiO2 in comparison to western Lunana leucogranites but a lower value of Al_2O_3.The value of SiO_2 > 70.1%, Al_2O_3>14.2%. The Sr/Sr ratios range from 0.754 to 0.758, Rb/Sr is 3.5-4.2 for the first group, and for the second group, the range is higher for both. These groups were divided from the Gophu La leucogranites as they were not homogeneous and Western Lunana resembles Group 1.

Recently, according to Hopkinson et al. (2020), the U-Pb and Hf isotopic composition of Oligocene-Miocene leucogranites from the Bhutan Himalayas, melt composition evolution extends from 32 to 12 Ma. Hopkinson et al. (2017) in his study suggested that the Himalayan leucogranites are purely crustal-derived melts and have no signature of mantle inputs. The geochemical characteristics of Bhutan leucogranites (Hopkinson,

2016) reveal that these leucogranites are peraluminous and record negative Eu anomalies. The trace and major composition suggest that the composition of leucogranites resembles the average composition of leucogranites in the Himalayas. The Sr, Nd, and Pb isotopic data from the above studies indicate that the majority of the data fall within the HHS field whereas some of the data indicate that the leucogranites fall under the LHS field. This suggests that the melt may have originated from the HHS, with some of the source material coming from the LHS. Greenwood et al. (2016) suggested that the leucogranite sheets in the Bhutan region associated with STD are of Miocene age ranging from ~17-20 Ma. The TSS and the GHS were juxtaposed by movement on the extensional north-directed STDS, which also involved the attenuation of isograds and inhomogeneous thinning along this zone, and post-kinematic mineral growth was also observed. In Bhutan, leucogranites are concordant and the majority of the leucogranite bodies occur in proximity to zones of marble and calc-silicate, also the leucogranites intrude the Cheka formation in the Chomolhari massif in western Bhutan (Grujic et al., 1996 and references therein). The comparison of geochemistry is presented in the figures below: Data sources Castelli and Lombardo (1988) region do not intrude Tethyan Himalayan sequence whereas leucogranites in the Garhwal region i.e., Malari leucogranite intrudes both into Himalayan and Martoli formation of Tethyan sequence. The Malari leucogranite is considered to be more evolved than other average granites consisting of >74% SiO_2 and other major geochemical data. These major element data and strong normative corundum indicate metasedimentary origin. The comparative data are presented in the figures below: Data sources Sachan et al. (2010).

10.2 Arunachal Pradesh Himalayas

In Arunachal Himalayas the Lesser Himalayan Crystallines are known as the Bomdila group and Higher Himalayan Crystallines are known as the Sela Group constitute gneiss, migmatites, and coarse to medium-grained leucogranites. According to Bikramaditya Singh (2013), geochemical data of western Arunachal Pradesh indicates that high Rb (154-412ppm) and low Sr (19-171ppm), high Rb/Sr (1-16) indicates towards typical crustal material. The total REE abundance ranges from (48-227 ppm), and LREE and HREE are enriched and depleted respectively as indicated in normalized chondrite REE pattern indicating metasedimentary origin. The value of Eu/Eu*values ranges from (0.37-0.82). The Ba, Nb, Sr, P, and Ti show negative values in primordial mantle-normalized values. The Higher Himalayan Leucogranites in this region are present in the form of sills, high silica content varies from 67-78 wt.%, normative corundum, and S-type. The depletion in HFSE suggests the generation of granites by partial melting of crust without any contribution from the mantle.

10.3 Comparative study of Geochemical characteristics

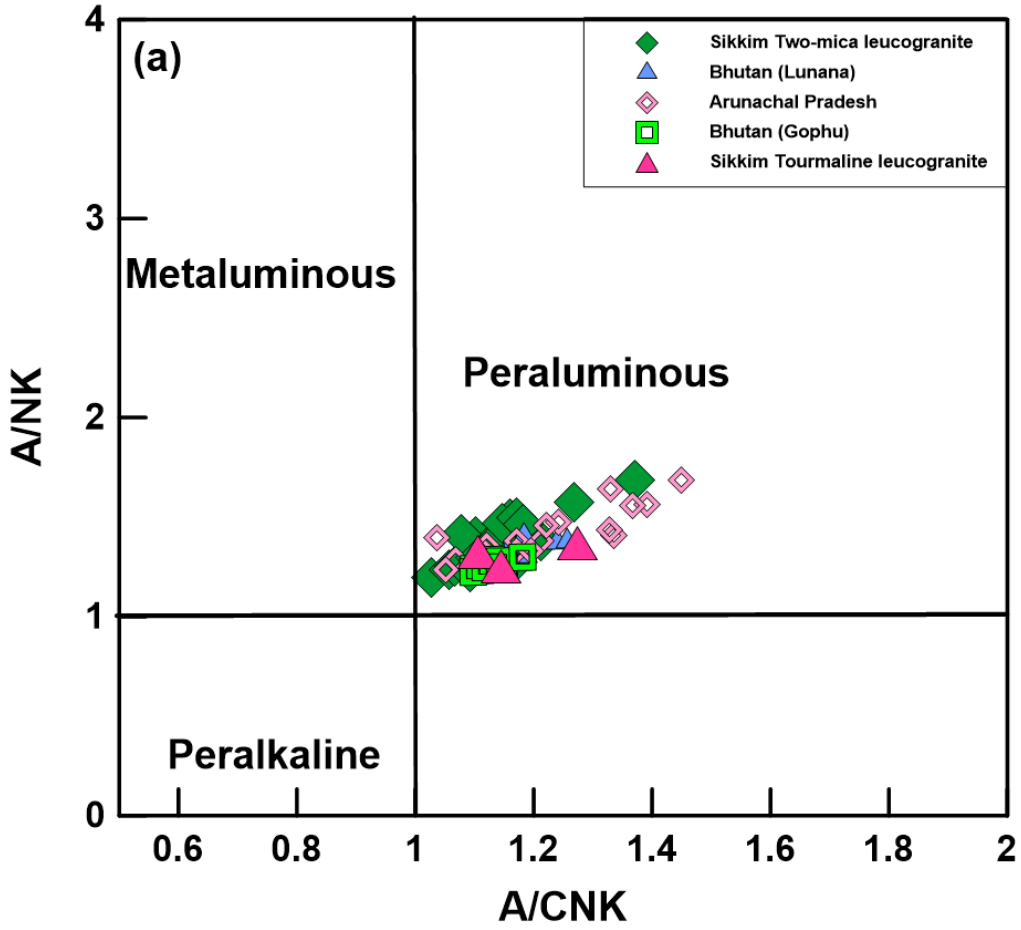

Figure 10.2. (a) A/NK versus A/CNK diagram (Shand 1943) Data Sources: Bikramaditya Singh (2013); Castelli and Lombardo (1988).

The comparative study of the leucogranites from Bhutan and Arunachal Pradesh suggests that leucogranites from all the areas are mostly peraluminous, similar to the leucogranites from Sikkim Himalayas.

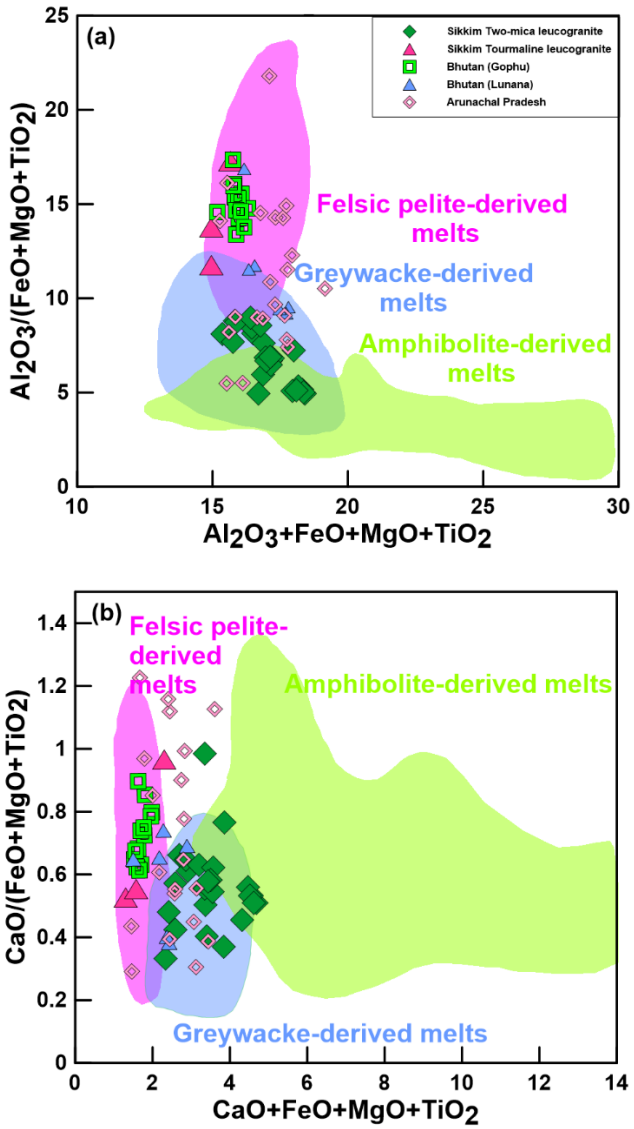

Figure 10.3. Correlation of Sikkim leucogranite with Eastern Himalayan leucogranites (a) Geochemical classification diagram Al_2O_3 /(FeOt + MgO + TiO_2versus (Al_2O_3 +FeO t + MgO +TiO_2) Patiño Douce (1999)(b) CaO/ (TFeO+MgO + TiO_2) versus CaO + TFeO+MgO + TiO_2 diagram from Patino and Douce (1999) Data Sources: Bikramaditya Singh (2013); Castelli and Lombardo (1988).

CHAPTER 11

DISCUSSIONS, MODEL, AND CONCLUSIONS

11.1 Discussions

There have been long periods of metamorphism, melting, and deformation in the Himalayan orogen, as documented by migmatites and leucogranites (King et al., 2011). Various studies have suggested HHS as the source of the Himalayan leucogranites (Aoya et al., 2005; Ji et al., 2022; Zeng et al., 2014), whilst some researchers have suggested mixing of LHS and HHS components (Guo and Wilson, 2012; Hopkinson et al., 2020). The metapelites (Deniel et al., 1987; Searle et al., 2009), metagraywacke (Guillot and Le Fort, 1995; Ji et al., 2022), amphibolites (Gao et al., 2013; Zeng et al., 2015, 2011), orthogneiss (Chen et al., 2022) felsic granulites (Zhang et al., 2017) have been reported as the potential source rocks for the generation of leucogranites. The present study from Sikkim Himalayas suggests that 2mg were generated from metagraywacke source and Tg were generated from pelitic sources.

The petrographic observations also indicate the presence of alumina-rich minerals such as tourmaline, and muscovites indicative that the leucogranites were derived from the pelitic sources.

The high SiO_2, Al_2O_3, and low MgO along with enrichment of Th, U, and Rb and leucogranites from the present study are characterized by the depletion of HFSE and enrichment of LILE suggesting that leucogranites were derived from the crustal sources. The primitive mantle normalized spider diagrams for the HHLG are characterized by negative Ti Sr, Ba, and Nb and enriched in Th, U, and Rb. The negative Nb and Ti are suggestive of fractionation of biotite whereas negative Sr is indicative of retention of plagioclase in the source.

Previous studies suggested that the leucogranites were produced by muscovite dehydration melting (Clemens and Stevens, 2015; Harris et al., 2004) or fluid-fluxed melting muscovite melting (Gao et al., 2013; Zeng et al., 2014) or biotite dehydration melting (Gou et al., 2019). The zircon saturation temperature suggests an average temperature of 754 ºC and 675º C for 2mg and Tg respectively. The basis of major, trace, and saturation temperature data of the Sikkim leucogranites suggests that leucogranites were derived from the muscovite breakdown melting in the absence of fluids.

In Sikkim the peraluminous nature of the pegmatites, the presence of tourmaline, and the high normal corundum content (> 1%), indicate that these pegmatites are likely S-type granitic, and also are classified as LCT pegmatites (enriched in lithium, caesium, and tantalum).

The Type 1 pegmatites are somewhat more fractionated $(La/Yb)_N$ than the Type 2 pegmatites in the Chondrite normalized REE diagrams (Fig. 4.17 a). The negative to positive Eu anomalies found in the examined pegmatites may result from feldspar accumulation or variable fractionation. Low HREE levels could be the result of garnet fractionation, and limited LREE enrichment could be caused by accessory minerals that are typically absent in the most recent solidified pegmatites. Alkali metals like Rb and K and alkaline earth metals like Sr and Ba show enrichment and depletion, respectively, in the primitive mantle normalized multi-element diagrams (Fig. 4.17 b), indicating a highly differentiated parent pluton. The Himalayan leucogranites possess scattered crystallization ages evident in zircons U-Pb dates (Aikman et al., 2012; Aoya et al., 2005) as well as in monazites U-Th-Pb (Lederer et al., 2013; Rubatto et al., 2013) and scattered ages probably reflect a prolonged period of crystallization. The zircons from

2mg show well-developed oscillatory zoning, have suggested that zircon morphology is closely related to the source and evolution of the parent magma, geological setting, and chemical composition. The LA-ICPMS U-Pb dates from the zircons yielded crystallization ages ranging from ~19-15 Ma indicates that leucogranites underwent prolonged crystallization while the pre-Tertiary ages ranging from ~145 to 2462 Ma record inheritance from the HHS and possibly from LHS. For monazites, both the leucogranites i.e., 2mg and Tg record the Miocene crystallization ages ~14-15 Ma. The chondrite normalized REE patterns of both samples illustrate the enrichment in LREE relative to HREE with marked Eu anomalies. The monazite Eu anomaly could also reflect the changes in oxygen fugacity of the system (Holder et al., 2020), and also negative Eu anomaly suggests co-crystallization of monazite with feldspar during melt crystallization, where Eu anomaly favorably partitions into feldspar. The isotopic composition of Sr and Nd in bulk rock samples is used to identify possible melt source regions. The Sr-Nd isotopic systematics in Sikkim leucogranites and gneiss suggests that Tg samples and granite gneiss samples all lie within the Himalayan orogen field defined by the HHS suggesting that they came from pelitic rocks within the HHS. As the 2mg samples are slightly more radiogenic in Sr isotope ratios and slightly lower in neodymium ratios, this suggests a source from metagraywacke rocks of the HHC, or from anatexis of the Lesser Himalayan Formation. The epsilon Nd values are negative indicating their origin from enriched mantle and crustal and crustal sources.

Since the isotopic compositions of tourmaline depend on boron sources, which might have varied boron isotopic signatures, tourmalines from various geological settings exhibit considerable ^{11}B variations (Jiang and Palmer, 1998). The pegmatitic tourmalines from the region near to Yumthang Valley in North Sikkim may have

resulted from fractionation during magmatic degassing from magmatic-hydrothermal fluids during the last magmatic stage, according to the lower ^{11}B values.

11.2 Tectonic Model for Sikkim Himalayas

The tectonic models which have been proposed to elucidate the evolution of Himalayas which have been briefly outlined in the Chapter 1, (Fig. 1.3). The channel flow model (Fig.11.1) explains the coeval extrusion of partially molten low-viscosity layer between the MCT and STDS, that depicts thrust sense and normal sense respectively (Fig.11.1). The data from the previous studies suggest that MCT was active around ~21-9 Ma. The STDS was active aound ~24-13 Ma (Kellett et al., 2013), which further indicates that there may have been contemporaneous movement on these structures in the Sikkim Himalaya over at least a portion of the Miocene, which is necessary for the channel flow concept. The U-Pb ages from monazite ages and zircon ages ~15-19 Ma from the present study suggest that emplacement of leucogranite with the Middle Miocene movement along the STDS, that might be coherent with channel flow model. It was suggested that MCT propagated structurally downwards through time resulting in progressive tectonic accretion of LHS material from the footwall to the hanging wall on the basis of kinematic, thermal models and petrochronological studies (Bollinger et al., 2006; Hopkinson et al., 2020; Mottram et al., 2015, 2014). The heat advected downward (Fig.11.2) from the overlying HHS material caused peak metamorphism in the MCT zone (Mottram et al., 2015) and exhumation along the MCT might have led to the decompression melting of LHS and HHS material (Hopkinson et al., 2020). The leucogranite formation is inextricably linked to decompression which enabled enhancing melt fraction and stress regime for melt extraction and eventual emplacement into the normal fault zone (Harris and Massey, 1994).

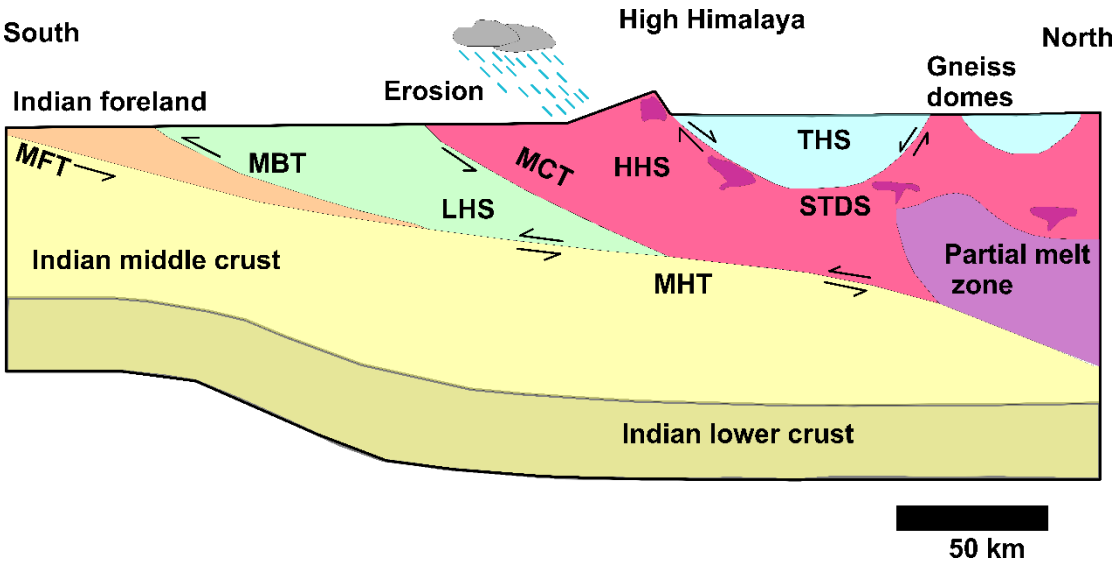

Figure 11.1 Schematic section demonstrating the channel flow model from Beaumont et al. (2002), where purple colour indicates melt-weakened middle crust.

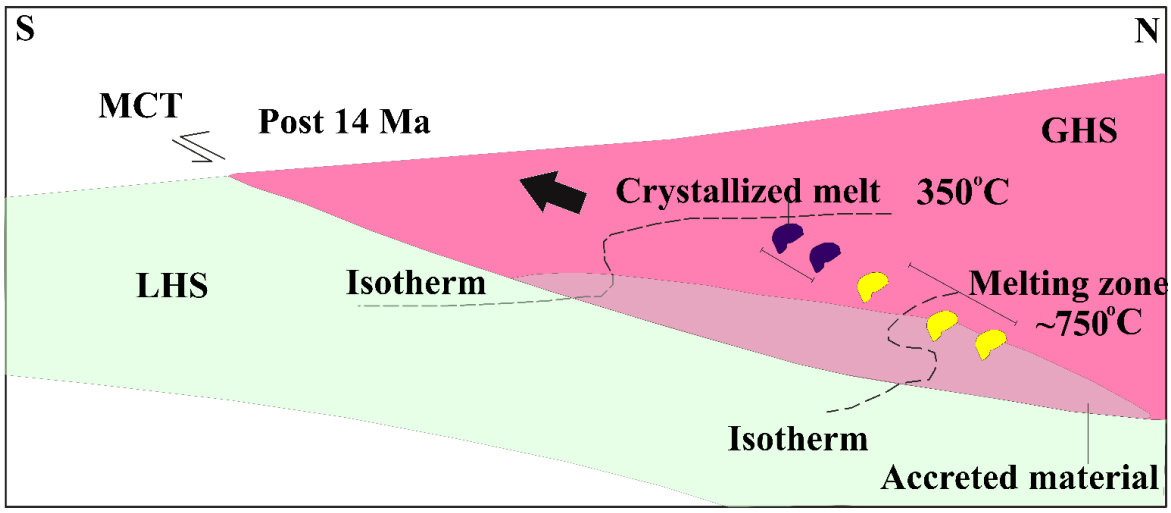

Figure 11.2. Tectonic diagram of Main Central Thrust (MCT) depicting the source for the generation of leucogranites modified after Hopkinson et al. (2020); Mottram et al. (2015) and references therein.

11.3 CONCLUSIONS

The petrological, geochemical, geochronological, and boron isotopic studies of Sikkim Himalayan leucogranites and pegmatites lead to the following conclusions:

1. The Higher Himalayan leucogranites from Sikkim, both 2mg and Tg have crystallized from crustal melts and are peraluminous.

2. The 2mg has been sourced from metagraywacke compositions, whilst Tg has been derived from metapelites.

3. The period of melting derived from the geochronological studies (19-14 Ma) from monazite and zircon dating is contemporaneous with the movement on MCT and STDS in the eastern Himalayas, enabling decompression melting as a viable method for melt formation.

4. The sillimanite-bearing gneiss from the Darjeeling region underwent intense melting and metamorphism from the early Oligocene to the Mid-Miocene, which peaked during the leucogranite crystallization phase.

5. The tourmalines from leucogranites and pegmatites belong to the alkali group and are schrols. The biotites and muscovites are mainly primary.

6. The Sr-Nd whole rock isotopic systematics suggest that the granitic gneiss and Tg have been sourced from the pelitic rocks and 2mg have been sourced from metagraywacke rocks of the HHS and might have minor contributions from anatexis of LHS. The epsilon Nd values indicates the crustal sources.

7. The studied pegmatites from the area near Yumthang valley suggest peraluminous nature and formed in a syn-collisional setting. Based on the geochemical composition and boron isotopic studies suggest that the pegmatitic tourmalines were derived from the continental crust.

8. The correlation of leucogranites from the eastern Himalayas with Sikkim Himalayan leucogranites based on major element geochemistry suggests that these leucogranites are peraluminous and are classified as S-type.

9. The zircon U-Pb ages, which overlap with crustal melting in the source HHS rocks, vary between~19 to 15 Ma. Leucogranite emplacement may have occurred contemporaneous with accretion along the MCT zone and migration along the South Tibetan Detachment System (STDS), according to 14 Ma monazite crystallization ages.

References

Abdel-Rahman, 1994. Nature of Biotites from Alkaline, Calc-alkaline, and Peraluminous Magmas. J. Petrol. 35. https://doi.org/10.1093/petrology/35.2.525

Acharyya, S., Ray, K.K., 1977. Geology of the Darjeeling-Sikkim Himalaya, guide to excursion No.4. 4thInternat. Gond. Symp. India.

Acharyya, S.K., 1989. The Daling Group, its nomenclature, tectono-stratigraphy and structural grain: with notes on their possible equivalents. Geol. Surv. India 22, 5-13(Spl. Pub.).

Acharyya, Subhrangsu K., Ghosh, S., Mandal, N., Bose, S., Pande, K., 2017. Pre-Himalayan tectono-magmatic imprints in the Darjeeling-Sikkim Himalaya (DSH) constrained by 40Ar/39Ar dating of muscovite. J. Asian Earth Sci. 146, 211–220. https://doi.org/10.1016/j.jseaes.2017.05.027

Aggarwal, J.K., Palmer, M.R., 1995. Boron isotope analysis. Analyst 120, 1301–1307. https://doi.org/10.1039/AN9952001301

Ahmad, I., Khan, S., Lapen, T., B, K., Jehan, N., 2013. Isotopic ages for alkaline igneous rocks, including a 26 Ma ignimbrite, from the Peshawar plain of northern Pakistan and their tectonic implications. J. Asian Earth Sci. 62, 414–424. https://doi.org/10.1016/j.jseaes.2012.10.025

Ahmad, T., Thakur, V.C., Islam, R., Khanna, P.P., Mukherjee, P.K., 1998. Geochemistry and geodynamic implications of magmatic rocks from the Trans-Himalayan arc. Geochem. J. 32, 383–404. https://doi.org/10.2343/geochemj.32.383

Aikman, A., Harrison, T., Ding, L., 2008. Evidence for Early (>44 Ma) Himalayan Crustal Thickening, Tethyan Himalaya, southeastern Tibet. Earth Planet. Sci. Lett. 274, 14–23. https://doi.org/10.1016/j.epsl.2008.06.038

Aikman, A.B., Harrison, T.M., Hermann, J., 2012. Age and thermal history of Eo- and Neohimalayan granitoids, eastern Himalaya, Journal of Asian Earth Sciences. https://doi.org/10.1016/j.jseaes.2012.01.011

Aoya, M., Wallis, S.R., Terada, K., Lee, J., Kawakami, T., Wang, Y., Heizler, M., 2005. North-south extension in the Tibetan crust triggered by granite emplacement. Geology 33, 853–856. https://doi.org/10.1130/G21806.1

Auden, J.B., 1935. Traverses in the Himalaya. Rec. G.S.I, LXIX, pt.1, PP. 123–167.

Baker, J., Peate, D., Waight, T., Meyzen, C., 2004. Pb Isotopic Analysis of Standards and Samples Using a 207Pb-204Pb Double Spike and Thallium to Correct for Mass Bias with a Double-Focusing MC-ICP-MS. Chem. Geol. 217, 275–303. https://doi.org/10.1016/j.chemgeo.2004.06.030

Barbarin, B., 1999. A review of the relationships between granitoid types, their origins and their geodynamic environments. Lithos 46, 605–626. https://doi.org/10.1016/S0024-4937(98)00085-1

Barbarin, B., 1990. Granitoids: Main petrogenetic classifications in relation to origin

and tectonic setting. Geol. J. 25, 227–238. https://doi.org/10.1002/gj.3350250306

Batchelor, R.A., Bowden, P., 1985. Petrogenetic interpretation of granitoid rock series using multicationic parameters. Chem. Geol. 48, 43–55. https://doi.org/https://doi.org/10.1016/0009-2541(85)90034-8

Bea, F., Bortnikov, N., Montero, P., Zinger, T., Sharkov, E., Silantyev, S., Skolotniev, S., Trukhalev, A., Molina, J., 2020. Zircon xenocryst evidence for crustal recycling at the Mid-Atlantic Ridge. Lithos 354–355, 105361. https://doi.org/10.1016/j.lithos.2019.105361

Beaumont, C., Jamieson, R.A., Nguyen, M.H., Lee, B., 2002. Himalayan tectonics explained by extrusion of a low-viscosity crustal channel coupled to focused surface denudation. Nature 414, 738–742. https://doi.org/10.1038/414738a

Beaumont, C., Nguyen, M.H., Lee, B., 2001. Himalayan tectonics explained by extrusion of a low-viscosity crustal channel coupled to focused surface denudation. Nature 414, 738–742. https://doi.org/10.1038/414738a

Bhattacharyya, K., Mitra, G., 2011. Strain softening along the MCT zone from the Sikkim Himalaya: Relative roles of Quartz and Micas. J. Struct. Geol. 33, 1105–1121. https://doi.org/10.1016/j.jsg.2011.03.008

Bhattacharyya, K., Mitra, G., 2009. A new kinematic evolutionary model for the growth of a duplex - an example from the Rangit duplex, Sikkim Himalaya, India. Gondwana Res. 16, 697–715. https://doi.org/10.1016/j.gr.2009.07.006

Bhattacharyya, K., Mitra, G., Kwon, S., 2015. Geometry and kinematics of the Darjeeling-Sikkim Himalaya, India: Implications for the evolution of the Himalayan fold-thrust belt. J. Asian Earth Sci. 113, 778–796. https://doi.org/10.1016/j.jseaes.2015.09.008

Bikramaditya Singh, R.K., 2013. Origin and emplacement of the Higher Himalayan Leucogranite in the eastern Himalaya: Constraints from geochemistry and mineral chemistry. J. Geol. Soc. India 81, 791–803. https://doi.org/10.1007/s12594-013-0104-9

Black, L., Kamo, S., Allen, C.M., Aleinikoff, J., Davis, D., Korsch, R., Foudoulis, C., 2003. TEMORA 1: A new zircon standard for Phanerozoic U-Pb geochronology. Chem. Geol. 200, 155–170. https://doi.org/10.1016/S0009-2541(03)00165-7

Bonin, B., Janoušek, V., Moyen, J.F., 2020. Chemical variation, modal composition and classification of granitoids, Geological Society Special Publication. https://doi.org/10.1144/SP491-2019-138

Boraiaha, C.K., Joshi, K.B., Kerr, A.C., Padhi, J.K., Mishra, S.S., Chandan, R., 2020. Field, petrographic and geochemical characteristics of Sullya alkaline complex in the Cauvery Shear Zone (CSZ), southern India: Implications for petrogenesis. J. Earth Syst. Sci. 129. https://doi.org/10.1007/s12040-020-1369-1

Brown, M., 2007. Crustal melting and melt extraction, ascent and emplacement in orogens: Mechanisms and consequences. J. Geol. Soc. - J GEOL SOC 164, 709–730. https://doi.org/10.1144/0016-76492006-171

Burchfiel, B., Chen, Z.L., Hodges, K., Yuping, L., Royden, L., Changrong, D., Jiene, X., 1992. The South Tibetan detachment system. Himal. orogen Ext. Contemp.

with parallel to shortening a collisional Mt. belt 20.

Cao, H.-W., Pei, Q., Santosh, M., Li, G.-M., Zhang, L.-K., Zhang, X.-F., Zhang, Y.-H., Zou, H., Dai, Z., Bin, L., Tang, L., Yu, X., 2022. Himalayan leucogranites: A review of geochemical and isotopic characteristics, timing of formation, genesis, and rare metal mineralization. Earth-Science Rev. 234, 104229. https://doi.org/10.1016/j.earscirev.2022.104229

Carosi, R., Lombardo, B., Molli, G., Musumeci, G., Pertusati, P.C., 1998. The south Tibetan detachment system in the Rongbuk Valley, Everest region. Deformation features and geological implications. J. Asian Earth Sci. 16, 299–311. https://doi.org/10.1016/S0743-9547(98)00014-2

Castelli, D., Lombardo, B., 1988. The Gophu La and Western Lunana granites: Miocene muscovite leucogranites of the Bhutan Himalaya. Lithos 21, 211–225. https://doi.org/10.1016/0024-4937(88)90010-2

Catanzaro, E.J., 1970. Boric acid: isotopic and assay standard reference materials. National Bureau of Standards, Institute for Materials Research.

Catlos, E.J., Dubey, C.S., Harrison, T.M., Edwards, M.A., 2004. Late Miocene movement within the Himalayan Main Central Thrust shear zone, Sikkim, north-east India. J. Metamorph. Geol. 22, 207–226. https://doi.org/10.1111/j.1525-1314.2004.00509.x

Cawood, P.A., Johnson, M.R.W., Nemchin, A.A., 2007. Early Palaeozoic orogenesis along the Indian margin of Gondwana: Tectonic response to Gondwana assembly. Earth Planet. Sci. Lett. 255, 70–84. https://doi.org/10.1016/j.epsl.2006.12.006

Célérier, J., Harrison, T.M., Webb, A.A.G., Yin, A., 2009. The Kumaun and Garwhal Lesser Himalaya, India: Part 1. Structure and stratigraphy. Bull. Geol. Soc. Am. 121, 1262–1280. https://doi.org/10.1130/B26344.1

Černý, P., 1991. Fertile granites of Precambrian rare-element pegmatite fields: is geochemistry controlled by tectonic setting or source lithologies? Precambrian Res. 51, 429–468. https://doi.org/10.1016/0301-9268(91)90111-M

Černý, P., Ercit, T.S., 2005. The classification of granitic pegmatites revisited. Can. Mineral. 43, 2005–2026. https://doi.org/10.2113/gscanmin.43.6.2005

Chakrabarti, B.K., 2016. Geology of the Himalayan Belt, Geology of the Himalayan Belt. https://doi.org/10.1016/c2014-0-00974-4

Chappell, B.W. and White, A.J.R. (1974), 1974. Two Contrasting Granite Types. Pacific Geol. 8, 173–174.

Chappell, B.W., White, A.J.R., 2001. Two contrasting granite types: 25 years later. Aust. J. Earth Sci. 48, 489–499. https://doi.org/10.1046/j.1440-0952.2001.00882.x

Chappell, B.W., White, A.J.R., 1992. I- and S-type granites in the Lachlan Fold Belt. Trans. R. Soc. Edinb. Earth Sci. 83, 1–26. https://doi.org/10.1017/S0263593300007720

Chen, H., Hu, G., Zeng, L., Yu, X., Li, Y., 2022. Miocene Crustal Anatexis of Paleozoic Orthogneiss in the Zhada Area, Western Himalaya. Acta Geol. Sin. - English Ed.

96. https://doi.org/10.1111/1755-6724.14897

Chen, S., Fan, W.-M., Shi, R.-D., Jifeng, X., Liu, Y.-M., 2021. The Tethyan Himalaya Igneous Province: Early Melting Products of the Kerguelen Mantle Plume. J. Petrol. 62. https://doi.org/10.1093/petrology/egab069

Chen, S., Fan, W.-M., Shi, R.-D., Liu, X.-H., Zhou, X.-J., 2018. 118–115 Ma magmatism in the Tethyan Himalaya igneous province: Constraints on Early Cretaceous rifting of the northern margin of Greater India. Earth Planet. Sci. Lett. 491, 21–33. https://doi.org/10.1016/j.epsl.2018.03.034

Chen, S.S., Shi, R.D., Gong, X.H., Liu, D.L., Huang, Q.S., Yi, G.D., Wu, K., Zou, H.B., 2017. A syn-collisional model for Early Cretaceous magmatism in the northern and central Lhasa subterranes. Gondwana Res. 41, 93–109. https://doi.org/10.1016/j.gr.2015.04.008

Chen, X., Zhang, G., Gao, R., Zhang, D., Yang, B., 2021. Petrogenesis of highly fractionated leucogranite in the Himalayas: The Early Miocene Cuonadong example. Geol. J. 56, 3791–3807. https://doi.org/10.1002/gj.4126

Cheng, L., Zhang, C., Yang, X., 2020. Petrogenesis of deformed tourmaline leucogranite in the Gurla Mandhata metamorphic core complex, Southwestern Tibet. Lithos 364–365, 105533. https://doi.org/10.1016/j.lithos.2020.105533

Cherniak, D.J., Watson, E.B., 2003. Diffusion in zircon. Rev. Mineral. geochemistry 53, 113–143.

Claiborne, L.L., Miller, C.F., Wooden, J.L., 2010. Trace element composition of igneous zircon: a thermal and compositional record of the accumulation and evolution of a large silicic batholith, Spirit Mountain, Nevada. Contrib. to Mineral. Petrol. 160, 511–531. https://doi.org/10.1007/s00410-010-0491-5

Clemens, J., Stevens, G., 2015. Comment on ‘Water-fluxed melting of the continental crust: A review’ by R.F. Weinberg and P. Hasalová. Lithos 234. https://doi.org/10.1016/j.lithos.2015.06.032

Colchen, M., P. Le Fort, and A.P., n.d. Notice explicative de la carte ge´ologique Annapurna-Manaslu-Ganesh (Himalaya du Ne´pal) au 1:200.000e (bilingue: Franc¸ais- English),. Cent. Natl. la Rech. Sci., Paris.

Coleman, M.E., Parrish, R., 1995. Constraints on Miocene high-temperature deformation and anatexis within the Greater Himalaya from U-Pb geochronology. Eos (Transactions, Am. Geophys. Union) 76, F708.

Copeland, P., Parrish, R.R., Harrison, T.M., 1988. Identification of inherited radiogenic Pb in monazite and its implications for U-Pb systematics. Nature 333, 760–763. https://doi.org/10.1038/333760a0

Corfu, F., 2003. Atlas of Zircon Textures. Rev. Mineral. Geochemistry - REV Miner. GEOCHEM 53, 469–500. https://doi.org/10.2113/0530469

Cottle, J., Lederer, G., Larson, K., 2019. The monazite record of pluton assembly: Mapping manaslu using petrochronology. Chem. Geol. 530, 119309. https://doi.org/10.1016/j.chemgeo.2019.119309

Cottle, J., Searle, M., Horstwood, M., Waters, D., 2009. Timing of Midcrustal

Metamorphism, Melting, and Deformation in the Mount Everest Region of Southern Tibet Revealed by U(-Th)-Pb Geochronology. Source J. Geol. 117, 643–664. https://doi.org/10.1086/605994

Cottle, J.M., Searle, M.P., Jessup, M.J., Crowley, J.L., Law, R.D., 2015. Rongbuk re-visited: Geochronology of leucogranites in the footwall of the South Tibetan Detachment System, Everest Region, Southern Tibet. Lithos 227, 94–106. https://doi.org/10.1016/j.lithos.2015.03.019

Dan, W., Wang, Q., Li, X.-H., Tang, G.-J., Zhang, C., Zhang, X.-Z., Wang, J., 2019. Low δ18O magmas in the Carboniferous intra-oceanic arc, Central Tibet: Implications for felsic magma generation and oceanic arc accretion. Lithos 326. https://doi.org/10.1016/j.lithos.2018.12.011

Dasgupta, S., Ganguly, J., Neogi, S., 2004. Inverted metamorphic sequence in the Sikkim Himalayas: Crystallization history, P-T gradient and implications. J. Metamorph. Geol. 22, 395–412. https://doi.org/10.1111/j.1525-1314.2004.00522.x

Davis, D., Suppe, J., Dahlen, F.A., 1983. Mechanics of Fold-and-Thrust Belts and Accretionary Wedges. J. Geophys. Res. 88, 1153–1172. https://doi.org/10.1029/JB088iB02p01153

DeCelles, P.G., Robinson, D.M., Zandt, G., 2002. Implications of shortening in the Himalayan fold-thrust belt for uplift of the Tibetan Plateau. Tectonics 21, 12-1-12–25. https://doi.org/10.1029/2001TC001322

Deer, W., Howie, R., Zussman, J., 1992. An Introduction to the Rock forming Minerals. 2nd ed. Longman, London.

Deniel, C., Vidal, P., Fernandez, A., Le Fort, P., Peucat, J.J., 1987. Isotopic study of the Manaslu granite (Himalaya, Nepal): inferences on the age and source of Himalayan leucogranites. Contrib. to Mineral. Petrol. 96, 78–92. https://doi.org/10.1007/BF00375529

Dèzes, P.J., Vannay, J.C., Steck, A., Bussy, F., Cosca, M., 1999. Synorogenic extension: Quantitative constraints on the age and displacement of the Zanskar shear zone (northwest Himalaya). Bull. Geol. Soc. Am. 111, 364–374. https://doi.org/10.1130/0016-7606(1999)111<0364:SEQCOT>2.3.CO;2

Dickin, A.P., 2013. Model Ages (Sm-Nd) BT - Encyclopedia of Scientific Dating Methods, in: Rink, W.J., Thompson, J. (Eds.), . Springer Netherlands, Dordrecht, pp. 1–7. https://doi.org/10.1007/978-94-007-6326-5_2-2

Dill, H.G., 2015. Pegmatites and aplites: Their genetic and applied ore geology. Ore Geol. Rev. 69, 417–561. https://doi.org/10.1016/j.oregeorev.2015.02.022

Dong, X., Zhang, Z., Fff, F., He, Z., Lin, Y., 2014. Late Paleozoic intrusive rocks from the southeastern Lhasa terrane, Tibetan Plateau, and their Late Mesozoic metamorphism and tectonic implications. Lithos 198. https://doi.org/10.1016/j.lithos.2014.04.001

Dutrow, B., Henry, D.J., 2018. Tourmaline : A powerful mineral monitor in metamorphic rocks 3–5.

Eby, G.N., 1990. The A-type granitoids: A review of their occurrence and chemical

characteristics and speculations on their petrogenesis. Lithos 26, 115–134. https://doi.org/10.1016/0024-4937(90)90043-Z

Eby, N., 1992. Chemical subdivision of the A-type granitoids:Petrogenetic and tectonic implications. Geology 20. https://doi.org/10.1130/0091-7613(1992)020<0641:CSOTAT>2.3.CO;2

Edwards, M.A., Harrison, T.M., 1997. When did the roof collapse? Late Miocene north-south extension in the high Himalaya revealed by Th-Pb monazite dating of the Khula Kangri granite. Geology 25, 543–546. https://doi.org/10.1130/0091-7613(1997)025<0543:WDTRCL>2.3.CO;2

Faak, K., Chakraborty, S., Dasgupta, S., 2012. Petrology and tectonic significance of metabasite slivers in the Lesser and Higher Himalayan domains of Sikkim, India. J. Metamorph. Geol. 30, 599–622. https://doi.org/10.1111/j.1525-1314.2012.00987.x

Fan, Y., Zhang, J., Lin, C., Wang, X., Zhang, B., 2021. Miocene granitic magmatism constrains the early E-W extension in the Himalayan Orogen: A case study of Kung Co leucogranite. Lithos 398–399, 106295. https://doi.org/10.1016/j.lithos.2021.106295

Ferry, J.M., Watson, E.B., 2007. New thermodynamic models and revised calibrations for the Ti-in-zircon and Zr-in-rutile thermometers. Contrib. to Mineral. Petrol. 154, 429–437. https://doi.org/10.1007/s00410-007-0201-0

Foster, M.D., 1960. Interpretation of the composition of trioctahedral mica. U.S. Geological Survey Professional Paper, v. 354-B, 11–48.

Frost, B.R., Barnes, C.G., Collins, W.J., Arculus, R.J., Ellis, D.J., Frost, C.D., 2001. A geochemical classification for granitic rocks. J. Petrol. 42, 2033–2048. https://doi.org/10.1093/petrology/42.11.2033

Frost, B.R., Frost, C.D., 2008. A geochemical classification for feldspathic igneous rocks. J. Petrol. 49, 1955–1969. https://doi.org/10.1093/petrology/egn054

Ganguly, J., Dasgupta, S., Cheng, W., Neogi, S., 2000. Exhumation history of a section of the Sikkim Himalayas, India: Records in the metamorphic mineral equilibria and compositional zoning of garnet. Earth Planet. Sci. Lett. 183, 471–486. https://doi.org/10.1016/S0012-821X(00)00280-6

Gansser, A., 1993. The Himalayas seen from Bhutan*) 335–346.

Gansser, A., 1964. The Geology of the Himalayas. Intersci. Publ., John Wiley Sons, New York 289.

Gao, L.E., Zeng, L., Asimow, P.D., 2017. Contrasting geochemical signatures of fluid-absent versus fluid-fluxed melting of muscovite in metasedimentary sources: The Himalayan leucogranites. Geology 45, 39–42. https://doi.org/10.1130/G38336.1

Gao, L.E., Zeng, L. Sen, Hou, K.J., Guo, C.L., Tang, S.H., Xie, K.J., Hu, G.Y., Wang, L., 2013. Episodic crustal anatexis and the formation of Paiku composite leucogranitic pluton in the Malashan Gneiss Dome, Southern Tibet. Chinese Sci. Bull. 58, 3546–3563. https://doi.org/10.1007/s11434-013-5792-4

Gao, P., Zheng, Y.F., Zhao, Z.F., Sun, G.C., 2021. Source diversity in controlling the

compositional diversity of Cenozoic granites in the Tethyan Himalaya. Lithos 388–389, 106072. https://doi.org/10.1016/j.lithos.2021.106072

Gehrels, G.E., DeCelles, P.G., Ojha, T.P., Upreti, B.N., 2006. Geologic and U-Th-Pb geochronologic evidence for early Paleozoic tectonism in the Kathmandu thrust sheet, central Nepal Himalaya. Bull. Geol. Soc. Am. 118, 185–198. https://doi.org/10.1130/B25753.1

Geisler-Wierwille, T., Pidgeon, R., Kurtz, R., Bronswijk, W., Schleicher, H., 2003. Experimental hydrothermal alteration of partially metamict zircon. Am. Mineral. 88, 1496–1513. https://doi.org/10.2138/am-2003-1013

Ghatak, A., Basu, A., 2011. Vestiges of the Kerguelen plume in the Sylhet Traps, northeastern India. Earth Planet. Sci. Lett. - EARTH PLANET SCI LETT 308, 52–64. https://doi.org/10.1016/j.epsl.2011.05.023

Godin, Laurent, Grujic, D., Law, R., Searle, M., 2006. Channel flow, ductile extrusion and exhumation in continental collision zones: An introduction. Geol. Soc. London Spec. Publ. 268, 1–23. https://doi.org/10.1144/GSL.SP.2006.268.01.01

Godin, L., Grujic, D., Law, R.D., Searle, M.P., 2006. Channel flow, ductile extrusion and exhumation in continental collision zones: An introduction. Geol. Soc. Spec. Publ. 268, 1–23. https://doi.org/10.1144/GSL.SP.2006.268.01.01

Godin, L., Parrish, R.R., Brown, R.L., Hodges, K. V., 2001. Crustal thickening leading to exhumation of the Himalayan metamorphic core of Central Nepal: Insight from U-Pb geochronology and 40Ar/39Ar thermochronology. Tectonics 20, 729–747. https://doi.org/10.1029/2000TC001204

Gou, Z., Dong, X., Wang, B., 2019. Petrogenesis and Tectonic Implications of the Paiku Leucogranites, Northern Himalaya. J. Earth Sci. 30, 525–534. https://doi.org/10.1007/s12583-019-1219-8

Gou, Z., Zhang, Z., Dong, X., Xiang, H., Ding, H., Tian, Z., Lei, H., 2016. Petrogenesis and tectonic implications of the Yadong leucogranites, southern Himalaya. Lithos 256–257, 300–310. https://doi.org/10.1016/j.lithos.2016.04.009

Goudie, D., Fisher, C., Hanchar, J., Crowley, J., Ayers, J., 2014. Simultaneous in situ determination of U-Pb and Sm-Nd isotopes in monazite by laser ablation ICP-MS. Geochemistry Geophys. Geosystems 15. https://doi.org/10.1002/2014GC005431

Greenwood, L. V, Argles, T.W., Parrish, R.R., Harris, N.B.W., Warren, C., Hall, W., Mk, M.K., 2016. The geology and tectonics of central Bhutan. https://doi.org/10.1144/jgs2015-031

Grujic, D., 2006. Channel flow and continental collision tectonics: An overview. Geol. Soc. London Spec. Publ. 268, 25–37. https://doi.org/10.1144/GSL.SP.2006.268.01.02

Grujic, D., Casey, M., Davidson, C., Hollister, L., Kündig, R., Pavlis, T., Schmid, S., 1996. Ductile extrusion of the Higher Himalayan Crystalline in Bhutan: Evidence from quartz microfabrics. Tectonophysics 260, 21–43. https://doi.org/10.1016/0040-1951(96)00074-1

Grujic, D., Hollister, L.S., Parrish, R.R., 2002. Himalayan metamorphic sequence as an orogenic channel: Insight from Bhutan. Earth Planet. Sci. Lett. 198, 177–191.

https://doi.org/10.1016/S0012-821X(02)00482-X

GSI, 2012. BRIEFING BOOK, Geological Survey of India.

Guillot, S., Hodges, K., Le Fort, P., Pecher, A., 1994. New constraints on the age of the Manaslu leucogranite: evidence for episodic tectonic denudation in the central Himalayas. Geology 22, 559–562. https://doi.org/10.1130/0091-7613(1994)022<0559:NCOTAO>2.3.CO;2

Guillot, S., Le Fort, P., 1995. Geochemical constraints on the bimodal origin of High Himalayan leucogranites. Lithos 35, 221–234. https://doi.org/10.1016/0024-4937(94)00052-4

Guo, R., Hu, X., Garzanti, E., Lai, W., 2021. Boron isotope composition of detrital tourmaline: A new tool in provenance analysis. Lithos 400–401, 106360. https://doi.org/10.1016/j.lithos.2021.106360

Guo, Z., Wilson, M., 2012. The Himalayan leucogranites: Constraints on the nature of their crustal source region and geodynamic setting. Gondwana Res. 22, 360–376. https://doi.org/10.1016/j.gr.2011.07.027

Halpin, J., Jensen, T., McGoldrick, P., Meffre, S., Berry, R., Everard, J., Calver, C., Thompson, J., Goemann, K., Whittaker, J., 2014. Authigenic monazite and detrital zircon dating from the Proterozoic Rocky Cape Group, Tasmania: Links to the Belt-Purcell Supergroup, North America. Precambrian Res. 250. https://doi.org/10.1016/j.precamres.2014.05.025

Harley, S., Kelly, N., Moeller, A., 2007. Zircon Behaviour and the Thermal Histories of Mountain Chains. Elements 3, 25–30. https://doi.org/10.2113/gselements.3.1.25

Harris, N., 2007. Channel flow and the Himalayan-Tibetan orogen: A critical review. J. Geol. Soc. London. 164, 511–523. https://doi.org/10.1144/0016-76492006-133

Harris, N., Ayres, M., Massey, J., 1995. Geochemistry of granitic melts produced during the incongruent melting of muscovite: implications for the extraction of Himalayan leucogranite magmas. J. Geophys. Res. 100. https://doi.org/10.1029/94jb02623

Harris, N.B.W., Caddick, M., Kosler, J., Goswami, S., Vance, D., Tindle, A.G., 2004. The pressure-temperature-time path of migmatites from the Sikkim Himalaya. J. Metamorph. Geol. 22, 249–264. https://doi.org/10.1111/j.1525-1314.2004.00511.x

Harris, N.B.W., Pearce, J.A., Tindle, A.G., 1986. Geochemical characteristics of collision-zone magmatism. Geol. Soc. Spec. Publ. 19, 67–81. https://doi.org/10.1144/GSL.SP.1986.019.01.04

Harrison, T., Lovera, O., Grove, M., 1997. New insights into the origin of two contrasting Himalayan granite belts. Geology 25. https://doi.org/10.1130/0091-7613(1997)025<0899:NIITOO>2.3.CO;2

Harrison, T.M., Grove, M., McKeegan, K.D., Coath, C.D., Lovera, O.M., Le Fort, P., 1999. Origin and episodic emplacement of the Manaslu intrusive complex, Central Himalaya. J. Petrol. 40, 3–19. https://doi.org/10.1093/petroj/40.1.3

Harrison, T.M., McKeegan, K.D., LeFort, P., 1995. Detection of inherited monazite in the Manaslu leucogranite by 208Pb232Th ion microprobe dating: Crystallization age and tectonic implications. Earth Planet. Sci. Lett. 133, 271–282. https://doi.org/10.1016/0012-821X(95)00091-P

Hawthorne, F.C., Henrys, D.J., 1999. Classification of the minerals of the tourmaline group. Eur. J. Mineral. 11, 201–216. https://doi.org/10.1127/ejm/11/2/0201

He, S.X., Liu, X.C., Yang, L., Wang, J.M., Hu, F.Y., Wu, F.Y., 2021. Multistage magmatism recorded in a single gneiss dome: Insights from the Lhagoi Kangri leucogranites, Himalayan orogen. Lithos 398–399. https://doi.org/10.1016/j.lithos.2021.106222

He, X., Tan, S., Zhou, J., Liu, Z., Zhao, Z., Yang, S., Zhang, Y., 2020. Identifying the leucogranites in the Ailaoshan-Red River shear zone: Constraints on the timing of the southeastward expansion of the Tibetan Plateau. Geosci. Front. 11, 765–781. https://doi.org/10.1016/j.gsf.2019.07.008

Healy, B., Collins, W.J., Richards, S.W., 2004. A hybrid origin for Lachlan S-type granites: the Murrumbidgee Batholith example. Lithos 78, 197–216. https://doi.org/https://doi.org/10.1016/j.lithos.2004.04.047

Heaman, L.M., Bowins, R., Crocket, J., 1990. The chemical composition of igneous zircon suites: implications for geochemical tracer studies. Geochim. Cosmochim. Acta 54, 1597–1607. https://doi.org/https://doi.org/10.1016/0016-7037(90)90394-Z

Henderson, A., Najman, Y., Parrish, R., Mark, D., Foster, G., 2011. Constraints to the timing of India–Eurasia collision; a re-evaluation of evidence from the Indus Basin sedimentary rocks of the Indus–Tsangpo Suture Zone, Ladakh, India. Earth-Science Rev. 106, 265–292. https://doi.org/10.1016/j.earscirev.2011.02.006

Henry, D.J., Dutrow, B.., 1996. Metamorphic tourmaline and its petrologic applications. In: Grew, E.S., Anovitz, L.M. (Eds.), Boron: Mineralogy, Petrology and Geochemistry: Reviews in Mineralogy 503–557.

Henry, D., Dutrow, B., 2012. Tourmaline at diagenetic to low-grade metamorphic conditions: Its petrologic applicability. Lithos 154, 16–32. https://doi.org/10.1016/j.lithos.2012.08.013

Henry, D.J., Dutrow, B.L., 2018. Tourmaline studies through time: Contributions to scientific advancements. J. Geosci. (Czech Republic) 63, 77–98. https://doi.org/10.3190/jgeosci.255

Henry, D.J., Guidotti, C. V., 1985. Tourmaline as a petrogenetic indicator mineral: an example from the staurolite-grade metapelites of NW Maine. Am. Mineral. 70, 1–15.

Henry, D.J., Novák, M., Hawthorne, F.C., Ertl, A., Dutrow, B.L., Uher, P., Pezzotta, F., 2011. Nomenclature of the tourmaline-supergroup minerals. Am. Mineral. 96, 895–913. https://doi.org/10.2138/am.2011.3636

Hinsberg, V., Henry, D., Marschall, H., 2011. Tourmaline: An ideal indicator of its host environment. Can. Mineral. 49, 1–16. https://doi.org/10.3749/canmin.49.1.1

Hodges, K., Parrish, R., Housh, T., Lux, D., Burchfiel, B., Royden, L., Chen, Z., 1992.

Simultaneous Miocene Extension and Shortening in the Himalayan Orogen. Science 258, 1466–1470. https://doi.org/10.1126/science.258.5087.1466

Hodges, K., Parrish, R., Searle, M., 1996. Tectonic evolution of the Central Annapurna Range, Nepalese Himalayas. Tectonics 15, 1264–1291. https://doi.org/10.1029/96TC01791

Hodges, K. V., 2000. Tectonics of the Himalaya and Southern Tibet from two perspectives. Bull. Geol. Soc. Am. 112, 324–350. https://doi.org/10.1130/0016-7606(2000)112<324:TOTHAS>2.0.CO;2

Holder, R.M., Yakymchuk, C., Viete, D.R., 2020. Accessory Mineral Eu Anomalies in Suprasolidus Rocks: Beyond Feldspar. Geochemistry, Geophys. Geosystems 21. https://doi.org/10.1029/2020GC009052

Hopkinson, T., Harris, N., Roberts, N.M.W., Warren, C.J., Hammond, S., Spencer, C.J., Parrish, R.R., 2020. Evolution of the melt source during protracted crustal anatexis: An example from the Bhutan Himalaya. Geology 48, 87–91. https://doi.org/10.1130/G47078.1

Hopkinson, T.N., 2016. Geochemical Insights into Crustal Melting in the Geochemical insights into crustal melting in the Bhutan Himalaya. https://doi.org/10.21954/ou.ro.0000bd2e

Hopkinson, T.N., Harris, N.B.W., Warren, C.J., Spencer, C.J., Roberts, N.M.W., Horstwood, M.S.A., Parrish, R.R., EIMF, 2017. The identification and significance of pure sediment-derived granites. Earth Planet. Sci. Lett. 467, 57–63. https://doi.org/10.1016/j.epsl.2017.03.018

Hoskin, P., Ireland, T., 2000. Rare earth chemistry of zircon and its use as a provenance indicator. Geology 28, 627. https://doi.org/10.1130/0091-7613(2000)28<627:REECOZ>2.0.CO;2

Hoskin, P., Schaltegger, U., 2003. The Composition of Zircon and Igneous and Metamorphic Petrogenesis. Rev. Mineral. Geochemistry - REV Miner. GEOCHEM 53, 27–62. https://doi.org/10.2113/0530027

Hoskin, P.W.O., 2005. Trace-element composition of hydrothermal zircon and the alteration of Hadean zircon from the Jack Hills, Australia. Geochim. Cosmochim. Acta 69, 637–648. https://doi.org/https://doi.org/10.1016/j.gca.2004.07.006

Hou, G., Santosh, M., Qian, X., Lister, G.S., Li, J., 2008. Configuration of the Late Paleoproterozoic supercontinent Columbia : Insights from radiating mafic dyke swarms. Gondwana Res. 14, 395–409. https://doi.org/10.1016/j.gr.2008.01.010

Hou, Z.Q., Zheng, Y.C., Zeng, L. Sen, Gao, L.E., Huang, K.X., Li, W., Li, Q.Y., Fu, Q., Liang, W., Sun, Q.Z., 2012. Eocene-Oligocene granitoids in southern Tibet: Constraints on crustal anatexis and tectonic evolution of the Himalayan orogen. Earth Planet. Sci. Lett. 349–350, 38–52. https://doi.org/10.1016/j.epsl.2012.06.030

Hu, G., Zeng, L., Gao, L.-E., Liu, Q., Chen, H., Guo, Y., 2018. Diverse magma sources for the Himalayan leucogranites: Evidence from B-Sr-Nd isotopes. Lithos 314–315, 88–99. https://doi.org/https://doi.org/10.1016/j.lithos.2018.05.022

Huang, C., Zhao, Z., Li, G., Zhu, D.C., Liu, D., Shi, Q., 2017. Leucogranites in Lhozag,

southern Tibet: Implications for the tectonic evolution of the eastern Himalaya. Lithos 294–295, 246–262. https://doi.org/10.1016/j.lithos.2017.09.014

Inger, S., Harris, N., 1993. Geochemical constraints on leucogranite magmatism in the Langtang Valley, Nepal Himalaya. J. Petrol. 34, 345–368. https://doi.org/10.1093/petrology/34.2.345

Irvine, T., Baragar, W., 1971. A Guide to the Chemical Classification of the Common Volcanic Rocks. Can. J. Earth Sci. - CAN J EARTH SCI 8, 523–548. https://doi.org/10.1139/e71-055

Islam, R., Ahmad, T., Khanna, P.P., 2005. An overview on the granitoids of the NW Himalaya. Himal. Geol. 26, 49–60.

Itano, K., Ueki, K., Iizuka, T., Kuwatani, T., 2020. Geochemical discrimination of monazite source rock based on machine learning techniques and multinomial logistic regression analysis. Geosci. 10. https://doi.org/10.3390/geosciences10020063

Jain, A.K., Ahmad, T., Singh, S., Ghosh, S.K., Patel, R.C., Kumar, R., Agarwal, K.K., Perumal, J., Islam, R., Bhargava, O.N., 2012. Evolution of the Himalaya. Proc. Indian Natl. Sci. Acad. 78, 259–275.

Jamieson, R.A., Beaumont, C., Nguyen, M.H., Grujic, D., 2006. Provenance of the Greater Himalayan Sequence and associated rocks: Predictions of channel flow models. Geol. Soc. Spec. Publ. 268, 165–182. https://doi.org/10.1144/GSL.SP.2006.268.01.07

Ji, M., Gao, X.Y., Zheng, Y.F., 2022. Geochemical evidence for partial melting of progressively varied crustal sources for leucogranites during the Oligocene–Miocene in the Himalayan orogen. Chem. Geol. 589, 120674. https://doi.org/10.1016/j.chemgeo.2021.120674

Ji, W.-Q., Wu, F.-Y., Chung, S.-L., Liu, C.-Z., 2012. Identification of Early Carboniferous Granitoids from Southern Tibet and Implications for Terrane Assembly Related to the Paleo-Tethyan Evolution. J. Geol. 120, 531–541. https://doi.org/10.1086/666742

Jiang, S.-Y., Palmer, M.R., 1998. Boron isotope systematics of tourmaline from granites and pegmatites: a synthesis. Eur. J. Mineral. 10, 1253–1266. https://doi.org/10.1127/ejm/10/6/1253

Kasemann, S., Erzinger, J., Franz, G., 2000. Boron recycling in the continental crust of the Central Andes from the Palaeozoic to Mesozoic, NW Argentina. Contrib. to Mineral. Petrol. 140, 328–343. https://doi.org/10.1007/s004100000189

Kawakami, T., Aoya, M., Wallis, S.R., Lee, J., Terada, K., Wang, Y., Heizler, M., 2007. Contact metamorphism in the Malashan dome, North Himalayan gneiss domes, southern Tibet: An example of shallow extensional tectonics in the Tethys Himalaya. J. Metamorph. Geol. 25, 831–853. https://doi.org/10.1111/j.1525-1314.2007.00731.x

Kellett, D., Grujic, D., Mottram, C., Mukul, M., 2014. Virtual field guide for the darjeeling-sikkim himalaya, India. J. Virtual Explor. 47. https://doi.org/10.3809/jvirtex.2014.00344

Kellett, D.A., Cottle, J.M., Larson, K.P., 2019. The South Tibetan detachment system: History, advances, definition and future directions. Geol. Soc. Spec. Publ. 483, 377–400. https://doi.org/10.1144/SP483.2

Kellett, D.A., Grujic, D., Coutand, I., Cottle, J., Mukul, M., 2013. The South Tibetan detachment system facilitates ultra rapid cooling of granulite-facies rocks in Sikkim Himalaya. Tectonics 32, 252–270. https://doi.org/10.1002/tect.20014

King, J., Harris, N., Argles, T., Parrish, R., Zhang, H., 2011. Contribution of crustal anatexis to the tectonic evolution of Indian crust beneath Southern Tibet. Bull. Geol. Soc. Am. 123, 218–239. https://doi.org/10.1130/B30085.1

Kohn, M., 2008. P-T-t data from central Nepal support critical taper and repudiate larger scale channel flow of the Great Himalayan Sequence. Geol. Soc. Am. Bull. - GEOL SOC AMER BULL 120. https://doi.org/10.1130/B26252.1

Kohn, M., Corrie, S., 2011. Preserved Zr-temperatures and U–Pb ages in high-grade metamorphic titanite: Evidence for a static hot channel in the Himalayan orogen. Earth Planet. Sci. Lett. 311, 136–143. https://doi.org/10.1016/j.epsl.2011.09.008

Kohn, M.J., Paul, S.K., Corrie, S.L., 2010. The lower lesser himalayan sequence: A paleoproterozoic arc on the northern margin of the Indian plate. Bull. Geol. Soc. Am. 122, 323–335. https://doi.org/10.1130/B26587.1

Kohn, M.J., Wieland, M.S., Parkinson, C.D., Upreti, B.N., 2005. Five generations of monazite in Langtang gneisses: Implications for chronology of the Himalayan metamorphic core. J. Metamorph. Geol. 23, 399–406. https://doi.org/10.1111/j.1525-1314.2005.00584.x

Konrad-Schmolke, M., Halama, R., 2014. Combined thermodynamic-geochemical modeling in metamorphic geology: Boron as tracer of fluid-rock interaction. Lithos 208–209, 393–414. https://doi.org/10.1016/j.lithos.2014.09.021

Larson, K., Cottle, J., Godin, L., 2011. Petrochronologic record of metamorphism and melting in the upper greater Himalayan sequence, Manaslu- Himal Chuli Himalaya, West-Central Nepal. Lithosphere 3, 379–392. https://doi.org/10.1130/L149.1

Laurent, O., Martin, H., Moyen, J.-F., Doucelance, R., 2014. The diversity and evolution of late- Archean granites:Evidence for the onset of a “modern-style” platetectonics between 3.0 and 2.5 Ga. Lithos 205, 208-235. https://doi.org/10.1016/j.lithos.201.

Le Fort, P., 1975. Himalayas: the collided range. Present knowledge of the continental arc. Am. J. Sci. 275, 1–44.

Le Fort, P., Cuney, M., Deniel, C., France-Lanord, C., Sheppard, S.M.F., Upreti, B.N., Vidal, P., 1987. Crustal generation of the Himalayan leucogranites. Tectonophysics 134, 39–57. https://doi.org/10.1016/0040-1951(87)90248-4

Lederer, G.W., Cottle, J.M., Jessup, M.J., Langille, J.M., Ahmad, T., 2013. Timescales of partial melting in the Himalayan middle crust: Insight from the Leo Pargil dome, northwest India. Contrib. to Mineral. Petrol. 166, 1415–1441. https://doi.org/10.1007/s00410-013-0935-9

Lee, J., Whitehouse, M.J., 2007. Onset of mid-crustal extensional flow in southern

Tibet: Evidence from U/Pb zircon ages. Geology 35, 45–48. https://doi.org/10.1130/G22842A.1

Lei, R., Wu, C., Chi, G., Gu, L., 2013. Journal of Asian Earth Sciences The Neoproterozoic Hongliujing A-type granite in Central Tianshan (NW China): LA-ICP-MS zircon U – Pb geochronology , geochemistry , Nd – Hf isotope and tectonic significance. J. Asian Earth Sci. 74, 142–154. https://doi.org/10.1016/j.jseaes.2013.03.025

Li, G.-J., Qingfei, W., Huang, Y.-H., Gao, L., Yu, L., 2015. Petrogenesis of middle Ordovician peraluminous granites in the Baoshan block: Implications for the early Paleozoic tectonic evolution along East Gondwana. Lithos 245. https://doi.org/10.1016/j.lithos.2015.10.012

Li, Z.X., Bogdanova, S. V., Collins, A.S., Davidson, A., De Waele, B., Ernst, R.E., Fitzsimons, I.C.W., Fuck, R.A., Gladkochub, D.P., Jacobs, J., Karlstrom, K.E., Lu, S., Natapov, L.M., Pease, V., Pisarevsky, S.A., Thrane, K., Vernikovsky, V., 2008. Assembly, configuration, and break-up history of Rodinia: A synthesis. Precambrian Res. 160, 179–210. https://doi.org/10.1016/j.precamres.2007.04.021

Liew, T.C., Hofmann, A.W., 1988. Precambrian crustal components, plutonic associations, plate environment of the Hercynian Fold Belt of central Europe: Indications from a Nd and Sr isotopic study. Contrib. to Mineral. Petrol. 98, 129–138. https://doi.org/10.1007/BF00402106

Lin, C., Zhang, J., Wang, X., Putthapiban, P., Zhang, B., Huang, T., 2020. Oligocene initiation of the South Tibetan Detachment System: Constraints from syn-tectonic leucogranites in the Kampa Dome, Northern Himalaya. Lithos 354–355, 105332.

Liu, J.H., Xie, C.M., Li, C., Wang, M., Wu, H., Li, X.K., Liu, Y.M., Zhang, T.Y., 2018. Early Carboniferous adakite-like and I-type granites in central Qiangtang, northern Tibet: Implications for intra-oceanic subduction and back-arc basin formation within the Paleo-Tethys Ocean. Lithos 296–299, 265–280. https://doi.org/10.1016/j.lithos.2017.11.005

Liu, Z.C., Wu, F.Y., Ding, L., Liu, X.C., Wang, J.G., Ji, W.Q., 2016. Highly fractionated Late Eocene (~ 35 Ma) leucogranite in the Xiaru Dome, Tethyan Himalaya, South Tibet. Lithos 240–243, 337–354. https://doi.org/10.1016/j.lithos.2015.11.026

Liu, Z.C., Wu, F.Y., Ji, W.Q., Wang, J.G., Liu, C.Z., 2014. Petrogenesis of the Ramba leucogranite in the Tethyan Himalaya and constraints on the channel flow model. Lithos 208, 118–136. https://doi.org/10.1016/j.lithos.2014.08.022

Liu, Z.C., Wu, F.Y., Qiu, Z.L., Wang, J.G., Liu, X.C., Ji, W.Q., Liu, C.Z., 2017. Leucogranite geochronological constraints on the termination of the South Tibetan Detachment in eastern Himalaya. Tectonophysics 721, 106–122. https://doi.org/10.1016/j.tecto.2017.08.019

Loiselle, M.C. and Wones, D.R. (1979), 1979. No Title. Charact. Anorogenic Granites. Geol. Soc. Am. Abstr. with Programs, 468.

London, D., 2018. Ore-forming processes within granitic pegmatites. Ore Geol. Rev. 101, 349–383. https://doi.org/10.1016/j.oregeorev.2018.04.020

London, D., Morgan, G.B., 2012. The pegmatite puzzle. Elements 8, 263–268. https://doi.org/10.2113/gselements.8.4.263

Lv, Z.H., Zhang, H., Tang, Y., 2021. Anatexis origin of rare metal/earth pegmatites: Evidences from the Permian pegmatites in the Chinese Altai. Lithos 380–381, 105865. https://doi.org/10.1016/j.lithos.2020.105865

Ma, L., Kerr, A., Wang, Q., Jiang, Z.-Q., Hu, W.-L., 2017a. Early Cretaceous (~ 140 Ma) aluminous A-type granites in the Tethyan Himalaya, Tibet: Products of crust-mantle interaction during lithospheric extension. Lithos 300. https://doi.org/10.1016/j.lithos.2017.11.023

Ma, L., Wang, Q., Kerr, A.C., Yang, J.H., Xia, X.P., Ou, Q., Yang, Z.Y., Sun, P., 2017b. Paleocene (c. 62 Ma) leucogranites in Southern Lhasa, Tibet: Products of syn-collisional crustal anatexis during slab roll-back? J. Petrol. 58, 2089–2114. https://doi.org/10.1093/petrology/egy001

Maner, J.L., London, D., 2017. The boron isotopic evolution of the Little Three pegmatites, Ramona, CA. Chem. Geol. 460, 70–83. https://doi.org/10.1016/j.chemgeo.2017.04.016

Marschall, H.R., Ludwig, T., Altherr, R., Kalt, A., Tonarini, S., 2006. Syros metasomatic tourmaline: Evidence for very high-δ11 B fluids in subduction zones. J. Petrol. 47, 1915–1942. https://doi.org/10.1093/petrology/egl031

Martin, A.J., 2017. A review of definitions of the Himalayan Main Central Thrust. Int. J. Earth Sci. 106, 2131–2145. https://doi.org/10.1007/s00531-016-1419-8

Matin, A., Mukul, M., 2010. Phases of deformation from cross-cutting structural relationships in external thrust sheets : insights from small-scale structures in the Ramgarh thrust sheet , Darjiling Himalaya , West Bengal.

McDonough, W.F., Sun, S. s., 1995. The composition of the Earth. Chem. Geol. 120, 223–253. https://doi.org/10.1016/0009-2541(94)00140-4

McQuarrie, N., Long, S.P., Tobgay, T., Nesbit, J.N., Gehrels, G., Ducea, M.N., 2013. Documenting basin scale, geometry and provenance through detrital geochemical data: Lessons from the Neoproterozoic to Ordovician Lesser, Greater, and Tethyan Himalayan strata of Bhutan. Gondwana Res. 23, 1491–1510. https://doi.org/10.1016/j.gr.2012.09.002

Middlemost, E.A.K., 1994. Naming materials in the magma/igneous rock system. Earth Sci. Rev. 37, 215–224. https://doi.org/10.1016/0012-8252(94)90029-9

Miller, C., Stoddard, E., Bradfish, L., Dollase, W., 1981. Composition of plutonic muscovite: Genetic implications. Can. Mineral. 19, 25–34.

Miller, C.F., McDowell, S.M., Mapes, R.W., 2003. Hot and cold granites: Implications of zircon saturation temperatures and preservation of inheritance. Geology 31, 529–532. https://doi.org/10.1130/0091-7613(2003)031<0529:HACGIO>2.0.CO;2

Miyashiro, A., 1974. Volcanic rock series in island arcs and active continental margins. Am. J. Sci. 274, 321–355. https://doi.org/10.2475/ajs.274.4.321

Montel, J.M., 1993. A model for monazite/melt equilibrium and application to the

generation of granitic magmas. Chem. Geol. 110, 127–146. https://doi.org/10.1016/0009-2541(93)90250-M

Mottram, C.M., Argles, T.W., Harris, N.B.W., Parrish, R.R., Horstwood, M.S.A., Warren, C.J., Gupta, S., 2014a. Tectonic interleaving along the Main Central Thrust, Sikkim Himalaya. J. Geol. Soc. London. 171, 255–268. https://doi.org/10.1144/jgs2013-064

Mottram, C.M., Parrish, R.R., Regis, D., Warren, C.J., Argles, T.W., Harris, N.B.W., Roberts, N.M.W., 2015. Using U-Th-Pb petrochronology to determine rates of ductile thrusting: Time windows into the Main Central Thrust, Sikkim Himalaya. Tectonics 34, 1355–1374. https://doi.org/10.1002/2014TC003743

Mottram, C.M., Warren, C.J., Regis, D., Roberts, N.M.W., Harris, N.B.W., Argles, T.W., Parrish, R.R., 2014b. Developing an inverted barrovian sequence; insights from monazite petrochronology. Earth Planet. Sci. Lett. 403, 418–431. https://doi.org/10.1016/j.epsl.2014.07.006

Moyen, J.F., Janoušek, V., Laurent, O., Bachmann, O., Jacob, J.B., Farina, F., Fiannacca, P., Villaros, A., 2021. Crustal melting vs. fractionation of basaltic magmas: Part 1, granites and paradigms. Lithos 402–403. https://doi.org/10.1016/j.lithos.2021.106291

Moyen, J.F., Laurent, O., Chelle-Michou, C., Couzinié, S., Vanderhaeghe, O., Zeh, A., Villaros, A., Gardien, V., 2017. Collision vs. subduction-related magmatism: Two contrasting ways of granite formation and implications for crustal growth. Lithos 277, 154–177. https://doi.org/10.1016/j.lithos.2016.09.018

Mukul, M., 2010. First-order kinematics of wedge-scale active Himalayan deformation: Insights from Darjiling-Sikkim-Tibet (DaSiT) wedge. J. Asian Earth Sci. 39, 645–657. https://doi.org/10.1016/j.jseaes.2010.04.029

Mukul, M., 2000. The geometry and kinematics of the Main Boundary Thrust and related neotectonics in the Darjiling Himalayan fold-and-thrust belt, West Bengal, India. J. Struct. Geol. 22, 1261–1283. https://doi.org/10.1016/S0191-8141(00)00032-8

Murphy, M.A., Harrison, T.M., 1999. Relationship between leucogranites and the Qomolangma detachment in the Rongbuk Valley, south Tibet. Geology 27, 831–834. https://doi.org/10.1130/0091-7613(1999)027<0831:RBLATQ<2.3.CO;2

Myrow, P.M., Hughes, N.C., Ryan McKenzie, N., Pelgay, P., Thomson, T.J., Haddad, E.E., Mark Fanning, C., 2016. Cambrian-Ordovician orogenesis in Himalayan equatorial Gondwana. Bull. Geol. Soc. Am. 128, 1679–1695. https://doi.org/10.1130/B31507.1

Nabelek, P.I., 2019. Geological Society, London, Special Publications.

Nabelek, P.I., Liu, M., 2004. Petrologic and thermal constraints on the origin of leucogranites in collisional orogens. Trans. R. Soc. Edinburgh, Earth Sci. 95, 73–85. https://doi.org/10.1017/s0263593300000936

Nachit, H., Ibhi, A., Abia, E., Ohoud, M., 2005. Discrimination between primary magmatic biotites, reequilibrated biotites and neoformed biotites. Comptes Rendus Geosci. 337, 1415–1420. https://doi.org/10.1016/j.crte.2005.09.002

Nakano, T., Nakamura, E., 2001. Boron isotope geochemistry of metasedimentary rocks and tourmalines in a subduction zone metamorphic suite 127, 233–252.

Nebel, O., 2013. Encyclopedia of Scientific Dating Methods. Encycl. Sci. Dating Methods 1–19. https://doi.org/10.1007/978-94-007-6326-5

Nelson, K.D., Zhao, W., Brown, L.D., Kuo, J., Che, J., Liu, X., Klemperer, S.L., Makovsky, Y., Meissner, R., Mechie, J., Kind, R., Wenzel, F., Ni, J., Nabelek, J., Chen, L., Tan, H., Wei, W., Jones, A.G., Booker, J., Unsworth, M., Kidd, W.S.F., Hauck, M., Alsdorf, D., Ross, A., Cogan, M., Wu, C., Sandvol, E., Edwards, M., 1996. Partially molten middle crust beneath southern Tibet: Synthesis of project INDEPTH results. Science (80-.). 274, 1684–1685. https://doi.org/10.1126/science.274.5293.1684

Neogi, S., Dasgupta, S., Fukuoka, M., 1998. High P-T polymetamorphism, dehydration melting, and generation of migmatites and granites in the Higher Himalayan Crystalline Complex, Sikkim, India. J. Petrol. 39, 61–99. https://doi.org/10.1093/petroj/39.1.61

Noble, S.R., Searle, M.P., 1995. Age of crustal melting and leucogranite formation from U-Pb zircon and monazite dating in the western Himalaya, Zanskar, India. Geology 23, 1135–1138. https://doi.org/10.1130/0091-7613(1995)023<1135:AOCMAL>2.3.CO;2

O'Connor, J.T., 1965. A classification of quartz-rich igneous rocks based on feldspar ratio. United States Geol. Surv. Prof. Pap. 525-B, 79–84.

Palin, R.M., Treloar, P.J., Searle, M.P., Wald, T., White, R.W., Mertz-Kraus, R., 2018. U-Pb monazite ages from the Pakistan Himalaya record pre-Himalayan Ordovician orogeny and Permian continental breakup. Bull. Geol. Soc. Am. 130, 2047–2061. https://doi.org/10.1130/B31943.1

Parui, C., Bhattacharyya, K., 2018. Duplex and along-strike structural variation: A case study from Sikkim Himalayan fold thrust belt. J. Struct. Geol. 113, 62–75. https://doi.org/10.1016/j.jsg.2018.05.017

Patiño Douce, A.E., 1999. What do experiments tell us about the relative contributions of crust and mantle to the origin of granitic magmas? Geol. Soc. Spec. Publ. 168, 55–75. https://doi.org/10.1144/GSL.SP.1999.168.01.05

Patiño Douce, A.E., Harris, N., 1998. Experimental constraints on Himalayan anatexis. J. Petrol. 39, 689–710. https://doi.org/10.1093/petroj/39.4.689

Patriat, P., Achache, J., 1984. India–Eurasia collision chronology has implications for crustal shortening and driving mechanism of plates. Nature 311, 615–621. https://doi.org/10.1038/311615a0

Paul, D.K., Chandy, K.C., Bhalla, J.K., Prasad, R., Sengupta, N.R., 1982. Geochronology and geochemistry of Lingtse Gneiss, Darjelling- Sikkim, Himalaya. Indian J. Earth Sci. 9, 11–17.

Paul, D.K., Mcnaughton, N.J., Chattopadhyay, S., Ray, K.K., 1996. Geochronology and geochemistry of the Lingtse Gneiss, Darjeeling - Sikkim Himalaya : Revisited. J. Geol. Soc. India 48, 497–506.

Pearce, J.A., Harris, N.B.W., Tindle, A.G., 1984. Trace element discrimination

diagrams for the tectonic interpretation of granitic rocks. J. Petrol. 25, 956–983. https://doi.org/10.1093/petrology/25.4.956

Peccerillo, S.K.O., 1976. SiO 2 K 2 O plot Peccerillo and Taylor 1976.

Pelleter, E., Cheilletz, A., Gasquet, D., Mouttaqi, A., Annich, M., Hakour, A., Deloule, E., Féraud, G., 2007. Hydrothermal zircons: A tool for ion microprobe U–Pb dating of gold mineralization (Tamlalt–Menhouhou gold deposit — Morocco). Chem. Geol. 245, 135–161. https://doi.org/10.1016/j.chemgeo.2007.07.026

Pettke, T., Audétat, A., Schaltegger, U., Heinrich, C.A., 2005. Magmatic-to-hydrothermal crystallization in the W–Sn mineralized Mole Granite (NSW, Australia): Part II: Evolving zircon and thorite trace element chemistry. Chem. Geol. 220, 191–213. https://doi.org/https://doi.org/10.1016/j.chemgeo.2005.02.017

Phukon, P., Sen, K., Srivastava, H.B., Singhal, S., Sen, A., 2018. U-Pb geochronology and geochemistry from the Kumaun Himalaya, NW India, reveal Paleoproterozoic arc magmatism related to formation of the Columbia supercontinent. Bull. Geol. Soc. Am. 130, 1164–1176. https://doi.org/10.1130/B31866.1

Pupin, J.P., 1980. Zircon and granite petrology. Contrib. to Mineral. Petrol. 73, 207–220. https://doi.org/10.1007/BF00381441

Raina, V. K. and Bhattacharya, U., 1962. Report on geological mapping in parts of northern and eastern Sikkim in sheet nos. 78A/NE & SE. Unpub. Report, G.S.I. (FS 1961-62). Raina, V.

Raina and Bhattacharya, 1965. Report on geological mapping in parts of north Sikkim (78A/NW, A/NE). Unpub. Report, GSI.

Rapp, R., Watson, E., 1986. Monazite solubility and dissolution kinetics: implications for the thorium and light rare earth chemistry of felsic magmas. Contrib. to Mineral. Petrol. 94, 304–316. https://doi.org/10.1007/BF00371439

Ray, S., 1976. Data for interpreting crustal tectonics in India. Misc. Pub. Geol. Surv. India , 34 (1), 75–83.

Ray, S.K., Neogi, S., 2011. Extent and analogues of the rangit window in the sikkim himalaya. Indian J. Geosci. 65, 275–286.

Rex, A.J., Searle, M.P., Tirrul, R., Crawford, M.B., Prior, D.J., Rex, D.C., Barnicoat, A., B., J.-M., 1988., 1998. The geochemical and tectonic evolution of the central Karakoram, north Pakistan. Philos. Trans. R. Soc. London, Series A 3, 229–255.

Richards, A., Argles, T., Harris, N., Parrish, R., Ahmad, T., Darbyshire, F., Draganits, E., 2005. Himalayan architecture constrained by isotopic tracers from clastic sediments. Earth Planet. Sci. Lett. 236, 773–796. https://doi.org/10.1016/j.epsl.2005.05.034

Richards, A., Parrish, R., Harris, N.B.W., Argles, T., Zhang, L., 2006. Correlation of lithotectonic units across the eastern Himalay, Bhutan. Geology 34, 341–344. https://doi.org/10.1130/G22169.1

Rogers, J.J.W., Santosh, M., 2002. Configuration of Columbia , a Mesoproterozoic Supercontinent 5–22.

Rollinson, H.R., 1993. Using geochemical data: evaluation. Present. Interpret. 796, 317–343.

Roy, & Purohit, R., 2018. Indian Shield: Precambrian Evolution and Phanerozoic Reconstitution, (1st ed.). ed. Elsevier.

Rubatto, D., Chakraborty, S., Dasgupta, S., 2013. Timescales of crustal melting in the Higher Himalayan Crystallines (Sikkim, Eastern Himalaya) inferred from trace element-constrained monazite and zircon chronology. Contrib. to Mineral. Petrol. 165, 349–372. https://doi.org/10.1007/s00410-012-0812-y

Rudnick, R., Fountain, D., 1995. Nature and Composition of the Continental-Crust—a Lower Crustal Perspective. Rev. Geophys. - REV Geophys 33. https://doi.org/10.1029/95RG01302

Rudnick, R., Gao, S., 2003. Composition of the Continental Crust. Treatise Geochem 3:1-64. Treatise on Geochemistry 3, 1–64. https://doi.org/10.1016/B0-08-043751-6/03016-4

Sachan, H.K., Kohn, M.J., Saxena, A., Corrie, S.L., 2010. The Malari leucogranite, Garhwal Himalaya, Northern India: Chemistry, age, and tectonic implications. Bull. Geol. Soc. Am. 122, 1865–1876. https://doi.org/10.1130/B30153.1

Saha, D., 2013. Lesser Himalayan sequences in Eastern Himalaya and their deformation: Implications for Paleoproterozoic tectonic activity along the northern margin of India. Geosci. Front. 4, 289–304. https://doi.org/10.1016/j.gsf.2013.01.004

Schärer, U., Hamet, J., Allègre, C.J., 1984. The Transhimalaya (Gangdese) plutonism in the Ladakh region: a UPb and RbSr study. Earth Planet. Sci. Lett. 67, 327–339. https://doi.org/10.1016/0012-821X(84)90172-9

Schärer, U., Xu, R.H., Allègre, C.J., 1986. U(Th)Pb systematics and ages of Himalayan leucogranites, South Tibet. Earth Planet. Sci. Lett. 77, 35–48. https://doi.org/10.1016/0012-821X(86)90130-5

Schelling, D., Arita, K., 1991. Thrust tectonics , Crustal shortening , and the Structure Schelling 1 and Kazunori Arita the last 20 years the techniques of restoring and balancing structural sections has led to an increased understanding of the structural geometry of compreszional terr. Tectonics 10, 851–862.

Schneider, D. A., Zeitler, P. K., Edwards, M. A., and Kidd, W.S.F., 1997. Geochronologic constraints on the geometry and timing of anatexis and exhumation at Nanga Parbat: A Prog. Rep. Eos (Transactions, Am. Geophys. Union), 78, 111.

Schneider, D., Zeitler, P., Kidd, W., Edwards, M.A., 2001. Geochronologic Constraints on the Tectonic Evolution and Exhumation of Nanga Parbat, Western Himalaya Syntaxis, Revisited. J. Geol. 109. https://doi.org/10.1086/322764

Schneider, D.A., Edwards, M.A., Kidd, W.S.F., Asif Khan, M., Seeber, L., Zeitler, P.K., 1999. Tectonics of Nanga Parbat, western Himalaya: Synkinematic plutonism within the doubly vergent shear zones of a crustal-scale pop-up structure. Geology 27, 999–1002. https://doi.org/10.1130/0091-7613(1999)027<0999:TONPWH>2.3.CO;2

Schulz, B., 2021. Monazite Microstructures and Their Interpretation in Petrochronology. Front. Earth Sci. 9, 1–22. https://doi.org/10.3389/feart.2021.668566

Searle, M., 2010. Low-angle normal faults in the compressional Himalayan orogen; Evidence from the Annapurna-Dhaulagiri Himalaya, Nepal. Geosphere 6, 296–315. https://doi.org/10.1130/GES00549.1

Searle, M.P., 2015. Mountain Building, Tectonic Evolution, Rheology, and Crustal Flow in the Himalaya, Karakoram, and Tibet, Treatise on Geophysics: Second Edition. Elsevier B.V. https://doi.org/10.1016/B978-0-444-53802-4.00121-4

Searle, M.P., Cottle, J.M., Streule, M.J., Waters, D.J., 2009. Crustal melt granites and migmatites along the Himalaya: Melt source, segregation, transport and granite emplacement mechanisms. Earth Environ. Sci. Trans. R. Soc. Edinburgh 100, 219–233. https://doi.org/10.1017/S175569100901617X

Searle, M.P., Godin, L., 2003. The South Tibetan detachment and the Manaslu leucogranite: A structural reinterpretation and restoration of the Annapurna-Manaslu Himalaya, Nepal. J. Geol. 111, 505–523. https://doi.org/10.1086/376763

Searle, M.P., Law, R.D., Godin, L., Larson, K.P., Streule, M.J., Cottle, J.M., Jessup, M.J., 2008. Defining the Himalayan Main Central Thrust in Nepal. J. Geol. Soc. London. 165, 523–534. https://doi.org/10.1144/0016-76492007-081

Searle, M.P., Parrish, R.R., Hodges, K. V., Hurford, A., Ayres, M.W., Whitehouse, M.J., 1997. Shisha Pangma leucogranite, south Tibetan Himalaya: Field relations, geochemistry, age, origin, and emplacement. J. Geol. 105, 295–317. https://doi.org/10.1086/515924

Searle, M.P., Rex, A.J., 1989. Thermal model for the Zanskar Himalaya. J. Metamorph. Geol. 7, 127–134. https://doi.org/10.1111/j.1525-1314.1989.tb00579.x

Searle, M.P., Simpson, R.L., Law, R.D., Parrish, R.R., Waters, D.J., 2003. The structural geometry, metamorphic and magmatic evolution of the Everest massif, High Himalaya of Nepal-South Tibet. J. Geol. Soc. London. 160, 345–366. https://doi.org/10.1144/0016-764902-126

Searle, M.P., Szulc, A.G., 2005. Channel flow and ductile extrusion of the high Himalayan slab-the Kangchenjunga-Darjeeling profile, Sikkim Himalaya. J. Asian Earth Sci. 25, 173–185. https://doi.org/10.1016/j.jseaes.2004.03.004

Shand, S.J., 1943. Eruptive Rocks: Their Genesis, Composition, Classification, and Their Relation to Ore-Deposits, with a Chapter on Meteorites.

Singh, Oinam, G., Chung, S.-L., Rk, B., Lee, H.-Y., Joshi, M., 2021. Magmatism in the Siang window of the Eastern Himalayan Syntaxis, NE India: a vestige of Kerguelen mantle plume activity. Geol. Soc. London Spec. Publ. SP518-2021. https://doi.org/10.1144/SP518-2021-13

Singh, P., Singhal, S., Das, A.N., 2020a. U–Pb (zircon) geochronologic constraint on tectono-magmatic evolution of Chaur granitoid complex (CGC) of Himachal Himalaya, NW India: implications for the Neoproterozoic magmatism related to Grenvillian orogeny and assembly of the Rodinia supercontinent. Int. J. Earth Sci. 109, 373–390. https://doi.org/10.1007/s00531-019-01808-5

Singh, P., Singhal, S., Das, A.N., 2020b. U–Pb (zircon) geochronologic constraint on tectono-magmatic evolution of Chaur granitoid complex (CGC) of Himachal Himalaya, NW India: implications for the Neoproterozoic magmatism related to Grenvillian orogeny and assembly of the Rodinia supercontinent. Int. J. Earth Sci. 109, 373–390. https://doi.org/10.1007/s00531-019-01808-5

Singh, S., 2020. Himalayan Magmatism through space and time. Episodes 43, 358–368. https://doi.org/10.18814/epiiugs/2020/020022

Singh, S., Claesson, S., Jain, A., Sjoberg, H., Gee, D., Manickavasagam, R.M., Andreasson, P.-G., 1994. Geochemistry of the Proterozoic peraluminous granitoids from the Higher Himalayan Crystalline. India. Abstr. Vol. Jour. Geol. Soc. Nepal 10. https://doi.org/10.1080/00144940.1994.11484119

Singh, S., Jain, A.K., 2003. Himalayan granitoids. J. Virtual Explor. 11. https://doi.org/10.3809/jvirtex.2003.00069

Sivakumar, R., Ghosh, S., 2017. Earthquake hazard assessment through geospatial model and development of EaHaAsTo tool for visualization: an integrated geological and geoinformatics approach. Environ. Earth Sci. 76, 1–22. https://doi.org/10.1007/s12665-017-6777-4

Slack, J.F., 1996. Tourmaline associations with hydrothermal ore deposits. Rev. Mineral. 33, 558–643.

Sláma, J., Košler, J., Condon, D., Crowley, J., Gerdes, A., Hanchar, J., Horstwood, M., Morris, G., Nasdala, L., Norberg, N., Schaltegger, U., Schoene, B., Tubrett, M., Whitehouse, M., 2008. Ple??ovice zircon - A new natural reference material for U-Pb and Hf isotopic microanalysis. Chem. Geol. 249, 1–35. https://doi.org/10.1016/j.chemgeo.2007.11.005

Sorcar, N., Hoppe, U., Dasgupta, S., Chakraborty, S., 2014. High-temperature cooling histories of migmatites from the High Himalayan Crystallines in Sikkim, India: Rapid cooling unrelated to exhumation? Contrib. to Mineral. Petrol. 167, 1–34. https://doi.org/10.1007/s00410-013-0957-3

Srikantia, S. V, 1981. The lithostratigraphy, sedimentation and structure of the Proterozoic and Phanerozoic formations of Spiti basin in the Higher Himalaya of H.P. Misc. Publ. Geol. Surv. India 41, 218–228.

Srivastava, P., Mitra, G., 1994. Thrust geometries and deep structure of the Outer and Lesser Himalaya, Kumaon and Garhwal (India): Implications for evolution of the Himalayan fold-and-thrust belt. Tectonics 13, 89–110. https://doi.org/10.1029/93TC01130

Srivastava, T., Joshi, K.B., Wanjari, N., 2022. Boron isotopic composition of pegmatitic tourmaline from Yumthang Valley, North Sikkim, in: Geochemical Treasures and Petrogenetic Processes. https://doi.org/10.1007/978-981-19-4782-7_8

Streckeisen, A.L. (1976), 1976. Classification and Nomenclature of Igneous Rocks. N. Jahrb. Miner. Abh., 144-240.

Streule, M.J., Searle, M.P., Waters, D.J., Horstwood, M.S.A., 2010. Metamorphism, melting, and channel flow in the Greater Himalayan Sequence and Makalu

leucogranite: Constraints from thermobarometry, metamorphic modeling, and U-Pb geochronology. Tectonics 29. https://doi.org/10.1029/2009TC002533

Sun, S.-S., McDonough, W.F., 1989. Chemical and isotopic systematics of oceanic basalts: implications for mantle composition and processes. Geol. Soc. London, Spec. Publ. 42, 313–345.

Sylvester, P.J., 1998. Post-collisional strongly peraluminous granites. Lithos 45, 29–44. https://doi.org/10.1016/S0024-4937(98)00024-3

Taylor, S.R., McLennan, S.M., 1985. The Continental Crust: its Composition and Evolution. An Examination of the Geochemical Record Preserved in Sedimentary Rocks. p. 328.

Thakur, V.C., 1984. Tectonics of the Himalayas and Karakoram conjugation area (Indus-Tsangpo Suture zone) Colloq. Int. Geol. Congr., Moscow 27, 137–152.

Thompson, J.M., Meffre, S., Danyushevsky, L., 2018. Impact of air, laser pulse width and fluence on U-Pb dating of zircons by LA-ICPMS. J. Anal. At. Spectrom. 33, 221–230. https://doi.org/10.1039/c7ja00357a

Tonarini, S., Pennisi, M., Leeman, W.P., 1997. Precise boron isotopic analysis of complex silicate (rock) samples using alkali carbonate fusion and ion-exchange separation. Chem. Geol. 142, 129–137. https://doi.org/10.1016/S0009-2541(97)00087-9

Trumbull, R.B., Beurlen, H., Wiedenbeck, M., Soares, D.R., 2013. The diversity of B-isotope variations in tourmaline from rare-element pegmatites in the Borborema Province of Brazil. Chem. Geol. 352, 47–62. https://doi.org/10.1016/j.chemgeo.2013.05.021

Trumbull, R.B., Slack, J.F., 2018. Boron isotopes in the continental crust: granites, pegmatites, felsic volcanic rocks, and related ore deposits. Adv. Isot. Geochemistry 249–272. https://doi.org/10.1007/978-3-319-64666-4_10

Valdiya, K.S., 1984. Evolution of the Himalaya. Tectonophysics 105, 229–248. https://doi.org/10.1016/0040-1951(84)90205-1

Van Hinsberg, V.J., Henry, D.J., Marschall, H.R., 2011. Tourmaline: An ideal indicator of its host environment. Can. Mineral. 49, 1–16. https://doi.org/10.3749/canmin.49.1.1

Vannay, J.-C., Grasemann, B., 2001. Himalayan inverted metamorphism and syn-convergence extension as a consequence of a general extrusion. Geol. Mag. - GEOL MAG 138. https://doi.org/10.1017/S0016756801005313

Viskupic, K., Hodges, K. V., Bowring, S.A., 2005. Timescales of melt generation and the thermal evolution of the Himalayan metamorphic core, Everest region, eastern Nepal. Contrib. to Mineral. Petrol. 149, 1–21. https://doi.org/10.1007/s00410-004-0628-5

Visonà, D., Lombardo, B., 2002. Two-mica and tourmaline leucogranites from the Everest-Makalu region (Nepal - Tibet). Himalayan leucogranite genesis by isobaric heating? Lithos 62, 125–150. https://doi.org/10.1016/S0024-

4937(02)00112-3

Wager, L.R., 1939. The Lachi series of North Sikkim and the age of the rocks forming Mount Everest. Rec. Geol. Surv. India 74, 171–188.

Wang, R.C., Wu, F.Y., Xie, L., Liu, X.C., Wang, J.M., Yang, L., Lai, W., Liu, C., 2017. A preliminary study of rare-metal mineralization in the Himalayan leucogranite belts, South Tibet. Sci. China Earth Sci. 60, 1655–1663. https://doi.org/10.1007/s11430-017-9075-8

Watson, E., Harrison, T., 1983. Watson, E. B. & Harrison, T. M. Zircon saturation revisited: temperature and composition effects in a variety of crustal magma types. Earth Planet. Sci. Lett. 64, 295-304. Earth Planet. Sci. Lett. 64, 295–304. https://doi.org/10.1016/0012-821X(83)90211-X

Watson, E.B., Harrison, T.M., 2005. Zircon thermometer reveals minimum melting conditions on earliest earth. Science (80-.). 308, 841–844. https://doi.org/10.1126/science.1110873

Watson, E.B., Harrison, T.M., 1983. Zircon saturation revisited: temperature and composition effects in a variety of crustal magma types. Earth Planet. Sci. Lett. 64, 295–304. https://doi.org/10.1016/0012-821X(83)90211-X

Webb, A.A., Schmitt, A., He, D., Weigand, E., 2011. Structural and geochronological evidence for the leading edge of the Greater Himalayan Crystalline complex in the central Nepal Himalaya. Earth Planet. Sci. Lett. 304, 483–495. https://doi.org/10.1016/j.epsl.2011.02.024

Webb, A.A.G., 2013. Preliminary balanced palinspastic reconstruction of cenozoic deformation across the Himachal Himalaya (northwestern India). Geosphere 9, 572–587. https://doi.org/10.1130/GES00787.1

Weinberg, R.F., 2016. Himalayan leucogranites and migmatites: nature, timing and duration of anatexis. J. Metamorph. Geol. 34, 821–843. https://doi.org/10.1111/jmg.12204

Whalen, J.B., Currie, K.L., Chappell, B.W., 1987. A-type granites: geochemical characteristics, discrimination and petrogenesis. Contrib. to Mineral. Petrol. 95, 407–419. https://doi.org/10.1007/BF00402202

White, A., Chappell, B., 1983. Granitoid types and their distribution in the Lachlan Fold Belt, Southeastern Australia, in: Circum-Pacific Plutonic Terranes. pp. 21–34. https://doi.org/10.1130/MEM159-p21

Whittaker, J., Williams, S., Halpin, J., Wild, T., Stilwell, J., Jourdan, F., Daczko, N., 2016. Eastern Indian Ocean microcontinent formation driven by plate motion changes. Earth Planet. Sci. Lett. 454. https://doi.org/10.1016/j.epsl.2016.09.019

Wiedenbeck, M., Alle, P., Corfu, F., Griffin, W., Meier, M., Ober, F., Quant, A., Roddick, J.C., Spiegel, J., 1995. Three natural zircon standards for U-Th-Pb, Lu-Hf, trace element and REE analysis. Geostand. Newsl. 19, 1–23.

Wu, C., Nelson, K.D., Wortman, G., Samson, S.D., Yue, Y., Li, J., Kidd, W.S.F., Edwards, M.A., 1998. Yadong cross structure and South Tibetan Detachment in the east central Himalaya (89°-90°E). Tectonics 17, 28–45. https://doi.org/10.1029/97TC03386

Wu, F.-Y., Clift, P., Yang, J.-H., 2007. Zircon Hf isotopic constraints on the sources of the Indus Molasse, Ladakh Himalaya, India. Tectonics 26. https://doi.org/10.1029/2006TC002051

Wu, F.Y., Liu, X.C., Liu, Z.C., Wang, R.C., Xie, L., Wang, J.M., Ji, W.Q., Yang, L., Liu, C., Khanal, G.P., He, S.X., 2020. Highly fractionated Himalayan leucogranites and associated rare-metal mineralization. Lithos 352–353, 105319. https://doi.org/10.1016/j.lithos.2019.105319

Wu, F.Y., Liu, Z.C., Liu, X.C., Ji, W.Q., 2015. Himalayan leucogranite: Petrogenesis and implications to orogenesis and plateau uplift. Acta Petrol. Sin. 31, 1–36.

Wu, X., Wang, Q., Zhu, D.-C., Zhao, Z., Chen, Y., Jia, L., Zheng, J., Mo, X., 2013. Origin of the Early Carboniferous granitoids in the southern margin of the Lhasa Terrane and its implication for the opening of the Songdo Tethyan Ocean. Acta Petrol. Sin. 29, 3716–3730.

Xavier, R., Wiedenbeck, M., Trumbull, R., Dreher, A., Monteiro, L., Rhede, D., Ganade, C., Torresi, I., 2008. Tourmaline B-isotopes fingerprint marine evaporites as the source of high-salinity ore fluids in iron oxide copper-gold deposits, Carajás Mineral Province (Brazil). Geology 36, 743–746. https://doi.org/10.1130/G24841A.1

Xie, J., Qiu, H., Bai, X., Zhang, W., Wang, Q., Xia, X., 2018. Geochronological and geochemical constraints on the Cuonadong leucogranite, eastern Himalaya. Acta Geochim. 37, 347–359. https://doi.org/10.1007/s11631-018-0273-8

Xie, L., Tao, X., Wang, R., Wu, F., Liu, C., Liu, X., Li, X., Zhang, R., 2020. Highly fractionated leucogranites in the eastern Himalayan Cuonadong dome and related magmatic Be–Nb–Ta and hydrothermal Be–W–Sn mineralization. Lithos 354–355, 105286. https://doi.org/10.1016/j.lithos.2019.105286

Xu, J., Xia, X.-P., Wang, Q., Spencer, C.J., Lai, C.-K., Ma, J.-L., Zhang, L., Cui, Z.-X., Zhang, W.-F., Zhang, Y.-Q., 2021. Pure sediment-derived granites in a subduction zone. GSA Bull. https://doi.org/10.1130/b36016.1

Yang, L., Liu, X.C., Wang, J.M., Wu, F.Y., 2019. Is Himalayan leucogranite a product by in situ partial melting of the Greater Himalayan Crystalline? A comparative study of leucosome and leucogranite from Nyalam, southern Tibet. Lithos 342–343, 542–556. https://doi.org/10.1016/j.lithos.2019.06.007

Yang, S.Y., Jiang, S.Y., 2012. Chemical and boron isotopic composition of tourmaline in the Xiangshan volcanic-intrusive complex, Southeast China: Evidence for boron mobilization and infiltration during magmatic-hydrothermal processes. Chem. Geol. 312–313, 177–189. https://doi.org/10.1016/j.chemgeo.2012.04.026

Yang, S.Y., Jiang, S.Y., Palmer, M.R., 2015. Chemical and boron isotopic compositions of tourmaline from the Nyalam leucogranites, South Tibetan Himalaya: Implication for their formation from B-rich melt to hydrothermal fluids. Chem. Geol. 419, 102–113. https://doi.org/10.1016/j.chemgeo.2015.10.026

Yang, X., Jin, Z., Ma, J., 2005. Anatexis in Himalayan crust: Evidence from geochemical and chronological investigations of higher Himalayan crystallines. Sci. China, Ser. D Earth Sci. 48, 1347–1356. https://doi.org/10.1360/03yd0254

Yin, A., 2006. Cenozoic tectonic evolution of the Himalayan orogen as constrained by along-strike variation of structural geometry, exhumation history, and foreland sedimentation. Earth-Science Rev. 76, 1–131. https://doi.org/10.1016/j.earscirev.2005.05.004

Yin, A., Dubey, C., Kelty, T., Webb, A.A., Harrison, T., Chou, C., Celerier, J., 2010. Geologic correlation of the Himalayan orogen and Indian craton: Part 2. Structural geology, geochronology, and tectonic evolution of the Eastern Himalaya. Geol. Soc. Am. Bull. - GEOL SOC AMER BULL 122, 360–395. https://doi.org/10.1130/B26461.1

Zeitler, P.K., Sutter, J.F., Williams, I.S., Zartman, R., Tahirkheli, R.A.K., 1989. Geochronology and temperature history of the Nanga Parbat-Haramosh Massif, Pakistan. Spec. Pap. Geol. Soc. Am. 232, 1–22. https://doi.org/10.1130/SPE232-p1

Zeng, L., Gao, L.E., Tang, S., Hou, K., Guo, C., Hu, G., 2015. Eocene magmatism in the Tethyan Himalaya, southern Tibet. Geol. Soc. Spec. Publ. 412, 287–316. https://doi.org/10.1144/SP412.8

Zeng, L., Gao, L.E., Tang, S., Hou, K., Guo, C., Hu, G., 2014. Eocene magmatism in the Tethyan Himalaya, southern Tibet. Geol. Soc. Spec. Publ. 412, 287–316. https://doi.org/10.1144/SP412.8

Zeng, L., Gao, L.E., Xie, K., Liu-Zeng, J., 2011. Mid-Eocene high Sr/Y granites in the Northern Himalayan Gneiss Domes: Melting thickened lower continental crust. Earth Planet. Sci. Lett. 303, 251–266. https://doi.org/10.1016/j.epsl.2011.01.005

Zhai, Q., Wang, J., Hu, P., Lee, H.-Y., Tang, Y., Wang, H., Tang, S., Chung, S.-L., 2018. Late Paleozoic granitoids from central Qiangtang, northern Tibetan plateau: A record of Paleo-Tethys Ocean subduction. J. Asian Earth Sci. 167. https://doi.org/10.1016/j.jseaes.2017.07.030

Zhang, H., Harris, N., Parrish, R., Kelley, S., Zhang, L., Rogers, N., Argles, T., King, J., 2004. Causes and consequences of protracted melting of the mid-crust exposed in the North Himalayan antiform. Earth Planet. Sci. Lett. 228, 195–212. https://doi.org/10.1016/j.epsl.2004.09.031

Zhang, J., Heckman, N., Cubranic, D., Kingsolver, J.G., Gaydos, T., Marron, J.S., 2014. Prinsimp. R J. 6, 27–42.

Zhang, L.K., Li, G.M., Cao, H.W., Zhang, Z., Dong, S.L., Liang, W., Fu, J.G., Huang, Y., Xia, X.B., Dai, Z.W., Pei, Q.M., Zhang, S.T., 2020. Activity of the south Tibetan detachment system: Constraints from leucogranite ages in the eastern Himalayas. Geol. J. 55, 5540–5573. https://doi.org/10.1002/gj.3756

Zhang, L.X., Wang, Q., Zhu, D.C., Li, S.M., Zhao, Z.D., Zhang, L.L., Chen, Y., Liu, S.A., Zheng, Y.C., Wang, R., Liao, Z.L., 2019. Generation of leucogranites via fractional crystallization: A case from the Late Triassic Luoza batholith in the Lhasa Terrane, southern Tibet. Gondwana Res. 66, 63–76. https://doi.org/10.1016/j.gr.2018.08.008

Zhang, L.Y., Ding, L., Yang, D., Xu, Q., Cai, F.L., Liu, D.L., 2012. Origin of middle Miocene leucogranites and rhyolites on the Tibetan Plateau: Constraints on the timing of crustal thickening and uplift of its northern boundary. Chinese Sci. Bull.

57, 511–524. https://doi.org/10.1007/s11434-011-4813-4

Zhang, W., Hu, Z., Spectroscopy, A., 2020. Estimation of Isotopic Reference Values for Pure Materials and Geological Reference Materials. At. Spectrosc. 41, 93–102. https://doi.org/10.46770/AS.2020.03.001

Zhang, Z., Xiang, H., Dong, X., Li, W., Ding, H., Gou, Z., Tian, Z., 2017. Oligocene HP metamorphism and anatexis of the Higher Himalayan Crystalline Sequence in Yadong region, east-central Himalaya. Gondwana Res. 41, 173–187. https://doi.org/10.1016/j.gr.2015.03.002

Zhao, G., Sun, M., Wilde, S.A., Li, S., 2004. A Paleo-Mesoproterozoic supercontinent : assembly , growth and breakup 67, 91–123. https://doi.org/10.1016/j.earscirev.2004.02.003

Zhao, S., Lai, S., Gao, L., Qin, J., Zhu, R., 2016. Evolution of the Proto-Tethys in the Baoshan block along the East Gondwana margin: constraints from early Palaeozoic magmatism. Int. Geol. Rev. 59, 1–15. https://doi.org/10.1080/00206814.2016.1198994

Zhu, D.C., Zhao, Z.D., Niu, Y., Dilek, Y., Mo, X.X., 2011. Lhasa terrane in Southern Tibet came from Australia. Geology 39, 727–730. https://doi.org/10.1130/G31895.1

APPENDIX A: 1.1 Details of the studied samples of leucogranites and gneiss

Sample	GPS		Rock type	Region	Location
LG2-I	88.50334	27.90203	2mg	North Sikkim	Thangu
LG2-III	88.50334	27.90203	2mg		Thangu
LG3-I	88.51339	27.91081	2mg		Thangu
LG3-II	88.51339	27.91081	2mg		Thangu
LG4-1	88.50999	27.90673	2mg		Thangu
LG4-III	88.50999	27.90673	2mg		Thangu
S-2	88.52110	27.89012	2mg		Thangu
LG-5	88.52110	27.89012	2mg		Thangu
ZY-LG-3 b	88.69361	27.86249	2mg		Between Yumthang and Yumesamdong
ZY-LG-2	88.69361	27.87306	2mg		Between Yumthang and Yumesamdong
Z-LG-4	88.73371	27.93058	2mg		Yumesamdong
L-2	88.72249	27.75611	2mg		Between Lachung and Yumthang transect
Y-LG-1	88.70556	27.79249	2mg		Near Yumthang
ZY-LG-3-a	88.73371	27.93058	2mg		Between Yumthang and Yumesamdong
Z-LG-1	88.73371	27.93058	2mg		Yumesamdong
Z-LG-2	88.73371	27.93058	2mg		Yumesamdong
Y-LG-2	88.72472	27.75472	2mg		Near Yumthang
Y-P-2	88.72479	27.75449	2mg		Near Yumthang
Z-LG-6	88.73339	27.93024	2mg		Yumesamdong
Z-LG-8	88.73339	27.93024	2mg		Yumesamdong
Z-LG-5	88.73339	27.93024	2mg		Yumesamdong
Z-LG-7	88.73339	27.93024	2mg		Yumesamdong
Z-1	88.73342	27.92989	2mg		Yumesamdong
Z-2	88.73342	27.92989	2mg		Yumesamdong
ZY-LGT-1	88.72046	27.92028	Tg		Yumesamdong

Y-G-1 b	88.72306	27.75361	Tg		Between Lachung and Yumthang transect
Y-TG-2	88.72280	27.75420	Tg		Between Lachung and Yumthang transect

APPENDIX A: 1.2 Major and trace elements data of two-mica leucogranites and tourmaline

	LG2-I	LG2-III	LG3-I	LG3-II	LG4-1	LG4-III	S2	LG5	ZY-LG-3 b	ZY-LG-2	Z-LG-4	L-2	Y-LG-1
Rock Type	**2mg**	**2mg**	**2mg**	**2mg**	**2mg**	**2mg**	**2mg**	**2mg**	**2mg**	**2mg**	**2mg**	**2mg**	**2mg**
Major Elements (wt.%)													
SiO_2	72.31	70.91	72.31	73.06	71.59	73.49	73.70	73.34	72.37	73.63	73.10	73.20	74.61
TiO_2	0.13	0.18	0.13	0.13	0.15	0.12	0.12	0.19	0.20	0.14	0.20	0.16	0.20
Al_2O_3	14.21	15.82	14.69	14.72	14.94	14.25	15.02	14.93	15.03	14.76	14.80	14.44	13.69
MnO	0.01	0.03	0.02	0.02	0.02	0.02	0.03	0.02	0.03	0.03	0.03	0.05	0.02
Fe_2O_3	1.29	1.61	1.50	1.48	1.58	1.45	1.49	1.78	1.73	1.36	1.70	2.19	1.23
CaO	1.07	1.67	1.10	1.13	1.23	0.78	0.58	1.12	1.37	0.94	1.20	0.98	1.66
MgO	0.33	0.56	0.32	0.28	0.39	0.21	0.30	0.45	0.45	0.28	0.43	0.30	0.38
Na_2O	3.34	3.47	3.70	3.74	3.46	3.82	3.96	3.94	3.57	3.56	3.67	3.70	2.45
K_2O	5.90	5.16	5.36	5.18	4.97	4.93	4.86	4.64	4.26	4.64	4.49	4.03	5.22
P_2O_5	0.07	0.08	0.09	0.08	0.06	0.14	0.15	0.10	0.09	0.12	0.12	0.12	0.07
Total	98.66	99.49	99.23	99.82	98.39	99.22	100.21	100.52	99.10	99.46	99.74	99.17	99.53
A/CNK	1.03	1.10	1.06	1.07	1.12	1.09	1.17	1.10	1.16	1.17	1.13	1.18	1.08
K_2O/Na_2O	1.76	1.49	1.45	1.39	1.43	1.29	1.23	1.18	1.19	1.30	1.22	1.09	2.13
Trace elements (ppm)													
Rb	308	282	271	298	261	236	327	219	206	304	248	266	198
Ba	546	559	339	350	357	542	295	490	603	385	508	419	947
Th	11.6	20.3	13	14.5	11.9	18.1	9.51	13.5	17.4	13.9	15.9	8.89	18.6
U	7.37	9.88	19.8	18.7	16.7	12.7	9.11	7.12	26.7	8.3	12.4	7	4.4
Nb	8.97	12.1	11.7	14	13.9	12.3	13.7	8.8	10.6	15.7	12	15.3	5.64
K	5.90	5.16	5.36	5.18	4.97	4.93	4.86	4.64	4.26	4.64	4.49	4.03	5.22
Pb	69	76	75	79	69	77	63	80	93	77	78	56	92
Sr	127	173	96	98.1	112	203	86.7	187	221	120	184	107	178
P	0.074	0.083	0.085	0.084	0.063	0.138	0.145	0.101	0.092	0.115	0.118	0.12	0.067
Zr	93	119	67	77.5	68.5	105	61	98.5	129	81	102	60.5	151
Ti	0.13	0.18	0.13	0.13	0.15	0.12	0.12	0.19	0.20	0.14	0.20	0.16	0.20
Y	18.7	20.3	22.1	24.6	20.6	20.2	16.9	20	20.3	20.3	20.2	15.7	8.08
La	18.2	33.2	21.8	24.4	20	33.5	16.3	25.5	31.2	24.4	29.1	17.1	32.8
Ce	35.1	66.2	42.3	47.7	38.8	64.7	33.2	49.4	61.8	48.6	56	33.3	61.1
Pr	4.14	7.87	4.91	5.67	4.57	7.62	4.04	5.77	7.35	5.73	6.66	3.96	7.33
Nd	15.3	28.1	17.9	20.2	16.9	28.5	14.9	20.9	26.7	19.6	24	14.3	25.7
Sm	3.47	6.41	4.38	4.91	3.98	5.99	3.56	4.4	5.87	4.46	5.18	3.29	5.19
Eu	0.76	0.98	0.78	0.79	0.75	0.96	0.57	0.76	1.02	0.68	0.89	0.65	1.51

Gd	3.31	5.22	4.21	4.73	3.87	5	3.36	3.92	5.09	4.2	4.76	3.09	3.84
Tb	0.6	0.82	0.76	0.81	0.66	0.74	0.59	0.64	0.76	0.72	0.71	0.5	0.49
Dy	3.43	4.28	4.27	4.82	3.85	3.93	3.26	3.6	4.01	4.08	3.78	2.93	2.22
Ho	0.67	0.76	0.78	0.87	0.72	0.73	0.59	0.69	0.77	0.69	0.73	0.58	0.31
Er	1.83	2.02	2.04	2.3	1.93	1.94	1.55	1.83	1.84	1.82	2.03	1.58	0.72
Tm	0.27	0.28	0.28	0.32	0.26	0.28	0.22	0.28	0.27	0.27	0.27	0.23	0.1
Yb	1.78	1.91	1.72	1.88	1.66	1.72	1.34	1.75	1.68	1.49	1.81	1.55	0.63
Lu	0.25	0.29	0.22	0.25	0.2	0.23	0.17	0.23	0.22	0.22	0.24	0.21	0.11
$(La/Yb)_N$	7.33	12.47	9.09	9.31	8.64	13.97	8.73	10.45	13.32	11.75	11.53	7.91	37.35
Eu/Eu*	0.69	0.52	0.56	0.50	0.58	0.54	0.50	0.56	0.57	0.48	0.55	0.62	1.03
Rb/Sr	2.43	1.63	2.82	3.04	2.33	1.16	3.77	1.17	0.93	2.53	1.35	2.49	1.11

Sample	**ZY-LG-3-a**	**Z-LG-1**	**Z-LG-2**	**Y-LG-2**	**Y-P-2**	**Z-LG-6**	**Z-LG-8**	**Z-LG-5**	**Z-LG-7**	**Z-1**	**Z-2**	**ZY-LGT-1**	**Y-G-1 b**	**Y-TG-2**
Rock Type	**2mg**	**2mg**	**2mg**	**2mg**	**2mg**	**2mg**	**2mg**	**2mg**	**2mg**	**2mg**	**2mg**	**Tg**	**Tg**	**Tg**
Major Elements (wt.%)														
SiO_2	73.34	73.12	73.39	74.32	74.46	71.60	71.30	71.34	71.61	71.17	71.77	74.90	74.38	74.58
TiO_2	0.21	0.20	0.19	0.18	0.19	0.29	0.27	0.28	0.28	0.29	0.27	0.07	0.09	0.06
Al_2O_3	14.85	14.78	14.96	13.95	13.88	15.32	15.33	15.31	15.00	15.31	15.14	14.80	13.78	13.95
MnO	0.03	0.03	0.03	0.03	0.05	0.04	0.03	0.03	0.03	0.04	0.04	0.02	0.03	0.03
Fe_2O_3	1.82	1.75	1.73	1.42	2.09	2.42	2.35	2.23	2.29	2.37	2.33	0.73	0.98	0.85
CaO	1.25	1.29	1.26	0.77	1.04	1.58	1.59	1.60	1.57	1.56	1.35	0.45	1.13	0.56
MgO	0.45	0.44	0.43	0.36	0.74	0.64	0.60	0.58	0.61	0.64	0.60	0.13	0.20	0.19
Na_2O	3.23	3.65	3.58	2.62	1.93	3.57	3.62	3.55	3.51	3.54	3.68	3.77	3.21	2.69
K_2O	3.81	4.25	4.20	5.36	4.67	4.10	4.04	4.11	4.10	4.08	3.96	4.25	4.74	6.22

P_2O_5	0.09	0.11	0.11	0.11	0.14	0.08	0.08	0.08	0.08	0.08	0.09	0.17	0.15	0.16
Total	99.08	99.62	99.88	99.12	99.19	99.64	99.21	99.11	99.08	99.08	99.23	99.29	98.69	99.29
A/CNK	1.27	1.14	1.18	1.21	1.37	1.16	1.16	1.16	1.15	1.17	1.18	1.27	1.11	1.15
K_2O/Na_2O	1.18	1.16	1.17	2.05	2.42	1.15	1.12	1.16	1.17	1.15	1.08	1.13	1.48	2.31
Trace elements (ppm)														
Rb	240	246	243	243	176	208	208	206	213	222	237	301	258	281
Ba	505	563	541	1190	619	767	764	747	741	812	761	65	194	342
Th	15.8	16.7	15	14.4	10.7	24.4	23.9	23.2	24.4	25	23.2	4.38	5.14	7.6
U	13	9.87	28.7	8.69	4.81	9.34	11.8	9.7	12	9.66	7.3	18.9	15.4	14.9
Nb	12.2	12.6	11.6	8.75	5.02	13	13.1	12.5	12.6	13.4	13	16.9	9.07	5.47
K	3.81	4.25	4.2	5.36	4.67	4.1	4.04	4.11	4.1	4.08	3.96	4.25	4.74	6.22
Pb	72	83	80	88	55	91	93	93	94	93	87	44	62	70
Sr	187	206	192	179	114	271	277	265	259	268	257	23.7	65.2	79.4
P	0.091	0.108	0.11	0.112	0.144	0.081	0.08	0.079	0.08	0.078	0.085	0.173	0.148	0.157
Zr	103	114	98	90	76.5	149	158	143	150	151	140	25	39.5	36.5
Ti	0.21	0.20	0.19	0.18	0.19	0.29	0.27	0.28	0.28	0.29	0.27	0.07	0.09	0.06
Y	20.1	20.9	19.2	21.8	14.4	24.6	24.3	22.6	23.4	21.7	20.9	11.2	12.1	24.5
La	29.5	31.5	27.7	26.6	18.7	47.8	46.8	45.4	47.2	49.1	44.7	5.12	8.49	11.4
Ce	58.1	61.2	54	53	38.5	90.9	90	86.2	90.3	95.8	86.7	10.7	16.8	23.5
Pr	6.95	7.41	6.51	6.29	4.7	11	10.4	9.96	10.7	11	10	1.35	1.99	2.9
Nd	24.2	25.4	22.6	23.3	16.4	37.8	36.8	35.9	36.9	38.6	34.9	4.79	7.49	10.6
Sm	5.34	5.56	4.75	5.15	3.84	7.45	7.57	7.23	7.5	7.75	6.99	1.71	2.11	3.01
Eu	0.85	0.9	0.9	1.13	0.89	1.31	1.21	1.19	1.23	1.27	1.11	0.11	0.39	0.52
Gd	4.43	4.6	4.37	4.64	3.4	6.24	5.75	5.89	5.95	6.18	5.69	1.67	2.11	3.49
Tb	0.72	0.74	0.68	0.7	0.58	0.88	0.9	0.84	0.89	0.87	0.82	0.38	0.39	0.7
Dy	3.95	4.08	3.75	3.87	3.16	4.81	4.84	4.49	4.63	4.5	4.35	2.23	2.3	4.44
Ho	0.75	0.75	0.7	0.76	0.55	0.91	0.91	0.82	0.89	0.8	0.8	0.36	0.4	0.89

Er	2	2.06	1.97	2.27	1.21	2.43	2.38	2.32	2.31	2.18	2.03	1.17	1.21	2.52
Tm	0.28	0.31	0.28	0.34	0.16	0.3	0.33	0.31	0.3	0.31	0.3	0.18	0.19	0.39
Yb	1.75	1.95	1.69	2.48	0.97	2.33	2.07	1.95	2.15	1.89	1.75	1.13	1.27	2.35
Lu	0.26	0.26	0.26	0.33	0.14	0.3	0.29	0.28	0.27	0.27	0.24	0.15	0.19	0.31
$(La/Yb)_N$	12.09	11.59	11.76	7.69	13.83	14.72	16.22	16.70	15.75	18.63	18.32	3.25	4.80	3.48
Eu/Eu*	0.53	0.54	0.60	0.71	0.75	0.59	0.56	0.56	0.56	0.56	0.54	0.20	0.57	0.49
Rb/Sr	1.28	1.19	1.27	1.36	1.54	0.77	0.75	0.78	0.82	0.83	0.92	12.70	3.96	3.54

APPENDIX A: 1.3 Major and Trace element concentrations of pegmatites

Major Elements (in wt.%)	Y-TP-3	Y-TP-1	Y-TG-1	TP-1
SiO_2	71.89	66.24	73.89	NA
TiO_2	0.37	0.19	0.08	NA
Al_2O_3	14.1	19.2	14.82	NA
Fe_2O_3	3.36	1.25	1.42	NA
MnO	0.05	0.03	0.03	NA
MgO	0.78	0.32	0.25	NA
CaO	1.38	1.92	0.39	NA
Na_2O	2.55	4.34	1.95	NA
K_2O	4.67	5.21	6.12	NA
P_2O_5	0.16	0.19	0.25	NA
LOI	0.34	0.88	0.43	NA
Total	99.65	99.77	99.63	NA
	TYPE 1		TYPE 2	
Trace Elements (ppm)	Y-TP-3	Y-TP-1	Y-TG-1	TP-1
V	44.8	16.4	1.7	0.7
Cr	29	14	5	10
Co	8.2	3.2	0.9	0.5
Ni	16	6	2	4
Zn	70	30	55	BDL
Ga	18.7	28.8	29.3	8.3
Rb	219	205	281	169
Sr	124	143	57.9	9.5
Y	32.6	50.1	4.76	1.68
Zr	199	198	21	4.5
Nb	10.9	8.46	7.12	0.84
Cs	16.5	8.79	10.1	3.46
Ba	624	404	152	17.5
Th	20.7	21	0.97	1.1
U	4.06	19.8	16.3	3.03
La	35.9	35.3	1.78	1.94
Ce	73.8	69.9	3.76	3.38
Pr	8.95	8.23	0.47	0.42
Nd	32.2	29.6	1.78	1.61
Sm	7.42	6.31	0.73	0.36
Eu	1.06	1.23	0.31	0.06
Gd	7.01	6.42	0.7	0.4
Tb	1.16	1.24	0.17	0.05

Dy	6.72	7.98	0.91	0.31
Ho	1.21	1.8	0.17	0.04
Er	3.35	5.53	0.41	0.12
Tm	0.43	0.86	0.08	0.02
Yb	2.95	5.93	0.68	0.21
Lu	0.42	0.89	0.1	0.02
$(La/Yb)_N$	8.73	4.27	1.88	6.63
(Eu/Eu*)	0.45	0.59	1.33	0.48

APPENDIX A 1.4 Boron isotopic composition of tourmaline pegmatites.

Sample Number	δ ^{11}B, ‰	2SD, ‰	^{11}B/^{10}Bratios
Y-TG-1	-12.78	0.84	3.9919
Y-TG-1, r.2	-12.55	0.91	3.9929
Y-TP-3	-12.86	0.84	3.9916
Y-TP-1	-13.03	0.41	3.9909
Y-TP-1, r.2	-12.59	0.44	3.9927
TP-1	-13.83	0.37	3.9877
TP-1, r.2	-14.13	0.40	3.9865

Appendix B: 1.1 Representative EPMA data in (wt.%) for tourmaline of the two-mica leucogranites, tourmaline leucogranites and pegmatites.

Sample: LG-4(I)-Two-mica leucogranite

SiO_2	35.51	35.5587	35.4264	35.0005	35.6134	35.5047	35.6808	35.0281	35.1475	35.5527	36.0744	35.2221
TiO_2	0	0	0	0	0	0	0	0.0011	0.0087	0.0109	0.0218	0.0034
Al_2O_3	34.0451	34.6674	34.2844	34.9099	34.2443	33.4839	33.4995	34.4379	34.0301	34.3677	26.7151	34.4015
V_2O_3	0	0	0	0	0	0	0	0	0	0	0	0
Cr_2O_3	0	0	0	0	0.044	0.0049	0	0	0.042	0	0	0.0475
Fe_2O_3	0	0	0	0	0	0	0	0	0	0	0	0
FeO	12.1798	12.5739	12.3793	11.8231	12.3693	11.4316	11.2104	11.2841	11.9012	12.0557	17.4537	10.7148
MgO	4.4929	4.324	4.4522	4.8262	4.3276	5.0809	5.288	5.3666	4.4563	4.4446	3.1177	5.6155
CaO	0.0473	0.0308	0.0213	0	0.0367	0.0083	0.0702	0.0392	0.0487	0.0261	0.3347	0.0703
MnO	0.9959	1.0471	0.9429	0.944	0.9074	0.8678	0.8297	0.6916	0.9014	0.9223	0.6718	0.58
ZnO	0	0	0	0	0	0	0	0	0	0	0	0
BaO	0	0	0	0	0	0	0	0	0	0	0	0
Na_2O	1.0943	1.2634	1.0895	1.0758	1.2077	1.1888	1.1165	0.8476	1.2291	1.2452	0.7412	0.8862
K_2O	0.0118	0.0157	0.0103	0	0.0236	0.0216	0	0.0044	0	0.0212	0.6064	0.0049
Rb_2O	0	0	0	0	0	0	0	0	0	0	0	0
Cs_2O	0	0	0	0	0	0	0	0	0	0	0	0
F	0	0	0	0	0	0	0.0222	0.2136	0.105	0.1687	0.0593	0.2241
Cl	0	0	0	0	0	0	0	0	0	0	0	0
H_2O	0	0	0	0	0	0	0	0	0	0	0	0
B_2O_3	8.4638	8.3546	9.118	9.7715	9.3568	9.3169	9.4943	8.3568	8.2759	8.0667	8.6427	8.8425
Li_2O	0	0	0	0	0	0	0	0	0	0	0	0
H_2O*	3.53909	3.53747	3.51684	3.54317	3.50259	3.50503	3.54955	3.52007	3.53404	3.55302	3.53937	3.57046
B_2O_3*	-	-	-	-	-	-	-	-	-	-	-	-
Li_2O*	0.40651	0.44897	0.4439	0.49303	0.41338	0.38	0.39956	0.48118	0.36867	0.43362	0.41968	0.35516
Total	99.831	99.9768	99.7243	100.078	99.5175	99.4619	100.224	99.9493	100.078	100.181	100.256	100.393

O=F	0	0	0	0	0	0	0.00935	0.08994	0.04421	0.07103	0.02497	0.09436
Total*	99.7802	99.9135	99.6512	100.018	99.4487	99.392	100.171	99.8734	100.018	100.132	100.194	100.354
B	3.14924	3.15087	3.14666	3.15642	3.13995	3.13782	3.14165	3.18012	3.13263	3.15858	3.14903	3.10916
T: Si	5.74057	5.74354	5.74874	5.75256	5.75097	5.72767	5.73618	5.69127	5.71179	5.72249	5.71876	5.74845
Al	0.25943	0.25646	0.25126	0.24744	0.24903	0.27233	0.26382	0.30873	0.28821	0.27751	0.28124	0.25155
Z: Al	6	6	6	6	6	6	6	6	6	6	6	6
Mg	0	0	0	0	0	0	0	0	0	0	0	0
Y: Al	0.04058	0.05052	0.08232	0.03799	0.05384	0.05265	0.05678	0.02773	0.0726	0.05217	0.03715	0.12919
Ti	0.07021	0.06904	0.06885	0.07348	0.07557	0.07254	0.07083	0.07173	0.07005	0.06846	0.07073	0.06665
V	0	0	0	0	0	0	0	0	0	0	0	0
Cr	0.00012	0.00014	0.00043	0.00087	0.00085	0	6.6E-05	0.0003	0.00039	0.00105	5.3E-05	0.00093
Fe^{3+}	0	0	0	0	0	0	0	0	0	0	0	0
Mg	1.19222	1.21616	1.16675	1.16617	1.14188	1.21723	1.18307	1.19786	1.17931	1.1501	1.19551	1.12561
Mn	0.00371	0.00439	0.00334	0.00211	0.00211	0.00123	0.00263	0.00193	0.00299	0.00298	0.00122	0.00509
Fe^{2+}	1.42065	1.35983	1.38099	1.39026	1.4476	1.40076	1.41988	1.37874	1.42797	1.43564	1.41512	1.43577
Zn	0	0	0	0	0	0	0	0	0	0	0	0
Li*	0.27252	0.29994	0.29735	0.32919	0.2782	0.25564	0.26679	0.32174	0.24674	0.28965	0.28024	0.23683
Y	3.00001	3.00002	3.00003	3.00005	3.00005	3.00005	3.00004	3.00001	3.00005	3.00005	3.00002	3.00006
X: Ca	0.14929	0.15581	0.14571	0.16444	0.15105	0.15408	0.15	0.16964	0.16683	0.15427	0.1683	0.15124
Ba	0	0	0	0	0	0	0	0	0	0	0	0
Na	0.58946	0.58757	0.58141	0.57617	0.58529	0.59271	0.59263	0.56374	0.57451	0.57881	0.58228	0.57895
K	0.01508	0.01579	0.01526	0.01633	0.01399	0.01577	0.01441	0.01559	0.01565	0.01378	0.01678	0.01585
Rb	0	0	0	0	0	0	0	0	0	0	0	0
Cs	0	0	0	0	0	0	0	0	0	0	0	0
X-vacancy	0.24618	0.24083	0.25762	0.24305	0.24967	0.23744	0.24296	0.25104	0.24301	0.25315	0.23264	0.25396
V+W site												
OH	3.93504	3.91981	3.90787	3.92455	3.91061	3.9118	3.93169	3.90384	3.92375	3.93723	3.9203	3.95005
F	0.06358	0.07907	0.09157	0.07379	0.0865	0.08789	0.06654	0.0947	0.07512	0.06137	0.07757	0.04899

SiO_2	35.0087	35.1155	35.8033	35.3671	35.8592	35.508	35.7282	35.8485	35.4433	35.9214	35.0257	35.8066	35.7133
TiO_2	0	0	0	0	0.0011	0.0008	0	0.0461	0.0098	0	0	0	0
Al_2O_3	34.2063	34.9307	34.7679	34.688	34.4473	34.5959	34.2077	34.4936	34.7673	34.1846	34.8689	34.3634	34.0893
V_2O_3	0	0	0	0	0	0	0	0	0	0	0	0	0
Cr_2O_3	0	0.0049	0	0	0	0	0.0227	0	0.0251	0.0091	0	0	0.0387
Fe_2O_3	0	0	0	0	0	0	0	0	0	0	0	0	0
FeO	12.0933	12.1988	12.3919	11.8618	12.0769	12.1526	12.3174	3.395	12.4336	9.4344	12.31	12.1043	12.2279
MgO	4.3421	4.4476	4.2725	4.3668	4.4627	4.1732	4.2666	0.8552	4.1272	3.6356	4.3588	4.923	4.4745
CaO	0.0095	0.0987	-0.0024	0.0476	0.0381	0.082	0.0143	16.4941	0.0512	0.38	0.0226	0.0417	0.0298
MnO	0.9506	0.9238	0.9737	0.9271	1.0594	1.0478	0.9537	0.1046	1.0287	0.6487	0.9305	0.9896	0.9391
ZnO	0	0	0	0	0	0	0	0	0	0	0	0	0
BaO	0	0	0	0	0	0	0	0	0	0	0	0	0
Na_2O	1.1835	1.1395	1.102	1.1539	1.1032	1.1557	1.2078	0.1897	1.22	1.1338	1.2291	1.558	0.9856
K_2O	0.0222	0.029	0	0.002	0	0.0049	0.0007	0.3004	0.0016	0.2379	0.0403	0.0518	0.0253
Rb_2O	0	0	0	0	0	0	0	0	0	0	0	0	0
Cs_2O	0	0	0	0	0	0	0	0	0	0	0	0	0
F	0	0	0.115	0	0.0395	0	0.3843	0.1941	0	0.035	0	0.0951	0.0213
Cl	0	0	0	0	0	0	0	0	0	0	0	0	0
H_2O	0	0	0	0	0	0	0	0	0	0	0	0	0
B_2O_3	8.4962	8.7808	8.9753	9.951	9.1408	9.8816	9.8299	9.0683	9.0078	6.5358	9.8633	6.7045	9.1786
Li_2O	0	0	0	0	0	0	0	0	0	0	0	0	0
H_2O*	3.5243	3.56911	3.55376	3.55309	3.58762	3.57506	3.5502	3.55359	3.57825	3.54932	3.56051	3.56881	3.55022
B_2O_3*	-	-	-	-	-	-	-	-	-	-	-	-	-
Li_2O*	0.38539	0.47352	0.3977	0.3165	0.38617	0.38801	0.46916	0.41163	0.5305	0.33354	0.32798	0.39954	0.41777
Total	100.431	100.719	100.415	100.157	100.671	100.449	100.533	100.573	100.628	100.428	100.402	100.812	100.323
O=F	0	0	0.04842	0	0.01663	0	0.16182	0.08173	0	0.01474	0	0.04004	0.00897
Total*	100.354	100.664	100.359	100.099	100.626	100.399	100.473	100.514	100.584	100.372	100.342	100.745	100.266
B	3.13483	3.16419	3.11773	3.089	3.1244	3.12132	3.15789	3.1231	3.17171	3.0774	3.10982	3.13002	3.12983

T: Si	5.74551	5.7209	5.75042	5.79355	5.77263	5.78111	5.71702	5.7455	5.72477	5.77625	5.75562	5.75589	5.7335
Al	0.25449	0.2791	0.24958	0.20645	0.22737	0.21889	0.28298	0.2545	0.27523	0.22375	0.24438	0.24411	0.2665
Z: Al	6	6	6	6	6	6	6	6	6	6	6	6	6
Mg	0	0	0	0	0	0	0	0	0	0	0	0	0
Y: Al	0.03076	0.05529	0.12979	0.25657	0.21157	0.2192	0.06601	0.10906	0.05562	0.16454	0.24904	0.20799	0.1094
Ti	0.07242	0.07001	0.06898	0.04393	0.0437	0.04324	0.07399	0.0743	0.07307	0.07351	0.04016	0.04132	0.07005
V	0	0	0	0	0	0	0	0	0	0	0	0	0
Cr	0.00171	0.00065	0.00085	0.00035	0.00053	0.00055	0.00128	0.0011	0.00095	0.00135	0.0008	0.00057	0.00059
Fe^{3+}	0	0	0	0	0	0	0	0	0	0	0	0	0
Mg	1.18745	1.13158	1.10492	1.09418	1.08833	1.0914	1.08086	1.08347	1.08323	1.08451	1.10666	1.11126	1.11606
Mn	0.00387	0.00525	0.00316	0.00227	0.01258	0.00227	0.00439	0.00439	0.00035	0.00298	0.00385	0.00295	0.00281
Fe^{2+}	1.44662	1.4228	1.42738	1.39187	1.38747	1.38586	1.46095	1.45363	1.43433	1.45064	1.38165	1.37164	1.42248
Zn	0	0	0	0	0	0	0	0	0	0	0	0	0
Li*	0.25723	0.31446	0.26498	0.21088	0.25589	0.25755	0.31255	0.2741	0.3525	0.22253	0.2179	0.2643	0.27864
Y	3.00004	3.00004	3.00006	3.00005	3.00006	3.00006	3.00004	3.00006	3.00004	3.00006	3.00006	3.00004	3.00004
X: Ca	0.16482	0.15725	0.1525	0.12049	0.11966	0.12012	0.16414	0.16428	0.16722	0.16491	0.12455	0.12571	0.1561
Ba	0	0	0	0	0	0	0	0	0	0	0	0	0
Na	0.58551	0.57789	0.57338	0.55136	0.55889	0.55395	0.56462	0.5581	0.55984	0.55667	0.54288	0.56477	0.57759
K	0.01463	0.01254	0.01419	0.01302	0.01213	0.01186	0.01355	0.01367	0.01547	0.01452	0.01048	0.01085	0.01566
Rb	0	0	0	0	0	0	0	0	0	0	0	0	0
Cs	0	0	0	0	0	0	0	0	0	0	0	0	0
X-vacancy	0.23504	0.25233	0.25993	0.31512	0.30931	0.31407	0.25769	0.26395	0.25746	0.26389	0.32209	0.29867	0.25065
V+W site													
OH	3.90241	3.93168	3.92842	3.92763	3.94387	3.93697	3.92345	3.92581	3.94411	3.92851	3.92464	3.91631	3.92799
F	0.09607	0.06753	0.07028	0.07217	0.05582	0.06292	0.0754	0.07349	0.05472	0.06969	0.07458	0.08325	0.07103

SiO_2	35.0548	35.9037	35.0544	35.1141	35.9439	35.8546	35.6742	35.8622
TiO_2	0	0.0029	0	0.0055	0.0153	0.0069	0	0
Al_2O_3	34.8141	34.3314	34.3736	34.4486	34.4413	34.2667	34.3131	34.1635
V_2O_3	0	0	0	0	0	0	0	0
Cr_2O_3	0.0007	0	0	0	0	0.0014	0	0
Fe_2O_3	0	0	0	0	0	0	0	0
FeO	11.8538	12.0928	11.9881	12.0384	12.3528	12.3087	12.0304	11.4406
MgO	4.4048	4.4001	4.4155	4.4805	4.4708	4.3952	4.4581	4.7754
CaO	0.0447	0.047	0.0344	0.0401	0.0229	0.0642	0.0459	0.1964
MnO	0.9329	1.0373	1.0363	1.0928	1.0018	1.0882	0.9861	0.9288
ZnO	0	0	0	0	0	0	0	0
BaO	0	0	0	0	0	0	0	0
Na_2O	0.9792	1.0712	1.0318	1.0462	0.9856	1.0977	1.1176	1.4058
K_2O	0	0.0078	0.0348	-0.0296	0.0077	0.0129	0.0126	0.0757
Rb_2O	0	0	0	0	0	0	0	0
Cs_2O	0	0	0	0	0	0	0	0
F	0	0	0.1938	0.08	0	0	0	0
Cl	0	0	0	0	0	0	0	0
H_2O	0	0	0	0	0	0	0	0
B_2O_3	9.5652	9.3842	8.3783	8.0827	8.876	9.5871	8.8734	9.6661
Li_2O	0	0	0	0	0	0	0	0
H_2O*	3.57046	3.5243	3.56911	3.55376	3.55309	3.58762	3.57506	3.5502
B_2O_3*	-	-	-	-	-	-	-	-
Li_2O*	0.35516	0.38539	0.47352	0.3977	0.3165	0.38617	0.38801	0.46916
Total	100.393	100.431	100.719	100.415	100.157	100.671	100.449	100.533

O=F	0	0	0.0816	0.03369	0	0	0	0
Total*	100.354	100.354	100.664	100.359	100.099	100.626	100.399	100.473
B	3.10916	3.13483	3.16419	3.11773	3.089	3.1244	3.12132	3.15789
T: Si	5.74845	5.74551	5.7209	5.75042	5.79355	5.77263	5.78111	5.71702
Al	0.25155	0.25449	0.2791	0.24958	0.20645	0.22737	0.21889	0.28298
Z: Al	6	6	6	6	6	6	6	6
Mg	0	0	0	0	0	0	0	0
Y: Al	0.12919	0.03076	0.05529	0.12979	0.25657	0.21157	0.2192	0.06601
Ti	0.06665	0.07242	0.07001	0.06898	0.04393	0.0437	0.04324	0.07399
V	0	0	0	0	0	0	0	0
Cr	0.00093	0.00171	0.00065	0.00085	0.00035	0.00053	0.00055	0.00128
Fe^{3+}	0	0	0	0	0	0	0	0
Mg	1.12561	1.18745	1.13158	1.10492	1.09418	1.08833	1.0914	1.08086
Mn	0.00509	0.00387	0.00525	0.00316	0.00227	0.01258	0.00227	0.00439
Fe^{2+}	1.43577	1.44662	1.4228	1.42738	1.39187	1.38747	1.38586	1.46095
Zn	0	0	0	0	0	0	0	0
Li*	0.23683	0.25723	0.31446	0.26498	0.21088	0.25589	0.25755	0.31255
Y	3.00006	3.00004	3.00004	3.00006	3.00005	3.00006	3.00006	3.00004
X: Ca	0.15124	0.16482	0.15725	0.1525	0.12049	0.11966	0.12012	0.16414
Ba	0	0	0	0	0	0	0	0
Na	0.57895	0.58551	0.57789	0.57338	0.55136	0.55889	0.55395	0.56462
K	0.01585	0.01463	0.01254	0.01419	0.01302	0.01213	0.01186	0.01355

Rb	0	0	0	0	0	0	0	0
Cs	0	0	0	0	0	0	0	0
X-vacancy	0.25396	0.23504	0.25233	0.25993	0.31512	0.30931	0.31407	0.25769
V+W site								
OH	3.95005	3.90241	3.93168	3.92842	3.92763	3.94387	3.93697	3.92345
F	0.04899	0.09607	0.06753	0.07028	0.07217	0.05582	0.06292	0.0754

Sample: LG-3 (I) Two-mica leucogranite

SiO_2	35.3253	35.1359	35.7728	35.1046	35.9814	35.4123	35.9207	35.4328	35.9236	35.0419	35.5732	35.8085	35.9885	35.5334	35.9254
TiO_2	0	0.0168	0	0	0.0037	0	0.0165	0	0.0121	0.0026	0	0	0	0.0172	0.0055
Al_2O_3	33.086	34.8877	34.9502	34.1411	34.1066	34.0803	34.2789	34.3232	34.2127	34.3305	34.2731	34.9619	34.7095	34.3694	34.1566
V_2O_3	0	0	0	0	0	0	0	0	0	0	0	0	0	0	0
Cr_2O_3	0.0428	0	0	0.021	0.0146	0.0044	0.0458	0	0.0044	0.0256	0.0178	0.0455	0	0	0
Fe_2O_3															
FeO	12.0188	12.2208	12.0631	11.7667	8.0101	10.6943	10.2691	10.7077	10.6238	10.7325	8.8496	10.9925	11.246	11.2149	11.6403
MgO	5.0175	4.565	4.5271	4.8075	2.7438	5.7251	5.9296	5.9978	5.9408	5.6828	1.7515	5.7554	5.7792	5.3801	5.3098
CaO	0.0632	0	0.0229	0	0.3987	0.0494	0.0472	0.0299	0.0357	0.0368	1.2682	0.0046	0.0737	0.0563	0.0218
MnO	0.9735	0.9217	0.8441	0.6808	0.3761	0.4891	0.4507	0.3565	0.3903	0.3948	0.1782	0.5147	0.5204	0.4716	0.6143
ZnO	0	0	0	0	0	0	0	0	0	0	0	0	0	0	0
BaO	0	0	0	0	0	0	0	0	0	0	0	0	0	0	0
Na_2O	1.4798	1.0535	1.0064	1.0157	0.5954	0.784	0.7746	0.8086	0.7591	0.7484	0.4311	0.7663	0.9089	0.8036	0.7867
K_2O	0.0272	0.0399	0.006	0.0056	0.1005	0	0	0	0	0.0044	0.4095	0.0018	0.0049	0.001	0
Rb_2O	0	0	0	0	0	0	0	0	0	0	0	0	0	0	0
Cs_2O	0	0	0	0	0	0	0	0	0	0	0	0	0	0	0
F	0	0	0.2136	0	0	0	0	0	0.0673	0.0203	0.0538	0	0	0	0.2149
Cl	0	0	0	0	0	0	0	0	0	0	0	0	0	0	0
H_2O	0	0	0	0	0	0	0	0	0	0	0	0	0	0	0
B_2O_3	8.5548	8.3929	8.2031	8.5239	8.4196	8.6355	8.1289	10.1364	8.8915	0	0.1693	8.531	9.264	8.8785	8.9445
Li_2O															
H_2O*	3.53909	3.53747	3.51684	3.54317	3.50259	3.50503	3.52007	3.53404	3.55302	3.53937	3.57046	3.5243	3.55376	3.55309	3.58762
B_2O_3*	-	-	-	-	-	-	-	-	-	-	-	-	-	-	-
Li_2O*	0.40651	0.44897	0.4439	0.49303	0.41338	0.38	0.48118	0.36867	0.43362	0.41968	0.35516	0.38539	0.3977	0.3165	0.38617
Total	99.831	99.9768	99.7243	100.078	99.5175	99.4619	99.9493	100.078	100.181	100.256	100.393	100.431	100.415	100.157	100.671

O=F	0	0	0.08994	0	0	0	0	0	0.02834	0.00855	0.02265	0	0	0	0.09049
Total*	99.7802	99.9135	99.6512	100.018	99.4487	99.392	99.8734	100.018	100.132	100.194	100.354	100.354	100.359	100.099	100.626
B	3	3	3	3	3	3	3	3	3	3	3	3	3	3	3
T: Si	5.74057	5.74354	5.74874	5.75256	5.75097	5.72767	5.69127	5.71179	5.72249	5.71876	5.74845	5.74551	5.75042	5.79355	5.77263
Al	0.25943	0.25646	0.25126	0.24744	0.24903	0.27233	0.30873	0.28821	0.27751	0.28124	0.25155	0.25449	0.24958	0.20645	0.22737
Z: Al	6	6	6	6	6	6	6	6	6	6	6	6	6	6	6
Mg	0	0	0	0	0	0	0	0	0	0	0	0	0	0	0
Y: Al	0.04058	0.05052	0.08232	0.03799	0.05384	0.05265	0.02773	0.0726	0.05217	0.03715	0.12919	0.03076	0.12979	0.25657	0.21157
Ti	0.07021	0.06904	0.06885	0.07348	0.07557	0.07254	0.07173	0.07005	0.06846	0.07073	0.06665	0.07242	0.06898	0.04393	0.0437
V	0	0	0	0	0	0	0	0	0	0	0	0	0	0	0
Cr	0.00012	0.00014	0.00043	0.00087	0.00085	0	0.0003	0.00039	0.00105	5.3E-05	0.00093	0.00171	0.00085	0.00035	0.00053
Fe^{3+}	0	0	0	0	0	0	0	0	0	0	0	0	0	0	0
Mg	1.19222	1.21616	1.16675	1.16617	1.14188	1.21723	1.19786	1.17931	1.1501	1.19551	1.12561	1.18745	1.10492	1.09418	1.08833
Mn	0.00371	0.00439	0.00334	0.00211	0.00211	0.00123	0.00193	0.00299	0.00298	0.00122	0.00509	0.00387	0.00316	0.00227	0.01258
Fe^{2+}	1.42065	1.35983	1.38099	1.39026	1.4476	1.40076	1.37874	1.42797	1.43564	1.41512	1.43577	1.44662	1.42738	1.39187	1.38747
Zn	0	0	0	0	0	0	0	0	0	0	0	0	0	0	0
Li*	0.27252	0.29994	0.29735	0.32919	0.2782	0.25564	0.32174	0.24674	0.28965	0.28024	0.23683	0.25723	0.26498	0.21088	0.25589
Y	3.00001	3.00002	3.00003	3.00005	3.00005	3.00005	3.00001	3.00005	3.00005	3.00002	3.00006	3.00004	3.00006	3.00005	3.00006

X: Ca	0.14929	0.15581	0.14571	0.16444	0.15105	0.15408	0.16964	0.16683	0.15427	0.1683	0.15124	0.16482	0.1525	0.12049	0.11966
Ba	0	0	0	0	0	0	0	0	0	0	0	0	0	0	0
Na	0.58946	0.58757	0.58141	0.57617	0.58529	0.59271	0.56374	0.57451	0.57881	0.58228	0.57895	0.58551	0.57338	0.55136	0.55889
K	0.01508	0.01579	0.01526	0.01633	0.01399	0.01577	0.01559	0.01565	0.01378	0.01678	0.01585	0.01463	0.01419	0.01302	0.01213
Rb	0	0	0	0	0	0	0	0	0	0	0	0	0	0	0
Cs	0	0	0	0	0	0	0	0	0	0	0	0	0	0	0
X-vacancy	0.24618	0.24083	0.25762	0.24305	0.24967	0.23744	0.25104	0.24301	0.25315	0.23264	0.25396	0.23504	0.25993	0.31512	0.30931
V+W site															
OH	3.93504	3.91981	3.90787	3.92455	3.91061	3.9118	3.90384	3.92375	3.93723	3.9203	3.95005	3.90241	3.92842	3.92763	3.94387
F	0.06358	0.07907	0.09157	0.07379	0.0865	0.08789	0.0947	0.07512	0.06137	0.07757	0.04899	0.09607	0.07028	0.07217	0.05582

SiO_2	35.5556	35.8496	35.4191	35.0255	35.234	35.0302	35.2204	35.4107	35.8194	35.4381	35.485	35.1164	35.6133	35.6138	35.9739
TiO_2	0.0132	0	0	0.0029	0.0208	0	0.0026	0	0	0.0084	0	0.0132	0	0.0066	0
Al_2O_3	34.7607	34.4803	28.7721	34.5547	34.5232	34.034	34.4338	34.8234	34.3641	34.6559	34.9567	34.423	34.538	34.3235	34.8499
V_2O_3	0	0	0	0	0	0	0	0	0	0	0	0	0	0	0
Cr_2O_3	0.0036	0.0216	0.0159	0	0	0.0268	0.031	0.0049	0	0.0131	0.0363	0.0247	0.0236	0.0175	0
Fe_2O_3															
FeO	10.9909	11.6199	12.0896	11.8284	11.8072	11.1758	10.9222	1.2254	10.8384	11.1031	10.8178	10.8297	10.6949	10.7122	11.0769
MgO	4.7705	4.8278	4.5271	5.2374	4.8899	4.9934	5.2249	1.0034	5.1933	5.3527	5.6864	5.2227	5.2256	5.1166	5.8478
CaO	0.0367	0.0057	0.0298	0.0688	0.0195	0.0241	0.0287	0	0.0574	0.031	0.0265	0.0103	0.0345	0.0299	0.054
MnO	0.6562	0.7614	0.7497	0.6989	0.768	0.5764	0.6341	0.0477	0.4908	0.5615	0.6501	0.5894	0.6346	0.5467	0.4419
ZnO	0	0	0	0	0	0	0	0	0	0	0	0	0	0	0
BaO	0	0	0	0	0	0	0	0	0	0	0	0	0	0	0
Na_2O	0.8599	1.0274	0.9402	1.1403	0.9101	0.8569	1.0175	0.9115	0.9575	0.8414	1.0226	1.0627	1.0398	0.9544	1.0352
K_2O	0.0143	0	0.0156	0.0004	0	0.0005	0.0161	8.1724	0	0.0108	0.0091	0.0027	0	0.0142	0.0071
Rb_2O	0	0	0	0	0	0	0	0	0	0	0	0	0	0	0
Cs_2O	0	0	0	0	0	0	0	0	0	0	0	0	0	0	0
F	0.0802	0.0206	0.2006	0	0.1271	0	0.0852	0.467	0	0	0	0.0084	0.0084	0	0.1717
Cl	0	0	0	0	0	0	0	0	0	0	0	0	0	0	0
H_2O	0	0	0	0	0	0	0	0	0	0	0	0	0	0	0
B_2O_3	8.3327	5.0243	9.8965	0.0001	9.1162	9.0141	0	8.1813	8.4623	9.6375	8.1367	8.4534	8.9092	8.0741	9.1717
Li_2O							0	0	0	0	0	0	0	0	0
H_2O*	3.57506	3.55359	3.57825	3.54932	3.56051	3.56881	3.53909	3.53747	3.51684	3.54317	3.50503	3.52007	3.55302	3.53937	3.55022
B_2O_3*	-	-	-	-	-	-	-	-	-	-	-	-	-	-	-
Li_2O*	0.38801	0.41163	0.5305	0.33354	0.32798	0.39954	0.40651	0.44897	0.4439	0.49303	0.38	0.48118	0.43362	0.41968	0.41777
Total	100.449	100.573	100.628	100.428	100.402	100.812	99.831	99.9768	99.7243	100.078	99.4619	99.9493	100.181	100.256	100.323
O=F	0.03377	0.00867	0.08447	0	0.05352	0	0.03588	0.19664	0	0	0	0.00354	0.00354	0	0.0723

Total*	100.399	100.514	100.584	100.372	100.342	100.745	99.7802	99.9135	99.6512	100.018	99.392	99.8734	100.132	100.194	100.266
B	3	3	3	3	3	3	3	3.15087	3.14666	3.15642	3.13782	3.18012	3.15858	3.14903	3.12983
T: Si	5.78111	5.7455	5.72477	5.77625	5.75562	5.75589	5.74057	5.74354	5.74874	5.75256	5.72767	5.69127	5.72249	5.71876	5.7335
Al	0.21889	0.2545	0.27523	0.22375	0.24438	0.24411	0.25943	0.25646	0.25126	0.24744	0.27233	0.30873	0.27751	0.28124	0.2665
Z: Al	6	6	6	6	6	6	6	6	6	6	6	6	6	6	6
Mg	0	0	0	0	0	0	0	0	0	0	0	0	0	0	0
Y: Al	0.2192	0.10906	0.05562	0.16454	0.24904	0.20799	0.04058	0.05052	0.08232	0.03799	0.05265	0.02773	0.05217	0.03715	0.1094
Ti	0.04324	0.0743	0.07307	0.07351	0.04016	0.04132	0.07021	0.06904	0.06885	0.07348	0.07254	0.07173	0.06846	0.07073	0.07005
V	0	0	0	0	0	0	0	0	0	0	0	0	0	0	0
Cr	0.00055	0.0011	0.00095	0.00135	0.0008	0.00057	0.00012	0.00014	0.00043	0.00087	0	0.0003	0.00105	5.3E-05	0.00059
Fe^{3+}	0	0	0	0	0	0	0	0	0	0	0	0	0	0	0
Mg	1.0914	1.08347	1.08323	1.08451	1.10666	1.11126	1.19222	1.21616	1.16675	1.16617	1.21723	1.19786	1.1501	1.19551	1.11606
Mn	0.00227	0.00439	0.00035	0.00298	0.00385	0.00295	0.00371	0.00439	0.00334	0.00211	0.00123	0.00193	0.00298	0.00122	0.00281
Fe^{2+}	1.38586	1.45363	1.43433	1.45064	1.38165	1.37164	1.42065	1.35983	1.38099	1.39026	1.40076	1.37874	1.43564	1.41512	1.42248
Zn	0	0	0	0	0	0	0	0	0	0	0	0	0	0	0
Li*	0.25755	0.2741	0.3525	0.22253	0.2179	0.2643	0.27252	0.29994	0.29735	0.32919	0.25564	0.32174	0.28965	0.28024	0.27864
?Y	3.00006	3.00006	3.00004	3.00006	3.00006	3.00004	3.00001	3.00002	3.00003	3.00005	3.00005	3.00001	3.00005	3.00002	3.00004

X: Ca	0.12012	0.16428	0.16722	0.16491	0.12455	0.12571	0.14929	0.15581	0.14571	0.16444	0.15408	0.16964	0.15427	0.1683	0.1561
Ba	0	0	0	0	0	0	0	0	0	0	0	0	0	0	0
Na	0.55395	0.5581	0.55984	0.55667	0.54288	0.56477	0.58946	0.58757	0.58141	0.57617	0.59271	0.56374	0.57881	0.58228	0.57759
K	0.01186	0.01367	0.01547	0.01452	0.01048	0.01085	0.01508	0.01579	0.01526	0.01633	0.01577	0.01559	0.01378	0.01678	0.01566
Rb	0	0	0	0	0	0	0	0	0	0	0	0	0	0	0
Cs	0	0	0	0	0	0	0	0	0	0	0	0	0	0	0
X-vacancy	0.31407	0.26395	0.25746	0.26389	0.32209	0.29867	0.24618	0.24083	0.25762	0.24305	0.23744	0.25104	0.25315	0.23264	0.25065
V+W site															
OH	3.93697	3.92581	3.94411	3.92851	3.92464	3.91631	3.93504	3.91981	3.90787	3.92455	3.9118	3.90384	3.93723	3.9203	3.92799
	0.06292	0.07349	0.05472	0.06969	0.07458	0.08325	0.06358	0.07907	0.09157	0.07379	0.08789	0.0947	0.06137	0.07757	0.07103

SiO_2	35.2924	35.2199	35.8111	35.7641	35.6205	35.0135	35.3694	35.8021	35.6345	35.304	35.3232	35.3405	35.2579	35.1872	35.0593	35.928
TiO_2	0.0252	0.0047	0	0	0	0	0	0.0263	0	0.0004	0	0	0	0.0117	0	0
Al_2O_3	28.5493	34.711	34.182	34.1664	34.3992	34.1717	34.1252	34.8537	34.0313	34.86	34.5319	34.4511	34.206	34.7815	34.4605	34.0587
V_2O_3	0	0	0	0	0	0	0	0	0	0	0	0	0	0	0	0
Cr_2O_3	0	0	0	0	0.036	0.0007	0.0602	0	0.0498	0.0275	0.0134	0.068	0.0261	0.004	0.0177	0
Fe_2O_3																
FeO	10.6378	10.9356	10.7188	10.9973	10.9659	10.8817	11.0043	10.7986	11.1039	10.9783	10.5806	10.6842	11.1346	10.571	11.277	11.3581
MgO	4.5791	5.4879	4.8421	5.6178	5.4653	5.4518	5.4994	5.2	5.2068	5.3317	4.8272	5.239	5.2119	4.2934	5.1954	5.1164
CaO	0.0929	0.0322	0.0826	0.0264	0.0355	0.054	0.031	0.0367	0.0367	0.0195	0.0126	0.023	0.0161	0.4624	0.031	0.0562
MnO	0.401	0.4555	0.5623	0.5432	0.5682	0.5711	0.6045	0.6397	0.7116	0.5671	1.0151	0.6476	0.7887	0.5342	0.5323	0.5904
ZnO	0	0	0	0	0	0	0	0	0	0	0	0	0	0	0	0
BaO	0	0	0	0	0	0	0	0	0	0	0	0	0	0	0	0
Na_2O	0.6738	0.8062	0.7674	0.7278	0.7162	0.7305	0.8216	0.8501	0.8289	0.9438	1.295	1.0614	0.8318	0.5806	0.6914	0.6761
K_2O	0.0398	0	0	0.0076	0	0	0.002	0.0234	0.0222	0.0012	0	0	0.0207	0.0411	0	0.0019
Rb_2O	0	0	0	0	0	0	0	0	0	0	0	0	0	0	0	0
Cs_2O	0	0	0	0	0	0	0	0	0	0	0	0	0	0	0	0
F	0.0838	0	0.2119	0.0463	0	0.1085	0.1018	0	0.1027	0	0	0.0947	0	0	0	0
Cl	0	0	0	0	0	0	0	0	0	0	0	0	0	0	0	0
H_2O	0	0	0	0	0	0	0	0	0	0	0	0	0	0	0	0
B_2O_3	9.4916	2.8476	8.8429	8.9508	0	9.2608	8.6718	8.8307	9.1669	6.1603	7.6922	9.1344	9.2844	9.6045	8.8882	8.4867
Li_2O	0	0	0	0	0	0	0	0	0	0	0	0	0	0	0	0
H_2O*	3.57046	3.5243	3.56911	3.55376	3.55309	3.58762	3.57506	3.5502	3.55359	3.57825	3.54932	3.56051	3.56881	3.55022	3.57046	3.5243
B_2O_3*	-	-	-	-	-	-	-	-	-	-	-	-	-	-	-	-
Li_2O*	0.35516	0.38539	0.47352	0.3977	0.3165	0.38617	0.38801	0.46916	0.41163	0.5305	0.33354	0.32798	0.39954	0.41777	0.35516	0.38539
Total	100.393	100.431	100.719	100.415	100.157	100.671	100.449	100.533	100.573	100.628	100.428	100.402	100.812	100.323	100.393	100.431
O=F	0.03529	0	0.08923	0.0195	0	0.04569	0.04287	0	0.04324	0	0	0.03988	0	0	0	0

Total*	100.354	100.354	100.664	100.359	100.099	100.626	100.399	100.473	100.514	100.584	100.372	100.342	100.745	100.266	100.354	100.354
B	3.10916	3.13483	3.16419	3.11773	3	3.1244	3.12132	3.15789	3.1231	3.17171	3.0774	3.10982	3.13002	3.12983	3.10916	3.13483
T: Si	5.74845	5.74551	5.7209	5.75042	5.79355	5.77263	5.78111	5.71702	5.7455	5.72477	5.77625	5.75562	5.75589	5.7335	5.74845	5.74551
Al	0.25155	0.25449	0.2791	0.24958	0.20645	0.22737	0.21889	0.28298	0.2545	0.27523	0.22375	0.24438	0.24411	0.2665	0.25155	0.25449
Z: Al	6	6	6	6	6	6	6	6	6	6	6	6	6	6	6	6
Mg	0	0	0	0	0	0	0	0	0	0	0	0	0	0	0	0
Y: Al	0.12919	0.03076	0.05529	0.12979	0.25657	0.21157	0.2192	0.06601	0.10906	0.05562	0.16454	0.24904	0.20799	0.1094	0.12919	0.03076
Ti	0.06665	0.07242	0.07001	0.06898	0.04393	0.0437	0.04324	0.07399	0.0743	0.07307	0.07351	0.04016	0.04132	0.07005	0.06665	0.07242
V	0	0	0	0	0	0	0	0	0	0	0	0	0	0	0	0
Cr	0.00093	0.00171	0.00065	0.00085	0.00035	0.00053	0.00055	0.00128	0.0011	0.00095	0.00135	0.0008	0.00057	0.00059	0.00093	0.00171
Fe^{3+}	0	0	0	0	0	0	0	0	0	0	0	0	0	0	0	0
Mg	1.12561	1.18745	1.13158	1.10492	1.09418	1.08833	1.0914	1.08086	1.08347	1.08323	1.08451	1.10666	1.11126	1.11606	1.12561	1.18745
Mn	0.00509	0.00387	0.00525	0.00316	0.00227	0.01258	0.00227	0.00439	0.00439	0.00035	0.00298	0.00385	0.00295	0.00281	0.00509	0.00387
Fe^{2+}	1.43577	1.44662	1.4228	1.42738	1.39187	1.38747	1.38586	1.46095	1.45363	1.43433	1.45064	1.38165	1.37164	1.42248	1.43577	1.44662
Zn	0	0	0	0	0	0	0	0	0	0	0	0	0	0	0	0
Li*	0.23683	0.25723	0.31446	0.26498	0.21088	0.25589	0.25755	0.31255	0.2741	0.3525	0.22253	0.2179	0.2643	0.27864	0.23683	0.25723
Y	3.00006	3.00004	3.00004	3.00006	3.00005	3.00006	3.00006	3.00004	3.00006	3.00004	3.00006	3.00006	3.00004	3.00004	3.00006	3.00004

X: Ca	0.15124	0.16482	0.15725	0.1525	0.12049	0.11966	0.12012	0.16414	0.16428	0.16722	0.16491	0.12455	0.12571	0.1561	0.15124	0.16482
Ba	0	0	0	0	0	0	0	0	0	0	0	0	0	0	0	0
Na	0.57895	0.58551	0.57789	0.57338	0.55136	0.55889	0.55395	0.56462	0.5581	0.55984	0.55667	0.54288	0.56477	0.57759	0.57895	0.58551
K	0.01585	0.01463	0.01254	0.01419	0.01302	0.01213	0.01186	0.01355	0.01367	0.01547	0.01452	0.01048	0.01085	0.01566	0.01585	0.01463
Rb	0	0	0	0	0	0	0	0	0	0	0	0	0	0	0	0
Cs	0	0	0	0	0	0	0	0	0	0	0	0	0	0	0	0
X-vacancy	0.25396	0.23504	0.25233	0.25993	0.31512	0.30931	0.31407	0.25769	0.26395	0.25746	0.26389	0.32209	0.29867	0.25065	0.25396	0.23504
V+W site																
OH	3.95005	3.90241	3.93168	3.92842	3.92763	3.94387	3.93697	3.92345	3.92581	3.94411	3.92851	3.92464	3.91631	3.92799	3.95005	3.90241
F	0.04899	0.09607	0.06753	0.07028	0.07217	0.05582	0.06292	0.0754	0.07349	0.05472	0.06969	0.07458	0.08325	0.07103	0.04899	0.09607

SiO_2	35.0965	35.1359	35.686	35.5312	35.4209	35.721	35.1607	35.6159	35.1769	35.3202	35.0613	35.7473	35.7473	35.1381
TiO_2	0	0	0	0	0	0	0	0.0139	0	0.0015	0	0.0058	0.0058	0
Al_2O_3	34.1981	34.5099	34.332	34.2952	34.1096	34.4981	34.3259	34.5062	34.5293	34.3774	34.5962	30.3119	30.3119	31.6032
V_2O_3	0	0	0	0	0	0	0	0	0	0	0	0	0	0
Cr_2O_3	0	0	0.0376	0	0	0.0241	0	0	0	0	0	0.0321	0.0321	0.025
Fe_2O_3														
FeO	11.1895	11.078	11.296	10.9184	10.8605	11.0869	10.4369	10.9052	10.8366	10.9318	11.0454	11.3008	11.3008	11.3077
MgO	5.167	5.1539	5.2153	5.1256	5.3782	5.105	5.3395	5.2031	5.1967	5.1136	5.1171	5.0315	5.0315	5.2146
CaO	0.0206	0.0652	0.0481	0.0286	0.0103	0.0652	0.0298	0	0.0229	0.0527	0.0229	0.0619	0.0619	0.039
MnO	0.6228	0.5655	0.5655	0.5845	0.5498	0.5813	0.6804	0.6797	0.6352	0.5189	0.6071	0.5334	0.5334	0.4398
ZnO	0	0	0	0	0	0	0	0	0	0	0	0	0	0
BaO	0	0	0	0	0	0	0	0	0	0	0	0	0	0
Na_2O	0.7474	0.7224	0.6948	0.8291	0.9416	0.8369	0.9279	0.9353	0.9175	0.817	0.8649	0.7917	0.7917	0.8192
K_2O	0.02	0	0.0018	0.01	0.014	0	0	0.0221	0	0	0	0.0254	0.0254	0
Rb_2O	0	0	0	0	0	0	0	0	0	0	0	0	0	0
Cs_2O	0	0	0	0	0	0	0	0	0	0	0	0	0	0
F	0	0	0.1183	0	0	0	0.0978	0.0632	0	0.0597	0.1225	0.0376	0.0376	0
Cl	0	0	0	0	0	0	0	0	0	0	0	0	0	0
H_2O	0	0	0	0	0	0	0	0	0	0	0	0	0	0
B_2O_3	8.9189	9.5304	8.5285	8.6931	8.4882	8.6029	8.3284	8.2626	8.2996	9.9662	8.5186	9.0262	9.0262	9.097
Li_2O	0	0	0	0	0	0	0	0	0	0	0		0.00	0.00
H_2O*	3.56911	3.55376	3.55309	3.58762	3.57506	3.5502	3.55359	3.57825	3.54932	3.56051	3.56881		3.54	3.54
B_2O_3*	-	-	-	-	-	-	-	-	-	-	-		-	-

Li_2O*	0.47352	0.3977	0.3165	0.38617	0.38801	0.46916	0.41163	0.5305	0.33354	0.32798	0.39954		0.41	0.45
Total	100.719	100.415	100.157	100.671	100.449	100.533	100.573	100.628	100.428	100.402	100.812	92.9056	99.83	99.98
O=F	0	0	0.04981	0	0	0	0.04118	0.02661	0	0.02514	0.05158	0.01583	0.02	0.00
Total*	100.664	100.359	100.099	100.626	100.399	100.473	100.514	100.584	100.372	100.342	100.745	92.8898	99.78	99.91
B	3.16419	3.11773	3.089	3.1244	3.12132	3.15789	3.1231	3.17171	3.0774	3.10982	3.13002	3	3.149	3.151
T: Si	5.7209	5.75042	5.79355	5.77263	5.78111	5.71702	5.7455	5.72477	5.77625	5.75562	5.75589	5.74354	5.741	5.744
Al	0.2791	0.24958	0.20645	0.22737	0.21889	0.28298	0.2545	0.27523	0.22375	0.24438	0.24411	0.25646	0.259	0.256
Z: Al	6	6	6	6	6	6	6	6	6	6	6	6	6.000	6.000
Mg	0	0	0	0	0	0	0	0	0	0	0	0	0.000	0.000
Y: Al	0.05529	0.12979	0.25657	0.21157	0.2192	0.06601	0.10906	0.05562	0.16454	0.24904	0.20799	0.05052	0.041	0.051
Ti	0.07001	0.06898	0.04393	0.0437	0.04324	0.07399	0.0743	0.07307	0.07351	0.04016	0.04132	0.06904	0.070	0.069
V	0	0	0	0	0	0	0	0	0	0	0	0	0.000	0.000
Cr	0.00065	0.00085	0.00035	0.00053	0.00055	0.00128	0.0011	0.00095	0.00135	0.0008	0.00057	0.00014	0.000	0.000
Fe^{3+}	0	0	0	0	0	0	0	0	0	0	0	0	0.000	0.000
Mg	1.13158	1.10492	1.09418	1.08833	1.0914	1.08086	1.08347	1.08323	1.08451	1.10666	1.11126	1.21616	1.192	1.216
Mn	0.00525	0.00316	0.00227	0.01258	0.00227	0.00439	0.00439	0.00035	0.00298	0.00385	0.00295	0.00439	0.004	0.004
Fe^{2+}	1.4228	1.42738	1.39187	1.38747	1.38586	1.46095	1.45363	1.43433	1.45064	1.38165	1.37164	1.35983	1.421	1.360
Zn	0	0	0	0	0	0	0	0	0	0	0	0	0.000	0.000
Li*	0.31446	0.26498	0.21088	0.25589	0.25755	0.31255	0.2741	0.3525	0.22253	0.2179	0.2643	0.29994	0.273	0.300

Y	3.00004	3.00006	3.00005	3.00006	3.00006	3.00004	3.00006	3.00004	3.00006	3.00006	3.00004	3.00002	3.000	3.000
X: Ca	0.15725	0.1525	0.12049	0.11966	0.12012	0.16414	0.16428	0.16722	0.16491	0.12455	0.12571	0.15581	0.149	0.156
Ba	0	0	0	0	0	0	0	0	0	0	0	0	0.000	0.000
Na	0.57789	0.57338	0.55136	0.55889	0.55395	0.56462	0.5581	0.55984	0.55667	0.54288	0.56477	0.58757	0.589	0.588
K	0.01254	0.01419	0.01302	0.01213	0.01186	0.01355	0.01367	0.01547	0.01452	0.01048	0.01085	0.01579	0.015	0.016
Rb	0	0	0	0	0	0	0	0	0	0	0	0	0.000	0.000
Cs	0	0	0	0	0	0	0	0	0	0	0	0	0.000	0.000
X-vacancy	0.25233	0.25993	0.31512	0.30931	0.31407	0.25769	0.26395	0.25746	0.26389	0.32209	0.29867	0.24083	0.246	0.241
V+W site														
OH	3.93168	3.92842	3.92763	3.94387	3.93697	3.92345	3.92581	3.94411	3.92851	3.92464	3.91631	3.91981	3.935	3.920
F	0.06753	0.07028	0.07217	0.05582	0.06292	0.0754	0.07349	0.05472	0.06969	0.07458	0.08325	0.07907	0.064	0.079

SiO_2	35.0965	35.1359	35.686	35.5312	35.4209	35.721	35.1607	35.6159	35.1769	35.3202	35.0613	35.7473	35.7473	35.1381
TiO_2	0	0	0	0	0	0	0	0.0139	0	0.0015	0	0.0058	0.0058	0
Al_2O_3	34.1981	34.5099	34.332	34.2952	34.1096	34.4981	34.3259	34.5062	34.5293	34.3774	34.5962	30.3119	30.3119	31.6032
V_2O_3	0	0	0	0	0	0	0	0	0	0	0	0	0	0
Cr_2O_3	0	0	0.0376	0	0	0.0241	0	0	0	0	0	0.0321	0.0321	0.025
Fe_2O_3														
FeO	11.1895	11.078	11.296	10.9184	10.8605	11.0869	10.4369	10.9052	10.8366	10.9318	11.0454	11.3008	11.3008	11.3077
MgO	5.167	5.1539	5.2153	5.1256	5.3782	5.105	5.3395	5.2031	5.1967	5.1136	5.1171	5.0315	5.0315	5.2146
CaO	0.0206	0.0652	0.0481	0.0286	0.0103	0.0652	0.0298	0	0.0229	0.0527	0.0229	0.0619	0.0619	0.039
MnO	0.6228	0.5655	0.5655	0.5845	0.5498	0.5813	0.6804	0.6797	0.6352	0.5189	0.6071	0.5334	0.5334	0.4398
ZnO	0	0	0	0	0	0	0	0	0	0	0	0	0	0
BaO	0	0	0	0	0	0	0	0	0	0	0	0	0	0
Na_2O	0.7474	0.7224	0.6948	0.8291	0.9416	0.8369	0.9279	0.9353	0.9175	0.817	0.8649	0.7917	0.7917	0.8192
K_2O	0.02	0	0.0018	0.01	0.014	0	0	0.0221	0	0	0	0.0254	0.0254	0
Rb_2O	0	0	0	0	0	0	0	0	0	0	0	0	0	0
Cs_2O	0	0	0	0	0	0	0	0	0	0	0	0	0	0
F	0	0	0.1183	0	0	0	0.0978	0.0632	0	0.0597	0.1225	0.0376	0.0376	0
Cl	0	0	0	0	0	0	0	0	0	0	0	0	0	0
H_2O	0	0	0	0	0	0	0	0	0	0	0	0	0	0
B_2O_3	8.9189	9.5304	8.5285	8.6931	8.4882	8.6029	8.3284	8.2626	8.2996	9.9662	8.5186	9.0262	9.0262	9.097
Li_2O	0	0	0	0	0	0	0	0	0	0	0		0.00	0.00
H_2O*	3.56911	3.55376	3.55309	3.58762	3.57506	3.5502	3.55359	3.57825	3.54932	3.56051	3.56881		3.54	3.54
B_2O_3*	-	-	-	-	-	-	-	-	-	-	-		-	-

Li_2O*	0.47352	0.3977	0.3165	0.38617	0.38801	0.46916	0.41163	0.5305	0.33354	0.32798	0.39954		0.41	0.45
Total	100.719	100.415	100.157	100.671	100.449	100.533	100.573	100.628	100.428	100.402	100.812	92.9056	99.83	99.98
O=F	0	0	0.04981	0	0	0	0.04118	0.02661	0	0.02514	0.05158	0.01583	0.02	0.00
Total*	100.664	100.359	100.099	100.626	100.399	100.473	100.514	100.584	100.372	100.342	100.745	92.8898	99.78	99.91
B	3.16419	3.11773	3.089	3.1244	3.12132	3.15789	3.1231	3.17171	3.0774	3.10982	3.13002	3	3.149	3.151
T: Si	5.7209	5.75042	5.79355	5.77263	5.78111	5.71702	5.7455	5.72477	5.77625	5.75562	5.75589	5.74354	5.741	5.744
Al	0.2791	0.24958	0.20645	0.22737	0.21889	0.28298	0.2545	0.27523	0.22375	0.24438	0.24411	0.25646	0.259	0.256
Z: Al	6	6	6	6	6	6	6	6	6	6	6	6	6.000	6.000
Mg	0	0	0	0	0	0	0	0	0	0	0	0	0.000	0.000
Y: Al	0.05529	0.12979	0.25657	0.21157	0.2192	0.06601	0.10906	0.05562	0.16454	0.24904	0.20799	0.05052	0.041	0.051
Ti	0.07001	0.06898	0.04393	0.0437	0.04324	0.07399	0.0743	0.07307	0.07351	0.04016	0.04132	0.06904	0.070	0.069
V	0	0	0	0	0	0	0	0	0	0	0	0	0.000	0.000
Cr	0.00065	0.00085	0.00035	0.00053	0.00055	0.00128	0.0011	0.00095	0.00135	0.0008	0.00057	0.00014	0.000	0.000
Fe^{3+}	0	0	0	0	0	0	0	0	0	0	0	0	0.000	0.000
Mg	1.13158	1.10492	1.09418	1.08833	1.0914	1.08086	1.08347	1.08323	1.08451	1.10666	1.11126	1.21616	1.192	1.216
Mn	0.00525	0.00316	0.00227	0.01258	0.00227	0.00439	0.00439	0.00035	0.00298	0.00385	0.00295	0.00439	0.004	0.004
Fe^{2+}	1.4228	1.42738	1.39187	1.38747	1.38586	1.46095	1.45363	1.43433	1.45064	1.38165	1.37164	1.35983	1.421	1.360
Zn	0	0	0	0	0	0	0	0	0	0	0	0	0.000	0.000

Li*	0.31446	0.26498	0.21088	0.25589	0.25755	0.31255	0.2741	0.3525	0.22253	0.2179	0.2643	0.29994	0.273	0.300
Y	3.00004	3.00006	3.00005	3.00006	3.00006	3.00004	3.00006	3.00004	3.00006	3.00006	3.00004	3.00002	3.000	3.000
X: Ca	0.15725	0.1525	0.12049	0.11966	0.12012	0.16414	0.16428	0.16722	0.16491	0.12455	0.12571	0.15581	0.149	0.156
Ba	0	0	0	0	0	0	0	0	0	0	0	0	0.000	0.000
Na	0.57789	0.57338	0.55136	0.55889	0.55395	0.56462	0.5581	0.55984	0.55667	0.54288	0.56477	0.58757	0.589	0.588
K	0.01254	0.01419	0.01302	0.01213	0.01186	0.01355	0.01367	0.01547	0.01452	0.01048	0.01085	0.01579	0.015	0.016
Rb	0	0	0	0	0	0	0	0	0	0	0	0	0.000	0.000
Cs	0	0	0	0	0	0	0	0	0	0	0	0	0.000	0.000
X-vacancy	0.25233	0.25993	0.31512	0.30931	0.31407	0.25769	0.26395	0.25746	0.26389	0.32209	0.29867	0.24083	0.246	0.241
V+W site														
OH	3.93168	3.92842	3.92763	3.94387	3.93697	3.92345	3.92581	3.94411	3.92851	3.92464	3.91631	3.91981	3.935	3.920
F	0.06753	0.07028	0.07217	0.05582	0.06292	0.0754	0.07349	0.05472	0.06969	0.07458	0.08325	0.07907	0.064	0.079

SiO_2	35.1381	35.2441	35.8742	35.852	35.9151	35.1956	35.3416	35.2386	35.1529
TiO_2	0	0	0	0	0.004	0	0	0	0.7287
Al_2O_3	31.6032	29.7106	31.0252	31.1918	31.0053	30.5775	30.3413	34.7386	34.754
V_2O_3	0	0	0	0	0	0	0	0	
Cr_2O_3	0.025	0	0.0069	0.0086	0	0	0	0.021	-0.0395
Fe_2O_3									0
FeO	11.3077	10.4302	11.2471	11.5026	11.5809	11.5464	11.5837	11.4493	10.1616
MgO	5.2146	4.3188	5.2717	5.0843	4.9741	4.8696	4.8584	4.6828	2.5882
CaO	0.039	0.2532	0.031	0.0366	0.0149	0.0229	0.0195	0.0034	0.2861
MnO	0.4398	0.5264	0.5687	0.649	0.6055	0.7559	0.8069	0.8337	0.0728
ZnO	0	0	0	0	0	0	0	0	
BaO	0	0	0	0	0	0	0	0	
Na_2O	0.8192	0.6987	0.8183	0.8508	0.8846	1.0065	1.0194	1.0305	1.8344
K_2O	0	0.0842	0.0099	0	0	0.0045	0.0069	0	-0.0108
Rb_2O	0	0	0	0	0	0	0	0	
Cs_2O	0	0	0	0	0	0	0	0	
F	0	0	0	0.1169	0	0	0	0	
Cl	0	0	0	0	0	0	0	0	
H_2O	0	0	0	0	0	0	0	0	
B_2O_3	9.097	8.8655	9.1133	0	9.9147	9.5042	8.3463	8.1456	
Li_2O	0.00	0.00	0.00	0.00	0.00	0.00	0.00	0.00	
H_2O*	3.54	3.52	3.54	3.50	3.51	3.55	3.52	3.53	
B_2O_3*	-	-	-	-	-	-	-	-	
Li_2O*	0.45	0.44	0.49	0.41	0.38	0.40	0.48	0.37	

Total	99.98	99.72	100.08	99.52	99.46	100.22	99.95	100.08	85.5284
O=F	0.00	0.00	0.00	0.05	0.00	0.00	0.00	0.00	0
Total*	99.91	99.65	100.02	99.45	99.39	100.17	99.87	100.02	85.5284
B	3.151	3.147	3.156	3.000	3.138	3.142	3.180	3.133	3
T: Si	5.744	5.749	5.753	5.751	5.728	5.736	5.691	5.712	5.81518
Al	0.256	0.251	0.247	0.249	0.272	0.264	0.309	0.288	0.18482
Z: Al	6.000	6.000	6.000	6.000	6.000	6.000	6.000	6.000	6
Mg	0.000	0.000	0.000	0.000	0.000	0.000	0.000	0.000	0
Y: Al	0.051	0.082	0.038	0.054	0.053	0.057	0.028	0.073	0.59101
Ti	0.069	0.069	0.073	0.076	0.073	0.071	0.072	0.070	0.09065
V	0.000	0.000	0.000	0.000	0.000	0.000	0.000	0.000	0
Cr	0.000	0.000	0.001	0.001	0.000	0.000	0.000	0.000	-0.0052
Fe^{3+}	0.000	0.000	0.000	0.000	0.000	0.000	0.000	0.000	0
Mg	1.216	1.167	1.166	1.142	1.217	1.183	1.198	1.179	0.63828
Mn	0.004	0.003	0.002	0.002	0.001	0.003	0.002	0.003	0.0102
Fe^{2+}	1.360	1.381	1.390	1.448	1.401	1.420	1.379	1.428	1.40579
Zn	0.000	0.000	0.000	0.000	0.000	0.000	0.000	0.000	0
Li*	0.300	0.297	0.329	0.278	0.256	0.267	0.322	0.247	0.26907
Y	3.000	3.000	3.000	3.000	3.000	3.000	3.000	3.000	2.99982
X: Ca	0.156	0.146	0.164	0.151	0.154	0.150	0.170	0.167	0.05071

Ba	0.000	0.000	0.000	0.000	0.000	0.000	0.000	0.000	0
Na	0.588	0.581	0.576	0.585	0.593	0.593	0.564	0.575	0.58836
K	0.016	0.015	0.016	0.014	0.016	0.014	0.016	0.016	-0.0023
Rb	0.000	0.000	0.000	0.000	0.000	0.000	0.000	0.000	0
Cs	0.000	0.000	0.000	0.000	0.000	0.000	0.000	0.000	0
X-vacancy	0.241	0.258	0.243	0.250	0.237	0.243	0.251	0.243	0.36321
V+W site									
OH	3.920	3.908	3.925	3.911	3.912	3.932	3.904	3.924	4
F	0.079	0.092	0.074	0.086	0.088	0.067	0.095	0.075	0

Sample LG-3 (II)

SiO_2	35.1529	36.2495	36.2509	36.3404	36.6125	36.1708	35.9514	34.4999	35.2851	35.9044	35.6166
TiO_2	0.7287	0.3262	0.2385	0.1995	0.2402	0.2282	0.26	0.4388	0.3967	0.3871	0.4252
Al_2O_3	34.754	35.3344	35.1472	34.7502	34.9164	34.8679	35.1616	34.7685	34.9415	34.9799	34.4413
V_2O_3											
Cr_2O_3	-0.0395	-0.0125	-0.0259	-0.107	-0.026	-0.0528	-0.026	-0.0663	-0.0259	-0.1338	-0.1067
Fe_2O_3	0	0	0	0	0	0	0	0	0	0	0
FeO	10.1616	10.0574	9.7468	9.6303	9.2723	10.5472	9.0714	9.907	9.8557	9.9349	10.2572
MgO	2.5882	2.2872	2.1422	2.2532	2.3054	2.2531	2.2735	2.5333	2.5907	2.6468	2.6615
CaO	0.2861	0.0573	0.0811	0.0076	0.0883	0.081	0.0527	0.2298	0.1874	0.2159	0.2321
MnO	0.0728	0.0729	0.0851	0.0127	-0.0595	-0.0473	0.049	0.085	0.1091	0.0611	0.097
ZnO											
BaO											
Na_2O	1.8344	1.6386	1.4974	1.6039	1.4766	1.5788	1.5492	1.7607	1.8686	1.8328	1.9183
K_2O	-0.0108	-0.0086	-0.0244	-0.0154	-0.0312	-0.0198	-0.0018	-0.0108	0.0028	0.0186	-0.0085
Rb_2O											
Cs_2O											
F											
Cl											
H_2O											
B_2O_3											
Li_2O											
H_2O*											
B_2O_3*											

Li_2O*		_	_	_	_	_	_	_	_	_	_
		_	_	_	_	_	_	_	_	_	_
Total	85.5284	86.0024	85.1389	84.6754	84.795	85.6071	84.341	84.1459	85.2117	85.8477	85.534
O=F	0	0	0	0	0	0	0	0	0	0	0
Total*	85.5284	86.0024	85.1389	84.6754	84.795	85.6071	84.341	84.1459	85.2117	85.8477	85.534
B	3	3	3	3	3	3	3	3	3	3	3
T: Si	5.81518	5.92772	5.96713	6.00462	6.01675	5.95622	5.95091	5.79626	5.84385	5.89255	5.88835
Al	0.18482	0.07228	0.03287	0	0	0.04378	0.04909	0.20374	0.15615	0.10745	0.11165
Z: Al	6	6	6	6	6	6	6	6	6	6	6
Mg	0	0	0	0	0	0	0	0	0	0	0
Y: Al	0.59101	0.73758	0.78571	0.7672	0.76266	0.72319	0.81039	0.68075	0.66417	0.65852	0.59918
Ti	0.09065	0.04011	0.02952	0.02479	0.02968	0.02826	0.03236	0.05544	0.04941	0.04777	0.05286
V	0	0	0	0	0	0	0	0	0	0	0
Cr	-0.0052	-0.0016	-0.0034	-0.014	-0.0034	-0.0069	-0.0034	-0.0088	-0.0034	-0.0174	-0.0139
Fe^{3+}	0	0	0	0	0	0	0	0	0	0	0
Mg	0.63828	0.55757	0.52567	0.55501	0.56479	0.5531	0.56101	0.63449	0.63964	0.64757	0.65596
Mn	0.0102	0.0101	0.01186	0.00178	-0.0083	-0.0066	0.00687	0.0121	0.0153	0.00849	0.01358
Fe^{2+}	1.40579	1.37539	1.34173	1.33074	1.27431	1.45247	1.25573	1.39196	1.36506	1.36356	1.41816
Zn	0	0	0	0	0	0	0	0	0	0	0
Li*	0.26907	0.28059	0.30857	0.33443	0.3801	0.25612	0.33673	0.23434	0.2696	0.29119	0.27406
Y	2.99982	2.99973	2.99969	2.99997	2.9999	2.99967	2.99969	3.00028	2.99978	2.99975	2.99986

X: Ca	0.05071	0.01004	0.0143	0.00135	0.01555	0.01429	0.00935	0.04137	0.03325	0.03796	0.04111
Ba	0	0	0	0	0	0	0	0	0	0	0
Na	0.58836	0.51952	0.47789	0.51383	0.47048	0.50407	0.49719	0.57354	0.60003	0.5832	0.6149
K	-0.0023	-0.0018	-0.0051	-0.0032	-0.0065	-0.0042	-0.0004	-0.0023	0.00059	0.00389	-0.0018
Rb	0	0	0	0	0	0	0	0	0	0	0
Cs	0	0	0	0	0	0	0	0	0	0	0
X-vacancy	0.36321	0.47223	0.51293	0.48807	0.52051	0.4858	0.49384	0.38741	0.36613	0.37494	0.34578
V+W site											
OH	4	4	4	4	4	4	4	4	4	4	4
F	0	0	0	0	0	0	0	0	0	0	0

SiO_2	35.4314	34.2193	35.2355	35.2004	35.3907	36.0591	35.5369	34.8175	35.187
TiO_2	0.5118	0.4087	0.3749	0.4655	0.3862	0.3878	0.4827	0.5501	0.5148
Al_2O_3	34.3973	35.2524	34.2341	34.3667	34.1714	34.4547	34.3715	33.9454	34.3902
V_2O_3									
Cr_2O_3	0.0821	0.0146	-0.0258	0.0281	-0.0662	-0.093	0.0013	-0.1739	-0.1067
Fe_2O_3	0	0	0	0	0	0	0	0	0
FeO	9.8991	9.8819	10.2113	9.7371	10.1116	10.3791	10.3387	10.1252	9.7618
MgO	2.5329	2.5538	2.5265	2.5253	2.5631	2.6878	2.7669	2.655	2.713
CaO	0.2158	0.2252	0.2228	0.2443	0.2583	0.1686	0.2158	0.2299	0.2301
MnO	0.0129	0.1934	0.0249	0.0009	0.1092	0.1213	0.1694	-0.0111	0.1455
ZnO									
BaO									
Na_2O	1.8852	1.8904	1.9013	1.7881	1.8787	1.8923	1.8741	1.8359	1.7994
K_2O	0.0119	0.0119	-0.013	-0.0085	0.0074	0.0052	0.0232	-0.0062	0.0097
Rb_2O	_	_	_	_	_	_	_	_	_
Cs_2O	_	_	_	_	_	_	_	_	_
F	_	_	_	_	_	_	_	_	_
Cl	_	_	_	_	_	_	_	_	_
H_2O									
B_2O_3	_	_	_	_	_	_	_	_	_
Li_2O	_	_	_	_	_	_	_	_	_
H_2O*	_	_	_	_	_	_	_	_	_
B_2O_3*	_	_	_	_	_	_	_	_	_
Li_2O*	_	_	_	_	_	_	_	_	_
	_	_	_	_	_	_	_	_	_

Total	84.9804	84.6516	84.6925	84.3479	84.8104	86.0629	85.7805	83.9678	84.6448
O=F	0	0	0	0	0	0	0	0	0
Total*	84.9804	84.6516	84.6925	84.3479	84.8104	86.0629	85.7805	83.9678	84.6448
B	3	3	3	3	3	3	3	3	3
T: Si	5.88066	5.72852	5.88185	5.87846	5.89674	5.92451	5.87213	5.86335	5.8661
Al	0.11934	0.27148	0.11815	0.12154	0.10326	0.07549	0.12787	0.13665	0.1339
Z: Al	6	6	6	6	6	6	6	6	6
Mg	0	0	0	0	0	0	0	0	0
Y: Al	0.60914	0.68382	0.61702	0.64255	0.60704	0.59628	0.5659	0.60065	0.62315
Ti	0.06388	0.05145	0.04706	0.05846	0.04839	0.04791	0.05998	0.06966	0.06454
V	0	0	0	0	0	0	0	0	0
Cr	0.01077	0.00193	-0.0034	0.00371	-0.0087	-0.0121	0.00017	-0.0232	-0.0141
Fe^{3+}	0	0	0	0	0	0	0	0	0
Mg	0.62671	0.63733	0.62873	0.62869	0.63664	0.65833	0.68158	0.66653	0.67426
Mn	0.00181	0.02742	0.00352	0.00013	0.01541	0.01688	0.02371	-0.0016	0.02055
Fe^{2+}	1.37401	1.38346	1.42551	1.35988	1.40896	1.42611	1.42869	1.42596	1.36098
Zn	0	0	0	0	0	0	0	0	0
Li*	0.31351	0.21471	0.28147	0.30669	0.29221	0.26621	0.23999	0.26214	0.2707
?Y	2.99984	3.00014	2.99991	3.00011	2.99993	2.99965	3.00002	3.00021	3.00012
X: Ca	0.03837	0.04039	0.03985	0.04371	0.04611	0.02968	0.03821	0.04148	0.0411

Ba	0	0	0	0	0	0	0	0	0
Na	0.60665	0.61358	0.61536	0.57897	0.60691	0.6028	0.60042	0.59944	0.58162
K	0.00252	0.00254	-0.0028	-0.0018	0.00157	0.00109	0.00489	-0.0013	0.00206
Rb	0	0	0	0	0	0	0	0	0
Cs	0	0	0	0	0	0	0	0	0
X-vacancy	0.35245	0.34349	0.34756	0.37913	0.3454	0.36643	0.35648	0.36041	0.37521
V+W site									
OH	4	4	4	4	4	4	4	4	4
F	0	0	0	0	0	0	0	0	0

Sample: ZY-LGT-1 Tourmaline leucogranite

SiO_2	35.595	35.3994	35.6283	35.068	35.5751	34.2535	34.8407	35.325	35.5553	35.3888	34.4044	35.4144
TiO_2	0.3719	0.3555	0.4623	0.4278	0.4387	0.4442	0.3887	0.4183	0.5214	0.4142	0.4206	0.4658
Al_2O_3	34.8386	34.3154	34.2914	34.1848	34.3248	34.0258	34.801	34.094	35.7477	35.9812	34.9227	34.8831
V_2O_3	0	0	0	0	0	0	0	0	0	0	0	0
Cr_2O_3	0.0191	0.0289	0.0342	0	0	0.0299	0	0	0.0428	0	0	0
Fe_2O_3	0	0	0	0	0	0	0	0	0	0	0	0
FeO	10.5304	10.8996	10.8623	10.9047	10.8297	11.1055	10.5766	10.9292	11.3179	11.122	10.7462	11.3851
MgO	2.5691	2.8647	2.7865	2.7632	2.7578	2.8776	2.6926	2.7455	2.5674	2.3091	2.8834	2.3112
CaO	0.267	0.1971	0.2125	0.2162	0.2143	0.195	0.1936	0.2116	0.2085	0.1686	0.293	0.1673
MnO	0.0874	0.0534	0.0766	0.0737	0.1196	0.0566	0.0912	0.1031	0.1554	0.16	0.1114	0.1747
ZnO	0	0	0	0	0	0	0	0	0	0	0	0
BaO	0	0	0	0	0	0	0	0	0	0	0	0
Na_2O	1.6403	1.7026	1.7052	1.6728	1.7032	1.7552	1.6148	1.7063	1.6357	1.6593	1.8851	1.6316
K_2O	0.0511	0.035	0.0122	0.0624	0.0048	0.0295	0.0388	0.0801	0.0496	0.0497	0.0736	0.0431
Rb_2O	0	0	0	0	0	0	0	0	0	0	0	0
Cs_2O	0	0	0	0	0	0	0	0	0	0	0	0
F	0.0563	0.1193	0.1822	0.0247	0.2359	0.1049	0	0.2709	0.459	0.0752	0.3136	0.4719
Cl												
H_2O												
B_2O_3	10.2931	9.9563	9.3824	10.8892	10.0366	10.1738		10.0202	8.4561	8.5102	9.4175	10.0209
Li_2O	0	0	0	0	0	0	0	0	0	0	0	0
H_2O*	3.539092	3.537474	3.516838	3.543168	3.502586	3.505028	3.549551	3.520073	3.534043	3.553016	3.539371	3.550217
B_2O_3*	-	-	-	-	-	-	-	-	-	-	-	-

Li_2O*	0.406505	0.448972	0.443896	0.49303	0.413378	0.380004	0.399555	0.481179	0.368671	0.433621	0.419683	0.417774
Total	99.831	99.97685	99.72433	100.0776	99.51746	99.46193	100.224	99.94925	100.0777	100.1812	100.2558	100.3232
O=F	0.023706	0.050234	0.076719	0.0104	0.099331	0.04417	0	0.114068	0.193272	0.031665	0.132048	0.198704
Total*	99.78022	99.91348	99.65115	100.0184	99.44866	99.39199	100.1707	99.87342	100.0176	100.1321	100.1936	100.2662
B	3.149239	3.150871	3.146657	3.156418	3.139953	3.137821	3.141648	3.180119	3.132633	3.158577	3.149032	3.129827
T: Si	5.74057	5.74354	5.748744	5.752562	5.750965	5.727668	5.736178	5.69127	5.711789	5.722494	5.718764	5.7335
Al	0.25943	0.25646	0.251256	0.247438	0.249035	0.272332	0.263822	0.30873	0.288211	0.277506	0.281236	0.2665
Z: Al	6	6	6	6	6	6	6	6	6	6	6	6
Mg	0	0	0	0	0	0	0	0	0	0	0	0
Y: Al	0.040583	0.050524	0.082317	0.037991	0.053839	0.05265	0.056776	0.027727	0.072598	0.052168	0.03715	0.109401
Ti	0.070209	0.069045	0.06885	0.073475	0.075573	0.072536	0.070829	0.071729	0.070045	0.068461	0.070727	0.070051
V	0	0	0	0	0	0	0	0	0	0	0	0
Cr	0.000119	0.000144	0.000435	0.000866	0.000847	0	6.56E-05	0.000302	0.000395	0.001051	5.25E-05	0.00059
Fe^{3+}	0	0	0	0	0	0	0	0	0	0	0	0
Mg	1.19222	1.216157	1.166747	1.166167	1.141876	1.217227	1.183068	1.197856	1.179311	1.150096	1.195507	1.116057
Mn	0.003713	0.00439	0.003344	0.00211	0.002112	0.001233	0.00263	0.001929	0.002989	0.002983	0.001224	0.00281
Fe^{2+}	1.42065	1.359826	1.380986	1.390256	1.447601	1.400759	1.419885	1.378735	1.42797	1.435642	1.415119	1.422485
Zn	0	0	0	0	0	0	0	0	0	0	0	0
Li*	0.27252	0.299936	0.297352	0.329188	0.2782	0.255641	0.266788	0.321736	0.246739	0.289649	0.280244	0.278642
Y	3.000013	3.000022	3.00003	3.000054	3.000049	3.000045	3.000042	3.000015	3.000047	3.00005	3.000024	3.000035

X: Ca	0.149286	0.155806	0.145713	0.164444	0.151053	0.154077	0.15	0.169637	0.166833	0.154266	0.168302	0.156104
Ba	0	0	0	0	0	0	0	0	0	0	0	0
Na	0.589459	0.587575	0.581407	0.576171	0.585286	0.592711	0.592632	0.563735	0.574507	0.578812	0.582279	0.577587
K	0.015077	0.015788	0.015259	0.016333	0.013986	0.015774	0.014405	0.01559	0.01565	0.013776	0.016777	0.015659
Rb	0	0	0	0	0	0	0	0	0	0	0	0
Cs	0	0	0	0	0	0	0	0	0	0	0	0
X-vacancy	0.246179	0.240831	0.257621	0.243052	0.249674	0.237438	0.242963	0.251038	0.243011	0.253146	0.232641	0.25065
V+W site												
OH	3.935039	3.919806	3.90787	3.924555	3.91061	3.911796	3.931688	3.903836	3.923753	3.937226	3.920296	3.927989
F	0.063577	0.079068	0.091565	0.073785	0.086497	0.087892	0.066539	0.094699	0.075119	0.061366	0.077565	0.071028

SiO_2	35.3652	35.7108	35.7569	35.781	35.3257	35.4567	35.4774	35.7784	35.9758	35.1947	35.6631	34.2024	34.0643
TiO_2	0.4532	0.3817	0.4193	0.4067	0.398	0.3909	0.3737	0.431	0.5164	0.4223	0.3998	0.4389	0.4564
Al_2O_3	34.802	34.7033	34.5067	34.5512	34.0793	34.0841	34.687	34.6139	34.6384	34.567	34.7878	34.8393	34.8354
V_2O_3	0	0	0	0	0	0	0	0	0	0	0	0	0
Cr_2O_3	0	0	0	0.0086	0	0	0.012	0.0254	0	0.027	0	0	0
Fe_2O_3	0	0	0	0	0	0	0	0	0	0	0	0	0
FeO	11.815	11.1511	10.8409	11.8247	10.9397	10.7451	10.6389	11.4533	11.299	11.6302	10.7058	11.1466	11.3369
MgO	2.1453	2.9453	3.0781	2.1418	2.7847	3	2.8103	2.7408	2.6076	2.8683	2.7895	2.5197	2.5131
CaO	0.1385	0.2218	0.2346	0.1234	0.1527	0.2184	0.1781	0.2007	0.2073	0.1741	0.1839	0.2229	0.2215
MnO	0.2252	0.1032	0.0344	0.1464	0.0779	0.0513	0.1026	0.0495	0.1524	0.1035	0.1008	0.1439	0.1835
ZnO	0	0	0	0	0	0	0	0	0	0	0	0	0
BaO	0	0	0	0	0	0	0	0	0	0	0	0	0
Na_2O	1.7025	1.7299	1.72	1.5916	1.6453	1.7679	1.7447	1.6667	1.7249	1.647	1.6265	1.661	1.7796
K_2O	0.0466	0.0123	0.0362	0.0506	0.0502	0.0252	0.0225	0.0099	0.0172	0.0288	0.0404	0.0378	0.0161
Rb_2O	0	0	0	0	0	0	0	0	0	0	0	0	0
Cs_2O	0	0	0	0	0	0	0	0	0	0	0	0	0
F	0.5841	0.3329	0.401	0.2019	0.3522	0.2724	0.3491	0.5656	0.4866	0.1237	0.5773	0.6875	0.6406
Cl													
H_2O													
B_2O_3	9.6398	9.3039	8.7463	9.5023	9.2337	9.7443	9.7574	8.6924	8.2942	9.2351	9.1443	9.244	10.942
Li_2O	0	0	0	0	0	0	0	0	0	0	0	0	0
H_2O*	3.570459	3.5243	3.569112	3.553763	3.553088	3.587622	3.575055	3.550196	3.553588	3.578248	3.549315	3.539092	3.537474
B_2O_3*	-	-	-	-	-	-	-	-	-	-	-	-	-
Li_2O*	0.355162	0.385386	0.47352	0.397699	0.316497	0.386172	0.388011	0.469157	0.411628	0.530503	0.333541	0.406505	0.448972

Total	100.393	100.4306	100.7186	100.4151	100.157	100.6715	100.4494	100.5335	100.5728	100.6284	100.4282	99.831	99.97685
O=F	0.245948	0.140175	0.16885	0.085014	0.148302	0.1147	0.146996	0.238158	0.204894	0.052087	0.243085	0.289487	0.269739
Total*	100.3537	100.3535	100.6642	100.3586	100.099	100.6264	100.3986	100.4729	100.5137	100.5843	100.3722	99.78022	99.91348
B	3.109158	3.134834	3.164191	3.117731	3.089004	3.124403	3.121323	3.157888	3.123101	3.171706	3.077396	3.149239	3.150871
T: Si	5.748454	5.745506	5.7209	5.750416	5.793552	5.772633	5.781106	5.71702	5.7455	5.724773	5.776248	5.74057	5.74354
Al	0.251546	0.254494	0.2791	0.249584	0.206448	0.227367	0.218894	0.28298	0.2545	0.275227	0.223752	0.25943	0.25646
Z: Al	6	6	6	6	6	6	6	6	6	6	6	6	6
Mg	0	0	0	0	0	0	0	0	0	0	0	0	0
Y: Al	0.129187	0.03076	0.055293	0.129793	0.256567	0.211574	0.219195	0.066008	0.109061	0.055618	0.164539	0.040583	0.050524
Ti	0.066652	0.072416	0.070006	0.068979	0.043929	0.043699	0.043242	0.073994	0.074305	0.073068	0.073509	0.070209	0.069045
V	0	0	0	0	0	0	0	0	0	0	0	0	0
Cr	0.000931	0.001706	0.000653	0.000852	0.000354	0.000534	0.000548	0.001284	0.0011	0.000954	0.001351	0.000119	0.000144
Fe^{3+}	0	0	0	0	0	0	0	0	0	0	0	0	0
Mg	1.125608	1.187447	1.131578	1.104915	1.094181	1.088325	1.091397	1.080863	1.083471	1.083234	1.084506	1.19222	1.216157
Mn	0.005085	0.003867	0.005245	0.003158	0.002274	0.012577	0.002265	0.004392	0.004391	0.00035	0.00298	0.003713	0.00439
Fe^{2+}	1.435767	1.446617	1.422804	1.427379	1.39187	1.387465	1.385861	1.460948	1.453633	1.434325	1.450638	1.42065	1.359826
Zn	0	0	0	0	0	0	0	0	0	0	0	0	0
Li*	0.236829	0.257232	0.314457	0.264983	0.210879	0.255886	0.257552	0.312551	0.274101	0.352497	0.222535	0.27252	0.299936

?Y	3.00006	3.000045	3.000037	3.000058	3.000053	3.00006	3.000061	3.000041	3.000061	3.000045	3.000058	3.000013	3.000022
X: Ca	0.15124	0.164818	0.157246	0.152504	0.120489	0.119663	0.120122	0.164143	0.164281	0.16722	0.164912	0.149286	0.155806
Ba	0	0	0	0	0	0	0	0	0	0	0	0	0
Na	0.578955	0.585513	0.577888	0.573381	0.551365	0.558892	0.553953	0.564621	0.558096	0.559844	0.556674	0.589459	0.587575
K	0.015848	0.014633	0.012536	0.014186	0.013023	0.012131	0.011858	0.013548	0.01367	0.015473	0.014522	0.015077	0.015788
Rb	0	0	0	0	0	0	0	0	0	0	0	0	0
Cs	0	0	0	0	0	0	0	0	0	0	0	0	0
X-vacancy	0.253957	0.235035	0.25233	0.25993	0.315124	0.309314	0.314068	0.257688	0.263953	0.257463	0.263892	0.246179	0.240831
V+W site													
OH	3.950053	3.902407	3.931684	3.928425	3.927634	3.943872	3.936972	3.923449	3.925811	3.944107	3.928509	3.935039	3.919806
F	0.048991	0.096074	0.067532	0.070283	0.072169	0.055821	0.062916	0.0754	0.073488	0.054716	0.069691	0.063577	0.079068
SiO_2	35.213	35.5538	35.2207	35.7138	35.9863	35.9481	35.4447	35.1371	35.2444	34.9226	34.1886	34.5409	34.5278
TiO_2	0.4874	0.4765	0.4688	0.495	0.4913	0.4867	0.5027	0.5016	0.5104	0.492	0.4723	0.4702	0.4664
Al_2O_3	34.4625	34.7049	34.6681	34.2385	34.8478	34.6806	34.822	34.1338	34.6927	34.6707	34.3668	34.7926	34.6332
V_2O_3	0	0	0	0	0	0	0	0	0	0	0	0	0
Cr_2O_3	0.0337	0	0	0.0028	0.0121	0	0.0202	0	0	0.0395	0.0296	0.023	0
Fe_2O_3	0	0	0	0	0	0	0	0	0	0	0	0	0
FeO	11.1464	11.2463	11.1155	11.4088	11.4226	11.2967	11.1045	11.2269	11.138	11.3352	11.0884	11.2847	11.2594
MgO	2.6097	2.6291	2.5987	2.632	2.6169	2.6379	2.6093	2.7517	2.6458	2.6292	2.6545	2.6535	2.6471
CaO	0.229	0.236	0.2648	0.3768	0.2167	0.1647	0.2099	0.287	0.2496	0.2031	0.2122	0.1824	0.1902
MnO	0.1793	0.0565	0.1085	0.1364	0.1097	0.1134	0.083	0.1297	0.0797	0.145	0.1467	0.1559	0.1476
ZnO	0	0	0	0	0	0	0	0	0	0	0	0	0

BaO	0	0	0	0	0	0	0	0	0	0	0	0	0
Na_2O	1.7884	1.7289	1.7618	1.8615	1.6778	1.7561	1.6596	1.8475	1.659	1.6215	1.7155	1.747	1.7082
K_2O	0.0258	0.0158	0.0577	0.0576	0.0407	0.0339	0.042	0.0487	0.0395	0.0366	0.0585	0.0392	0.056
Rb_2O	0	0	0	0	0	0	0	0	0	0	0	0	0
Cs_2O	0	0	0	0	0	0	0	0	0	0	0	0	0
F	0.6707	0.1968	0.335	0.3041	0.3761	0.2933	0.0822	0.5792	0.3018	0.2167	0.4423	0.5849	0.6728
Cl													
H_2O													
B_2O_3	10.011	10.0273	10.7937	10.658	9.6853	9.3478	9.6675	9.875	9.869	10.8501	10.3424	10.3608	11.7707
Li_2O	0	0	0	0	0	0	0	0	0	0	0	0	0
H_2O*	3.516838	3.543168	3.502586	3.505028	3.549551	3.520073	3.534043	3.553016	3.539371	3.550217	3.570459	3.5243	3.569112
B_2O_3*	-	-	-	-	-	-	-	-	-	-	-	-	-
Li_2O*	0.443896	0.49303	0.413378	0.380004	0.399555	0.481179	0.368671	0.433621	0.419683	0.417774	0.355162	0.385386	0.47352
Total	99.72433	100.0776	99.51746	99.46193	100.224	99.94925	100.0777	100.1812	100.2558	100.3232	100.393	100.4306	100.7186
O=F	0.282413	0.082867	0.141059	0.128048	0.158365	0.1235	0.034612	0.243885	0.12708	0.091246	0.18624	0.246285	0.283297
Total*	99.65115	100.0184	99.44866	99.39199	100.1707	99.87342	100.0176	100.1321	100.1936	100.2662	100.3537	100.3535	100.6642
B	3.146657	3.156418	3.139953	3.137821	3.141648	3.180119	3.132633	3.158577	3.149032	3.129827	3.109158	3.134834	3.164191
T: Si	5.748744	5.752562	5.750965	5.727668	5.736178	5.69127	5.711789	5.722494	5.718764	5.7335	5.748454	5.745506	5.7209
Al	0.251256	0.247438	0.249035	0.272332	0.263822	0.30873	0.288211	0.277506	0.281236	0.2665	0.251546	0.254494	0.2791
Z: Al	6	6	6	6	6	6	6	6	6	6	6	6	6

Mg	0	0	0	0	0	0	0	0	0	0	0	0	0
Y: Al	0.082317	0.037991	0.053839	0.05265	0.056776	0.027727	0.072598	0.052168	0.03715	0.109401	0.129187	0.03076	0.055293
Ti	0.06885	0.073475	0.075573	0.072536	0.070829	0.071729	0.070045	0.068461	0.070727	0.070051	0.066652	0.072416	0.070006
V	0	0	0	0	0	0	0	0	0	0	0	0	0
Cr	0.000435	0.000866	0.000847	0	6.56E-05	0.000302	0.000395	0.001051	5.25E-05	0.00059	0.000931	0.001706	0.000653
Fe^{3+}	0	0	0	0	0	0	0	0	0	0	0	0	0
Mg	1.166747	1.166167	1.141876	1.217227	1.183068	1.197856	1.179311	1.150096	1.195507	1.116057	1.125608	1.187447	1.131578
Mn	0.003344	0.00211	0.002112	0.001233	0.00263	0.001929	0.002989	0.002983	0.001224	0.00281	0.005085	0.003867	0.005245
Fe^{2+}	1.380986	1.390256	1.447601	1.400759	1.419885	1.378735	1.42797	1.435642	1.415119	1.422485	1.435767	1.446617	1.422804
Zn	0	0	0	0	0	0	0	0	0	0	0	0	0
Li*	0.297352	0.329188	0.2782	0.255641	0.266788	0.321736	0.246739	0.289649	0.280244	0.278642	0.236829	0.257232	0.314457
?Y	3.00003	3.000054	3.000049	3.000045	3.000042	3.000015	3.000047	3.00005	3.000024	3.000035	3.00006	3.000045	3.000037
X: Ca	0.145713	0.164444	0.151053	0.154077	0.15	0.169637	0.166833	0.154266	0.168302	0.156104	0.15124	0.164818	0.157246
Ba	0	0	0	0	0	0	0	0	0	0	0	0	0
Na	0.581407	0.576171	0.585286	0.592711	0.592632	0.563735	0.574507	0.578812	0.582279	0.577587	0.578955	0.585513	0.577888
K	0.015259	0.016333	0.013986	0.015774	0.014405	0.01559	0.01565	0.013776	0.016777	0.015659	0.015848	0.014633	0.012536
Rb	0	0	0	0	0	0	0	0	0	0	0	0	0
Cs	0	0	0	0	0	0	0	0	0	0	0	0	0
X-vacancy	0.257621	0.243052	0.249674	0.237438	0.242963	0.251038	0.243011	0.253146	0.232641	0.25065	0.253957	0.235035	0.25233

V+W site													
OH	3.90787	3.924555	3.91061	3.911796	3.931688	3.903836	3.923753	3.937226	3.920296	3.927989	3.950053	3.902407	3.931684
F	0.091565	0.073785	0.086497	0.087892	0.066539	0.094699	0.075119	0.061366	0.077565	0.071028	0.048991	0.096074	0.067532

SiO_2	35.213	35.5538	35.2207	35.7138	35.9863	35.9481	35.4447	35.1371	35.2444	34.9226	34.1886	34.5409	34.5278	34.5663
TiO_2	0.4874	0.4765	0.4688	0.495	0.4913	0.4867	0.5027	0.5016	0.5104	0.492	0.4723	0.4702	0.4664	0.4702
Al_2O_3	34.4625	34.7049	34.6681	34.2385	34.8478	34.6806	34.822	34.1338	34.6927	34.6707	34.3668	34.7926	34.6332	34.3737
V_2O_3	0	0	0	0	0	0	0	0	0	0	0	0	0	0
Cr_2O_3	0.0337	0	0	0.0028	0.0121	0	0.0202	0	0	0.0395	0.0296	0.023	0	0
Fe_2O_3	0	0	0	0	0	0	0	0	0	0	0	0	0	0
FeO	11.1464	11.2463	11.1155	11.4088	11.4226	11.2967	11.1045	11.2269	11.138	11.3352	11.0884	11.2847	11.2594	11.3589
MgO	2.6097	2.6291	2.5987	2.632	2.6169	2.6379	2.6093	2.7517	2.6458	2.6292	2.6545	2.6535	2.6471	2.7804
CaO	0.229	0.236	0.2648	0.3768	0.2167	0.1647	0.2099	0.287	0.2496	0.2031	0.2122	0.1824	0.1902	0.2043
MnO	0.1793	0.0565	0.1085	0.1364	0.1097	0.1134	0.083	0.1297	0.0797	0.145	0.1467	0.1559	0.1476	0.1284
ZnO	0	0	0	0	0	0	0	0	0	0	0	0	0	0
BaO	0	0	0	0	0	0	0	0	0	0	0	0	0	0
Na_2O	1.7884	1.7289	1.7618	1.8615	1.6778	1.7561	1.6596	1.8475	1.659	1.6215	1.7155	1.747	1.7082	1.7918
K_2O	0.0258	0.0158	0.0577	0.0576	0.0407	0.0339	0.042	0.0487	0.0395	0.0366	0.0585	0.0392	0.056	0.0177
Rb_2O	0	0	0	0	0	0	0	0	0	0	0	0	0	0
Cs_2O	0	0	0	0	0	0	0	0	0	0	0	0	0	0
F	0.6707	0.1968	0.335	0.3041	0.3761	0.2933	0.0822	0.5792	0.3018	0.2167	0.4423	0.5849	0.6728	0.0323
Cl														
H_2O														
B_2O_3	10.011	10.0273	10.7937	10.658	9.6853	9.3478	9.6675	9.875	9.869	10.8501	10.3424	10.3608	11.7707	11.7929
Li_2O	0	0	0	0	0	0	0	0	0	0	0	0	0	0
H_2O*	3.516838	3.543168	3.502586	3.505028	3.549551	3.520073	3.534043	3.553016	3.539371	3.550217	3.570459	3.5243	3.569112	3.553763
B_2O_3*	-	-	-	-	-	-	-	-	-	-	-	-	-	-
Li_2O*	0.443896	0.49303	0.413378	0.380004	0.399555	0.481179	0.368671	0.433621	0.419683	0.417774	0.355162	0.385386	0.47352	0.397699

Total	99.72433	100.0776	99.51746	99.46193	100.224	99.94925	100.0777	100.1812	100.2558	100.3232	100.393	100.4306	100.7186	100.4151
O=F	0.282413	0.082867	0.141059	0.128048	0.158365	0.1235	0.034612	0.243885	0.12708	0.091246	0.18624	0.246285	0.283297	0.013601
Total*	99.65115	100.0184	99.44866	99.39199	100.1707	99.87342	100.0176	100.1321	100.1936	100.2662	100.3537	100.3535	100.6642	100.3586
B	3.146657	3.156418	3.139953	3.137821	3.141648	3.180119	3.132633	3.158577	3.149032	3.129827	3.109158	3.134834	3.164191	3.117731
T: Si	5.748744	5.752562	5.750965	5.727668	5.736178	5.69127	5.711789	5.722494	5.718764	5.7335	5.748454	5.745506	5.7209	5.750416
Al	0.251256	0.247438	0.249035	0.272332	0.263822	0.30873	0.288211	0.277506	0.281236	0.2665	0.251546	0.254494	0.2791	0.249584
Z: Al	6	6	6	6	6	6	6	6	6	6	6	6	6	6
Mg	0	0	0	0	0	0	0	0	0	0	0	0	0	0
Y: Al	0.082317	0.037991	0.053839	0.05265	0.056776	0.027727	0.072598	0.052168	0.03715	0.109401	0.129187	0.03076	0.055293	0.129793
Ti	0.06885	0.073475	0.075573	0.072536	0.070829	0.071729	0.070045	0.068461	0.070727	0.070051	0.066652	0.072416	0.070006	0.068979
V	0	0	0	0	0	0	0	0	0	0	0	0	0	0
Cr	0.000435	0.000866	0.000847	0	6.56E-05	0.000302	0.000395	0.001051	5.25E-05	0.00059	0.000931	0.001706	0.000653	0.000852
Fe^{3+}	0	0	0	0	0	0	0	0	0	0	0	0	0	0
Mg	1.166747	1.166167	1.141876	1.217227	1.183068	1.197856	1.179311	1.150096	1.195507	1.116057	1.125608	1.187447	1.131578	1.104915
Mn	0.003344	0.00211	0.002112	0.001233	0.00263	0.001929	0.002989	0.002983	0.001224	0.00281	0.005085	0.003867	0.005245	0.003158
Fe^{2+}	1.380986	1.390256	1.447601	1.400759	1.419885	1.378735	1.42797	1.435642	1.415119	1.422485	1.435767	1.446617	1.422804	1.427379
Zn	0	0	0	0	0	0	0	0	0	0	0	0	0	0
Li*	0.297352	0.329188	0.2782	0.255641	0.266788	0.321736	0.246739	0.289649	0.280244	0.278642	0.236829	0.257232	0.314457	0.264983
?Y	3.00003	3.000054	3.000049	3.000045	3.000042	3.000015	3.000047	3.00005	3.000024	3.000035	3.00006	3.000045	3.000037	3.000058

X: Ca	0.145713	0.164444	0.151053	0.154077	0.15	0.169637	0.166833	0.154266	0.168302	0.156104	0.15124	0.164818	0.157246	0.152504
Ba	0	0	0	0	0	0	0	0	0	0	0	0	0	0
Na	0.581407	0.576171	0.585286	0.592711	0.592632	0.563735	0.574507	0.578812	0.582279	0.577587	0.578955	0.585513	0.577888	0.573381
K	0.015259	0.016333	0.013986	0.015774	0.014405	0.01559	0.01565	0.013776	0.016777	0.015659	0.015848	0.014633	0.012536	0.014186
Rb	0	0	0	0	0	0	0	0	0	0	0	0	0	0
Cs	0	0	0	0	0	0	0	0	0	0	0	0	0	0
X-vacancy	0.257621	0.243052	0.249674	0.237438	0.242963	0.251038	0.243011	0.253146	0.232641	0.25065	0.253957	0.235035	0.25233	0.25993
V+W site														
OH	3.90787	3.924555	3.91061	3.911796	3.931688	3.903836	3.923753	3.937226	3.920296	3.927989	3.950053	3.902407	3.931684	3.928425
F	0.091565	0.073785	0.086497	0.087892	0.066539	0.094699	0.075119	0.061366	0.077565	0.071028	0.048991	0.096074	0.067532	0.070283

SiO_2	35.213	35.5538	35.2207	35.7138	35.9863	35.9481	35.4447	35.1371	35.2444	34.9226	34.1886	34.5409	34.5278	34.5663
TiO_2	0.4874	0.4765	0.4688	0.495	0.4913	0.4867	0.5027	0.5016	0.5104	0.492	0.4723	0.4702	0.4664	0.4702
Al_2O_3	34.4625	34.7049	34.6681	34.2385	34.8478	34.6806	34.822	34.1338	34.6927	34.6707	34.3668	34.7926	34.6332	34.3737
V_2O_3	0	0	0	0	0	0	0	0	0	0	0	0	0	0
Cr_2O_3	0.0337	0	0	0.0028	0.0121	0	0.0202	0	0	0.0395	0.0296	0.023	0	0
Fe_2O_3	0	0	0	0	0	0	0	0	0	0	0	0	0	0
FeO	11.1464	11.2463	11.1155	11.4088	11.4226	11.2967	11.1045	11.2269	11.138	11.3352	11.0884	11.2847	11.2594	11.3589
MgO	2.6097	2.6291	2.5987	2.632	2.6169	2.6379	2.6093	2.7517	2.6458	2.6292	2.6545	2.6535	2.6471	2.7804
CaO	0.229	0.236	0.2648	0.3768	0.2167	0.1647	0.2099	0.287	0.2496	0.2031	0.2122	0.1824	0.1902	0.2043
MnO	0.1793	0.0565	0.1085	0.1364	0.1097	0.1134	0.083	0.1297	0.0797	0.145	0.1467	0.1559	0.1476	0.1284
ZnO	0	0	0	0	0	0	0	0	0	0	0	0	0	0
BaO	0	0	0	0	0	0	0	0	0	0	0	0	0	0
Na_2O	1.7884	1.7289	1.7618	1.8615	1.6778	1.7561	1.6596	1.8475	1.659	1.6215	1.7155	1.747	1.7082	1.7918
K_2O	0.0258	0.0158	0.0577	0.0576	0.0407	0.0339	0.042	0.0487	0.0395	0.0366	0.0585	0.0392	0.056	0.0177
Rb_2O	0	0	0	0	0	0	0	0	0	0	0	0	0	0
Cs_2O	0	0	0	0	0	0	0	0	0	0	0	0	0	0
F	0.6707	0.1968	0.335	0.3041	0.3761	0.2933	0.0822	0.5792	0.3018	0.2167	0.4423	0.5849	0.6728	0.0323
Cl														
H_2O														
B_2O_3	10.011	10.0273	10.7937	10.658	9.6853	9.3478	9.6675	9.875	9.869	10.8501	10.3424	10.3608	11.7707	11.7929
Li_2O	0	0	0	0	0	0	0	0	0	0	0	0	0	0
H_2O*	3.516838	3.543168	3.502586	3.505028	3.549551	3.520073	3.534043	3.553016	3.539371	3.550217	3.570459	3.5243	3.569112	3.553763
B_2O_3*	-	-	-	-	-	-	-	-	-	-	-	-	-	-

Li_2O*	0.443896	0.49303	0.413378	0.380004	0.399555	0.481179	0.368671	0.433621	0.419683	0.417774	0.355162	0.385386	0.47352	0.397699
Total	99.72433	100.0776	99.51746	99.46193	100.224	99.94925	100.0777	100.1812	100.2558	100.3232	100.393	100.4306	100.7186	100.4151
O=F	0.282413	0.082867	0.141059	0.128048	0.158365	0.1235	0.034612	0.243885	0.12708	0.091246	0.18624	0.246285	0.283297	0.013601
Total*	99.65115	100.0184	99.44866	99.39199	100.1707	99.87342	100.0176	100.1321	100.1936	100.2662	100.3537	100.3535	100.6642	100.3586
B	3.146657	3.156418	3.139953	3.137821	3.141648	3.180119	3.132633	3.158577	3.149032	3.129827	3.109158	3.134834	3.164191	3.117731
T: Si	5.748744	5.752562	5.750965	5.727668	5.736178	5.69127	5.711789	5.722494	5.718764	5.7335	5.748454	5.745506	5.7209	5.750416
Al	0.251256	0.247438	0.249035	0.272332	0.263822	0.30873	0.288211	0.277506	0.281236	0.2665	0.251546	0.254494	0.2791	0.249584
Z: Al	6	6	6	6	6	6	6	6	6	6	6	6	6	6
Mg	0	0	0	0	0	0	0	0	0	0	0	0	0	0
Y: Al	0.082317	0.037991	0.053839	0.05265	0.056776	0.027727	0.072598	0.052168	0.03715	0.109401	0.129187	0.03076	0.055293	0.129793
Ti	0.06885	0.073475	0.075573	0.072536	0.070829	0.071729	0.070045	0.068461	0.070727	0.070051	0.066652	0.072416	0.070006	0.068979
V	0	0	0	0	0	0	0	0	0	0	0	0	0	0
Cr	0.000435	0.000866	0.000847	0	6.56E-05	0.000302	0.000395	0.001051	5.25E-05	0.00059	0.000931	0.001706	0.000653	0.000852
Fe^{3+}	0	0	0	0	0	0	0	0	0	0	0	0	0	0
Mg	1.166747	1.166167	1.141876	1.217227	1.183068	1.197856	1.179311	1.150096	1.195507	1.116057	1.125608	1.187447	1.131578	1.104915
Mn	0.003344	0.00211	0.002112	0.001233	0.00263	0.001929	0.002989	0.002983	0.001224	0.00281	0.005085	0.003867	0.005245	0.003158

Fe^{2+}	1.380986	1.390256	1.447601	1.400759	1.419885	1.378735	1.42797	1.435642	1.415119	1.422485	1.435767	1.446617	1.422804	1.427379
Zn	0	0	0	0	0	0	0	0	0	0	0	0	0	0
Li*	0.297352	0.329188	0.2782	0.255641	0.266788	0.321736	0.246739	0.289649	0.280244	0.278642	0.236829	0.257232	0.314457	0.264983
?Y	3.00003	3.000054	3.000049	3.000045	3.000042	3.000015	3.000047	3.00005	3.000024	3.000035	3.00006	3.000045	3.000037	3.000058
X: Ca	0.145713	0.164444	0.151053	0.154077	0.15	0.169637	0.166833	0.154266	0.168302	0.156104	0.15124	0.164818	0.157246	0.152504
Ba	0	0	0	0	0	0	0	0	0	0	0	0	0	0
Na	0.581407	0.576171	0.585286	0.592711	0.592632	0.563735	0.574507	0.578812	0.582279	0.577587	0.578955	0.585513	0.577888	0.573381
K	0.015259	0.016333	0.013986	0.015774	0.014405	0.01559	0.01565	0.013776	0.016777	0.015659	0.015848	0.014633	0.012536	0.014186
Rb	0	0	0	0	0	0	0	0	0	0	0	0	0	0
Cs	0	0	0	0	0	0	0	0	0	0	0	0	0	0
X-vacancy	0.257621	0.243052	0.249674	0.237438	0.242963	0.251038	0.243011	0.253146	0.232641	0.25065	0.253957	0.235035	0.25233	0.25993
V+W site														
OH	3.90787	3.924555	3.91061	3.911796	3.931688	3.903836	3.923753	3.937226	3.920296	3.927989	3.950053	3.902407	3.931684	3.928425
F	0.091565	0.073785	0.086497	0.087892	0.066539	0.094699	0.075119	0.061366	0.077565	0.071028	0.048991	0.096074	0.067532	0.070283

SiO_2	34.7073	34.2103	34.4739	34.897	34.4722	34.237	36.1806	35.1813	35.0989	35.6193	35.9173	35.5941	36.3724
TiO_2	0.5059	0.4803	0.4502	0.4761	0.4589	0.5121	0.2408	0.5195	0.5007	0.3092	0.1908	0.2156	0.2718
Al_2O_3	34.3185	34.4018	34.8116	34.3111	34.5972	34.6172	34.36	32.8584	33.31	33.9625	33.917	34.3964	34.4867
V_2O_3	0	0	0	0	0	0							
Cr_2O_3	0	0	0.0269	0	0.0302	0.0043	0	0.0308	0.0001	0.0157	-0.0153	0.0618	0.0775
Fe_2O_3	0	0	0	0	0	0	0	0	0	0	0	0	0
FeO	11.3947	11.3761	11.33	11.3212	11.3826	11.5061	10.5216	10.7733	11.4807	10.27	10.6414	11.1437	10.396
MgO	2.7368	2.6468	2.746	2.6047	2.6537	2.7118	2.3418	2.7726	2.8513	2.4628	2.3766	2.3067	2.3357
CaO	0.1522	0.1917	0.2264	0.2371	0.256	0.2084	0.0842	0.1979	0.2656	0.1089	0.0816	0.0734	0.0817
MnO	0.1742	0.1283	0.0978	0.1036	0.1129	0.1444	0.0967	0.1932	0.0966	0.2076	0.0968	0.0415	0.2905
ZnO	0	0	0	0	0	0							
BaO	0	0	0	0	0	0							
Na_2O	1.7408	1.6699	1.6898	1.7052	1.7149	1.7185	1.574	2.0669	1.9337	1.7529	1.6356	1.6126	1.7158
K_2O	0.0418	0.0325	0.0457	0.003	0.0378	0.0429	-0.0078	0.0026	0.013	0.0261	-0.0025	0.0338	-0.0103
Rb_2O	0	0	0	0	0	0	_	_	_	_	_	_	_
Cs_2O	0	0	0	0	0	0	_	_	_	_	_	_	_
F	0.525	0.0924	0.2385	0.3607	0.3785	0.3022	_	_	_	_	_	_	_
Cl													
H_2O													
B_2O_3	13.5692	5.9483	10.2797	11.2446	10.9939	9.3951	_	_	_	_	_	_	_
Li_2O	0	0	0	0	0	0	_	_	_	_	_	_	_
H_2O*	3.553088	3.587622	3.575055	3.550196	3.553588	3.578248	_	_	_	_	_	_	_
B_2O_3*	-	-	-	-	-	-	_	_	_	_	_	_	_
Li_2O*	0.316497	0.386172	0.388011	0.469157	0.411628	0.530503	_	_	_	_	_	_	_

Total	100.157	100.6715	100.4494	100.5335	100.5728	100.6284	85.3919	84.5965	85.5506	84.735	84.8393	85.4796	86.0178
O=F	0.221063	0.038907	0.100426	0.151881	0.159376	0.127248	0	0	0	0	0	0	0
Total*	100.099	100.6264	100.3986	100.4729	100.5137	100.5843	85.3919	84.5965	85.5506	84.735	84.8393	85.4796	86.0178
B	3.089004	3.124403	3.121323	3.157888	3.123101	3.171706	3	3	3	3	3	3	3
T: Si	5.793552	5.772633	5.781106	5.71702	5.7455	5.724773	5.98111	5.92284	5.87252	5.94424	5.98703	5.916	5.97266
Al	0.206448	0.227367	0.218894	0.28298	0.2545	0.275227	0.01889	0.07716	0.12748	0.05576	0.01297	0.084	0.02734
Z: Al	6	6	6	6	6	6	6	6	6	6	6	6	6
Mg	0	0	0	0	0	0	0	0	0	0	0	0	0
Y: Al	0.256567	0.211574	0.219195	0.066008	0.109061	0.055618	0.67557	0.44243	0.44095	0.62409	0.65019	0.65381	0.64692
Ti	0.043929	0.043699	0.043242	0.073994	0.074305	0.073068	0.02994	0.06577	0.063	0.0388	0.02392	0.02695	0.03356
V	0	0	0	0	0	0	0	0	0	0	0	0	0
Cr	0.000354	0.000534	0.000548	0.001284	0.0011	0.000954	0	0.0041	1.3E-05	0.00207	-0.002	0.00812	0.01006
Fe^{3+}	0	0	0	0	0	0	0	0	0	0	0	0	0
Mg	1.094181	1.088325	1.091397	1.080863	1.083471	1.083234	0.57712	0.69585	0.71118	0.6127	0.59057	0.57154	0.57177
Mn	0.002274	0.012577	0.002265	0.004392	0.004391	0.00035	0.01354	0.02755	0.01369	0.02934	0.01367	0.00584	0.0404
Fe^{2+}	1.39187	1.387465	1.385861	1.460948	1.453633	1.434325	1.4546	1.51678	1.60641	1.4333	1.48341	1.54894	1.42764
Zn	0	0	0	0	0	0	0	0	0	0	0	0	0
Li*	0.210879	0.255886	0.257552	0.312551	0.274101	0.352497	0.24923	0.24752	0.16476	0.25969	0.24026	0.18479	0.26964
?Y	3.000053	3.00006	3.000061	3.000041	3.000061	3.000045	3	3	3	3	3	3	3

X: Ca	0.120489	0.119663	0.120122	0.164143	0.164281	0.16722	0.01491	0.0357	0.04761	0.01947	0.01457	0.01307	0.01437
Ba	0	0	0	0	0	0	0	0	0	0	0	0	0
Na	0.551365	0.558892	0.553953	0.564621	0.558096	0.559844	0.5045	0.67466	0.62729	0.56717	0.52861	0.51967	0.54627
K	0.013023	0.012131	0.011858	0.013548	0.01367	0.015473	-0.0016	0.00056	0.00277	0.00556	-0.0005	0.00717	-0.0022
Rb	0	0	0	0	0	0	0	0	0	0	0	0	0
Cs	0	0	0	0	0	0	0	0	0	0	0	0	0
X-vacancy	0.315124	0.309314	0.314068	0.257688	0.263953	0.257463	0.48224	0.28909	0.32233	0.4078	0.45735	0.4601	0.44151
V+W site													
OH	3.927634	3.943872	3.936972	3.923449	3.925811	3.944107	4	4	4	4	4	4	4
F	0.072169	0.055821	0.062916	0.0754	0.073488	0.054716	0	0	0	0	0	0	0

SiO_2	32.7959	36.265	35.9671	36.1396	35.9887	34.975	35.3728	34.6129	35.4142	35.1284	35.4796	35.4224	35.9142	36.0484
TiO_2	0.2901	0.2032	0.183	0.1896	0.3758	0.8052	0.2222	0.5816	0.4611	0.1361	0.027	0.0214	0.0165	0.1804
Al_2O_3	32.2592	34.4185	34.4466	34.6932	34.307	33.4617	34.1719	33.2989	34.7735	34.974	34.9451	35.0186	34.4325	35.2612
V_2O_3														
Cr_2O_3	0.1236	0.1085	-0.0617	0.0002	-0.0927	0.0155	-0.077	-0.0153	-0.1085	-0.0622	-0.1247	0.0002	-0.031	-0.1248
Fe_2O_3	0	0	0	0	0	0	0	0	0	0	0	0	0	0
FeO	10.3116	10.4005	10.3882	10.3323	10.1421	11.3076	10.9308	12.3826	9.8811	8.3709	8.2977	8.256	8.9646	8.6284
MgO	2.2885	2.3029	2.2915	2.2789	2.7013	1.7644	2.3509	2.9015	3.4327	4.0653	3.9397	4.0466	3.8773	3.3906
CaO	0.3829	0.1035	0.0763	0.0546	0.1334	0.1625	0.106	0.2192	0.3728	0.426	0.426	0.4399	0.3739	0.0818
MnO	0.1106	0.1385	0.0555	0.1109	0.0555	0.2345	0.1797	0.179	0.0416	0.1391	0.0835	0.1252	0.0695	0.0694
ZnO														
BaO														
Na_2O	1.4945	1.5306	1.6857	1.4962	1.6766	1.3719	1.2523	1.5946	1.3963	1.4593	1.4464	1.3709	1.454	1.76
K_2O	0.0753	-0.0155	0.0131	-0.0259	0.0183	0.0466	0.0701	0.0388	0.0546	0.0105	0.0131	0.034	0.06	-0.0287
Rb_2O	_	_	_	_	_	_	_	_						
Cs_2O	_	_	_	_	_	_	_	_						
F	_	_	_	_	_	_	_	_						
Cl														
H_2O														
B_2O_3	_	_	_	_	_	_	_	_						
Li_2O	_	_	_	_	_	_	_	_						
H_2O*	_	_	_	_	_	_	_	_						
B_2O_3*	_	_	_	_	_	_	_	_						
Li_2O*	_	_	_	_	_	_	_	_						

Total	80.1322	85.4557	85.0453	85.2696	85.306	84.1449	84.5797	85.7938	85.7194	84.6474	84.5334	84.7352	85.1315	85.2667
O=F	0	0	0	0	0	0	0	0	0	0	0	0	0	0
Total*	80.1322	85.4557	85.0453	85.2696	85.306	84.1449	84.5797	85.7938	85.7194	84.6474	84.5334	84.7352	85.1315	85.2667
B	3	3	3	3	3	3	3	3	3	3	3	3	3	3
T: Si	5.83129	5.9863	5.96495	5.97231	5.95001	5.91638	5.93654	5.8242	5.8431	5.82711	5.8761	5.85931	5.92972	5.91098
Al	0.16871	0.0137	0.03505	0.02769	0.04999	0.08362	0.06346	0.1758	0.1569	0.17289	0.1239	0.14069	0.07028	0.08902
Z: Al	6	6	6	6	6	6	6	6	6	6	6	6	6	6
Mg	0	0	0	0	0	0	0	0	0	0	0	0	0	0
Y: Al	0.59142	0.68234	0.69786	0.72939	0.63483	0.58754	0.69563	0.42784	0.60502	0.6646	0.69718	0.68621	0.62999	0.72535
Ti	0.03879	0.02522	0.02282	0.02356	0.04672	0.10243	0.02804	0.07359	0.05721	0.01698	0.00336	0.00266	0.00205	0.02224
V	0	0	0	0	0	0	0	0	0	0	0	0	0	0
Cr	0.01738	0.01416	-0.0081	2.6E-05	-0.0121	0.00207	-0.0102	-0.002	-0.0142	-0.0082	-0.0163	2.6E-05	-0.004	-0.0162
Fe^{3+}	0	0	0	0	0	0	0	0	0	0	0	0	0	0
Mg	0.6066	0.5667	0.56654	0.56143	0.66578	0.44494	0.58817	0.72783	0.84433	1.0053	0.97271	0.99786	0.95435	0.82882
Mn	0.01666	0.01936	0.0078	0.01552	0.00777	0.0336	0.02554	0.02551	0.00581	0.01954	0.01171	0.01754	0.00972	0.00964
Fe^{2+}	1.5333	1.43576	1.44078	1.42795	1.40228	1.59965	1.53416	1.74247	1.36341	1.16124	1.14928	1.14207	1.23781	1.1832
Zn	0	0	0	0	0	0	0	0	0	0	0	0	0	0
Li*	0.19585	0.25646	0.27229	0.24212	0.25473	0.22976	0.13866	0.00479	0.13837	0.14049	0.18209	0.15363	0.17013	0.24692
?Y	3	3	3	3	3	3	3	3	3	3	3	3	3	3

X: Ca	0.07294	0.0183	0.01356	0.00967	0.02363	0.02945	0.01906	0.03952	0.0659	0.07571	0.07559	0.07796	0.06614	0.01437
Ba	0	0	0	0	0	0	0	0	0	0	0	0	0	0
Na	0.51521	0.48987	0.54204	0.4794	0.53744	0.44995	0.40749	0.52023	0.44667	0.46934	0.46446	0.43966	0.46546	0.55954
K	0.01708	-0.0033	0.00277	-0.0055	0.00386	0.01006	0.01501	0.00833	0.01149	0.00222	0.00277	0.00717	0.01264	-0.006
Rb	0	0	0	0	0	0	0	0	0	0	0	0	0	0
Cs	0	0	0	0	0	0	0	0	0	0	0	0	0	0
X-vacancy	0.39476	0.49509	0.44163	0.5164	0.43507	0.51054	0.55844	0.43192	0.47593	0.45273	0.45718	0.4752	0.45576	0.43209
V+W site														
OH	4	4	4	4	4	4	4	4	4	4	4	4	4	4
F	0	0	0	0	0	0	0	0	0	0	0	0	0	0

Sample Y-TG-1 Tourmaline Pegmatite

SiO_2	34.501	34.5347	34.8261	34.4271	34.6821	34.8166	34.3161	34.7535	34.555	34.49
TiO_2	0.5463	0.7371	0.8598	0.6638	0.7722	0.754	0.5965	0.7864	0.6928	0.5171
Al_2O_3	34.5746	34.4977	34.5901	34.762	34.5838	34.6036	34.8341	34.3924	34.7595	34.4488
V_2O_3	0	0	0	0	0	0	0	0	0	0
Cr_2O_3	0	0.0065	0.0693	0.0057	0	0	0	0	0.0062	0
Fe_2O_3	0	0	0	0	0	0	0	0	0	0
FeO	11.0694	11.0126	10.7657	11.1892	10.8153	10.8968	10.7582	11.2495	10.7423	10.6023
MgO	2.2043	2.4103	2.2051	2.3677	2.2191	2.292	2.325	2.1377	2.1325	2.4217
CaO	0.2364	0.2935	0.3235	0.299	0.2637	0.2203	0.2756	0.3083	0.2779	0.2915
MnO	0.0911	0.116	0.1007	0.1323	0.1467	0.0686	0.0901	0.184	0.1403	0.0737
ZnO	0	0	0	0	0	0	0	0	0	0
BaO	0	0	0	0	0	0	0	0	0	0
Na_2O	1.5137	1.5797	1.4788	1.5964	1.5043	1.5093	1.5566	1.5376	1.5049	1.4931
K_2O	0.0288	0.0261	0.0336	0.0439	0.0448	0.0233	0.0009	0.0332	0.0441	0
Rb_2O	0	0	0	0	0	0	0	0	0	0
Cs_2O	0	0	0	0	0	0	0	0	0	0
F	0	0	1.0709	0.2548	0.1534	0.3956	0.133	0.1704	0.24	0.156
Cl										
H_2O										
B_2O_3	10.7108	10.9612	9.5478	10.2021	9.9293	11.003	9.7378	9.7378	10.7595	9.5284
Li_2O										
H_2O*										

B_2O_3*										
Li_2O*										
Total	95.4764	96.1754	95.8714	95.944	95.1147	96.5831	94.6239	95.2908	95.855	94.0226
O=F	0	0	0.45093	0.10729	0.06459	0.16658	0.056	0.07175	0.10106	0.06569
Total*	95.4764	96.1754	95.4205	95.8367	95.0501	96.4165	94.5679	95.219	95.7539	93.9569
B	3.14165	3.18012	3.13263	3.15858	3.14903	3.12983	3.10916	3.13483	3.16419	3.11773
T: Si	5.73618	5.69127	5.71179	5.72249	5.71876	5.7335	5.74845	5.74551	5.7209	5.75042
Al	0.26382	0.30873	0.28821	0.27751	0.28124	0.2665	0.25155	0.25449	0.2791	0.24958
Z: Al	6	6	6	6	6	6	6	6	6	6
Mg	0	0	0	0	0	0	0	0	0	0
Y: Al	0.05678	0.02773	0.0726	0.05217	0.03715	0.1094	0.12919	0.03076	0.05529	0.12979
Ti	0.07083	0.07173	0.07005	0.06846	0.07073	0.07005	0.06665	0.07242	0.07001	0.06898
V	0	0	0	0	0	0	0	0	0	0
Cr	6.6E-05	0.0003	0.00039	0.00105	5.3E-05	0.00059	0.00093	0.00171	0.00065	0.00085
Fe^{3+}	0	0	0	0	0	0	0	0	0	0
Mg	1.18307	1.19786	1.17931	1.1501	1.19551	1.11606	1.12561	1.18745	1.13158	1.10492
Mn	0.00263	0.00193	0.00299	0.00298	0.00122	0.00281	0.00509	0.00387	0.00525	0.00316
Fe^{2+}	1.41988	1.37874	1.42797	1.43564	1.41512	1.42248	1.43577	1.44662	1.4228	1.42738
Zn	0	0	0	0	0	0	0	0	0	0
Li*	0.26679	0.32174	0.24674	0.28965	0.28024	0.27864	0.23683	0.25723	0.31446	0.26498

Y	3.00004	3.00001	3.00005	3.00005	3.00002	3.00004	3.00006	3.00004	3.00004	3.00006
X: Ca	0.15	0.16964	0.16683	0.15427	0.1683	0.1561	0.15124	0.16482	0.15725	0.1525
Ba	0	0	0	0	0	0	0	0	0	0
Na	0.59263	0.56374	0.57451	0.57881	0.58228	0.57759	0.57895	0.58551	0.57789	0.57338
K	0.01441	0.01559	0.01565	0.01378	0.01678	0.01566	0.01585	0.01463	0.01254	0.01419
Rb	0	0	0	0	0	0	0	0	0	0
Cs	0	0	0	0	0	0	0	0	0	0
X-vacancy	0.24296	0.25104	0.24301	0.25315	0.23264	0.25065	0.25396	0.23504	0.25233	0.25993
V+W site										
OH	3.93169	3.90384	3.92375	3.93723	3.9203	3.92799	3.95005	3.90241	3.93168	3.92842
F	0.06654	0.0947	0.07512	0.06137	0.07757	0.07103	0.04899	0.09607	0.06753	0.07028

Sample Y-TP-3 Tourmaline Pegmatite

SiO_2	34.8072	34.5459	34.5857	34.8453	35.3426	35.4334	35.0924	34.9258	35.3629	35.2191	35.6355	35.3795
TiO_2	1.0029	0.9976	0.9917	1.0286	0.3188	0.3273	0.261	0.2696	0.2757	0.2996	0.2814	0.2525
Al_2O_3	33.0995	32.925	32.8253	32.4579	34.0985	34.1671	34.5606	34.0241	33.9461	34.2309	33.8677	34.2234
V_2O_3												
Cr_2O_3	0.0416	0.028	0.0416	0.0551	0.0961	0.0011	0.0417	0.0011	0.0554	0.0825	0.0557	0.0
Fe_2O_3	0	0	0	0	0	0	0	0	0	0	0	0
FeO	9.1751	9.4273	9.5595	9.8868	9.1178	9.3841	9.8198	9.5447	9.1709	9.4085	8.8775	9.6567
MgO	3.7664	3.9757	3.4902	3.4946	3.0542	3.0101	2.8725	2.8429	2.8279	2.9537	2.8866	2.815
CaO	0.676	0.6994	0.7329	0.7563	0.2911	0.3078	0.3287	0.3265	0.3079	0.3457	0.3299	0.2415
MnO	0.0975	0.1338	0.0252	0.0493	0.0374	0.0495	0.1219	0.0978	0.0254	0.0979	0.0498	0.0618
ZnO												
BaO												
Na_2O	1.8208	1.9133	1.9266	1.8698	1.5879	1.5136	1.5344	1.4641	1.463	1.5637	1.489	1.4849
K_2O	0.0	0.0	0.0031	0.0642	0.0123	0.0	0.0395	0.0	0.0	0.0056	0.008	0.00
Rb_2O												
Cs_2O												
F												
Cl												
H_2O												
B_2O_3												
Li_2O												
H_2O*												
B_2O_3*												

Li_2O*												
Total	84.4674	84.6107	84.1818	84.5079	83.9567	84.1791	84.6725	83.4953	83.4248	84.2072	83.4811	84.0882
O=F	0	0	0	0	0	0	0	0	0	0	0	0
Total*	84.4674	84.6107	84.1818	84.5079	83.9567	84.1791	84.6725	83.4953	83.4248	84.2072	83.4811	84.0882
B	3	3	3	3	3	3	3	3	3	3	3	3
T: Si	5.82707	5.79661	5.82243	5.85639	5.91356	5.91922	5.85667	5.89533	5.94617	5.8905	5.97339	5.92399
Al	0.17293	0.20339	0.17757	0.14361	0.08644	0.08078	0.14333	0.10467	0.05383	0.1095	0.02661	0.07601
Z: Al	6	6	6	6	6	6	6	6	6	6	6	6
Mg	0	0	0	0	0	0	0	0	0	0	0	0
Y: Al	0.35774	0.30778	0.33529	0.28566	0.63778	0.64614	0.65457	0.66402	0.67338	0.63808	0.66421	0.67769
Ti	0.12626	0.12588	0.12555	0.13	0.04011	0.04112	0.03276	0.03422	0.03486	0.03768	0.03547	0.03179
V	0	0	0	0	0	0	0	0	0	0	0	0
Cr	0.00551	0.00371	0.00554	0.00732	0.01271	0.00015	0.0055	0.00015	0.00737	0.01091	0.00738	-0.0034
Fe^{3+}	0	0	0	0	0	0	0	0	0	0	0	0
Mg	0.93997	0.99449	0.87592	0.87557	0.76183	0.74962	0.71467	0.71537	0.70886	0.73646	0.72133	0.70267
Mn	0.01383	0.01902	0.00359	0.00702	0.0053	0.007	0.01723	0.01398	0.00362	0.01387	0.00707	0.00876
Fe^{2+}	1.28454	1.32288	1.34586	1.38962	1.27584	1.31099	1.37055	1.34735	1.28961	1.31598	1.24447	1.35222
Zn	0	0	0	0	0	0	0	0	0	0	0	0
Li*	0.27215	0.22624	0.30825	0.30481	0.26642	0.24498	0.20472	0.22491	0.28231	0.24702	0.32006	0.2303
Y	3	3	3	3	3	3	3	3	3	3	3	3

X: Ca	0.12125	0.12574	0.13219	0.13619	0.05219	0.05509	0.05878	0.05905	0.05547	0.06195	0.05925	0.04332
Ba	0	0	0	0	0	0	0	0	0	0	0	0
Na	0.591	0.62245	0.62885	0.60929	0.51513	0.49024	0.4965	0.47916	0.47696	0.50708	0.48393	0.48207
K	-0.0042	-0.0076	0.00067	0.01377	0.00263	-0.0032	0.00841	-0.0003	-0.0022	0.00119	0.00171	-0.0003
Rb	0	0	0	0	0	0	0	0	0	0	0	0
Cs	0	0	0	0	0	0	0	0	0	0	0	0
X-vacancy	0.29193	0.25937	0.23829	0.24075	0.43005	0.45784	0.43631	0.46207	0.4698	0.42978	0.45511	0.47487
V+W site												
OH	0	0	0	0	0	0	0	0	0	0	0	0
F	0	0	0	0	0	0	0	0	0	0	0	0

SiO_2	33.8501	34.403	34.7513	34.8999	34.9915	35.2926	34.8971	35.1694	35.233
TiO_2	0.8957	0.8884	0.8454	0.8377	0.919	0.8082	0.8486	0.7957	0.8594
Al_2O_3	34.1644	32.6275	33.3659	33.5472	33.9234	33.5858	33.823	33.5741	33.9548
V_2O_3									
Cr_2O_3	0.0	0.1234	0.0014	0.0559	0.0695	0.0832	0.0561	0.1105	0.0833
Fe_2O_3	0	0	0	0	0	0	0	0	0
FeO	8.6552	9.5293	8.9188	8.8674	8.9805	8.9344	8.3046	9.3599	9.1396
MgO	3.4717	3.3723	3.7888	3.7765	3.5174	3.5532	3.4919	3.6747	3.6171
CaO	0.6335	0.5924	0.4773	0.5272	0.4677	0.5347	0.4543	0.4731	0.511
MnO	0.1224	-0.0107	0.0984	0.147	0.1227	0.05	0.0258	0.0259	0.1229
ZnO									
BaO									
Na_2O	1.7588	1.8265	1.8771	1.9125	1.7715	1.7221	1.7306	1.779	1.7556
K_2O	0.0397	0.00	0.0149	0.0	0.0	0.0	0.0104	0.0241	0.0
Rb_2O	_	_	_	_	_	_	_	_	_
Cs_2O	_	_	_	_	_	_	_	_	_
F	_	_	_	_	_	_	_	_	_
Cl	_	_	_	_	_	_	_	_	_

H_2O									
B_2O_3									
Li_2O									
H_2O*									
B_2O_3*									
Li_2O*									
Total	83.5791	83.351	84.1393	84.5589	84.7395	84.5768	83.6424	84.9864	85.2667
O=F	0	0	0	0	0	0	0	0	0
Total*	83.5791	83.351	84.1393	84.5589	84.7395	84.5768	83.6424	84.9864	85.2667
B	3	3	3	3	3	3	3	3	3
T: Si	5.71402	5.84521	5.82952	5.82392	5.82095	5.87315	5.84671	5.849	5.83125
Al	0.28598	0.15479	0.17048	0.17608	0.17905	0.12685	0.15329	0.151	0.16875
Z: Al	6	6	6	6	6	6	6	6	6
Mg	0	0	0	0	0	0	0	0	0

Y: Al	0.51093	0.37868	0.42612	0.42177	0.47194	0.46031	0.52539	0.42977	0.45446
Ti	0.1137	0.11351	0.10665	0.10512	0.11497	0.10114	0.10692	0.09951	0.10696
V	0	0	0	0	0	0	0	0	0
Cr	-0.0017	0.01658	0.00019	0.00738	0.00914	0.01095	0.00743	0.01453	0.0109
Fe^{3+}	0	0	0	0	0	0	0	0	0
Mg	0.87364	0.85416	0.94748	0.93948	0.87229	0.88149	0.87215	0.91106	0.89244
Mn	0.0175	-0.0015	0.01398	0.02078	0.01729	0.00705	0.00366	0.00365	0.01723
Fe^{2+}	1.22184	1.35401	1.25119	1.23749	1.24936	1.24339	1.16358	1.3018	1.26501
Zn	0	0	0	0	0	0	0	0	0
Li*	0.26404	0.28461	0.25439	0.26797	0.26502	0.29567	0.32086	0.23968	0.253
Y	3	3	3	3	3	3	3	3	3
X: Ca	0.11457	0.10784	0.08578	0.09426	0.08336	0.09534	0.08155	0.0843	0.09061
Ba	0	0	0	0	0	0	0	0	0
Na	0.57563	0.60169	0.61051	0.61878	0.57137	0.55564	0.56217	0.57364	0.56336
K	0.00855	-0.0002	0.00319	-0.0026	-0.005	0.00267	0.00222	0.00511	-0.0021
Rb	0	0	0	0	0	0	0	0	0

Cs	0	0	0	0	0	0	0	0	0
X-vacancy	0.30124	0.29071	0.30051	0.2896	0.3503	0.34635	0.35406	0.33695	0.34814
V+W site									
OH	0	0	0	0	0	0	0	0	0
F	0	0	0	0	0	0	0	0	0

APPENDIX B: 1.2 Representative EPMA data in (wt.%) for biotite of the two-mica leucogranites.

Sample LG-3 (I) Two mica leucogranite

SiO_2	34.9151	35.0321	34.689	34.3029	35.1225	34.6811	35.5174	34.3208	35.2215	34.5593	35.405	35.3293	35.1202
TiO_2	2.4177	2.4606	2.4682	2.4073	2.0969	1.9996	2.336	2.2837	2.5019	2.4249	2.6063	2.1356	2.6446
Al_2O_3	19.0241	19.4519	19.0013	18.9769	19.4114	19.2804	20.7474	19.4357	19.8457	19.3836	19.4404	21.4113	19.0384
Cr_2O_3	0.0399	0.0229	0.0667	0.0139	0	0.0581	0	0.0198	0.3277	0.3044	0.3735	0.3527	0.3878
Fe_2O_3													
FeO	21.2466	21.3133	21.4452	20.8076	21.3239	21.4372	20.858	21.4711	20.922	20.8524	21.0796	20.4543	21.1614
MnO	0.3019	0.358	0.2699	0.4629	0.3531	0.3452	0.3524	0.3469	0.3277	0.3044	0.3735	0.3527	0.3878
MgO	5.3424	5.4802	5.537	5.2012	5.575	5.5543	5.2824	5.0927	5.681	5.4955	5.4202	5.2667	5.4657
CaO	0	0	0	0	0	0	0	0	0	0	0	0	0
Na_2O	0.3498	0.3246	0.2884	0.3356	0.2241	0.2314	0.1618	0.2533	0.1815	0.2269	0.159	0.1185	0.1493
K_2O	8.264	8.0814	8.2665	8.0768	8.2222	8.1608	8.2832	8.2739	8.4686	8.2132	8.3822	7.8769	8.3244
H_2O													
Total	91.9015	92.525	92.0322	90.5851	92.3291	91.7481	93.5386	91.4979	93.4776	91.7646	93.2397	93.298	92.6796
Si	5.536239	5.507061	5.500926	5.515845	5.534194	5.510694	5.491657	5.478331	5.476057	5.479917	5.521491	5.452903	5.520262
Ti	0.288404	0.290999	0.294457	0.291211	0.248567	0.239031	0.271726	0.274238	0.292635	0.289268	0.305783	0.247976	0.312723
Al	3.55517	3.603882	3.551257	3.596344	3.604795	3.61064	3.780773	3.656334	3.63648	3.622415	3.573154	3.894848	3.526858
Cr	0.005002	0.002846	0.008363	0.001767	0	0.007299	0	0.002499	0.040282	0.038162	0.046053	0.04304	0.048193
Fe^{+3}	0	0	0	0	0	0	0	0	0	0	0	0	0
Fe^{+2}	2.81747	2.80203	2.844084	2.798153	2.809985	2.848721	2.697138	2.866246	2.720393	2.765244	2.749302	2.640254	2.781733
Mn	0.040546	0.047668	0.036252	0.063046	0.047125	0.046459	0.046151	0.046901	0.043154	0.040883	0.049337	0.046109	0.051629
Mg	1.262841	1.284283	1.308969	1.246796	1.309557	1.31569	1.217599	1.211852	1.316726	1.299053	1.260137	1.211831	1.280735

Ca	0	0	0	0	0	0	0	0	0	0	0	0	0
Na	0.107539	0.098934	0.088671	0.104628	0.068463	0.071289	0.048505	0.078392	0.054712	0.069757	0.048077	0.035461	0.0455
K	1.671661	1.620678	1.67233	1.656826	1.652774	1.654255	1.633867	1.684836	1.679686	1.661414	1.667655	1.550974	1.669214
H	0	0	0	0	0	0	0	0	0	0	0	0	0
Total	15.28487	15.25838	15.30531	15.27462	15.27546	15.30408	15.18742	15.29963	15.26013	15.26611	15.22099	15.12339	15.23685
Al (iv)	2.463761	2.492939	2.499074	2.484155	2.465806	2.489306	2.508343	2.521669	2.523943	2.520083	2.478509	2.547097	2.479738
Al (vi)	1.091409	1.110943	1.052183	1.112188	1.138989	1.121335	1.27243	1.134665	1.112537	1.102332	1.094645	1.347751	1.04712

SiO_2	34.6547	35.1127	35.37	35.311	35.2362	34.9495	35.1408	34.9208	34.543	35.059	35.0407	34.7831	35.1516	35.6335
TiO_2	2.7727	2.525	1.6525	2.2461	2.4243	2.5214	2.0083	2.201	2.1097	2.125	2.1127	2.0915	2.1126	1.8723
Al_2O_3	19.3888	19.2784	23.0106	19.5347	19.4078	19.3354	19.5999	19.481	18.3951	18.9819	18.7938	19.1503	19.3189	20.2487
Cr_2O_3	0.2994	0.3648	0.1993	0.3591	0.333	0.3975	0.3182	0.4059	0.3587	0.3481	0.3543	0.3994	0.3691	0.2164
Fe_2O_3														
FeO	21.7795	21.2948	14.6765	20.8272	21.3758	21.4149	21.6305	22.0983	21.5835	21.6792	21.5117	21.9813	21.5508	21.2652
MnO	0.2994	0.3648	0.1993	0.3591	0.333	0.3975	0.3182	0.4059	0.3587	0.3481	0.3543	0.3994	0.3691	0.2164
MgO	5.1726	5.3549	3.5209	5.5062	5.4367	5.3088	5.7168	5.5064	6.0357	5.8811	6.0078	5.7423	5.6588	6.0872
CaO	0	0	0	0	0	0	0	0	0	0	0	0	0	0
Na_2O	0.1712	0.1473	0.13	0.0993	0.1546	0.1591	0.1362	0.2375	0.2171	0.2086	0.2029	0.1964	0.1889	0.2092
K_2O	8.4126	8.5169	7.2172	8.196	8.5038	8.3357	8.3714	8.2302	8.2558	8.2484	8.1311	8.3787	8.2782	8.2162
H_2O														
Total	92.9509	92.9596	85.9763	92.4387	93.2052	92.8198	93.2403	93.487	91.8573	92.8794	92.5093	93.1224	92.998	93.9651
Si	5.452589	5.50925	5.698009	5.540295	5.511019	5.492928	5.495275	5.464611	5.505489	5.511567	5.524742	5.471446	5.511704	5.496556
Ti	0.328201	0.298048	0.200275	0.265124	0.28525	0.298127	0.236267	0.259115	0.252961	0.251323	0.250596	0.247508	0.249204	0.217272
Al	3.595392	3.564955	4.368887	3.612305	3.577453	3.581549	3.612322	3.592866	3.455356	3.516981	3.492276	3.550293	3.57008	3.681155
Cr	0.037245	0.045254	0.025385	0.044546	0.041178	0.049394	0.039342	0.050219	0.0452	0.043267	0.044166	0.049672	0.045757	0.026391
Fe^{+3}	0	0	0	0	0	0	0	0	0	0	0	0	0	0
Fe^{+2}	2.865872	2.794282	1.977329	2.73289	2.795977	2.814799	2.828868	2.892026	2.876909	2.850278	2.836497	2.891715	2.826002	2.743279
Mn	0.039901	0.048481	0.027195	0.047723	0.044114	0.052916	0.042147	0.0538	0.048423	0.046352	0.047315	0.053214	0.04902	0.028273
Mg	1.213278	1.252536	0.845576	1.28791	1.26762	1.243856	1.332728	1.284557	1.434083	1.378303	1.4121	1.346575	1.322744	1.399782
Ca	0	0	0	0	0	0	0	0	0	0	0	0	0	0
Na	0.052226	0.04481	0.040605	0.030208	0.046881	0.048482	0.041295	0.072058	0.067087	0.063582	0.062025	0.059899	0.057427	0.062566
K	1.688602	1.704772	1.483246	1.640519	1.696728	1.671327	1.670061	1.643016	1.678616	1.654252	1.635479	1.681384	1.655896	1.616812

H	0	0	0	0	0	0	0	0	0	0	0	0	0	0
Total	15.27331	15.26239	14.66651	15.20152	15.26622	15.25338	15.2983	15.31227	15.36412	15.3159	15.30519	15.35171	15.28783	15.27209
Al (iv)	2.547411	2.49075	2.301991	2.459705	2.488981	2.507072	2.504725	2.535389	2.494511	2.488433	2.475258	2.528554	2.488296	2.503444
Al (vi)	1.047981	1.074205	2.066896	1.1526	1.088472	1.074477	1.107597	1.057477	0.960845	1.028548	1.017018	1.021739	1.081784	1.177711

SiO_2	35.4233	35.1166	33.82	34.50	33.88	33.47	34.40	31.34	34.29
TiO_2	1.7618	1.9691	2.49	1.95	2.65	2.20	2.36	2.26	2.40
$A_{l2}O_3$	19.8947	19.543	19.16	19.05	19.07	19.31	19.80	18.23	18.98
Cr_2O_3	0.3291	0.3368	0.05	0.01	0.00	0.00	0.00	0.00	0.00
Fe_2O_3									
FeO	20.7362	20.9494	22.11	22.01	21.99	22.72	22.22	20.06	21.67
MnO	0.3291	0.3368	0.3511	0.4453	0.3868	0.32	0.35	0.31	0.35
MgO	6.0372	5.9138	5.06	5.29	5.14	5.05	5.10	4.49	4.98
CaO	0	0	-0.02	0.00	-0.01	0.03	0.03	0.06	0.06
Na_2O	0.1982	0.1633	0.14	0.12	0.22	0.17	0.24	0.28	0.14
K_2O	8.2203	8.4301	9.41	8.83	9.05	8.99	8.90	8.36	8.93
H_2O									
Total	92.9299	92.7589	92.58	92.21	92.38	92.27	93.41	85.39	91.80
Si	5.522538	5.506457	5.400227	5.497924	5.408341	5.37018	5.414093	5.398737	5.487375
Ti	0.206635	0.232287	0.299702	0.234042	0.318423	0.265929	0.279036	0.292644	0.288923
Al	3.655458	3.611651	3.60591	3.578429	3.586937	3.65084	3.672892	3.70095	3.579443
Cr	0.040565	0.041755	0.006539	0.001651	0	0	0	0	0
Fe^{+3}	0	0	0	0	0	0	0	0	0
Fe^{+2}	2.70363	2.74726	2.952988	2.932887	2.936182	3.048641	2.924427	2.89047	2.899322
Mn	0.043457	0.044732	0.047485	0.060105	0.0523	0.043047	0.047017	0.044636	0.047829

Mg	1.403124	1.382411	1.205103	1.256435	1.224081	1.206916	1.196577	1.153536	1.187656
Ca	0	0	-0.00397	1.71E-05	-0.00236	0.005655	0.005582	0.011278	0.010064
Na	0.05991	0.049647	0.043188	0.037076	0.068619	0.053935	0.074058	0.094058	0.044613
K	1.63491	1.686355	1.916534	1.795936	1.843111	1.840587	1.787546	1.837726	1.822126
H	0	0	0	0	0	0	0	0	0
Total	15.27023	15.30255	15.47371	15.3945	15.43563	15.48573	15.40123	15.42404	15.36735
Al (iv)	2.477462	2.493543	2.599773	2.502076	2.591659	2.62982	2.585907	2.601263	2.512625
Al (vi)	1.177996	1.118108	1.006138	1.076353	0.995277	1.021021	1.086984	1.099687	1.066818

Sample Z-2 Two mica leucogranite

SiO_2	34.95	34.42	34.48
TiO_2	3.27	1.88	3.01
Al_2O_3	19.06	17.47	18.31
Cr_2O_3	0.07	0.19	0.07
Fe_2O_3			
FeO	21.08	21.76	20.51
MnO	0.33	0.34	0.36
MgO	6.70	7.05	6.49
CaO	0.00	0.01	0.00
Na_2O	0.17	0.05	0.15
K_2O	9.31	9.03	9.18
H_2O			
Total	94.92	92.21	92.57
Si	5.392616	5.50303	5.454068
Ti	0.379765	0.22624	0.358501
Al	3.465796	3.292197	3.412769
Cr	0.007942	0.024573	0.008153
Fe^{+3}	0	0	0
Fe^{+2}	2.71972	2.909221	2.712662
Mn	0.042958	0.046014	0.048792
Mg	1.541004	1.681025	1.53132
Ca	-0.00038	0.002398	0.000797
Na	0.050707	0.014476	0.046644
K	1.831952	1.840819	1.853173
H	0	0	0
Total	15.43208	15.53999	15.42688
Al (iv)	2.607384	2.49697	2.545932
Al (vi)	0.858413	0.795227	0.866836

Sample : ZY-LG-2 Two-mica leucogranite

SiO_2	35.7779	34.7354	35.0977	34.7802	34.5558	35.007	35.281	35.0428	35.4605	33.7541	35.2324	35.1488	35.447	35.4325	35.3071
TiO_2	1.8184	1.7775	1.9842	2.2392	2.3684	2.6882	2.7033	2.584	1.9338	2.7478	2.6801	2.6324	2.5662	2.6162	2.595
Al_2O_3	19.5952	19.5222	19.6025	19.9146	19.4935	18.7958	18.8094	19.4117	19.7297	18.72	18.739	18.664	18.9837	18.9425	19.1068
Cr_2O_3	0.0199	0	0	0	0	0.016	0.033	0.0229	0.0113	0	0	0	0.0154	0.0332	0.0073
Fe_2O_3															
FeO	21.311	21.6154	21.2647	21.5986	21.4563	21.2204	21.3117	21.6953	21.5636	22.0673	21.4166	21.121	21.0907	20.9686	21.239
MnO	0.3652	0.2817	0.3196	0.3127	0.3346	0.329	0.2921	0.3035	0.2671	0.3807	0.3646	0.3655	0.342	0.3879	0.3022
MgO	5.8069	5.6397	5.8454	5.5257	5.4884	5.315	5.5054	5.4196	5.7569	5.2189	5.3701	5.4034	5.4371	5.6332	5.551
CaO	0	0	0	0	0	0	0	0	0	0	0	0	0	0	0
Na_2O	0.106	0.1713	0.1914	0.1469	0.1965	0.4224	0.2946	0.369	0.1977	0.5026	0.4313	0.4698	0.4756	0.4795	0.4518
K_2O	8.3208	8.5251	8.3776	8.4331	8.5009	8.3086	8.0518	8.2426	8.5163	8.1801	8.2979	8.1973	8.2814	8.2091	8.2911
H_2O	0	0	0	0	0	0	0	0	0	0	0	0	0	0	0
Total	93.1213	92.2683	92.6831	92.951	92.3944	92.1024	92.2823	93.0914	93.4369	91.5715	92.532	92.0022	92.6391	92.7027	92.8513
Si	5.576205	5.498289	5.510108	5.456778	5.463007	5.542108	5.559236	5.490507	5.52542	5.420383	5.553915	5.564469	5.565838	5.556373	5.535386
Ti	0.213211	0.211671	0.234349	0.264298	0.281684	0.320168	0.320454	0.304581	0.226688	0.33196	0.317837	0.313518	0.303137	0.308644	0.30607
Al	3.599385	3.64199	3.627001	3.682396	3.63208	3.506999	3.493043	3.584528	3.623228	3.542942	3.481434	3.482352	3.513069	3.500915	3.530438
Cr	0.002452	0	0	0	0	0.002003	0.004111	0.002837	0.001392	0	0	0	0.001912	0.004116	0.000905
Fe^{+3}	0	0	0	0	0	0	0	0	0	0	0	0	0	0	0
Fe^{+2}	2.777768	2.861455	2.791959	2.833989	2.836835	2.809584	2.808411	2.842809	2.810024	2.96361	2.823423	2.796379	2.769558	2.749966	2.784763
Mn	0.04821	0.037768	0.042499	0.041555	0.044805	0.044117	0.038984	0.040277	0.035252	0.051781	0.048681	0.04901	0.045484	0.051522	0.04013
Mg	1.349208	1.330828	1.368064	1.292416	1.293503	1.254394	1.293224	1.265877	1.337272	1.249376	1.261973	1.275237	1.272709	1.316908	1.297382
Ca	0	0	0	0	0	0	0	0	0	0	0	0	0	0	0
Na	0.032031	0.052572	0.05826	0.044686	0.060231	0.129655	0.090002	0.112094	0.059727	0.156484	0.13182	0.144202	0.14479	0.145788	0.137333

K	1.654418	1.721516	1.677867	1.687904	1.714479	1.678048	1.61854	1.647533	1.692886	1.675786	1.668713	1.655543	1.658866	1.642258	1.658267
H	0	0	0	0	0	0	0	0	0	0	0	0	0	0	0
Total	15.25289	15.35609	15.31011	15.30402	15.32662	15.28707	15.226	15.29104	15.31189	15.39232	15.2878	15.28071	15.27536	15.27649	15.29067
Al (iv)	2.423795	2.501711	2.489892	2.543222	2.536993	2.457892	2.440764	2.509493	2.47458	2.579617	2.446085	2.435531	2.434162	2.443627	2.464614
Al (vi)	1.17559	1.140279	1.137109	1.139174	1.095087	1.049106	1.052278	1.075035	1.148648	0.963325	1.03535	1.046821	1.078907	1.057288	1.065824

SiO_2	35.2878	34.9332	34.6279	36.4784	34.5038	34.2636	34.2802	34.0844	34.0033	34.2853	34.6839	34.8013	34.7944
TiO_2	2.5968	2.6288	2.6118	2.5566	2.5051	2.4333	2.4445	2.4002	2.4088	2.3901	2.4246	2.4141	2.4303
$A_{l2}O_3$	18.8649	18.998	19.1032	20.3869	19.7297	19.485	19.4586	19.3458	19.427	19.8016	19.2534	18.874	21.066
Cr_2O_3	0.0549	0.0627	0	0	0.0174	0	0.0315	0	0	0	0.0348	0.0225	0
Fe_2O_3													
FeO	21.0378	21.3105	20.9636	21.3242	22.0637	21.4508	21.8226	21.247	21.5862	21.4963	20.9859	20.9411	19.6084
MnO	0.3453	0.3233	0.3338	0.3477	0.3118	0.3372	0.3747	0.3731	0.3454	0.2885	0.3111	0.3193	0.2464
MgO	5.4959	5.4538	5.4561	5.7794	5.341	5.2565	5.268	5.1884	5.1975	5.4125	5.4341	5.4246	5.2114
CaO	0	0	0	0	0	0	0	0	0	0	0	0	0
Na_2O	0.4973	0.5097	0.519	0.5095	0.488	0.4799	0.3771	0.4155	0.3654	0.313	0.372	0.3877	0.3545
K_2O	8.181	8.5023	8.3741	8.4976	8.3387	8.3306	8.2652	8.2653	8.2344	8.4029	8.1694	8.3949	7.8261
H_2O	0	0	0	0	0	0	0	0	0	0	0	0	0
Total	92.3617	92.7223	91.9895	95.8803	93.2992	92.0369	92.3224	91.3197	91.568	92.3902	91.6692	91.5795	91.5375
Si	5.557991	5.504223	5.490531	5.515532	5.416334	5.44356	5.436022	5.454477	5.433602	5.42149	5.506129	5.538833	5.459926
Ti	0.307701	0.311611	0.311548	0.290811	0.295842	0.290832	0.291625	0.288963	0.289577	0.284331	0.289571	0.289051	0.286902
Al	3.50189	3.527933	3.569842	3.632934	3.650176	3.648423	3.636673	3.648706	3.658704	3.690334	3.602306	3.540311	3.895957
Cr	0.006837	0.007811	0	0	0.00216	0	0.003949	0	0	0	0.004368	0.002831	0
Fe^{+3}	0	0	0	0	0	0	0	0	0	0	0	0	0
Fe^{+2}	2.771162	2.808146	2.779856	2.696452	2.896578	2.850112	2.894094	2.843567	2.884771	2.842777	2.786213	2.787344	2.573285
Mn	0.046066	0.043147	0.044829	0.044529	0.041457	0.045376	0.050328	0.050572	0.046749	0.03864	0.041832	0.043044	0.032749
Mg	1.290455	1.281054	1.289678	1.302702	1.24989	1.244966	1.245358	1.237775	1.238146	1.275908	1.286047	1.287067	1.219109
Ca	0	0	0	0	0	0	0	0	0	0	0	0	0
Na	0.151864	0.15571	0.159551	0.149362	0.148526	0.147824	0.115941	0.128918	0.113209	0.095962	0.1145	0.119636	0.107854
K	1.643827	1.709033	1.69388	1.639096	1.669911	1.688429	1.672044	1.687378	1.67863	1.695104	1.654493	1.704491	1.566676
H	0	0	0	0	0	0	0	0	0	0	0	0	0
Total	15.27779	15.34867	15.33972	15.27142	15.37087	15.35952	15.34603	15.34036	15.34339	15.34455	15.28546	15.31261	15.14246

Al (iv)	2.442009	2.495777	2.509469	2.484468	2.583666	2.55644	2.563978	2.545523	2.566398	2.57851	2.493871	2.461167	2.540074
Al (vi)	1.059881	1.032155	1.060373	1.148466	1.06651	1.091984	1.072695	1.103183	1.092306	1.111824	1.108435	1.079144	1.355883

SiO_2	34.7796	34.9013	34.7596	35.2553	35.1708	35.266	35.5295	35.3796	34.8136	34.9327	35.5238	35.2849	35.2322
TiO_2	2.4759	2.5428	2.4854	2.6383	2.6986	2.743	2.81	2.7828	2.8712	2.9237	2.9486	2.861	2.6751
Al_2O_3	19.4538	19.3219	19.538	19.1082	18.9029	18.9454	19.2421	18.9309	18.581	18.7626	18.9925	18.9617	19.2263
Cr_2O_3	0.001	0	0.0208	0.008	0	0	0.0374	0	0	0	0	0	0.0185
Fe_2O_3													
FeO	21.6639	21.3556	21.0241	20.9165	20.6867	21.132	20.8191	21.0673	20.8337	20.7997	21.1544	20.8623	20.6047
MnO	0.3369	0.3303	0.263	0.3389	0.2978	0.3776	0.3701	0.3601	0.3685	0.3855	0.3047	0.3996	0.3899
MgO	5.2609	5.51	5.2821	5.6907	5.6637	5.6033	5.6682	5.5163	5.4398	5.5048	5.6187	5.6011	5.6302
CaO	0	0	0	0	0	0	0	0	0	0	0	0	0
Na_2O	0.4171	0.4548	0.5096	0.5007	0.493	0.355	0.3904	0.4449	0.4419	0.4741	0.3925	0.396	0.464
K_2O	8.3002	8.3925	8.1697	8.2042	8.1597	8.3594	8.4707	8.331	8.1962	8.5051	8.4393	8.6485	8.3795
H_2O	0	0	0	0	0	0	0	0	0	0	0	0	0
Total	92.6893	92.8092	92.0523	92.6608	92.0732	92.7817	93.3375	92.8129	91.5459	92.2882	93.3745	93.0151	92.6204
Si	5.174905	5.480171	5.487045	5.493269	5.530163	5.534915	5.534915	5.53165	5.547526	5.538065	5.519125	5.536845	5.527703
Ti	0.192556	0.293494	0.30075	0.295494	0.31134	0.323875	0.323875	0.329131	0.328266	0.343613	0.34751	0.345745	0.337187
Al	5.24364	3.612674	3.580152	3.639074	3.532548	3.504397	3.504397	3.530798	3.498424	3.483638	3.493702	3.48883	3.500966
Cr	0.002461	0.000125	0	0.002599	0.000992	0	0	0.004604	0	0	0	0	0
Fe^{+3}	0	0	0	0	0	0	0	0	0	0	0	0	0
Fe^{+2}	1.797571	2.854792	2.80787	2.778701	2.743916	2.773727	2.773727	2.71079	2.762636	2.771685	2.748296	2.757478	2.733294
Mn	0.029574	0.044963	0.043984	0.035204	0.045027	0.050196	0.050196	0.048806	0.047825	0.049652	0.051588	0.040226	0.053023
Mg	0.938987	1.235777	1.291395	1.244438	1.33073	1.31102	1.31102	1.315593	1.289452	1.290039	1.296553	1.305538	1.308097
Ca	0	0	0	0	0	0	0	0	0	0	0	0	0
Na	0.098253	0.127425	0.138631	0.156146	0.152277	0.108026	0.108026	0.117847	0.135255	0.136294	0.145229	0.118612	0.120281
K	1.161338	1.668455	1.683234	1.647095	1.641747	1.673733	1.673733	1.682447	1.666479	1.663329	1.714249	1.678053	1.728435
H	0	0	0	0	0	0	0	0	0	0	0	0	0
Total	14.63928	15.31788	15.33306	15.29202	15.28874	15.27989	15.27989	15.27167	15.27586	15.27631	15.31625	15.27133	15.30898

Al (iv)	2.825095	2.519829	2.512955	2.506731	2.469837	-62.3416	2.465085	2.46835	2.452474	2.461935	2.480875	2.463155	2.472297
Al (vi)	2.418545	1.092844	1.067197	1.132343	1.062711	100.1474	1.039313	1.062448	1.045951	1.021703	1.012827	1.025676	1.028669

SiO_2	35.4115	34.9529	34.8413	32.455	33.7546	34.7655	34.9343	36.7424	36.7338	36.2887	35.4936	36.1935	36.1304	36.2261
TiO_2	2.6788	2.5793	2.4838	2.4279	2.4955	2.5009	2.4979	2.9303	2.8297	2.582	2.1568	2.2546	2.4512	2.5131
Al_2O_3	19.1019	19.7831	19.8104	20.3161	18.9579	18.8175	19.0992	18.3818	18.1488	18.5345	18.797	18.54	18.582	18.0663
Cr_2O_3	0.0494	0	0.0348	0.0343	0	0	0.0216	0	0.018	0.034	0.0071	0	0	0
Fe_2O_3														
FeO	20.9641	21.4608	21.3794	21.313	21.6764	21.2279	21.0653	22.3336	22.2558	21.9633	22.6713	22.0886	21.9834	21.7767
MnO	0.2932	0.3488	0.3182	0.3779	0.4042	0.3329	0.429	0.3869	0.4273	0.4435	0.482	0.4456	0.3731	0.3535
MgO	5.5683	5.4784	5.5665	4.9736	5.1083	5.3781	5.4465	4.3922	4.557	4.6788	4.8833	4.9968	4.9708	4.8479
CaO	0	0	0	0	0	0	0	0	0	0	0	0	0	0
Na_2O	0.4555	0.3945	0.409	0.3657	0.3771	0.4213	0.4798	0.1595	0.1264	0.1759	0.2652	0.1194	0.1791	0.1826
K_2O	8.3863	8.3578	8.5129	8.1453	8.2302	8.2775	8.5062	8.4898	9.5058	8.1158	7.8153	8.2586	8.3364	8.4679
H_2O	0	0	0	0	0	0	0							
Total	92.909	93.3556	93.3563	90.4088	91.0042	91.7216	92.4798	93.8165	94.6026	92.8165	92.5716	92.8971	93.0064	92.4341
Si	5.526583	5.542719	5.458126	5.445609	5.26445	5.441101	5.530247	5.71206	5.69978	5.630716	5.603112	5.677883	5.661395	5.713527
Ti	0.315685	0.315439	0.303011	0.292056	0.296278	0.302627	0.299288	0.342716	0.330316	0.301401	0.256145	0.266086	0.288952	0.298187
Al	3.554409	3.523789	3.640906	3.64922	3.883886	3.601628	3.527871	3.367968	3.318906	3.389439	3.497217	3.427838	3.43161	3.358201
Cr	0.002294	0.006113	0	0.0043	0.004399	0	0	0	0.002208	0.004171	0.000886	0	0	0
Fe^{+3}	0	0	0	0	0	0	0	0	0	0	0	0	0	0
Fe^{+2}	2.703034	2.744246	2.802687	2.794576	2.891241	2.922196	2.824044	2.903704	2.888044	2.850087	2.993119	2.89796	2.880805	2.872388
Mn	0.051803	0.038871	0.046134	0.042125	0.05192	0.055187	0.044853	0.050946	0.056158	0.058287	0.064448	0.059209	0.049518	0.047223
Mg	1.316593	1.299307	1.275336	1.297015	1.202688	1.227555	1.275368	1.01793	1.0541	1.082274	1.14922	1.16858	1.161148	1.139848
Ca	0	0	0	0	0	0	0	0	0	0	0	0	0	0
Na	0.141117	0.138233	0.11944	0.123942	0.115011	0.117857	0.129937	0.048076	0.038026	0.052918	0.08117	0.036317	0.054411	0.055838
K	1.676839	1.674578	1.664979	1.697407	1.685524	1.692469	1.679777	1.683756	1.881643	1.606497	1.573915	1.652794	1.666424	1.703785
H	0	0	0	0	0	0	0	0	0	0	0	0	0	0
Total	15.28836	15.2833	15.31062	15.34625	15.3954	15.36062	15.31139	15.12716	15.26918	14.97579	15.21923	15.18667	15.19427	15.189

Al (iv)	2.473417	2.457281	2.541874	2.554391	2.73555	2.558899	2.469753	2.28794	2.30022	2.369284	2.396888	2.322117	2.338605	2.286473
Al (vi)	1.080992	1.066508	1.099031	1.094829	1.148336	1.042729	1.058119	1.080028	1.018686	1.020156	1.100329	1.105721	1.093005	1.071727

SiO_2	36.65	36.6572	36.8961
TiO_2	2.0249	2.099	2.0848
Al_2O_3	18.6335	18.5581	18.4759
Cr_2O_3	0.0101	0.0775	0.0136
Fe_2O_3			
FeO	21.9559	21.0621	22.777
MnO	0.4114	0.4609	0.495
MgO	4.966	4.9622	4.6533
CaO	0	0	0
Na_2O	0.2834	0.2046	0.4292
K_2O	7.9742	8.3146	8.0011
H_2O			
Total	92.9094	92.3962	93.826
Si	5.72759	5.749052	5.735181
Ti	0.238067	0.247655	0.243797
Al	3.431999	3.430245	3.384753
Cr	0.001248	0.00961	0.001671
Fe^{+3}	0	0	0
Fe^{+2}	2.869575	2.76253	2.960953
Mn	0.054456	0.061225	0.065172
Mg	1.156952	1.160171	1.078297
Ca	0	0	0
Na	0.08587	0.062214	0.129351
K	1.589796	1.663545	1.586619
H	0	0	0
Total	15.15555	15.14625	15.18579
Al (iv)	2.27241	2.250948	2.264819
Al (vi)	1.159589	1.179297	1.119935

APPENDIX B 1.3: Representative EPMA data in (wt.%) for muscovite of the two-mica leucogranites, tourmaline leucogranites and pegmatites.

Sample ZY-LG-2 Two-mica leucogranite

SiO_2	46.4701	43.9852	45.4971	45.8274	45.4935	45.793	45.075
TiO_2	0	0.2379	0.5773	0.0605	0.3175	0.0351	0.5309
Al_2O_3	34.9493	33.373	33.4776	35.4096	33.9989	33.9196	34.3479
Cr_2O_3	0.0317	0.0334	0	0	0	0	0.03
Fe_2O_3							
FeO	1.422	4.3892	1.4238	0.7573	1.953	0.3606	1.354
MnO	0.0264	0	0.0268	0.0197	0	0.0197	0
MgO	1.0008	0.7686	0.8041	0.1579	1.0045	0.314	0.7535
CaO	0	0	0	0	0	0.9946	0
Na_2O	0.6299	0.7686	0.7896	0.7589	0.6791	1.759	0.6819
K_2O	8.9087	10.2739	9.895	10.0112	8.8284	9.551	8.7997
H_2O							
Total	93.4389	93.8298	92.4913	93.0025	92.2749	92.7466	91.5729
Si	6.242941	6.067629	6.234982	6.209994	6.216882	6.247606	6.18868
Ti	0	0.024689	0.059518	0.006168	0.032641	0.003603	0.054837
Al	5.533614	5.425783	5.407052	5.655119	5.475741	5.454061	5.557983
Cr	0.003367	0.003643	0	0	0	0	0.003257
Fe^{+3}	0	0	0	0	0	0	0
Fe^{+2}	0.159766	0.506368	0.163181	0.085823	0.2232	0.041144	0.155471
Mn	91.1072	0.6604	73.518	0	0	3.7162	0.056
Mg	0.200435	0.158061	0.164275	0.031898	0.204637	0.063864	0.154226
Ca	0	0	0	0	0	0.072695	0
Na	0.164071	0.205569	0.209799	0.199386	0.179929	0.465291	0.181521
K	1.526815	1.808024	1.729911	1.730647	1.539082	1.66234	1.541298

H	0	0	0	0	0	0	0

Sample ZY-LGT-1 Tourmaline leucogranite

SiO_2	45.7528	45.496	45.7228	45.3715	45.3522	45.5805	45.3029	45.5536	45.1033	45.7101	45.593	45.7559	45.6916
TiO_2	0.5169	0.5615	0.3935	0.5035	0.3505	0.2392	0.2784	0.3302	0.6163	0.3994	0.3389	0.3805	0.5895
Al_2O_3	34.466	34.8429	36.3383	36.5109	36.245	36.5359	36.1147	36.759	36.6117	36.4383	31.7645	36.6064	36.8233
Cr_2O_3	0.0026	0.027	0.0099	0.0191	0	0.0011	0.0524	0	0.0191	0	0.0316	0.0254	0
Fe_2O_3													
FeO	2.4108	2.3485	2.0513	2.1007	2.317	1.9185	1.8361	1.8581	2.1763	1.9587	2.188	1.8689	2.1034
MnO	0.0461	0.0684	0.0117	0.0568	0.0449	0.0299	0.0167	0.028	0.0672	0.0442	0.0638	0.0586	0.0049
MgO	0.5161	0.5376	0.5408	0.5484	0.5694	0.5141	0.4863	0.3895	0.4186	0.4634	0.5365	0.4898	0.5537
CaO	0	0	0	0	0	0	0	0	0	0	0	0	0
Na_2O	0.7408	0.6931	0.8071	0.7757	0.7771	0.757	0.5829	0.5185	0.7227	0.5474	0.6235	0.7468	0.6859
K_2O	9.9092	9.2496	8.7623	8.9773	8.7832	8.8478	9.1222	9.2516	9.0281	9.2557	9	8.764	8.9295
H_2O													
Total	94.3613	93.8246	94.6377	94.8639	94.4393	94.424	93.7926	94.6885	94.7633	94.8172	90.1398	94.6963	95.3818
Si	6.172169	6.145794	6.089237	6.043312	5.60077	6.081601	6.092422	6.06827	6.019576	6.085845	6.392198	6.082865	6.043945
Ti	0.052459	0.057063	0.039425	0.050453	0.024498	0.02401	0.028166	0.033091	0.061879	0.040005	0.035745	0.038055	0.058663
Al	5.479814	5.5472	5.703605	5.731512	6.217374	5.74531	5.724041	5.771127	5.758803	5.717702	5.248665	5.735521	5.740657
Cr	0.000277	0.002884	0.001042	0.002011	0	0.000116	0.005571	0	0.002015	0	0.003503	0.00267	0
Fe^{+3}	0	0	0	0	0	0	0	0	0	0	0	0	0
Fe^{+2}	0.271988	0.265316	0.228469	0.234005	0.20013	0.214077	0.206504	0.207004	0.24291	0.218095	0.256547	0.207786	0.232688
Mn	0.003004	0	0.00562	0.000827	0.000623	0.003521	0.002726	0.006554	0	0.003111	0.002261	0	0.002276
Mg	0.103792	0.108262	0.107369	0.108893	0.156275	0.102258	0.097494	0.07735	0.083285	0.091976	0.112133	0.097071	0.109187
Ca	0	0	0	0	0	0	0	0	0	0	0	0	0
Na	0.193761	0.181529	0.208402	0.200323	0.360757	0.19583	0.151986	0.133917	0.187008	0.141305	0.169486	0.192491	0.175909
K	1.705356	1.593985	1.488691	1.525436	1.765285	1.506019	1.56502	1.572228	1.537129	1.572079	1.609722	1.486346	1.506842
H	0	0	0	0	0	0	0	0	0	0	0	0	0

SiO_2	45.7936	45.1729	45.303	45.4318	45.0007	45.9054	45.8806	45.5848	45.2959	45.0865	45.3244	45.572
TiO_2	0.2725	0.4169	0.4501	0.4298	0.2454	0.3934	0.2911	0.3588	0.3271	0.4483	0.4063	0.4131
Al_2O_3	36.7538	36.854	36.6925	36.2443	36.6683	36.0619	36.3988	36.0647	36.3744	36.9905	36.3939	36.9598
Cr_2O_3	0.0267	0	0	0	0	0.0506	0.0085	0	0.0484	0.0169	0.0265	0
Fe_2O_3												
FeO	1.8776	1.6803	2.2723	2.1855	2.1254	1.6419	2.0507	1.7313	2.0316	1.5985	2.1223	1.9438
MnO	0.0454	0	0.0308	0.0729	0.0339	0.0661	0.0387	0	0.0403	0	0.0258	0.069
MgO	0.4731	0.3888	0.5107	0.5748	0.504	0.3856	0.5151	0.4248	0.5412	0.3695	0.5277	0.425
CaO	0	0	0	0	0	0	0	0	0	0	0	0
Na_2O	0.6241	0.5668	0.7479	0.6507	0.6913	0.5981	0.6783	0.6667	0.6944	0.5512	0.6804	0.6641
K_2O	9.1605	8.9364	9.033	9.0218	8.9344	8.8462	8.9931	8.592	8.741	9.1138	9.0265	9.0793
H_2O												
Total	95.0273	94.0161	95.0403	94.6116	94.2034	93.9492	94.8549	93.4231	94.0943	94.1752	94.5338	95.1261
Si	6.077587	6.046505	6.028534	6.067991	6.032214	6.141516	6.100163	6.127194	6.067598	6.029927	6.056788	6.044841
Ti	0.027208	0.041981	0.04506	0.043187	0.024747	0.039595	0.029117	0.036282	0.032964	0.045106	0.040846	0.041223
Al	5.748882	5.813877	5.754622	5.705313	5.792993	5.686109	5.703667	5.71319	5.742599	5.830563	5.731835	5.777915
Cr	0.002802	0	0	0	0	0.005352	0.000894	0	0.005126	0.001787	0.0028	0
Fe^{+3}	0	0	0	0	0	0	0	0	0	0	0	0
Fe^{+2}	0.2084	0.188097	0.252882	0.24412	0.238268	0.183707	0.228025	0.194618	0.227596	0.178791	0.237184	0.215629
Mn	0	0.005268	0.007826	0.00132	0.006408	0.003978	0.003379	0.001902	0.003159	0.007596	0.004984	0.007576
Mg	0.093603	0.077582	0.101312	0.114449	0.100716	0.076906	0.102097	0.085121	0.108075	0.07367	0.105126	0.08404
Ca	0	0	0	0	0	0	0	0	0	0	0	0
Na	0.160592	0.147096	0.192962	0.168504	0.179667	0.155142	0.174855	0.173747	0.180348	0.142929	0.176286	0.170791
K	1.550965	1.525968	1.533462	1.537215	1.527845	1.509819	1.52538	1.473303	1.493741	1.554968	1.538814	1.536369
H	0	0	0	0	0	0	0	0	0	0	0	0

SiO_2	45.2857	45.437	45.1027	45.4884	46.5704	45.3819	45.84	45.28	45.37	44.78
TiO_2	0.5141	0.6258	0.4671	0.4072	0.4165	0.4351	0.32	0.39	0.36	0.35
Al_2O_3	36.5396	36.4309	36.3139	36.3157	36.6664	36.858	34.15	34.84	34.58	33.53
Cr_2O_3	0	0	0	0.0182	0	0	0.00	0.03	0.00	0.00
Fe_2O_3										
FeO	2.1214	1.5906	2.4082	2.6892	2.007	1.5265	1.64	1.36	2.14	1.73
MnO	0.0289	0.0224	0.064	0.0351	0.0413	0.0206	0.14	0.00	0.00	0.03
MgO	0.5189	0.3367	0.5532	0.5428	0.497	0.3338	0.42	0.31	0.53	0.48
CaO	0	0	0	0	0	0	0.01	0.02	0.03	0.06
Na_2O	0.7698	0.7224	0.6507	0.9449	0.6114	0.6118	0.65	0.11	0.19	0.23
K_2O	8.747	9.0601	8.7745	8.5159	9.0061	8.9511	10.05	10.23	9.96	9.82
H_2O										
Total	94.5254	94.2259	94.3343	94.9574	95.8161	94.1188	93.2106	92.5761	93.1593	91.0179
Si	6.043977	6.074812	6.042019	6.056026	6.121095	6.062961	6.237019	6.185775	6.177918	6.230776
Ti	0.051619	0.062944	0.047075	0.040784	0.041184	0.043731	0.032377	0.040341	0.037002	0.036345
Al	5.747517	5.740475	5.733334	5.698181	5.67992	5.803481	5.476907	5.610329	5.549684	5.498879
Cr	0	0	0	0.001916	0	0	0	0.003489	0	0
Fe^{+3}	0	0	0	0	0	0	0	0	0	0
Fe^{+2}	0.236784	0.177849	0.269799	0.299418	0.220615	0.170556	0.1867	0.155832	0.243647	0.201283
Mn	0.006598	0.000549	0.005104	0	0.003472	0.008247	0.016169	0	1.15E-05	0.003312
Mg	0.103242	0.067108	0.110477	0.10773	0.097384	0.066481	0.084402	0.062892	0.107041	0.100004
Ca	0	0	0	0	0	0	0.000816	0.002474	0.004902	0.009601
Na	0.199198	0.18726	0.169007	0.243903	0.155808	0.158473	0.170316	0.028077	0.0504	0.06267
K	1.489283	1.545299	1.499541	1.446352	1.510123	1.52558	1.745204	1.783611	1.729663	1.74381
H	0	0	0	0	0	0	0	0	0	0

Sample Y-TG-1 Tourmaline pegmatite

SiO_2	45.936	45.480	45.524	45.183	45.598	45.033	45.995
TiO_2	0.136	0.231	0.027	0.116	0.242	0.053	0.141
Al_2O_3	36.049	36.012	36.831	36.833	36.618	36.060	36.865
Cr_2O_3	0.003	0.032	0.000	0.000	0.000	0.001	0.010
Fe_2O_3							
FeO	1.090	1.318	0.746	1.026	1.017	1.029	1.118
MnO	0.000	0.049	0.007	0.006	0.031	0.024	0.059
MgO	0.292	0.307	0.156	0.369	0.331	0.260	0.350
CaO	0.000	0.000	0.000	0.000	0.000	0.000	0.000
Na_2O	0.572	0.492	0.474	0.513	0.684	0.550	0.748
K_2O	10.667	10.000	10.811	10.887	10.670	10.995	10.532
H_2O							
Total	94.7451	93.92	94.5758	94.9326	95.1905	94.0046	95.817
Si	6.1429	6.12095	6.0914	6.04232	6.07479	6.08891	6.08345
Ti	0.01363	0.02335	0.00268	0.0117	0.02422	0.00536	0.01404
Al	5.68155	5.71214	5.80821	5.80522	5.7496	5.74626	5.74658
Cr	0.0003	0.00337	0	0	0	8.6E-05	0.00101
Fe^{+3}	0	0	0	0	0	0	0
Fe^{+2}	0.12194	0.14837	0.08347	0.11476	0.11331	0.11637	0.12368

Mn	0	0.00562	0.00083	0.00062	0.00352	0.00273	0.00655
Mg	0.05813	0.06152	0.03102	0.07356	0.06568	0.05249	0.06893
Ca	0	0	0	0	0	0	0
Na	0.14836	0.1283	0.12299	0.13304	0.17671	0.14426	0.19192
K	1.81982	1.71694	1.8454	1.85732	1.81341	1.89646	1.77703
H	0	0	0	0	0	0	0

APPENDIX B 1.4 : Representative EPMA data in (wt.%) for K-feldspar and plagioclase of the two-mica leucogranites, tourmaline leucogranites and pegmatites.

Sample LG-3 (I) Two mica leucogranite

SiO_2	64.5032	64.6345	65.2471	59.6246	65.4173	65.2237	65.7515	65.5692	65.5374	66.5561	65.6668
TiO_2	0.0169	0	0.0064	0	0.0083	0.0072	0	0	0.007	0	0.0156
Al_2O_3	18.9255	18.9213	18.8015	18.7925	18.4339	18.8342	18.8004	18.4748	18.511	18.2038	18.5248
Cr_2O_3	0	0.0098	0.0238	0.0292	0.003	0.0068	0	0.0189	0	0.0226	0
Fe_2O_3											
FeO	0	0	0.0837	0.0717	0.0526	0.0542	0.0203	0.1585	0.0566	0	0.046
MnO	0	0.0274	0.0429	0.0052	0	0	0	0	0	0.0636	0
MgO	0.0098	0.0115	0	0.045	0	0	0	0.0067	0	0.0101	0
CaO	0	0	0.0961	0.165	0	0	0	0	0	0	0
Na_2O	1.3548	1.4367	1.6363	1.3027	1.494	1.8544	1.8397	1.5651	1.8091	1.2284	2.052
K_2O	12.8112	12.8033	12.3083	11.9784	12.95	12.5197	12.0181	12.9448	12.5221	12.6835	12.1452
H_2O											
Si	3.000339	3.00049	3.009954	2.949561	3.021729	3.005852	3.019489	3.019217	3.020182	3.0483	3.021232
Ti	0.000591	0	0.000222	0	0.000288	0.00025	0	0	0.000243	0	0.00054
Al	1.037507	1.035222	1.022223	1.095649	1.003541	1.022973	1.017536	1.002603	1.005376	0.982622	1.004492
Cr	0	0.00036	0.000868	0.001142	0.00011	0.000248	0	0.000688	0	0.000818	0
Fe^{+3}	0	0	0	0	0	0	0	0	0	0	0
Fe^{+2}	0	0	0.003229	0.002966	0.002032	0.002089	0.00078	0.006104	0.002181	0	0.00177
Mn	0	0.001077	0.001676	0.000218	0	0	0	0	0	0.002467	0
Mg	0.00068	0.000796	0	0.003319	0	0	0	0.00046	0	0.00069	0
Ca	0	0	0.00475	0.008746	0	0	0	0	0	0	0
Na	0.122182	0.129312	0.146354	0.124946	0.133801	0.165695	0.163802	0.139727	0.161641	0.109082	0.183046
K	0.760213	0.758239	0.724358	0.75594	0.763113	0.736059	0.704077	0.760407	0.736169	0.74108	0.712852

H	0	0	0	0	0	0	0	0	0	0	0
An	0	0	0.00	0.983046	0	0	0	0	0	0	0
Ab	13.84698	14.56984	65.83	14.04497	14.91821	18.37516	18.87423	15.52327	18.00429	12.83104	20.43198
Or	86.15302	85.43016	34.17	84.97199	85.08179	81.62484	81.12577	84.47673	81.99571	87.16896	79.56802

Sample LG-4 (I) Two-mica leucogranite

SiO_2	65.636	66.1008	65.9627	69.0735	65.6134	66.8958
TiO_2	0.0027	0.0047	0.0024	0	0	0
Al_2O_3	18.3716	18.6928	18.5157	19.6966	18.8893	19.0018
Cr_2O_3	0.034	0	0.037	0	0	0.0224
Fe_2O_3						
FeO	0.0126	0	0.0351	0.0056	0.0589	0
MnO	0	0.0213	0.0125	0.0196	0	0.0268
MgO	0.0068	0.0124	0.0097	0.0124	0.0564	0.0052
CaO	0	0	0	0	0	0
Na_2O	1.6857	1.6788	1.8698	1.286	2.3193	3.8379
K_2O	12.6492	12.7097	12.4574	9.676	11.9351	9.2236
H_2O						
Si	3.026131	3.021305	3.023748	3.062684	3.006084	3.022772
Ti	0	0.000162	0	0	0	0
Al	0.998268	1.006971	1.000327	1.029287	1.019951	1.011943
Cr	0.001239	0	0.001341	0	0	0.0008
Fe^{+3}	0	0	0	0	0	0
Fe^{+2}	0.000486	0	0.001346	0.000208	0.002257	0
Mn	0	0.000825	0.000485	0.000736	0	0.001026
Mg	0.000467	0.000845	0.000663	0.00082	0.003852	0.00035
Ca	0	0	0	0	0	0
Na	0.150685	0.148775	0.166183	0.110554	0.20602	0.336236
K	0.743986	0.741105	0.728502	0.547322	0.697575	0.531696
H	0	0	0	0	0	0

An	0	0	0	0	0	0
Ab	16.84287	16.71896	18.57486	16.8051	22.80051	38.74054
Or	83.15713	83.28104	81.42514	83.1949	77.19949	61.25946

Sample ZY-LGT-1 Tourmaline leucogranite

SiO_2	64.8221	62.1507	64.248	63.9216	64.2518	64.2186	64.6745	64.4661	64.4236	64.4661	64.1891	64.6089	64.7789	64.8833	64.435
TiO_2	0	0.0182	0.0059	0	0	0.0007	0	0	0	0	0	0	0.0061	0	0.0109
Al_2O_3	19.0293	19.3382	19.0926	19.4938	19.0367	19.2668	19.2192	19.092	19.5683	19.092	19.2395	19.944	19.3992	19.1373	19.2554
Cr_2O_3	0	0.0085	0.0256	0.0327	0	0	0.0145	0.0343	0	0.0343	0	0	0	0.0573	0
Fe_2O_3															
FeO	0.0494	0	0.0379	0.0091	0.0273	0	0.0356	0.003	0	0.003	0.0029	0.041	0.0352	0.0308	0.0029
MnO	0	0.0135	0.0202	0.0371	0.0352	0.023	0.0099	0	0	0	0	0.0179	0	0	0.0191
MgO	0	0.0196	0.0119	0.0145	0.0129	0.0014	0.0098	0.0046	0.0126	0.0046	0	0	0	0	0.0018
CaO	0	0	0	0	0	0	0	0	0	0	0	0	0	0	0
Na_2O	1.3741	1.4509	1.2127	1.6596	1.3825	1.243	1.2443	1.1921	1.3036	1.1921	1.3862	1.4598	1.8983	1.5947	1.4963
K_2O	13.9599	12.8563	13.2384	12.6458	13.868	13.0983	13.1662	13.1192	13.0028	13.1192	12.6355	12.5007	12.0174	12.4793	13.5061
H_2O															
Si	2.987829	2.956501	2.988721	2.971717	2.981251	2.985513	2.990726	2.993933	2.978823	2.993933	2.989072	2.97199	2.988697	2.99695	2.979413
Ti	0	0.000651	0.000206	0	0	0	0	0	0	0	0	0	0.000212	0	0.000379
Al	1.033737	1.084183	1.046756	1.068098	1.041022	1.055656	1.047451	1.045001	1.066369	1.045001	1.055902	1.08124	1.054841	1.041794	1.049344
Cr	0	0.00032	0.000942	0.001202	0	0	0.00053	0.001259	0	0.001259	0	0	0	0.002093	0
Fe^{+3}	0	0	0	0	0	0	0	0	0	0	0	0	0	0	0
Fe^{+2}	0.001904	0	0.001474	0.000354	0.001059	0	0.001377	0.000117	0	0.000117	0.000113	0.001577	0.001358	0.00119	0.000112
Mn	0	0.000544	0.000796	0.001461	0.001383	0.000906	0.000388	0	0	0	0	0.000697	0	0	0.000748
Mg	0	0.00139	0.000825	0.001005	0.000892	0	0.000676	0.000318	0.000869	0.000318	0	0	0	0	0.000124
Ca	0	0	0	0	0	0	0	0	0	0	0	0	0	0	0

Na	0.122799	0.133818	0.109376	0.149592	0.124372	0.11204	0.111561	0.107341	0.116866	0.107341	0.125154	0.130194	0.169808	0.142814	0.134144
K	0.820864	0.780197	0.785629	0.750002	0.820887	0.776836	0.776713	0.777274	0.766996	0.777274	0.750626	0.733577	0.707319	0.735348	0.796701
H	0	0	0	0	0	0	0	0	0	0	0	0	0	0	0
An	0	0	0	0	0	0	0	0	0	0	0	0	0	0	0.00
Ab	13.01332	14.64098	12.22103	16.62917	13.15775	12.60498	12.55961	12.13453	13.22251	12.13453	14.2909	15.07313	19.35996	16.26315	13.04
Or	86.98668	85.35902	87.77897	83.37083	86.84225	87.39502	87.44039	87.86547	86.77749	87.86547	85.7091	84.92687	80.64004	83.73685	86.96

Sample Y-TG-1 Tourmaline pegmatite

SiO_2	64.474	64.055	64.838	64.248	64.4083	64.2253	64.8652	64.6358	64.15
TiO_2	0.000	0.000	0.009	0	0.004	0.0016	0	0	0.002
Al_2O_3	18.153	19.300	19.331	19.2311	19.2354	19.0626	19.1929	19.2958	19.2845
Cr_2O_3	0.000	0.000	0.003	0.0156	0	0	0.0257	0	0.0101
Fe_2O_3									
FeO	0.000	0.000	0.008	0.0213	0	0.0329	0	0.0944	0.0299
MnO	0.018	0.000	0.038	0	0	0.0091	0	0.0459	0.0073
MgO	0.013	0.000	0.007	0	0.0114	0.0672	0.0041	0.0057	0.012
CaO	0.000	0.000	0.000	0	0	0.0089	0	0	0
Na_2O	2.342	1.763	1.804	1.9302	1.329	1.2881	1.742	0.8004	1.1579
K_2O	13.115	13.558	12.033	13.294	12.735	12.8067	12.1705	13.4112	12.6804
H_2O									
Si	3.003852	2.969159	2.992391	2.97305	2.991274	2.992174	2.996965	2.991698	2.989508
Ti	0	0	0.000319	0	0.00014	0	0	0	0
Al	0.99677	1.054385	1.051455	1.048823	1.052859	1.046689	1.045118	1.052597	1.059171
Cr	0	0	0.000102	0.000571	0	0	0.000939	0	0.000372
Fe^{+3}	0	0	0	0	0	0	0	0	0
Fe^{+2}	0	0	0.000316	0.000824	0	0.001282	0	0.003654	0.001165
Mn	0.000714	0	0.001485	0	0	0.000359	0	0.001799	0.000288
Mg	0.000896	0	0.000495	0	0.000789	0.004667	0.000282	0.000393	0.000834
Ca	0	0	0	0	0	0.000444	0	0	0
Na	0.21153	0.158472	0.161452	0.173177	0.11967	0.116352	0.156049	0.071828	0.104621
K	0.779533	0.801736	0.70844	0.784793	0.754518	0.761157	0.717356	0.791897	0.753863

H	0	0	0	0	0	0	0	0	0
An	0	0	0.00	0	0	0.050602	0	0	0
Ab	21.3442	16.5043	18.56	18.07787	13.68954	13.25296	17.86717	8.316313	12.18699
Or	78.6558	83.4957	81.44	81.92213	86.31046	86.69644	82.13283	91.68369	87.81301

Sample LG-3 (I) Two-mica leucogranite (Plagioclase)

SiO_2	55.1472	63.6977	73.8581	62.7213	62.7593	63.5898	62.9088	63.13	60.6845	62.8513	60.3145
TiO_2	0	0	0.0105	0	0	0.0068	0	0	0.0046	0.0066	0.0081
Al_2O_3	21.0073	23.1147	15.1742	24.1114	23.34	22.6927	23.7288	23.7895	24.7366	23.7828	25.1789
Cr_2O_3	0.0242	0.0264	0	0.0141	0.0562	0.0333	0	0	0.0256	0	0.0404
Fe_2O_3											
FeO	0.0568	0	0.038	0.0109	0.0246	0.2482	0.1023	0.0355	0.0403	0	0.0181
MnO	0.0189	0	0	0.0121	0.0365	0.0505	0.0243	0.0468	0.0636	0.048	0.0282
MgO	0	0	0.0097	0	0.0306	0.022	0	0.0086	0	0	0

CaO	4.4085	3.8321	1.321	5.3837	4.5136	3.5724	4.6744	5.0707	5.8273	4.5892	6.7784
Na_2O	6.5528	8.9315	8.5146	8.0967	8.7139	9.008	8.2966	8.2452	7.9256	8.6238	7.207
K_2O	0.2351	0.2363	0.1505	0.2124	0.2006	0.2577	0.2279	0.1943	0.2523	0.242	0.1493
H_2O											
Total	87.4508	99.8387	99.0766	100.5626	99.6753	99.4814	99.9631	100.5206	99.5604	100.1437	99.7229
Si	2.779066	2.81218	3.204784	2.759147	2.783803	2.820659	2.779433	2.77573	2.707431	2.774443	2.686834
Ti	0	0	0.000343	0	0	0.000227	0	0	0.000154	0.000219	0.000271
Al	1.247672	1.202714	0.775999	1.250077	1.220158	1.186326	1.235593	1.232768	1.300692	1.237312	1.321937
Cr	0.000964	0.000922	0	0.00049	0.001971	0.001168	0	0	0.000903	0	0.001423
Fe^{+3}	0	0	0	0	0	0	0	0	0	0	0
Fe^{+2}	0.002394	0	0.001379	0.000401	0.000913	0.009207	0.00378	0.001305	0.001504	0	0.000674
Mn	0.000807	0	0	0.000451	0.001371	0.001897	0.000909	0.001743	0.002403	0.001795	0.001064
Mg	0	0	0.000627	0	0.002023	0.001455	0	0.000564	0	0	0
Ca	0.238035	0.181272	0.061415	0.253755	0.214515	0.169784	0.221281	0.238882	0.278561	0.217056	0.323534
Na	0.640245	0.764519	0.716323	0.690577	0.749406	0.774704	0.710705	0.702889	0.685577	0.738082	0.622469
K	0.015114	0.013309	0.008331	0.01192	0.011351	0.014583	0.012845	0.010899	0.01436	0.013628	0.008485
H	0	0	0	0	0	0	0	0	0	0	0
An	26.64314	18.89965	7.812708	26.5357	21.99475	17.70245	23.41953	25.07431	28.46752	22.40481	33.89527
Ab	71.66512	79.71274	91.1275	72.2178	76.84135	80.77709	75.22096	73.7817	70.06495	76.18848	65.21581
Or	1.691742	1.387611	1.059796	1.246497	1.163896	1.52046	1.359514	1.143987	1.467529	1.406717	0.888912

Sample LG-4 (I) Two-mica leucogranite

SiO_2	63.7138	65.3199	64.0681
TiO_2	0.0051	0.0121	0.0008
Al_2O_3	23.1811	22.3722	21.376
Cr_2O_3	0	0.0244	0.0114
Fe_2O_3			
FeO	0.0378	0.0155	0.0047
MnO	0.057	0	0
MgO	0	0	0
CaO	4.0896	3.0349	2.215
Na_2O	8.6926	9.2902	9.8253
K_2O	0.2995	0.2392	0.2794
H_2O			
Total	100.0765	100.3084	97.7807
Si	2.80839	2.860812	2.879128
Ti	0.000169	0.000399	0
Al	1.204239	1.154801	1.13214
Cr	0	0.000845	0.000405
Fe^{+3}	0	0	0
Fe^{+2}	0.001393	0.000568	0.000177
Mn	0.002128	0	0
Mg	0	0	0
Ca	0.193143	0.142417	0.106651
Na	0.742879	0.788884	0.85607
K	0.016841	0.013365	0.016018

H	0	0	0
An	20.26915	15.07545	10.89647
Ab	77.96343	83.50981	87.467
Or	1.767416	1.414732	1.636536

Sample ZY-LG-2 Two-mica leucogranite

SiO_2	65.7184	65.8905	65.6876	67.6574
TiO_2	0	0	0.0078	0
Al_2O_3	23.0044	20.7051	19.26	21.1649
Cr_2O_3	0	0.0322	0.0047	0
Fe_2O_3				
FeO	0	0.0048	0	0
MnO	0	0.0089	0.0412	0
MgO	0.0166	0	0.0144	0.0016
CaO	0.6671	4.1525	2.517	3.5439
Na_2O	9.8095	8.5722	9.2595	8.2762
K_2O	0.0931	0.2727	0.1787	0.2393
H_2O				
Total	99.3091	99.6389	96.9709	100.8833
Si	2.88217	2.906385	2.964159	2.930374
Ti	0	0	0.000265	0
Al	1.189045	1.076372	1.024305	1.080385
Cr	0	0.001123	0.000168	0
Fe^{+3}	0	0	0	0
Fe^{+2}	0	0.000177	0	0
Mn	0	0.000333	0.001575	0
Mg	0.001085	0	0.000969	0.000103
Ca	0.031347	0.196252	0.121696	0.164461
Na	0.834111	0.733106	0.810121	0.694997
K	0.005209	0.015345	0.010287	0.013222

H	0	0	0	0
An	3.600229	20.77332	12.91703	18.84495
Ab	95.80153	77.60237	85.99105	79.63994
Or	0.598241	1.624308	1.09192	1.515107

Sample ZY-LGT-1 Tourmaline leucogranite

SiO_2	66.9192	65.912
TiO_2	0.0049	0.0025
Al_2O_3	21.7981	22.1267
Cr_2O_3	0	0.024
Fe_2O_3		
FeO	0.0015	0.0418
MnO	0	0
MgO	0	0.0084
CaO	1.4918	1.4734
Na_2O	9.0403	9.0687
K_2O	0.3658	0.3797
H_2O		
Total	99.6216	99.0372
Si	2.925774	2.903089
Ti	0.000161	0
Al	1.123216	1.148596
Cr	0	0.000836
Fe^{+3}	0	0
Fe^{+2}	5.48E-05	0.00154
Mn	0	0
Mg	0	0.000552
Ca	0.069884	0.069533
Na	0.766332	0.774435
K	0.020403	0.021335
H	0	0
An	8.15779	8.035402
Ab	89.46048	89.49904
Or	2.381731	2.465555

Sample Y-TG-1 Tourmaline pegmatite

SiO_2	66.287	66.840	61.520	66.562	66.6766
TiO_2	0.0131	0	0	0.0056	0
Al_2O_3	21.5287	21.8491	19.0623	21.531	21.9322
Cr_2O_3	0	0.0092	0	0.0368	
Fe2O3					
FeO	0.0364	0	0	0.0758	0.0448
MnO	0	0	0.0128	0	0
MgO	0.0225	0	0.0022	0	0
CaO	0.113	0.1206	0.2423	0.1903	0.3338
Na_2O	10.1933	10.1426	10.0394	10.1774	10.2519
K_2O	0.1207	0.2012	0.1112	0.1112	0.1503
H_2O	0	0	0	0	0
Total	98.315	99.162	90.990	98.690	99.390
Si	2.933101	2.931463	2.95031	2.934761	2.921921
Ti	0.000436	0	0	0.000186	0
Al	1.122721	1.129377	1.077409	1.11884	1.132744
Cr	0	0.000319	0	0.001283	0
Fe^{+3}	0	0	0	0	0
Fe+2	0.001347	0	0	0.002795	0.001642
Mn	0	0	0.00052	0	0
Mg	0.001484	0	0.000157	0	0
Ca	0.005357	0.005667	0.01245	0.00899	0.015673
Na	0.874497	0.86247	0.933475	0.870022	0.871051

K	0.006813	0.011257	0.006803	0.006255	0.008403
H	0	0	0	0	0
An	0.604192	0.644425	1.306752	1.015481	1.750875
Ab	98.6274	98.07549	97.97919	98.278	97.31045
Or	0.768406	1.280088	0.714055	0.706521	0.938674

APPENDIX C: 1.1 U-Pb isotope (LA-ICPMS) data for two-mica leucogranite (ZY-LG-2) and REE variation in zircons.

Analysis	Source Filename	Comment	Preferred Age	Preferred Age	207 corr 206Pb/238U	207 corr 206Pb/238U	238U/206Pb	238U/206Pb
			Ma	2s%	Age	2s%	ratio	1s%
ZY-LG-2 (Two-mica leucogranite)								
2021-G-080	C21MAY14A0268.csv	concordant	13.93032798	2.240508051	13.93032798	2.2405081	463.3450337	1.081297846
2021-G-080	C21MAY14A0241.csv	minor common Pb	14.94542525	2.375572027	14.94542525	2.375572	429.2908565	1.122164955
2021-G-080	C21FEB25A0034.csv	young, some common Pb	15.33244243	2.41850947	15.33244243	2.4185095	420.2372437	1.196424331
2021-G-080	C21MAY14A0260.csv	concordant	15.43091607	2.122977082	15.43091607	2.1229771	418.4802708	1.05030678
2021-G-080	C21FEB25A0007.csv	high U, young concordant	15.50014543	1.934418865			415.3201824	0.959368173
2021-G-080	C21MAY14A0242.csv	minor common Pb	16.74713184	2.839678833	16.74713184	2.8396788	383.776992	1.338091241
2021-G-080	C21MAY14A0234.csv	concordant	18.91268728	2.886098985			339.9764358	1.44246036
2021-G-080	C21MAY14A0264.csv	younger	24.86720439	9.216753754	24.86720439	9.2167538	246.075041	3.693377821
2021-G-080	C21FEB25A0032.csv	comm Pb or Pb loss	28.76381981	2.529062414			224.0078749	1.151043211
2021-G-080	C21MAY14A0232.csv	High common Pb	41.52561938	5.704207217	41.52561938	5.7042072	144.8284333	2.90283357

2021-G-080	C21MAY14A0228.csv	older	144.2353677	2.604341941	144.2353677	2.6043419	44.13149984	1.331062384
2021-G-080	C21FEB25A0020.csv	Comm Pb or Pb loss	149.6068234	2.401434229	149.6068234	2.4014342	37.31828109	1.2700699
2021-G-080	C21MAY14A0230.csv	younger	346.2312729	4.08503102	346.2312729	4.085031	18.09531765	2.038548285
2021-G-080	C21MAY14A0269.csv	younger	349.6257965	6.868200882	349.6257965	6.8682009	18.00975496	4.157007096
2021-G-080	C21MAY14A0225.csv	minor common Pb	389.9822582	3.004278001	389.9822582	3.004278	15.84299546	1.511650274
2021-G-080	C21FEB25A0008.csv	moderate U, concordant	437.7931483	2.75933648	437.7931483	2.7593365	14.2102561	1.47577253
2021-G-080	C21MAY14A0236.csv	minor common Pb	446.4415003	1.970429955	446.4415003	1.97043	13.90496575	0.997912551
2021-G-080	C21MAY14A0230.csv	older	481.3249659	2.379307229			12.98093177	1.146416823
2021-G-080	C21FEB25A0033.csv	comm Pb or Pb loss	511.2376973	2.703119015	511.2376973	2.703119	11.79896239	1.39286673
2021-G-080	C21FEB25A0033.csv	comm Pb or Pb loss	597.4727037	2.282607751	597.4727037	2.2826078	9.899544448	1.135938529
2021-G-080	C21FEB25A0033.csv	comm Pb or Pb loss	643.1756009	1.948674418	643.1756009	1.9486744	9.157185883	1.034011855
2021-G-080	C21MAY14A0266.csv	concordant	773.3925808	1.934645859	773.3925808	1.9346459	7.838005725	0.994744855
2021-G-080	C21MAY14A0229.csv	Pb loss; use 7-6 ratio	784.8648525	5.694690384	333.4190163	5.3050194	18.60919447	3.317751568
2021-G-080	C21FEB25A0022.csv	minor common Pb	785.0881341	1.454573363	785.0881341	1.4545734	7.712388515	0.750779665
2021-G-080	C21MAY14A0267.csv	concordant	806.6917876	2.06569884	806.6917876	2.0656988	7.500588537	1.083575012
2021-G-080	C21MAY14A0233.csv	Pb loss; use 7-6 ratio	813.997749	2.720163671	750.9806315	1.9475474	8.068894137	1.008090424
2021-G-080	C21MAY14A0231.csv	Pb loss; use 7-6 ratio	816.5871887	3.237988072	709.0687744	2.1713113	8.580185065	1.151789253

2021-G-080	C21FEB25A0006.csv	high U, Pb loss, use 7/6	829.7085105	2.22347296	787.2017605	1.5562147	7.689662572	0.828248321
2021-G-080	C21MAY14A0263.csv	Pb loss; use 7-6 ratio	882.0060301	2.934829878	607.9657453	2.5771779	10.02135169	1.261595441
2021-G-080	C21MAY14A0270.csv	Pb loss; use 7-6 ratio	960.5552447	10.41532171	767.2955383	2.4525437	7.893109381	1.223972247
2021-G-080	C21FEB25A0009.csv	high U, Pb loss, use 7/6	965.0511889	3.176723913	916.9339144	1.7146539	6.507871939	0.878170158
2021-G-080	C21MAY14A0240.csv	Pb loss; use 7-6 ratio	1054.468059	5.870399608	948.9194636	2.5680074	6.286742449	1.425914789
2021-G-080	C21MAY14A0226.csv	high U, Pb loss, common Pb	1144.791977	2.751046664	271.4630221	3.3320252	22.40504745	1.878434354
2021-G-080	C21FEB25A0024.csv	Pb loss, use 7/6	1236.902926	1.70585345	667.2509406	3.3783754	8.91154182	1.645756184
2021-G-080	C21FEB25A0029.csv	Comm Pb or Pb loss	1279.786882	1.482904909	1279.786882	1.4829049	4.392326627	0.765431709
2021-G-080	C21FEB25A0033.csv	high U, Pb loss, use 7/6	1446.045658	1.826748722	528.465771	1.8614992	11.24981159	0.923361449
2021-G-080	C21FEB25A0031.csv	Comm Pb or Pb loss	1447.227368	1.507183028	1447.227368	1.507183	3.816833336	0.786907939
2021-G-080	C21MAY14A0264.csv	Pb loss; use 7-6 ratio	1546.515508	3.496478671	1333.721718	5.6308432	4.356350383	3.010986661
2021-G-080	C21MAY14A0261.csv	Pb loss; use 7-6 ratio	1718.480585	1.515267295	688.9526645	3.3734993	8.408700902	1.978936139
2021-G-080	C21MAY14A0269.csv	older	1727.869639	3.398673591	1727.869639	3.3986736	3.224343565	1.610190419
2021-G-080	C21MAY14A0249.csv	Pb loss; use 7-6 ratio	1737.603161	1.83135133	801.2882859	3.4232454	7.204010244	1.744593681
2021-G-080	C21MAY14A0238.csv	Pb loss; use 7-6 ratio	1752.574967	4.04941381	475.620786	2.7568969	12.28087922	1.435441972
2021-G-080	C21FEB25A0019.csv	Pb loss likely, use 7/6	1758.452394	0.955440893	1722.346558	1.5392732	3.257216907	0.794962113
2021-G-080	C21MAY14A0255.csv	Pb loss; use 7-6 ratio	1774.940806	1.121627614	1431.032572	1.9752472	3.935153887	1.016569386

2021-G-080	C21MAY14A0257.csv	Pb loss; use 7-6 ratio	1778.000239	1.027511159	1507.090753	2.3871643	3.730748658	1.257472259
2021-G-080	C21FEB25A0011.csv	high U, Pb loss, use 7/6	1806.146911	1.080076453	1585.030845	1.68583	3.533686175	0.868106186
2021-G-080	C21FEB25A0010.csv	high U, Pb loss, use 7/6	1808.401803	1.349631104	1326.29309	1.9237211	4.252143972	1.016389355
2021-G-080	C21FEB25A0023.csv	high U, Pb loss, use 7/6	1809.578985	0.993409611	646.5087163	4.1852374	8.888043178	2.648898974
2021-G-080	C21FEB25A0030.csv	high U, Pb loss, use 7/6	1826.950185	0.576253885	1693.91632	1.52849	3.298381522	0.812373002
2021-G-080	C21MAY14A0253.csv	Pb loss; use 7-6 ratio	1827.855934	1.171204574	1723.56797	1.9314955	3.238072408	0.996274888
2021-G-080	C21FEB25A0005.csv	high U, Pb loss, use 7/6	1832.38787	0.722223759	1590.289153	2.021415	3.52583968	1.077187221
2021-G-080	C21FEB25A0018.csv	Pb mobility, use 7/6	1842.274573	0.828578383			2.975431438	0.756537668
2021-G-080	C21MAY14A0254.csv	Pb loss; use 7-6 ratio	1843.499798	0.795581132	1697.113682	1.9488831	3.288687434	1.020484327
2021-G-080	C21MAY14A0251.csv	use 7-6 ratio	1843.934973	1.343438164	1763.512263	1.8398324	3.16021469	0.937581182
2021-G-080	C21MAY14A0259.csv	Pb loss; use 7-6 ratio	1843.990377	0.998312788	1334.905756	4.5956084	4.215582243	2.263151919
2021-G-080	C21MAY14A0258.csv	Pb loss; use 7-6 ratio	1844.420445	1.246929253	1406.098611	6.8262256	4.011648499	14.77716183
2021-G-080	C21MAY14A0262.csv	Pb loss; use 7-6 ratio	1846.360846	1.42731043	1550.976555	2.7576555	3.60748018	1.519213143
2021-G-080	C21MAY14A0239.csv	Pb loss; use 7-6 ratio	1846.946171	1.097057519	1819.203838	1.8999464	3.073483577	0.969491854
2021-G-080	C21MAY14A0265.csv	Pb loss; use 7-6 ratio	1983.659618	0.883362738	1346.834649	2.5684773	4.130168516	1.406821436
2021-G-080	C21MAY14A0235.csv	Pb loss; use 7-6 ratio	2135.82399	1.779231589	385.2494597	4.5124377	14.70589333	2.232870828
2021-G-080	C21MAY14A0250.csv	Pb loss; use 7-6 ratio	2142.300872	1.228186976	2034.885604	1.9183528	2.670929029	0.945298972

2021-G-080	C21MAY14A0252.csv	Pb loss; use 7-6 ratio	2462.826651	0.593393925	2267.771206	1.9557624	2.324918542	0.959235145
2021-G-080	*C21FEB25A0021.csv*	*do not use*	*1491.075386*	*2.670094837*	*1491.075386*	*2.6700948*	*3.800642535*	*1.403396953*
2021-G-080	*C21FEB25A0021.csv*	*do not use*	*1685.68398*	*1.511892641*	*1685.68398*	*1.5118926*	*3.321688633*	*0.79604065*
2021-G-080	*C21MAY14A0227.csv*	*do not use, inclusions*			*115.8619087*	*18.332298*	*54.58595233*	*12.03063362*
2021-G-080	*C21MAY14A0237.csv*	*do not use, inclusions*			*137.8069166*	*14.138017*	*45.87903092*	*13.675208*
2021-G-080	*C21MAY14A0256.csv*	*do not use, inclusions*			*76.19903501*	*8.892064*	*70.52981004*	*6.037766769*

Analysis	Source Filename	Comment	207Pb/206Pb	207Pb/206Pb	207Pb/235U(calc)	207Pb/235U(calc)	206Pb/238U	206Pb/238U
			ratio	1s%	ratio	1s%	ratio	1s%
ZY-LG-2 (Two-mica leucogranite)								
2021-G-080	C21MAY14A0268.csv	concordant	0.046727	2.485116	0.013027	3.159155	0.002164	1.111401
2021-G-080	C21MAY14A0241.csv	minor common Pb	0.049514	3.176611	0.014933	3.642959	0.00233	1.171801
2021-G-080	C21FEB25A0034.csv	young, some common Pb	0.048507	4.318158	0.014833	4.58031	0.002388	1.180691
2021-G-080	C21MAY14A0260.csv	concordant	0.04713	2.570367	0.014689	3.190315	0.002399	1.051219
2021-G-080	C21FEB25A0007.csv	high U, young concordant	0.045455	3.18479	0.013869	3.585924	0.002407	0.967209
2021-G-080	C21MAY14A0242.csv	minor common Pb	0.047871	4.757311	0.016985	5.142891	0.002606	1.391466
2021-G-080	C21MAY14A0234.csv	concordant	0.045107	5.445755	0.018062	5.676343	0.002938	1.443049
2021-G-080	C21MAY14A0264.csv	younger	0.068982	17.9432	0.037678	20.16905	0.003978	4.323921
2021-G-080	C21FEB25A0032.csv	comm Pb or Pb loss	0.044581	4.68394	0.025301	5.06284	0.004472	1.264531
2021-G-080	C21MAY14A0232.csv	High common Pb	0.080175	4.986487	0.068984	5.831214	0.006746	2.808767
2021-G-080	C21MAY14A0228.csv	older	0.054417	1.937618	0.15941	2.740936	0.022784	1.305048
2021-G-080	C21FEB25A0020.csv	Comm Pb or Pb loss	0.149411	0.680114	0.511296	2.10754	0.026859	1.187558
2021-G-080	C21MAY14A0230.csv	younger	0.056692	2.967841	0.430723	3.500029	0.055403	2.066502
2021-G-080	C21MAY14A0269.csv	younger	0.056374	2.69516	0.417487	4.681787	0.055934	3.487667
2021-G-080	C21MAY14A0225.csv	minor common Pb	0.059985	2.708447	0.513309	3.615029	0.062793	1.516946

2021-G-080	C21FEB25A0008.csv	moderate U, concordant	0.056195	1.178023	0.536405	2.401398	0.070321	1.406022
2021-G-080	C21MAY14A0236.csv	minor common Pb	0.058443	1.340877	0.572663	2.419654	0.071939	1.001381
2021-G-080	C21MAY14A0230.csv	older	0.055131	2.225532	0.575203	3.142044	0.077524	1.189654
2021-G-080	C21FEB25A0033.csv	comm Pb or Pb loss	0.081513	0.977909	0.889612	2.957695	0.085042	1.379466
2021-G-080	C21FEB25A0033.csv	comm Pb or Pb loss	0.090672	0.736865	1.167829	2.255252	0.100915	1.167956
2021-G-080	C21FEB25A0033.csv	comm Pb or Pb loss	0.093868	0.715433	1.306377	1.906982	0.109279	0.997147
2021-G-080	C21MAY14A0266.csv	concordant	0.0657	1.167274	1.138859	2.293171	0.127579	0.994188
2021-G-080	C21MAY14A0229.csv	Pb loss; use 7-6 ratio	0.065356	1.06415	0.479768	3.333927	0.053903	2.694469
2021-G-080	C21FEB25A0022.csv	minor common Pb	0.066285	0.957901	1.169716	2.006175	0.129663	0.747017
2021-G-080	C21MAY14A0267.csv	concordant	0.0666	0.815091	1.206841	2.212283	0.1334	1.065026
2021-G-080	C21MAY14A0233.csv	Pb loss; use 7-6 ratio	0.06627	0.529639	1.06923	2.043521	0.123851	1.003687
2021-G-080	C21MAY14A0231.csv	Pb loss; use 7-6 ratio	0.066353	0.632731	1.023519	2.110677	0.116744	1.117535
2021-G-080	C21FEB25A0006.csv	high U, Pb loss, use 7/6	0.066771	0.44239	1.098205	1.864499	0.1301	0.802689
2021-G-080	C21MAY14A0263.csv	Pb loss; use 7-6 ratio	0.068474	0.625875	0.92948	2.278434	0.099921	1.32256
2021-G-080	C21MAY14A0270.csv	Pb loss; use 7-6 ratio	0.071141	2.448655	1.236301	3.082653	0.127381	1.247621
2021-G-080	C21FEB25A0009.csv	high U, Pb loss, use 7/6	0.071298	0.750866	1.483748	1.996899	0.153163	0.885439
2021-G-080	C21MAY14A0240.csv	Pb loss; use 7-6 ratio	0.074512	1.536866	1.615739	2.700152	0.159314	1.323184

2021-G-080	C21MAY14A0226.csv	high U, Pb loss, common Pb	0.077953	0.79248	0.459222	2.586055	0.044465	1.686228
2021-G-080	C21FEB25A0024.csv	Pb loss, use 7/6	0.081677	0.538081	1.216566	2.472083	0.111757	1.737392
2021-G-080	C21FEB25A0029.csv	Comm Pb or Pb loss	0.113049	0.494896	3.50396	1.85653	0.227499	0.76569
2021-G-080	C21FEB25A0033.csv	high U, Pb loss, use 7/6	0.091014	0.69359	1.026547	1.992299	0.089041	0.948633
2021-G-080	C21FEB25A0031.csv	Comm Pb or Pb loss	0.124518	0.45924	4.443329	1.854795	0.261875	0.77637
2021-G-080	C21MAY14A0264.csv	Pb loss; use 7-6 ratio	0.095979	1.439015	3.046786	4.126924	0.232627	2.91681
2021-G-080	C21MAY14A0261.csv	Pb loss; use 7-6 ratio	0.105285	0.708495	1.702457	2.545374	0.11898	1.733324
2021-G-080	C21MAY14A0269.csv	older	0.117762	2.851244	5.04149	3.441911	0.311682	1.698526
2021-G-080	C21MAY14A0249.csv	Pb loss; use 7-6 ratio	0.106388	0.867894	2.02634	2.601124	0.139155	1.763298
2021-G-080	C21MAY14A0238.csv	Pb loss; use 7-6 ratio	0.107261	1.93921	1.191285	2.980948	0.081656	1.380268
2021-G-080	C21FEB25A0019.csv	Pb loss likely, use 7/6	0.107606	0.459418	4.494795	1.848698	0.307032	0.787392
2021-G-080	C21MAY14A0255.csv	Pb loss; use 7-6 ratio	0.108582	0.5455	3.750764	2.076784	0.253976	1.020713
2021-G-080	C21MAY14A0257.csv	Pb loss; use 7-6 ratio	0.108764	0.500777	3.963245	2.24271	0.267983	1.232873
2021-G-080	C21FEB25A0011.csv	high U, Pb loss, use 7/6	0.110458	0.536586	4.24571	1.916355	0.282841	0.866924
2021-G-080	C21FEB25A0010.csv	high U, Pb loss, use 7/6	0.110595	0.671524	3.524678	2.042703	0.235353	0.993655
2021-G-080	C21FEB25A0023.csv	high U, Pb loss, use 7/6	0.110667	0.494675	1.64279	2.90919	0.112241	2.149867
2021-G-080	C21FEB25A0030.csv	high U, Pb loss, use 7/6	0.111731	0.29032	4.34794	1.826458	0.303279	0.784149

2021-G-080	C21MAY14A0253.csv	Pb loss; use 7-6 ratio	0.111787	0.590417	4.694569	2.05663	0.308743	0.987662
2021-G-080	C21FEB25A0005.csv	high U, Pb loss, use 7/6	0.112066	0.365185	4.110259	2.087713	0.284342	1.041588
2021-G-080	C21FEB25A0018.csv	Pb mobility, use 7/6	0.11268	0.421729	5.151487	1.849445	0.336077	0.748113
2021-G-080	C21MAY14A0254.csv	Pb loss; use 7-6 ratio	0.112756	0.405264	4.530182	2.071163	0.304228	0.99945
2021-G-080	C21MAY14A0251.csv	use 7-6 ratio	0.112783	0.684537	4.854834	2.068997	0.316432	0.937334
2021-G-080	C21MAY14A0259.csv	Pb loss; use 7-6 ratio	0.112787	0.5087	3.58766	2.878423	0.237557	2.38341
2021-G-080	C21MAY14A0258.csv	Pb loss; use 7-6 ratio	0.112814	0.635566	3.838628	4.028816	0.250666	3.537546
2021-G-080	C21MAY14A0262.csv	Pb loss; use 7-6 ratio	0.112935	0.728444	4.256894	2.303495	0.27739	1.42111
2021-G-080	C21MAY14A0239.csv	Pb loss; use 7-6 ratio	0.112971	0.560113	5.059894	2.03311	0.32671	0.966281
2021-G-080	C21MAY14A0265.csv	Pb loss; use 7-6 ratio	0.121916	0.492327	4.014339	2.346423	0.242404	1.32981
2021-G-080	C21MAY14A0235.csv	Pb loss; use 7-6 ratio	0.132898	1.086356	1.241149	3.037918	0.068198	2.286017
2021-G-080	C21MAY14A0250.csv	Pb loss; use 7-6 ratio	0.133391	0.752717	6.796284	2.096904	0.374547	0.954688
2021-G-080	C21MAY14A0252.csv	Pb loss; use 7-6 ratio	0.160751	0.432516	9.403365	2.069185	0.430016	0.949491
2021-G-080	*C21FEB25A0021.csv*	*do not use*	*0.10223*	*0.7487*	*3.67454*	*2.35709*	*0.26302*	*1.37852*
2021-G-080	*C21FEB25A0021.csv*	*do not use*	*0.11161*	*0.61662*	*4.56832*	*1.87669*	*0.30172*	*0.7727*
2021-G-080	*C21MAY14A0227.csv*	*do not use, inclusions*	*0.06809*	*1.31794*	*0.1643*	*9.53513*	*0.0186*	*9.22061*
2021-G-080	*C21MAY14A0237.csv*	*do not use, inclusions*	*0.06809*	*2.15251*	*0.20149*	*8.00479*	*0.02214*	*7.11685*

2021-G-080	*C21MAY14A0256.csv*	*do not use, inclusions*	*0.17096*	*3.37592*	*0.31602*	*6.59154*	*0.01408*	*4.3739*

Analysis	Source Filename	Comment					Rho	208Pb/232Th	208Pb/232Th
								ratio	1s%
ZY-LG-2 (Two-mica leucogranite)									
2021-G-080	C21MAY14A0268.csv	concordant	0.0	2.7	0.0	1.1	0.4	0.00082	7.014577
2021-G-080	C21MAY14A0241.csv	minor common Pb	0.0	3.4	0.0	1.1	0.3	0.001127	8.966042
2021-G-080	C21FEB25A0034.csv	young, some common Pb	0.0	4.5	0.0	1.2	0.3	0.000995	11.41972
2021-G-080	C21MAY14A0260.csv	concordant	0.0	2.8	0.0	1.1	0.4	0.00071	8.479409
2021-G-080	C21FEB25A0007.csv	high U, young concordant	0.0	3.3	0.0	1.0	0.3	0.000753	10.01183
2021-G-080	C21MAY14A0242.csv	minor common Pb	0.0	4.9	0.0	1.3	0.3	0.001106	11.18899
2021-G-080	C21MAY14A0234.csv	concordant	0.0	5.6	0.0	1.4	0.3	0.001435	17.97526
2021-G-080	C21MAY14A0264.csv	younger	0.0	18.3	0.0	3.7	0.2	0.001952	31.57124
2021-G-080	C21FEB25A0032.csv	comm Pb or Pb loss	0.0	4.8	0.0	1.2	0.2	0.001309	19.31914
2021-G-080	C21MAY14A0232.csv	High common Pb	0.1	5.8	0.0	2.9	0.5	0.026144	9.439131
2021-G-080	C21MAY14A0228.csv	older	0.2	2.4	0.0	1.3	0.6	0.002576	21.3517
2021-G-080	C21FEB25A0020.csv	Comm Pb or Pb loss	0.6	1.4	0.0	1.3	0.9	0.051338	2.214905

2021-G-080	C21MAY14A0230.csv	younger		0.4	3.6	0.1	2.0	0.6	0.022183	5.561137
2021-G-080	C21MAY14A0269.csv	younger		0.4	5.0	0.1	4.2	0.8	0.041849	9.441626
2021-G-080	C21MAY14A0225.csv	minor common Pb		0.5	3.1	0.1	1.5	0.5	0.02197	4.238772
2021-G-080	C21FEB25A0008.csv	moderate U, concordant		0.5	1.9	0.1	1.5	0.8	0.023207	3.939065
2021-G-080	C21MAY14A0236.csv	minor common Pb		0.6	1.7	0.1	1.0	0.6	0.020406	4.118616
2021-G-080	C21MAY14A0230.csv	older		0.6	2.5	0.1	1.1	0.5	0.023101	3.863949
2021-G-080	C21FEB25A0033.csv	comm Pb or Pb loss		1.0	1.7	0.1	1.4	0.8	0.031292	4.899996
2021-G-080	C21FEB25A0033.csv	comm Pb or Pb loss		1.3	1.4	0.1	1.1	0.8	0.042072	3.123479
2021-G-080	C21FEB25A0033.csv	comm Pb or Pb loss		1.4	1.3	0.1	1.0	0.8	0.037525	3.158709
2021-G-080	C21MAY14A0266.csv	concordant		1.2	1.5	0.1	1.0	0.6	0.039323	3.327583
2021-G-080	C21MAY14A0229.csv	Pb loss; use 7-6 ratio		0.5	3.5	0.1	3.3	1.0	0.030403	3.670883
2021-G-080	C21FEB25A0022.csv	minor common Pb		1.2	1.2	0.1	0.8	0.6	0.038814	1.591524
2021-G-080	C21MAY14A0267.csv	concordant		1.2	1.4	0.1	1.1	0.8	0.037543	3.254428
2021-G-080	C21MAY14A0233.csv	Pb loss; use 7-6 ratio		1.1	1.1	0.1	1.0	0.9	0.02994	3.743826
2021-G-080	C21MAY14A0231.csv	Pb loss; use 7-6 ratio		1.1	1.3	0.1	1.2	0.9	0.039186	3.34317
2021-G-080	C21FEB25A0006.csv	high U, Pb loss, use 7/6		1.2	0.9	0.1	0.8	0.9	0.043841	1.773624

2021-G-080	C21MAY14A0263.csv	Pb loss; use 7-6 ratio	0.9	1.4	0.1	1.3	0.9	0.037603	3.165797
2021-G-080	C21MAY14A0270.csv	Pb loss; use 7-6 ratio	1.2	2.7	0.1	1.2	0.4	0.041302	3.965139
2021-G-080	C21FEB25A0009.csv	high U, Pb loss, use 7/6	1.5	1.2	0.2	0.9	0.8	0.046247	1.734173
2021-G-080	C21MAY14A0240.csv	Pb loss; use 7-6 ratio	1.6	2.1	0.2	1.4	0.7	0.048266	3.735745
2021-G-080	C21MAY14A0226.csv	high U, Pb loss, common Pb	0.5	2.0	0.0	1.9	0.9	0.031578	3.380074
2021-G-080	C21FEB25A0024.csv	Pb loss, use 7/6	1.3	1.7	0.1	1.6	1.0	0.036596	1.868078
2021-G-080	C21FEB25A0029.csv	Comm Pb or Pb loss	3.5	0.9	0.2	0.8	0.8	0.065544	1.834257
2021-G-080	C21FEB25A0033.csv	high U, Pb loss, use 7/6	1.1	1.2	0.1	0.9	0.8	0.041968	2.705411
2021-G-080	C21FEB25A0031.csv	Comm Pb or Pb loss	4.5	0.9	0.3	0.8	0.9	0.093323	1.401809
2021-G-080	C21MAY14A0264.csv	Pb loss; use 7-6 ratio	3.0	3.3	0.2	3.0	0.9	0.068528	3.802665
2021-G-080	C21MAY14A0261.csv	Pb loss; use 7-6 ratio	1.7	2.1	0.1	2.0	0.9	0.071723	3.460644
2021-G-080	C21MAY14A0269.csv	older	5.0	3.3	0.3	1.6	0.5	0.094609	3.981772
2021-G-080	C21MAY14A0249.csv	Pb loss; use 7-6 ratio	2.0	1.9	0.1	1.7	0.9	0.069592	3.41202
2021-G-080	C21MAY14A0238.csv	Pb loss; use 7-6 ratio	1.2	2.4	0.1	1.4	0.6	0.05577	4.647849
2021-G-080	C21FEB25A0019.csv	Pb loss likely, use 7/6	4.6	0.9	0.3	0.8	0.9	0.091576	1.496438

2021-G-080	C21MAY14A0255.csv	Pb loss; use 7-6 ratio	3.8	1.2	0.3	1.0	0.9	0.076873	3.26751
2021-G-080	C21MAY14A0257.csv	Pb loss; use 7-6 ratio	4.0	1.4	0.3	1.3	0.9	0.080355	3.176056
2021-G-080	C21FEB25A0011.csv	high U, Pb loss, use 7/6	4.3	1.0	0.3	0.9	0.9	0.092213	1.638533
2021-G-080	C21FEB25A0010.csv	high U, Pb loss, use 7/6	3.6	1.2	0.2	1.0	0.8	0.077202	1.919478
2021-G-080	C21FEB25A0023.csv	high U, Pb loss, use 7/6	1.7	2.7	0.1	2.6	1.0	0.107054	2.241686
2021-G-080	C21FEB25A0030.csv	high U, Pb loss, use 7/6	4.7	0.9	0.3	0.8	0.9	0.088211	1.310957
2021-G-080	C21MAY14A0253.csv	Pb loss; use 7-6 ratio	4.8	1.2	0.3	1.0	0.9	0.094576	3.558093
2021-G-080	C21FEB25A0005.csv	high U, Pb loss, use 7/6	4.4	1.1	0.3	1.1	0.9	0.090436	1.500086
2021-G-080	C21FEB25A0018.csv	Pb mobility, use 7/6	5.2	0.9	0.3	0.8	0.9	0.096742	1.435948
2021-G-080	C21MAY14A0254.csv	Pb loss; use 7-6 ratio	4.7	1.1	0.3	1.0	0.9	0.08736	3.263455
2021-G-080	C21MAY14A0251.csv	use 7-6 ratio	4.9	1.2	0.3	0.9	0.8	0.087829	3.22916
2021-G-080	C21MAY14A0259.csv	Pb loss; use 7-6 ratio	3.7	2.3	0.2	2.3	1.0	0.08325	3.383854
2021-G-080	C21MAY14A0258.csv	Pb loss; use 7-6 ratio	3.9	14.8	0.2	14.8	1.0	0.078596	3.796889
2021-G-080	C21MAY14A0262.csv	Pb loss; use 7-6 ratio	4.3	1.7	0.3	1.5	0.9	0.086362	3.530554

2021-G-080	C21MAY14A0239.csv	Pb loss; use 7-6 ratio	5.1	1.1	0.3	1.0	0.9	0.084021	3.186129
2021-G-080	C21MAY14A0265.csv	Pb loss; use 7-6 ratio	4.1	1.5	0.2	1.4	0.9	0.08099	3.2767
2021-G-080	C21MAY14A0235.csv	Pb loss; use 7-6 ratio	1.2	2.5	0.1	2.2	0.9	0.052202	4.2362
2021-G-080	C21MAY14A0250.csv	Pb loss; use 7-6 ratio	6.9	1.2	0.4	0.9	0.8	0.103601	3.478313
2021-G-080	C21MAY14A0252.csv	Pb loss; use 7-6 ratio	9.5	1.1	0.4	1.0	0.9	0.110078	3.264056
2021-G-080	*C21FEB25A0021.csv*	*do not use*	*3.7*	*1.6*	*0.3*	*1.4*	*0.9*	*0.08453*	*1.98175*
2021-G-080	*C21FEB25A0021.csv*	*do not use*	*4.6*	*1.0*	*0.3*	*0.8*	*0.8*	*0.08184*	*1.89064*
2021-G-080	*C21MAY14A0227.csv*	*do not use, inclusions*	*0.2*	*12.1*	*0.0*	*12.0*	*1.0*	*0.01004*	*10.1186*
2021-G-080	*C21MAY14A0237.csv*	*do not use, inclusions*	*0.2*	*13.8*	*0.0*	*13.7*	*1.0*	*0.02848*	*6.22138*
2021-G-080	*C21MAY14A0256.csv*	*do not use, inclusions*	*0.3*	*6.9*	*0.0*	*6.0*	*0.9*	*0.21816*	*8.4105*

Analysis	Source Filename	Comment	Time (s)	SiO4	31P	49Ti	56Fe	89Y	91Zr	93Nb	139La	140Ce
				ppm	ppm	ppm	ppm	ppm	ppm	ppm	ppm	ppm
ZY-LG-2 (Two-mica leucogranite)												
2021-G-080	C21MAY14A0268.csv	concordant	19.267	498831.3	3681.292	5.019517	<4.771	9243.671	460734.8	9.696385	0.022472	2.298654
2021-G-080	C21MAY14A0241.csv	minor common Pb	26.356	500512.3	3551.926	4.813347	11.69722	5698.373	468959	3.643037	0.559257	7.372805
2021-G-080	C21FEB25A0034.csv	young, some common Pb	7.999	499196.1	1150.322	6.941214	8.917802	2690.66	480069.6	3.703059	0.018226	1.73222
2021-G-080	C21MAY14A0260.csv	concordant	15.781	497665.2	1750.65	3.812347	<4.961	4128.176	472253.5	9.088045	0.004726	1.011232
2021-G-080	C21FEB25A0007.csv	high U, young concordant	26.103	498953	827.8345	4.606549	<2.949	1656.047	481811.6	2.342158	<0.001	0.873163
2021-G-080	C21MAY14A0242.csv	minor common Pb	26.356	499173.1	580.7224	3.856885	<4.539	899.3744	484417.4	2.057865	<0.002	0.850172
2021-G-080	C21MAY14A0234.csv	concordant	26.356	499112.9	149.7221	5.399758	<4.649	222.1419	486992.3	1.815729	<0.002	0.881767
2021-G-080	C21MAY14A0264.csv	younger	1.785	499226.4	554.1942	5.228917	<17.182	1200.968	484349.8	2.198579	<0.008	0.621363

2021-G-080	C21FEB25A0032.csv	comm Pb or Pb loss	10.504	498793.5	325.9385	2.076525	<3.651	478.8033	484947.2	0.700858	<0.001	0.315209
2021-G-080	C21MAY14A0232.csv	High common Pb	5.122	498458	790.0618	9.237237	34.56186	1420.688	481175.7	5.650226	0.180056	5.102022
2021-G-080	C21MAY14A0228.csv	older	9.636	498528.4	423.5921	1.610767	8.637281	449.0572	483998.5	1.270188	<0.003	1.270405
2021-G-080	C21FEB25A0020.csv	Comm Pb or Pb loss	26.103	498523.2	92.49359	3.410286	<2.918	139.8098	485647.7	1.57832	0.00118	1.376412
2021-G-080	C21MAY14A0230.csv	younger	6.888	499429.9	1053.639	4.680365	<6.613	2571.749	480793.7	1.464975	0.005497	1.661274
2021-G-080	C21MAY14A0269.csv	younger	4.934	499023	423.608	1.133663	<13.122	691.8678	484952.1	4.044773	<0.006	0.937945
2021-G-080	C21MAY14A0225.csv	minor common Pb	11.736	500188.2	1025.594	5.509404	<6.229	2116.721	483718.1	0.851654	0.014179	1.906672
2021-G-080	C21FEB25A0008.csv	moderate U, concordant	10.486	499218.5	1091.977	4.836068	<4.378	2357.569	480314.5	1.394454	0.011969	0.424884
2021-G-080	C21MAY14A0236.csv	minor common Pb	26.356	500011.2	1487.544	4.866725	<4.587	3180.581	479790.6	1.067461	<0.002	0.6433
2021-G-080	C21MAY14A0230.csv	older	9.875	500390	1954.281	4.270634	<8.821	3816.548	477972	2.86932	<0.004	5.392911
2021-G-080	C21FEB25A0033.csv	comm Pb or Pb loss	4.719	496522.4	1380.07	1.869475	8.759461	2536.399	471669.2	4.191981	0.042728	0.635535
2021-G-080	C21FEB25A0033.csv	comm Pb or Pb loss	6.141	496524.6	1422.133	3.303426	9.54197	2867.367	471136.8	4.768177	0.073058	1.668546
2021-G-080	C21FEB25A0033.csv	comm Pb or Pb loss	4.605	496714.8	1518.954	2.395462	14.09063	2959.065	471111.6	4.483113	0.245367	2.66376
2021-G-080	C21MAY14A0266.csv	concordant	26.356	499426.2	329.9101	4.755335	<4.834	2048.923	484928.9	17.19212	0.007352	19.42031
2021-G-080	C21MAY14A0229.csv	Pb loss; use 7-6 ratio	26.356	498378.4	317.0764	3.551683	11.11685	813.6326	483327.3	4.388609	0.070412	4.036018

2021-G-080	C21FEB25A0022.csv	minor common Pb	26.103	499624.3	475.9273	7.120423	<2.907	989.2194	485934.7	1.186561	0.007571	6.41066
2021-G-080	C21MAY14A0267.csv	concordant	26.356	499499.8	330.2807	8.402142	<4.791	1938.186	485522.2	6.909907	0.025412	63.55284
2021-G-080	C21MAY14A0233.csv	Pb loss; use 7-6 ratio	26.356	498359.9	984.0613	194.8598	1080.196	2114.421	476189.4	8.843252	0.206976	2.913997
2021-G-080	C21MAY14A0231.csv	Pb loss; use 7-6 ratio	18.416	499332.8	1747.109	10.61494	52.59377	3914.962	476045.7	5.271629	0.132247	2.022471
2021-G-080	C21FEB25A0006.csv	high U, Pb loss, use 7/6	16.194	498170.6	780.6341	7.685107	8.184904	2009.317	479451.4	14.08137	0.029075	2.667795
2021-G-080	C21MAY14A0263.csv	Pb loss; use 7-6 ratio	26.356	500953.5	2668.694	9.48668	89.4786	2439.899	477856.3	9.757718	26.93482	139.1849
2021-G-080	C21MAY14A0270.csv	Pb loss; use 7-6 ratio	7.845	499649.5	182.0579	11.36874	35.64013	720.8569	487677	2.019154	0.037129	22.41295
2021-G-080	C21FEB25A0009.csv	high U, Pb loss, use 7/6	10.169	499370.3	701.5485	8.085849	<3.716	1701.728	483451.4	2.188308	0.001673	5.083543
2021-G-080	C21MAY14A0240.csv	Pb loss; use 7-6 ratio	26.356	500045.4	84.31437	5.854263	<4.690	575.8581	489581.5	5.936483	<0.002	13.94588
2021-G-080	C21MAY14A0226.csv	high U, Pb loss, common Pb	26.356	499691.2	1190.711	7.215547	16.6548	2784.426	481072.3	3.195143	0.220691	3.553813
2021-G-080	C21FEB25A0024.csv	Pb loss, use 7/6	26.103	499010.6	583.7251	5.587706	<2.904	1126.553	483547.2	1.106598	0.003759	0.73584
2021-G-080	C21FEB25A0029.csv	Comm Pb or Pb loss	26.103	499126	428.4511	5.413003	6.475726	814.5119	484879.8	0.660005	0.031544	0.650267

2021-G-080	C21FEB25A0033.csv	high U, Pb loss, use 7/6	6.739	496659	1243.363	3.980177	10.90425	2788.839	472397.8	4.774835	0.108417	1.667912
2021-G-080	C21FEB25A0031.csv	Comm Pb or Pb loss	26.103	499286	266.9563	6.264501	4.780809	668.2784	486364.5	3.83033	0.010234	6.563847
2021-G-080	C21MAY14A0264.csv	Pb loss; use 7-6 ratio	3.97	498491.6	430.861	10.80857	<8.542	2419.454	481335.8	23.59249	0.025922	14.76781
2021-G-080	C21MAY14A0261.csv	Pb loss; use 7-6 ratio	26.356	499790.2	1154.304	5.151139	<4.897	2603.37	481523	1.504089	0.055278	1.904219
2021-G-080	C21MAY14A0269.csv	older	3.289	500321.8	783.3293	14.8703	<10.896	3052.606	484254.9	2.337375	0.075104	6.017995
2021-G-080	C21MAY14A0249.csv	Pb loss; use 7-6 ratio	13.116	499043.5	296.6374	8.535986	22.13912	2273.539	483757.5	5.497338	0.095125	13.91018
2021-G-080	C21MAY14A0238.csv	Pb loss; use 7-6 ratio	19.138	499000.6	144.7793	4.605864	<5.777	227.5069	486466.3	1.669451	0.187104	4.07183
2021-G-080	C21FEB25A0019.csv	Pb loss likely, use 7/6	26.103	499694.3	888.3772	6.524987	7.607988	1964.415	483087.1	0.91441	0.032659	1.376
2021-G-080	C21MAY14A0255.csv	Pb loss; use 7-6 ratio	26.356	499426.5	582.7644	6.539586	24.49424	1417.454	484459.8	2.781229	0.033436	3.885682
2021-G-080	C21MAY14A0257.csv	Pb loss; use 7-6 ratio	26.356	499675.7	1132.785	13.24275	9.026393	3587.406	480280.4	4.270218	0.035689	17.60088
2021-G-080	C21FEB25A0011.csv	high U, Pb loss, use 7/6	25.074	499302.7	512.8649	4.68141	3.489433	994.1642	484802.9	1.071342	0.013373	1.242001
2021-G-080	C21FEB25A0010.csv	high U, Pb loss, use 7/6	12.751	499193.7	742.592	8.857746	23.82947	1411.572	482916.2	2.090456	0.04349	1.08079

2021-G-080	C21FEB25A0023.csv	high U, Pb loss, use 7/6	26.103	499230.7	645.5004	3.899286	<2.924	1339.222	483690	2.137832	0.017936	2.356002
2021-G-080	C21FEB25A0030.csv	high U, Pb loss, use 7/6	26.103	499072.8	1328.461	5.950984	14.97895	3112.384	478288.7	1.850507	0.019983	1.112813
2021-G-080	C21MAY14A0253.csv	Pb loss; use 7-6 ratio	26.356	499540.1	759.3576	5.106223	6.94768	1557.817	483737.7	1.019356	0.02515	1.159345
2021-G-080	C21FEB25A0005.csv	high U, Pb loss, use 7/6	22.077	499287.8	913.5725	7.339131	8.886451	2575.108	481259	2.938248	0.066055	5.778682
2021-G-080	C21FEB25A0018.csv	Pb mobility, use 7/6	26.103	499560.1	778.6688	4.930304	6.98665	1774.226	483439.7	0.772596	0.00618	1.350606
2021-G-080	C21MAY14A0254.csv	Pb loss; use 7-6 ratio	26.356	499476.1	1834.839	54.27179	530.8897	3985.324	474788.1	2.977902	0.048037	1.129888
2021-G-080	C21MAY14A0251.csv	use 7-6 ratio	26.356	499744.6	195.0815	4.939823	<4.696	790.3529	487945.8	1.679034	0.017579	10.07961
2021-G-080	C21MAY14A0259.csv	Pb loss; use 7-6 ratio	26.356	499150.3	888.3791	4.625944	18.88095	2057.882	481593.2	2.16611	0.026903	1.220081
2021-G-080	C21MAY14A0258.csv	Pb loss; use 7-6 ratio	26.356	499658.2	1144.236	7.418281	7.620868	2523.601	481208.7	0.985813	1.173116	3.329313
2021-G-080	C21MAY14A0262.csv	Pb loss; use 7-6 ratio	26.356	500734.8	510.5231	354.1912	2208.664	2001.009	482029.5	6.172361	0.345028	9.238881
2021-G-080	C21MAY14A0239.csv	Pb loss; use 7-6 ratio	13.06	498791.1	290.1693	7.560078	25.7842	1767.618	484148.9	3.763479	0.045943	22.29584
2021-G-080	C21MAY14A0265.csv	Pb loss; use 7-6 ratio	26.356	498985	399.2789	9.310252	6.614267	1283.529	484245.6	6.417836	0.795208	19.98851

2021-G-080	C21MAY14A0235.csv	Pb loss; use 7-6 ratio	7.445	498745.2	433.0785	6.118127	<6.215	1082.367	483640	3.457429	0.012108	8.520563
2021-G-080	C21MAY14A0250.csv	Pb loss; use 7-6 ratio	26.356	499509.8	76.04414	3.905747	<4.689	650.7936	487922.9	0.800982	0.015011	4.346227
2021-G-080	C21MAY14A0252.csv	Pb loss; use 7-6 ratio	26.356	498726.4	457.746	3.525494	5.916818	957.7886	483427	2.196545	0.007169	5.240421
2021-G-080	*C21FEB25A0021.csv*	*do not use*	*11.967*	*499300*	*611.762*	*6.22202*	*3.90531*	*1299.95*	*484004*	*0.98554*	*0.00126*	*1.05269*
2021-G-080	*C21FEB25A0021.csv*	*do not use*	*12.28*	*499537*	*735.069*	*7.61504*	*4.83807*	*1512.35*	*483845*	*0.8932*	*0.01913*	*1.47408*
2021-G-080	*C21MAY14A0227.csv*	*do not use, inclusions*	*17.482*	*499486*	*2101.48*	*12.9188*	*83.0509*	*5187.73*	*473649*	*2.72275*	*8.32122*	*24.3557*
2021-G-080	*C21MAY14A0237.csv*	*do not use, inclusions*	*26.356*	*499976*	*652.073*	*17.2502*	*215.011*	*1603.79*	*485146*	*3.73685*	*0.38131*	*10.4505*
2021-G-080	*C21MAY14A0256.csv*	*do not use, inclusions*	*26.356*	*504293*	*1698.46*	*247.711*	*13482.3*	*1098.43*	*462954*	*27.6022*	*5.55009*	*11.3766*

Analysis	Source Filename	Comment	141Pr	146Nd	147Sm	153Eu	157Gd	159Tb	163Dy	165Ho	166Er	169Tm	172Yb
			ppm	ppm	ppm	ppm	ppm	ppm	ppm	ppm	ppm	ppm	ppm
ZY-LG-2 (Two-mica leucogranite)													
2021-G-080	C21MAY14A0268.csv	concordant	0.157185	2.027433	13.11545	0.8273	136.9731	61.6916	813.0584	285.866	1278.163	247.7525	2026.364
2021-G-080	C21MAY14A0241.csv	minor common Pb	2.680364	31.40621	75.71698	1.073433	274.845	84.53087	732.3763	168.933	620.2417	116.795	980.5495
2021-G-080	C21FEB25A0034.csv	young, some common Pb	0.102419	1.615757	7.600898	0.473178	58.60667	22.9861	248.3739	75.09779	325.6787	59.31921	491.9981
2021-G-080	C21MAY14A0260.csv	concordant	0.067789	1.497959	6.431428	0.50286	67.11889	29.55831	386.8897	128.4685	539.2608	99.91762	807.1441
2021-G-080	C21FEB25A0007.csv	high U, young concordant	0.034907	0.595498	2.977778	0.156809	31.47107	13.45063	160.0876	49.42069	212.0847	39.74479	334.7341
2021-G-080	C21MAY14A0242.csv	minor common Pb	0.021306	0.301654	2.515347	0.581114	23.24599	8.45257	91.16869	27.98376	122.1337	23.33528	192.6644
2021-G-080	C21MAY14A0234.csv	concordant	0.005507	0.34004	1.778631	0.561814	12.85509	3.446533	27.5711	6.827538	24.3703	3.970074	30.17807
2021-G-080	C21MAY14A0264.csv	younger	0.064195	0.949672	7.175043	0.59295	20.86437	8.857014	102.2053	35.51033	162.1145	30.50788	282.5234
2021-G-080	C21FEB25A0032.csv	comm Pb or Pb loss	0.01191	0.213683	0.646675	0.327648	10.71587	4.542349	49.79229	14.7395	64.42759	11.55621	97.87315
2021-G-080	C21MAY14A0232.csv	High common Pb	0.167182	0.84614	2.779384	0.395011	25.6573	10.6631	129.674	43.30827	192.2464	44.46821	401.3929
2021-G-080	C21MAY14A0228.csv	older	0.011506	0.119802	0.890669	0.260211	6.310491	2.431244	36.74147	12.21348	67.76376	17.90086	190.122
2021-G-080	C21FEB25A0020.csv	Comm Pb or Pb loss	0.017209	0.319214	1.617846	0.435435	11.91893	2.531669	17.02148	4.031142	16.82481	3.201659	29.26086
2021-G-080	C21MAY14A0230.csv	younger	0.042513	0.355506	3.355704	0.138486	32.55784	13.39154	198.4037	81.20394	424.4088	91.08129	821.7296
2021-G-080	C21MAY14A0269.csv	younger	0.041883	0.418037	0.483941	0.061965	7.640851	2.481635	52.90893	22.19817	125.0799	31.70047	341.9403
2021-G-080	C21MAY14A0225.csv	minor common Pb	0.169695	3.564243	9.159457	0.136777	58.3902	17.30346	198.2252	68.72272	310.5991	59.29163	509.1267

2021-G-080	C21FEB25A0008.csv	moderate U, concordant	0.019032	0.293435	2.640666	0.087289	21.48255	13.21272	190.3045	69.07757	335.2405	71.52539	657.7093
2021-G-080	C21MAY14A0236.csv	minor common Pb	0.021632	0.683913	3.718795	0.121778	37.68907	17.05247	247.1929	98.07263	495.2662	102.5374	906.1252
2021-G-080	C21MAY14A0230.csv	older	0.039016	2.015285	6.159933	0.718516	58.07012	22.66564	303.8421	122.6042	607.2946	124.6782	1081.767
2021-G-080	C21FEB25A0033.csv	comm Pb or Pb loss	0.146914	1.161388	3.527877	0.173948	36.21618	17.79644	243.9055	72.35184	335.7015	83.84095	902.4876
2021-G-080	C21FEB25A0033.csv	comm Pb or Pb loss	0.349959	3.197477	8.153023	0.218486	51.37833	23.58379	280.0326	78.72973	349.9263	80.59118	845.8387
2021-G-080	C21FEB25A0033.csv	comm Pb or Pb loss	0.794041	8.599724	13.34918	0.320277	68.60074	28.30928	312.3602	82.09661	356.8523	81.26181	854.8684
2021-G-080	C21MAY14A0266.csv	concordant	0.111098	2.570512	6.355497	0.437345	43.19993	13.55367	182.5233	68.03349	318.9711	62.37791	499.4889
2021-G-080	C21MAY14A0229.csv	Pb loss; use 7-6 ratio	0.035437	0.475242	1.997732	0.102632	12.39257	4.780805	65.47436	25.21483	129.1145	26.54416	252.0316
2021-G-080	C21FEB25A0022.csv	minor common Pb	0.051186	1.287717	3.298891	0.244021	20.52607	6.895768	82.83275	31.07855	150.0338	30.19224	264.4619
2021-G-080	C21MAY14A0267.csv	concordant	0.554932	8.663014	13.94703	1.125215	61.86216	17.40445	189.9664	63.47024	282.0801	53.82781	450.2487
2021-G-080	C21MAY14A0233.csv	Pb loss; use 7-6 ratio	0.153302	1.399688	2.383972	0.05955	24.08274	11.02718	158.1535	64.15156	344.1238	79.35003	761.2363
2021-G-080	C21MAY14A0231.csv	Pb loss; use 7-6 ratio	0.140919	1.632503	6.245101	0.088779	45.23374	20.8808	298.2524	121.4423	625.4858	133.3499	1193.483
2021-G-080	C21FEB25A0006.csv	high U, Pb loss, use 7/6	0.026175	0.543215	1.376485	0.016946	15.37163	8.349945	139.7825	60.06305	344.5097	80.76614	787.1504

2021-G-080	C21MAY14A0263.csv	Pb loss; use 7-6 ratio	10.39724	50.30612	24.67163	1.669406	76.52958	21.57587	229.3137	76.78153	343.4514	66.52746	558.0032
2021-G-080	C21MAY14A0270.csv	Pb loss; use 7-6 ratio	0.130292	2.165022	2.484974	0.586135	16.02583	4.989947	61.69822	22.42572	106.322	22.44976	197.4444
2021-G-080	C21FEB25A0009.csv	high U, Pb loss, use 7/6	0.047691	1.385765	3.710105	0.144085	27.31675	11.1724	150.4775	54.92412	254.0677	49.56401	426.6387
2021-G-080	C21MAY14A0240.csv	Pb loss; use 7-6 ratio	0.094467	2.418967	3.524319	0.390761	17.0937	5.340399	59.24591	19.95762	88.54199	15.24312	127.2767
2021-G-080	C21MAY14A0226.csv	high U, Pb loss, common Pb	0.194526	2.699313	8.655489	0.603469	58.36304	21.21555	263.2314	89.81183	391.9331	72.7792	605.0308
2021-G-080	C21FEB25A0024.csv	Pb loss, use 7/6	0.043602	0.573276	3.279562	0.087209	28.68045	10.79195	117.9429	35.2035	151.482	28.0873	230.238
2021-G-080	C21FEB25A0029.csv	Comm Pb or Pb loss	0.036322	0.314724	1.98056	0.056544	18.459	7.08448	79.83736	23.56947	93.93828	16.93854	137.6834
2021-G-080	C21FEB25A0033.csv	high U, Pb loss, use 7/6	0.312717	4.844693	7.571283	0.207764	51.29074	24.15251	278.7429	73.9416	324.612	73.09649	753.2613
2021-G-080	C21FEB25A0031.csv	Comm Pb or Pb loss	0.051677	0.659101	2.140441	0.143062	12.82451	4.314741	54.49131	20.54766	107.1645	23.80151	226.8858
2021-G-080	C21MAY14A0264.csv	Pb loss; use 7-6 ratio	0.166153	1.599003	4.41923	0.644745	42.17498	14.52821	189.4938	78.98201	410.2893	90.20669	851.613
2021-G-080	C21MAY14A0261.csv	Pb loss; use 7-6 ratio	0.095999	2.579905	6.902679	0.369324	50.13772	18.72423	235.2039	82.82992	381.7333	75.34805	625.9542
2021-G-080	C21MAY14A0269.csv	older	0.722752	9.72733	13.6913	1.024174	90.7198	23.25581	272.8077	105.4035	477.4056	89.83299	685.1423

2021-G-080	C21MAY14A0249.csv	Pb loss; use 7-6 ratio	0.11769	2.5471	7.707854	0.42684	55.38067	18.22678	216.2735	77.2631	342.354	61.96872	493.4813
2021-G-080	C21MAY14A0238.csv	Pb loss; use 7-6 ratio	0.047266	0.750942	0.812547	0.288357	5.230257	1.863862	20.38546	7.366922	36.13092	7.715422	74.14709
2021-G-080	C21FEB25A0019.csv	Pb loss likely, use 7/6	0.05047	0.91115	3.45334	0.14445	31.55227	12.48277	164.802	59.97731	295.4066	58.35524	516.1173
2021-G-080	C21MAY14A0255.csv	Pb loss; use 7-6 ratio	0.086069	1.764289	5.15116	0.261893	34.87373	12.03077	143.2852	44.01672	182.4437	33.3758	272.7811
2021-G-080	C21MAY14A0257.csv	Pb loss; use 7-6 ratio	0.240676	4.41718	10.51656	2.140307	77.66067	24.35105	307.245	113.5856	532.9834	105.1892	930.5419
2021-G-080	C21FEB25A0011.csv	high U, Pb loss, use 7/6	0.036836	0.8507	2.739624	0.110777	21.55125	8.205976	98.82832	30.91123	131.6027	24.21303	205.1836
2021-G-080	C21FEB25A0010.csv	high U, Pb loss, use 7/6	0.055622	0.958975	4.034259	0.227844	31.07288	12.14525	142.7282	39.96863	168.5704	30.38394	253.8526
2021-G-080	C21FEB25A0023.csv	high U, Pb loss, use 7/6	0.041824	0.986356	2.96742	0.104721	23.58938	9.923955	125.1952	40.89093	176.9252	33.54849	279.6245
2021-G-080	C21FEB25A0030.csv	high U, Pb loss, use 7/6	0.044574	1.026521	5.487689	0.164228	57.96967	26.03918	302.3638	83.21664	313.4001	53.17516	405.8311
2021-G-080	C21MAY14A0253.csv	Pb loss; use 7-6 ratio	0.045989	0.714179	2.590357	0.067953	25.77791	10.57748	138.2266	47.3449	209.7489	39.21437	335.1325
2021-G-080	C21FEB25A0005.csv	high U, Pb loss, use 7/6	0.145622	2.290622	6.182122	0.228028	44.44466	18.18569	232.0769	78.14676	351.7347	65.44126	526.5853

2021-G-080	C21FEB25A0018.csv	Pb mobility, use 7/6	0.05128	1.171914	3.353308	0.156626	31.78204	12.68534	161.4161	54.09327	241.6748	44.23424	364.8015
2021-G-080	C21MAY14A0254.csv	Pb loss; use 7-6 ratio	0.07411	1.291379	5.339521	0.130553	50.47871	23.7808	327.5115	122.4131	593.6313	119.5222	1033.584
2021-G-080	C21MAY14A0251.csv	use 7-6 ratio	0.067754	1.099976	2.775876	0.367869	17.56359	5.483942	66.33015	25.62215	121.3365	24.62841	218.6634
2021-G-080	C21MAY14A0259.csv	Pb loss; use 7-6 ratio	0.053531	0.888668	4.342264	0.092016	37.40492	15.39963	187.9939	60.37205	252.4949	46.49935	375.902
2021-G-080	C21MAY14A0258.csv	Pb loss; use 7-6 ratio	0.383922	2.334103	5.10125	0.232105	47.11471	18.53785	225.5023	79.21176	361.8843	67.41538	577.8232
2021-G-080	C21MAY14A0262.csv	Pb loss; use 7-6 ratio	0.309401	4.465725	7.141987	0.598414	48.51834	15.70363	186.9166	66.13069	312.0172	59.5854	499.0642
2021-G-080	C21MAY14A0239.csv	Pb loss; use 7-6 ratio	0.221314	3.747218	10.15829	2.075853	58.31896	16.47983	172.9549	58.35981	251.7814	46.77865	391.1001
2021-G-080	C21MAY14A0265.csv	Pb loss; use 7-6 ratio	0.356527	1.85245	3.04382	0.481958	21.50522	7.695543	99.50879	40.05733	202.8959	43.01481	393.8
2021-G-080	C21MAY14A0235.csv	Pb loss; use 7-6 ratio	0.038272	0.486432	2.556471	0.330352	19.97177	7.499761	94.81167	33.54113	160.8836	32.85593	298.9154
2021-G-080	C21MAY14A0250.csv	Pb loss; use 7-6 ratio	0.091334	1.599684	2.980366	0.940526	16.68938	4.546457	56.20021	20.39488	100.9553	21.62499	210.3615
2021-G-080	C21MAY14A0252.csv	Pb loss; use 7-6 ratio	0.011437	0.420934	1.182819	0.175203	11.50982	4.624284	65.17767	29.65025	161.5631	39.24823	394.9171
2021-G-080	*C21FEB25A0021.csv*	*do not use*	*0.04475*	*0.73012*	*2.50878*	*0.16007*	*22.9102*	*9.18816*	*113.516*	*39.8215*	*190.281*	*39.4656*	*364.973*

2021-G-080	*C21FEB25A0021.csv*	*do not use*	*0.04792*	*1.0652*	*3.34426*	*0.10534*	*29.0082*	*11.6144*	*135.569*	*47.2307*	*217.569*	*39.537*	*337.716*
2021-G-080	*C21MAY14A0227.csv*	*do not use, inclusions*	*2.16102*	*9.15433*	*14.1127*	*0.49075*	*100.545*	*38.9306*	*461.621*	*155.061*	*692.637*	*135.509*	*1136.98*
2021-G-080	*C21MAY14A0237.csv*	*do not use, inclusions*	*0.25437*	*3.24488*	*4.46329*	*0.62398*	*31.3931*	*11.0725*	*138.797*	*50.0131*	*251.291*	*50.0502*	*443.804*
2021-G-080	*C21MAY14A0256.csv*	*do not use, inclusions*	*1.1413*	*5.64774*	*2.01481*	*0.79368*	*10.8712*	*5.04344*	*78.4742*	*30.401*	*170.475*	*42.1432*	*412.001*

Analysis	Source Filename	Comment	175Lu	178Hf	181Ta	204Pb	206Pb	207Pb	208Pb	232Th	235U	238U
			ppm	ppm	ppm	ppm	ppm	ppm	ppm	ppm	ppm	ppm
ZY-LG-2 (Two-mica leucogranite)												
2021-G-080	C21MAY14A0268.csv	concordant	356.5529	13538.06	6.173539	<0.045	16.77955	0.787297	0.2795	375.2362	64.30072	8267.729
2021-G-080	C21MAY14A0241.csv	minor common Pb	171.9402	14498.38	4.420277	<0.045	7.572651	0.376084	0.124678	115.3926	26.1428	3336.802
2021-G-080	C21FEB25A0034.csv	young, some common Pb	92.64512	12508.63	2.505476	<0.025	6.022151	0.294425	0.101945	112.2958	19.60943	2838.072
2021-G-080	C21MAY14A0260.csv	concordant	131.6916	13576.27	6.896853	<0.048	17.60482	0.833245	0.209843	329.1253	62.43499	7996.665
2021-G-080	C21FEB25A0007.csv	high U, young concordant	62.11347	13886.62	2.178695	<0.018	4.05406	0.1856	0.045606	66.04066	13.05308	1864.614
2021-G-080	C21MAY14A0242.csv	minor common Pb	36.99224	12914.59	2.198956	<0.045	3.523131	0.169239	0.075941	71.72973	10.9045	1390.073
2021-G-080	C21MAY14A0234.csv	concordant	5.25419	12381.27	2.030206	<0.046	2.818548	0.127512	0.028845	21.00005	7.616815	982.8516
2021-G-080	C21MAY14A0264.csv	younger	50.13759	12604.99	1.861561	<0.166	5.237926	0.36223	0.131747	67.80423	9.721124	1269.043
2021-G-080	C21FEB25A0032.csv	comm Pb or Pb loss	16.07292	13853.96	0.413904	<0.022	4.953118	0.222787	0.027222	23.64132	8.91734	1288.394
2021-G-080	C21MAY14A0232.csv	High common Pb	70.2136	13137.63	4.571328	<0.091	24.76523	1.987225	3.217432	130.0916	29.49417	3847.23
2021-G-080	C21MAY14A0228.csv	older	39.70371	13556.95	3.33365	<0.055	51.97716	2.835873	0.045005	19.8906	19.97967	2558.181
2021-G-080	C21FEB25A0020.csv	Comm Pb or Pb loss	6.060647	14131.84	2.378888	<0.018	31.20115	4.694607	1.51878	32.12508	8.885967	1284.567
2021-G-080	C21MAY14A0230.csv	younger	162.8748	13697.72	1.599013	<0.066	24.66199	1.404085	1.395016	72.81806	3.989907	510.0937
2021-G-080	C21MAY14A0269.csv	younger	76.11733	12775.78	4.481254	<0.124	80.79019	4.599838	0.840023	19.50718	10.34713	1345.829
2021-G-080	C21MAY14A0225.csv	minor common Pb	99.31757	11138.37	0.61438	<0.061	18.96704	1.140045	2.736581	132.1849	2.433348	312.6422
2021-G-080	C21FEB25A0008.csv	moderate U, concordant	132.319	14433.62	1.158554	<0.027	62.62716	3.544645	0.978225	45.13093	6.548536	963.2515
2021-G-080	C21MAY14A0236.csv	minor common Pb	173.306	12705.9	1.029373	<0.045	42.95147	2.517071	1.387135	70.96566	4.832395	612.1883

2021-G-080	C21MAY14A0230.csv	older	213.4723	12398.64	1.381784	<0.087	48.56152	2.687093	6.068631	254.9709	4.470803	594.5724
2021-G-080	C21FEB25A0033.csv	comm Pb or Pb loss	189.3896	19761.71	11.98761	0.046037	458.0318	37.62528	1.529585	49.82516	38.97919	5630.065
2021-G-080	C21FEB25A0033.csv	comm Pb or Pb loss	163.0754	19754.29	14.41389	<0.030	519.4545	47.48992	3.251624	83.2571	39.36728	5683.161
2021-G-080	C21FEB25A0033.csv	comm Pb or Pb loss	171.8182	19328.05	13.94587	<0.036	565.6279	53.60642	3.11213	88.49058	38.78854	5600.822
2021-G-080	C21MAY14A0266.csv	concordant	94.36852	11323.44	4.67469	<0.046	45.20812	2.982789	6.749265	182.2217	2.858695	364.6212
2021-G-080	C21MAY14A0229.csv	Pb loss; use 7-6 ratio	50.92539	15155.34	4.86827	<0.045	62.04572	4.065472	4.342719	149.4614	9.247904	1181.978
2021-G-080	C21FEB25A0022.csv	minor common Pb	52.08302	11899.06	0.802529	<0.018	31.82378	2.125494	3.844522	107.5361	1.815551	271.2051
2021-G-080	C21MAY14A0267.csv	concordant	85.70243	9686.609	3.199334	<0.046	94.61462	6.334005	29.73978	843.1276	5.676779	732.4888
2021-G-080	C21MAY14A0233.csv	Pb loss; use 7-6 ratio	155.164	15318.67	8.322906	<0.046	413.2575	27.45749	7.082516	247.1448	26.69752	3415.236
2021-G-080	C21MAY14A0231.csv	Pb loss; use 7-6 ratio	224.8996	13140.21	5.939847	<0.047	270.6535	18.00355	10.14335	281.3018	19.24022	2472.194
2021-G-080	C21FEB25A0006.csv	high U, Pb loss, use 7/6	160.3823	14916.94	17.22515	<0.020	294.3544	19.8017	4.251098	108.5398	18.05327	2577.901
2021-G-080	C21MAY14A0263.csv	Pb loss; use 7-6 ratio	106.5812	11276.01	5.075642	<0.045	162.8215	11.18933	37.66646	1058.943	12.97882	1676.277
2021-G-080	C21MAY14A0270.csv	Pb loss; use 7-6 ratio	37.06867	10769.73	0.74072	<0.067	28.20761	2.014761	5.816726	165.1961	1.995639	251.6293
2021-G-080	C21FEB25A0009.csv	high U, Pb loss, use 7/6	78.08794	12471.33	1.817262	<0.023	118.3912	8.502754	7.814166	193.0928	6.042054	895.1425
2021-G-080	C21MAY14A0240.csv	Pb loss; use 7-6 ratio	22.28342	9075.557	3.243698	<0.047	23.34792	1.744949	3.09619	66.9511	1.182419	150.6551
2021-G-080	C21MAY14A0226.csv	high U, Pb loss, common Pb	107.8026	11293.47	2.549669	<0.045	85.03886	6.646888	7.229633	240.32	15.44238	1957.517
2021-G-080	C21FEB25A0024.csv	Pb loss, use 7/6	43.66643	13949.48	1.015716	<0.018	92.45481	7.61288	3.458025	102.5496	6.16736	911.7351

2021-G-080	C21FEB25A0029.csv	Comm Pb or Pb loss	24.53797	13687.58	0.694146	<0.017	100.818	11.48899	2.297212	38.00523	3.322805	489.3431
2021-G-080	C21FEB25A0033.csv	high U, Pb loss, use 7/6	143.3931	19303.95	12.53193	<0.026	399.4805	36.54621	3.144102	86.9996	36.53042	5274.934
2021-G-080	C21FEB25A0031.csv	Comm Pb or Pb loss	49.00651	12069.35	1.915081	<0.017	134.6126	16.89218	7.690009	89.33473	3.873313	567.0469
2021-G-080	C21MAY14A0264.csv	Pb loss; use 7-6 ratio	179.0884	13861.87	35.74292	<0.080	203.7905	19.62098	14.28988	246.0053	8.09967	1020.491
2021-G-080	C21MAY14A0261.csv	Pb loss; use 7-6 ratio	118.8239	12059.23	2.158195	<0.047	116.8362	12.34166	7.030982	103.3833	8.108296	1012.654
2021-G-080	C21MAY14A0269.csv	older	135.1684	9263.824	0.788146	<0.103	41.68502	4.925172	16.2113	189.5653	1.147846	140.9833
2021-G-080	C21MAY14A0249.csv	Pb loss; use 7-6 ratio	92.25064	12065.6	2.745954	<0.057	103.1069	10.99871	12.13459	194.6532	6.2695	815.1911
2021-G-080	C21MAY14A0238.csv	Pb loss; use 7-6 ratio	17.80607	13722.12	0.590625	<0.057	16.88784	1.816038	1.595479	28.87133	1.561009	204.2714
2021-G-080	C21FEB25A0019.csv	Pb loss likely, use 7/6	103.5805	12379.21	0.901524	<0.017	137.8514	14.95811	5.277105	62.6176	3.826182	497.8544
2021-G-080	C21MAY14A0255.csv	Pb loss; use 7-6 ratio	50.32913	12077.88	1.958418	<0.047	200.9897	21.88686	11.95785	163.0652	6.296324	811.3096
2021-G-080	C21MAY14A0257.csv	Pb loss; use 7-6 ratio	180.6861	11112.99	1.996955	<0.046	255.4595	27.88963	42.85833	560.536	7.667757	980.5078
2021-G-080	C21FEB25A0011.csv	high U, Pb loss, use 7/6	40.06378	13195.09	0.944159	<0.018	113.0577	12.57185	3.794559	44.58884	3.022489	439.4751
2021-G-080	C21FEB25A0010.csv	high U, Pb loss, use 7/6	48.97786	13921.97	2.563401	<0.027	171.303	19.07966	4.846819	66.05424	5.417725	775.8123
2021-G-080	C21FEB25A0023.csv	high U, Pb loss, use 7/6	50.72467	13215.58	1.814022	<0.018	92.52743	10.31904	9.529232	96.60188	6.307566	908.984
2021-G-080	C21FEB25A0030.csv	high U, Pb loss, use 7/6	71.39304	13801.25	1.862375	<0.017	600.2731	67.59593	13.64526	167.7373	15.15151	2186.114
2021-G-080	C21MAY14A0253.csv	Pb loss; use 7-6 ratio	60.53716	12667.96	0.824661	<0.046	172.8629	19.39038	6.607765	73.20107	4.480999	575.3938
2021-G-080	C21FEB25A0005.csv	high U, Pb loss, use 7/6	96.08814	12887.02	2.01193	<0.019	294.9304	33.27775	12.2688	145.6486	7.907692	1134.935

2021-G-080	C21FEB25A0018.csv	Pb mobility, use 7/6	67.08067	12717.24	0.553268	<0.017	147.6107	16.75496	6.535019	73.43523	3.318385	485.3045
2021-G-080	C21MAY14A0254.csv	Pb loss; use 7-6 ratio	189.256	13460.12	2.825917	<0.046	715.2724	80.89633	12.84727	154.1058	18.80088	2414.393
2021-G-080	C21MAY14A0251.csv	use 7-6 ratio	43.3065	10241.3	0.725956	<0.046	85.25599	9.642925	12.75401	151.9315	2.17893	276.4094
2021-G-080	C21MAY14A0259.csv	Pb loss; use 7-6 ratio	67.23228	13291.33	2.107221	<0.049	334.3093	37.78963	8.52887	107.7651	11.19664	1441.581
2021-G-080	C21MAY14A0258.csv	Pb loss; use 7-6 ratio	107.406	12737.73	0.836838	<0.046	209.5202	23.67518	8.029085	107.3103	6.589624	858.0464
2021-G-080	C21MAY14A0262.csv	Pb loss; use 7-6 ratio	95.17303	10281.16	1.703208	<0.049	78.36438	8.882508	14.14056	172.9083	2.251829	290.5289
2021-G-080	C21MAY14A0239.csv	Pb loss; use 7-6 ratio	71.01218	10120.87	1.575387	<0.051	525.9912	59.43887	95.90498	1273.881	13.96022	1768.203
2021-G-080	C21MAY14A0265.csv	Pb loss; use 7-6 ratio	80.37224	12674.03	2.734528	<0.046	220.0975	26.93034	20.18181	264.1519	7.239371	933.5096
2021-G-080	C21MAY14A0235.csv	Pb loss; use 7-6 ratio	58.25411	13798.3	2.388485	<0.062	79.0911	10.53785	6.786004	149.3959	10.02419	1314.635
2021-G-080	C21MAY14A0250.csv	Pb loss; use 7-6 ratio	46.30502	11020.45	0.409979	<0.046	69.14983	9.25041	5.271361	53.16467	1.501563	189.4958
2021-G-080	C21MAY14A0252.csv	Pb loss; use 7-6 ratio	87.68145	14567.47	1.809915	<0.046	258.0705	41.61336	12.20278	116.0366	4.803561	616.0221
2021-G-080	*C21FEB25A0021.csv*	*do not use*	*71.1273*	*13132.3*	*1.08502*	*<0.022*	*132.684*	*13.6657*	*3.69471*	*49.4352*	*4.02361*	*580.412*
2021-G-080	*C21FEB25A0021.csv*	*do not use*	*66.3556*	*12829.7*	*0.6868*	*<0.026*	*121.238*	*13.6283*	*5.03093*	*64.6365*	*2.93088*	*428.252*
2021-G-080	*C21MAY14A0227.csv*	*do not use, inclusions*	*218.287*	*12136.9*	*4.0093*	*<0.051*	*68.4635*	*4.66457*	*2.44538*	*266.43*	*30.9292*	*3965.1*
2021-G-080	*C21MAY14A0237.csv*	*do not use, inclusions*	*86.8323*	*10090.4*	*2.22147*	*<0.048*	*20.5805*	*1.40431*	*5.71709*	*209.551*	*7.46478*	*965.745*
2021-G-080	*C21MAY14A0256.csv*	*do not use, inclusions*	*87.4733*	*12787.8*	*5.53092*	*0.18881*	*33.1563*	*5.69735*	*11.554*	*55.5978*	*18.7661*	*2417.56*

Analysis	Source Filename	Comment	CommPb at 206Pb/238U Age		206Pb/238U Age (Ma)	206Pb/238U Age (Ma)	206Pb/238U Age (Ma)
					Age	2s%	2s_sys%
ZY-LG-2 (Two-mica leucogranite)							
2021-G-080	C21MAY14A0268.csv	concordant	0.836510262		13.93757645	2.22280217	2.440061165
2021-G-080	C21MAY14A0241.csv	minor common Pb	0.836578658		15.00572871	2.343602088	2.550592039
2021-G-080	C21FEB25A0034.csv	young, some common Pb	0.836602277		15.37450651	2.361382621	2.361382621
2021-G-080	C21MAY14A0260.csv	concordant	0.836606873		15.44626441	2.102437782	2.330942648
2021-G-080	C21FEB25A0007.csv	high U, young concordant	0.836610324		15.50014543	1.934418865	1.934418865
2021-G-080	C21MAY14A0242.csv	minor common Pb	0.836692247		16.77897441	2.782932663	2.959351822
2021-G-080	C21MAY14A0234.csv	concordant	0.836828998		18.91268728	2.886098985	3.056569377
2021-G-080	C21MAY14A0264.csv	younger	0.837257624		25.59258667	8.64784273	8.706218059
2021-G-080	C21FEB25A0032.csv	comm Pb or Pb loss	0.83746138		28.76381981	2.529062414	2.529062414
2021-G-080	C21MAY14A0232.csv	High common Pb	0.838400444		43.34453266	5.617533789	5.706990001
2021-G-080	C21MAY14A0228.csv	older	0.845065544		145.2257063	2.610096722	2.797437023

2021-G-080	C21FEB25A0020.csv	Comm Pb or Pb loss	0.846771198		170.8568344	2.375116607	2.375116607
2021-G-080	C21MAY14A0230.csv	younger	0.858857447		347.609576	4.133004249	4.253795143
2021-G-080	C21MAY14A0269.csv	younger	0.859084216		350.8474117	6.975333484	7.047575911
2021-G-080	C21MAY14A0225.csv	minor common Pb	0.862025266		392.5887926	3.033891166	3.196489419
2021-G-080	C21FEB25A0008.csv	moderate U, concordant	0.86526837		438.0854584	2.812043163	2.812043163
2021-G-080	C21MAY14A0236.csv	minor common Pb	0.86596772		447.824704	2.002762465	2.241451871
2021-G-080	C21MAY14A0230.csv	older	0.868387149		481.3249659	2.379307229	2.583437998
2021-G-080	C21FEB25A0033.csv	comm Pb or Pb loss	0.871658129		526.1479252	2.758931218	2.758931218
2021-G-080	C21FEB25A0033.csv	comm Pb or Pb loss	0.878616334		619.7664696	2.335912901	2.335912901
2021-G-080	C21FEB25A0033.csv	comm Pb or Pb loss	0.882311084		668.5543919	1.994293643	1.994293643
2021-G-080	C21MAY14A0266.csv	concordant	0.89046233		774.0344494	1.988375173	2.228606028
2021-G-080	C21MAY14A0229.csv	Pb loss; use 7-6 ratio	0.858215979		338.4354491	5.388937157	5.482124832
2021-G-080	C21FEB25A0022.csv	minor common Pb	0.891396384		785.9383682	1.494033351	1.494033351
2021-G-080	C21MAY14A0267.csv	concordant	0.893074339		807.2309326	2.130052131	2.355880108
2021-G-080	C21MAY14A0233.csv	Pb loss; use 7-6 ratio	0.888794759		752.6903202	2.007373403	2.245572751
2021-G-080	C21MAY14A0231.csv	Pb loss; use 7-6 ratio	0.885625359		711.7934137	2.235070076	2.45124198
2021-G-080	C21FEB25A0006.csv	high U, Pb loss, use 7/6	0.891592396		788.431756	1.605378325	1.605378325
2021-G-080	C21MAY14A0263.csv	Pb loss; use 7-6 ratio	0.878178658		613.9454269	2.645120974	2.830143807
2021-G-080	C21MAY14A0270.csv	Pb loss; use 7-6 ratio	0.890373848		772.9048905	2.495241389	2.690590751
2021-G-080	C21FEB25A0009.csv	high U, Pb loss, use 7/6	0.902007906		918.6651467	1.770878092	1.770878092
2021-G-080	C21MAY14A0240.csv	Pb loss; use 7-6 ratio	0.904809078		952.9601899	2.64636827	2.831309594
2021-G-080	C21MAY14A0226.csv	high U, Pb loss, common Pb	0.854197823		280.4517328	3.372455078	3.519446299
2021-G-080	C21FEB25A0024.csv	Pb loss, use 7/6	0.883409867		682.9437525	3.474783138	3.474783138
2021-G-080	C21FEB25A0029.csv	Comm Pb or Pb loss	0.936464516		1321.372581	1.531380409	1.531380409
2021-G-080	C21FEB25A0033.csv	high U, Pb loss, use 7/6	0.873404334		549.8605128	1.897265868	1.897265868
2021-G-080	C21FEB25A0031.csv	Comm Pb or Pb loss	0.952796191		1499.421297	1.552740284	1.552740284
2021-G-080	C21MAY14A0264.csv	Pb loss; use 7-6 ratio	0.93888654		1348.247176	5.833619759	5.919811525
2021-G-080	C21MAY14A0261.csv	Pb loss; use 7-6 ratio	0.88662101		724.6880412	3.466648827	3.609806517
2021-G-080	C21MAY14A0269.csv	older	0.976798056		1748.974086	3.397051905	3.543022812
2021-G-080	C21MAY14A0249.csv	Pb loss; use 7-6 ratio	0.895665208		839.8791904	3.526595107	3.667413537
2021-G-080	C21MAY14A0238.csv	Pb loss; use 7-6 ratio	0.870182946		505.9990579	2.76053613	2.938300313
2021-G-080	C21FEB25A0019.csv	Pb loss likely, use 7/6	0.97454376		1726.081723	1.574784958	1.574784958
2021-G-080	C21MAY14A0255.csv	Pb loss; use 7-6 ratio	0.949024535		1458.944221	2.04142563	2.27606406

2021-G-080	C21MAY14A0257.csv	Pb loss; use 7-6 ratio	0.955720158		1530.55013	2.465745493	2.663259251
2021-G-080	C21FEB25A0011.csv	high U, Pb loss, use 7/6	0.962857329		1605.649382	1.733847852	1.733847852
2021-G-080	C21FEB25A0010.csv	high U, Pb loss, use 7/6	0.940176234		1362.488437	1.987310422	1.987310422
2021-G-080	C21FEB25A0023.csv	high U, Pb loss, use 7/6	0.883624547		685.7488176	4.299733286	4.299733286
2021-G-080	C21FEB25A0030.csv	high U, Pb loss, use 7/6	0.972725827		1707.543345	1.568297182	1.568297182
2021-G-080	C21MAY14A0253.csv	Pb loss; use 7-6 ratio	0.97537256		1734.510404	1.975324253	2.216969758
2021-G-080	C21FEB25A0005.csv	high U, Pb loss, use 7/6	0.963580164		1613.187544	2.083176734	2.083176734
2021-G-080	C21FEB25A0018.csv	Pb mobility, use 7/6	0.988658844		1867.764345	1.496225541	1.496225541
2021-G-080	C21MAY14A0254.csv	Pb loss; use 7-6 ratio	0.973185205		1712.234451	1.998900974	2.238002257
2021-G-080	C21MAY14A0251.csv	use 7-6 ratio	0.979103253		1772.27594	1.874667394	2.127775091
2021-G-080	C21MAY14A0259.csv	Pb loss; use 7-6 ratio	0.941220246		1373.982081	4.766820355	4.871922136
2021-G-080	C21MAY14A0258.csv	Pb loss; use 7-6 ratio	0.947446932		1441.902757	7.075092352	7.146326385
2021-G-080	C21MAY14A0262.csv	Pb loss; use 7-6 ratio	0.960234999		1578.199018	2.842220856	3.015173029
2021-G-080	C21MAY14A0239.csv	Pb loss; use 7-6 ratio	0.984098663		1822.410834	1.932562226	2.178955199
2021-G-080	C21MAY14A0265.csv	Pb loss; use 7-6 ratio	0.943518765		1399.178718	2.659620347	2.843699948
2021-G-080	C21MAY14A0235.csv	Pb loss; use 7-6 ratio	0.864352023		425.2859897	4.572033908	4.681510766
2021-G-080	C21MAY14A0250.csv	Pb loss; use 7-6 ratio	1.007433134		2050.751881	1.90937565	2.158417099
2021-G-080	C21MAY14A0252.csv	Pb loss; use 7-6 ratio	1.034459634		2305.782881	1.898982785	2.149228843
2021-G-080	*C21FEB25A0021.csv*	*do not use*	0.953342349		1505.252182	2.757041219	2.757041219
2021-G-080	*C21FEB25A0021.csv*	*do not use*	0.971972943		1699.845276	1.54539264	1.54539264
2021-G-080	*C21MAY14A0227.csv*	*do not use, inclusions*	0.84331832		118.7860479	18.44121265	18.46865921
2021-G-080	*C21MAY14A0237.csv*	*do not use, inclusions*	0.844798302		141.1938119	14.23369143	14.26923336
2021-G-080	*C21MAY14A0256.csv*	*do not use, inclusions*	0.841438451		90.12828608	8.747793071	8.805505812

Analysis	Source Filename	Comment	207Pb/206Pb Age (Ma)	207Pb/206Pb Age (Ma)	207Pb/206Pb Age (Ma)	207Pb/235U(calc) Age (Ma)	207Pb/235U(calc) Age (Ma)	207Pb/235U(calc) Age (Ma)
			Age	2s%	2s_sys%	Age	2s%	2_sys%
ZY-LG-2 (Two-mica leucogranite)								
2021-G-080	C21MAY14A0268.csv	concordant	34.20499	347.9223	347.9227	13.14219	6.318309	6.398681847
2021-G-080	C21MAY14A0241.csv	minor common Pb	171.2072	86.61422	86.61583	15.05059	7.285917	7.355724474
2021-G-080	C21FEB25A0034.csv	young, some common Pb	123.0121	165.3336	165.3336	14.95023	9.160619	9.160619056
2021-G-080	C21MAY14A0260.csv	concordant	54.76784	223.8787	223.8793	14.80678	6.380631	6.46022797
2021-G-080	C21FEB25A0007.csv	high U, young concordant	7.28E-08	2.12E+11	2.12E+11	13.98601	7.171848	7.171847672
2021-G-080	C21MAY14A0242.csv	minor common Pb	91.85401	245.3526	245.3532	17.10136	10.28578	10.33534715
2021-G-080	C21MAY14A0234.csv	concordant	7.28E-08	3.64E+11	3.64E+11	18.17621	11.35269	11.39761344
2021-G-080	C21MAY14A0264.csv	younger	897.2769	82.50916	82.51086	37.55411	40.3381	40.35076334
2021-G-080	C21FEB25A0032.csv	comm Pb or Pb loss	7.28E-08	3.15E+11	3.15E+11	25.37017	10.12568	10.12568085
2021-G-080	C21MAY14A0232.csv	High common Pb	1200.416	16.37482	16.38337	67.73521	11.66243	11.70616595
2021-G-080	C21MAY14A0228.csv	older	387.3653	22.461	22.46723	150.1867	5.481873	5.574318525
2021-G-080	C21FEB25A0020.csv	Comm Pb or Pb loss	2338.435	0.995359	0.995359	419.3205	4.215079	4.215079347
2021-G-080	C21MAY14A0230.csv	younger	478.5937	27.40723	27.41234	363.6896	7.000058	7.072687498
2021-G-080	C21MAY14A0269.csv	younger	466.1394	25.60901	25.61448	354.2522	9.363574	9.417994472

2021-G-080	C21MAY14A0225.csv	minor common Pb	602.0583	19.47001	19.4772	420.6722	7.230059	7.300400578
2021-G-080	C21FEB25A0008.csv	moderate U, concordant	459.1072	11.37867	11.37867	436.0515	4.802796	4.802796137
2021-G-080	C21MAY14A0236.csv	minor common Pb	545.4423	10.74161	10.75464	459.7351	4.839308	4.943783309
2021-G-080	C21MAY14A0230.csv	older	416.5502	23.86871	23.87457	461.3743	6.284087	6.364892075
2021-G-080	C21FEB25A0033.csv	comm Pb or Pb loss	1232.971	3.111866	3.111866	646.1609	5.915391	5.915390724
2021-G-080	C21FEB25A0033.csv	comm Pb or Pb loss	1438.863	1.952313	1.952313	785.6284	4.510504	4.510503919
2021-G-080	C21FEB25A0033.csv	comm Pb or Pb loss	1504.611	1.796719	1.796719	848.5331	3.813964	3.813964303
2021-G-080	C21MAY14A0266.csv	concordant	795.896	6.149086	6.17181	771.9679	4.586341	4.696447969
2021-G-080	C21MAY14A0229.csv	Pb loss; use 7-6 ratio	784.8649	5.69469	5.71922	397.9135	6.667855	6.744062717
2021-G-080	C21FEB25A0022.csv	minor common Pb	814.4611	4.916499	4.916499	786.5123	4.012349	4.012349346
2021-G-080	C21MAY14A0267.csv	concordant	824.3698	4.126718	4.160502	803.7391	4.424566	4.538598898
2021-G-080	C21MAY14A0233.csv	Pb loss; use 7-6 ratio	813.9977	2.720164	2.771149	738.3627	4.087042	4.210226794
2021-G-080	C21MAY14A0231.csv	Pb loss; use 7-6 ratio	816.5872	3.237988	3.280936	715.6806	4.221354	4.34072838
2021-G-080	C21FEB25A0006.csv	high U, Pb loss, use 7/6	829.7085	2.223473	2.223473	752.4822	3.728998	3.728998461
2021-G-080	C21MAY14A0263.csv	Pb loss; use 7-6 ratio	882.006	2.93483	2.982147	667.3609	4.556868	4.667670051
2021-G-080	C21MAY14A0270.csv	Pb loss; use 7-6 ratio	960.5552	10.41532	10.42875	817.204	6.165307	6.247648067
2021-G-080	C21FEB25A0009.csv	high U, Pb loss, use 7/6	965.0512	3.176724	3.176724	923.764	3.993798	3.993798188

2021-G-080	C21MAY14A0240.csv	Pb loss; use 7-6 ratio	1054.468	5.8704	5.894198	976.3383	5.400303	5.494121637
2021-G-080	C21MAY14A0226.csv	high U, Pb loss, common Pb	1144.792	2.751047	2.80147	383.7169	5.172111	5.269992949
2021-G-080	C21FEB25A0024.csv	Pb loss, use 7/6	1236.903	1.705853	1.705853	808.2033	4.944165	4.944165306
2021-G-080	C21FEB25A0029.csv	Comm Pb or Pb loss	1848.197	0.968518	0.968518	1528.108	3.713061	3.71306077
2021-G-080	C21FEB25A0033.csv	high U, Pb loss, use 7/6	1446.046	1.826749	1.826749	717.1992	3.984599	3.984598696
2021-G-080	C21FEB25A0031.csv	Comm Pb or Pb loss	2021.169	0.805197	0.805197	1720.456	3.709589	3.709589047
2021-G-080	C21MAY14A0264.csv	Pb loss; use 7-6 ratio	1546.516	3.496479	3.536289	1419.427	8.253849	8.315534356
2021-G-080	C21MAY14A0261.csv	Pb loss; use 7-6 ratio	1718.481	1.515267	1.604995	1009.455	5.090749	5.190165375
2021-G-080	C21MAY14A0269.csv	older	1921.731	5.31931	5.345562	1826.32	6.883822	6.957665306
2021-G-080	C21MAY14A0249.csv	Pb loss; use 7-6 ratio	1737.603	1.831351	1.906259	1124.388	5.202249	5.299574377
2021-G-080	C21MAY14A0238.csv	Pb loss; use 7-6 ratio	1752.575	4.049414	4.083837	796.5558	5.961897	6.047008086
2021-G-080	C21FEB25A0019.csv	Pb loss likely, use 7/6	1758.452	0.955441	0.955441	1730.011	3.697396	3.697396091
2021-G-080	C21MAY14A0255.csv	Pb loss; use 7-6 ratio	1774.941	1.121628	1.240171	1582.277	4.153568	4.274835758
2021-G-080	C21MAY14A0257.csv	Pb loss; use 7-6 ratio	1778	1.027511	1.155748	1626.704	4.48542	4.597943562
2021-G-080	C21FEB25A0011.csv	high U, Pb loss, use 7/6	1806.147	1.080076	1.080076	1682.907	3.832709	3.832709225
2021-G-080	C21FEB25A0010.csv	high U, Pb loss, use 7/6	1808.402	1.349631	1.349631	1532.768	4.085405	4.085405065

2021-G-080	C21FEB25A0023.csv	high U, Pb loss, use 7/6	1809.579	0.99341	0.99341	986.7849	5.81838	5.818380341
2021-G-080	C21FEB25A0030.csv	high U, Pb loss, use 7/6	1826.95	0.576254	0.576254	1702.505	3.652917	3.652916621
2021-G-080	C21MAY14A0253.csv	Pb loss; use 7-6 ratio	1827.856	1.171205	1.285183	1766.272	4.113259	4.235681333
2021-G-080	C21FEB25A0005.csv	high U, Pb loss, use 7/6	1832.388	0.722224	0.722224	1656.344	4.175427	4.175426742
2021-G-080	C21FEB25A0018.csv	Pb mobility, use 7/6	1842.275	0.828578	0.828578	1844.64	3.698889	3.698889238
2021-G-080	C21MAY14A0254.csv	Pb loss; use 7-6 ratio	1843.5	0.795581	0.955471	1736.529	4.142326	4.263913938
2021-G-080	C21MAY14A0251.csv	use 7-6 ratio	1843.935	1.343438	1.443884	1794.454	4.137994	4.259705461
2021-G-080	C21MAY14A0259.csv	Pb loss; use 7-6 ratio	1843.99	0.998313	1.129869	1546.804	5.756846	5.844944145
2021-G-080	C21MAY14A0258.csv	Pb loss; use 7-6 ratio	1844.42	1.246929	1.354551	1600.885	8.057632	8.12080826
2021-G-080	C21MAY14A0262.csv	Pb loss; use 7-6 ratio	1846.361	1.42731	1.522232	1685.069	4.60699	4.716614439
2021-G-080	C21MAY14A0239.csv	Pb loss; use 7-6 ratio	1846.946	1.097058	1.217994	1829.408	4.06622	4.190016935
2021-G-080	C21MAY14A0265.csv	Pb loss; use 7-6 ratio	1983.66	0.883363	1.029711	1637.104	4.692847	4.800510871
2021-G-080	C21MAY14A0235.csv	Pb loss; use 7-6 ratio	2135.824	1.779232	1.856244	819.4028	6.075836	6.159373192
2021-G-080	C21MAY14A0250.csv	Pb loss; use 7-6 ratio	2142.301	1.228187	1.337318	2085.239	4.193808	4.313945139
2021-G-080	C21MAY14A0252.csv	Pb loss; use 7-6 ratio	2462.827	0.593394	0.795042	2378.159	4.13837	4.260070972
2021-G-080	*C21FEB25A0021.csv*	*do not use*	1664.242	1.664839	1.664839	1565.854	4.714175	4.714174796
2021-G-080	*C21FEB25A0021.csv*	*do not use*	1824.937	1.225578	1.225578	1743.508	3.753372	3.753371544

2021-G-080	*C21MAY14A0227.csv*	*do not use, inclusions*	870.281	6.274863	6.297132	154.4611	19.07026	19.09704434
2021-G-080	*C21MAY14A0237.csv*	*do not use, inclusions*	870.4509	10.24605	10.25971	186.3871	16.00958	16.04147211
2021-G-080	*C21MAY14A0256.csv*	*do not use, inclusions*	2566.325	4.399447	4.431152	278.8353	13.18308	13.22179278

Analysis	**Source Filename**	**Comment**	**208Pb/232Th Age (Ma)**	**208Pb/232Th Age (Ma)**	**208Pb/232Th Age (Ma)**	**206Pb/204Pb**	**206Pb/204Pb**
			Age	**2s%**	**2s_sys%**	**ratio**	**1s%**
ZY-LG-2 (Two-mica leucogranite)							
2021-G-080	C21MAY14A0268.csv	concordant	16.61738	14.02915	14.115		
2021-G-080	C21MAY14A0241.csv	minor common Pb	22.83875	17.93208	17.99933		
2021-G-080	C21FEB25A0034.csv	young, some common Pb	20.16301	22.83945	22.83945		
2021-G-080	C21MAY14A0260.csv	concordant	14.38414	16.95882	17.02991		
2021-G-080	C21FEB25A0007.csv	high U, young concordant	15.2493	20.02367	20.02367		
2021-G-080	C21MAY14A0242.csv	minor common Pb	22.39619	22.37797	22.43189		
2021-G-080	C21MAY14A0234.csv	concordant	29.05696	35.95052	35.98411		
2021-G-080	C21MAY14A0264.csv	younger	39.52728	63.14249	63.16162		
2021-G-080	C21FEB25A0032.csv	comm Pb or Pb loss	26.51708	38.63828	38.63828		
2021-G-080	C21MAY14A0232.csv	High common Pb	523.1315	18.87826	18.94215		
2021-G-080	C21MAY14A0228.csv	older	52.15488	42.70341	42.73169		
2021-G-080	C21FEB25A0020.csv	Comm Pb or Pb loss	1014.792	4.42981	4.42981		
2021-G-080	C21MAY14A0230.csv	younger	444.7406	11.12227	11.23037		
2021-G-080	C21MAY14A0269.csv	younger	830.995	18.88325	18.94712		
2021-G-080	C21MAY14A0225.csv	minor common Pb	440.5146	8.477544	8.618868		
2021-G-080	C21FEB25A0008.csv	moderate U, concordant	465.0277	7.87813	7.87813		
2021-G-080	C21MAY14A0236.csv	minor common Pb	409.4635	8.237232	8.382609		

2021-G-080	C21MAY14A0230.csv	older	462.9215	7.727899	7.882674		
2021-G-080	C21FEB25A0033.csv	comm Pb or Pb loss	624.5725	9.799993	9.799993	9879.153	17.98901
2021-G-080	C21FEB25A0033.csv	comm Pb or Pb loss	835.3451	6.246957	6.246957		
2021-G-080	C21FEB25A0033.csv	comm Pb or Pb loss	746.6961	6.317419	6.317419		
2021-G-080	C21MAY14A0266.csv	concordant	781.8076	6.655167	6.83428		
2021-G-080	C21MAY14A0229.csv	Pb loss; use 7-6 ratio	607.0815	7.341766	7.50451		
2021-G-080	C21FEB25A0022.csv	minor common Pb	771.8783	3.183047	3.183047		
2021-G-080	C21MAY14A0267.csv	concordant	747.0555	6.508856	6.691887		
2021-G-080	C21MAY14A0233.csv	Pb loss; use 7-6 ratio	597.9677	7.487652	7.647292		
2021-G-080	C21MAY14A0231.csv	Pb loss; use 7-6 ratio	779.1223	6.68634	6.86464		
2021-G-080	C21FEB25A0006.csv	high U, Pb loss, use 7/6	869.722	3.547248	3.547248		
2021-G-080	C21MAY14A0263.csv	Pb loss; use 7-6 ratio	748.2336	6.331594	6.519603		
2021-G-080	C21MAY14A0270.csv	Pb loss; use 7-6 ratio	820.3518	7.930278	8.081178		
2021-G-080	C21FEB25A0009.csv	high U, Pb loss, use 7/6	916.3858	3.468347	3.468347		
2021-G-080	C21MAY14A0240.csv	Pb loss; use 7-6 ratio	955.4612	7.471491	7.631469		
2021-G-080	C21MAY14A0226.csv	high U, Pb loss, common Pb	630.1862	6.760149	6.936552		
2021-G-080	C21FEB25A0024.csv	Pb loss, use 7/6	728.5368	3.736156	3.736156		
2021-G-080	C21FEB25A0029.csv	Comm Pb or Pb loss	1286.85	3.668514	3.668514		
2021-G-080	C21FEB25A0033.csv	high U, Pb loss, use 7/6	833.3151	5.410821	5.410821		
2021-G-080	C21FEB25A0031.csv	Comm Pb or Pb loss	1808.508	2.803618	2.803618		
2021-G-080	C21MAY14A0264.csv	Pb loss; use 7-6 ratio	1343.533	7.605331	7.762551		
2021-G-080	C21MAY14A0261.csv	Pb loss; use 7-6 ratio	1404.052	6.921288	7.093685		
2021-G-080	C21MAY14A0269.csv	older	1832.346	7.963544	8.113826		
2021-G-080	C21MAY14A0249.csv	Pb loss; use 7-6 ratio	1363.699	6.82404	6.998833		
2021-G-080	C21MAY14A0238.csv	Pb loss; use 7-6 ratio	1100.045	9.295698	9.424762		

2021-G-080	C21FEB25A0019.csv	Pb loss likely, use 7/6	1776.094	2.992875	2.992875		
2021-G-080	C21MAY14A0255.csv	Pb loss; use 7-6 ratio	1501.208	6.53502	6.717338		
2021-G-080	C21MAY14A0257.csv	Pb loss; use 7-6 ratio	1566.645	6.352113	6.539532		
2021-G-080	C21FEB25A0011.csv	high U, Pb loss, use 7/6	1787.927	3.277065	3.277065		
2021-G-080	C21FEB25A0010.csv	high U, Pb loss, use 7/6	1507.401	3.838955	3.838955		
2021-G-080	C21FEB25A0023.csv	high U, Pb loss, use 7/6	2061.496	4.483372	4.483372		
2021-G-080	C21FEB25A0030.csv	high U, Pb loss, use 7/6	1713.506	2.621913	2.621913		
2021-G-080	C21MAY14A0253.csv	Pb loss; use 7-6 ratio	1831.737	7.116185	7.283971		
2021-G-080	C21FEB25A0005.csv	high U, Pb loss, use 7/6	1754.913	3.000172	3.000172		
2021-G-080	C21FEB25A0018.csv	Pb mobility, use 7/6	1871.795	2.871896	2.871896		
2021-G-080	C21MAY14A0254.csv	Pb loss; use 7-6 ratio	1697.66	6.526909	6.709448		
2021-G-080	C21MAY14A0251.csv	use 7-6 ratio	1706.395	6.45832	6.642744		
2021-G-080	C21MAY14A0259.csv	Pb loss; use 7-6 ratio	1620.899	6.767708	6.943919		
2021-G-080	C21MAY14A0258.csv	Pb loss; use 7-6 ratio	1533.623	7.593778	7.751232		
2021-G-080	C21MAY14A0262.csv	Pb loss; use 7-6 ratio	1679.038	7.061108	7.230172		
2021-G-080	C21MAY14A0239.csv	Pb loss; use 7-6 ratio	1635.322	6.372258	6.559101		
2021-G-080	C21MAY14A0265.csv	Pb loss; use 7-6 ratio	1578.554	6.553399	6.73522		
2021-G-080	C21MAY14A0235.csv	Pb loss; use 7-6 ratio	1031.436	8.4724	8.613809		
2021-G-080	C21MAY14A0250.csv	Pb loss; use 7-6 ratio	1998.174	6.956626	7.128169		
2021-G-080	C21MAY14A0252.csv	Pb loss; use 7-6 ratio	2116.79	6.528113	6.710618		
2021-G-080	*C21FEB25A0021.csv*	*do not use*	1644.844	3.963493	3.963493		
2021-G-080	*C21FEB25A0021.csv*	*do not use*	1594.449	3.781274	3.781274		
2021-G-080	*C21MAY14A0227.csv*	*do not use, inclusions*	202.4102	20.23712	20.29672		

2021-G-080	*C21MAY14A0237.csv*	*do not use, inclusions*	569.1945	12.44275	12.53947		
2021-G-080	*C21MAY14A0256.csv*	*do not use, inclusions*	4000.116	16.82099	16.89266	201.3406	8.82825

Analysis	**Source Filename**	**Comment**	**207Pb/204Pb**	**207Pb/204Pb**	**208Pb/204Pb**	**208Pb/204Pb**	**Spot Size (μm)**
			ratio	**1s%**	**ratio**	**1s%**	
ZY-LG-2 (Two-mica leucogranite)							
2021-G-080	C21MAY14A0268.csv	concordant					20
2021-G-080	C21MAY14A0241.csv	minor common Pb					20

2021-G-080	C21FEB25A0034.csv	young, some common Pb					30
2021-G-080	C21MAY14A0260.csv	concordant					20
2021-G-080	C21FEB25A0007.csv	high U, young concordant					30
2021-G-080	C21MAY14A0242.csv	minor common Pb					20
2021-G-080	C21MAY14A0234.csv	concordant					20
2021-G-080	C21MAY14A0264.csv	younger					20
2021-G-080	C21FEB25A0032.csv	comm Pb or Pb loss					30
2021-G-080	C21MAY14A0232.csv	High common Pb					20
2021-G-080	C21MAY14A0228.csv	older					20
2021-G-080	C21FEB25A0020.csv	Comm Pb or Pb loss					30
2021-G-080	C21MAY14A0230.csv	younger					20
2021-G-080	C21MAY14A0269.csv	younger					20
2021-G-080	C21MAY14A0225.csv	minor common Pb					20
2021-G-080	C21FEB25A0008.csv	moderate U, concordant					30
2021-G-080	C21MAY14A0236.csv	minor common Pb					20
2021-G-080	C21MAY14A0230.csv	older					20
2021-G-080	C21FEB25A0033.csv	comm Pb or Pb loss	785.2044	17.76905	31.36906	18.19154	30
2021-G-080	C21FEB25A0033.csv	comm Pb or Pb loss					30
2021-G-080	C21FEB25A0033.csv	comm Pb or Pb loss					30
2021-G-080	C21MAY14A0266.csv	concordant					20
2021-G-080	C21MAY14A0229.csv	Pb loss; use 7-6 ratio					20
2021-G-080	C21FEB25A0022.csv	minor common Pb					30
2021-G-080	C21MAY14A0267.csv	concordant					20
2021-G-080	C21MAY14A0233.csv	Pb loss; use 7-6 ratio					20
2021-G-080	C21MAY14A0231.csv	Pb loss; use 7-6 ratio					20
2021-G-080	C21FEB25A0006.csv	high U, Pb loss, use 7/6					30
2021-G-080	C21MAY14A0263.csv	Pb loss; use 7-6 ratio					20
2021-G-080	C21MAY14A0270.csv	Pb loss; use 7-6 ratio					20

2021-G-080	C21FEB25A0009.csv	high U, Pb loss, use 7/6				30
2021-G-080	C21MAY14A0240.csv	Pb loss; use 7-6 ratio				20
2021-G-080	C21MAY14A0226.csv	high U, Pb loss, common Pb				20
2021-G-080	C21FEB25A0024.csv	Pb loss, use 7/6				30
2021-G-080	C21FEB25A0029.csv	Comm Pb or Pb loss				30
2021-G-080	C21FEB25A0033.csv	high U, Pb loss, use 7/6				30
2021-G-080	C21FEB25A0031.csv	Comm Pb or Pb loss				30
2021-G-080	C21MAY14A0264.csv	Pb loss; use 7-6 ratio				20
2021-G-080	C21MAY14A0261.csv	Pb loss; use 7-6 ratio				20
2021-G-080	C21MAY14A0269.csv	older				20
2021-G-080	C21MAY14A0249.csv	Pb loss; use 7-6 ratio				20
2021-G-080	C21MAY14A0238.csv	Pb loss; use 7-6 ratio				20
2021-G-080	C21FEB25A0019.csv	Pb loss likely, use 7/6				30
2021-G-080	C21MAY14A0255.csv	Pb loss; use 7-6 ratio				20
2021-G-080	C21MAY14A0257.csv	Pb loss; use 7-6 ratio				20
2021-G-080	C21FEB25A0011.csv	high U, Pb loss, use 7/6				30
2021-G-080	C21FEB25A0010.csv	high U, Pb loss, use 7/6				30
2021-G-080	C21FEB25A0023.csv	high U, Pb loss, use 7/6				30
2021-G-080	C21FEB25A0030.csv	high U, Pb loss, use 7/6				30
2021-G-080	C21MAY14A0253.csv	Pb loss; use 7-6 ratio				20
2021-G-080	C21FEB25A0005.csv	high U, Pb loss, use 7/6				30
2021-G-080	C21FEB25A0018.csv	Pb mobility, use 7/6				30
2021-G-080	C21MAY14A0254.csv	Pb loss; use 7-6 ratio				20
2021-G-080	C21MAY14A0251.csv	use 7-6 ratio				20
2021-G-080	C21MAY14A0259.csv	Pb loss; use 7-6 ratio				20
2021-G-080	C21MAY14A0258.csv	Pb loss; use 7-6 ratio				20
2021-G-080	C21MAY14A0262.csv	Pb loss; use 7-6 ratio				20
2021-G-080	C21MAY14A0239.csv	Pb loss; use 7-6 ratio				20

2021-G-080	C21MAY14A0265.csv	Pb loss; use 7-6 ratio					20
2021-G-080	C21MAY14A0235.csv	Pb loss; use 7-6 ratio					20
2021-G-080	C21MAY14A0250.csv	Pb loss; use 7-6 ratio					20
2021-G-080	C21MAY14A0252.csv	Pb loss; use 7-6 ratio					20
2021-G-080	*C21FEB25A0021.csv*	*do not use*					30
2021-G-080	*C21FEB25A0021.csv*	*do not use*					30
2021-G-080	*C21MAY14A0227.csv*	*do not use, inclusions*					20
2021-G-080	*C21MAY14A0237.csv*	*do not use, inclusions*					20
2021-G-080	*C21MAY14A0256.csv*	*do not use, inclusions*	32.82976	8.715695	64.99834	8.649354	20

Analysis	Source Filename	Comment	SiO4	31P	49Ti	56Fe	89Y	91Zr	93Nb	139La	140Ce
			1s%	1s%	1s%	1s%	1s%	1s%	1s%	1s%	1s%
ZY-LG-2 (Two-mica leucogranite)											
2021-G-080	C21MAY14A0268.csv	concordant		2.289741	10.15009	8.547129	1.496643	0.378258	3.521972	37.46811	5.898011
2021-G-080	C21MAY14A0241.csv	minor common Pb		10.15365	9.302247	3.325361	9.034546	0.356564	4.939365	6.841185	3.099491
2021-G-080	C21FEB25A0034.csv	young, some common Pb		2.544371	10.13398	4.806834	1.923111	0.525121	5.954192	46.22552	8.04988
2021-G-080	C21MAY14A0260.csv	concordant		5.318514	12.5808	17.62066	5.027517	0.394077	5.113501	88.407	9.522902
2021-G-080	C21FEB25A0007.csv	high U, young concordant		2.284046	6.791927	10.09298	1.571268	0.417468	4.752408	1.46113	6.234069
2021-G-080	C21MAY14A0242.csv	minor common Pb		5.737033	10.34742	7.227265	5.789506	0.356564	6.449476	91.73454	8.594774
2021-G-080	C21MAY14A0234.csv	concordant		3.074465	8.905494	5.71249	2.485449	0.356564	6.944875	230.4475	8.564237
2021-G-080	C21MAY14A0264.csv	younger		5.497781	36.21419	27.50805	4.954687	0.852482	25.06088	353.4677	40.93704
2021-G-080	C21FEB25A0032.csv	comm Pb or Pb loss		4.571629	14.95863	7.790057	5.463326	0.487579	11.42561	1.46113	15.00185
2021-G-080	C21MAY14A0232.csv	High common Pb		8.682524	14.97079	4.195962	12.89534	0.546035	8.627567	26.51142	7.867515
2021-G-080	C21MAY14A0228.csv	older		4.117376	24.17247	5.537945	2.024981	0.449766	12.21647	151.7771	10.60759
2021-G-080	C21FEB25A0020.csv	Comm Pb or Pb loss		2.944484	7.858794	8.66633	2.305352	0.417468	5.259171	104.0944	5.021615
2021-G-080	C21MAY14A0230.csv	younger		3.569044	16.80264	26.2102	2.628131	0.494553	13.44611	121.2652	10.97488
2021-G-080	C21MAY14A0269.csv	younger		7.906002	51.02347	20.80993	2.803376	0.566313	12.4876	214.5361	22.43103
2021-G-080	C21MAY14A0225.csv	minor common Pb		3.140619	12.8996	7.238267	2.852655	0.426256	14.83417	63.58254	8.651117

2021-G-080	C21FEB25A0008.csv	moderate U, concordant		2.484728	10.63015	1.876202	1.670028	0.490251	8.82768	53.01167	14.08989
2021-G-080	C21MAY14A0236.csv	minor common Pb		2.255361	9.30287	7.265697	1.833049	0.356564	8.921644	111.0059	9.9332
2021-G-080	C21MAY14A0230.csv	older		3.071873	18.28583	12.75308	2.559339	0.446378	10.15087	149.8149	6.472854
2021-G-080	C21FEB25A0033.csv	comm Pb or Pb loss		2.658041	27.10838	6.993717	2.115257	0.61692	8.324537	45.58939	18.64832
2021-G-080	C21FEB25A0033.csv	comm Pb or Pb loss		2.734154	16.21667	5.338187	2.10253	0.563995	7.539339	27.00379	9.003563
2021-G-080	C21FEB25A0033.csv	comm Pb or Pb loss		2.623162	22.56233	5.231862	1.987884	0.61692	8.363123	17.52074	8.68057
2021-G-080	C21MAY14A0266.csv	concordant		3.476066	9.484361	9.131453	1.53566	0.356564	3.239263	59.65944	2.32126
2021-G-080	C21MAY14A0229.csv	Pb loss; use 7-6 ratio		4.447556	10.80628	3.397559	2.87657	0.356564	4.534441	19.00192	4.484354
2021-G-080	C21FEB25A0022.csv	minor common Pb		2.617183	5.521909	1.876202	1.500384	0.417468	6.009637	41.10116	2.674633
2021-G-080	C21MAY14A0267.csv	concordant		4.674753	7.154429	8.028453	4.702796	0.356564	4.632203	31.95007	4.874831
2021-G-080	C21MAY14A0233.csv	Pb loss; use 7-6 ratio		2.478347	1.97123	1.336621	2.273715	0.356564	4.32083	11.26099	4.795291
2021-G-080	C21MAY14A0231.csv	Pb loss; use 7-6 ratio		2.450411	7.220308	2.098353	2.157938	0.381461	5.339365	15.82685	6.409661
2021-G-080	C21FEB25A0006.csv	high U, Pb loss, use 7/6		2.912191	6.420226	3.706721	1.915273	0.448222	2.806195	25.59758	4.807517
2021-G-080	C21MAY14A0263.csv	Pb loss; use 7-6 ratio		3.206343	6.673844	5.478647	1.531725	0.356564	3.653271	3.98954	2.288437
2021-G-080	C21MAY14A0270.csv	Pb loss; use 7-6 ratio		6.407833	10.73349	3.383726	1.94214	0.47857	11.41386	46.41305	4.206964
2021-G-080	C21FEB25A0009.csv	high U, Pb loss, use 7/6		2.519881	9.236916	7.492023	1.765929	0.493042	6.643233	132.1658	4.116191
2021-G-080	C21MAY14A0240.csv	Pb loss; use 7-6 ratio		3.760477	8.585887	8.962944	2.65381	0.356564	5.125435	111.0136	2.732379

2021-G-080	C21MAY14A0226.csv	high U, Pb loss, common Pb		2.362215	7.653376	2.879749	2.055503	0.356564	5.258713	10.80263	4.326024
2021-G-080	C21FEB25A0024.csv	Pb loss, use 7/6		2.44681	6.208574	5.835829	1.463678	0.417468	6.224077	58.42565	6.735313
2021-G-080	C21FEB25A0029.csv	Comm Pb or Pb loss		2.624077	6.270009	3.501105	1.480658	0.417468	7.924805	20.07685	7.096241
2021-G-080	C21FEB25A0033.csv	high U, Pb loss, use 7/6		2.711318	13.18999	4.57102	1.915817	0.545213	5.489578	19.77226	8.638411
2021-G-080	C21FEB25A0031.csv	Comm Pb or Pb loss		3.400185	5.904381	3.946699	1.580161	0.417468	3.980872	35.50447	2.956025
2021-G-080	C21MAY14A0264.csv	Pb loss; use 7-6 ratio		4.009543	16.10563	9.690611	3.217645	0.619571	5.652816	73.96384	6.650942
2021-G-080	C21MAY14A0261.csv	Pb loss; use 7-6 ratio		2.213355	9.194871	6.531841	1.788965	0.356564	7.688521	21.95519	5.946938
2021-G-080	C21MAY14A0269.csv	older		5.317832	14.6123	17.68382	2.132945	0.655761	17.09414	50.97224	8.984687
2021-G-080	C21MAY14A0249.csv	Pb loss; use 7-6 ratio		4.358146	9.735155	3.36071	1.650183	0.412804	5.54916	22.73431	3.151631
2021-G-080	C21MAY14A0238.csv	Pb loss; use 7-6 ratio		3.587559	11.83269	7.966523	1.783104	0.3793	8.884954	14.61655	5.2221
2021-G-080	C21FEB25A0019.csv	Pb loss likely, use 7/6		2.497949	5.713105	3.29977	1.737463	0.417468	6.753277	19.69623	5.833269
2021-G-080	C21MAY14A0255.csv	Pb loss; use 7-6 ratio		2.633075	8.11554	2.509389	2.248596	0.356564	5.681908	27.96577	4.200793
2021-G-080	C21MAY14A0257.csv	Pb loss; use 7-6 ratio		2.770644	5.752789	3.752213	2.380847	0.356564	4.634427	26.93646	3.817055
2021-G-080	C21FEB25A0011.csv	high U, Pb loss, use 7/6		2.433494	6.95155	4.533092	1.904342	0.419035	6.452929	31.75893	5.415587
2021-G-080	C21FEB25A0010.csv	high U, Pb loss, use 7/6		2.479608	7.428364	3.020265	1.5465	0.46967	7.086853	26.33267	8.440133
2021-G-080	C21FEB25A0023.csv	high U, Pb loss, use 7/6		2.392553	7.398611	1.876202	2.663459	0.417468	4.595715	26.83376	3.969017

2021-G-080	C21FEB25A0030.csv	high U, Pb loss, use 7/6		2.177527	5.969435	2.697767	1.442435	0.417468	4.851422	25.08649	5.485778
2021-G-080	C21MAY14A0253.csv	Pb loss; use 7-6 ratio		3.352253	9.077632	4.202424	2.175302	0.356564	9.131911	31.94942	7.440628
2021-G-080	C21FEB25A0005.csv	high U, Pb loss, use 7/6		2.394277	5.896336	3.333939	1.943489	0.426983	4.58691	15.30922	3.162431
2021-G-080	C21FEB25A0018.csv	Pb mobility, use 7/6		2.720405	6.517801	3.393171	1.809732	0.417468	7.310079	45.11331	5.305044
2021-G-080	C21MAY14A0254.csv	Pb loss; use 7-6 ratio		2.598685	3.049899	1.3751	1.555774	0.356564	5.446195	23.0893	7.520855
2021-G-080	C21MAY14A0251.csv	use 7-6 ratio		5.048234	9.262209	19.15615	1.532021	0.356564	7.189946	38.33649	3.295093
2021-G-080	C21MAY14A0259.csv	Pb loss; use 7-6 ratio		2.651613	9.854582	2.823216	3.117785	0.356564	6.549702	31.9497	7.500497
2021-G-080	C21MAY14A0258.csv	Pb loss; use 7-6 ratio		4.844917	7.592093	4.045696	5.970601	0.356564	9.319586	4.852538	4.495486
2021-G-080	C21MAY14A0262.csv	Pb loss; use 7-6 ratio		3.688517	1.724322	1.31755	2.251476	0.356564	4.018493	8.964983	4.525106
2021-G-080	C21MAY14A0239.csv	Pb loss; use 7-6 ratio		4.16644	9.826413	3.020469	1.921554	0.412804	6.881919	31.02481	2.915594
2021-G-080	C21MAY14A0265.csv	Pb loss; use 7-6 ratio		4.221442	6.83291	4.331667	2.699643	0.356564	4.027096	5.858564	3.051637
2021-G-080	C21MAY14A0235.csv	Pb loss; use 7-6 ratio		4.736587	13.99242	9.937179	2.497349	0.483599	10.15478	77.69044	5.513678
2021-G-080	C21MAY14A0250.csv	Pb loss; use 7-6 ratio		3.89352	10.39941	5.629967	5.408994	0.356564	10.31556	41.50088	3.968952
2021-G-080	C21MAY14A0252.csv	Pb loss; use 7-6 ratio		3.095379	10.86519	4.510766	1.643846	0.356564	6.284946	59.65525	3.626386
2021-G-080	*C21FEB25A0021.csv*	*do not use*		*2.66481*	*8.19068*	*5.67394*	*1.673*	*0.47365*	*9.10155*	*141.575*	*7.83877*
2021-G-080	*C21FEB25A0021.csv*	*do not use*		*2.76729*	*8.01571*	*5.5339*	*1.68843*	*0.47162*	*10.3168*	*39.2852*	*7.97329*
2021-G-080	*C21MAY14A0227.csv*	*do not use, inclusions*		*3.17406*	*6.95205*	*6.90053*	*2.63454*	*0.38612*	*6.77989*	*7.46227*	*7.05748*

2021-G-080	*C21MAY14A0237.csv*	*do not use, inclusions*		*10.4068*	*5.20186*	*1.49262*	*5.62319*	*0.35656*	*5.03495*	*8.51642*	*2.74574*
2021-G-080	*C21MAY14A0256.csv*	*do not use, inclusions*		*2.22454*	*2.52556*	*1.30595*	*2.22248*	*0.35656*	*9.58473*	*3.79326*	*4.07209*

Analysis	Source Filename	Comment	141Pr	146Nd	147Sm	153Eu	157Gd	159Tb	163Dy
			1s%	1s%	1s%	1s%	1s%	1s%	1s%
ZY-LG-2 (Two-mica leucogranite)									
2021-G-080	C21MAY14A0268.csv	concordant	12.64418	13.37763	5.849339	11.66593	2.995578274	2.455507	1.641119
2021-G-080	C21MAY14A0241.csv	minor common Pb	2.942781	3.411324	2.699724	9.226282	13.04469591	11.9726	10.91294
2021-G-080	C21FEB25A0034.csv	young, some common Pb	17.04245	16.2994	8.912243	16.31808	3.646270092	2.949488	2.292202
2021-G-080	C21MAY14A0260.csv	concordant	20.79526	16.80587	8.814424	16.13747	5.551635695	4.947521	4.596474
2021-G-080	C21FEB25A0007.csv	high U, young concordant	16.8146	15.53653	7.447491	16.61472	3.073420568	2.450701	1.78102
2021-G-080	C21MAY14A0242.csv	minor common Pb	30.62847	30.85016	11.55138	12.43995	5.596129959	4.951821	5.025515
2021-G-080	C21MAY14A0234.csv	concordant	61.10373	29.4886	13.8913	12.83282	5.510308016	4.875861	3.442217
2021-G-080	C21MAY14A0264.csv	younger	72.37528	71.28296	27.81826	50.21666	16.56627332	9.482716	7.498548
2021-G-080	C21FEB25A0032.csv	comm Pb or Pb loss	42.56677	38.17776	23.07919	17.01348	6.004154847	6.779291	5.891286
2021-G-080	C21MAY14A0232.csv	High common Pb	24.47138	41.18091	24.37007	33.54367	8.289337592	4.981852	11.73446
2021-G-080	C21MAY14A0228.csv	older	63.01599	73.96538	29.08822	27.95997	11.1552557	7.267381	3.584055
2021-G-080	C21FEB25A0020.csv	Comm Pb or Pb loss	23.79255	21.02805	9.925307	9.975293	4.784182146	3.572504	2.79549
2021-G-080	C21MAY14A0230.csv	younger	38.80815	50.83189	17.79009	45.32384	6.262112587	3.872652	2.608661
2021-G-080	C21MAY14A0269.csv	younger	60.2696	72.25911	71.91013	104.4297	18.38781705	11.93926	6.150897
2021-G-080	C21MAY14A0225.csv	minor common Pb	16.38443	13.60176	9.18532	38.40294	4.648434976	4.123066	2.877656
2021-G-080	C21FEB25A0008.csv	moderate U, concordant	36.67036	35.61678	12.53446	35.85081	5.30804063	2.995265	2.13475
2021-G-080	C21MAY14A0236.csv	minor common Pb	30.62197	20.67374	9.618677	27.22434	3.701001985	2.73429	1.864572
2021-G-080	C21MAY14A0230.csv	older	42.63209	22.51514	13.8619	20.98414	4.906042827	3.928308	2.786451
2021-G-080	C21FEB25A0033.csv	comm Pb or Pb loss	21.46357	28.96758	17.51123	41.17311	8.406750603	4.365809	2.90535
2021-G-080	C21FEB25A0033.csv	comm Pb or Pb loss	10.82607	13.56167	9.226998	29.04744	4.738943097	3.760689	2.849891
2021-G-080	C21FEB25A0033.csv	comm Pb or Pb loss	14.0985	14.70638	9.954527	27.87176	7.442016742	3.589033	2.75619
2021-G-080	C21MAY14A0266.csv	concordant	13.69501	10.86418	7.517353	14.57691	3.721233028	2.733865	1.700861
2021-G-080	C21MAY14A0229.csv	Pb loss; use 7-6 ratio	23.80541	24.64503	12.95753	29.4885	5.536409544	5.010879	3.391634
2021-G-080	C21FEB25A0022.csv	minor common Pb	13.83632	10.52795	7.059813	13.26363	3.380453131	2.63788	1.932161
2021-G-080	C21MAY14A0267.csv	concordant	6.174726	6.035695	5.206516	9.116117	6.257494594	5.630944	5.130472
2021-G-080	C21MAY14A0233.csv	Pb loss; use 7-6 ratio	11.62255	14.58967	12.02218	39.15946	4.624489585	3.568962	2.518227

2021-G-080	C21MAY14A0231.csv	Pb loss; use 7-6 ratio	13.64252	15.21399	8.459252	36.1386	4.072017865	3.399099	2.173547
2021-G-080	C21FEB25A0006.csv	high U, Pb loss, use 7/6	23.5284	19.71865	13.04025	61.14268	4.58497188	3.242908	2.392905
2021-G-080	C21MAY14A0263.csv	Pb loss; use 7-6 ratio	3.755368	4.679278	4.036114	7.448729	2.90779968	2.54642	1.639878
2021-G-080	C21MAY14A0270.csv	Pb loss; use 7-6 ratio	22.06133	20.53225	20.53015	21.94253	8.69259119	6.39842	3.297958
2021-G-080	C21FEB25A0009.csv	high U, Pb loss, use 7/6	21.62822	15.32773	9.919395	26.03375	4.11765691	3.036875	2.259511
2021-G-080	C21MAY14A0240.csv	Pb loss; use 7-6 ratio	14.83636	11.18593	9.971632	15.40356	5.01436687	4.119035	3.169867
2021-G-080	C21MAY14A0226.csv	high U, Pb loss, common Pb	10.22779	10.4591	6.415277	12.25761	3.109566052	3.319711	2.193077
2021-G-080	C21FEB25A0024.csv	Pb loss, use 7/6	15.00846	15.73213	7.091159	22.14716	3.189590319	2.373877	1.837562
2021-G-080	C21FEB25A0029.csv	Comm Pb or Pb loss	16.31984	21.03752	8.95229	27.28812	3.637471484	2.73907	1.917178
2021-G-080	C21FEB25A0033.csv	high U, Pb loss, use 7/6	10.21043	9.856918	10.39164	25.9801	6.284462163	3.319587	1.976122
2021-G-080	C21FEB25A0031.csv	Comm Pb or Pb loss	13.82527	14.69708	8.698869	17.34228	4.317193811	3.236292	2.231052
2021-G-080	C21MAY14A0264.csv	Pb loss; use 7-6 ratio	26.01319	31.76907	20.50886	27.84614	6.959639046	4.591579	3.362033
2021-G-080	C21MAY14A0261.csv	Pb loss; use 7-6 ratio	14.83889	10.92621	7.281637	15.97024	3.595796759	2.929915	2.027414
2021-G-080	C21MAY14A0269.csv	older	14.65798	15.17177	13.72611	25.91309	5.690122442	5.532961	3.355931
2021-G-080	C21MAY14A0249.csv	Pb loss; use 7-6 ratio	18.18964	14.8657	9.258615	20.1472	4.139892312	3.204647	1.980982
2021-G-080	C21MAY14A0238.csv	Pb loss; use 7-6 ratio	25.80383	24.54759	25.27283	22.04821	10.19944115	6.464293	4.423171
2021-G-080	C21FEB25A0019.csv	Pb loss likely, use 7/6	13.83985	12.40861	6.867072	17.08846	2.97096234	2.537631	2.011007
2021-G-080	C21MAY14A0255.csv	Pb loss; use 7-6 ratio	15.53051	13.05512	8.299338	18.77602	3.686092442	3.12163	2.642822
2021-G-080	C21MAY14A0257.csv	Pb loss; use 7-6 ratio	9.282702	8.300953	5.909174	6.679679	4.161396277	3.621425	2.746793
2021-G-080	C21FEB25A0011.csv	high U, Pb loss, use 7/6	16.79367	13.34305	7.937791	20.25191	3.397727082	2.648745	2.165103
2021-G-080	C21FEB25A0010.csv	high U, Pb loss, use 7/6	20.31745	18.66004	9.656458	21.01365	4.443192124	3.216963	1.941773
2021-G-080	C21FEB25A0023.csv	high U, Pb loss, use 7/6	15.35435	12.05238	7.44865	20.26354	3.575506356	3.26805	2.911693
2021-G-080	C21FEB25A0030.csv	high U, Pb loss, use 7/6	14.6777	11.64846	5.534244	15.97858	2.608101797	2.230889	1.755619
2021-G-080	C21MAY14A0253.csv	Pb loss; use 7-6 ratio	21.033	20.2489	11.47784	36.44901	4.140410605	3.235858	2.520673
2021-G-080	C21FEB25A0005.csv	high U, Pb loss, use 7/6	9.053542	8.717069	5.753755	15.04431	2.880833721	2.723563	2.178192

2021-G-080	C21FEB25A0018.csv	Pb mobility, use 7/6	13.71292	10.94699	6.953706	16.39469	3.330229943	2.582344	2.095198
2021-G-080	C21MAY14A0254.csv	Pb loss; use 7-6 ratio	16.55068	15.06672	8.07371	26.26637	3.261093893	2.450238	1.588747
2021-G-080	C21MAY14A0251.csv	use 7-6 ratio	17.39797	16.39756	11.13324	15.77457	4.809993871	3.785732	2.303063
2021-G-080	C21MAY14A0259.csv	Pb loss; use 7-6 ratio	20.16643	18.785	9.227275	32.406	4.889859541	4.286494	3.426541
2021-G-080	C21MAY14A0258.csv	Pb loss; use 7-6 ratio	7.380015	11.32257	8.299274	19.84119	6.623857939	6.191417	6.094183
2021-G-080	C21MAY14A0262.csv	Pb loss; use 7-6 ratio	8.41363	8.465382	7.247414	12.72983	4.465923109	3.802587	2.811519
2021-G-080	C21MAY14A0239.csv	Pb loss; use 7-6 ratio	12.61284	11.6724	7.714234	8.771531	4.412381628	3.285641	2.481015
2021-G-080	C21MAY14A0265.csv	Pb loss; use 7-6 ratio	7.687505	12.7426	10.69983	13.87353	6.123029077	4.699023	3.484073
2021-G-080	C21MAY14A0235.csv	Pb loss; use 7-6 ratio	38.88522	41.32139	19.36104	27.91985	7.214769949	4.752654	3.7255
2021-G-080	C21MAY14A0250.csv	Pb loss; use 7-6 ratio	15.00193	13.63228	10.75902	9.93696	4.916655853	3.694239	6.064631
2021-G-080	C21MAY14A0252.csv	Pb loss; use 7-6 ratio	42.02592	26.27497	16.83947	22.67062	5.747195348	3.730319	2.454964
2021-G-080	*C21FEB25A0021.csv*	*do not use*	*20.7136*	*19.7085*	*11.2563*	*23.131*	*4.340715787*	*3.21963*	*2.37414*
2021-G-080	*C21FEB25A0021.csv*	*do not use*	*21.6614*	*17.4967*	*10.4686*	*30.5348*	*4.220903689*	*3.12409*	*2.07385*
2021-G-080	*C21MAY14A0227.csv*	*do not use, inclusions*	*3.84142*	*6.95882*	*6.09112*	*16.3559*	*3.409896389*	*3.57945*	*2.63723*
2021-G-080	*C21MAY14A0237.csv*	*do not use, inclusions*	*9.24345*	*9.86069*	*9.0501*	*12.4401*	*10.88985099*	*8.68566*	*6.71811*
2021-G-080	*C21MAY14A0256.csv*	*do not use, inclusions*	*7.12508*	*12.0946*	*21.5668*	*17.8664*	*9.539288047*	*5.38103*	*2.82739*

Analysis	Source Filename	Comment	165Ho	166Er	169Tm	172Yb	175Lu	178Hf	181Ta
			1s%	1s%	1s%	1s%	1s%	1s%	1s%
ZY-LG-2 (Two-mica leucogranite)									
2021-G-080	C21MAY14A0268.csv	concordant	1.834662	1.77508	2.702454	1.80686	1.963642181	1.905749	3.703675
2021-G-080	C21MAY14A0241.csv	minor common Pb	8.887177	7.274663	7.084791	6.273148	5.709873506	3.131856	6.424734
2021-G-080	C21FEB25A0034.csv	young, some common Pb	2.432469	2.099131	2.388057	2.388282	3.237564732	1.957113	5.638257
2021-G-080	C21MAY14A0260.csv	concordant	4.83751	5.161704	4.998889	4.533464	4.513141678	1.888887	4.330967
2021-G-080	C21FEB25A0007.csv	high U, young concordant	1.924325	1.822101	2.073378	2.031462	3.058973099	1.753392	4.016024
2021-G-080	C21MAY14A0242.csv	minor common Pb	5.862404	5.864991	6.744688	6.236886	6.472019515	1.71832	4.777325
2021-G-080	C21MAY14A0234.csv	concordant	3.736677	3.638566	5.477263	4.636851	5.096034424	1.727173	5.005589
2021-G-080	C21MAY14A0264.csv	younger	6.386675	6.978433	5.955382	5.166301	8.338189269	3.447399	19.72215
2021-G-080	C21FEB25A0032.csv	comm Pb or Pb loss	6.26926	6.495036	5.969572	6.139923	6.535046029	1.833909	10.67884
2021-G-080	C21MAY14A0232.csv	High common Pb	12.86694	13.56997	15.84704	15.71241	14.51574741	2.170003	7.068654
2021-G-080	C21MAY14A0228.csv	older	4.02146	3.05229	4.310728	2.818376	2.999108875	1.962513	6.481237
2021-G-080	C21FEB25A0020.csv	Comm Pb or Pb loss	3.169513	2.996281	4.27843	3.683814	4.313785376	1.726436	3.578379
2021-G-080	C21MAY14A0230.csv	younger	2.811152	2.668766	3.270112	2.733099	3.184928535	2.217226	10.264
2021-G-080	C21MAY14A0269.csv	younger	4.959159	5.224912	5.272786	4.540392	4.722629382	2.127205	9.225073
2021-G-080	C21MAY14A0225.csv	minor common Pb	3.636463	2.935968	3.558066	3.089282	2.980475318	1.981392	12.66487
2021-G-080	C21FEB25A0008.csv	moderate U, concordant	2.18977	1.959231	2.222255	2.138488	3.057381067	1.924053	7.524174
2021-G-080	C21MAY14A0236.csv	minor common Pb	1.940443	2.042151	2.997796	2.422179	2.421291373	1.735874	6.732609
2021-G-080	C21MAY14A0230.csv	older	2.697322	2.476486	3.081291	2.400208	2.448819447	1.937557	10.60781
2021-G-080	C21FEB25A0033.csv	comm Pb or Pb loss	2.586077	2.135417	2.273381	2.822673	3.80610705	2.188136	4.309316

2021-G-080	C21FEB25A0033.csv	comm Pb or Pb loss	2.485422	2.586149	2.471927	2.457126	3.448636099	1.988963	3.138257
2021-G-080	C21FEB25A0033.csv	comm Pb or Pb loss	2.434868	2.264685	2.447552	2.076569	3.301727495	2.222373	4.438107
2021-G-080	C21MAY14A0266.csv	concordant	1.763492	1.805772	2.697054	1.84771	1.910200607	1.722914	3.790407
2021-G-080	C21MAY14A0229.csv	Pb loss; use 7-6 ratio	3.182339	3.038825	3.605011	2.7112	2.746170006	1.712317	3.66599
2021-G-080	C21FEB25A0022.csv	minor common Pb	1.94845	1.72684	1.97579	1.95703	2.987650324	1.726191	5.429433
2021-G-080	C21MAY14A0267.csv	concordant	4.863564	4.595517	4.801926	4.184422	4.107926844	1.70013	4.152601
2021-G-080	C21MAY14A0233.csv	Pb loss; use 7-6 ratio	2.270165	2.206771	2.87015	2.035204	1.928653534	1.748014	2.97757
2021-G-080	C21MAY14A0231.csv	Pb loss; use 7-6 ratio	2.21921	2.251259	2.8262	2.261808	2.027639951	1.801731	5.245756
2021-G-080	C21FEB25A0006.csv	high U, Pb loss, use 7/6	2.362693	2.036193	2.16719	2.080016	3.137141183	1.803229	2.782512
2021-G-080	C21MAY14A0263.csv	Pb loss; use 7-6 ratio	1.803104	1.823957	2.699006	1.830449	2.002816497	1.813123	3.592137
2021-G-080	C21MAY14A0270.csv	Pb loss; use 7-6 ratio	3.074874	2.699262	3.775161	2.441018	3.013674689	1.990812	13.63577
2021-G-080	C21FEB25A0009.csv	high U, Pb loss, use 7/6	2.221207	2.000144	2.414163	2.076096	3.169885645	1.903538	5.814512
2021-G-080	C21MAY14A0240.csv	Pb loss; use 7-6 ratio	2.926078	3.07421	3.608294	3.333073	3.773478992	1.82807	4.134762
2021-G-080	C21MAY14A0226.csv	high U, Pb loss, common Pb	2.219981	2.20623	2.981119	2.27321	2.246066724	1.759026	4.509736
2021-G-080	C21FEB25A0024.csv	Pb loss, use 7/6	1.95357	1.776963	2.061167	1.972751	3.066054983	1.754978	4.916719
2021-G-080	C21FEB25A0029.csv	Comm Pb or Pb loss	2.10689	1.956841	2.299612	2.151318	3.22938354	1.747528	5.757814
2021-G-080	C21FEB25A0033.csv	high U, Pb loss, use 7/6	2.202678	2.411489	2.25717	2.246005	3.356255025	2.018448	3.264979
2021-G-080	C21FEB25A0031.csv	Comm Pb or Pb loss	2.114276	1.868967	2.143509	2.008481	3.041751558	1.761389	3.882319

2021-G-080	C21MAY14A0264.csv	Pb loss; use 7-6 ratio	3.274484	3.343283	4.14461	3.020624	3.052814152	2.610224	3.456956
2021-G-080	C21MAY14A0261.csv	Pb loss; use 7-6 ratio	2.174392	2.241177	3.867738	2.405214	2.494443708	1.715544	4.929381
2021-G-080	C21MAY14A0269.csv	older	4.385967	2.637111	3.302518	3.10058	3.020419318	2.394479	20.5298
2021-G-080	C21MAY14A0249.csv	Pb loss; use 7-6 ratio	1.905886	1.919775	2.769245	2.016211	2.328163224	1.868201	6.093958
2021-G-080	C21MAY14A0238.csv	Pb loss; use 7-6 ratio	4.076666	3.390082	4.111619	3.096916	3.199921347	1.737526	10.78905
2021-G-080	C21FEB25A0019.csv	Pb loss likely, use 7/6	2.233324	1.919668	2.11695	2.078146	3.147215747	1.798806	5.134938
2021-G-080	C21MAY14A0255.csv	Pb loss; use 7-6 ratio	2.504846	2.778986	3.62828	3.11501	3.185479501	1.768296	5.096052
2021-G-080	C21MAY14A0257.csv	Pb loss; use 7-6 ratio	2.743917	2.586876	3.047988	2.324104	2.401756244	1.774375	5.033518
2021-G-080	C21FEB25A0011.csv	high U, Pb loss, use 7/6	2.25827	2.046777	2.201425	2.430926	3.22655928	1.786054	5.200594
2021-G-080	C21FEB25A0010.csv	high U, Pb loss, use 7/6	2.342452	1.89514	2.243392	2.211439	3.190625571	1.765678	4.775266
2021-G-080	C21FEB25A0023.csv	high U, Pb loss, use 7/6	3.038264	3.024402	3.237428	3.203231	3.919392612	1.762214	3.963424
2021-G-080	C21FEB25A0030.csv	high U, Pb loss, use 7/6	1.82017	1.749681	1.936103	1.971672	3.022016507	1.734683	3.955597
2021-G-080	C21MAY14A0253.csv	Pb loss; use 7-6 ratio	2.311431	2.408654	3.165908	2.493667	2.745093086	1.721272	7.469534
2021-G-080	C21FEB25A0005.csv	high U, Pb loss, use 7/6	2.330857	2.047717	2.379162	2.282662	3.221814359	1.753883	4.618935
2021-G-080	C21FEB25A0018.csv	Pb mobility, use 7/6	2.373165	2.240337	2.591351	2.565247	3.612733	1.747647	6.359007
2021-G-080	C21MAY14A0254.csv	Pb loss; use 7-6 ratio	1.750247	1.74239	2.722453	1.91977	2.249683866	1.690717	4.331229
2021-G-080	C21MAY14A0251.csv	use 7-6 ratio	2.160463	1.902831	3.022937	1.936673	2.050379581	1.766772	7.954651
2021-G-080	C21MAY14A0259.csv	Pb loss; use 7-6 ratio	3.310548	3.162484	3.897095	3.253686	3.323755331	1.721553	5.047678

2021-G-080	C21MAY14A0258.csv	Pb loss; use 7-6 ratio	6.114237	6.116116	6.462043	6.032337	5.911864624	1.762621	7.451314
2021-G-080	C21MAY14A0262.csv	Pb loss; use 7-6 ratio	2.628571	2.591031	3.096187	2.404626	2.582975721	1.721213	5.52191
2021-G-080	C21MAY14A0239.csv	Pb loss; use 7-6 ratio	2.157612	2.046381	2.888045	2.275035	2.683027879	1.906131	7.113162
2021-G-080	C21MAY14A0265.csv	Pb loss; use 7-6 ratio	3.324002	2.66137	3.260066	2.316871	2.303048296	1.766571	4.434373
2021-G-080	C21MAY14A0235.csv	Pb loss; use 7-6 ratio	3.406909	3.274218	3.640156	3.081264	3.194776654	2.212561	7.41233
2021-G-080	C21MAY14A0250.csv	Pb loss; use 7-6 ratio	5.922493	5.171912	5.191374	4.52381	3.69943224	1.964765	10.45943
2021-G-080	C21MAY14A0252.csv	Pb loss; use 7-6 ratio	2.00158	1.976876	2.716434	1.928249	2.026767526	1.723789	5.219402
2021-G-080	*C21FEB25A0021.csv*	*do not use*	*2.17789*	*1.95844*	*2.09714*	*2.17503*	*3.291621358*	*1.85308*	*8.28426*
2021-G-080	*C21FEB25A0021.csv*	*do not use*	*2.12472*	*2.03834*	*2.31863*	*2.16694*	*3.203542816*	*1.8456*	*8.54266*
2021-G-080	*C21MAY14A0227.csv*	*do not use, inclusions*	*2.71392*	*2.72389*	*3.19388*	*2.79525*	*2.929864226*	*1.79749*	*5.87461*
2021-G-080	*C21MAY14A0237.csv*	*do not use, inclusions*	*5.64276*	*4.90701*	*4.81612*	*4.3021*	*4.007363172*	*2.48122*	*7.28419*
2021-G-080	*C21MAY14A0256.csv*	*do not use, inclusions*	*2.49181*	*3.85793*	*4.77308*	*3.9673*	*3.72894697*	*1.97757*	*5.03812*

Analysis	Source Filename	Comment	204Pb	206Pb	207Pb	208Pb	232Th	235U	238U
			1s%	1s%	1s%	1s%	1s%	1s%	1s%
ZY-LG-2 (Two-mica leucogranite)									
2021-G-080	C21MAY14A0268.csv	concordant	15.04794	1.462357	3.171051	6.374547	2.090258	4.369185051	1.25877
2021-G-080	C21MAY14A0241.csv	minor common Pb	13.98336	4.72226	6.189073	8.471276	3.015412	5.899890761	4.161264
2021-G-080	C21FEB25A0034.csv	young, some common Pb	3.280398	2.093059	4.541066	11.48077	1.618771	4.262690975	2.053304
2021-G-080	C21MAY14A0260.csv	concordant	14.67616	2.936804	3.879591	7.957801	2.648351	4.838272366	2.423888
2021-G-080	C21FEB25A0007.csv	high U, young concordant	1.955188	1.904601	3.675015	10.08128	1.119914	4.110516337	1.698469
2021-G-080	C21MAY14A0242.csv	minor common Pb	10.68392	5.318184	6.612029	10.79431	6.053477	6.321305028	4.572181
2021-G-080	C21MAY14A0234.csv	concordant	15.97323	2.085404	5.430697	17.72304	3.519676	4.481783393	1.418627
2021-G-080	C21MAY14A0264.csv	younger	33.58183	3.561954	19.56181	31.4077	3.977986	5.765186534	2.832074
2021-G-080	C21FEB25A0032.csv	comm Pb or Pb loss	2.00357	2.962134	4.79665	19.34725	3.36825	4.653178245	2.766398
2021-G-080	C21MAY14A0232.csv	High common Pb	23.25876	12.09276	13.34569	14.62889	16.06924	14.50017735	13.70091
2021-G-080	C21MAY14A0228.csv	older	23.63216	1.554538	2.556078	21.12616	1.634757	4.482395742	1.575888
2021-G-080	C21FEB25A0020.csv	Comm Pb or Pb loss	3.271844	1.89725	1.994746	2.53685	1.659786	4.127834171	1.731609
2021-G-080	C21MAY14A0230.csv	younger	22.4238	2.904791	3.608083	4.692154	3.019575	4.816572136	1.585457
2021-G-080	C21MAY14A0269.csv	younger	42.98081	3.283615	3.949735	8.78727	2.718445	4.669450969	1.35966
2021-G-080	C21MAY14A0225.csv	minor common Pb	55.76839	2.351338	3.715334	3.288258	2.173959	4.756674533	1.747407

2021-G-080	C21FEB25A0008.csv	moderate U, concordant	2.036537	1.95548	2.150345	4.318316	1.397472	4.288727817	1.963341
2021-G-080	C21MAY14A0236.csv	minor common Pb	13.94103	1.213433	1.745419	3.150271	1.41152	4.487915193	1.241161
2021-G-080	C21MAY14A0230.csv	older	35.15228	2.532571	3.258722	4.573315	4.219526	5.680146636	2.705932
2021-G-080	C21FEB25A0033.csv	comm Pb or Pb loss	18.28321	1.903257	2.137768	4.981839	2.019769	4.268941166	2.051867
2021-G-080	C21FEB25A0033.csv	comm Pb or Pb loss	2.272042	2.054733	2.123049	4.074141	3.444156	4.1852948	1.877453
2021-G-080	C21FEB25A0033.csv	comm Pb or Pb loss	32.02328	2.027069	2.117043	3.355869	2.239361	4.24649956	2.00611
2021-G-080	C21MAY14A0266.csv	concordant	15.06547	1.528442	1.89537	1.682195	0.968545	4.509828531	1.160821
2021-G-080	C21MAY14A0229.csv	Pb loss; use 7-6 ratio	13.91265	1.746746	1.918894	3.843953	2.654456	4.663056963	1.984758
2021-G-080	C21FEB25A0022.csv	minor common Pb	1.959131	1.766412	1.963689	2.031932	1.04877	4.212559791	1.690054
2021-G-080	C21MAY14A0267.csv	concordant	16.49062	4.336578	4.417905	6.224712	6.284021	6.024564544	4.240792
2021-G-080	C21MAY14A0233.csv	Pb loss; use 7-6 ratio	14.39022	1.321519	1.46531	2.540687	7.633477	4.520033095	1.662033
2021-G-080	C21MAY14A0231.csv	Pb loss; use 7-6 ratio	27.71547	1.406947	1.641137	2.755483	2.401938	4.526661541	1.704306
2021-G-080	C21FEB25A0006.csv	high U, Pb loss, use 7/6	2.474686	2.23958	2.318741	3.017084	2.252382	4.190343133	1.882354
2021-G-080	C21MAY14A0263.csv	Pb loss; use 7-6 ratio	66.27822	1.167881	1.418355	1.333737	1.224003	4.386925821	1.14989
2021-G-080	C21MAY14A0270.csv	Pb loss; use 7-6 ratio	23.49195	1.385	2.602758	2.56309	1.316653	5.46414269	1.436684
2021-G-080	C21FEB25A0009.csv	high U, Pb loss, use 7/6	29.84113	1.90207	2.060902	2.129351	1.357445	4.286761089	1.886833
2021-G-080	C21MAY14A0240.csv	Pb loss; use 7-6 ratio	20.78189	3.056579	3.550718	3.59958	2.459085	5.611800882	3.427672
2021-G-080	C21MAY14A0226.csv	high U, Pb loss, common Pb	15.53266	1.207777	1.477658	1.941594	1.501936	5.144383075	2.924081
2021-G-080	C21FEB25A0024.csv	Pb loss, use 7/6	1.832116	2.313687	2.301535	2.538114	1.079786	4.212153288	1.840923
2021-G-080	C21FEB25A0029.csv	Comm Pb or Pb loss	1.713652	2.050974	2.12771	2.52688	1.251454	4.188278432	1.732847
2021-G-080	C21FEB25A0033.csv	high U, Pb loss, use 7/6	1.966859	2.031742	1.932433	3.283236	1.943651	4.182509358	1.880805
2021-G-080	C21FEB25A0031.csv	Comm Pb or Pb loss	2.20127	1.831274	1.873299	2.400156	1.361751	4.177066943	1.704549
2021-G-080	C21MAY14A0264.csv	Pb loss; use 7-6 ratio	22.18465	1.852718	2.709725	4.204803	3.324843	4.878661725	2.234994
2021-G-080	C21MAY14A0261.csv	Pb loss; use 7-6 ratio	15.92904	1.380407	1.561287	2.782015	2.343351	4.882197229	1.664712

2021-G-080	C21MAY14A0269.csv	older	23.76781	1.993528	2.618941	2.874203	2.023226	9.474605392	2.556976
2021-G-080	C21MAY14A0249.csv	Pb loss; use 7-6 ratio	269.711	1.203753	1.597447	1.84826	1.075232	4.723224091	1.660109
2021-G-080	C21MAY14A0238.csv	Pb loss; use 7-6 ratio	18.99224	1.401355	2.360537	3.98063	1.528139	4.93273838	1.384237
2021-G-080	C21FEB25A0019.csv	Pb loss likely, use 7/6	2.193106	4.011034	3.904353	2.851796	2.012749	11.00444561	3.55752
2021-G-080	C21MAY14A0255.csv	Pb loss; use 7-6 ratio	16.59775	1.284174	1.359752	4.087357	4.26462	4.533201057	1.559887
2021-G-080	C21MAY14A0257.csv	Pb loss; use 7-6 ratio	37.26325	2.659703	2.693498	2.985402	2.291818	4.7483002	2.09277
2021-G-080	C21FEB25A0011.csv	high U, Pb loss, use 7/6	2.92736	2.413861	2.435095	2.182013	1.210171	4.871410327	2.947909
2021-G-080	C21FEB25A0010.csv	high U, Pb loss, use 7/6	60.87334	1.779797	1.868506	2.368994	1.285255	4.194371703	1.709642
2021-G-080	C21FEB25A0023.csv	high U, Pb loss, use 7/6	1.823487	1.838961	1.854417	3.187797	2.793743	4.887646295	3.129039
2021-G-080	C21FEB25A0030.csv	high U, Pb loss, use 7/6	2.210651	1.788973	1.769331	2.018689	1.248252	4.133164447	1.754967
2021-G-080	C21MAY14A0253.csv	Pb loss; use 7-6 ratio	9.148802	2.786631	2.851189	4.981091	3.221049	4.686993314	1.868913
2021-G-080	C21FEB25A0005.csv	high U, Pb loss, use 7/6	12.38016	1.887046	1.87976	1.9523	1.533098	4.535846023	2.49939
2021-G-080	C21FEB25A0018.csv	Pb mobility, use 7/6	2.422361	1.910311	1.935098	3.513763	2.937648	4.289969429	1.960456
2021-G-080	C21MAY14A0254.csv	Pb loss; use 7-6 ratio	37.46759	1.341172	1.434415	1.636979	1.738766	4.363963176	1.156057
2021-G-080	C21MAY14A0251.csv	use 7-6 ratio	29.39882	1.440268	1.685607	1.730531	1.334137	4.518459322	1.196468
2021-G-080	C21MAY14A0259.csv	Pb loss; use 7-6 ratio	20.23709	3.877027	3.897127	4.364133	4.769436	4.924160202	2.537791
2021-G-080	C21MAY14A0258.csv	Pb loss; use 7-6 ratio	14.85135	5.509293	5.561359	6.673008	7.16894	6.145910326	4.43302
2021-G-080	C21MAY14A0262.csv	Pb loss; use 7-6 ratio	20.925	2.335168	2.682782	3.745629	2.660239	5.281175849	2.774294
2021-G-080	C21MAY14A0239.csv	Pb loss; use 7-6 ratio	20.94052	1.484264	1.68074	1.59432	1.138196	4.425943133	1.302037
2021-G-080	C21MAY14A0265.csv	Pb loss; use 7-6 ratio	11.37246	1.810301	1.806414	2.695373	2.561828	4.630285728	1.902392
2021-G-080	C21MAY14A0235.csv	Pb loss; use 7-6 ratio	37.90723	1.745094	2.039444	3.036491	1.241632	4.815448224	1.870938
2021-G-080	C21MAY14A0250.csv	Pb loss; use 7-6 ratio	11.79011	1.61385	1.797916	5.255554	5.840728	4.804112249	1.615797
2021-G-080	C21MAY14A0252.csv	Pb loss; use 7-6 ratio	19.75479	1.795826	1.847666	1.752601	1.207892	4.488816988	1.337842

2021-G-080	*C21FEB25A0021.csv*	*do not use*	*1.77889*	*1.8309*	*1.94084*	*2.86787*	*1.91603*	*4.460927773*	*2.21001*
2021-G-080	*C21FEB25A0021.csv*	*do not use*	*3.72248*	*1.98013*	*1.90091*	*2.21486*	*1.26686*	*4.425653746*	*2.00788*
2021-G-080	*C21MAY14A0227.csv*	*do not use, inclusions*	*16.2171*	*7.10226*	*7.41041*	*7.96287*	*2.15151*	*5.507236382*	*3.58541*
2021-G-080	*C21MAY14A0237.csv*	*do not use, inclusions*	*19.0211*	*3.60536*	*4.88152*	*6.59532*	*2.88609*	*14.19223017*	*13.4274*
2021-G-080	*C21MAY14A0256.csv*	*do not use, inclusions*	*10.0474*	*5.95911*	*8.08488*	*8.83796*	*2.32688*	*5.058362205*	*2.65808*

APPENDIX C 1.2 U-Th-Pb isotope (LA-ICPMS) data for two-mica leucogranite (ZY-LG-2) and tourmaline leucogranites (ZY-LGT-1) and REE variations in monazites.

Analysis	Source Filename	Comment	Preferred Age	Preferred Age	207 corr $^{206}Pb/^{238}U$	207 corr $^{206}Pb/^{238}U$	$^{238}U/^{206}Pb$	$^{238}U/^{206}Pb$	$^{207}Pb/^{206}Pb$
			Ma	2s%	Age	2s%	ratio	1s%	ratio
	ZY-LG-2								
2021-G-604	C21DEC08A0054.csv		13.94347799	2.893478536	13.94347799	2.8934785	454.865815	1.351354367	0.058765823
2021-G-604	C21DEC08A0021.csv		13.98382854	1.553414285	13.98382854	1.5534143	453.574097	0.742498417	0.057861929
2021-G-604	C21DEC08A0055.csv	high common Pb	14.05623752	4.715393969	14.05623752	4.715394	371.0613646	1.801950513	0.197073753
2021-G-604	C21DEC08A0045.csv	high common Pb	14.09531258	3.65261381	14.09531258	3.6526138	443.6901603	1.611129087	0.070701918
2021-G-604	C21DEC08A0011.csv	high common Pb	14.13247128	5.748491864	14.13247128	5.7484919	343.6580033	2.066990165	0.242452056
2021-G-604	C21DEC08A0047.csv		14.14057763	1.727556428	14.14057763	1.7275564	448.8304815	0.840170426	0.056667573
2021-G-604	C21DEC08A0022.csv		14.23630945	2.985210352	14.23630945	2.9852104	443.6487629	1.521699465	0.062059725
2021-G-604	C21DEC08A0046.csv		14.31338548	1.83649627	14.31338548	1.8364963	439.9792455	0.901757698	0.063288444
2021-G-604	C21DEC08A0018.csv		14.34930197	2.097768472	14.34930197	2.0977685	439.3179394	1.027174492	0.061876057
2021-G-604	C21DEC08A0056.csv		14.40638951	4.123219798	14.40638951	4.1232198	430.1843593	1.977663398	0.075438056
2021-G-604	C21DEC08A0022.csv	high common Pb	14.48316241	2.741607598	14.48316241	2.7416076	417.5106136	1.290232805	0.095607552
2021-G-604	C21DEC08A0023.csv		14.50213687	2.713947286	14.50213687	2.7139473	425.0470321	1.355392676	0.078322377

2021-G-604	C21DEC08A0059.csv		14.5286062	2.268803186	14.5286062	2.2688032	434.2474997	1.025662007	0.061979486
2021-G-604	C21DEC08A0029.csv	high common Pb	14.97144551	6.567209481	14.97144551	6.5672095	265.1800722	1.80970323	0.351692337
2021-G-604	C21DEC08A0044.csv		14.57031533	2.177404293	14.57031533	2.1774043	432.7512077	0.995971604	0.062386595
2021-G-604	C21DEC08A0035.csv		14.57293253	2.149075475	14.57293253	2.1490755	429.1245419	0.958077611	0.068452895
2021-G-604	C21DEC08A0032.csv		14.63849947	2.275294765	14.63849947	2.2752948	429.1182289	1.00711689	0.065360092
2021-G-604	C21DEC08A0011.csv		14.64007804	2.757566847	14.64007804	2.7575668	423.7646607	1.213556748	0.075108162
2021-G-604	C21DEC08A0030.csv		14.65315101	2.045017182	14.65315101	2.0450172	425.8213029	0.941936621	0.070870318
2021-G-604	C21DEC08A0006.csv		14.67632913	2.532479293	14.67632913	2.5324793	417.3767465	1.194999454	0.084945888
2021-G-604	C21DEC08A0009.csv		14.72375517	2.295024598	14.72375517	2.2950246	425.7751788	1.005298026	0.067956987
2021-G-604	C21DEC08A0024.csv		14.78668091	2.312389876	14.78668091	2.3123899	409.6097247	1.043298028	0.092962183
2021-G-604	C21DEC08A0034.csv		14.79658408	2.093337091	14.79658408	2.0933371	420.4650028	0.994434629	0.071003282
2021-G-604	C21DEC08A0007.csv		14.81030083	2.36607899	14.81030083	2.366079	413.7952757	1.107350818	0.082819871
2021-G-604	C21DEC08A0005.csv		14.85779869	2.273017686	14.85779869	2.2730177	424.6869173	1.043535072	0.062146845
2021-G-604	C21DEC08A0023.csv	high common Pb	14.87049988	5.694894381	14.87049988	5.6948944	380.8465859	2.030876294	0.147769272
2021-G-604	C21DEC08A0043.csv		14.90127906	2.2654163	14.90127906	2.2654163	418.3495859	1.059231907	0.07027703
2021-G-604	C21DEC08A0057.csv		14.95898796	2.692560095	14.95898796	2.6925601	415.4481747	1.11505374	0.073591606

2021-G-604	C21DEC08A0048.csv		14.96364664	3.329032323	14.96364664	3.3290323	419.9961362	1.592682028	0.061620862
2021-G-604	C21DEC08A0033.csv		14.9809814	2.54115181	14.9809814	2.5411518	411.1987224	1.164783421	0.080357016
2021-G-604	C21DEC08A0010.csv		15.03243007	1.899172463	15.03243007	1.8991725	419.3963001	0.929013857	0.063729418
2021-G-604	C21DEC08A0031.csv		15.07973143	2.511479218	15.07973143	2.5114792	417.8668032	1.159496537	0.063838156
2021-G-604	C21DEC08A0055.csv		15.13168099	2.637511785	15.13168099	2.6375118	413.2235218	1.197864152	0.071068338
2021-G-604	C21DEC08A0020.csv		15.13601322	1.878702163	15.13601322	1.8787022	418.4219823	0.859520677	0.059681524
2021-G-604	C21DEC08A0058.csv		15.14672348	2.427360501	15.14672348	2.4273605	415.4981874	1.093553935	0.061102854
2021-G-604	C21DEC08A0019.csv		15.36566074	2.289969184	15.36566074	2.2899692	413.371701	1.048171496	0.055903568
2021-G-604	C21DEC08A0042.csv		15.40006299	3.65263302	15.40006299	3.652633	412.0382357	1.703381203	0.060134707
2021-G-604	C21DEC08A0042.csv	high common Pb	15.4678675	5.573811342	15.4678675	5.5738113	401.0276489	2.049962013	0.078825538
2021-G-604	C21DEC08A0029.csv		15.76926182	4.668569468	15.76926182	4.6685695	358.6486687	1.770633639	0.140894443
2021-G-604	C21DEC08A0008.csv		17.50703567	1.8595705	17.50703567	1.8595705	365.546027	0.919431063	0.050996208
2021-G-604	C21DEC08A0053.csv		472.2835245	1.742612905	472.2835245	1.7426129	13.14105453	0.920520623	0.056679619

Analysis	Source Filename	Comment	$^{207}Pb/^{206}Pb$	$^{207}Pb/^{235U}$(calc)	$^{207}Pb/^{235}U$(calc)	$^{206}Pb/^{238}U$
			1s%	ratio	1s%	ratio
	ZY-LG-2					
2021-G-604	C21DEC08A0054.csv		4.783618585	0.016961712	4.798940701	0.002199992
2021-G-604	C21DEC08A0021.csv		1.953527745	0.016488154	2.337087379	0.002203802
2021-G-604	C21DEC08A0055.csv	high common Pb	4.205204767	0.072993001	4.010259111	0.002697323
2021-G-604	C21DEC08A0045.csv	high common Pb	6.222680747	0.021898481	6.539020174	0.002258627
2021-G-604	C21DEC08A0011.csv	high common Pb	4.07802412	0.096876367	3.835940618	0.002918934
2021-G-604	C21DEC08A0047.csv		2.548669632	0.016201104	2.658102757	0.002225111
2021-G-604	C21DEC08A0022.csv		4.850251814	0.018143636	5.335809209	0.002255782
2021-G-604	C21DEC08A0046.csv		2.509422597	0.018661122	2.688479335	0.002271608
2021-G-604	C21DEC08A0018.csv		2.799243789	0.0184008	2.948009248	0.00227316
2021-G-604	C21DEC08A0056.csv		6.932449085	0.024143967	6.781847971	0.002322874
2021-G-604	C21DEC08A0022.csv	high common Pb	2.506343203	0.029145102	2.65879198	0.002398823
2021-G-604	C21DEC08A0023.csv		3.798216941	0.024200199	3.894900743	0.002347218
2021-G-604	C21DEC08A0059.csv		3.472356601	0.018757261	3.590317144	0.002301894
2021-G-604	C21DEC08A0029.csv	high common Pb	3.467181688	0.182295794	3.579646962	0.003787605
2021-G-604	C21DEC08A0044.csv		3.088176436	0.018494553	3.208028174	0.002309721
2021-G-604	C21DEC08A0035.csv		3.41218029	0.02119418	3.389994773	0.00232838
2021-G-604	C21DEC08A0032.csv		3.447647745	0.020706715	3.529254172	0.002329485
2021-G-604	C21DEC08A0011.csv		4.055879633	0.023715077	4.075535841	0.002359559

2021-G-604	C21DEC08A0030.csv		3.349167625	0.021259538	3.446164263	0.002348598
2021-G-604	C21DEC08A0006.csv		3.804162337	0.027785663	3.825707536	0.002396363
2021-G-604	C21DEC08A0009.csv		3.319498428	0.020902677	3.429443157	0.002350978
2021-G-604	C21DEC08A0024.csv		3.181731668	0.031023787	3.307826525	0.002440419
2021-G-604	C21DEC08A0034.csv		3.260289079	0.023013944	3.350222155	0.002372016
2021-G-604	C21DEC08A0007.csv		3.875651079	0.027213629	3.958464481	0.002411434
2021-G-604	C21DEC08A0005.csv		4.019011137	0.019982393	4.15115571	0.002354599
2021-G-604	C21DEC08A0023.csv	high common Pb	5.346388089	0.053588935	5.122556259	0.002649488
2021-G-604	C21DEC08A0043.csv		3.563703134	0.022964232	3.62795461	0.002386548
2021-G-604	C21DEC08A0057.csv		3.723220475	0.024280451	3.802766219	0.002406205
2021-G-604	C21DEC08A0048.csv		6.120381217	0.019906841	6.049648431	0.002369777
2021-G-604	C21DEC08A0033.csv		3.783417552	0.026732706	3.813360542	0.002431301
2021-G-604	C21DEC08A0010.csv		2.576496886	0.019716644	2.742419711	0.002387173
2021-G-604	C21DEC08A0031.csv		4.187729364	0.020911213	4.216232216	0.002395028
2021-G-604	C21DEC08A0055.csv		4.053037771	0.02212775	4.340967278	0.002425982
2021-G-604	C21DEC08A0020.csv		2.903225872	0.018725481	3.213060544	0.002391112
2021-G-604	C21DEC08A0058.csv		3.70807008	0.019660383	3.776603336	0.002397191
2021-G-604	C21DEC08A0019.csv		3.573160543	0.017523865	3.771900938	0.002415674
2021-G-604	C21DEC08A0042.csv		6.770991463	0.020050396	6.672008963	0.002434279
2021-G-604	C21DEC08A0042.csv	high common Pb	7.331567825	0.027059927	7.159240711	0.002505307
2021-G-604	C21DEC08A0029.csv		5.472816425	0.053791647	6.334967654	0.002781968
2021-G-604	C21DEC08A0008.csv		2.892531964	0.018057877	3.051126912	0.002735441

2021-G-604	C21DEC08A0053.csv		0.631256932	0.565223601	1.491256336	0.076029796

Analysis	Source Filename	Comment					Rho	$^{208}Pb/^{232}Th$	$^{208}Pb/^{232}Th$
								ratio	1s%
	ZY-LG-2								
2021-G-604	C21DEC08A0054.csv		0.017813	4.970831	0.002198	1.351354	0.271857	0.000718	2.19665
2021-G-604	C21DEC08A0021.csv		0.017589	2.089874	0.002205	0.742498	0.355284	0.000683	1.162283
2021-G-604	C21DEC08A0055.csv	high common Pb	0.073229	4.575016	0.002695	1.801951	0.393868	0.000821	1.866117
2021-G-604	C21DEC08A0045.csv	high common Pb	0.021971	6.427868	0.002254	1.611129	0.250647	0.000688	1.406828
2021-G-604	C21DEC08A0011.csv	high common Pb	0.097275	4.57195	0.00291	2.06699	0.452103	0.000843	1.977355
2021-G-604	C21DEC08A0047.csv		0.017408	2.68358	0.002228	0.84017	0.313078	0.00067	1.180111
2021-G-604	C21DEC08A0022.csv		0.019287	5.083356	0.002254	1.521699	0.299349	0.000674	1.539585
2021-G-604	C21DEC08A0046.csv		0.019833	2.666527	0.002273	0.901758	0.338177	0.000679	1.163385
2021-G-604	C21DEC08A0018.csv		0.01942	2.981753	0.002276	1.027174	0.344487	0.000689	1.164961
2021-G-604	C21DEC08A0056.csv		0.024179	7.209022	0.002325	1.977663	0.274332	0.000724	1.803165
2021-G-604	C21DEC08A0022.csv	high common Pb	0.031574	2.818946	0.002395	1.290233	0.4577	0.000748	1.53738
2021-G-604	C21DEC08A0023.csv		0.025407	4.032808	0.002353	1.355393	0.336092	0.000692	1.365549
2021-G-604	C21DEC08A0059.csv		0.019679	3.620669	0.002303	1.025662	0.28328	0.000682	1.250874
2021-G-604	C21DEC08A0029.csv	high common Pb	0.182862	3.911058	0.003771	1.809703	0.462714	0.00087	1.655475
2021-G-604	C21DEC08A0044.csv		0.019877	3.24481	0.002311	0.995972	0.306943	0.00068	1.258484
2021-G-604	C21DEC08A0035.csv		0.021994	3.544134	0.00233	0.958078	0.270328	0.000696	1.161504
2021-G-604	C21DEC08A0032.csv		0.021001	3.591735	0.00233	1.007117	0.280398	0.000692	1.163427
2021-G-604	C21DEC08A0011.csv		0.024438	4.233542	0.00236	1.213557	0.286653	0.000686	1.246059
2021-G-604	C21DEC08A0030.csv		0.022948	3.479105	0.002348	0.941937	0.270741	0.000692	1.214334
2021-G-604	C21DEC08A0006.csv		0.028062	3.98744	0.002396	1.194999	0.299691	0.000691	1.166339
2021-G-604	C21DEC08A0009.csv		0.022007	3.468385	0.002349	1.005298	0.289846	0.000713	1.202157
2021-G-604	C21DEC08A0024.csv		0.031292	3.348416	0.002441	1.043298	0.31158	0.000701	1.15181
2021-G-604	C21DEC08A0034.csv		0.023284	3.408575	0.002378	0.994435	0.291745	0.00069	1.135006
2021-G-604	C21DEC08A0007.csv		0.027596	4.030744	0.002417	1.107351	0.274726	0.00069	1.206007
2021-G-604	C21DEC08A0005.csv		0.020177	4.152278	0.002355	1.043535	0.251316	0.000682	1.133112

2021-G-604	C21DEC08A0023.csv	high common Pb	0.053498	5.719119	0.002626	2.030876	0.355103	0.000779	2.038286
2021-G-604	C21DEC08A0043.csv		0.023162	3.717789	0.00239	1.059232	0.284909	0.000687	1.18186
2021-G-604	C21DEC08A0057.csv		0.024424	3.886607	0.002407	1.115054	0.286896	0.00069	1.147655
2021-G-604	C21DEC08A0048.csv		0.020229	6.324216	0.002381	1.592682	0.251839	0.000701	1.330754
2021-G-604	C21DEC08A0033.csv		0.026945	3.958657	0.002432	1.164783	0.294237	0.000688	1.145453
2021-G-604	C21DEC08A0010.csv		0.020952	2.738869	0.002384	0.929014	0.339196	0.000691	1.15815
2021-G-604	C21DEC08A0031.csv		0.021064	4.345286	0.002393	1.159497	0.26684	0.000684	1.198313
2021-G-604	C21DEC08A0055.csv		0.023713	4.226345	0.00242	1.197864	0.283428	0.000701	1.362601
2021-G-604	C21DEC08A0020.csv		0.019666	3.027787	0.00239	0.859521	0.283877	0.00071	1.183713
2021-G-604	C21DEC08A0058.csv		0.020277	3.86596	0.002407	1.093554	0.282867	0.000698	1.177101
2021-G-604	C21DEC08A0019.csv		0.018647	3.723727	0.002419	1.048171	0.281485	0.000683	1.230416
2021-G-604	C21DEC08A0042.csv		0.020123	6.981965	0.002427	1.703381	0.243969	0.000685	1.33377
2021-G-604	C21DEC08A0042.csv	high common Pb	0.027102	7.612768	0.002494	2.049962	0.269279	0.000691	1.514524
2021-G-604	C21DEC08A0029.csv		0.054166	5.752118	0.002788	1.770634	0.307823	0.000725	1.460264
2021-G-604	C21DEC08A0008.csv		0.019235	3.035143	0.002736	0.919431	0.302928	0.000692	1.164919
2021-G-604	C21DEC08A0053.csv		0.5947	1.116174	0.076097	0.920521	0.824711	0.023961	1.194395

Analysis	Source Filename	Comment	Preferred Age	Preferred Age	207 corr $^{206}Pb/^{238}U$	207 corr $^{206}Pb/^{238}U$	$^{238}U/^{206}Pb$	$^{238}U/^{206}Pb$	$^{207}Pb/^{206}Pb$
			Ma	2s%	Age	2s%	ratio	1s%	ratio
	ZY-LGT-1								
2021-G-605	C21DEC08A0114.csv		13.34136102	1.752010507	13.34136	1.752011	474.1462	0.887306	0.06166
2021-G-605	C21DEC08A0082.csv		13.37682016	1.276273722	13.37682	1.276274	479.7981	0.631521	0.049248
2021-G-605	C21DEC08A0077.csv		13.38294125	1.445591556	13.38294	1.445592	478.4717	0.714752	0.050507
2021-G-605	C21DEC08A0096.csv		13.46711302	1.504486947	13.46711	1.504487	474.609	0.765724	0.052501
2021-G-605	C21DEC08A0081.csv		13.48314571	1.443288974	13.48315	1.443289	474.403	0.710193	0.051515
2021-G-605	C21DEC08A0068.csv		13.55514902	1.689618229	13.55515	1.689618	472.4093	0.839823	0.05062
2021-G-605	C21DEC08A0101.csv		13.56110968	1.403991817	13.56111	1.403992	471.5499	0.700586	0.051285
2021-G-605	C21DEC08A0092.csv		13.57321069	1.659318658	13.57321	1.659319	469.9091	0.834605	0.053133
2021-G-605	C21DEC08A0102.csv		13.61487876	1.424889601	13.61488	1.42489	470.5214	0.675059	0.050122
2021-G-605	C21DEC08A0083.csv		13.68782559	1.677319826	13.68783	1.67732	461.7927	0.807171	0.061353
2021-G-605	C21DEC08A0071.csv	high common Pb	13.70106356	2.402065342	13.70106	2.402065	430.5031	1.106346	0.114939
2021-G-605	C21DEC08A0114.csv	high common Pb	14.08002155	5.230828778	14.08002	5.230829	248.689	1.283425	0.407634
2021-G-605	C21DEC08A0095.csv		13.82464996	1.638415295	13.82465	1.638415	459.5929	0.783163	0.05607
2021-G-605	C21DEC08A0094.csv		13.84909616	2.01248873	13.8491	2.012489	458.3274	1.012238	0.059891
2021-G-605	C21DEC08A0119.csv		13.86101834	1.619030273	13.86102	1.61903	460.9507	0.781677	0.052704

2021-G-605	C21DEC08A0116.csv		13.91128933	1.498455923	13.91129	1.498456	458.6562	0.726282	0.053476
2021-G-605	C21DEC08A0071.csv		13.94392242	1.800809145	13.94392	1.800809	459.0236	0.907961	0.052912
2021-G-605	C21DEC08A0093.csv		13.94896146	1.671060889	13.94896	1.671061	454.1831	0.813496	0.059106
2021-G-605	C21DEC08A0069.csv	high common Pb	13.9805688	4.272253543	13.98057	4.272254	399.8821	1.750879	0.151166
2021-G-605	C21DEC08A0090.csv		14.02734391	1.732396649	14.02734	1.732397	455.3081	0.921663	0.054205
2021-G-605	C21DEC08A0080.csv		14.16081884	2.219149651	14.16082	2.21915	451.3842	1.053921	0.053641
2021-G-605	C21DEC08A0078.csv		14.17292983	1.483438587	14.17293	1.483439	450.2331	0.709853	0.053094
2021-G-605	C21DEC08A0104.csv		14.18766815	2.70611471	14.18767	2.706115	429.7541	1.192453	0.088556
2021-G-605	C21DEC08A0118.csv		14.22970863	1.930349168	14.22971	1.930349	446.6699	0.913217	0.055871
2021-G-605	C21DEC08A0107.csv		14.31502541	1.848672964	14.31503	1.848673	434.9223	0.892228	0.069233
2021-G-605	C21DEC08A0067.csv		14.50829108	2.550839151	14.50829	2.550839	442.019	1.247739	0.053251
2021-G-605	C21DEC08A0103.csv		14.51923035	2.162645036	14.51923	2.162645	435.277	1.036685	0.060794
2021-G-605	C21DEC08A0079.csv		14.5392118	2.019582516	14.53921	2.019583	433.7539	0.926762	0.062744
2021-G-605	C21DEC08A0070.csv		14.54736166	3.7972485	14.54736	3.797248	436.6933	1.909976	0.06107
2021-G-605	C21DEC08A0115.csv		14.55586956	1.428940376	14.55587	1.42894	440.6529	0.701894	0.050028
2021-G-605	C21DEC08A0105.csv		14.5612557	2.245730804	14.56126	2.245731	438.6289	1.077443	0.052695
2021-G-605	C21DEC08A0072.csv		14.65841208	2.309375885	14.65841	2.309376	423.2283	1.103412	0.074832

2021-G-605	C21DEC08A0066.csv		14.77332642	1.870446508	14.77333	1.870447	429.6463	0.9286	0.058381
2021-G-605	C21DEC08A0120.csv		14.80961428	2.225951196	14.80961	2.225951	421.6304	0.939712	0.067881
2021-G-605	C21DEC08A0091.csv		14.82363862	2.426106302	14.82364	2.426106	421.3372	1.123559	0.069221
2021-G-605	C21DEC08A0106.csv		14.86539659	2.210092581	14.8654	2.210093	422.0363	0.980976	0.068161
2021-G-605	C21DEC08A0069.csv		14.92820575	3.373944175	14.92821	3.373944	418.9086	1.43807	0.066336
2021-G-605	C21DEC08A0117.csv		15.3016775	2.979112746	15.30168	2.979113	404.0964	1.347426	0.078035

Analysis	Source Filename	Comment	$^{207}Pb/^{206}Pb$	$^{207}Pb/^{235}U$(calc)	$^{207}Pb/^{235}U$(calc)	$^{206}Pb/^{238}U$	$^{206}Pb/^{238}U$	
			1s%	ratio	1s%	ratio	1s%	
	ZY-LGT-1							
2021-G-605	C21DEC08A0114.csv		1.96938	0.017036	2.420155	0.002113	0.862139	0.017931
2021-G-605	C21DEC08A0082.csv		0.984506	0.01322	1.497847	0.002085	0.635597	0.014152
2021-G-605	C21DEC08A0077.csv		1.378879	0.013633	1.759109	0.002089	0.717831	0.014554
2021-G-605	C21DEC08A0096.csv		1.624172	0.014193	1.95736	0.002108	0.744817	0.015252
2021-G-605	C21DEC08A0081.csv		1.552745	0.013966	1.883569	0.002108	0.714887	0.014972
2021-G-605	C21DEC08A0068.csv		1.585931	0.013597	1.930402	0.002117	0.839195	0.014774
2021-G-605	C21DEC08A0101.csv		1.551188	0.014195	1.893438	0.002119	0.695112	0.014996
2021-G-605	C21DEC08A0092.csv		1.637685	0.014694	1.941862	0.002126	0.82272	0.01559
2021-G-605	C21DEC08A0102.csv		1.567155	0.013726	1.910275	0.002124	0.705902	0.014688
2021-G-605	C21DEC08A0083.csv		3.289406	0.017279	3.514603	0.002167	0.797489	0.018319
2021-G-605	C21DEC08A0071.csv	high common Pb	2.528156	0.034017	2.945832	0.00233	1.126035	0.036812
2021-G-605	C21DEC08A0114.csv	high common Pb	2.018051	0.212164	2.758967	0.004025	1.433253	0.226004
2021-G-605	C21DEC08A0095.csv		2.224659	0.015687	2.451839	0.002174	0.803924	0.016821
2021-G-605	C21DEC08A0094.csv		3.027092	0.016953	3.139643	0.002188	0.979305	0.018017
2021-G-605	C21DEC08A0119.csv		1.833349	0.014799	2.226595	0.00217	0.800611	0.015765
2021-G-605	C21DEC08A0116.csv		1.794409	0.014951	2.093266	0.00218	0.73961	0.016076
2021-G-605	C21DEC08A0071.csv		2.597449	0.014812	2.648707	0.002184	0.883774	0.015894
2021-G-605	C21DEC08A0093.csv		1.940706	0.016758	2.20704	0.002202	0.822766	0.017943
2021-G-605	C21DEC08A0069.csv	high common Pb	5.071461	0.052023	5.327448	0.002503	1.811515	0.052122
2021-G-605	C21DEC08A0090.csv		2.876145	0.015473	3.042953	0.0022	0.843531	0.016415
2021-G-605	C21DEC08A0080.csv		2.360441	0.015341	2.573295	0.00222	1.098506	0.016385
2021-G-605	C21DEC08A0078.csv		1.914491	0.015195	2.112791	0.00222	0.730769	0.016259
2021-G-605	C21DEC08A0104.csv		3.832863	0.028339	3.845345	0.002328	1.273784	0.028412

2021-G-605	C21DEC08A0118.csv	2.635887	0.01598	2.809066	0.002237	0.947178	0.017247
2021-G-605	C21DEC08A0107.csv	2.565522	0.020655	2.731045	0.002289	0.894813	0.021948
2021-G-605	C21DEC08A0067.csv	3.389467	0.015732	3.504376	0.002273	1.255383	0.016611
2021-G-605	C21DEC08A0103.csv	3.651738	0.01795	3.532142	0.002297	1.043366	0.019257
2021-G-605	C21DEC08A0079.csv	3.160444	0.0187	3.311016	0.002306	0.977173	0.019945
2021-G-605	C21DEC08A0070.csv	5.343066	0.018119	5.315086	0.002302	1.852764	0.019282
2021-G-605	C21DEC08A0115.csv	1.844186	0.01473	2.048494	0.002271	0.705311	0.015654
2021-G-605	C21DEC08A0105.csv	3.09993	0.015129	3.235725	0.00228	1.104196	0.016564
2021-G-605	C21DEC08A0072.csv	3.602633	0.023285	3.658114	0.002362	1.099042	0.024379
2021-G-605	C21DEC08A0066.csv	2.736044	0.017566	2.96408	0.00233	0.912964	0.018735
2021-G-605	C21DEC08A0120.csv	3.069478	0.022024	3.181303	0.002364	1.079787	0.022198
2021-G-605	C21DEC08A0091.csv	3.073855	0.021194	3.18547	0.002371	1.181318	0.022652
2021-G-605	C21DEC08A0106.csv	3.253959	0.021795	3.347998	0.002374	1.066987	0.022268
2021-G-605	C21DEC08A0069.csv	5.076876	0.020993	4.937951	0.002379	1.630383	0.021834
2021-G-605	C21DEC08A0117.csv	4.545582	0.02656	4.522603	0.002476	1.414551	0.026626

Analysis	Source Filename	Comment				Rho	$^{208}Pb/^{232}Th$	$^{208}Pb/^{232}Th$
							ratio	1s%
	ZY-LGT-1							
2021-G-605	C21DEC08A0114.csv		2.16004	0.002109	0.887306	0.410782344	0.000740089	1.468820588
2021-G-605	C21DEC08A0082.csv		1.169646	0.002084	0.631521	0.539925183	0.00077837	1.430704642
2021-G-605	C21DEC08A0077.csv		1.553119	0.00209	0.714752	0.460204293	0.000667212	1.186719493
2021-G-605	C21DEC08A0096.csv		1.795625	0.002107	0.765724	0.426438782	0.000682697	1.363698767
2021-G-605	C21DEC08A0081.csv		1.707452	0.002108	0.710193	0.415937535	0.000664883	1.155434956
2021-G-605	C21DEC08A0068.csv		1.79457	0.002117	0.839823	0.467980029	0.000712055	1.31067893
2021-G-605	C21DEC08A0101.csv		1.702059	0.002121	0.700586	0.411610763	0.000662271	1.172556725
2021-G-605	C21DEC08A0092.csv		1.838091	0.002128	0.834605	0.454060779	0.00067895	1.164751571
2021-G-605	C21DEC08A0102.csv		1.706365	0.002125	0.675059	0.395612428	0.000655163	1.148074045
2021-G-605	C21DEC08A0083.csv		3.386993	0.002165	0.807171	0.238315085	0.000677009	1.465167924
2021-G-605	C21DEC08A0071.csv	high common Pb	2.759633	0.002323	1.106346	0.400903258	0.000838661	2.012219284
2021-G-605	C21DEC08A0114.csv	high common Pb	2.391591	0.004021	1.283425	0.536640507	0.003920703	3.164906982
2021-G-605	C21DEC08A0095.csv		2.358485	0.002176	0.783163	0.332061715	0.000662945	1.236693819
2021-G-605	C21DEC08A0094.csv		3.191851	0.002182	1.012238	0.317132002	0.000692174	1.328903768
2021-G-605	C21DEC08A0119.csv		1.993035	0.002169	0.781677	0.392204435	0.000649746	1.143961407
2021-G-605	C21DEC08A0116.csv		1.935818	0.00218	0.726282	0.375180973	0.000679829	1.230529465
2021-G-605	C21DEC08A0071.csv		2.75157	0.002179	0.907961	0.329979391	0.000684831	1.275710458
2021-G-605	C21DEC08A0093.csv		2.104309	0.002202	0.813496	0.386586032	0.000666167	1.211637337
2021-G-605	C21DEC08A0069.csv	high common Pb	5.365193	0.002501	1.750879	0.326340314	0.000733827	1.679642797
2021-G-605	C21DEC08A0090.csv		3.020211	0.002196	0.921663	0.305165243	0.00067616	1.332613639
2021-G-605	C21DEC08A0080.csv		2.585039	0.002215	1.053921	0.407700094	0.000660909	1.235305491
2021-G-605	C21DEC08A0078.csv		2.041854	0.002221	0.709853	0.347651155	0.000656563	1.134256902
2021-G-605	C21DEC08A0104.csv		4.014073	0.002327	1.192453	0.29706802	0.000682114	1.150021588
2021-G-605	C21DEC08A0118.csv		2.789599	0.002239	0.913217	0.327364783	0.000678405	1.372241985
2021-G-605	C21DEC08A0107.csv		2.716243	0.002299	0.892228	0.328478858	0.000671966	1.132640473
2021-G-605	C21DEC08A0067.csv		3.611833	0.002262	1.247739	0.345458566	0.000687172	1.351351147
2021-G-605	C21DEC08A0103.csv		3.796038	0.002297	1.036685	0.273096443	0.000674997	1.266759785
2021-G-605	C21DEC08A0079.csv		3.293523	0.002305	0.926762	0.281389172	0.000681217	1.188913668

2021-G-605	C21DEC08A0070.csv	5.674184	0.00229	1.909976	0.336608017	0.000703028	1.545645462
2021-G-605	C21DEC08A0115.csv	1.97324	0.002269	0.701894	0.355706221	0.000663482	1.132947062
2021-G-605	C21DEC08A0105.csv	3.281837	0.00228	1.077443	0.328304988	0.000661404	1.372425451
2021-G-605	C21DEC08A0072.csv	3.767822	0.002363	1.103412	0.292851535	0.00069563	1.377118183
2021-G-605	C21DEC08A0066.csv	2.889331	0.002327	0.9286	0.321389239	0.000698129	1.307039191
2021-G-605	C21DEC08A0120.csv	3.210102	0.002372	0.939712	0.292735876	0.000676065	1.167191601
2021-G-605	C21DEC08A0091.csv	3.272762	0.002373	1.123559	0.34330597	0.000694645	1.203341376
2021-G-605	C21DEC08A0106.csv	3.398612	0.002369	0.980976	0.288640123	0.000680544	1.169930052
2021-G-605	C21DEC08A0069.csv	5.27662	0.002387	1.43807	0.272536259	0.000684968	1.353068669
2021-G-605	C21DEC08A0117.csv	4.741084	0.002475	1.347426	0.284202186	0.000688343	1.297402447

Analysis	Source Filename	Comment	PO4	89Y	139La	140Ce	141Pr	146Nd	147Sm	153Eu	157Gd
			ppm	ppm	ppm	ppm	ppm	ppm	ppm	ppm	ppm
	ZY-LG-2										
2021-G-604	C21DEC08A0054.csv		392560	27447.1	93645.16	208615.2	25888.8	100198.8	25684.18	179.6963	20818.73
2021-G-604	C21DEC08A0021.csv		393828.6	32614.76	99478.79	207754.7	24731.24	94318.86	21788.14	278.3287	18277.23
2021-G-604	C21DEC08A0055.csv	high common Pb	395281.3	13859.08	124281.4	240540.8	27234.51	101683	17353.18	310.4675	11699.91
2021-G-604	C21DEC08A0045.csv	high common Pb	395674.4	11135.86	127830.9	248019.2	27391.89	102018.2	16117.97	260.1031	10474.09
2021-G-604	C21DEC08A0011.csv	high common Pb	393116.9	12009	121764.8	243317.4	26301.75	97336.04	16215.02	251.9993	10880.2
2021-G-604	C21DEC08A0047.csv		396042.5	28083.33	103710.7	222244.8	25971.05	98582.96	21059.43	271.9271	18531.9
2021-G-604	C21DEC08A0022.csv		393834.8	28163.71	98034.77	216360.5	25557.44	97925.87	21699.46	249.8343	19051.43
2021-G-604	C21DEC08A0046.csv		393534.4	21027.9	100857.4	225701.8	26625.44	102022.6	23409.28	157.5105	17867
2021-G-604	C21DEC08A0018.csv		395776.2	25238.89	106212.9	225939	25800.7	99259.8	21556.68	252.8052	17675.17
2021-G-604	C21DEC08A0056.csv		397330.7	10960.41	135782.3	248659.1	28027.56	103416.3	15163.65	260.4766	9714.006
2021-G-604	C21DEC08A0022.csv	high common Pb	393400	25922.67	99426.43	216979.3	25653.99	98565.8	23238.39	215.7425	18569.19
2021-G-604	C21DEC08A0023.csv		392891.7	20885.46	105681.8	222445.6	25813.52	100036.2	21705.06	213.3981	17375.71
2021-G-604	C21DEC08A0059.csv		393588.5	13277.92	128353.8	238602.3	26146.93	94755.18	15664.05	239.2384	10996.89
2021-G-604	C21DEC08A0029.csv	high common Pb	394479.3	8853.609	127182	250903.3	27446.37	101096.1	15002.26	285.3969	9575.717
2021-G-604	C21DEC08A0044.csv		392578	19934.5	95989.81	226427.9	26605.14	101490.7	26162.52	100.6063	18210.35

2021-G-604	C21DEC08A0035.csv		393524.8	13985.73	118119	236346.4	26731.31	102364.8	17734.66	268.8682	12435.83
2021-G-604	C21DEC08A0032.csv		395031.2	12498.39	129369	245371.2	27109.73	96146.75	15443.12	281.8212	10681.27
2021-G-604	C21DEC08A0011.csv		394071.9	13087.68	123357.4	238376.8	26573.09	102468.2	16033.6	249.7151	11664.85
2021-G-604	C21DEC08A0030.csv		393084.3	24246.31	102768.7	219820.5	25889.36	97454.57	21629.02	195.0687	17270.22
2021-G-604	C21DEC08A0006.csv		393320.4	10152.29	122852.1	241034.4	27415.44	104358.4	16371.77	232.7265	10343.9
2021-G-604	C21DEC08A0009.csv		393284.9	18483.36	106921.8	228987.4	25966.79	102377.5	21276.69	214.0807	15867.39
2021-G-604	C21DEC08A0024.csv		395053.5	17144.94	113054.3	236850.3	27140.87	103507.8	19271.76	272.9337	13901.36
2021-G-604	C21DEC08A0034.csv		393774.3	11086.13	124565.7	243588.2	26533.32	100895.1	15820.03	242.3959	10584.79
2021-G-604	C21DEC08A0007.csv		392694.1	10580.25	126235.6	238567	26223.01	100278.5	15691.09	234.5569	10504.43
2021-G-604	C21DEC08A0005.csv		393024.9	10316.89	120368.3	242909.1	26891.46	103873.1	15912.08	209.7388	10458.5
2021-G-604	C21DEC08A0023.csv	high common Pb	392270.3	21948.82	102870.1	219936.2	25390.02	97732.52	22930.57	233.1121	18101.07
2021-G-604	C21DEC08A0043.csv		393211.6	9718.951	127313.3	243738	26447.41	99504.64	15223.59	234.1525	10116.58
2021-G-604	C21DEC08A0057.csv		392701.3	10063.64	124805.3	240585.2	26483.18	101901	15238.37	223.9499	9987.745
2021-G-604	C21DEC08A0048.csv		394381.2	10784.2	134187.2	244272	26073.41	97496.86	13804.95	253.3739	8998.924
2021-G-604	C21DEC08A0033.csv		394001.2	8990.938	124152.3	245582.4	27688.78	104935.6	16282.03	250.4164	10526.8
2021-G-604	C21DEC08A0010.csv		393141.5	20883.72	105514.9	225344.2	25936.49	99981.05	21003.62	210.7207	16284.4
2021-G-604	C21DEC08A0031.csv		394329.2	6975.857	142394.4	251681.3	26567.17	94377.27	11686.97	235.4598	7015.087

2021-G-604	C21DEC08A0055.csv		393299.9	16208.05	111898.2	232603.5	26615.11	100535.6	20753.89	208.1462	14654.77
2021-G-604	C21DEC08A0020.csv		391565.5	14839.03	115895.6	227109.9	25904.74	101192.2	17938.59	326.1049	13158.73
2021-G-604	C21DEC08A0058.csv		394600.3	15211.23	120544.5	237882.1	26839.31	99327.28	18259.12	242.4117	12871.03
2021-G-604	C21DEC08A0019.csv		392015.1	14372.71	117150.8	230519.6	26384.48	100209.5	17156.82	335.5666	13097.98
2021-G-604	C21DEC08A0042.csv		393908.8	10542.82	125474.1	247689.8	26581.56	101006.7	13862.9	255.5904	8674.532
2021-G-604	C21DEC08A0042.csv	high common Pb	394237.8	11898.33	126177.9	244507	27060.05	100688.3	14210.32	260.4432	9011.115
2021-G-604	C21DEC08A0029.csv		393216.2	8908.864	129808.4	238349.9	26994.52	104368.5	15460.88	227.6104	9752.95
2021-G-604	C21DEC08A0008.csv		394308	23959.72	109332.5	225215.2	25403.2	97465.73	18734.92	180.8456	14917.13
2021-G-604	C21DEC08A0053.csv		392973.4	22758.8	108721.3	223601	25640.99	98595.96	17498.8	332.04	12583.44

Analysis	Source Filename	Comment	159Tb	163Dy	165Ho	166Er	169Tm	172Yb	175Lu
			ppm	ppm	ppm	ppm	ppm	ppm	ppm
	ZY-LG-2								
2021-G-604	C21DEC08A0054.csv		2602.223	9828.058	1062.488	1539	105.5697	358.754	25.36608
2021-G-604	C21DEC08A0021.csv		2400.225	9827.506	1233.177	2088.776	162.9904	609.697	50.30004
2021-G-604	C21DEC08A0055.csv	high common Pb	1180.667	4355.255	551.4208	874.9176	63.21003	221.181	18.67502
2021-G-604	C21DEC08A0045.csv	high common Pb	965.4887	3411.144	422.0685	732.272	53.51957	193.5834	18.51569
2021-G-604	C21DEC08A0011.csv	high common Pb	1076.14	3915.064	465.9306	779.8933	53.47336	205.1486	14.89087
2021-G-604	C21DEC08A0047.csv		2238.163	8896.597	1093.623	1772.206	123.3734	411.5653	31.21889
2021-G-604	C21DEC08A0022.csv		2272.042	9061.724	1098.223	1744.856	122.5874	421.5549	33.69271
2021-G-604	C21DEC08A0046.csv		2013.816	7441.407	821.4064	1253.292	90.86979	315.8547	24.79267
2021-G-604	C21DEC08A0018.csv		2025.967	8080.146	945.9355	1532.684	103.6213	350.4713	26.95192
2021-G-604	C21DEC08A0056.csv		868.7586	3191.205	417.4738	701.3644	53.58309	208.9642	17.82942
2021-G-604	C21DEC08A0022.csv	high common Pb	2266.223	8780.076	994.1389	1542.693	113.0978	371.9131	29.06371
2021-G-604	C21DEC08A0023.csv		1954.59	6985.093	806.182	1203.213	81.71199	270.7116	20.59628
2021-G-604	C21DEC08A0059.csv		1157.418	4247.893	492.9002	783.6471	57.12941	201.3791	15.79856
2021-G-604	C21DEC08A0029.csv	high common Pb	869.9644	2972.709	353.8194	528.2159	36.98446	124.0036	10.12393
2021-G-604	C21DEC08A0044.csv		2109.19	7418.394	760.0499	1145.554	85.1502	304.4102	22.47013
2021-G-604	C21DEC08A0035.csv		1227.106	4367.854	536.5766	851.2879	58.24441	207.4775	17.95231
2021-G-604	C21DEC08A0032.csv		1078.129	3988.676	474.5392	763.1711	52.76031	182.8779	15.25834
2021-G-604	C21DEC08A0011.csv		1080.389	4122.774	500.75	800.7339	59.11792	218.6083	17.8699
2021-G-604	C21DEC08A0030.csv		2020.072	7816.972	919.2298	1475.207	102.4448	346.4033	27.77593
2021-G-604	C21DEC08A0006.csv		971.6371	3294.295	404.1807	626.1859	44.21944	156.5359	12.41393
2021-G-604	C21DEC08A0009.csv		1667.311	6290.663	727.155	1141.22	77.52524	260.0555	20.4124
2021-G-604	C21DEC08A0024.csv		1404.53	5433.063	675.5918	1070.456	75.11827	256.6594	20.25416
2021-G-604	C21DEC08A0034.csv		974.1658	3497.15	415.4951	682.6667	48.92651	170.9684	15.24111
2021-G-604	C21DEC08A0007.csv		977.653	3449.908	398.4703	629.3207	46.18321	153.5444	13.38243
2021-G-604	C21DEC08A0005.csv		951.7328	3359.49	392.1854	620.2318	44.57064	153.8302	12.4487

2021-G-604	C21DEC08A0023.csv	high common Pb	2063.063	7573.232	800.3511	1335.521	86.04688	290.4372	23.544
2021-G-604	C21DEC08A0043.csv		916.7638	3168.98	371.4764	579.3567	41.72435	139.9491	11.98149
2021-G-604	C21DEC08A0057.csv		904.5664	3179.413	375.3773	600.3269	42.73574	142.1718	12.56942
2021-G-604	C21DEC08A0048.csv		912.6952	3318.128	410.1666	658.2213	46.22958	171.9664	14.00688
2021-G-604	C21DEC08A0033.csv		902.7397	3010.637	344.7057	537.5211	36.56598	125.06	10.31566
2021-G-604	C21DEC08A0010.csv		1850.565	6899.268	799.4425	1270.563	89.43396	312.8862	24.28083
2021-G-604	C21DEC08A0031.csv		628.979	2262.468	267.7253	429.0567	29.87249	106.233	8.740192
2021-G-604	C21DEC08A0055.csv		1576.35	5695.112	618.2425	928.1389	70.822	234.6463	18.7388
2021-G-604	C21DEC08A0020.csv		1328.736	4797.063	548.5044	863.3755	60.7166	215.3963	18.38307
2021-G-604	C21DEC08A0058.csv		1349.361	5042.616	590.1923	904.4761	62.45759	206.9849	17.02974
2021-G-604	C21DEC08A0019.csv		1333.185	4744.966	529.673	783.1613	52.59098	188.1752	15.59486
2021-G-604	C21DEC08A0042.csv		822.0688	3228.492	426.7162	745.3327	57.33353	208.4557	17.20345
2021-G-604	C21DEC08A0042.csv	high common Pb	868.9951	3331.583	458.351	782.8952	62.73605	228.7359	19.06707
2021-G-604	C21DEC08A0029.csv		878.5356	3028.388	353.4029	551.4249	37.2228	123.0313	10.08221
2021-G-604	C21DEC08A0008.csv		1755.88	7243.993	937.9943	1600.603	118.5753	422.6029	34.41389
2021-G-604	C21DEC08A0053.csv		1446.709	6252.34	854.7795	1579.48	135.9939	557.2123	46.81109

Analysis	Source Filename	Comment	204Pb	206Pb	207Pb	208Pb	232Th	235U	238U
			ppm	ppm	ppm	ppm	ppm	ppm	ppm
	ZY-LG-2								
2021-G-604	C21DEC08A0054.csv		<0.147	32.32539	1.902319	35.67596	71593.41	126.576	17650.92
2021-G-604	C21DEC08A0021.csv		<0.094	35.48001	2.055605	38.77653	72594	126.3824	17760.02
2021-G-604	C21DEC08A0055.csv	high common Pb	<0.253	13.81639	2.724491	36.56993	54908.85	38.92433	5490.197
2021-G-604	C21DEC08A0045.csv	high common Pb	<0.107	6.597103	0.468034	25.73788	51811.51	24.10017	3412.326
2021-G-604	C21DEC08A0011.csv	high common Pb	<0.285	15.26928	3.714449	46.22806	66571.8	40.71997	5618.616
2021-G-604	C21DEC08A0047.csv		<0.093	19.95392	1.13236	31.77328	60916.9	70.83341	9893.979
2021-G-604	C21DEC08A0022.csv		<0.226	26.17995	1.626498	39.77233	71786.91	88.43866	12424.57
2021-G-604	C21DEC08A0046.csv		<0.093	17.44918	1.106671	36.05391	68218.76	60.76328	8501.1
2021-G-604	C21DEC08A0018.csv		<0.092	17.20142	1.066308	32.01946	60660.21	60.09476	8451.351
2021-G-604	C21DEC08A0056.csv		<0.128	6.676546	0.505197	21.2497	41760.61	24.34517	3413.103
2021-G-604	C21DEC08A0022.csv	high common Pb	<0.109	26.22501	2.514819	39.53953	71235	89.23573	12538.68
2021-G-604	C21DEC08A0023.csv		<0.110	13.20346	1.036797	37.94941	75020.15	46.28612	6510.877
2021-G-604	C21DEC08A0059.csv		<0.095	12.47734	0.775412	33.52057	65218.79	43.85568	6109.695
2021-G-604	C21DEC08A0029.csv	high common Pb	<0.203	9.683885	3.419212	41.03946	57454.28	19.74841	2751.884
2021-G-604	C21DEC08A0044.csv		<0.095	17.0985	1.070153	36.75098	72112.62	60.23015	8427.442
2021-G-604	C21DEC08A0035.csv		<0.089	11.32906	0.777164	35.32753	65737.44	38.30937	5398.913
2021-G-604	C21DEC08A0032.csv		<0.089	8.625563	0.564814	30.95396	57349.66	28.64511	4093.632
2021-G-604	C21DEC08A0011.csv		<0.098	8.816069	0.663334	32.24247	62980.78	29.78865	4264.21
2021-G-604	C21DEC08A0030.csv		<0.090	15.46505	1.098633	40.83616	77425.02	52.72585	7398.698
2021-G-604	C21DEC08A0006.csv		<0.095	6.497831	0.551943	34.91159	65329.98	21.29765	3015.896
2021-G-604	C21DEC08A0009.csv		<0.095	12.46349	0.848232	38.42822	70401.25	42.01398	5940.778
2021-G-604	C21DEC08A0024.csv		<0.092	7.921824	0.738137	33.53549	61205.58	25.06751	3593.738
2021-G-604	C21DEC08A0034.csv		<0.088	8.895791	0.632772	33.87788	62896.28	29.44332	4136.245
2021-G-604	C21DEC08A0007.csv		<0.095	8.006612	0.664159	37.0184	69560.04	25.83108	3691.478

2021-G-604	C21DEC08A0005.csv		<0.095	7.81542	0.486428	35.69544	66767.6	25.72077	3664.135
2021-G-604	C21DEC08A0023.csv	high common Pb	<0.340	18.70698	2.775342	49.38057	78715.35	53.83268	7575.12
2021-G-604	C21DEC08A0043.csv		<0.091	7.682784	0.54062	35.14427	65644.63	24.88167	3548.71
2021-G-604	C21DEC08A0057.csv		<0.092	7.291382	0.53772	36.92728	69318.81	23.67905	3365.887
2021-G-604	C21DEC08A0048.csv		<0.113	8.081429	0.499255	30.06597	60142.68	28.73764	4006.436
2021-G-604	C21DEC08A0033.csv		<0.088	5.869542	0.472504	32.16342	59895.93	18.87772	2668.796
2021-G-604	C21DEC08A0010.csv		<0.098	16.52677	1.054882	39.35254	72687.41	54.31484	7654.304
2021-G-604	C21DEC08A0031.csv		<0.090	6.01846	0.384941	31.04934	58165.19	19.62275	2781.875
2021-G-604	C21DEC08A0055.csv		<0.103	11.80349	0.841538	34.81357	68339.21	40.50239	5653.74
2021-G-604	C21DEC08A0020.csv		<0.101	16.08479	0.961284	42.56089	76695.88	52.68378	7429.264
2021-G-604	C21DEC08A0058.csv		<0.095	10.73008	0.657129	32.19603	60948.34	35.84162	5021.945
2021-G-604	C21DEC08A0019.csv		<0.092	13.47947	0.755395	39.01523	74764.07	44.45996	6248.33
2021-G-604	C21DEC08A0042.csv		<0.144	5.525391	0.332905	35.5516	63998.43	17.51537	2440.176
2021-G-604	C21DEC08A0042.csv	high common Pb	<0.124	5.413819	0.427982	31.68198	63609.75	17.64308	2531.398
2021-G-604	C21DEC08A0029.csv		<0.109	6.598481	0.932149	33.7794	65078.56	20.31198	2789.955
2021-G-604	C21DEC08A0008.csv		<0.095	16.57102	0.846933	38.77767	71560.78	47.63156	6704.151
2021-G-604	C21DEC08A0053.csv		<0.093	455.071	25.8623	1411.119	77739.98	48.38165	6740.526

Analysis	Source Filename	Comment	**PO4**	**89Y**	**139La**	**140Ce**	**141Pr**	**146Nd**	**147Sm**	**153Eu**	**157Gd**
			ppm	**ppm**	**ppm**	**ppm**	**ppm**	**ppm**	**ppm**	**ppm**	**ppm**
	ZY-LGT-1										
2021-G-605	C21DEC08A0114.csv		385532.9	24860.12	78396.51	198076.9	24855.17	92865.9	31462.59	82.75801	21208.13
2021-G-605	C21DEC08A0082.csv		388951.4	24201.35	64610.5	189449.8	27200.34	109297.4	52065.77	81.75502	30973.01
2021-G-605	C21DEC08A0077.csv		385722	28662.21	75246	191545.3	24579.24	90918.59	32841.23	61.38158	22724.55
2021-G-605	C21DEC08A0096.csv		386805.9	25534.36	82699.94	197702.7	25403.66	93076.28	31085.96	85.16555	21475.59
2021-G-605	C21DEC08A0081.csv		384000.5	25966.83	74107.41	188898.8	24330.61	93924.17	32238.42	70.81984	22298.16
2021-G-605	C21DEC08A0068.csv		388503.5	25650.1	78763.13	203274.8	26594.35	96337.73	34442.14	88.27897	21854.14
2021-G-605	C21DEC08A0101.csv		383162.7	27552.5	72998.65	183849.6	23876.67	90604.94	32329.84	68.5485	23005.64
2021-G-605	C21DEC08A0092.csv		390115	21517.85	100564.1	217907.9	25145.25	92588.69	24267.3	221.8825	16704.52
2021-G-605	C21DEC08A0102.csv		382992.2	25789.53	71067.72	187347.5	24120.43	93141.27	32601.07	50.60509	22476.59
2021-G-605	C21DEC08A0083.csv		387767.8	21948.56	83591.84	205897.7	25681.4	98495.06	31215.64	77.27243	20771.21
2021-G-605	C21DEC08A0071.csv	high common Pb	382932	28989.38	71654.32	183637.7	23356.38	89573.69	31249.86	74.20509	22076.44
2021-G-605	C21DEC08A0114.csv	high common Pb	389760.3	25449.17	83542.08	204366.1	26504.38	101190.3	30016.16	73.49651	22090.85
2021-G-605	C21DEC08A0095.csv		386513.4	24416.43	76921.2	196044.8	25562.27	98414.72	33237.42	85.15725	22691.55
2021-G-605	C21DEC08A0094.csv		386257.7	23540.09	79232.62	197341.9	25673.22	98393.94	31023.47	66.5008	21769.56
2021-G-605	C21DEC08A0119.csv		385387.6	20962.1	80976.08	198717.1	25392.39	95245.08	33784.32	64.22053	22018.23
2021-G-605	C21DEC08A0116.csv		381660.1	28170.61	72742.48	180505.9	23034.14	89829.59	29374.13	51.09115	21066.45

2021-G-605	C21DEC08A0071.csv		383627.4	33689.37	72223.58	177567.7	22883.05	86786.54	29873.11	61.2563	22929.88
2021-G-605	C21DEC08A0093.csv		387075.3	24545.3	82470.79	197955.2	25461.83	96499.21	30617.73	124.284	21778.15
2021-G-605	C21DEC08A0069.csv	high common Pb	392886.2	14090	116724.9	235304.7	27045.77	100139.7	18242.31	172.6351	12458.35
2021-G-605	C21DEC08A0090.csv		382629.8	23810.88	70904.03	188026.9	23515.37	95889.33	33713.93	52.08972	22188.79
2021-G-605	C21DEC08A0080.csv		382101	21122.61	71845.62	185758.7	24685.37	97557.56	36643.03	85.45874	23081.65
2021-G-605	C21DEC08A0078.csv		382749.3	20953.68	69782.92	191427	25325.41	96700.3	37069.9	85.21331	23117.75
2021-G-605	C21DEC08A0104.csv		394659.4	13456.67	120074.4	237180.2	27063.12	106452.3	17961.12	264.9455	12552.09
2021-G-605	C21DEC08A0118.csv		382622.8	25432.34	74712.36	185861.6	24021.85	93114.05	29793.67	41.65275	21432.99
2021-G-605	C21DEC08A0107.csv		391393.7	24303.33	96771.44	212912.6	26172.81	100269.5	22705.1	199.0345	17712.39
2021-G-605	C21DEC08A0067.csv		381356.9	21975.77	70532.68	185070.2	24141.78	90844.83	38646.85	86.6073	23854.98
2021-G-605	C21DEC08A0103.csv		392060.1	18513.09	101858.3	225287.7	26227.55	100982.9	24067.39	148.3422	17030.34
2021-G-605	C21DEC08A0079.csv		392138.9	20838.04	97411.92	221472.9	26343.64	102644.5	24359.26	130.4732	17874.71
2021-G-605	C21DEC08A0070.csv		394668.7	17854.13	112015.9	232495.1	26917.6	101958.3	21412.1	198.2108	15172.92
2021-G-605	C21DEC08A0115.csv		380814.3	20352.25	70480.18	184506.1	24661.13	92699.94	38506.37	100.3247	23980.15
2021-G-605	C21DEC08A0105.csv		386705.7	23098.51	80349.23	199954.1	24992.7	100517.6	30219.19	58.54996	20886.92
2021-G-605	C21DEC08A0072.csv		395366	12976.47	120194.1	243670.2	27665.88	104550.8	18042.65	205.9867	11937.66
2021-G-605	C21DEC08A0066.csv		390582.6	16163.99	110304.6	225687.1	26439.55	96268.87	20316.88	166.9143	13676.73

2021-G-605	C21DEC08A0120.csv	392990.6	21695.25	101970.7	222210.1	26473.81	101221.4	22475.23	160.4476	17139.68
2021-G-605	C21DEC08A0091.csv	392164.1	23894.65	101841	217251.7	25265.84	98506.4	20888.66	209.5567	17305.31
2021-G-605	C21DEC08A0106.csv	393808.6	15843.27	114814.7	234744.1	26852.88	102123.9	18641.75	233.0634	13237.32
2021-G-605	C21DEC08A0069.csv	393563.9	14082.69	117766.9	237533	26406.3	102340.4	17501.83	182.6575	11764.68
2021-G-605	C21DEC08A0117.csv	393740.6	11229.45	127023	241971.1	26783.66	99545.08	15621.41	196.771	10130.91

Analysis	**Source Filename**	**Comment**	**159Tb**	**163Dy**	**165Ho**	**166Er**	**169Tm**	**172Yb**	**175Lu**
			ppm	**ppm**	**ppm**	**ppm**	**ppm**	**ppm**	**ppm**
	ZY-LGT-1								
2021-G-605	C21DEC08A0114.csv		2728.734	9698.315	878.8993	1406.663	134.4113	592.3433	48.71633
2021-G-605	C21DEC08A0082.csv		3986.733	10982.6	838.3062	1193.448	115.2106	546.0258	38.12996
2021-G-605	C21DEC08A0077.csv		2970.303	10367.76	987.4446	1633.826	156.4841	697.2838	55.02049
2021-G-605	C21DEC08A0096.csv		2655.647	9477.208	890.4236	1424.429	135.3463	557.6675	43.88317
2021-G-605	C21DEC08A0081.csv		2870.899	9810.501	940.3168	1508.002	135.0866	602.4215	45.67183
2021-G-605	C21DEC08A0068.csv		2898.537	9601.126	887.8627	1388.346	133.1823	594.5536	44.98083
2021-G-605	C21DEC08A0101.csv		3013.135	10320.31	986.4964	1603.553	154.2881	689.1594	55.63896
2021-G-605	C21DEC08A0092.csv		2072.583	7437.022	769.3112	1238.958	106.0585	425.5858	34.38964
2021-G-605	C21DEC08A0102.csv		2869.612	9701.01	930.1906	1500.453	139.3966	616.7873	50.75538
2021-G-605	C21DEC08A0083.csv		2574.232	8432.268	812.8232	1292.224	115.3046	467.9457	36.31948
2021-G-605	C21DEC08A0071.csv	high common Pb	2852.226	10579.53	1029.315	1730.716	159.8537	699.4332	55.25931
2021-G-605	C21DEC08A0114.csv	high common Pb	2727.733	9321.184	921.906	1402.949	128.9998	566.0426	41.76046

2021-G-605	C21DEC08A0095.csv		2905.867	9574.749	910.2875	1378.306	127.7008	550.609	40.36104
2021-G-605	C21DEC08A0094.csv		2650.716	9137.472	877.8377	1365.021	117.5256	487.1183	35.51695
2021-G-605	C21DEC08A0119.csv		2717.313	8695.432	763.9415	1140.584	105.4526	452.9748	34.8745
2021-G-605	C21DEC08A0116.csv		2808.597	10032.38	1016.807	1623.469	146.4602	613.437	47.9538
2021-G-605	C21DEC08A0071.csv		3112.544	11525.97	1213.917	2028.408	201.2671	885.7676	74.80721
2021-G-605	C21DEC08A0093.csv		2667.763	9243.487	907.7011	1442.688	127.4123	513.6951	42.18494
2021-G-605	C21DEC08A0069.csv	high common Pb	1293.458	4634.374	540.2611	860.908	69.34217	244.0027	19.89114
2021-G-605	C21DEC08A0090.csv		2746.913	9371.903	866.5208	1350.908	120.5233	523.7633	41.64695
2021-G-605	C21DEC08A0080.csv		2821.985	8658.177	752.2195	1162.582	113.0011	475.9519	37.97562
2021-G-605	C21DEC08A0078.csv		2804.169	8701.77	743.5095	1127.97	100.7373	446.0296	32.9889
2021-G-605	C21DEC08A0104.csv		1210.629	4330.842	518.8225	828.0093	58.65273	201.3958	16.35128
2021-G-605	C21DEC08A0118.csv		2664.864	9264.575	931.9616	1521.257	132.2496	542.5337	44.27451
2021-G-605	C21DEC08A0107.csv		1997.568	7707.329	947.5449	1459.448	105.2672	354.5825	27.66618
2021-G-605	C21DEC08A0067.csv		2855.816	9268.173	776.9636	1212.006	117.1377	555.1871	42.23644
2021-G-605	C21DEC08A0103.csv		1921.162	6678.99	724.5715	1100.944	83.88638	326.0569	25.29848
2021-G-605	C21DEC08A0079.csv		1994.283	7211.447	809.7809	1240.427	93.11779	330.0377	26.18265
2021-G-605	C21DEC08A0070.csv		1681.151	6261.13	698.7866	1128.717	89.86083	334.2334	27.54404
2021-G-605	C21DEC08A0115.csv		2901.197	8819.613	731.8192	1092.938	109.8249	505.352	38.89829
2021-G-605	C21DEC08A0105.csv		2603.777	8664.65	875.7216	1373.45	113.9149	480.7181	38.22313
2021-G-605	C21DEC08A0072.csv		1181.058	4316.621	508.8467	804.0476	60.13572	215.2879	18.05643
2021-G-605	C21DEC08A0066.csv		1539.066	5456.242	602.7432	986.6603	83.85144	338.3018	31.37364
2021-G-605	C21DEC08A0120.csv		1953.642	7289.185	853.4627	1347.188	93.70601	307.7946	22.54248
2021-G-605	C21DEC08A0091.csv		1964.95	7596.647	916.0527	1406.509	100.491	316.3124	24.29579
2021-G-605	C21DEC08A0106.csv		1360.192	5018.862	618.2247	987.9102	71.18053	247.2874	18.6343
2021-G-605	C21DEC08A0069.csv		1253.607	4546.609	543.9432	902.0084	69.88439	251.7241	20.77308
2021-G-605	C21DEC08A0117.csv		967.4566	3548.323	442.0947	713.3504	52.40405	178.648	14.65583

Analysis	Source Filename	Comment	204Pb	206Pb	207Pb	208Pb	232Th	235U	238U
			ppm	ppm	ppm	ppm	ppm	ppm	ppm
	ZY-LGT-1								
2021-G-605	C21DEC08A0114.csv		<0.182	114.2805	7.054851	40.62672	68669.47	420.9146	57918.58
2021-G-605	C21DEC08A0082.csv		<0.101	155.3901	7.666191	7.335538	12174.65	595.2131	82527.93
2021-G-605	C21DEC08A0077.csv		<0.098	89.25396	4.51471	42.0535	82676.31	343.4992	47675.8
2021-G-605	C21DEC08A0096.csv		<0.103	79.2232	4.16933	39.32796	77810.72	308.9264	42703.47
2021-G-605	C21DEC08A0081.csv		<0.096	77.7524	4.011769	48.86739	96619.74	297.1474	41203.86
2021-G-605	C21DEC08A0068.csv		<0.105	99.12854	5.024021	28.5349	54667.33	386.5677	53756.69
2021-G-605	C21DEC08A0101.csv		<0.103	66.18632	3.400192	56.62206	110796.2	250.3504	34555.55
2021-G-605	C21DEC08A0092.csv		<0.098	58.16313	3.094006	35.87043	68370.16	218.3901	30198.03
2021-G-605	C21DEC08A0102.csv		<0.102	59.52535	2.988817	57.2407	113243.4	224.7521	31017.05
2021-G-605	C21DEC08A0083.csv		<0.105	42.29564	2.601041	43.28241	88131.71	161.8589	22440.64
2021-G-605	C21DEC08A0071.csv	high common Pb	0.346836	90.0909	10.35697	72.04692	106744	303.3256	42129.47
2021-G-605	C21DEC08A0114.csv	high common Pb	3.309937	143.733	58.74687	164.2205	59205.22	306.1172	42015.3
2021-G-605	C21DEC08A0095.csv		<0.103	42.28711	2.376442	47.82092	98129.81	160.922	22241.93
2021-G-605	C21DEC08A0094.csv		<0.118	36.30005	2.177627	50.80044	102394.7	140.3221	19405.52
2021-G-605	C21DEC08A0119.csv		<0.102	47.88979	2.528707	49.3894	98799.02	177.9361	24465.5
2021-G-605	C21DEC08A0116.csv		<0.105	67.66152	3.624763	60.67748	121479.2	257.3654	35407.81
2021-G-605	C21DEC08A0071.csv		<0.124	79.58824	4.219179	52.94454	108089.8	307.84	42781.12
2021-G-605	C21DEC08A0093.csv		<0.097	39.09512	2.310332	49.68573	98443.87	143.5158	19848.8
2021-G-605	C21DEC08A0069.csv	high common Pb	<0.213	12.87174	1.951407	41.50057	69719.07	38.75717	5459.023
2021-G-605	C21DEC08A0090.csv		<0.119	45.11096	2.449666	57.7546	119913.2	173.8286	24054.43

2021-G-605	C21DEC08A0080.csv	<0.111	48.62556	2.602444	56.34335	117520.8	182.3905	25286.32
2021-G-605	C21DEC08A0078.csv	<0.099	46.76473	2.487094	58.60717	115258.7	167.896	23296.93
2021-G-605	C21DEC08A0104.csv	<0.099	5.980217	0.530262	31.70917	60270.91	20.34276	2841.507
2021-G-605	C21DEC08A0118.csv	<0.113	41.06288	2.29975	61.56273	126254.6	155.2587	21350.2
2021-G-605	C21DEC08A0107.csv	<0.099	15.85418	1.099866	45.16373	87199.23	55.54915	7643.795
2021-G-605	C21DEC08A0067.csv	<0.143	44.93986	2.401121	60.04142	124720.1	170.057	23664.39
2021-G-605	C21DEC08A0103.csv	<0.105	19.19341	1.166657	36.26841	73319.2	69.10287	9518.539
2021-G-605	C21DEC08A0079.csv	<0.095	18.01404	1.133665	39.68798	76215.83	62.97579	8742.735
2021-G-605	C21DEC08A0070.csv	<0.135	14.65808	0.896192	29.23904	59381.9	54.68251	7604.189
2021-G-605	C21DEC08A0115.csv	<0.099	52.49303	2.630657	63.22671	123774	186.1759	25621.13
2021-G-605	C21DEC08A0105.csv	<0.116	35.99131	1.893	47.35044	100397.1	133.7467	18450.97
2021-G-605	C21DEC08A0072.csv	<0.098	10.70479	0.802152	27.45251	53067.88	36.79815	5142.534
2021-G-605	C21DEC08A0066.csv	<0.104	27.14573	1.586083	41.18526	78107.57	94.0485	13083.02
2021-G-605	C21DEC08A0120.csv	<0.101	11.31671	0.769987	39.74328	76408.47	38.23013	5296.639
2021-G-605	C21DEC08A0091.csv	<0.097	15.06058	1.044962	43.08905	83043.49	51.97734	7192.786
2021-G-605	C21DEC08A0106.csv	<0.096	9.700242	0.662367	35.02907	66765.86	32.44834	4534.501
2021-G-605	C21DEC08A0069.csv	<0.105	9.424864	0.626371	33.28461	66635.13	32.83675	4557.805
2021-G-605	C21DEC08A0117.csv	<0.100	6.479724	0.506923	33.10033	64803.8	21.37271	2975.859

Analysis	Source Filename	Comment	PO4	89Y	139La	140Ce	141Pr	146Nd	147Sm	153Eu
			1s%	1s%	1s%	1s%	1s%	1s%	1s%	1s%
	ZY-LG-2									
2021-G-604	C21DEC08A0054.csv			2.371944	2.316597	0.483028	3.291092	3.396513	2.919639	4.234191
2021-G-604	C21DEC08A0021.csv			1.481214	1.350339	0.205306	1.484507	1.898373	1.822147	2.640804
2021-G-604	C21DEC08A0055.csv	high common Pb		2.465092	2.033677	0.380367	2.44051	2.79518	2.267178	3.727491
2021-G-604	C21DEC08A0045.csv	high common Pb		1.899318	2.113536	0.329114	2.147883	2.400229	2.71985	3.141903
2021-G-604	C21DEC08A0011.csv	high common Pb		3.241788	2.42478	0.411133	2.93829	2.924815	2.979389	3.890185
2021-G-604	C21DEC08A0047.csv			1.426777	1.3284	0.205306	1.508093	1.96339	1.808282	2.517246
2021-G-604	C21DEC08A0022.csv			1.699179	2.257512	0.351711	2.499354	2.6808	2.360264	3.286115
2021-G-604	C21DEC08A0046.csv			1.339347	1.373857	0.205306	1.538791	1.851415	1.85676	3.03466
2021-G-604	C21DEC08A0018.csv			1.57633	1.629826	0.23704	1.678247	1.984971	1.962419	2.71193
2021-G-604	C21DEC08A0056.csv			2.315257	2.077551	0.418309	2.200684	2.836034	2.103636	4.776201
2021-G-604	C21DEC08A0022.csv	high common Pb		1.946446	1.984963	0.322584	2.002468	2.287526	2.203795	3.169945
2021-G-604	C21DEC08A0023.csv			2.326273	2.005013	0.310727	2.078563	2.368775	2.277943	2.889505
2021-G-604	C21DEC08A0059.csv			2.657232	1.701307	0.250065	1.682812	2.041596	2.288276	2.756639
2021-G-604	C21DEC08A0029.csv	high common Pb		2.12052	1.869936	0.336106	2.098067	2.113203	2.302058	3.043024
2021-G-604	C21DEC08A0044.csv			1.753704	1.511367	0.259858	1.850189	2.022256	2.253772	4.95262
2021-G-604	C21DEC08A0035.csv			1.434354	1.494334	0.221035	1.566654	1.937476	1.82983	2.570538
2021-G-604	C21DEC08A0032.csv			1.776899	1.407471	0.205306	1.52456	1.897496	1.909633	2.555247
2021-G-604	C21DEC08A0011.csv			2.133998	1.794995	0.276582	1.882324	2.302928	2.016115	2.863259
2021-G-604	C21DEC08A0030.csv			1.413454	1.436209	0.239225	1.550497	2.047597	1.990661	3.111656

2021-G-604	C21DEC08A0006.csv			1.659685	1.61325	0.225319	1.737847	2.008543	1.902228	2.565567
2021-G-604	C21DEC08A0009.csv			2.115989	1.524373	0.239225	1.789232	2.123921	2.004523	2.859852
2021-G-604	C21DEC08A0024.csv			1.690728	1.412533	0.205306	1.556028	1.913072	1.864617	2.589421
2021-G-604	C21DEC08A0034.csv			1.358391	1.297923	0.205306	1.619735	1.91818	1.801594	2.523106
2021-G-604	C21DEC08A0007.csv			1.608284	1.565987	0.228046	1.636629	2.037781	1.933078	2.735192
2021-G-604	C21DEC08A0005.csv			1.403936	1.459021	0.205306	1.648649	1.928388	1.856621	2.642316
2021-G-604	C21DEC08A0023.csv	high common Pb		2.517084	2.843904	0.471807	2.325891	3.076353	2.625727	4.638533
2021-G-604	C21DEC08A0043.csv			1.57037	1.493994	0.205306	1.592811	1.949057	1.775333	2.668399
2021-G-604	C21DEC08A0057.csv			1.396451	1.486029	0.216281	1.70339	2.010176	1.86257	2.547788
2021-G-604	C21DEC08A0048.csv			2.610528	2.056022	0.369983	2.36934	2.475921	2.551443	3.375647
2021-G-604	C21DEC08A0033.csv			1.658874	1.373518	0.205306	1.606139	1.97228	1.912514	2.663658
2021-G-604	C21DEC08A0010.csv			1.434969	1.400539	0.205306	1.612269	1.98567	1.955679	3.173135
2021-G-604	C21DEC08A0031.csv			1.452433	1.461324	0.205306	1.587543	1.933897	1.828879	2.626872
2021-G-604	C21DEC08A0055.csv			1.791141	1.92941	0.313553	1.90017	2.299082	2.247952	3.02261
2021-G-604	C21DEC08A0020.csv			1.538255	1.363643	0.205306	1.559412	1.91946	1.87604	2.619151
2021-G-604	C21DEC08A0058.csv			1.960927	1.550047	0.243828	1.886539	2.088326	2.124969	2.917811
2021-G-604	C21DEC08A0019.csv			1.583535	1.510029	0.240346	1.576418	1.993821	1.782622	2.726152
2021-G-604	C21DEC08A0042.csv			1.57303	1.552371	0.258374	1.76534	2.191505	1.94953	2.871479
2021-G-604	C21DEC08A0042.csv	high common Pb		2.09775	1.976549	0.391761	2.440358	2.43982	2.495644	3.158707
2021-G-604	C21DEC08A0029.csv			2.325291	2.345984	0.360468	2.373939	2.819173	2.613992	3.618217
2021-G-604	C21DEC08A0008.csv			1.349195	1.461594	0.205306	1.632318	1.912129	1.818399	2.809351
2021-G-604	C21DEC08A0053.csv			2.120639	1.420684	0.242647	1.70054	2.036649	1.945331	3.222222

Analysis	**Source Filename**	**Comment**	157Gd	159Tb	163Dy	165Ho	166Er	169Tm	172Yb	175Lu
			1s%	1s%	1s%	1s%	1s%	1s%	1s%	1s%
	ZY-LG-2									
2021-G-604	C21DEC08A0054.csv		3.680565	3.484743	2.897806	3.373602	2.956016	4.831645	4.280104	5.953943
2021-G-604	C21DEC08A0021.csv		2.206177	1.929593	2.052713	2.438014	2.376888	2.837316	2.598534	3.997661
2021-G-604	C21DEC08A0055.csv	high common Pb	3.071427	2.568668	2.52575	3.321021	3.308015	4.234778	4.299775	6.838952
2021-G-604	C21DEC08A0045.csv	high common Pb	2.546782	2.446002	2.332578	2.865505	2.905564	3.819044	3.740007	4.867118
2021-G-604	C21DEC08A0011.csv	high common Pb	2.710536	3.575854	3.228681	3.47842	3.543041	5.101433	4.600179	7.511883
2021-G-604	C21DEC08A0047.csv		2.290795	1.868228	2.112026	2.383246	2.302499	2.782369	2.359825	4.077745
2021-G-604	C21DEC08A0022.csv		2.728551	2.486518	2.490072	2.836076	3.213117	3.616979	3.738444	5.738959
2021-G-604	C21DEC08A0046.csv		2.238702	1.894789	2.003954	2.361758	2.333845	2.856739	2.47496	4.255717
2021-G-604	C21DEC08A0018.csv		2.31867	1.982198	2.148149	2.424018	2.509722	2.980688	2.692851	4.473484
2021-G-604	C21DEC08A0056.csv		2.897762	2.779834	3.1218	3.041007	2.963097	3.9164	3.514009	6.028994
2021-G-604	C21DEC08A0022.csv	high common Pb	2.646813	2.407974	2.50617	2.868665	2.546798	3.4212	2.674013	4.587487
2021-G-604	C21DEC08A0023.csv		2.621108	2.65215	2.513413	2.685697	2.899732	3.313976	2.982622	5.126201
2021-G-604	C21DEC08A0059.csv		2.815576	3.073269	3.148338	3.427789	3.328968	3.809906	3.577389	5.371296
2021-G-604	C21DEC08A0029.csv	high common Pb	2.630744	2.324201	2.454296	2.674529	3.193128	4.434518	4.216386	7.124873
2021-G-604	C21DEC08A0044.csv		2.489825	2.347535	2.401192	2.523972	2.57355	3.117608	2.655348	4.637003
2021-G-604	C21DEC08A0035.csv		2.267637	1.964876	2.052735	2.451209	2.357213	3.081839	2.773295	4.495171
2021-G-604	C21DEC08A0032.csv		2.476228	2.259582	2.405944	2.701959	2.784057	2.987673	2.701121	4.589634

2021-G-604	C21DEC08A0011.csv		2.675229	2.435625	2.679502	2.871172	2.833912	3.694574	3.140735	4.952798
2021-G-604	C21DEC08A0030.csv		2.370498	2.061794	2.078486	2.37437	2.32182	2.84956	2.459922	4.312328
2021-G-604	C21DEC08A0006.csv		2.435378	2.109054	2.245265	2.493039	2.558827	3.219053	2.798271	4.905768
2021-G-604	C21DEC08A0009.csv		2.48482	2.160879	2.544495	2.883172	2.843011	3.526552	3.21641	5.164609
2021-G-604	C21DEC08A0024.csv		2.366098	2.153312	2.382767	2.655933	2.657772	3.159612	2.650586	4.276129
2021-G-604	C21DEC08A0034.csv		2.27099	1.908007	2.076943	2.3564	2.367683	2.917645	2.697184	4.610401
2021-G-604	C21DEC08A0007.csv		2.356603	2.086357	2.275209	2.50319	2.566609	3.245376	2.80446	4.864711
2021-G-604	C21DEC08A0005.csv		2.257231	1.898837	2.140265	2.400009	2.346167	2.990407	2.819447	4.523987
2021-G-604	C21DEC08A0023.csv	high common Pb	3.183421	2.9032	2.943718	3.491718	3.2127	5.178308	4.788435	7.71117
2021-G-604	C21DEC08A0043.csv		2.321712	2.032884	2.077845	2.467922	2.517252	3.057477	3.043178	4.46344
2021-G-604	C21DEC08A0057.csv		2.242167	1.990471	2.160152	2.464275	2.45085	3.018682	2.903347	4.517355
2021-G-604	C21DEC08A0048.csv		3.033556	2.396367	3.043177	3.037711	2.855428	4.197021	3.840378	6.058283
2021-G-604	C21DEC08A0033.csv		2.271962	2.040716	2.310871	2.554904	2.662239	3.222164	3.075946	4.984273
2021-G-604	C21DEC08A0010.csv		2.327818	2.034635	2.08086	2.402954	2.354479	2.76467	2.574421	4.336583
2021-G-604	C21DEC08A0031.csv		2.259702	2.00497	2.147908	2.39031	2.422398	3.16969	2.90915	4.743736
2021-G-604	C21DEC08A0055.csv		2.503081	2.271137	2.404022	2.649873	2.902294	3.380053	3.139919	4.966083
2021-G-604	C21DEC08A0020.csv		2.307695	1.937995	2.12795	2.450597	2.498623	2.853147	2.627605	4.447759
2021-G-604	C21DEC08A0058.csv		2.5542	2.315909	2.427295	2.642867	2.533232	3.152496	3.032123	5.029739
2021-G-604	C21DEC08A0019.csv		2.39095	1.951366	2.145606	2.463817	2.431382	3.04799	2.785529	4.483985
2021-G-604	C21DEC08A0042.csv		2.395302	2.086633	2.248872	2.526797	2.631515	3.442151	3.226862	5.096854
2021-G-604	C21DEC08A0042.csv	high common Pb	2.976402	2.823595	2.775352	2.979097	2.911523	3.621846	3.552791	5.751344

2021-G-604	C21DEC08A0029.csv	2.857777	2.72673	2.967129	3.091629	2.997402	3.986132	4.019944	5.914928
2021-G-604	C21DEC08A0008.csv	2.221356	1.931056	2.053942	2.34586	2.331679	2.755853	2.248234	4.041354
2021-G-604	C21DEC08A0053.csv	2.344896	1.94976	2.310196	2.698082	2.89731	3.699192	3.366695	4.995536

Analysis	**Source Filename**	**Comment**	204Pb	206Pb	207Pb	208Pb	232Th	235U	238U
			1s%	1s%	1s%	1s%	1s%	1s%	1s%
	ZY-LG-2								
2021-G-604	C21DEC08A0054.csv		33.47241	2.041557	4.745931	2.474633	2.151058	5.910718	2.433095
2021-G-604	C21DEC08A0021.csv		14.61621	1.662948	2.442438	1.271544	1.156691	5.668504	1.719412
2021-G-604	C21DEC08A0055.csv	high common Pb	34.89326	3.416477	3.963104	2.049092	2.717754	6.247348	2.695794
2021-G-604	C21DEC08A0045.csv	high common Pb	23.06146	2.306709	6.677675	1.774601	1.784063	5.867756	1.68804
2021-G-604	C21DEC08A0011.csv	high common Pb	46.38555	3.506879	4.974201	2.357827	1.882675	6.200215	2.599817
2021-G-604	C21DEC08A0047.csv		18.93534	1.381636	2.586412	1.522226	1.26057	5.579157	1.395765
2021-G-604	C21DEC08A0022.csv		30.47857	2.13305	5.754934	1.880376	1.557783	5.734812	1.923173
2021-G-604	C21DEC08A0046.csv		26.45452	1.597554	2.852925	1.527762	1.282613	5.594307	1.45193
2021-G-604	C21DEC08A0018.csv		16.96286	1.502325	2.883535	1.608971	1.373751	5.611906	1.52179
2021-G-604	C21DEC08A0056.csv		95.70132	2.58402	6.754071	1.789994	1.876465	5.713471	1.685144
2021-G-604	C21DEC08A0022.csv	high common Pb	28.1414	1.818987	2.809573	1.520843	1.513671	5.653083	1.661257
2021-G-604	C21DEC08A0023.csv		27.48642	2.488219	4.85545	2.16586	1.640098	5.860759	2.266301
2021-G-604	C21DEC08A0059.csv		17.89698	2.307573	3.99076	1.502288	1.248402	5.794705	2.076311
2021-G-604	C21DEC08A0029.csv	high common Pb	28.92741	2.365122	3.011066	1.745359	1.714874	5.900452	1.802049
2021-G-604	C21DEC08A0044.csv		19.18808	2.76914	3.490879	2.011627	1.666469	5.8641	2.278931
2021-G-604	C21DEC08A0035.csv		15.16241	1.990235	3.627908	1.267103	1.276897	5.710288	1.794331
2021-G-604	C21DEC08A0032.csv		18.47973	1.622652	3.475579	1.296693	1.150335	5.679095	1.594601
2021-G-604	C21DEC08A0011.csv		65.67015	1.795606	4.029145	1.676047	1.447473	5.711	1.610625
2021-G-604	C21DEC08A0030.csv		35.21295	2.701172	3.947949	1.627747	1.322444	5.965864	2.530328

2021-G-604	C21DEC08A0006.csv		28.63803	1.81247	4.103077	1.445601	1.257436	5.667441	1.519148
2021-G-604	C21DEC08A0009.csv		38.53589	1.559472	3.757361	1.369179	1.38251	5.655683	1.642897
2021-G-604	C21DEC08A0024.csv		26.29124	2.263363	4.132225	1.313193	1.195305	5.752801	1.887713
2021-G-604	C21DEC08A0034.csv		21.55191	1.614484	3.293631	1.343494	1.177164	5.610769	1.34512
2021-G-604	C21DEC08A0007.csv		13.3751	1.533372	4.012309	1.390657	1.248763	5.646328	1.410126
2021-G-604	C21DEC08A0005.csv		11.47931	1.607833	4.579832	1.453151	1.14019	5.615572	1.32887
2021-G-604	C21DEC08A0023.csv	high common Pb	40.43625	2.865929	5.085725	1.814262	2.05632	5.88286	1.673744
2021-G-604	C21DEC08A0043.csv		13.85226	1.546167	3.575761	1.36031	1.297346	5.622864	1.36817
2021-G-604	C21DEC08A0057.csv		16.34371	1.806629	3.876093	1.417766	1.219847	5.648284	1.410358
2021-G-604	C21DEC08A0048.csv		53.64089	1.913724	6.018493	1.788106	1.706322	5.900795	1.919976
2021-G-604	C21DEC08A0033.csv		19.53411	1.783306	3.763739	1.314066	1.172718	5.730305	1.625996
2021-G-604	C21DEC08A0010.csv		20.26205	2.297975	3.398733	1.560014	1.258246	5.837817	2.21488
2021-G-604	C21DEC08A0031.csv		17.59427	1.84017	4.171406	1.403708	1.159739	5.666013	1.474988
2021-G-604	C21DEC08A0055.csv		35.7918	2.983842	4.994259	1.612555	1.544313	5.957012	2.510153
2021-G-604	C21DEC08A0020.csv		16.7792	1.427603	3.362	1.374486	1.191632	5.586124	1.324625
2021-G-604	C21DEC08A0058.csv		17.30231	1.721678	3.726493	1.376491	1.503308	5.65201	1.622366
2021-G-604	C21DEC08A0019.csv		15.95171	1.766743	4.242703	1.413207	1.209747	5.607924	1.511669
2021-G-604	C21DEC08A0042.csv		14.75587	2.091353	6.643773	1.566434	1.380239	5.829988	1.493472
2021-G-604	C21DEC08A0042.csv	high common Pb	49.03061	3.110004	7.097942	1.740194	1.632628	5.926945	1.682784
2021-G-604	C21DEC08A0029.csv		30.70451	2.769304	7.077534	1.874063	1.85169	5.80857	1.834473
2021-G-604	C21DEC08A0008.csv		27.70983	2.221291	3.618257	1.583092	1.243223	5.774218	1.981221
2021-G-604	C21DEC08A0053.csv		21.85764	5.373336	5.218812	2.688567	2.265178	7.689907	5.493612

Analysis	**Source Filename**	**Comment**		PO4	89Y	139La	140Ce	141Pr	146Nd	147Sm	153Eu	157Gd
				1s%	1s%	1s%	1s%	1s%	1s%	1s%	1s%	1s%
	ZY-LGT-1											
2021-G-605	C21DEC08A0114.csv				1.872818	2.016675	0.339792	2.27035	2.507625	2.393403	4.014451	2.770306
2021-G-605	C21DEC08A0082.csv				1.461088	1.438791	0.205306	1.559199	1.912762	1.87457	2.895037	2.332399
2021-G-605	C21DEC08A0077.csv				1.402513	1.473726	0.228983	1.635118	2.003108	1.877622	2.966377	2.28674
2021-G-605	C21DEC08A0096.csv				1.732928	1.750595	0.267761	1.88494	2.319408	2.057024	3.241365	2.390939
2021-G-605	C21DEC08A0081.csv				1.714059	1.637412	0.230902	1.590037	2.022033	2.021491	3.247562	2.311732
2021-G-605	C21DEC08A0068.csv				2.094012	1.822367	0.290838	2.166842	2.292293	2.167768	3.304467	2.468302
2021-G-605	C21DEC08A0101.csv				1.298434	1.373837	0.205306	1.534199	1.887062	1.819637	3.083641	2.217008
2021-G-605	C21DEC08A0092.csv				1.693307	1.34854	0.205306	1.551395	1.981946	2.094326	3.681518	2.365577
2021-G-605	C21DEC08A0102.csv				1.302903	1.405536	0.205306	1.547861	1.927434	1.802701	3.098518	2.25972
2021-G-605	C21DEC08A0083.csv				1.830337	1.946198	0.295403	2.075391	2.204754	2.151882	4.528436	2.650427
2021-G-605	C21DEC08A0071.csv	high common Pb			5.781182	2.463852	0.425902	2.696209	2.873215	3.021585	5.580691	3.151566
2021-G-605	C21DEC08A0114.csv	high common Pb			3.770658	3.230016	0.619125	3.173893	3.256458	2.647069	6.386822	4.795326
2021-G-605	C21DEC08A0095.csv				1.950776	1.808358	0.278472	1.843474	2.256583	2.057071	3.194567	2.509412
2021-G-605	C21DEC08A0094.csv				1.954885	2.133201	0.329114	2.141645	2.154862	2.394552	3.740621	2.461455
2021-G-605	C21DEC08A0119.csv				1.930605	1.288057	0.205306	1.542364	1.873788	1.799519	3.389197	2.306725

2021-G-605	C21DEC08A0116.csv			1.683854	1.713854	0.272933	1.70516	1.986654	2.193075	3.301768	2.590187
2021-G-605	C21DEC08A0071.csv			2.37196	2.567945	0.360468	2.596481	3.034134	2.662295	4.210742	2.852456
2021-G-605	C21DEC08A0093.csv			1.546658	1.655327	0.233896	1.806945	1.966342	1.952761	3.405231	2.296771
2021-G-605	C21DEC08A0069.csv	high common Pb		2.309705	1.946999	0.391761	2.320396	2.500564	2.687974	3.939195	2.660885
2021-G-605	C21DEC08A0090.csv			3.08664	2.692766	0.343616	2.374138	2.870172	2.609033	4.083573	3.307418
2021-G-605	C21DEC08A0080.csv			2.077801	2.08108	0.307984	2.373909	2.275049	2.267446	3.735393	2.56714
2021-G-605	C21DEC08A0078.csv			1.357161	1.390326	0.205306	1.535248	1.941021	1.742169	2.877358	2.223943
2021-G-605	C21DEC08A0104.csv			2.199094	1.37871	0.205306	1.564012	1.92833	2.187876	2.583734	2.682657
2021-G-605	C21DEC08A0118.csv			1.843205	1.867389	0.316469	2.164675	2.332732	2.14445	4.103023	2.620442
2021-G-605	C21DEC08A0107.csv			1.418862	1.373037	0.205306	1.618546	1.937568	1.85503	2.580819	2.2186
2021-G-605	C21DEC08A0067.csv			2.669182	2.743094	0.433954	2.737582	3.177735	2.924363	3.843289	3.486441
2021-G-605	C21DEC08A0103.csv			2.422301	1.650863	0.28239	1.88312	2.117861	2.90901	3.656015	3.261501
2021-G-605	C21DEC08A0079.csv			1.532567	1.528543	0.224437	1.739388	1.999709	2.162106	3.180234	2.43712
2021-G-605	C21DEC08A0070.csv			2.106873	2.34519	0.418309	2.354773	2.630871	2.643653	3.809485	2.807267
2021-G-605	C21DEC08A0115.csv			1.322397	1.315224	0.205306	1.607857	1.923771	1.796608	2.789029	2.215626
2021-G-605	C21DEC08A0105.csv			2.109162	2.319051	0.336106	2.380782	2.456777	2.145321	3.701473	2.655491
2021-G-605	C21DEC08A0072.csv			1.613406	1.67746	0.262919	1.70581	2.120764	1.980011	2.820512	2.367061

2021-G-605	C21DEC08A0066.csv			2.3719	1.745511	0.24503	1.808108	2.197575	3.31584	3.099802	3.632149
2021-G-605	C21DEC08A0120.csv			1.474893	1.321408	0.205306	1.488161	1.892881	1.839991	2.798278	2.240178
2021-G-605	C21DEC08A0091.csv			1.60337	1.772825	0.254098	1.702875	2.078698	1.849807	2.793774	2.374455
2021-G-605	C21DEC08A0106.csv			1.637092	1.325834	0.205306	1.543734	1.927457	1.907804	2.655743	2.453063
2021-G-605	C21DEC08A0069.csv			1.767983	1.895016	0.302736	1.998478	2.291697	2.411211	3.10141	2.53794
2021-G-605	C21DEC08A0117.csv			1.984281	1.678044	0.25692	1.905026	2.013982	2.283667	2.733409	2.497854

Analysis	**Source Filename**	**Comment**	159Tb	163Dy	165Ho	166Er	169Tm	172Yb	175Lu
			1s%	1s%	1s%	1s%	1s%	1s%	1s%
	ZY-LGT-1								
2021-G-605	C21DEC08A0114.csv		2.43147	2.530812	2.828444	3.110818	3.530632	3.050645	4.714521
2021-G-605	C21DEC08A0082.csv		1.851545	2.062502	2.38281	2.362372	2.859655	2.359462	4.167265
2021-G-605	C21DEC08A0077.csv		2.00569	2.097355	2.478004	2.374659	2.829885	2.370483	3.953753
2021-G-605	C21DEC08A0096.csv		2.203665	2.306256	2.627255	2.438097	2.958928	2.709355	4.261758
2021-G-605	C21DEC08A0081.csv		1.941851	2.118219	2.539932	2.568021	3.031759	2.457603	4.052504
2021-G-605	C21DEC08A0068.csv		2.24076	2.432707	2.60179	2.578152	3.257075	2.955092	4.156465
2021-G-605	C21DEC08A0101.csv		1.832885	1.990907	2.312554	2.297304	2.704659	2.206675	4.009477
2021-G-605	C21DEC08A0092.csv		2.087685	2.177335	2.511293	2.473328	2.934135	2.510158	4.195919
2021-G-605	C21DEC08A0102.csv		1.884093	2.044193	2.310409	2.32131	2.747241	2.263726	4.061791
2021-G-605	C21DEC08A0083.csv		2.088758	2.372596	2.682005	2.631046	3.184535	2.537283	4.312291
2021-G-605	C21DEC08A0071.csv	high common Pb	3.175121	4.416287	5.99014	6.261471	6.970958	7.366039	8.077456
2021-G-605	C21DEC08A0114.csv	high common Pb	2.897722	3.688056	3.655051	3.765797	5.359142	5.115609	6.879928
2021-G-605	C21DEC08A0095.csv		2.297988	2.387763	2.558431	2.665324	3.091671	2.636161	4.200285
2021-G-605	C21DEC08A0094.csv		2.278849	2.494947	2.66537	2.65833	3.512037	3.001255	4.405843
2021-G-605	C21DEC08A0119.csv		1.968513	2.264869	2.761287	2.764493	3.288087	2.816353	4.464344
2021-G-605	C21DEC08A0116.csv		2.127759	2.250827	2.57622	2.495155	2.959553	2.409386	4.432048
2021-G-605	C21DEC08A0071.csv		3.058784	2.867807	2.889593	2.795491	3.011467	3.144894	4.59571
2021-G-605	C21DEC08A0093.csv		2.031724	2.066835	2.474188	2.364901	2.954327	2.568062	4.299808
2021-G-605	C21DEC08A0069.csv	high common Pb	2.81006	2.926593	2.792409	3.085259	4.040207	3.861055	6.025704
2021-G-605	C21DEC08A0090.csv		2.817413	3.145953	3.108585	2.988496	3.912291	2.946132	4.552116
2021-G-605	C21DEC08A0080.csv		2.537409	2.504526	2.815432	2.707637	3.427539	2.840689	4.763656
2021-G-605	C21DEC08A0078.csv		1.849178	2.000104	2.380408	2.275738	2.764201	2.27509	4.149228
2021-G-605	C21DEC08A0104.csv		2.689811	2.89068	2.886699	2.630272	3.004949	2.527584	4.420174
2021-G-605	C21DEC08A0118.csv		2.158358	2.329759	2.617223	2.543852	3.057506	2.746812	4.191774
2021-G-605	C21DEC08A0107.csv		1.919131	2.094408	2.383121	2.274613	2.757714	2.382877	4.128588
2021-G-605	C21DEC08A0067.csv		3.002422	3.207451	3.599741	3.537341	3.695431	3.514343	5.341375

2021-G-605	C21DEC08A0103.csv	3.334212	3.438891	3.198663	3.023205	3.43693	3.320939	4.878661
2021-G-605	C21DEC08A0079.csv	2.277121	2.253895	2.470003	2.431324	3.124922	2.989112	4.643474
2021-G-605	C21DEC08A0070.csv	2.410491	2.845093	2.920092	2.989653	3.515535	3.725438	6.327165
2021-G-605	C21DEC08A0115.csv	1.837116	1.993913	2.376284	2.278223	2.719347	2.218962	4.000176
2021-G-605	C21DEC08A0105.csv	2.217604	2.707399	2.783458	2.867396	3.604287	2.687435	4.583416
2021-G-605	C21DEC08A0072.csv	2.180991	2.192804	2.457047	2.472253	3.2154	2.831718	4.750772
2021-G-605	C21DEC08A0066.csv	3.953366	3.195758	3.123308	2.897156	3.772167	3.540001	5.00224
2021-G-605	C21DEC08A0120.csv	1.889031	2.049978	2.436534	2.336267	2.703252	2.443891	4.405364
2021-G-605	C21DEC08A0091.csv	2.054083	2.259169	2.427053	2.538027	2.893577	2.466265	4.534632
2021-G-605	C21DEC08A0106.csv	2.316967	2.381522	2.615105	2.461695	2.99926	2.645731	4.396218
2021-G-605	C21DEC08A0069.csv	2.391511	2.574225	2.850588	2.667543	3.374294	3.063973	5.009195
2021-G-605	C21DEC08A0117.csv	2.321518	2.544329	2.744661	2.678919	3.320553	3.103239	5.268762

Analysis	**Source Filename**	**Comment**	204Pb	206Pb	207Pb	208Pb	232Th	235U	238U
			1s%	1s%	1s%	1s%	1s%	1s%	1s%
	ZY-LGT-1								
2021-G-605	C21DEC08A0114.csv		25.06662	1.651171	2.389938	1.964017	1.73102	5.715552	1.898456
2021-G-605	C21DEC08A0082.csv		22.42569	1.456196	1.580453	1.834976	1.174808	5.576571	1.394463
2021-G-605	C21DEC08A0077.csv		17.21451	1.418733	1.92051	1.648953	1.317811	5.581352	1.407375
2021-G-605	C21DEC08A0096.csv		63.9827	1.945689	2.417012	1.469456	1.518981	5.696587	1.82161
2021-G-605	C21DEC08A0081.csv		23.70413	1.702813	2.305779	1.448211	1.466173	5.75504	1.990974
2021-G-605	C21DEC08A0068.csv		18.66774	1.89618	2.214434	2.696912	2.086171	5.668755	1.733875
2021-G-605	C21DEC08A0101.csv		26.27727	1.329833	2.008405	1.214019	1.107227	5.561107	1.324737
2021-G-605	C21DEC08A0092.csv		19.06394	2.576271	3.144737	1.436106	1.254844	6.226898	3.093415
2021-G-605	C21DEC08A0102.csv		20.89334	1.410876	2.085453	1.363882	1.117814	5.579766	1.403535
2021-G-605	C21DEC08A0083.csv		4881.133	2.485261	5.795671	1.396303	1.775011	5.831002	2.201971
2021-G-605	C21DEC08A0071.csv	high common Pb	17.72291	2.620024	2.746781	2.730119	3.996745	6.136343	2.929406
2021-G-605	C21DEC08A0114.csv	high common Pb	10.31633	3.07177	3.824532	3.377247	2.223107	6.261109	2.999291
2021-G-605	C21DEC08A0095.csv		17.02305	1.577179	2.373927	1.450334	1.407669	5.648882	1.662855
2021-G-605	C21DEC08A0094.csv		113.758	1.665608	2.906781	1.667642	1.374881	5.652994	1.69294
2021-G-605	C21DEC08A0119.csv		38.22204	2.353848	2.727327	1.93751	1.706749	5.865115	2.28553
2021-G-605	C21DEC08A0116.csv		19.1834	1.371447	2.051104	1.358305	1.333964	5.61788	1.563461
2021-G-605	C21DEC08A0071.csv		39.52039	1.753538	3.142746	1.676603	1.760019	5.763055	2.049964
2021-G-605	C21DEC08A0093.csv		20.40903	2.002504	2.636697	1.386985	1.390097	5.700986	1.818561
2021-G-605	C21DEC08A0069.csv	high common Pb	29.2678	2.537377	6.445341	1.908637	1.652554	5.777607	2.002086
2021-G-605	C21DEC08A0090.csv		91.85246	2.05672	3.301101	1.920938	2.126599	5.766606	2.064862
2021-G-605	C21DEC08A0080.csv		35.08737	1.860038	2.512944	1.72273	1.434312	5.664416	1.707286

2021-G-605	C21DEC08A0078.csv	16.47387	1.247588	2.092954	1.451966	1.202513	5.579009	1.399173
2021-G-605	C21DEC08A0104.csv	38.05035	1.717883	3.833271	1.343275	1.145854	5.659045	1.564067
2021-G-605	C21DEC08A0118.csv	21.94553	1.857233	2.959563	1.668546	1.61838	5.65552	1.696336
2021-G-605	C21DEC08A0107.csv	65.89158	1.728326	2.693501	1.531743	1.279294	5.690173	1.707619
2021-G-605	C21DEC08A0067.csv	61.62322	2.158236	3.583529	1.986002	2.075834	5.870522	2.310856
2021-G-605	C21DEC08A0103.csv	22.33116	3.582835	5.084466	1.621275	2.05357	6.920315	4.34265
2021-G-605	C21DEC08A0079.csv	20.90652	4.811724	4.499323	1.929152	1.576306	7.241415	4.825373
2021-G-605	C21DEC08A0070.csv	41.48199	1.989748	5.279598	1.687504	1.641349	5.786983	2.078129
2021-G-605	C21DEC08A0115.csv	53.08266	1.258395	2.066839	1.224839	1.156642	5.559617	1.314726
2021-G-605	C21DEC08A0105.csv	20.04777	2.010352	3.361817	1.63664	1.459937	5.683553	1.782778
2021-G-605	C21DEC08A0072.csv	38.66719	1.710375	3.606357	1.581882	1.41103	5.629266	1.539341
2021-G-605	C21DEC08A0066.csv	23.03906	1.670557	3.132441	1.508528	1.806606	5.753229	1.985867
2021-G-605	C21DEC08A0120.csv	14.55666	3.544754	4.005757	1.362224	1.127738	6.321917	3.132874
2021-G-605	C21DEC08A0091.csv	20.79393	1.715852	3.174742	1.454144	1.274198	5.598172	1.47508
2021-G-605	C21DEC08A0106.csv	24.69378	3.240286	3.291369	1.38159	1.239851	6.285741	3.303595
2021-G-605	C21DEC08A0069.csv	26.32077	1.851703	5.165162	1.736886	1.523659	5.708066	1.871768
2021-G-605	C21DEC08A0117.csv	49.50603	2.345572	4.480843	1.683288	1.329339	5.887897	1.949468

Analysis	Source Filename	Comment	CommPb at 206Pb/238U Age		206Pb/238U Age (Ma)	206Pb/238U Age (Ma)	206Pb/238U Age (Ma)	207Pb/206Pb Age (Ma)	207Pb/206Pb Age (Ma)
					Age	2s%	2s_sys%	Age	2s%
	ZY-LG-2								
2021-G-604	C21DEC08A0054.csv		0.836525		14.16644	2.803649	2.978842	557.4581	37.41878055
2021-G-604	C21DEC08A0021.csv		0.836526		14.19095	1.526757	1.828671	523.5589	16.36438834
2021-G-604	C21DEC08A0055.csv	high common Pb	0.83673		17.3646	3.898499	4.026332	2801.386	4.910572694
2021-G-604	C21DEC08A0045.csv	high common Pb	0.836549		14.54358	3.469158	3.612216	947.8943	26.87400787
2021-G-604	C21DEC08A0011.csv	high common Pb	0.836821		18.78919	4.618343	4.726748	3135.429	4.134382121
2021-G-604	C21DEC08A0047.csv		0.836535		14.32801	1.68838	1.965624	477.6331	23.58752774
2021-G-604	C21DEC08A0022.csv		0.836548		14.52529	2.884119	3.0547	675.2132	30.71356783
2021-G-604	C21DEC08A0046.csv		0.836554		14.62707	1.790542	2.054042	716.9898	14.8625584
2021-G-604	C21DEC08A0018.csv		0.836555		14.63706	2.050564	2.284264	668.8725	17.91258482
2021-G-604	C21DEC08A0056.csv		0.836576		14.9568	3.889636	4.01775	1079.301	25.77467159
2021-G-604	C21DEC08A0022.csv	high common Pb	0.836607		15.44524	2.661084	2.845069	1539.233	6.124540546
2021-G-604	C21DEC08A0023.csv		0.836586		15.11336	2.598038	2.786189	1154.177	13.06007747
2021-G-604	C21DEC08A0059.csv		0.836567		14.82186	2.200914	2.420139	672.4462	22.08877688
2021-G-604	C21DEC08A0029.csv	high common Pb	0.837179		24.37027	3.928482	4.055369	3713.667	2.843317421

2021-G-604	C21DEC08A0044.csv		0.83657		14.8722	2.120841	2.347555	686.4351	19.20028881
2021-G-604	C21DEC08A0035.csv		0.836578		14.99221	2.061676	2.294245	881.3746	16.01332609
2021-G-604	C21DEC08A0032.csv		0.836578		14.99931	2.199919	2.419234	785.0117	18.44584745
2021-G-604	C21DEC08A0011.csv		0.836591		15.19273	2.639455	2.824849	1070.501	15.22364355
2021-G-604	C21DEC08A0030.csv		0.836586		15.12223	1.948766	2.193339	952.7626	14.37940442
2021-G-604	C21DEC08A0006.csv		0.836606		15.42942	2.380602	2.58463	1313.438	11.23465946
2021-G-604	C21DEC08A0009.csv		0.836587		15.13754	2.21941	2.436972	866.3174	15.88668275
2021-G-604	C21DEC08A0024.csv		0.836624		15.71274	2.167396	2.389698	1486.272	8.108977842
2021-G-604	C21DEC08A0034.csv		0.836596		15.27284	2.004146	2.242688	956.5958	13.93348898
2021-G-604	C21DEC08A0007.csv		0.836612		15.52634	2.206094	2.424851	1264.103	11.975792
2021-G-604	C21DEC08A0005.csv		0.836589		15.16083	2.180836	2.401894	678.212	25.32481114
2021-G-604	C21DEC08A0023.csv	high common Pb	0.83671		17.05706	5.204263	5.300698	2319.507	7.904082015
2021-G-604	C21DEC08A0043.csv		0.836602		15.3663	2.169508	2.391613	935.543	15.62362282
2021-G-604	C21DEC08A0057.csv		0.83661		15.49271	2.595659	2.783971	1029.388	14.62335614
2021-G-604	C21DEC08A0048.csv		0.836595		15.25844	3.185952	3.341159	660.02	39.7481637
2021-G-604	C21DEC08A0033.csv		0.83662		15.65411	2.410051	2.61178	1204.885	12.37004265
2021-G-604	C21DEC08A0010.csv		0.836602		15.37032	1.851712	2.107579	731.7173	14.91686112

2021-G-604	C21DEC08A0031.csv		0.836605		15.42083	2.415708	2.617001	735.3278	24.11203892
2021-G-604	C21DEC08A0055.csv		0.836618		15.6199	2.528777	2.721721	958.4678	17.28264358
2021-G-604	C21DEC08A0020.csv		0.836604		15.39565	1.826025	2.085046	591.0799	21.29701343
2021-G-604	C21DEC08A0058.csv		0.836606		15.43475	2.357503	2.56337	641.8972	24.83601442
2021-G-604	C21DEC08A0019.csv		0.836614		15.55361	2.233767	2.450054	447.5487	35.47586855
2021-G-604	C21DEC08A0042.csv		0.836621		15.67325	3.50167	3.643452	607.46	48.19769595
2021-G-604	C21DEC08A0042.csv	high common Pb	0.836651		16.13	5.36475	5.45835	1166.874	24.88884591
2021-G-604	C21DEC08A0029.csv		0.836765		17.90877	4.099079	4.22084	2237.459	8.461394492
2021-G-604	C21DEC08A0008.csv		0.836745		17.60966	1.822979	2.082379	239.6292	55.65000915

Analysis	Source Filename	Comment	207Pb/206Pb Age (Ma)	207Pb/235U(calc) Age (Ma)	207Pb/235U(calc) Age (Ma)	207Pb/235U(calc) Age (Ma)	208Pb/232Th Age (Ma)	208Pb/232Th Age (Ma)	208Pb/232Th Age (Ma)
			2s_sys%	Age	2s%	2_sys%	Age	2s%	2s_sys%
	ZY-LG-2								
2021-G-604	C21DEC08A0054.csv		37.42252	17.07821	9.597881	9.65098	14.55719	4.3933	4.66017432
2021-G-604	C21DEC08A0021.csv		16.37294	16.60527	4.674175	4.782259	13.84177	2.324566	2.796380677
2021-G-604	C21DEC08A0055.csv	high common Pb	4.938998	71.53572	8.020518	8.083985	16.63904	3.732235	4.042983363
2021-G-604	C21DEC08A0045.csv	high common Pb	26.87922	21.99539	13.07804	13.11706	13.9378	2.813657	3.214468093
2021-G-604	C21DEC08A0011.csv	high common Pb	4.168104	93.8889	7.671881	7.738208	17.07608	3.95471	4.249220104
2021-G-604	C21DEC08A0047.csv		23.59346	16.31849	5.316206	5.411482	13.57611	2.360221	2.826089795
2021-G-604	C21DEC08A0022.csv		30.71813	18.25761	10.67162	10.7194	13.66434	3.079169	3.449264121
2021-G-604	C21DEC08A0046.csv		14.87197	18.77356	5.376959	5.471177	13.75666	2.326769	2.798212858
2021-G-604	C21DEC08A0018.csv		17.9204	18.51404	5.896018	5.982067	13.95595	2.329922	2.800835009
2021-G-604	C21DEC08A0056.csv		25.7801	24.22411	13.5637	13.60132	14.66343	3.60633	3.927054119
2021-G-604	C21DEC08A0022.csv	high common Pb	6.147355	29.1704	5.317584	5.412836	15.16262	3.074761	3.44532901

2021-G-604	C21DEC08A0023.csv		13.07079	24.27986	7.789801	7.855132	14.02659	2.731098	3.142456888
2021-G-604	C21DEC08A0059.csv		22.09511	18.86939	7.180634	7.251455	13.81139	2.501749	2.945316018
2021-G-604	C21DEC08A0029.csv	high common Pb	2.892132	170.0342	7.159294	7.230324	17.62892	3.31095	3.657667625
2021-G-604	C21DEC08A0044.csv		19.20758	18.60751	6.416056	6.495219	13.7777	2.516968	2.958254311
2021-G-604	C21DEC08A0035.csv		16.02207	21.29533	6.77999	6.854951	14.1066	2.323008	2.795086067
2021-G-604	C21DEC08A0032.csv		18.45344	20.81053	7.058508	7.130542	14.01549	2.326854	2.798283602
2021-G-604	C21DEC08A0011.csv		15.23284	23.7988	8.151072	8.213529	13.90582	2.492118	2.937140134
2021-G-604	C21DEC08A0030.csv		14.38914	21.36032	6.892329	6.966081	14.01854	2.428668	2.883499149
2021-G-604	C21DEC08A0006.csv		11.24711	27.82825	7.651415	7.717917	14.00549	2.332679	2.803128771
2021-G-604	C21DEC08A0009.csv		15.89549	21.00545	6.858886	6.932995	14.45591	2.404314	2.863016464
2021-G-604	C21DEC08A0024.csv		8.126223	31.02227	6.615653	6.692456	14.20606	2.303619	2.778993021
2021-G-604	C21DEC08A0034.csv		13.94353	23.10313	6.700444	6.776286	13.98869	2.270013	2.751199212
2021-G-604	C21DEC08A0007.csv		11.98748	27.26296	7.916929	7.981219	13.97406	2.412014	2.869485826
2021-G-604	C21DEC08A0005.csv		25.33034	20.08973	8.302311	8.36364	13.82068	2.266225	2.748074801
2021-G-604	C21DEC08A0023.csv	high common Pb	7.921773	53.00541	10.24511	10.29487	15.77959	4.076571	4.362862878
2021-G-604	C21DEC08A0043.csv		15.63258	23.05379	7.255909	7.326003	13.92061	2.363719	2.829011804

2021-G-604	C21DEC08A0057.csv		14.63293	24.35942	7.605532	7.672432	13.98918	2.295309	2.772108415
2021-G-604	C21DEC08A0048.csv		39.75169	20.01451	12.0993	12.14146	14.20918	2.661509	3.082169445
2021-G-604	C21DEC08A0033.csv		12.38135	26.78746	7.626721	7.693437	13.9444	2.290905	2.768462978
2021-G-604	C21DEC08A0010.csv		14.92624	19.82514	5.484839	5.577236	14.00454	2.3163	2.789513579
2021-G-604	C21DEC08A0031.csv		24.11784	21.01394	8.432464	8.492853	13.85839	2.396625	2.856562846
2021-G-604	C21DEC08A0055.csv		17.29074	22.22317	8.681935	8.7406	14.20906	2.725201	3.137333442
2021-G-604	C21DEC08A0020.csv		21.30359	18.83771	6.426121	6.505162	14.37868	2.367426	2.832109878
2021-G-604	C21DEC08A0058.csv		24.84165	19.76912	7.553207	7.620566	14.14869	2.354203	2.821065652
2021-G-604	C21DEC08A0019.csv		35.47981	17.63933	7.543802	7.611244	13.84579	2.460832	2.91064191
2021-G-604	C21DEC08A0042.csv		48.2006	20.15742	13.34402	13.38226	13.87339	2.66754	3.087378829
2021-G-604	C21DEC08A0042.csv	high common Pb	24.89447	27.11102	14.31848	14.35413	14.00152	3.029048	3.404595411
2021-G-604	C21DEC08A0029.csv		8.477923	53.20075	12.66994	12.71021	14.68085	2.920528	3.308416744
2021-G-604	C21DEC08A0008.csv		55.65252	18.17208	6.102254	6.185434	14.01705	2.329839	2.800765546
2021-G-604	C21DEC08A0053.csv		5.859906	454.9208	2.982513	3.149203	479.958	2.388789	2.849991952

Analysis	Source Filename	Comment	206Pb/204Pb	206Pb/204Pb	207Pb/204Pb	207Pb/204Pb	208Pb/204Pb	208Pb/204Pb	Spot Size (μm)	Time (s)
			ratio	1s%	ratio	1s%	ratio	1s%		
	ZY-LG-2									
2021-G-604	C21DEC08A0054.csv								13	3.976
2021-G-604	C21DEC08A0021.csv								13	26.736
2021-G-604	C21DEC08A0055.csv	high common Pb							13	6.643
2021-G-604	C21DEC08A0045.csv	high common Pb							13	8.987
2021-G-604	C21DEC08A0011.csv	high common Pb							13	5.546
2021-G-604	C21DEC08A0047.csv								13	26.736
2021-G-604	C21DEC08A0022.csv								13	7.968
2021-G-604	C21DEC08A0046.csv								13	26.736
2021-G-604	C21DEC08A0018.csv								13	18.866
2021-G-604	C21DEC08A0056.csv								13	5.406
2021-G-604	C21DEC08A0022.csv	high common Pb							13	9.338
2021-G-604	C21DEC08A0023.csv								13	10.161
2021-G-604	C21DEC08A0059.csv								13	16.647
2021-G-604	C21DEC08A0029.csv	high common Pb							13	8.672
2021-G-604	C21DEC08A0044.csv								13	15.119
2021-G-604	C21DEC08A0035.csv								13	22.267
2021-G-604	C21DEC08A0032.csv								13	26.736
2021-G-604	C21DEC08A0011.csv								13	13.217

2021-G-604	C21DEC08A0030.csv							13	18.35
2021-G-604	C21DEC08A0006.csv							13	21.229
2021-G-604	C21DEC08A0009.csv							13	18.377
2021-G-604	C21DEC08A0024.csv							13	26.736
2021-G-604	C21DEC08A0034.csv							13	26.736
2021-G-604	C21DEC08A0007.csv							13	20.653
2021-G-604	C21DEC08A0005.csv							13	26.736
2021-G-604	C21DEC08A0023.csv	high common Pb						13	4.227
2021-G-604	C21DEC08A0043.csv							13	26.736
2021-G-604	C21DEC08A0057.csv							13	23.362
2021-G-604	C21DEC08A0048.csv							13	7.049
2021-G-604	C21DEC08A0033.csv							13	26.736
2021-G-604	C21DEC08A0010.csv							13	26.736
2021-G-604	C21DEC08A0031.csv							13	26.736
2021-G-604	C21DEC08A0055.csv							13	9.995
2021-G-604	C21DEC08A0020.csv							13	26.736
2021-G-604	C21DEC08A0058.csv							13	17.54
2021-G-604	C21DEC08A0019.csv							13	18.289
2021-G-604	C21DEC08A0042.csv							13	15.537
2021-G-604	C21DEC08A0042.csv	high common Pb						13	6.14
2021-G-604	C21DEC08A0029.csv							13	7.337
2021-G-604	C21DEC08A0008.csv							13	26.736
2021-G-604	C21DEC08A0053.csv							13	17.791

Analysis	Source Filename	Comment	CommPb at 206Pb/238U Age	206Pb/238U Age (Ma)	206Pb/238U Age (Ma)	206Pb/238U Age (Ma)	207Pb/206Pb Age (Ma)	207Pb/206Pb Age (Ma)
					Age	2s%	2s_sys%	Age	2s%
	ZY-LGT-1								
2021-G-605	C21DEC08A0114.csv		0.836489		13.6055	1.724279	1.996544	661.3916	12.76051
2021-G-605	C21DEC08A0082.csv		0.836478		13.42678	1.271193	1.621413	158.5937	29.04606
2021-G-605	C21DEC08A0077.csv		0.836479		13.45442	1.435662	1.753332	217.3602	29.36493
2021-G-605	C21DEC08A0096.csv		0.836487		13.57341	1.489633	1.797792	306.2599	24.15811
2021-G-605	C21DEC08A0081.csv		0.836487		13.57251	1.429775	1.748515	262.8972	27.11534
2021-G-605	C21DEC08A0068.csv		0.836491		13.62944	1.678391	1.95705	222.5158	32.9609
2021-G-605	C21DEC08A0101.csv		0.836492		13.64698	1.390224	1.716325	252.6411	28.24003
2021-G-605	C21DEC08A0092.csv		0.836494		13.69134	1.645441	1.928866	333.4849	22.26224

2021-G-605	C21DEC08A0102.csv		0.836494		13.68082	1.411805	1.733852	199.6186	36.45847
2021-G-605	C21DEC08A0083.csv		0.836511		13.95316	1.594978	1.886002	650.6743	21.70307
2021-G-605	C21DEC08A0071.csv	high common Pb	0.836578		15.00253	2.252071	2.466753	1878.129	4.851232
2021-G-605	C21DEC08A0114.csv	high common Pb	0.837277		25.89711	2.866506	3.038076	3936.81	1.538716
2021-G-605	C21DEC08A0095.csv		0.836514		13.99729	1.607848	1.896898	454.1496	21.74146
2021-G-605	C21DEC08A0094.csv		0.83652		14.09094	1.958609	2.20209	598.6626	21.89652
2021-G-605	C21DEC08A0119.csv		0.836513		13.97389	1.601223	1.891286	315.0397	26.46795
2021-G-605	C21DEC08A0116.csv		0.836517		14.03838	1.479219	1.789172	348.0554	23.31125
2021-G-605	C21DEC08A0071.csv		0.836518		14.06118	1.767548	2.03403	324.0116	36.40263
2021-G-605	C21DEC08A0093.csv		0.836526		14.17821	1.645531	1.928943	570.0492	14.81388
2021-G-605	C21DEC08A0069.csv	high common Pb	0.83665		16.11634	3.623029	3.760238	2358.402	7.344016

2021-G-605	C21DEC08A0090.csv		0.836525		14.16863	1.687061	1.964491	378.5803	34.16685
2021-G-605	C21DEC08A0080.csv		0.836533		14.2931	2.197013	2.416591	354.9916	30.02854
2021-G-605	C21DEC08A0078.csv		0.836533		14.29534	1.461539	1.774583	331.7915	26.16576
2021-G-605	C21DEC08A0104.csv		0.836578		14.98782	2.547568	2.739188	1393.717	10.54899
2021-G-605	C21DEC08A0118.csv		0.83654		14.40359	1.894356	2.145142	446.2546	26.252
2021-G-605	C21DEC08A0107.csv		0.836562		14.74195	1.789626	2.053244	904.7788	11.68567
2021-G-605	C21DEC08A0067.csv		0.836555		14.63641	2.510766	2.704994	338.5073	45.35141
2021-G-605	C21DEC08A0103.csv		0.836565		14.7897	2.086733	2.316787	631.0042	24.92602
2021-G-605	C21DEC08A0079.csv		0.836569		14.84732	1.954346	2.198299	698.6212	19.26829
2021-G-605	C21DEC08A0070.csv		0.836567		14.82361	3.705528	3.83979	640.7453	35.85813
2021-G-605	C21DEC08A0115.csv		0.836554		14.62427	1.410622	1.732889	195.2396	43.90072

2021-G-605	C21DEC08A0105.csv		0.836558		14.67941	2.208391	2.42694	314.6785	44.80776
2021-G-605	C21DEC08A0072.csv		0.836591		15.20623	2.198085	2.417566	1063.082	13.6319
2021-G-605	C21DEC08A0066.csv		0.836578		15.0018	1.825927	2.08496	543.099	22.02146
2021-G-605	C21DEC08A0120.csv		0.836593		15.22427	2.159575	2.382606	863.9962	14.73497
2021-G-605	C21DEC08A0091.csv		0.836595		15.26527	2.362635	2.568092	904.4237	14.00734
2021-G-605	C21DEC08A0106.csv		0.836597		15.28716	2.133973	2.359426	872.5299	15.44704
2021-G-605	C21DEC08A0069.csv		0.836598		15.3154	3.260765	3.412571	816.0746	25.99925
2021-G-605	C21DEC08A0117.csv		0.836639		15.94018	2.829102	3.00281	1146.888	15.74604

Analysis	Source Filename	Comment	CommPb at 206Pb/238U Age	206Pb/238U Age (Ma)	206Pb/238U Age (Ma)	206Pb/238U Age (Ma)	207Pb/206Pb Age (Ma)	207Pb/206Pb Age (Ma)
				Age	2s%	2s_sys%	Age	2s%
	ZY-LGT-1							
2021-G-605	C21DEC08A0114.csv		0.836489	13.6055	1.724279	1.996544	661.3916	12.76051
2021-G-605	C21DEC08A0082.csv		0.836478	13.42678	1.271193	1.621413	158.5937	29.04606
2021-G-605	C21DEC08A0077.csv		0.836479	13.45442	1.435662	1.753332	217.3602	29.36493
2021-G-605	C21DEC08A0096.csv		0.836487	13.57341	1.489633	1.797792	306.2599	24.15811
2021-G-605	C21DEC08A0081.csv		0.836487	13.57251	1.429775	1.748515	262.8972	27.11534
2021-G-605	C21DEC08A0068.csv		0.836491	13.62944	1.678391	1.95705	222.5158	32.9609
2021-G-605	C21DEC08A0101.csv		0.836492	13.64698	1.390224	1.716325	252.6411	28.24003
2021-G-605	C21DEC08A0092.csv		0.836494	13.69134	1.645441	1.928866	333.4849	22.26224
2021-G-605	C21DEC08A0102.csv		0.836494	13.68082	1.411805	1.733852	199.6186	36.45847
2021-G-605	C21DEC08A0083.csv		0.836511	13.95316	1.594978	1.886002	650.6743	21.70307
2021-G-605	C21DEC08A0071.csv	high common Pb	0.836578	15.00253	2.252071	2.466753	1878.129	4.851232
2021-G-605	C21DEC08A0114.csv	high common Pb	0.837277	25.89711	2.866506	3.038076	3936.81	1.538716
2021-G-605	C21DEC08A0095.csv		0.836514	13.99729	1.607848	1.896898	454.1496	21.74146

2021-G-605	C21DEC08A0094.csv		0.83652		14.09094	1.958609	2.20209	598.6626	21.89652
2021-G-605	C21DEC08A0119.csv		0.836513		13.97389	1.601223	1.891286	315.0397	26.46795
2021-G-605	C21DEC08A0116.csv		0.836517		14.03838	1.479219	1.789172	348.0554	23.31125
2021-G-605	C21DEC08A0071.csv		0.836518		14.06118	1.767548	2.03403	324.0116	36.40263
2021-G-605	C21DEC08A0093.csv		0.836526		14.17821	1.645531	1.928943	570.0492	14.81388
2021-G-605	C21DEC08A0069.csv	high common Pb	0.83665		16.11634	3.623029	3.760238	2358.402	7.344016
2021-G-605	C21DEC08A0090.csv		0.836525		14.16863	1.687061	1.964491	378.5803	34.16685
2021-G-605	C21DEC08A0080.csv		0.836533		14.2931	2.197013	2.416591	354.9916	30.02854
2021-G-605	C21DEC08A0078.csv		0.836533		14.29534	1.461539	1.774583	331.7915	26.16576
2021-G-605	C21DEC08A0104.csv		0.836578		14.98782	2.547568	2.739188	1393.717	10.54899
2021-G-605	C21DEC08A0118.csv		0.83654		14.40359	1.894356	2.145142	446.2546	26.252
2021-G-605	C21DEC08A0107.csv		0.836562		14.74195	1.789626	2.053244	904.7788	11.68567
2021-G-605	C21DEC08A0067.csv		0.836555		14.63641	2.510766	2.704994	338.5073	45.35141
2021-G-605	C21DEC08A0103.csv		0.836565		14.7897	2.086733	2.316787	631.0042	24.92602
2021-G-605	C21DEC08A0079.csv		0.836569		14.84732	1.954346	2.198299	698.6212	19.26829
2021-G-605	C21DEC08A0070.csv		0.836567		14.82361	3.705528	3.83979	640.7453	35.85813
2021-G-605	C21DEC08A0115.csv		0.836554		14.62427	1.410622	1.732889	195.2396	43.90072

2021-G-605	C21DEC08A0105.csv		0.836558		14.67941	2.208391	2.42694	314.6785	44.80776
2021-G-605	C21DEC08A0072.csv		0.836591		15.20623	2.198085	2.417566	1063.082	13.6319
2021-G-605	C21DEC08A0066.csv		0.836578		15.0018	1.825927	2.08496	543.099	22.02146
2021-G-605	C21DEC08A0120.csv		0.836593		15.22427	2.159575	2.382606	863.9962	14.73497
2021-G-605	C21DEC08A0091.csv		0.836595		15.26527	2.362635	2.568092	904.4237	14.00734
2021-G-605	C21DEC08A0106.csv		0.836597		15.28716	2.133973	2.359426	872.5299	15.44704
2021-G-605	C21DEC08A0069.csv		0.836598		15.3154	3.260765	3.412571	816.0746	25.99925
2021-G-605	C21DEC08A0117.csv		0.836639		15.94018	2.829102	3.00281	1146.888	15.74604

Analysis	Source Filename	Comment	207Pb/206Pb Age (Ma)	207Pb/235U(calc) Age (Ma)	207Pb/235U(calc) Age (Ma)	207Pb/235U(calc) Age (Ma)	208Pb/232Th Age (Ma)	208Pb/232Th Age (Ma)	208Pb/232Th Age (Ma)
			2s_sys%	Age	2s%	2_sys%	Age	2s%	2s_sys%
	ZY-LGT-1								
2021-G-605	C21DEC08A0114.csv		12.77148	17.1526	4.840309	4.944764	14.99596	2.937641	3.323534
2021-G-605	C21DEC08A0082.csv		29.05087	13.33496	2.995693	3.161689	15.77131	2.861409	3.256348
2021-G-605	C21DEC08A0077.csv		29.36969	13.74903	3.518219	3.660595	13.51978	2.373439	2.837138
2021-G-605	C21DEC08A0096.csv		24.16391	14.30993	3.91472	4.043159	13.83345	2.727398	3.139241
2021-G-605	C21DEC08A0081.csv		27.12051	14.0828	3.767137	3.900438	13.47261	2.31087	2.785006
2021-G-605	C21DEC08A0068.csv		32.96514	13.7133	3.860804	3.990978	14.42812	2.621358	3.047566
2021-G-605	C21DEC08A0101.csv		28.24499	14.31203	3.786877	3.919507	13.4197	2.345113	2.813485
2021-G-605	C21DEC08A0092.csv		22.26853	14.81167	3.883725	4.013155	13.75755	2.329503	2.800487
2021-G-605	C21DEC08A0102.csv		36.46231	13.8421	3.820549	3.952049	13.27571	2.296148	2.772803
2021-G-605	C21DEC08A0083.csv		21.70952	17.39543	7.029206	7.101537	13.71824	2.930336	3.317078
2021-G-605	C21DEC08A0071.csv	high common Pb	4.880003	33.96607	5.891664	5.977775	16.99242	4.024439	4.314191
2021-G-605	C21DEC08A0114.csv	high common Pb	1.627151	195.3667	5.517934	5.609786	79.31673	6.329814	6.517874
2021-G-605	C21DEC08A0095.csv		21.7479	15.80469	4.903678	5.006811	13.43335	2.473388	2.921264
2021-G-605	C21DEC08A0094.csv		21.90291	17.06955	6.279286	6.360151	14.02541	2.657808	3.078974

2021-G-605	C21DEC08A0119.csv		26.47324	14.91665	4.45319	4.566508	13.16599	2.287923	2.765995
2021-G-605	C21DEC08A0116.csv		23.31725	15.06833	4.186532	4.306872	13.77536	2.461059	2.910833
2021-G-605	C21DEC08A0071.csv		36.40647	14.92918	5.297413	5.393022	13.87669	2.551421	2.987623
2021-G-605	C21DEC08A0093.csv		14.82333	16.87474	4.414079	4.528376	13.49863	2.423275	2.878958
2021-G-605	C21DEC08A0069.csv	high common Pb	7.363053	51.49468	10.6549	10.70275	14.86912	3.359286	3.701478
2021-G-605	C21DEC08A0090.csv		34.17095	15.59045	6.085906	6.169307	13.70103	2.665227	3.085381
2021-G-605	C21DEC08A0080.csv		30.0332	15.45887	5.14659	5.244949	13.39212	2.470611	2.918914
2021-G-605	C21DEC08A0078.csv		26.17111	15.31232	4.225582	4.34484	13.30407	2.268514	2.749963
2021-G-605	C21DEC08A0104.csv		10.56226	28.37487	7.69069	7.756856	13.82165	2.300043	2.776029
2021-G-605	C21DEC08A0118.csv		26.25733	16.09728	5.618133	5.708372	13.74652	2.744484	3.154098
2021-G-605	C21DEC08A0107.csv		11.69764	20.75957	5.462089	5.554864	13.61609	2.265281	2.747296
2021-G-605	C21DEC08A0067.csv		45.35449	15.84972	7.008751	7.081292	13.9241	2.702702	3.11781
2021-G-605	C21DEC08A0103.csv		24.93164	18.06498	7.064283	7.136259	13.67748	2.53352	2.972349
2021-G-605	C21DEC08A0079.csv		19.27555	18.81191	6.622031	6.698761	13.80348	2.377827	2.84081
2021-G-605	C21DEC08A0070.csv		35.86203	18.23342	10.63017	10.67814	14.24528	3.091291	3.46009
2021-G-605	C21DEC08A0115.csv		43.90391	14.84711	4.096988	4.219882	13.44424	2.265894	2.747802
2021-G-605	C21DEC08A0105.csv		44.81088	15.24716	6.471449	6.549943	13.40213	2.744851	3.154417

2021-G-605	C21DEC08A0072.csv		13.64217	23.37173	7.316227	7.385748	14.09543	2.754236	3.162587
2021-G-605	C21DEC08A0066.csv		22.02781	17.68152	5.928159	6.013748	14.14603	2.614078	3.041307
2021-G-605	C21DEC08A0120.csv		14.74447	22.12048	6.362606	6.442426	13.69912	2.334383	2.804547
2021-G-605	C21DEC08A0091.csv		14.01733	21.29471	6.37094	6.450656	14.07548	2.406683	2.865006
2021-G-605	C21DEC08A0106.csv		15.4561	21.89228	6.695997	6.771888	13.78983	2.33986	2.809108
2021-G-605	C21DEC08A0069.csv		26.00463	21.09534	9.875902	9.927515	13.87946	2.706137	3.120788
2021-G-605	C21DEC08A0117.csv		15.75492	26.6163	9.045205	9.101529	13.94782	2.594805	3.024757

Analysis	Source Filename	Comment	206Pb/204Pb	206Pb/204Pb	207Pb/204Pb	207Pb/204Pb	208Pb/204Pb	208Pb/204Pb	Spot Size (µm)	Time (s)
			ratio	1s%	ratio	1s%	ratio	1s%		
	ZY-LGT-1									
2021-G-605	C21DEC08A0114.csv								13	8.482
2021-G-605	C21DEC08A0082.csv								13	26.736
2021-G-605	C21DEC08A0077.csv								13	20.445
2021-G-605	C21DEC08A0096.csv								13	14.246
2021-G-605	C21DEC08A0081.csv								13	19.989
2021-G-605	C21DEC08A0068.csv								13	11.775
2021-G-605	C21DEC08A0101.csv								13	26.736
2021-G-605	C21DEC08A0092.csv								13	26.736
2021-G-605	C21DEC08A0102.csv								13	26.736
2021-G-605	C21DEC08A0083.csv								13	11.42
2021-G-605	C21DEC08A0071.csv	high common Pb	276.7262	17.08546	31.51949	17.11853	217.5918	16.99469	13	5.323
2021-G-605	C21DEC08A0114.csv	high common Pb	44.4062	7.535472	18.06084	7.345959	50.26936	6.986084	13	2.286

2021-G-605	C21DEC08A0095.csv								13	12.986
2021-G-605	C21DEC08A0094.csv								13	8.923
2021-G-605	C21DEC08A0119.csv								13	26.736
2021-G-605	C21DEC08A0116.csv								13	13.62
2021-G-605	C21DEC08A0071.csv								13	7.416
2021-G-605	C21DEC08A0093.csv								13	19.413
2021-G-605	C21DEC08A0069.csv	high common Pb							13	6.226
2021-G-605	C21DEC08A0090.csv								13	8.217
2021-G-605	C21DEC08A0080.csv								13	10.364
2021-G-605	C21DEC08A0078.csv								13	26.736
2021-G-605	C21DEC08A0104.csv								13	26.736
2021-G-605	C21DEC08A0118.csv								13	9.873
2021-G-605	C21DEC08A0107.csv								13	26.736
2021-G-605	C21DEC08A0067.csv								13	5.003
2021-G-605	C21DEC08A0103.csv								13	12.536
2021-G-605	C21DEC08A0079.csv								13	21.35
2021-G-605	C21DEC08A0070.csv								13	5.297

2021-G-605	C21DEC08A0115.csv								13	26.736
2021-G-605	C21DEC08A0105.csv								13	8.577
2021-G-605	C21DEC08A0072.csv								13	14.86
2021-G-605	C21DEC08A0066.csv								13	17.334
2021-G-605	C21DEC08A0120.csv								13	26.736
2021-G-605	C21DEC08A0091.csv								13	15.963
2021-G-605	C21DEC08A0106.csv								13	26.736
2021-G-605	C21DEC08A0069.csv								13	10.853
2021-G-605	C21DEC08A0117.csv								13	15.552

APPENDIX C 1.3 Zircon images of two two-mica leucogranites (ZY-LG-2)

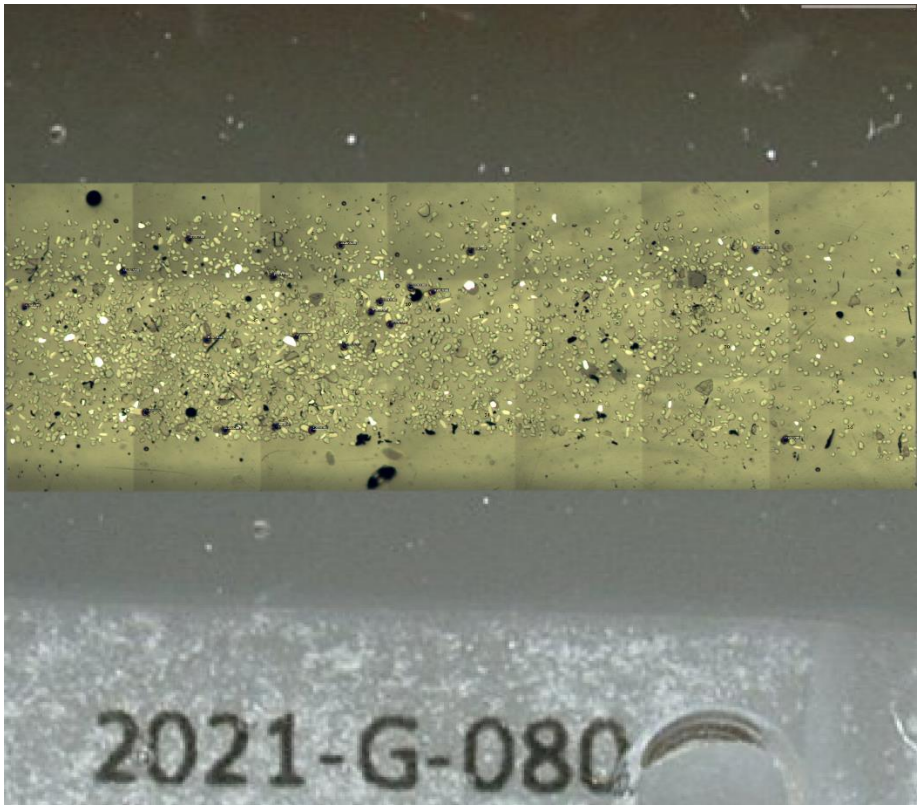

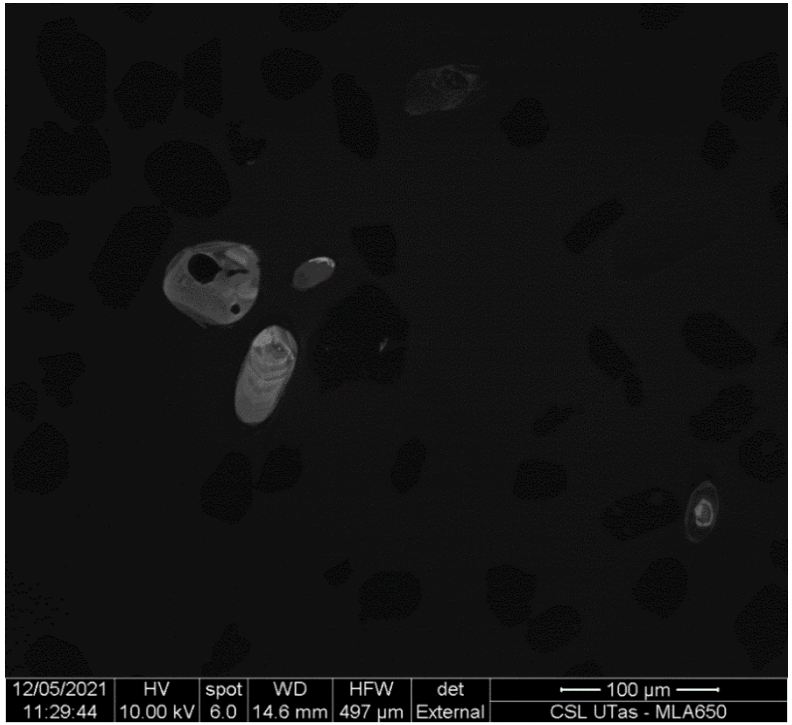
12/05/2021
11:29:44
HV
10.00 kV
spot
6.0
WD
14.6 mm
HFW
497 µm
det
External
100 µm
CSL UTas - MLA650

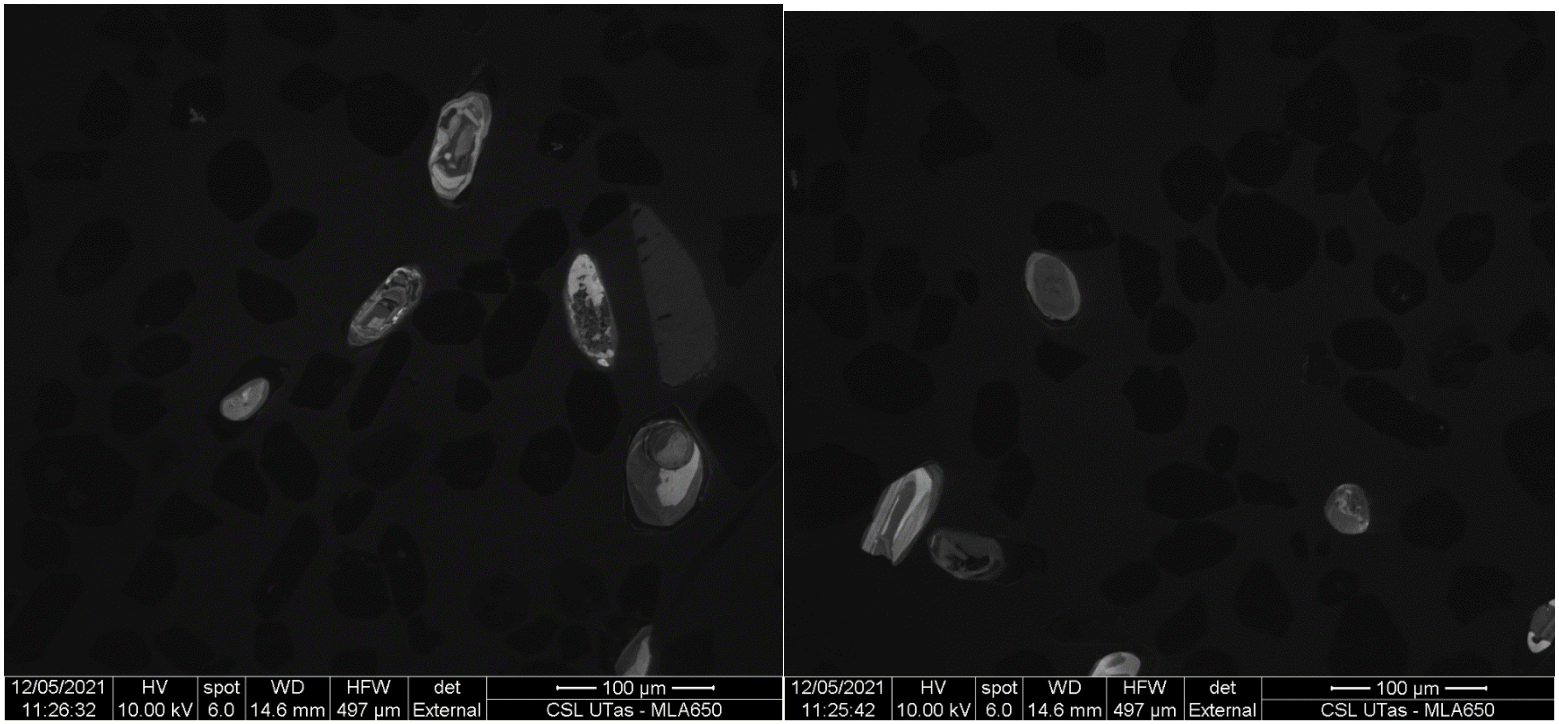
12/05/2021 HV spot WD HFW det 100 µm
11:26:32 10.00 kV 6.0 14.6 mm 497 µm External CSL UTas - MLA650
12/05/2021 HV spot WD HFW det 100 µm
11:25:42 10.00 kV 6.0 14.6 mm 497 µm External CSL UTas - MLA650

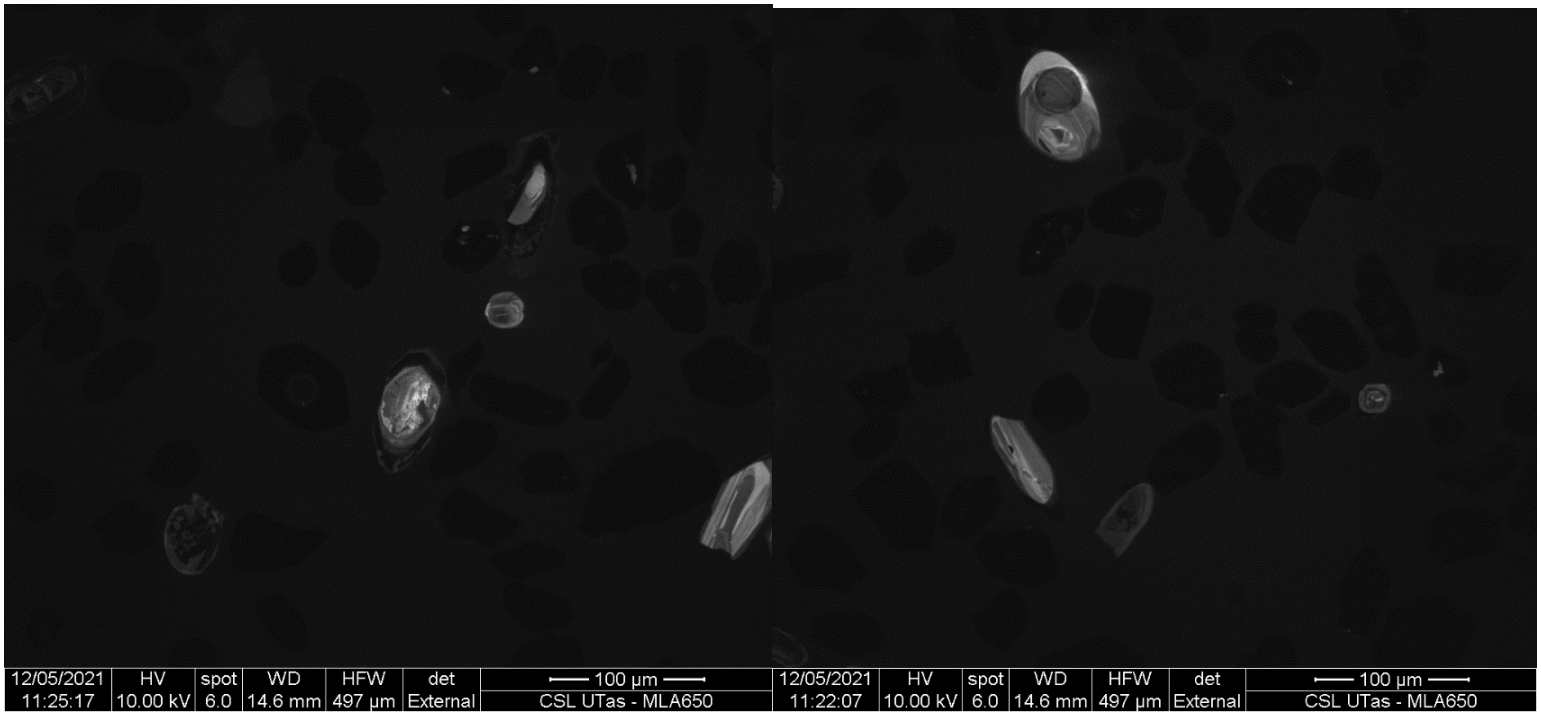
12/05/2021 11:25:17
HV 10.00 kV
spot 6.0
WD 14.6 mm
HFW 497 µm
det External
100 µm
CSL UTas - MLA650
12/05/2021 11:22:07
HV 10.00 kV
spot 6.0
WD 14.6 mm
HFW 497 µm
det External
100 µm
CSL UTas - MLA650

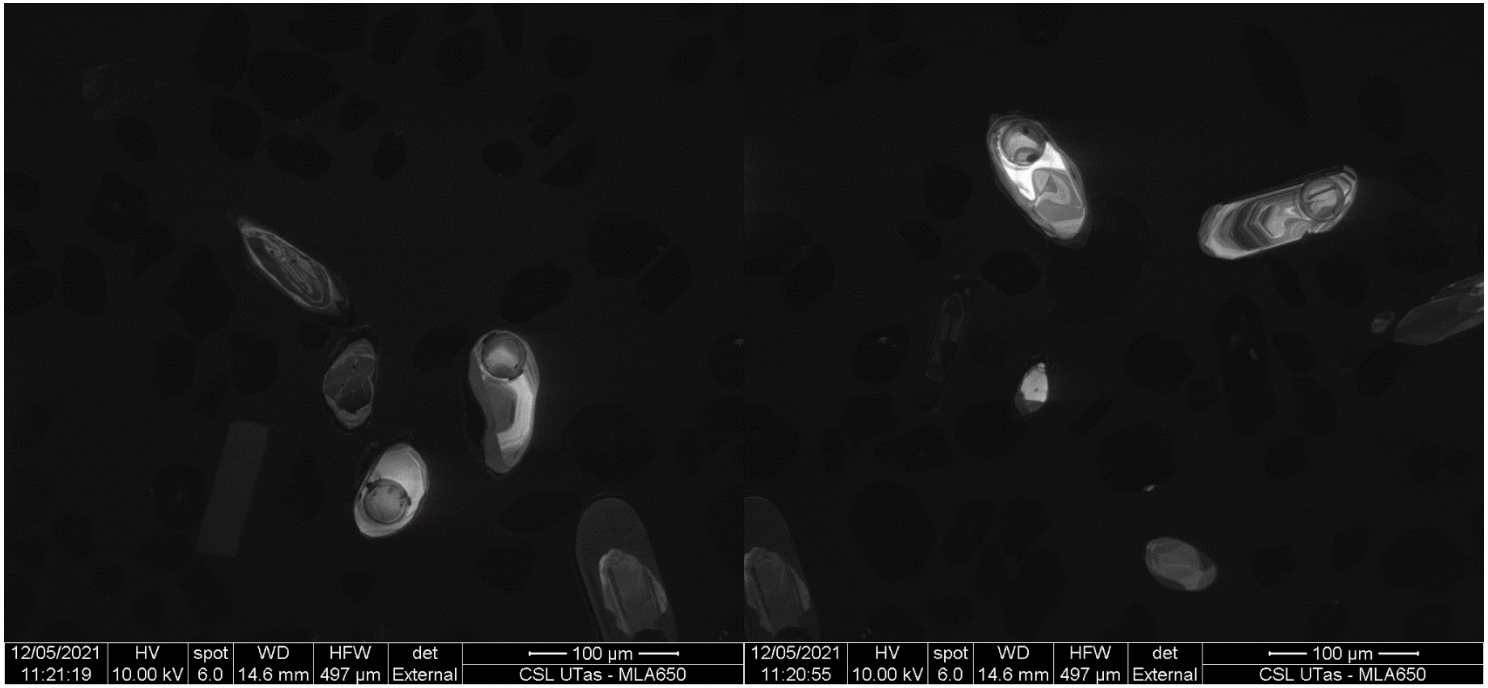
12/05/2021 | HV | spot | WD | HFW | det | 100 µm
11:21:19 | 10.00 kV | 6.0 | 14.6 mm | 497 µm | External | CSL UTas - MLA650
12/05/2021 | HV | spot | WD | HFW | det | 100 µm
11:20:55 | 10.00 kV | 6.0 | 14.6 mm | 497 µm | External | CSL UTas - MLA650

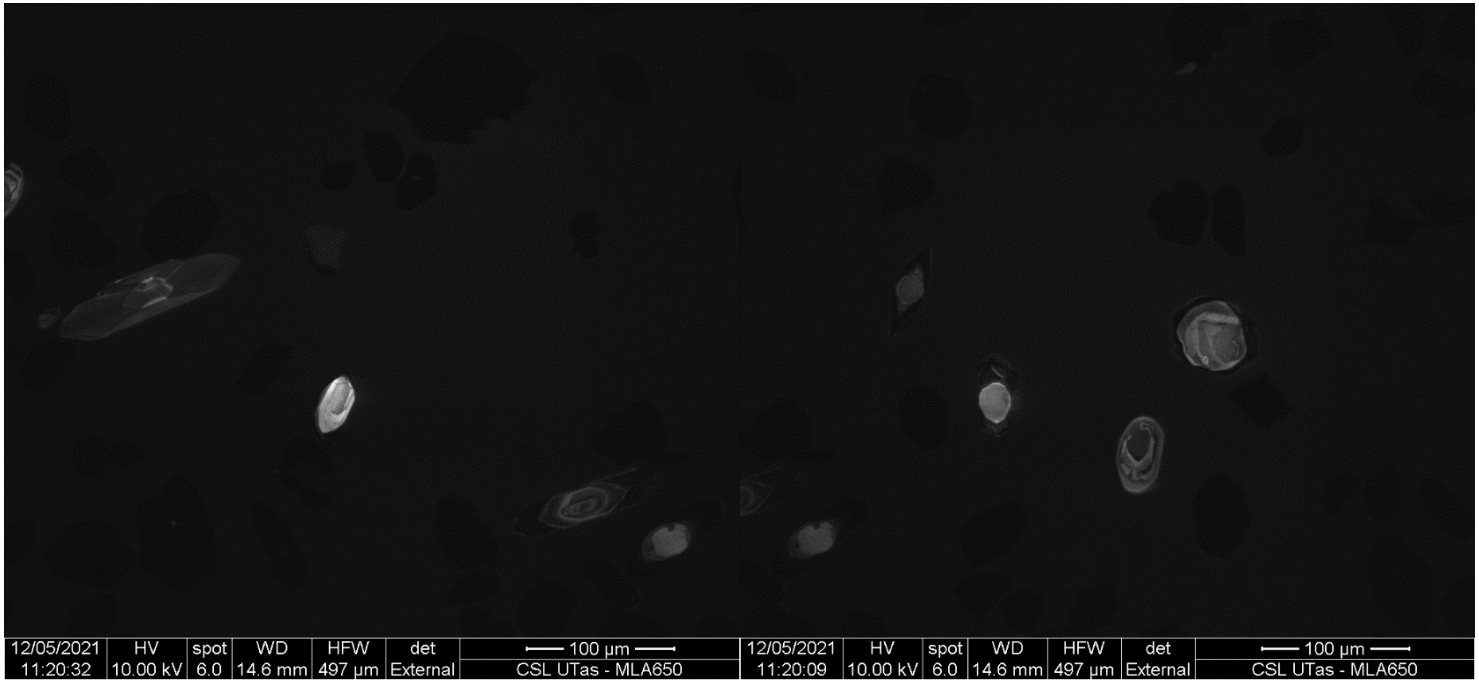
12/05/2021 11:20:32 | HV 10.00 kV | spot 6.0 | WD 14.6 mm | HFW 497 µm | det External | 100 µm | CSL UTas - MLA650
12/05/2021 11:20:09 | HV 10.00 kV | spot 6.0 | WD 14.6 mm | HFW 497 µm | det External | 100 µm | CSL UTas - MLA650

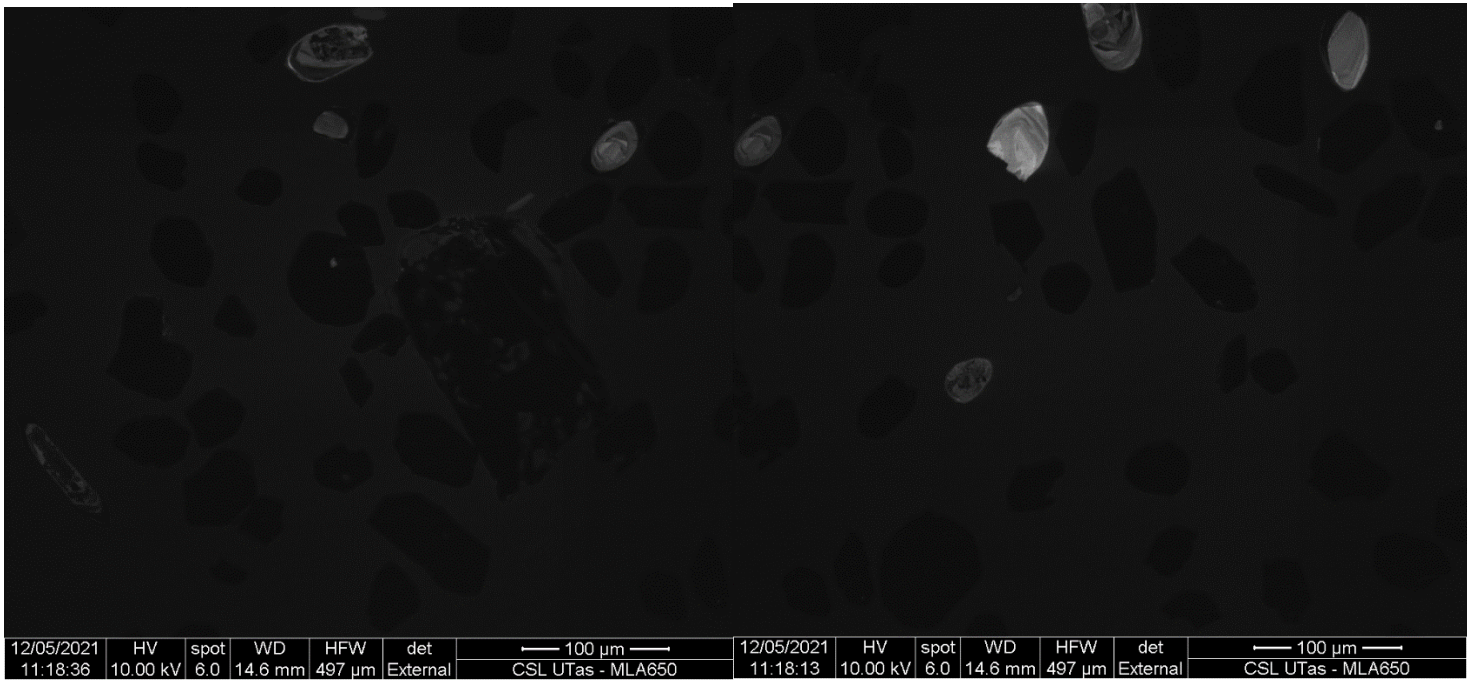
12/05/2021 11:18:36
HV 10.00 kV
spot 6.0
WD 14.6 mm
HFW 497 µm
det External
100 µm
CSL UTas - MLA650
12/05/2021 11:18:13
HV 10.00 kV
spot 6.0
WD 14.6 mm
HFW 497 µm
det External
100 µm
CSL UTas - MLA650

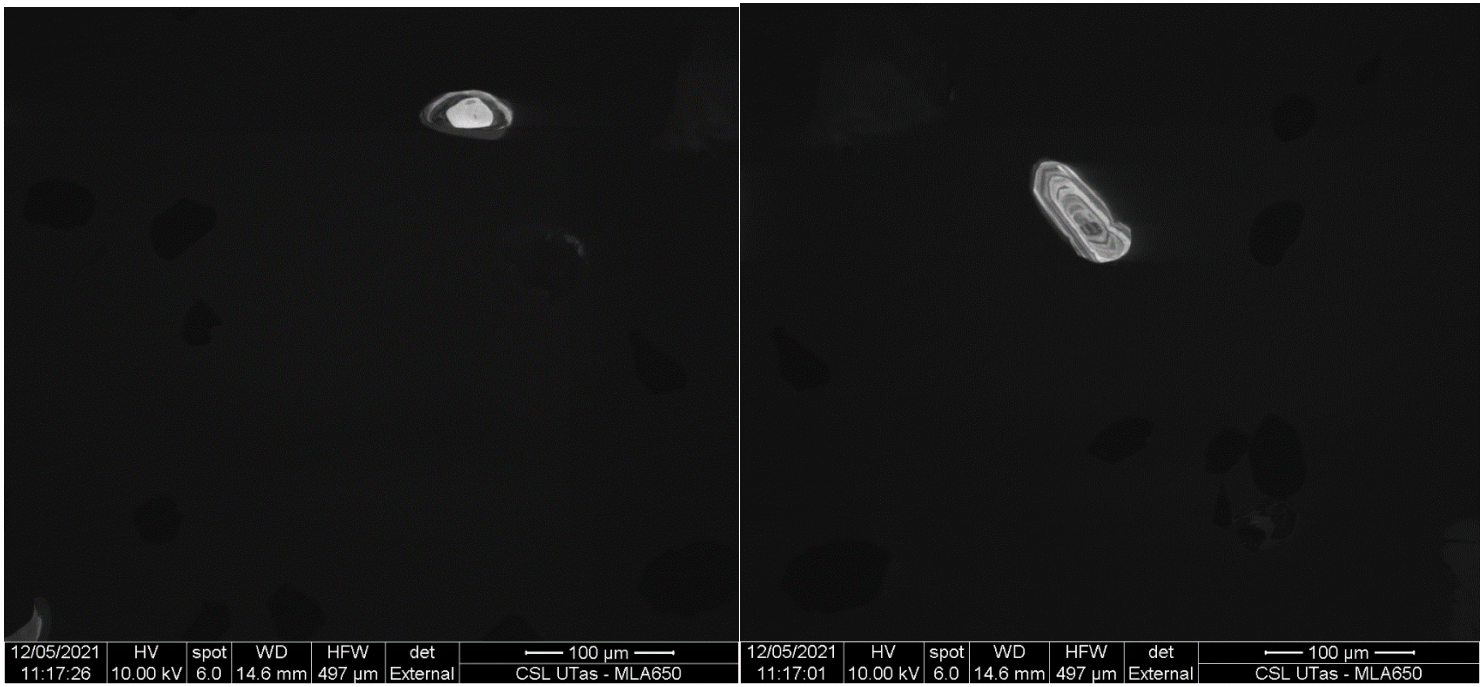
12/05/2021 HV spot WD HFW det 100 µm
11:17:26 10.00 kV 6.0 14.6 mm 497 µm External CSL UTas - MLA650
12/05/2021 HV spot WD HFW det 100 µm
11:17:01 10.00 kV 6.0 14.6 mm 497 µm External CSL UTas - MLA650

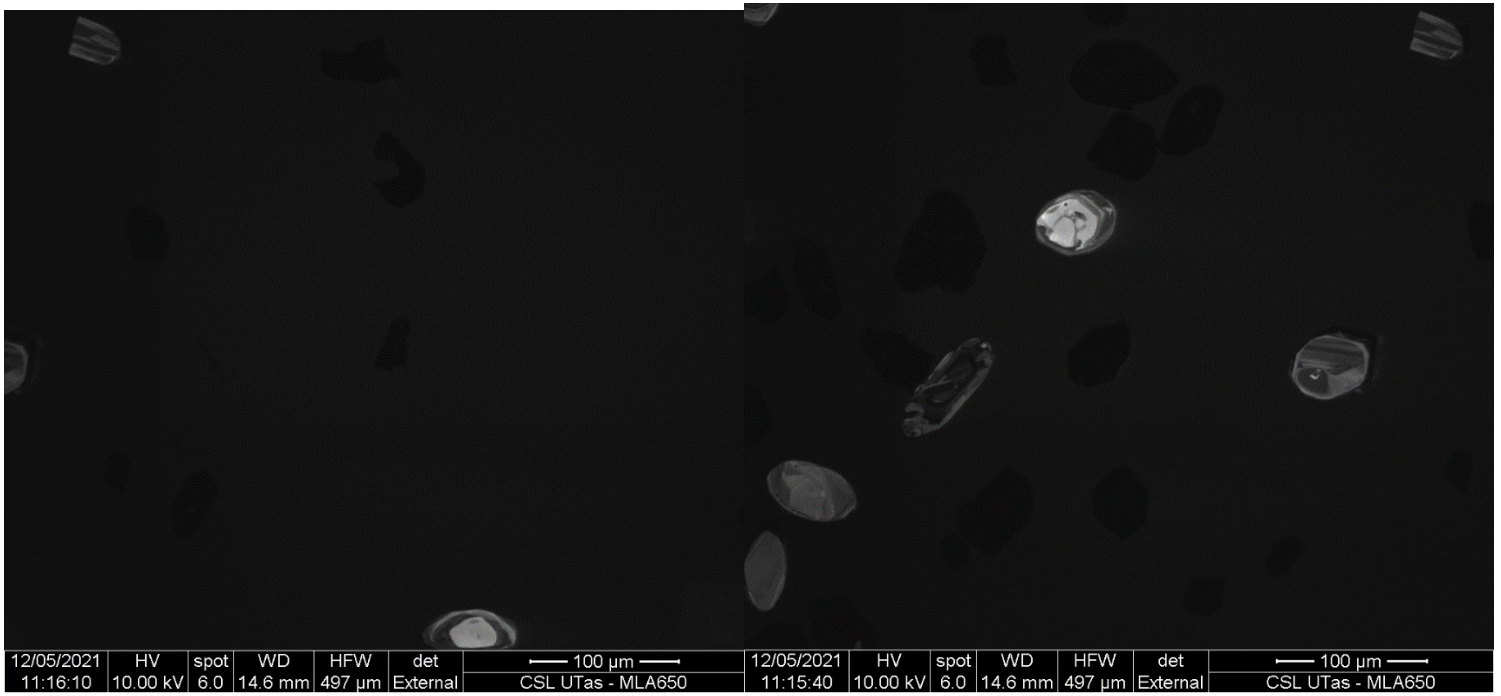
12/05/2021 11:16:10
HV 10.00 kV
spot 6.0
WD 14.6 mm
HFW 497 µm
det External
100 µm
CSL UTas - MLA650
12/05/2021 11:15:40
HV 10.00 kV
spot 6.0
WD 14.6 mm
HFW 497 µm
det External
100 µm
CSL UTas - MLA650

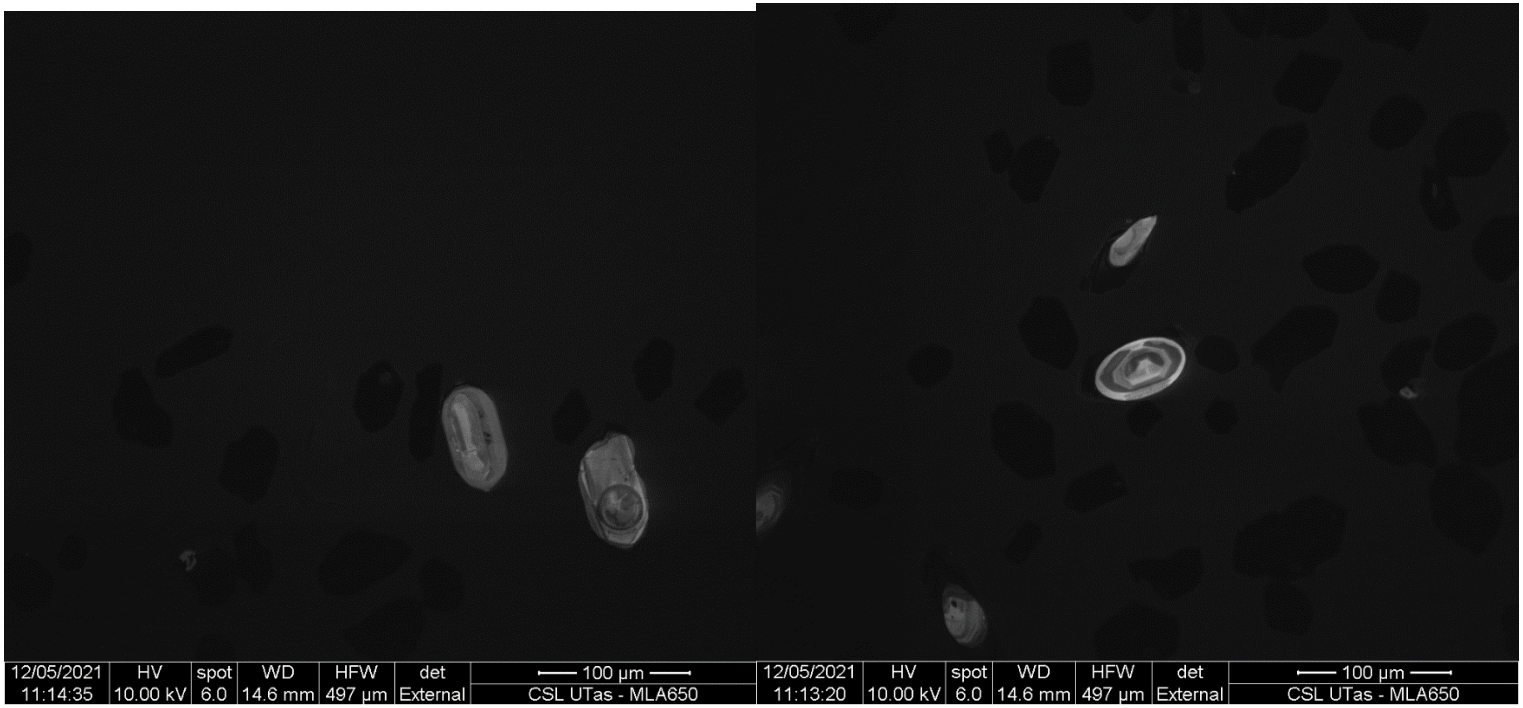
12/05/2021 11:14:35
HV 10.00 kV
spot 6.0
WD 14.6 mm
HFW 497 µm
det External
100 µm
CSL UTas - MLA650
12/05/2021 11:13:20
HV 10.00 kV
spot 6.0
WD 14.6 mm
HFW 497 µm
det External
100 µm
CSL UTas - MLA650

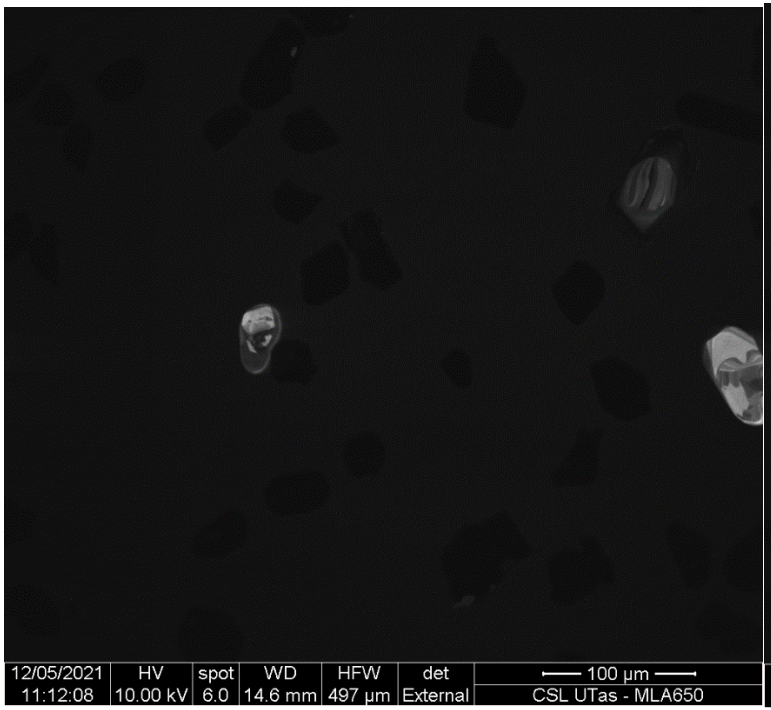
12/05/2021
11:12:08
HV
10.00 kV
spot
6.0
WD
14.6 mm
HFW
497 µm
det
External
100 µm
CSL UTas - MLA650

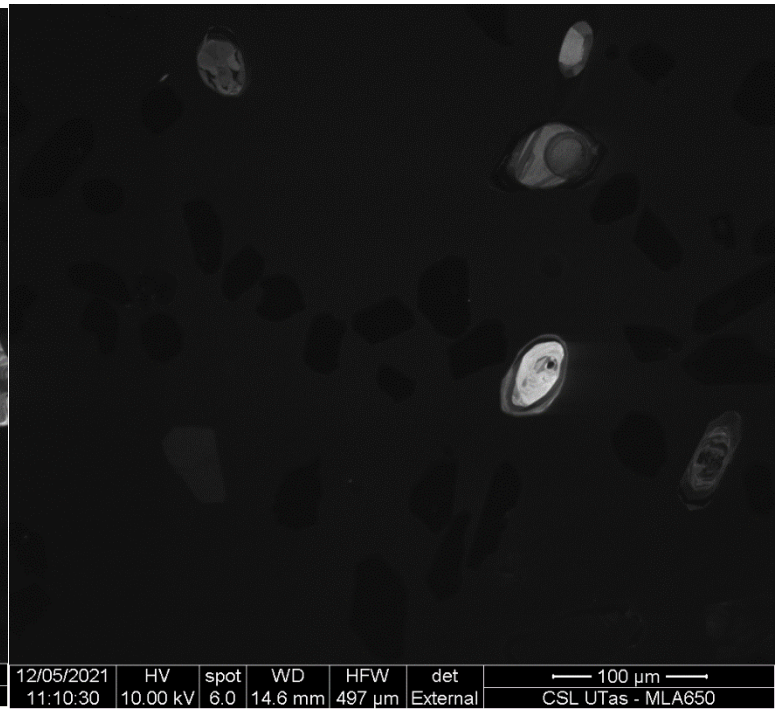
12/05/2021
11:10:30
HV
10.00 kV
spot
6.0
WD
14.6 mm
HFW
497 µm
det
External
100 µm
CSL UTas - MLA650

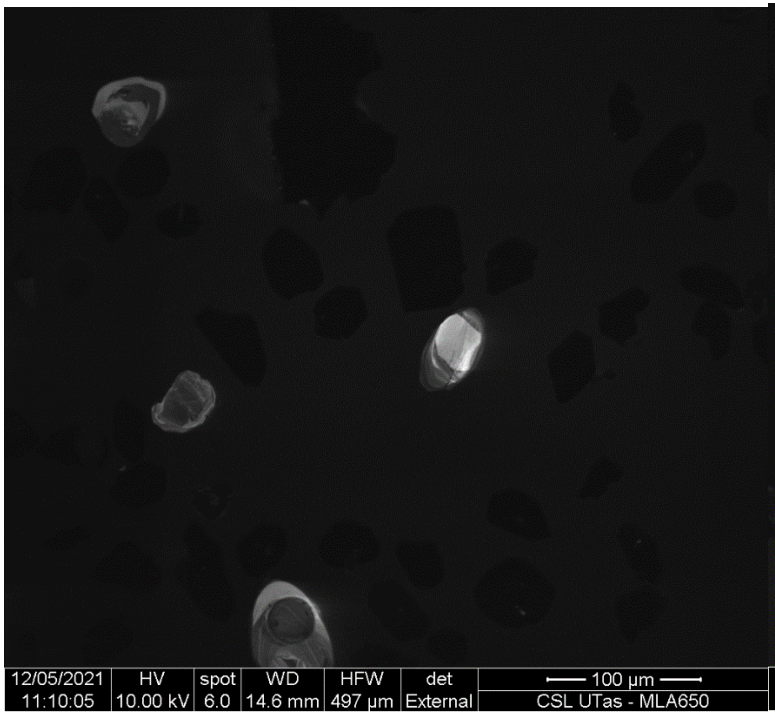
12/05/2021
11:10:05
HV
10.00 kV
spot
6.0
WD
14.6 mm
HFW
497 µm
det
External
100 µm
CSL UTas - MLA650

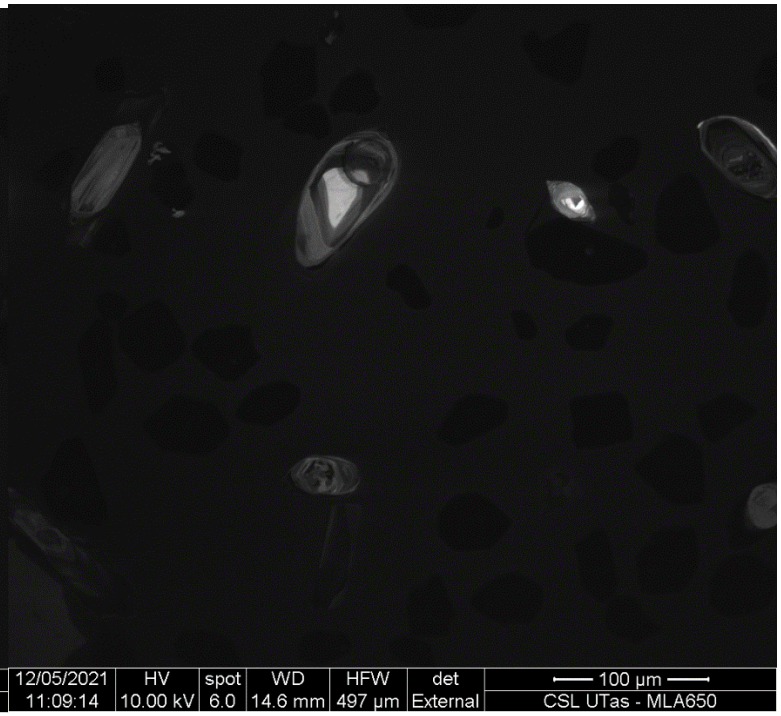
12/05/2021
11:09:14
HV
10.00 kV
spot
6.0
WD
14.6 mm
HFW
497 µm
det
External
100 µm
CSL UTas - MLA650

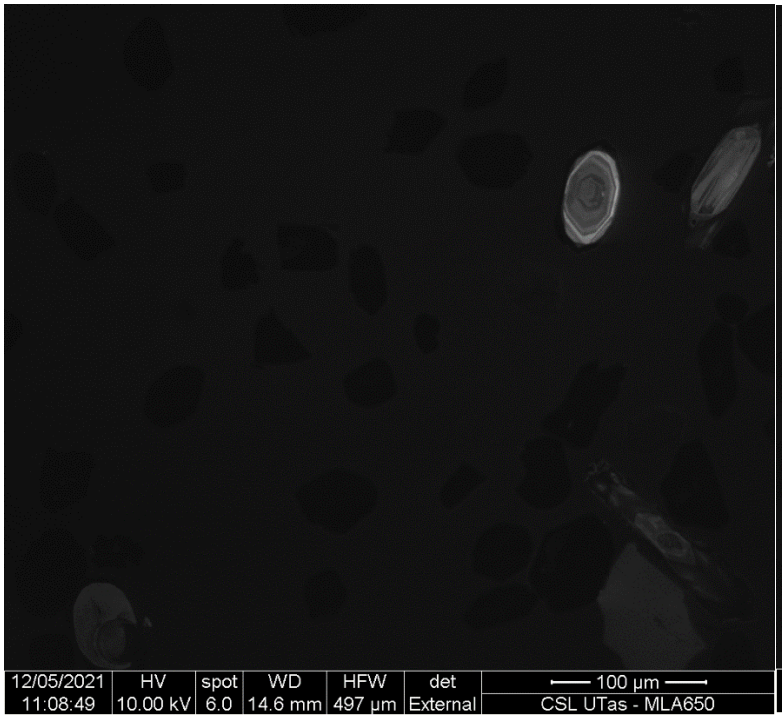
12/05/2021 | HV | spot | WD | HFW | det | 100 µm
11:08:49 | 10.00 kV | 6.0 | 14.6 mm | 497 µm | External | CSL UTas - MLA650

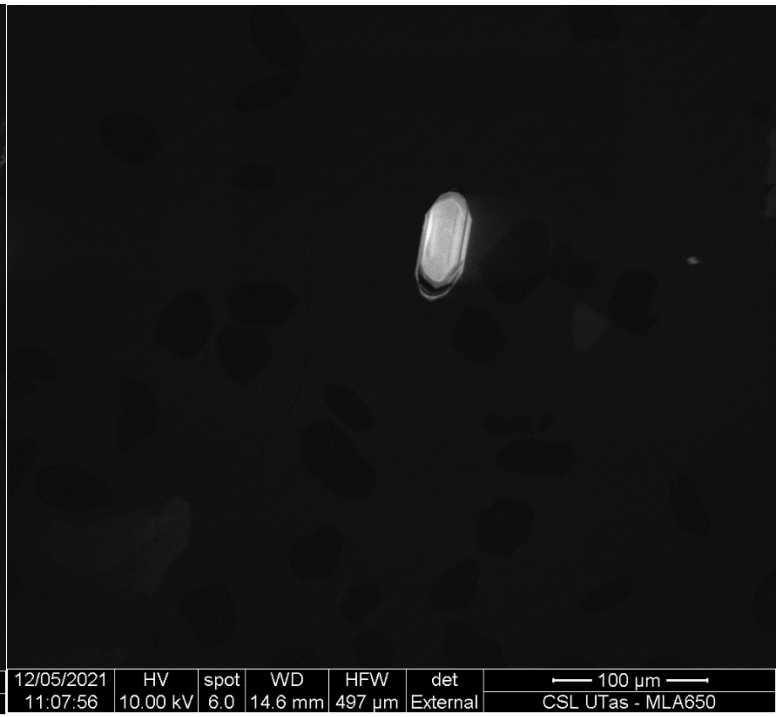
12/05/2021 | HV | spot | WD | HFW | det | 100 µm
11:07:56 | 10.00 kV | 6.0 | 14.6 mm | 497 µm | External | CSL UTas - MLA650

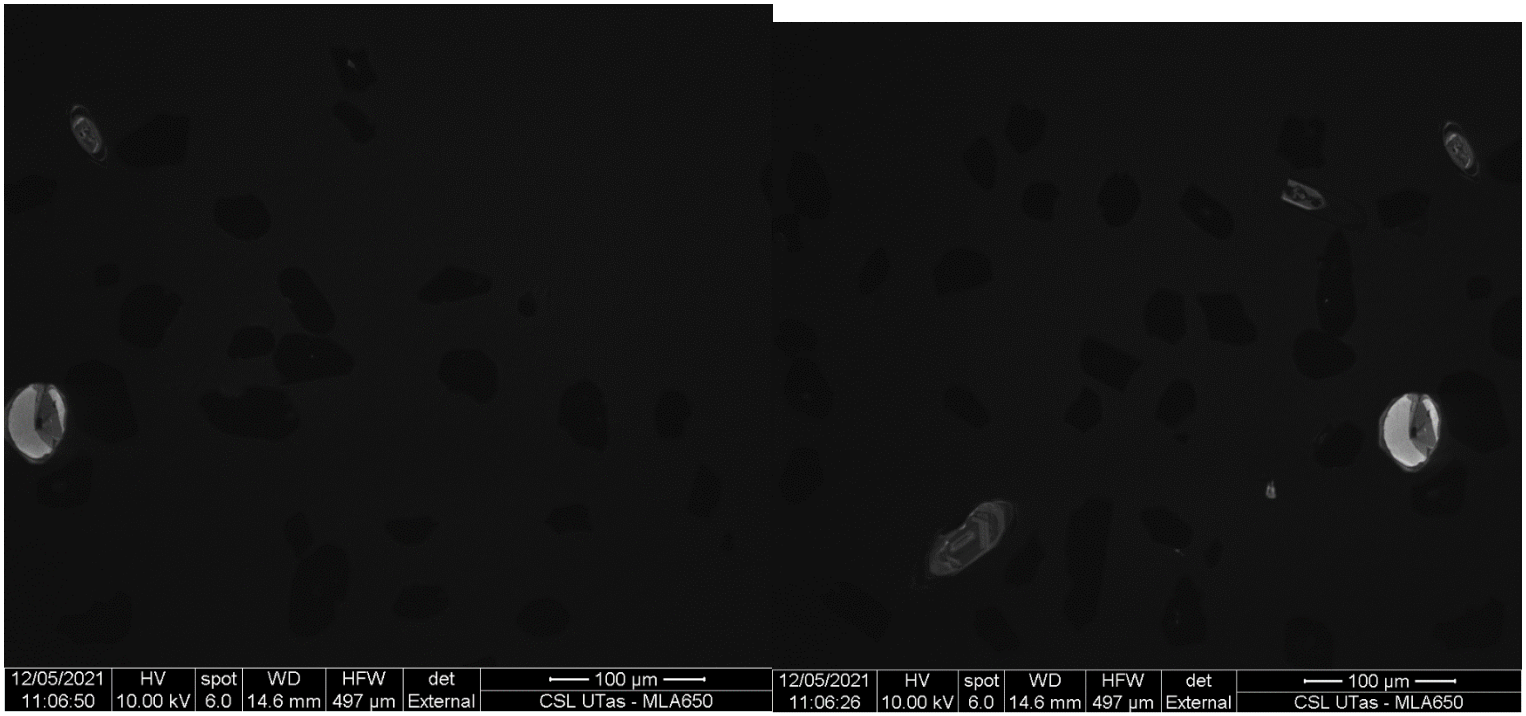
12/05/2021 11:06:50
HV 10.00 kV
spot 6.0
WD 14.6 mm
HFW 497 µm
det External
100 µm
CSL UTas - MLA650
12/05/2021 11:06:26
HV 10.00 kV
spot 6.0
WD 14.6 mm
HFW 497 µm
det External
100 µm
CSL UTas - MLA650

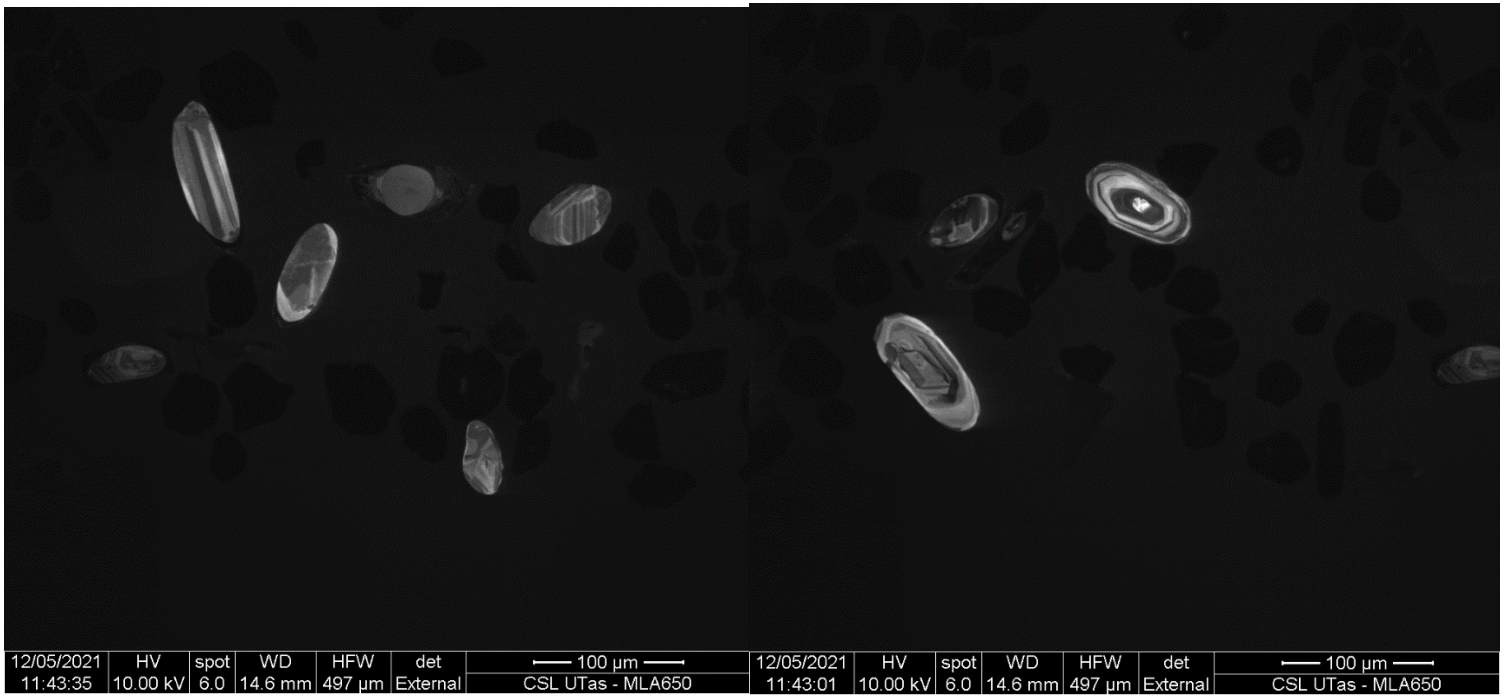
12/05/2021 11:43:35
HV 10.00 kV
spot 6.0
WD 14.6 mm
HFW 497 µm
det External
100 µm
CSL UTas - MLA650
12/05/2021 11:43:01
HV 10.00 kV
spot 6.0
WD 14.6 mm
HFW 497 µm
det External
100 µm
CSL UTas - MLA650

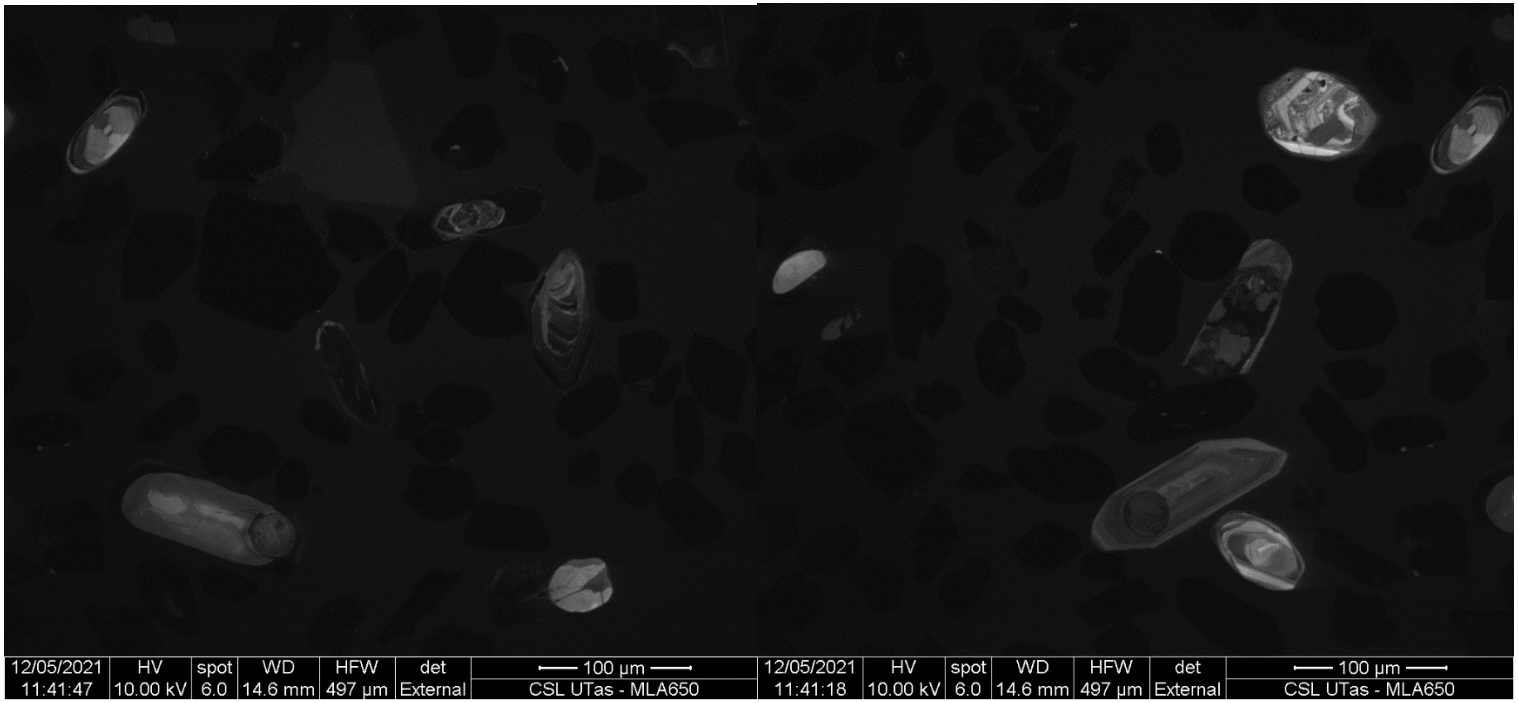
12/05/2021 HV spot WD HFW det 100 µm
11:41:47 10.00 kV 6.0 14.6 mm 497 µm External CSL UTas - MLA650
12/05/2021 HV spot WD HFW det 100 µm
11:41:18 10.00 kV 6.0 14.6 mm 497 µm External CSL UTas - MLA650

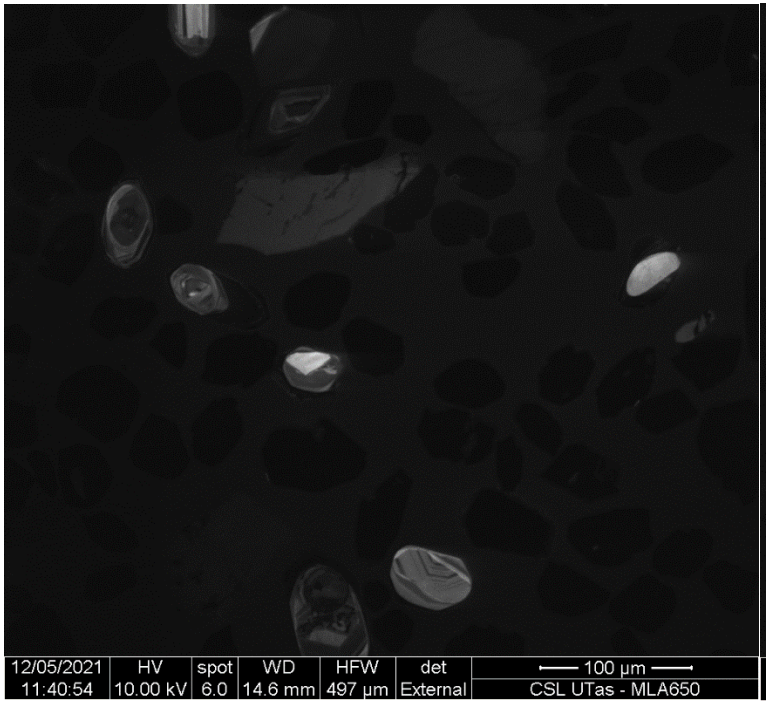
12/05/2021 HV spot WD HFW det 100 µm
11:40:54 10.00 kV 6.0 14.6 mm 497 µm External CSL UTas - MLA650

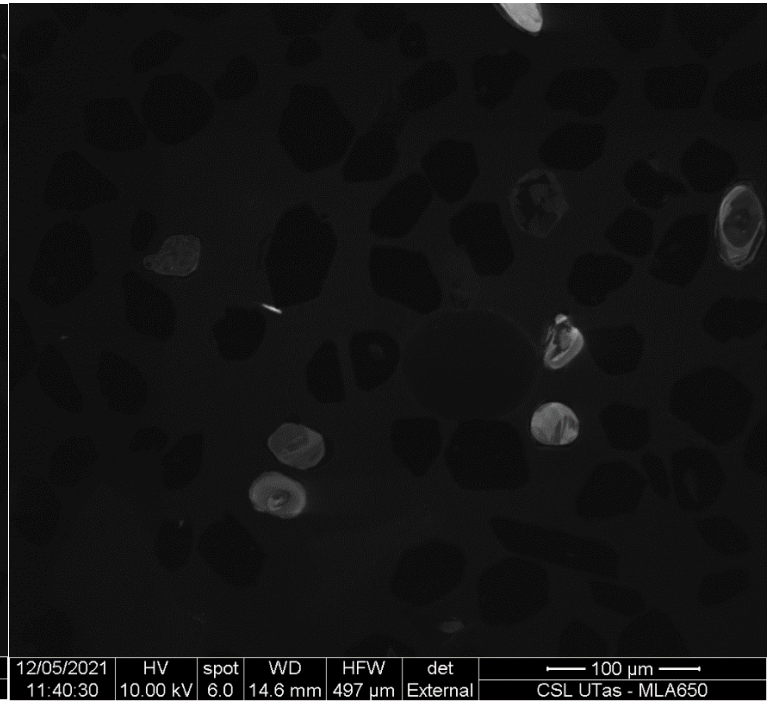
12/05/2021 HV spot WD HFW det 100 µm
11:40:30 10.00 kV 6.0 14.6 mm 497 µm External CSL UTas - MLA650

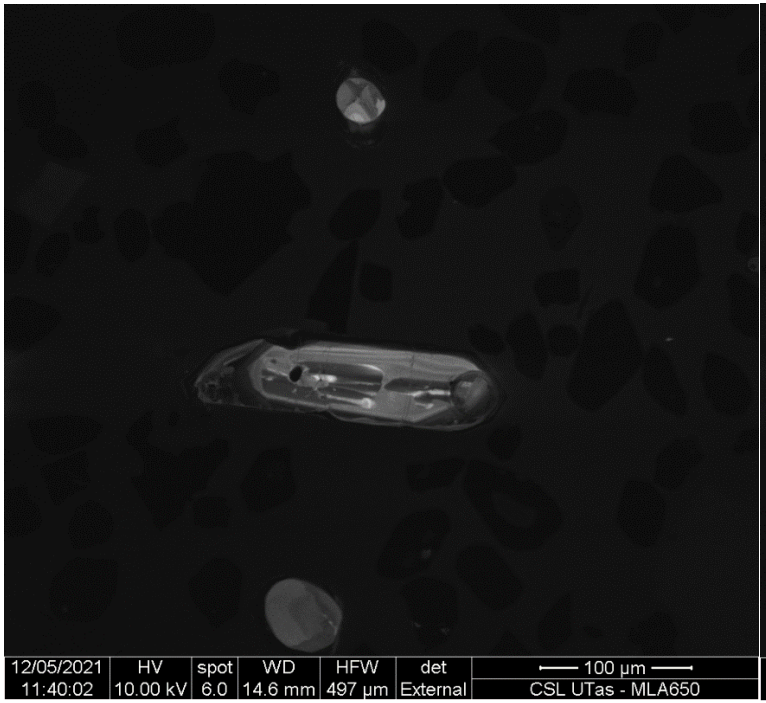
12/05/2021 | HV | spot | WD | HFW | det | 100 µm
11:40:02 | 10.00 kV | 6.0 | 14.6 mm | 497 µm | External | CSL UTas - MLA650

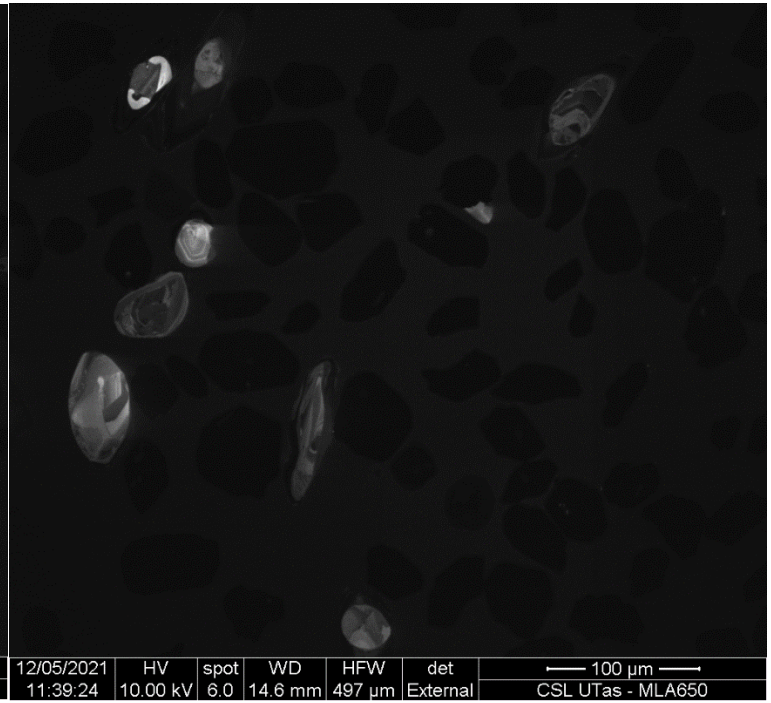
12/05/2021 | HV | spot | WD | HFW | det | 100 µm
11:39:24 | 10.00 kV | 6.0 | 14.6 mm | 497 µm | External | CSL UTas - MLA650

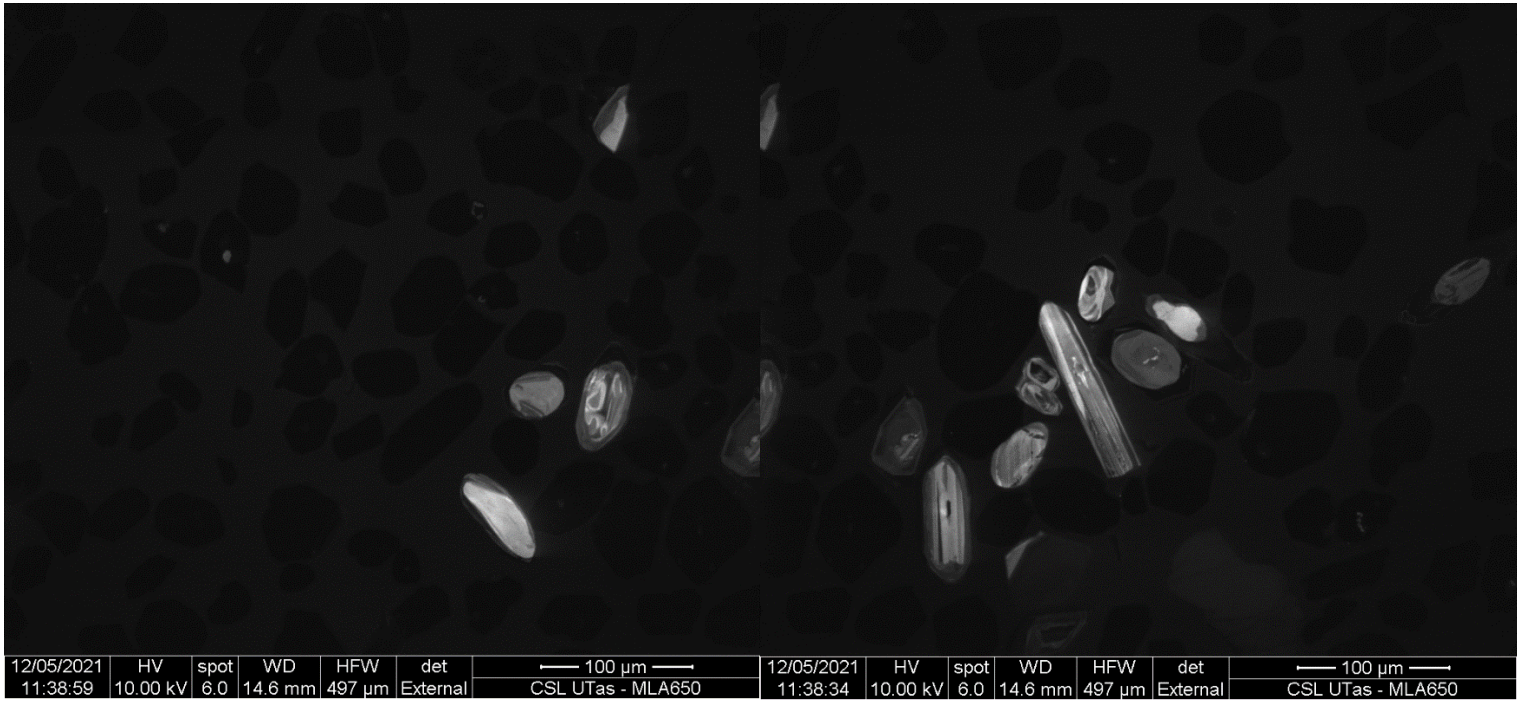
12/05/2021 11:38:59 HV 10.00 kV spot 6.0 WD 14.6 mm HFW 497 µm det External 100 µm CSL UTas - MLA650
12/05/2021 11:38:34 HV 10.00 kV spot 6.0 WD 14.6 mm HFW 497 µm det External 100 µm CSL UTas - MLA650

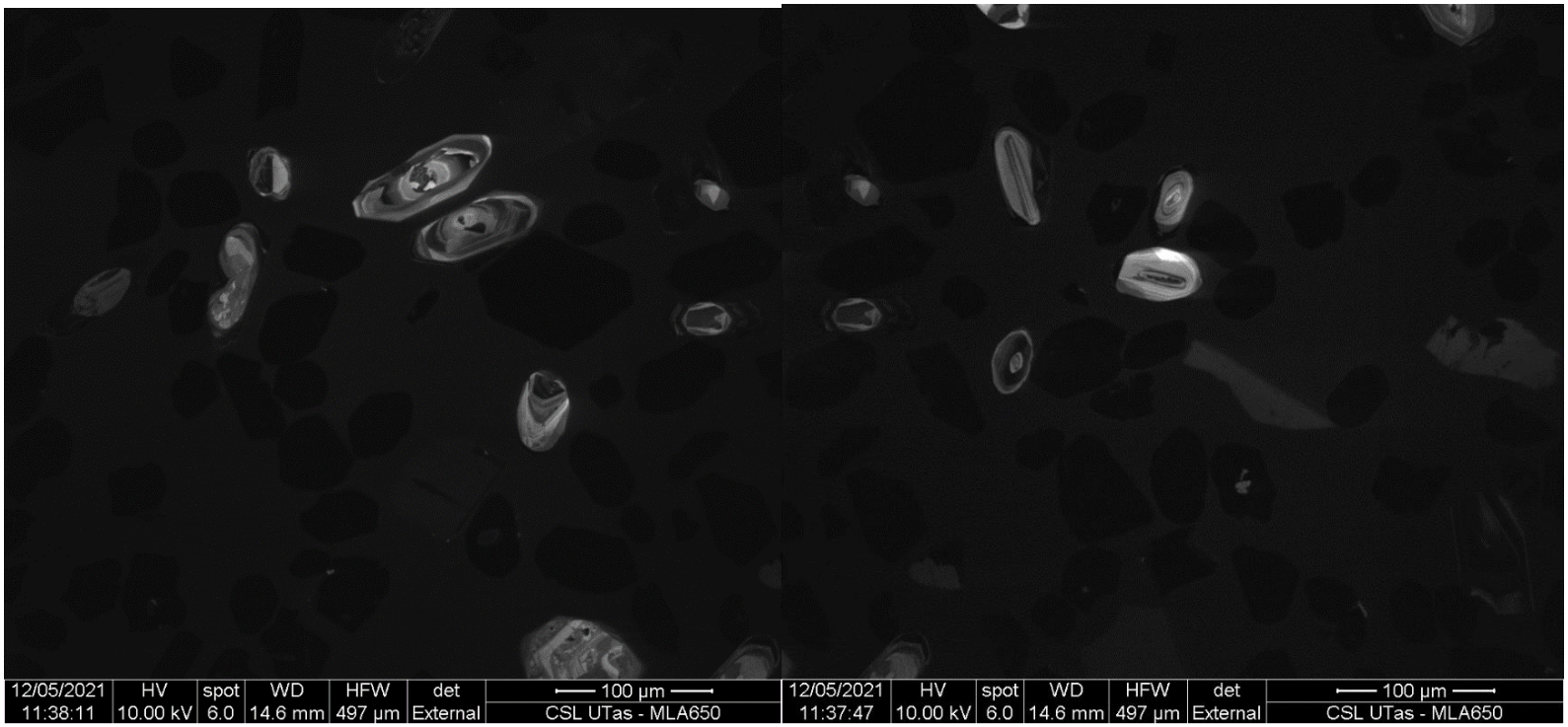
12/05/2021 HV spot WD HFW det 100 µm
11:38:11 10.00 kV 6.0 14.6 mm 497 µm External CSL UTas - MLA650
12/05/2021 HV spot WD HFW det 100 µm
11:37:47 10.00 kV 6.0 14.6 mm 497 µm External CSL UTas - MLA650

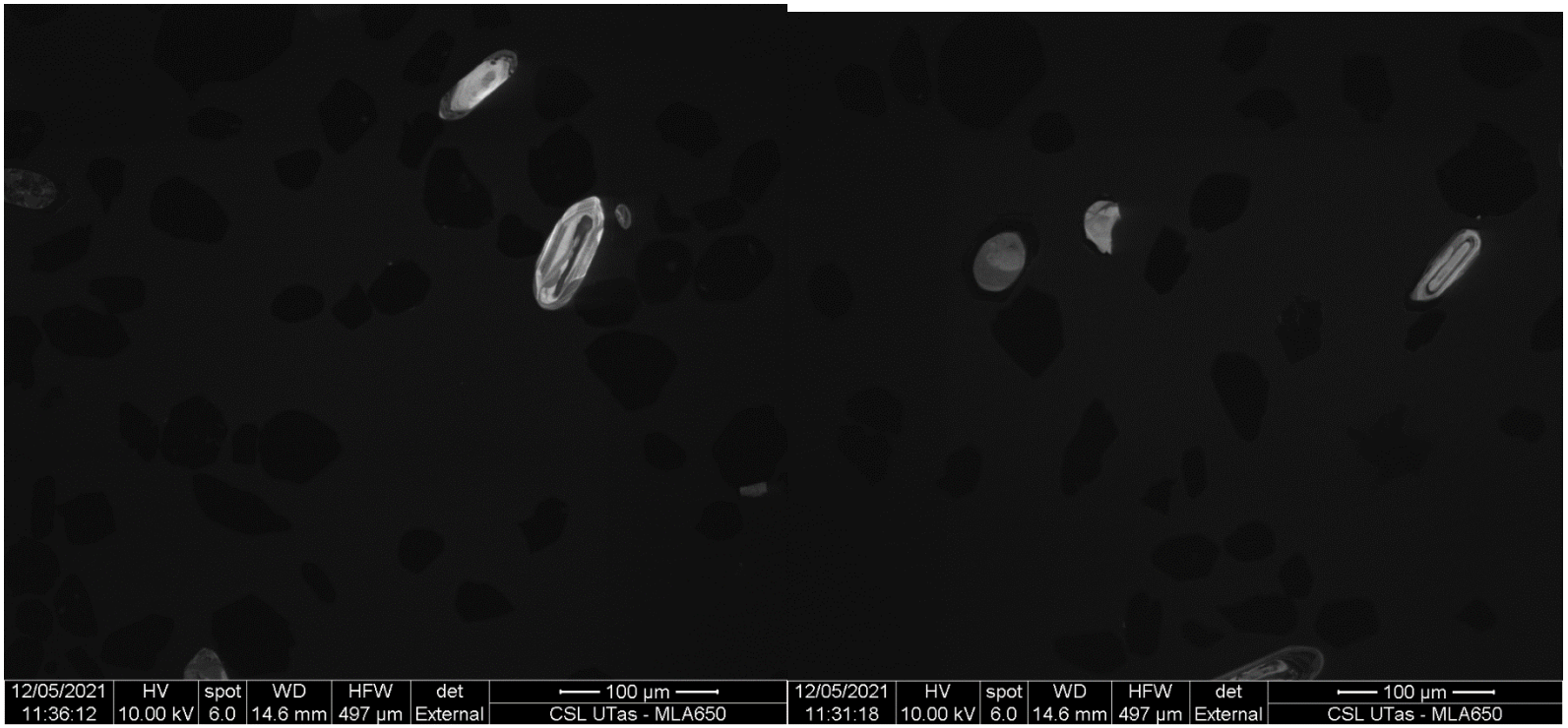
12/05/2021 11:36:12
HV 10.00 kV
spot 6.0
WD 14.6 mm
HFW 497 µm
det External
100 µm
CSL UTas - MLA650
12/05/2021 11:31:18
HV 10.00 kV
spot 6.0
WD 14.6 mm
HFW 497 µm
det External
100 µm
CSL UTas - MLA650

APPENDIX C 1.4 Cathodoluminescence images (with spots)

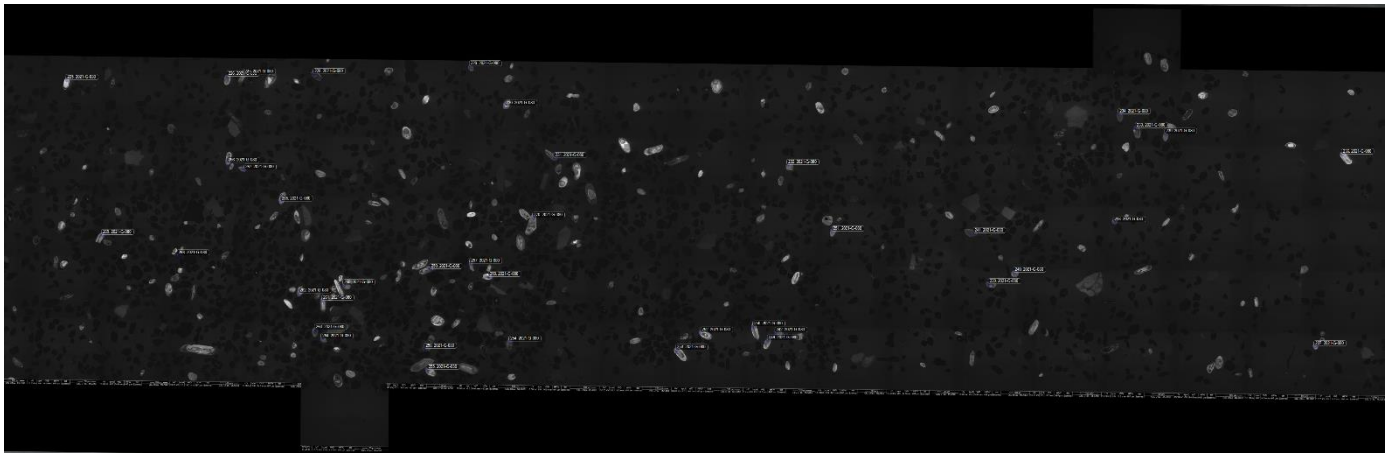

APPENDIX C 1.5 BSE images of zircons

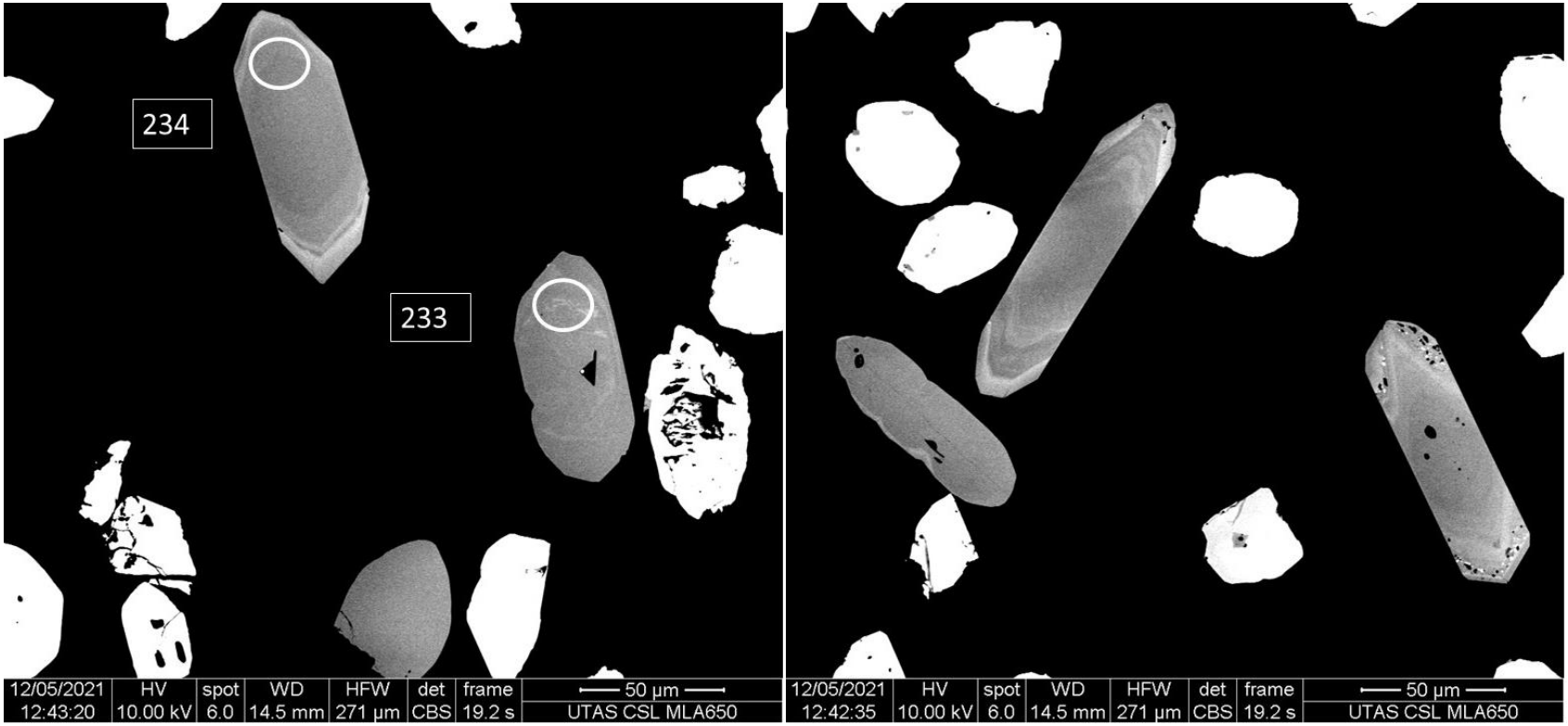

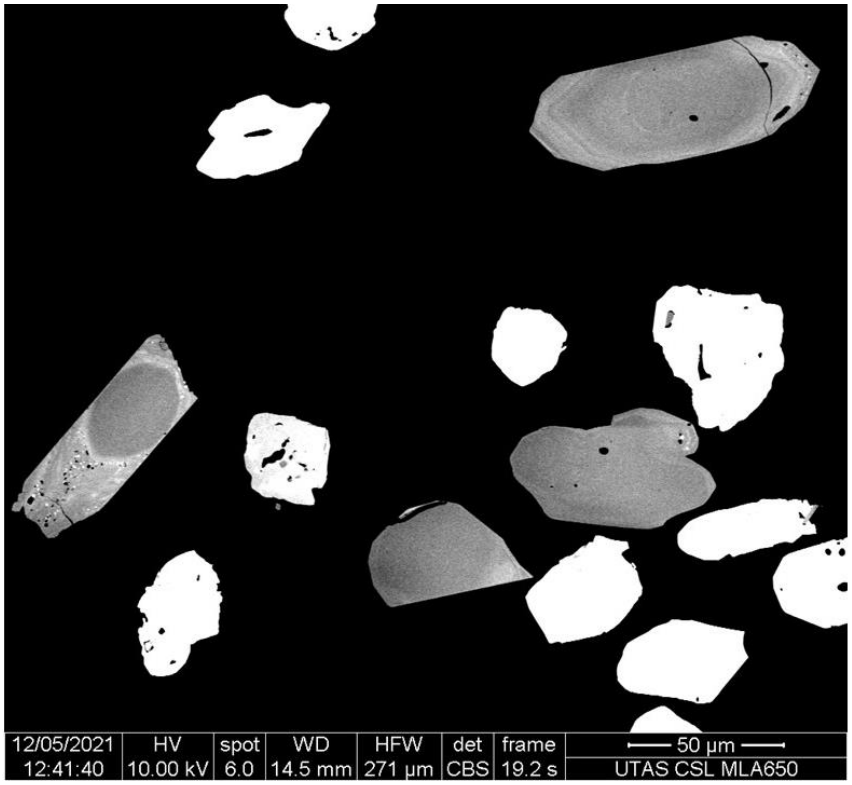
12/05/2021
12:41:40
HV
10.00 kV
spot
6.0
WD
14.5 mm
HFW
271 µm
det
CBS
frame
19.2 s
50 µm
UTAS CSL MLA650

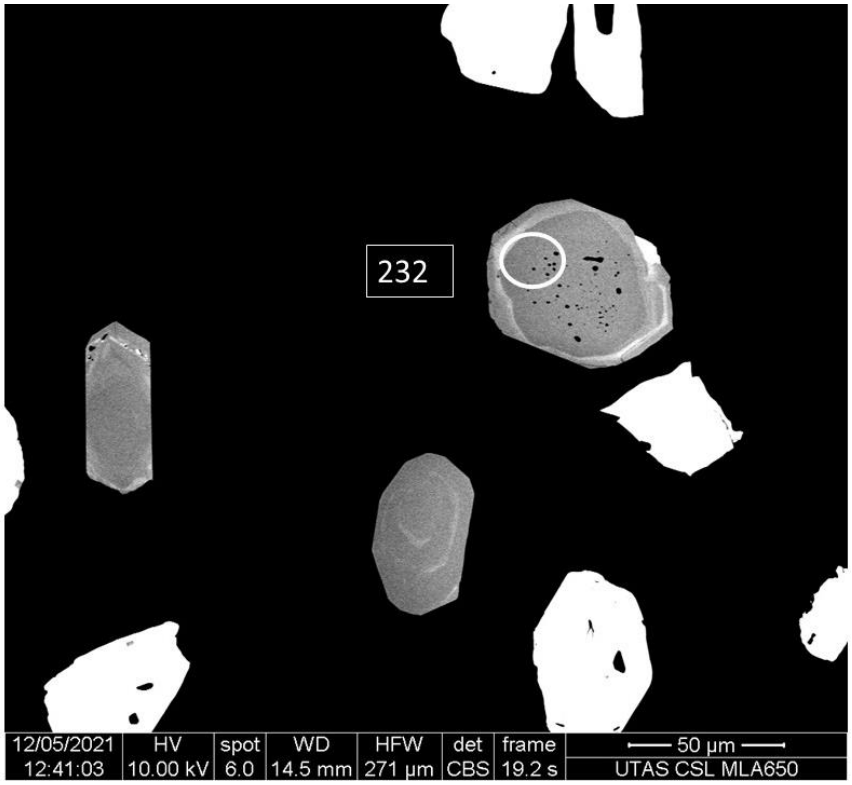
232
12/05/2021
12:41:03
HV
10.00 kV
spot
6.0
WD
14.5 mm
HFW
271 µm
det
CBS
frame
19.2 s
50 µm
UTAS CSL MLA650

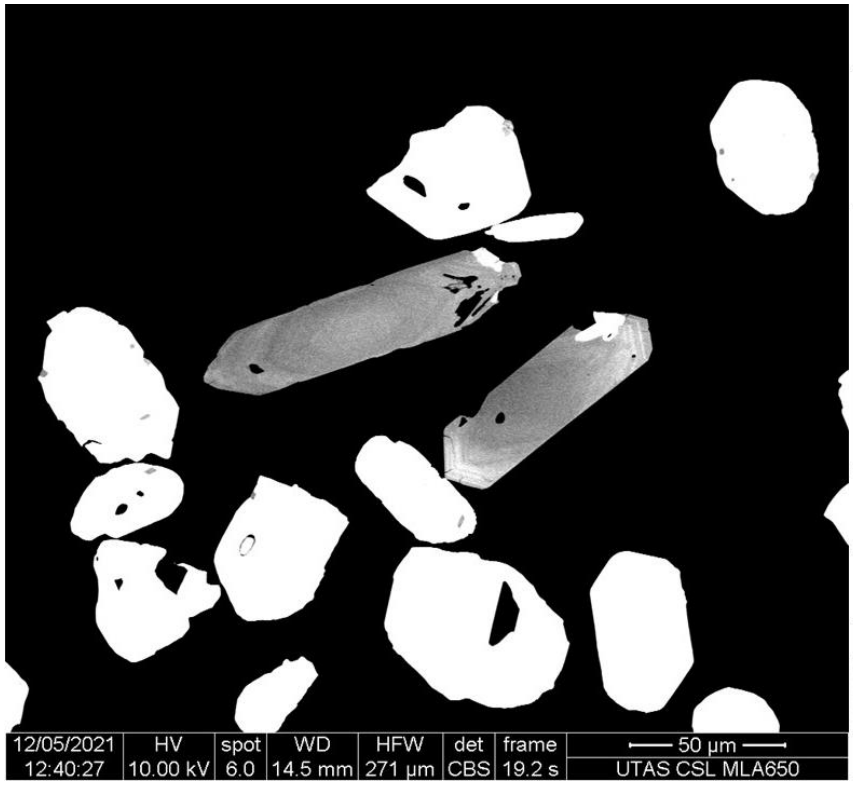
12/05/2021 12:40:27
HV 10.00 kV
spot 6.0
WD 14.5 mm
HFW 271 µm
det CBS
frame 19.2 s
50 µm
UTAS CSL MLA650

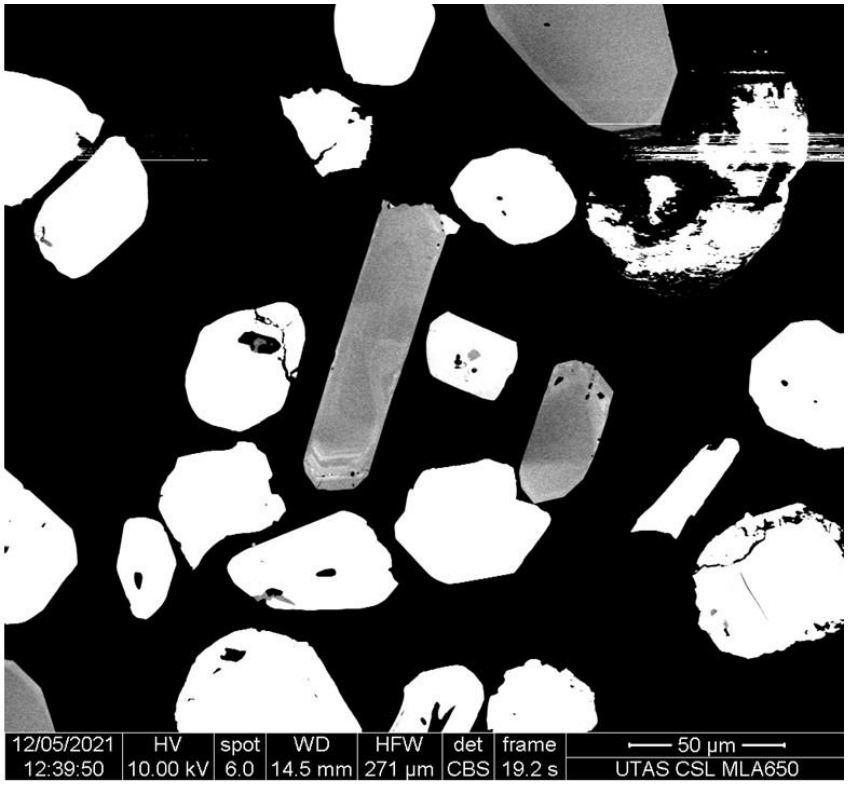
12/05/2021 12:39:50
HV 10.00 kV
spot 6.0
WD 14.5 mm
HFW 271 µm
det CBS
frame 19.2 s
50 µm
UTAS CSL MLA650

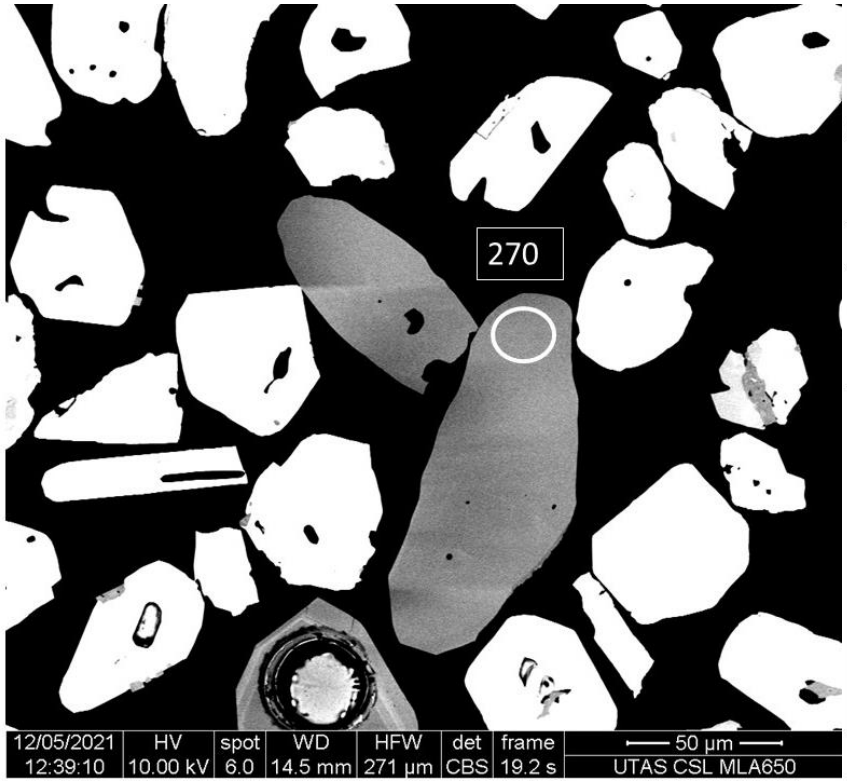
270
12/05/2021 12:39:10
HV 10.00 kV
spot 6.0
WD 14.5 mm
HFW 271 µm
det CBS
frame 19.2 s
50 µm
UTAS CSL MLA650

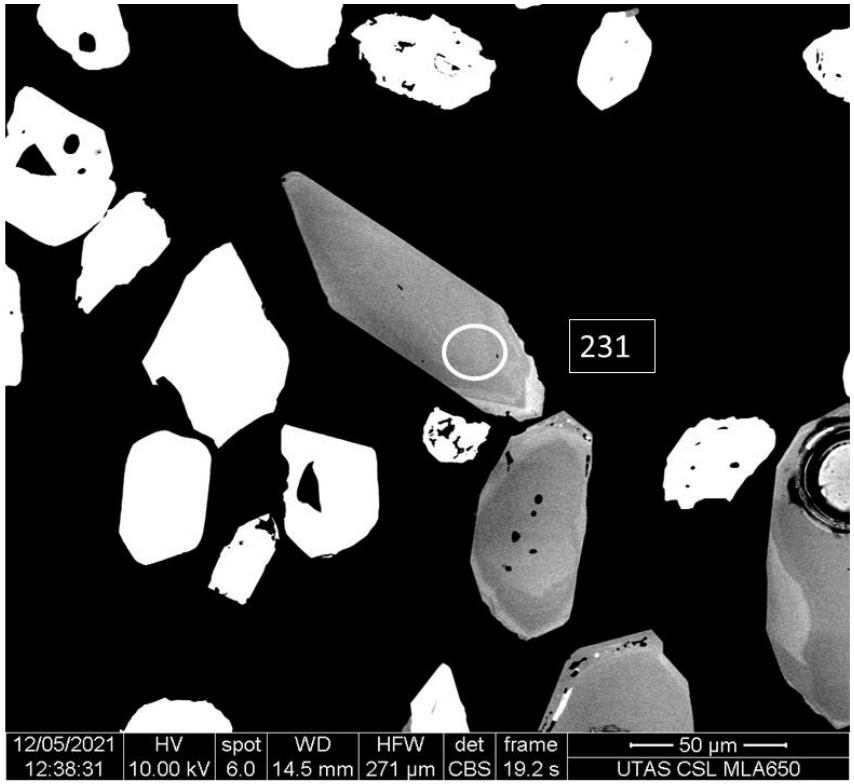
231
12/05/2021 12:38:31
HV 10.00 kV
spot 6.0
WD 14.5 mm
HFW 271 µm
det CBS
frame 19.2 s
50 µm
UTAS CSL MLA650

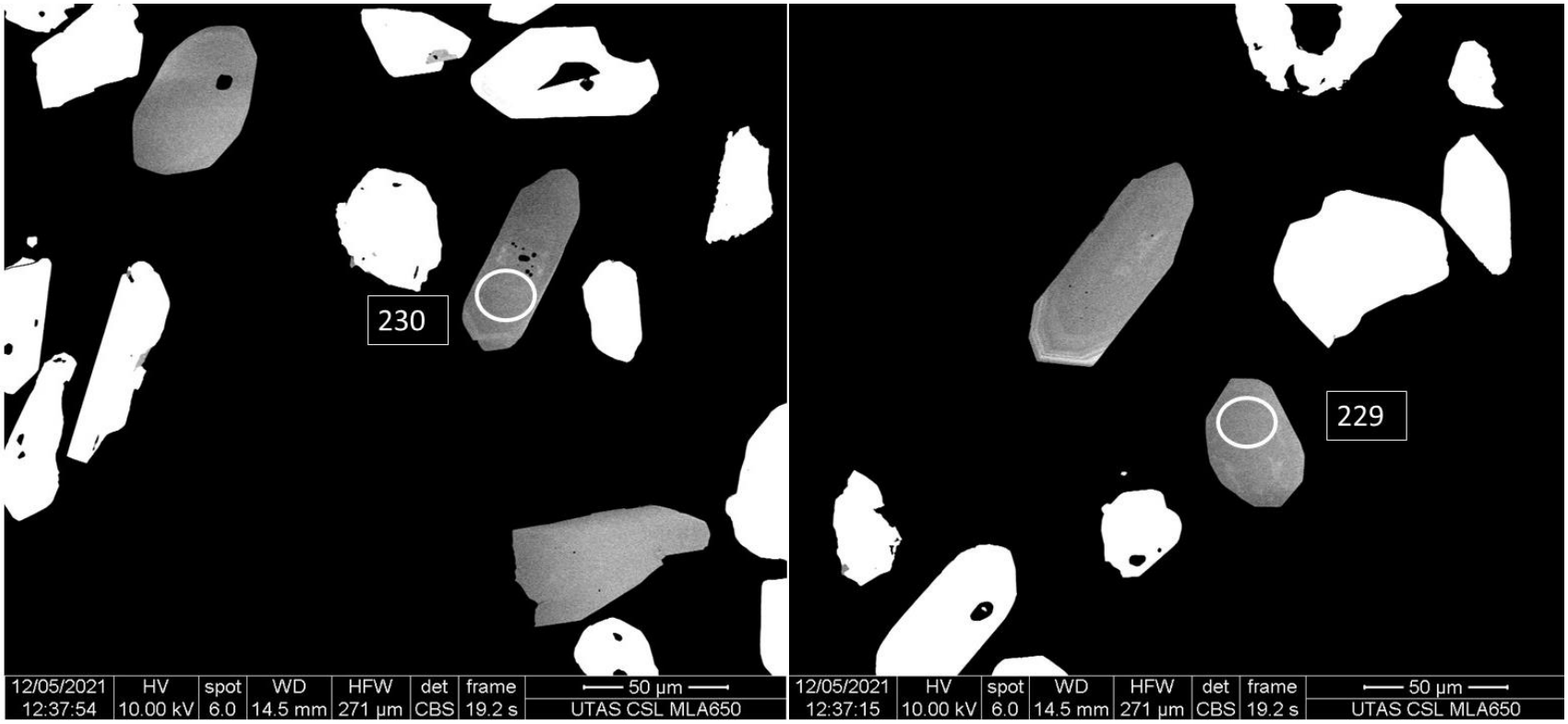
230
12/05/2021 12:37:54
HV 10.00 kV
spot 6.0
WD 14.5 mm
HFW 271 µm
det CBS
frame 19.2 s
50 µm
UTAS CSL MLA650
229
12/05/2021 12:37:15
HV 10.00 kV
spot 6.0
WD 14.5 mm
HFW 271 µm
det CBS
frame 19.2 s
50 µm
UTAS CSL MLA650

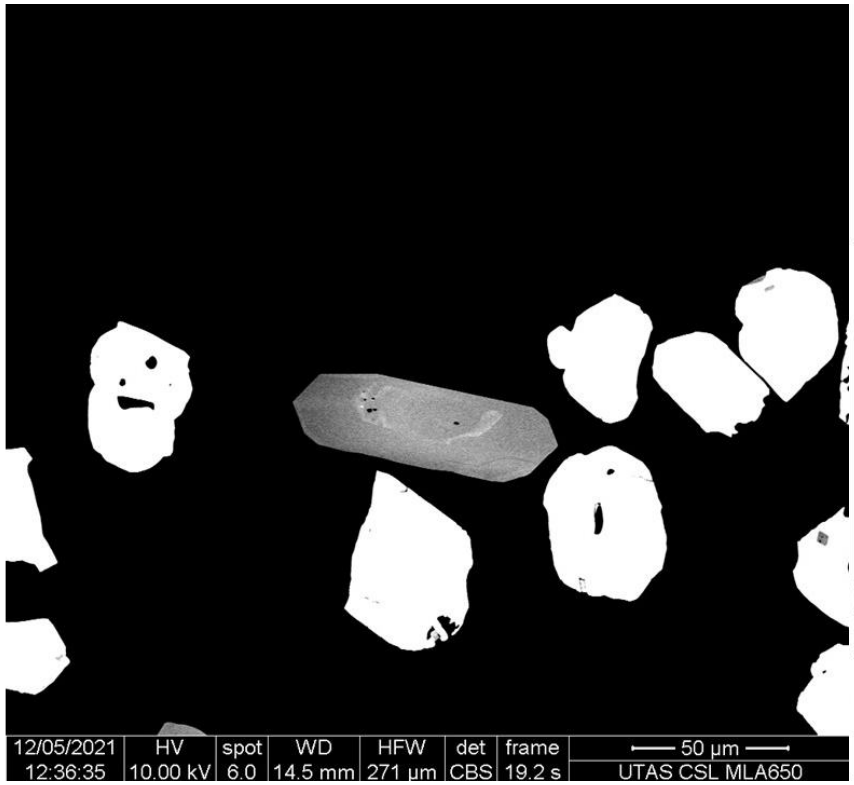
12/05/2021
12:36:35
HV
10.00 kV
spot
6.0
WD
14.5 mm
HFW
271 µm
det
CBS
frame
19.2 s
50 µm
UTAS CSL MLA650

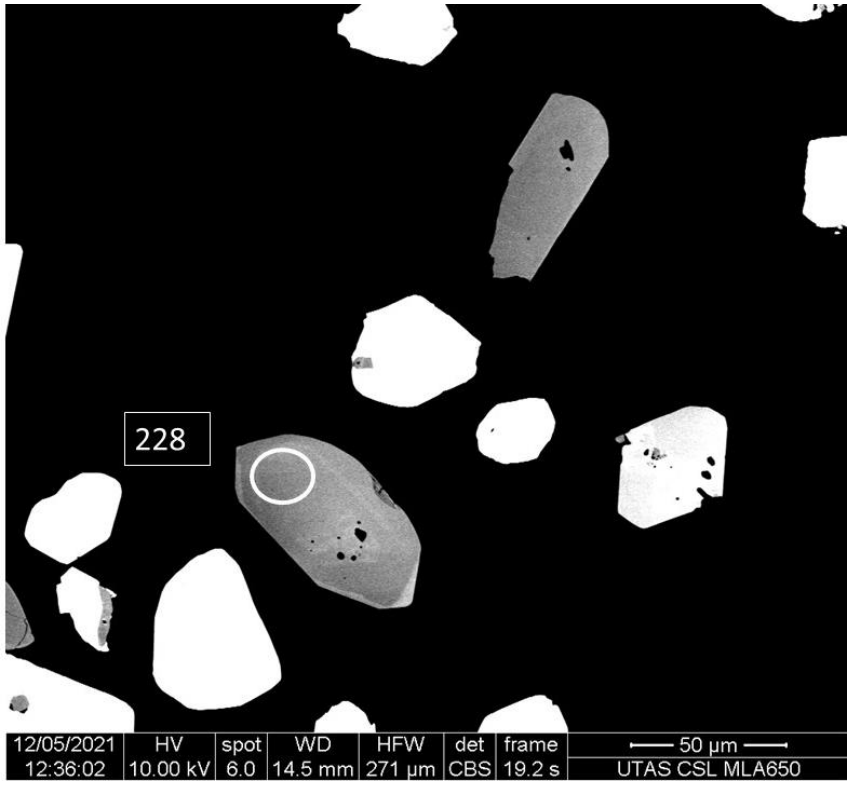
228
12/05/2021
12:36:02
HV
10.00 kV
spot
6.0
WD
14.5 mm
HFW
271 µm
det
CBS
frame
19.2 s
50 µm
UTAS CSL MLA650

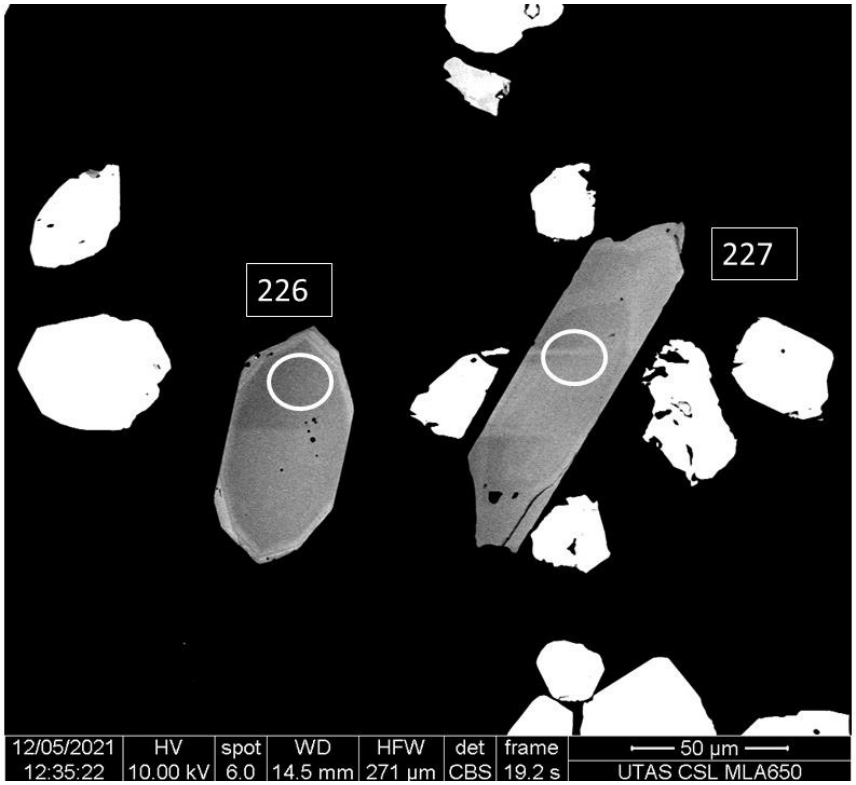
226
227
12/05/2021 12:35:22
HV 10.00 kV
spot 6.0
WD 14.5 mm
HFW 271 µm
det CBS
frame 19.2 s
50 µm
UTAS CSL MLA650


225
12/05/2021 12:34:26
HV 10.00 kV
spot 6.0
WD 14.5 mm
HFW 373 µm
det CBS
frame 19.2 s
100 µm
UTAS CSL MLA650


12/05/2021 | HV | spot | WD | HFW | det | frame | 100 µm
12:32:54 | 10.00 kV | 6.0 | 14.5 mm | 373 µm | CBS | 19.2 s | UTAS CSL MLA650

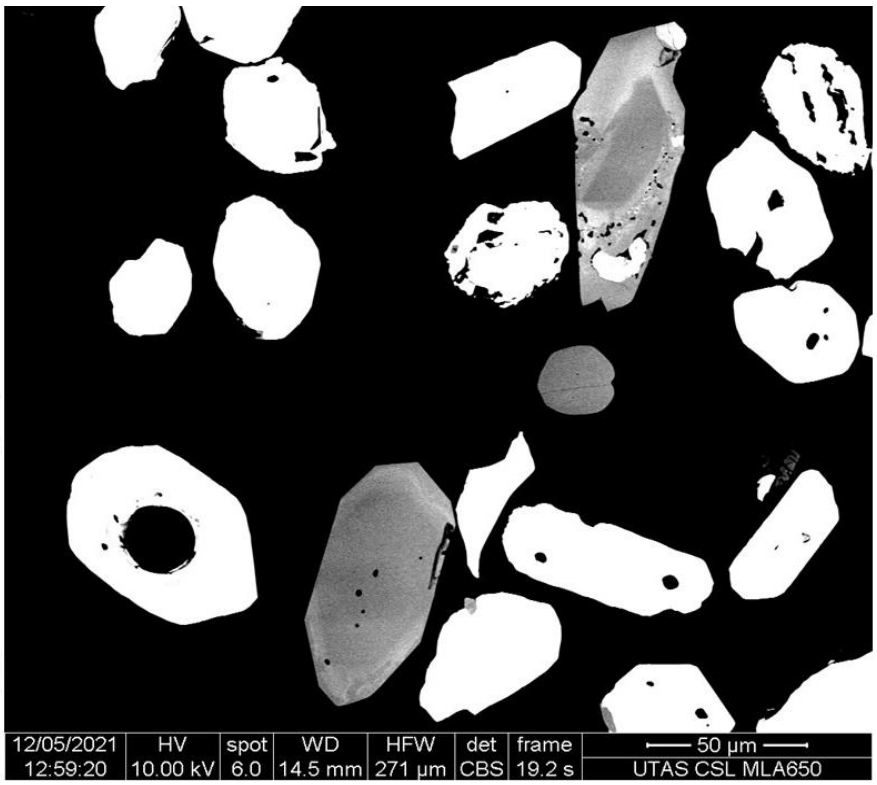
12/05/2021 | HV | spot | WD | HFW | det | frame | 50 µm
12:59:20 | 10.00 kV | 6.0 | 14.5 mm | 271 µm | CBS | 19.2 s | UTAS CSL MLA650

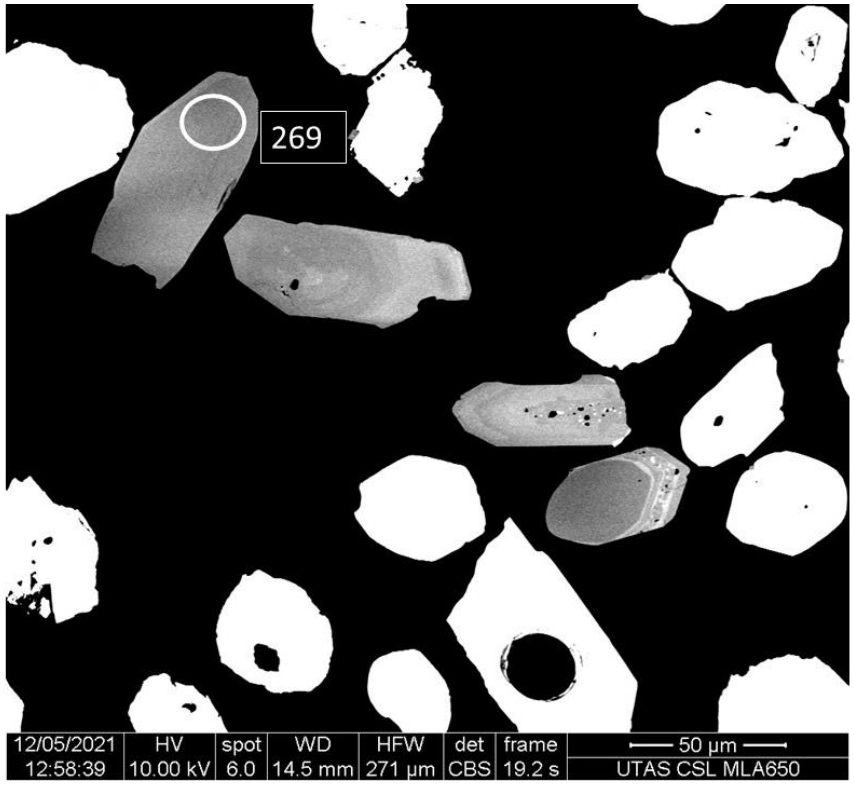
269
12/05/2021
12:58:39
HV
10.00 kV
spot
6.0
WD
14.5 mm
HFW
271 µm
det
CBS
frame
19.2 s
50 µm
UTAS CSL MLA650

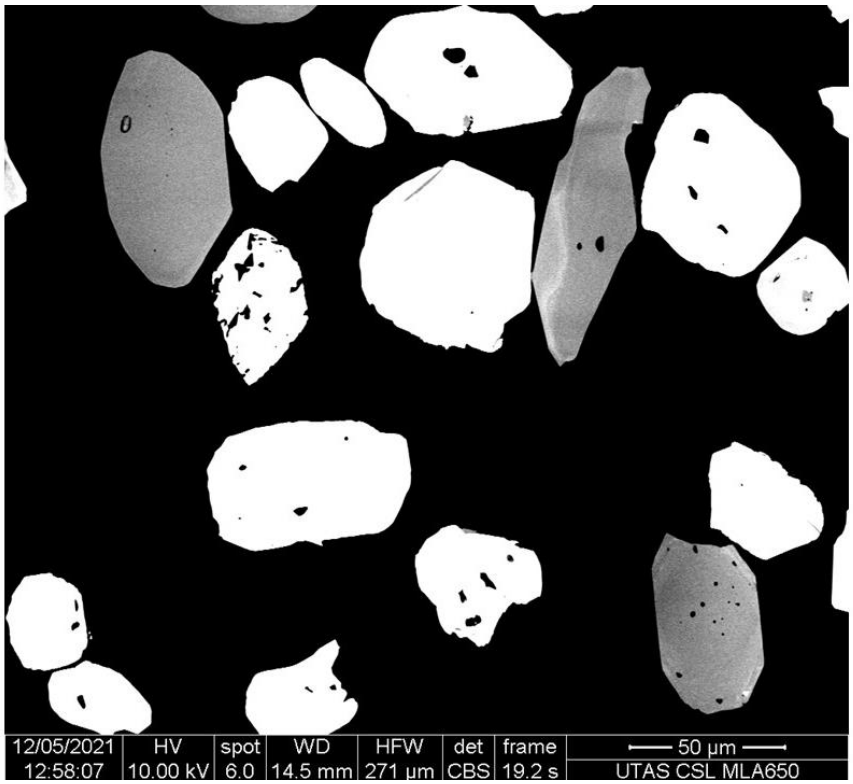
12/05/2021
12:58:07
HV
10.00 kV
spot
6.0
WD
14.5 mm
HFW
271 µm
det
CBS
frame
19.2 s
50 µm
UTAS CSL MLA650

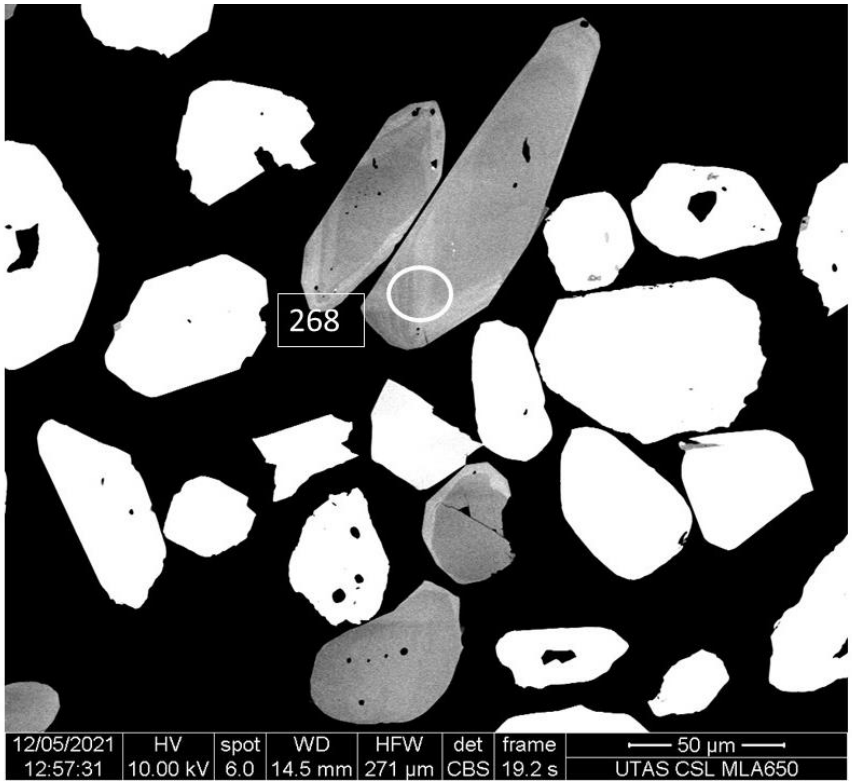
268
12/05/2021 12:57:31
HV 10.00 kV
spot 6.0
WD 14.5 mm
HFW 271 µm
det CBS
frame 19.2 s
50 µm
UTAS CSL MLA650

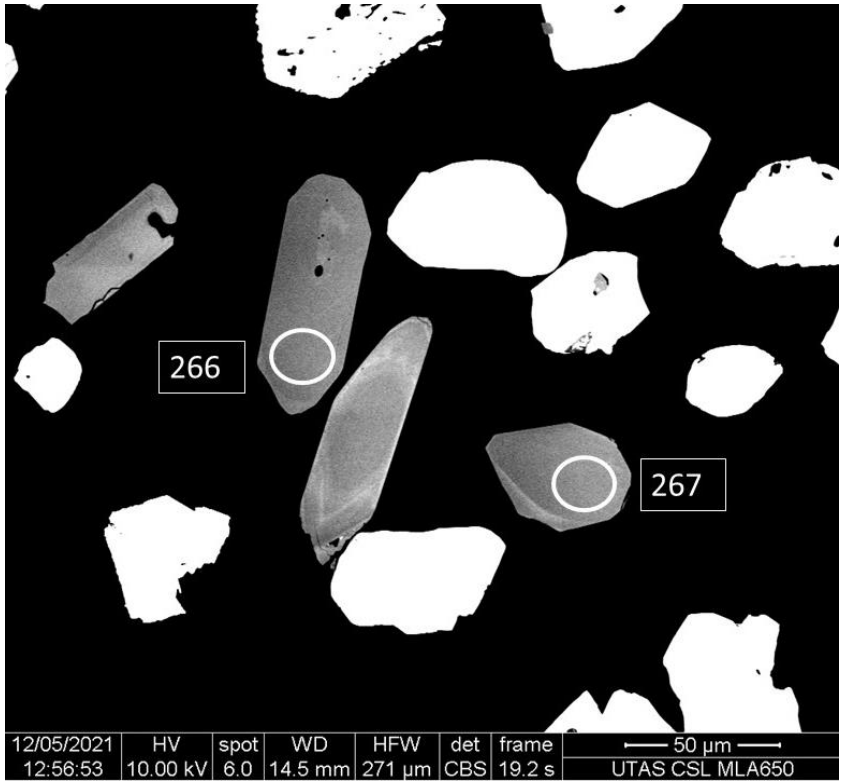
266
267
12/05/2021 12:56:53
HV 10.00 kV
spot 6.0
WD 14.5 mm
HFW 271 µm
det CBS
frame 19.2 s
50 µm
UTAS CSL MLA650

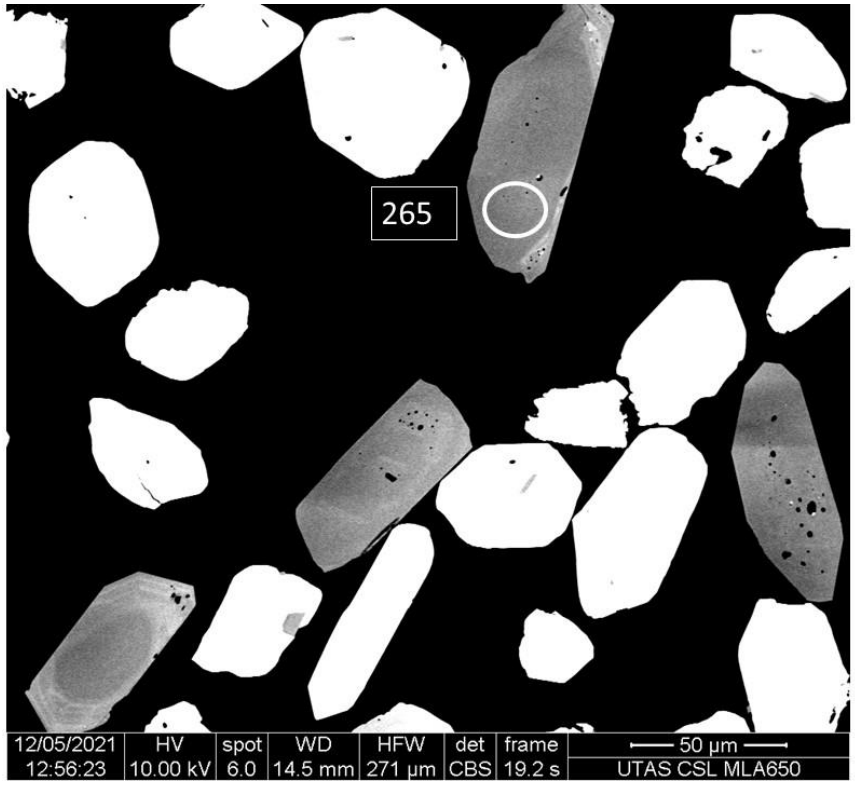
265
12/05/2021 12:56:23
HV 10.00 kV
spot 6.0
WD 14.5 mm
HFW 271 µm
det CBS
frame 19.2 s
50 µm
UTAS CSL MLA650

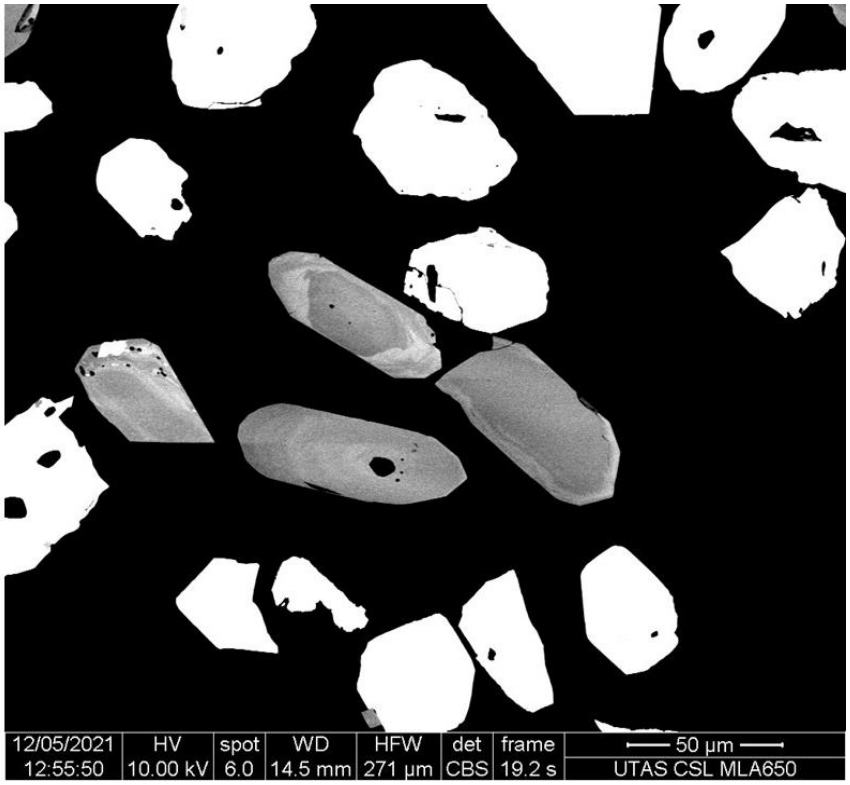
12/05/2021 12:55:50
HV 10.00 kV
spot 6.0
WD 14.5 mm
HFW 271 µm
det CBS
frame 19.2 s
50 µm
UTAS CSL MLA650

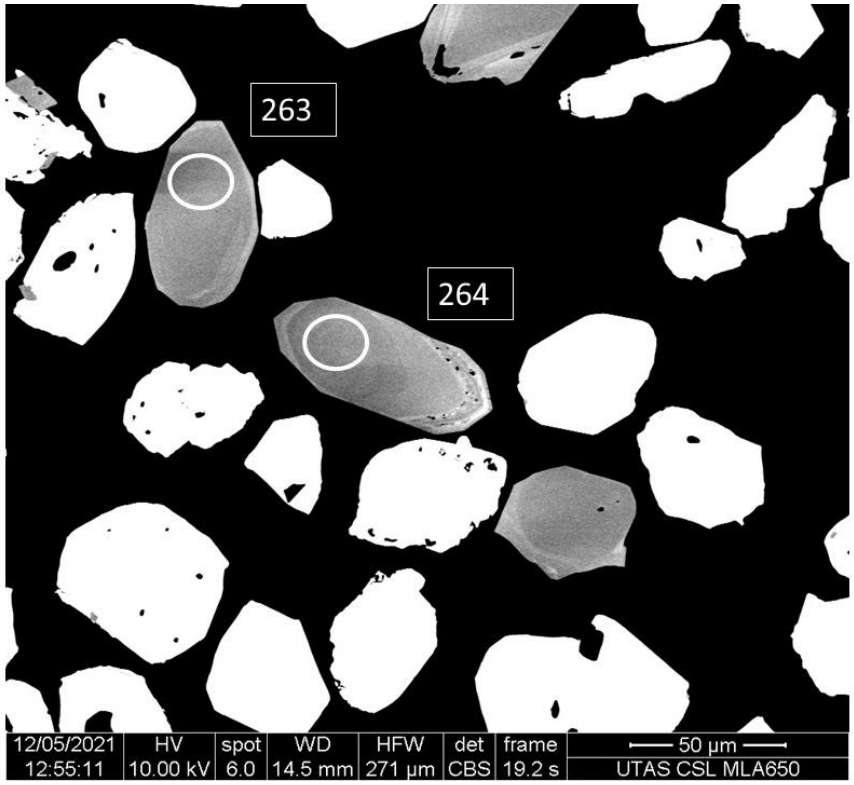
263
264
12/05/2021 12:55:11
HV 10.00 kV
spot 6.0
WD 14.5 mm
HFW 271 µm
det CBS
frame 19.2 s
50 µm
UTAS CSL MLA650


262
261
12/05/2021 12:54:39
HV 10.00 kV
spot 6.0
WD 14.5 mm
HFW 271 µm
det CBS
frame 19.2 s
50 µm
UTAS CSL MLA650


260
12/05/2021 12:54:03
HV 10.00 kV
spot 6.0
WD 14.5 mm
HFW 271 µm
det CBS
frame 19.2 s
50 µm
UTAS CSL MLA650

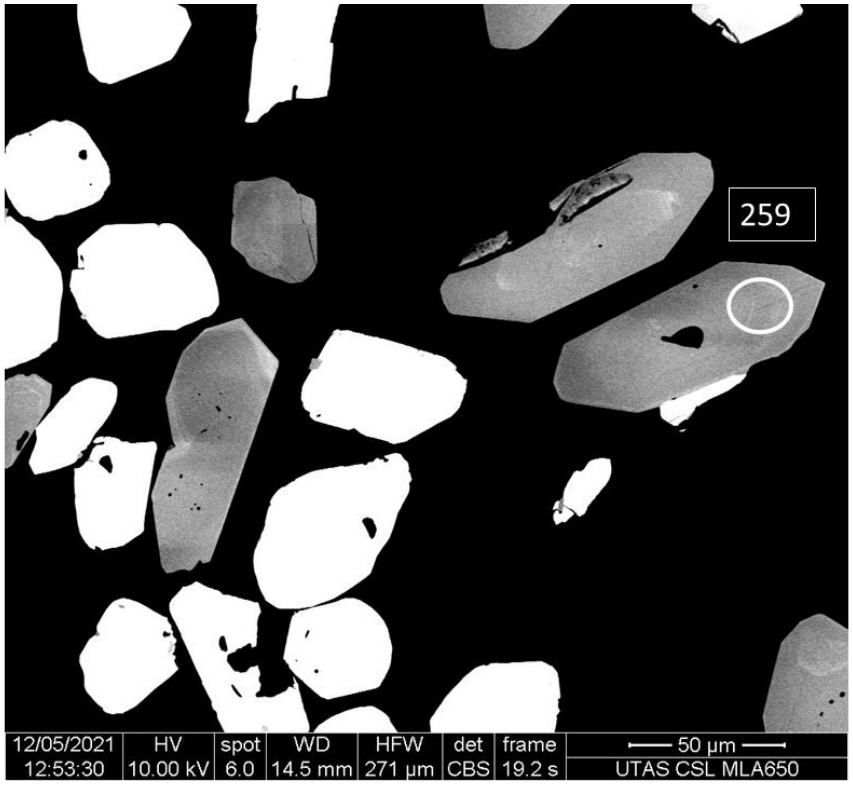
259
12/05/2021 12:53:30
HV 10.00 kV
spot 6.0
WD 14.5 mm
HFW 271 µm
det CBS
frame 19.2 s
50 µm
UTAS CSL MLA650

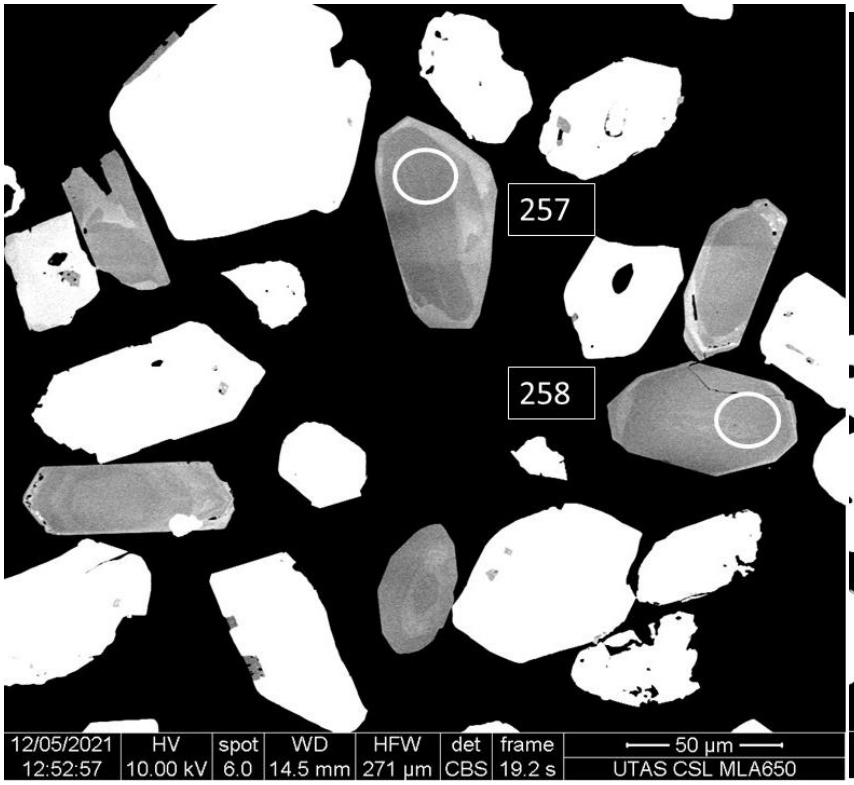
257
258
12/05/2021
12:52:57
HV
10.00 kV
spot
6.0
WD
14.5 mm
HFW
271 µm
det
CBS
frame
19.2 s
50 µm
UTAS CSL MLA650

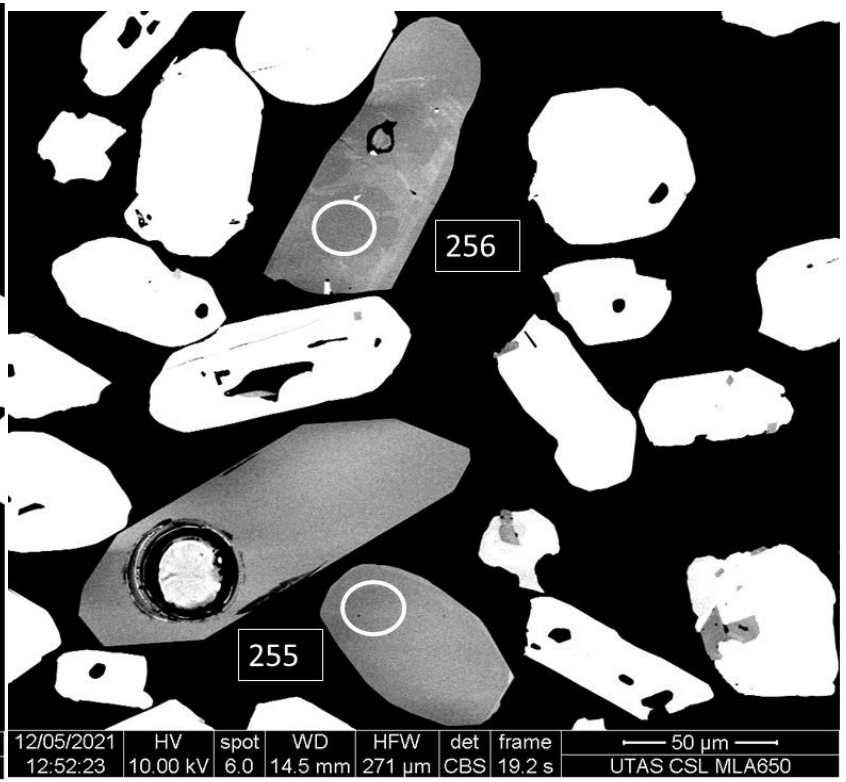
256
255
12/05/2021
12:52:23
HV
10.00 kV
spot
6.0
WD
14.5 mm
HFW
271 µm
det
CBS
frame
19.2 s
50 µm
UTAS CSL MLA650

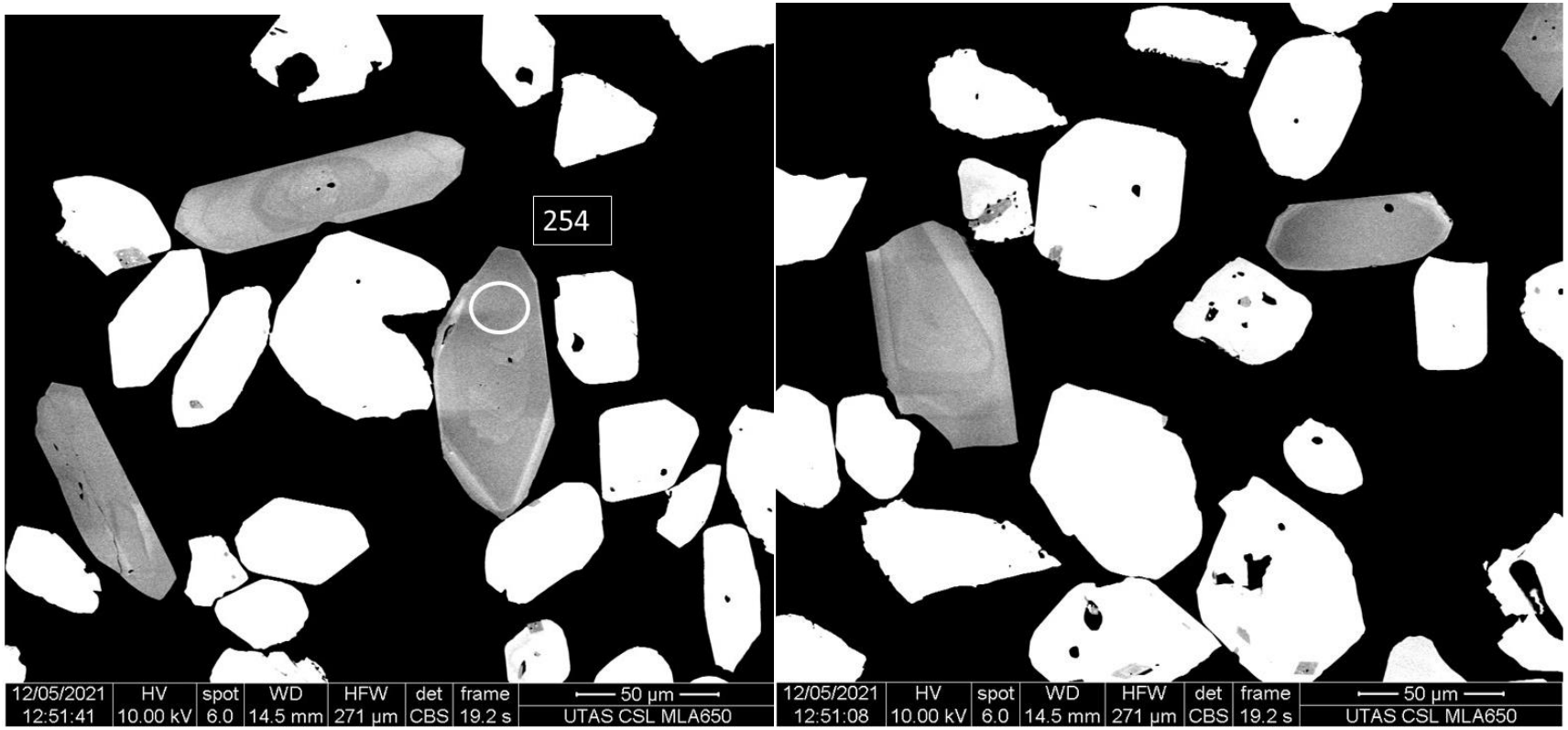
254
12/05/2021 12:51:41
HV 10.00 kV
spot 6.0
WD 14.5 mm
HFW 271 µm
det CBS
frame 19.2 s
50 µm
UTAS CSL MLA650
12/05/2021 12:51:08
HV 10.00 kV
spot 6.0
WD 14.5 mm
HFW 271 µm
det CBS
frame 19.2 s
50 µm
UTAS CSL MLA650

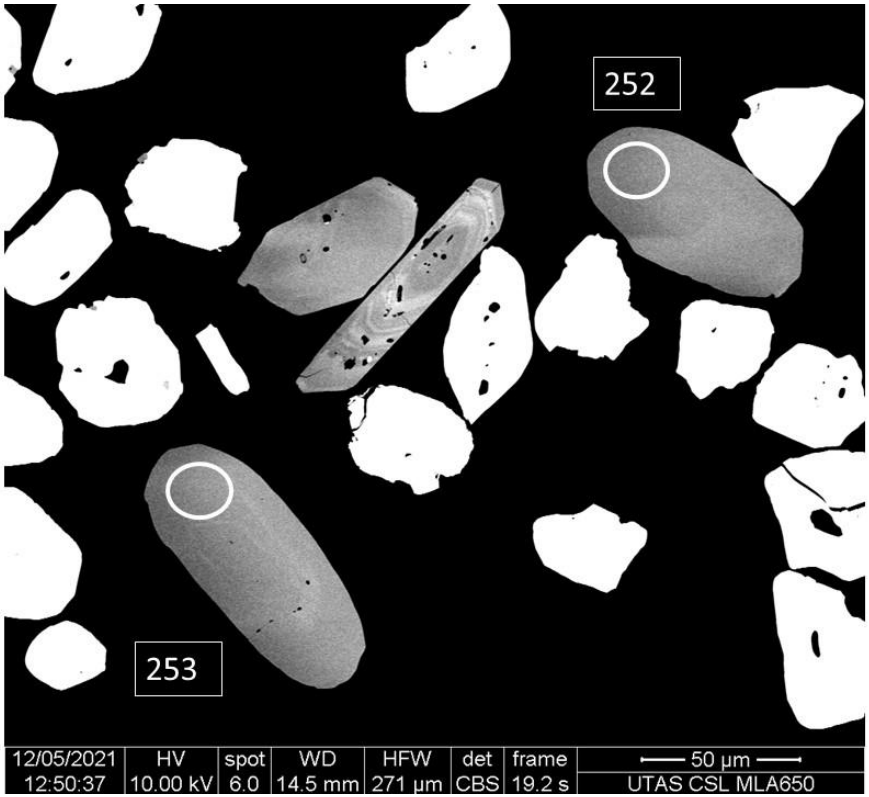
252
253
12/05/2021 12:50:37
HV 10.00 kV
spot 6.0
WD 14.5 mm
HFW 271 µm
det CBS
frame 19.2 s
50 µm
UTAS CSL MLA650


251
12/05/2021 12:49:24
HV 10.00 kV
spot 6.0
WD 14.5 mm
HFW 271 µm
det CBS
frame 19.2 s
50 µm
UTAS CSL MLA650

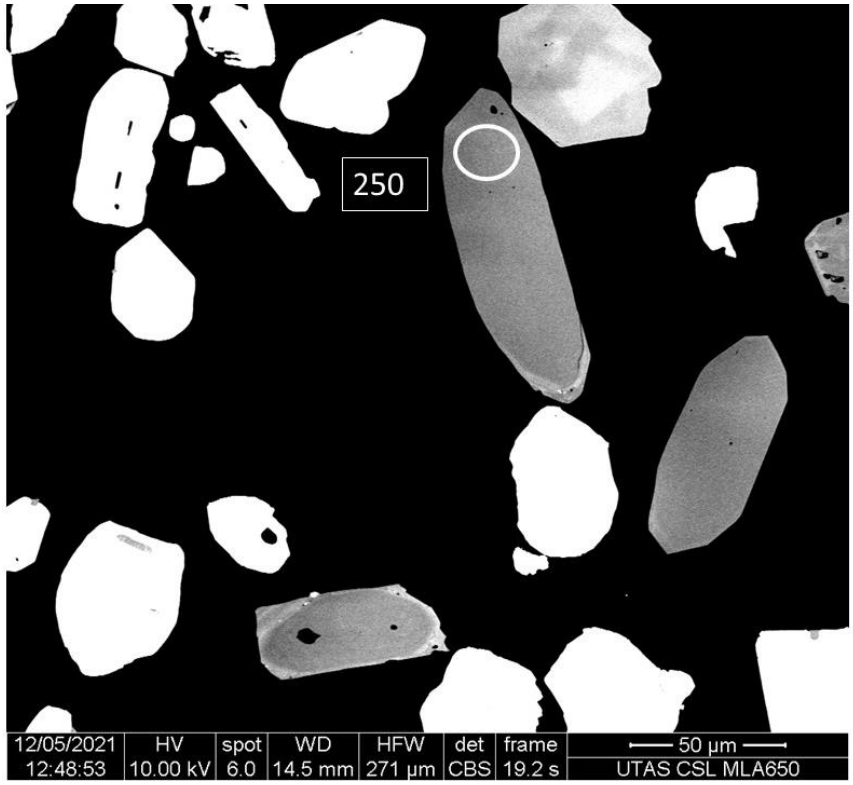
250
12/05/2021 12:48:53
HV 10.00 kV
spot 6.0
WD 14.5 mm
HFW 271 µm
det CBS
frame 19.2 s
50 µm
UTAS CSL MLA650

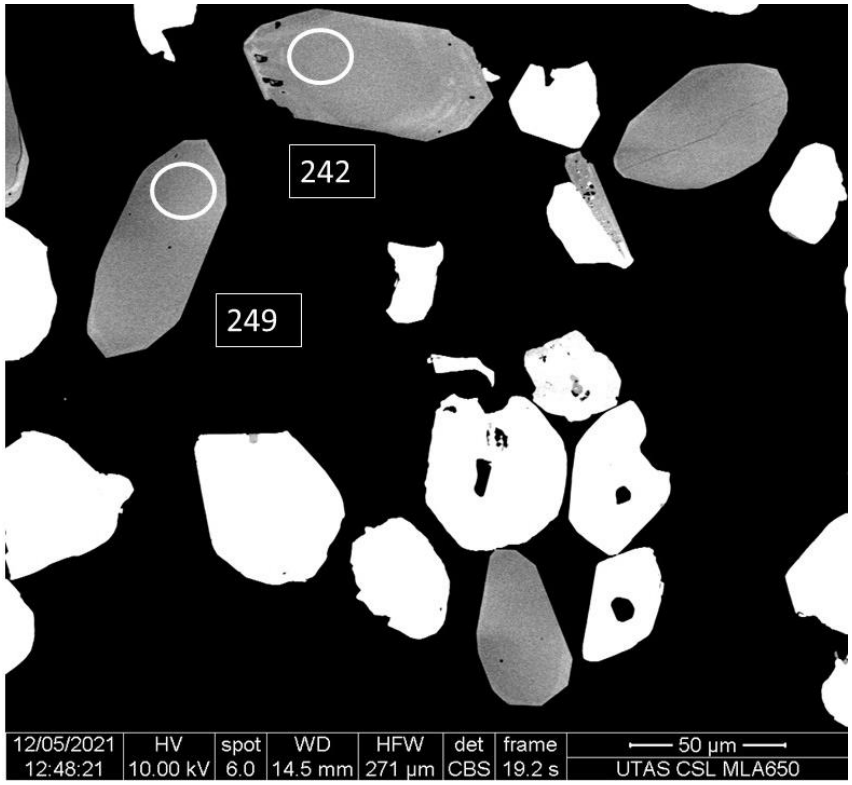
242
249
12/05/2021 12:48:21
HV 10.00 kV
spot 6.0
WD 14.5 mm
HFW 271 µm
det CBS
frame 19.2 s
50 µm
UTAS CSL MLA650

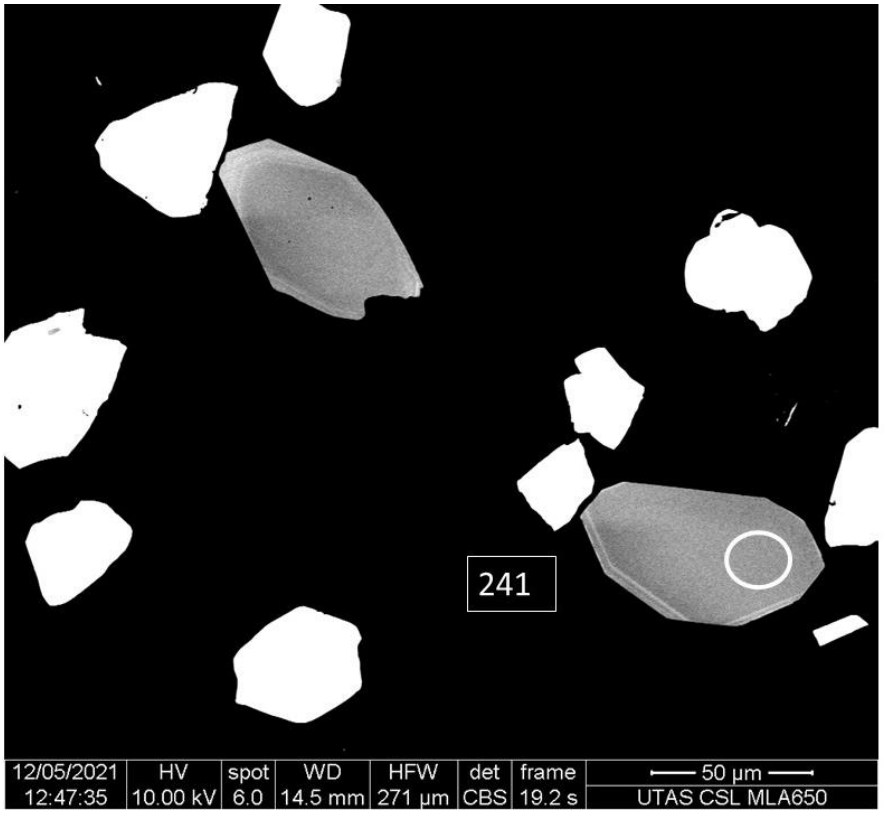
241
12/05/2021 12:47:35
HV 10.00 kV
spot 6.0
WD 14.5 mm
HFW 271 µm
det CBS
frame 19.2 s
50 µm
UTAS CSL MLA650

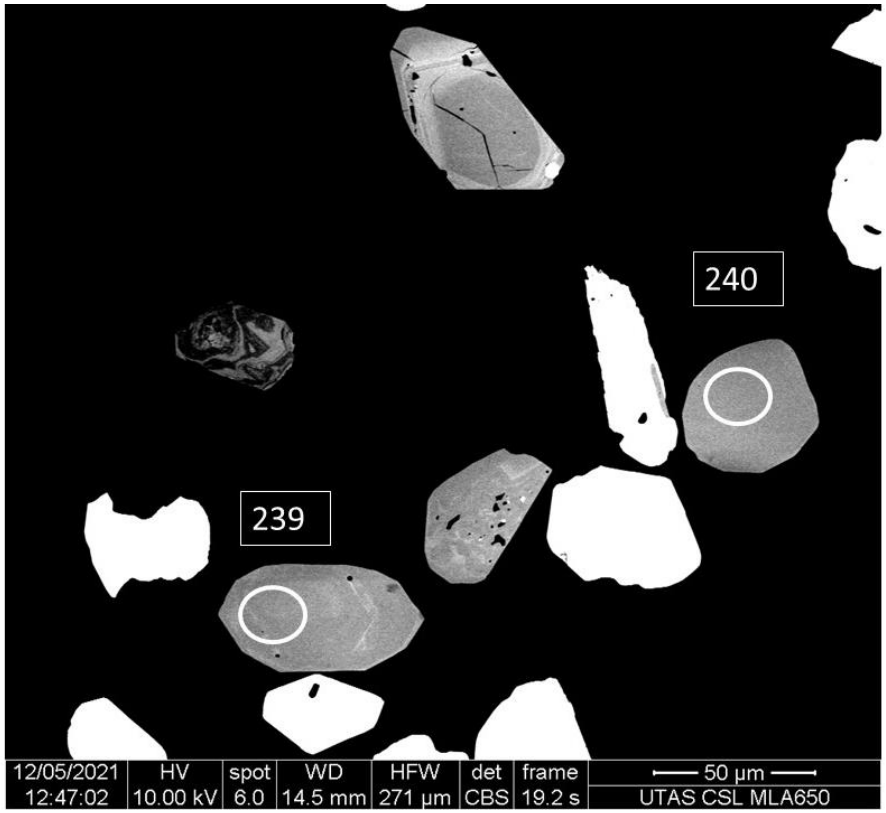
240
239
12/05/2021 12:47:02
HV 10.00 kV
spot 6.0
WD 14.5 mm
HFW 271 µm
det CBS
frame 19.2 s
50 µm
UTAS CSL MLA650

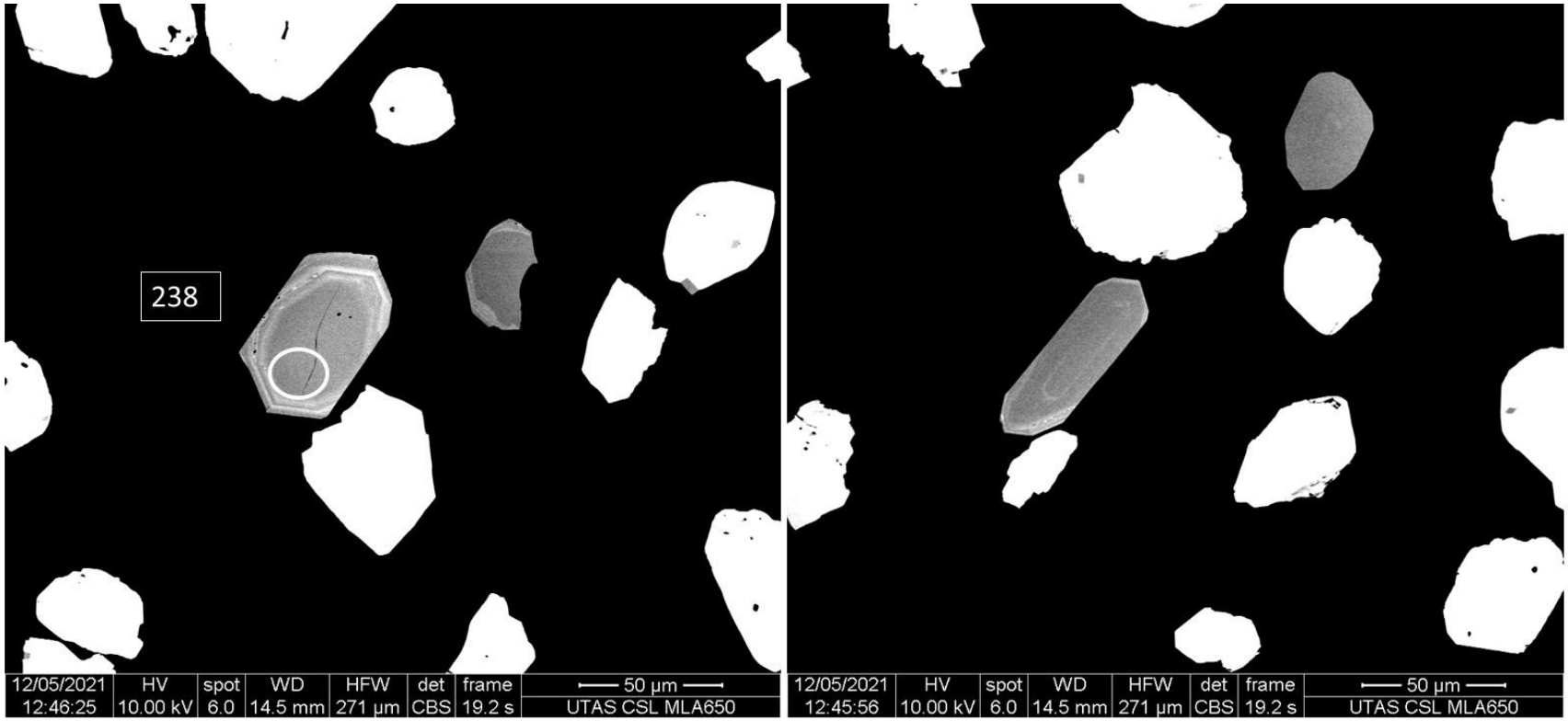
238
12/05/2021 12:46:25 | HV 10.00 kV | spot 6.0 | WD 14.5 mm | HFW 271 µm | det CBS | frame 19.2 s | 50 µm | UTAS CSL MLA650
12/05/2021 12:45:56 | HV 10.00 kV | spot 6.0 | WD 14.5 mm | HFW 271 µm | det CBS | frame 19.2 s | 50 µm | UTAS CSL MLA650

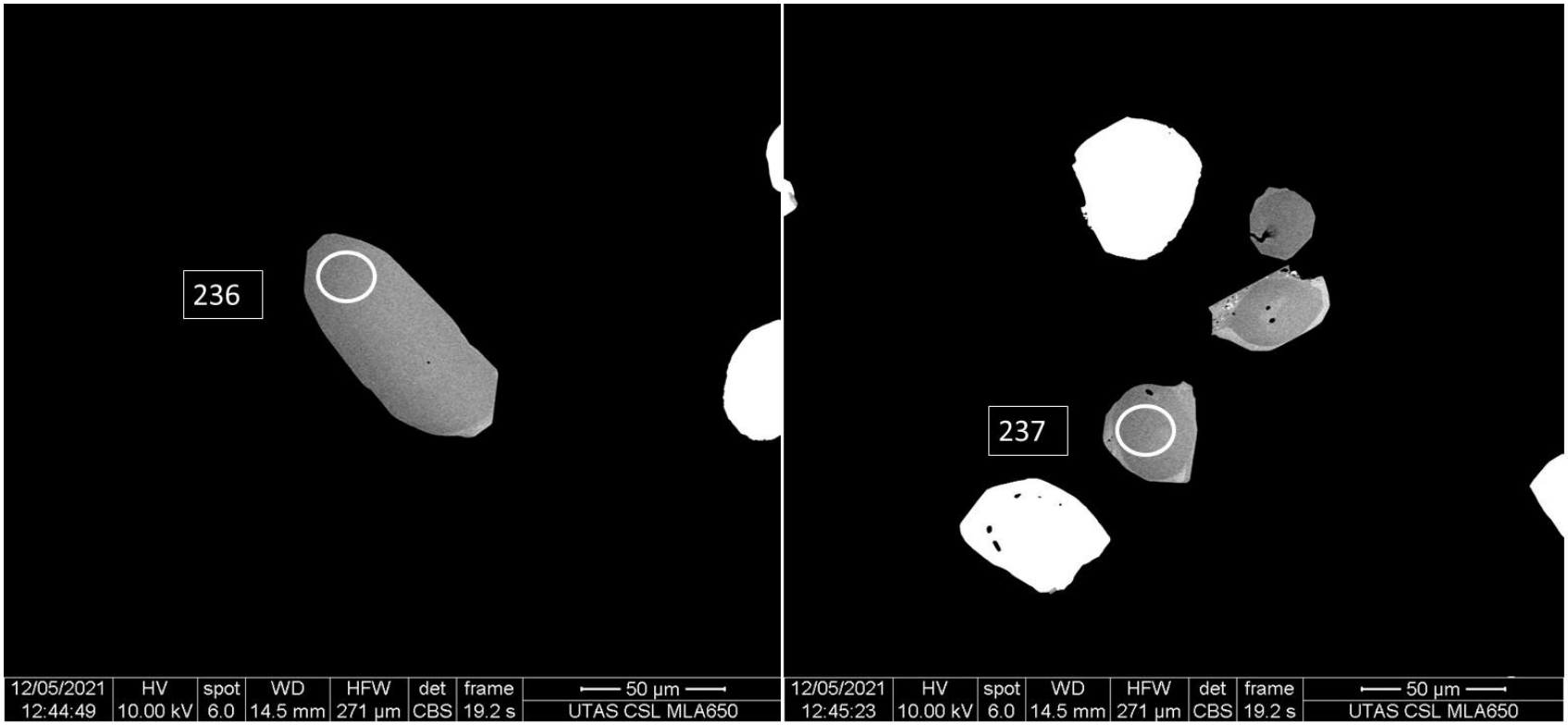
236
237
12/05/2021 12:44:49 | HV 10.00 kV | spot 6.0 | WD 14.5 mm | HFW 271 µm | det CBS | frame 19.2 s | 50 µm | UTAS CSL MLA650
12/05/2021 12:45:23 | HV 10.00 kV | spot 6.0 | WD 14.5 mm | HFW 271 µm | det CBS | frame 19.2 s | 50 µm | UTAS CSL MLA650

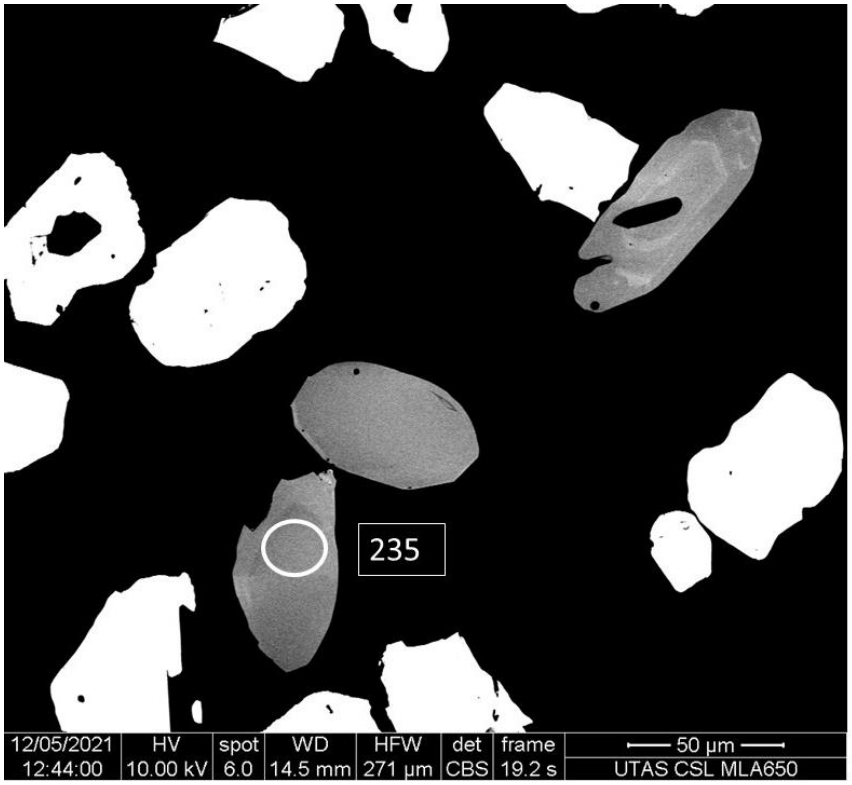
235
12/05/2021
12:44:00
HV
10.00 kV
spot
6.0
WD
14.5 mm
HFW
271 µm
det
CBS
frame
19.2 s
50 µm
UTAS CSL MLA650

APPENDIX C 1.6 Monazite images of two-mica leucogranites (ZY-LG-2) and tourmaline leucogranite (ZY-LGT-1)

2021-G-605_29
BSE

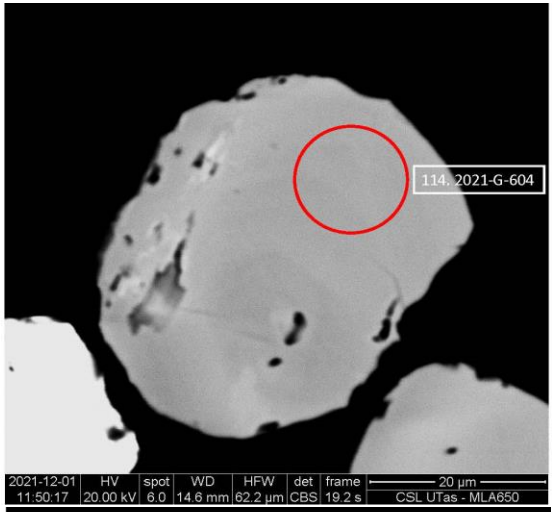

2021-G-605_28
BSE

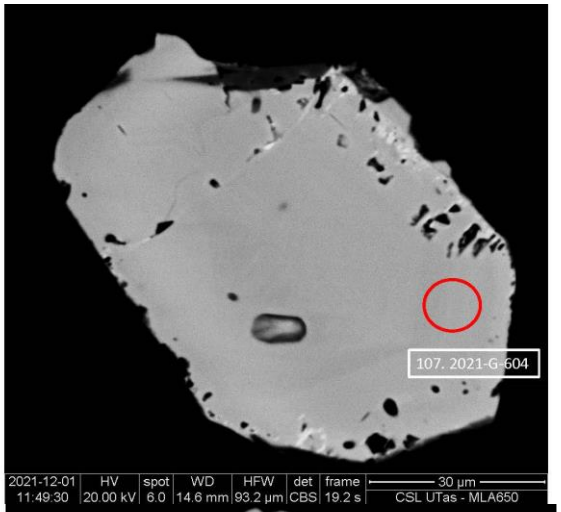

2021-G-605_27
BSE

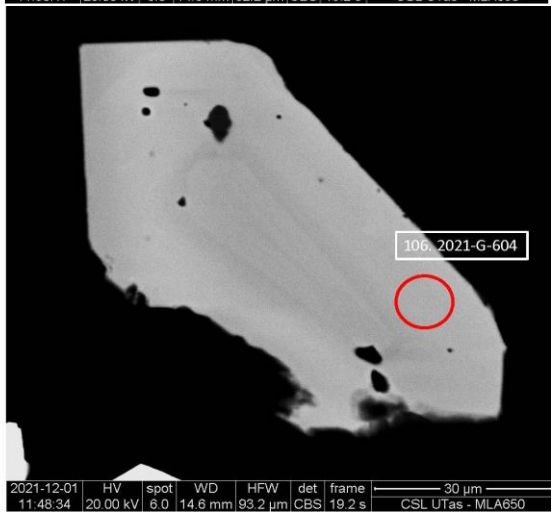

2021-G-605_26
BSE

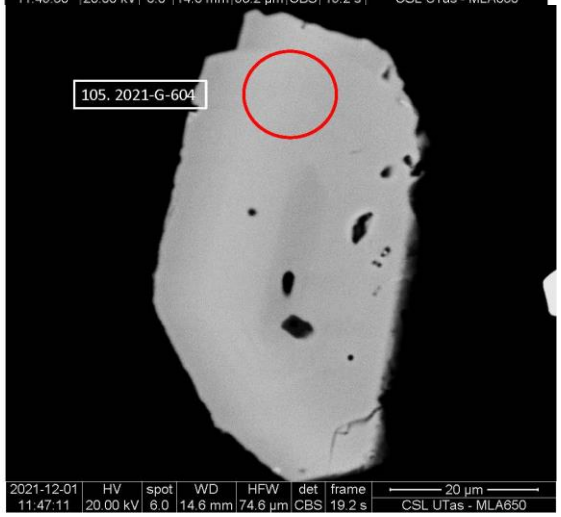

2021-G-605_25
BSE

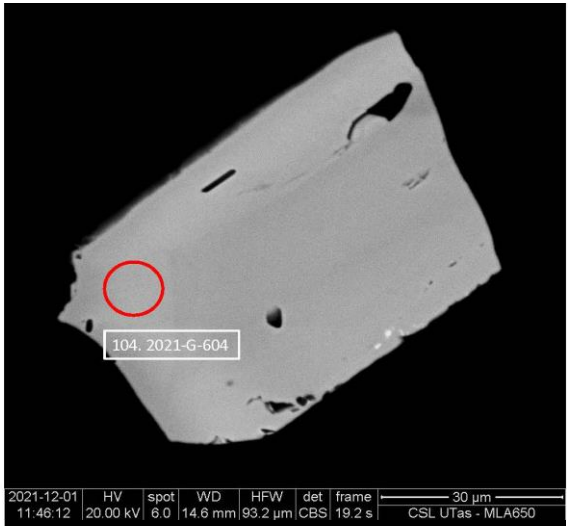

2021-G-605_24
BSE

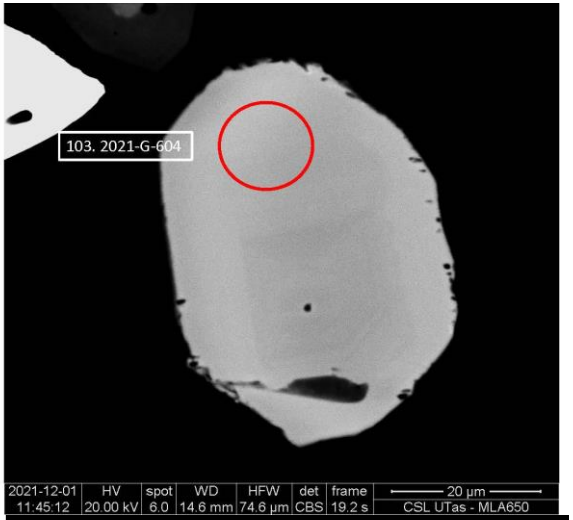

2021-G-605_23
BSE

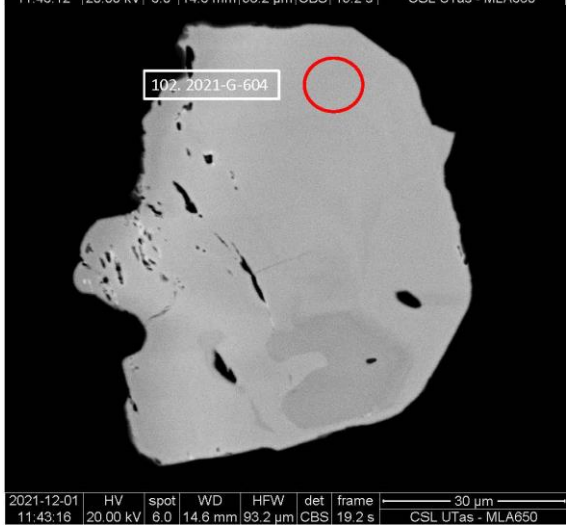

2021-G-605_22
BSE

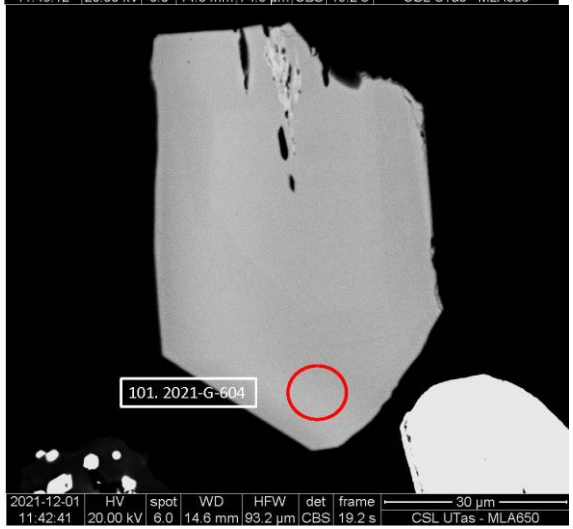

2021-G-605_21
BSE

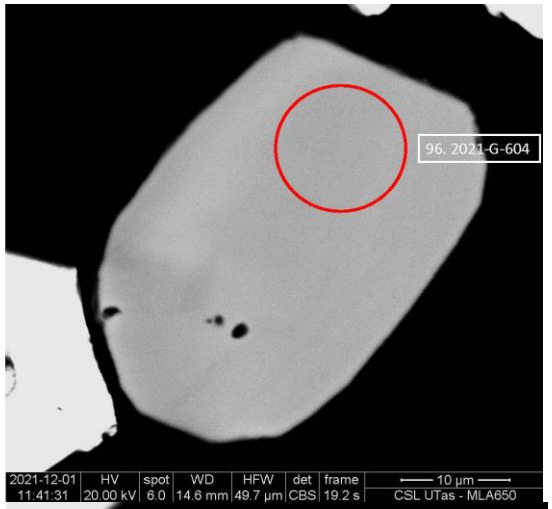

2021-G-605_20
BSE

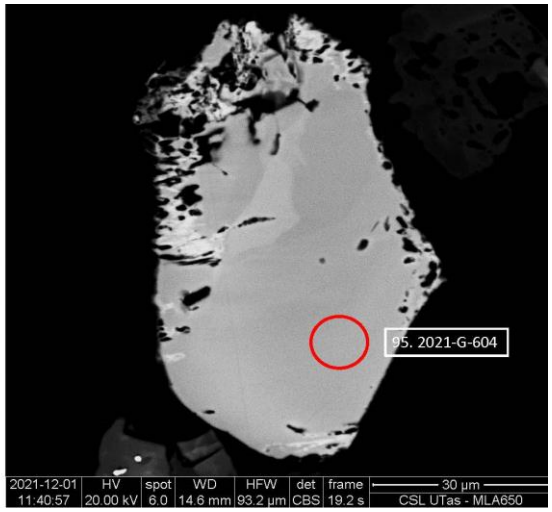

2021-G-605_19
BSE

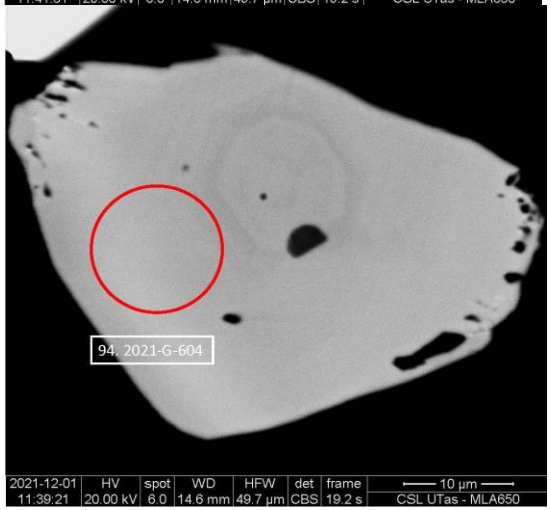

2021-G-605_18
BSE

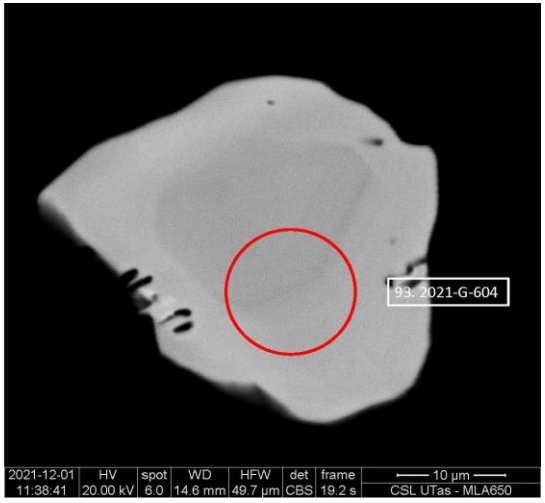

2021-G-605_17
BSE

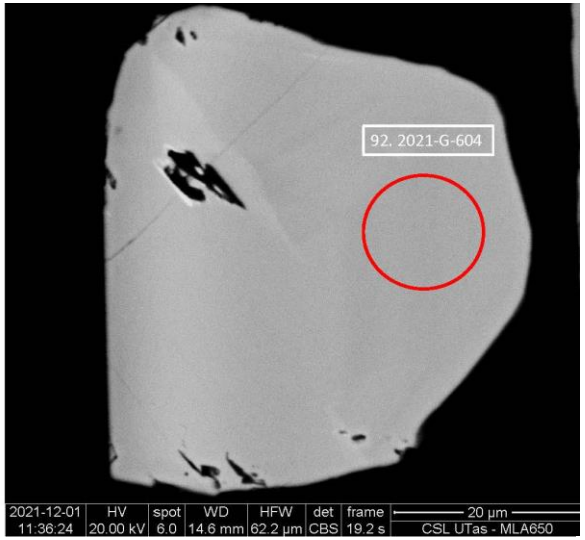

2021-G-605_16
BSE

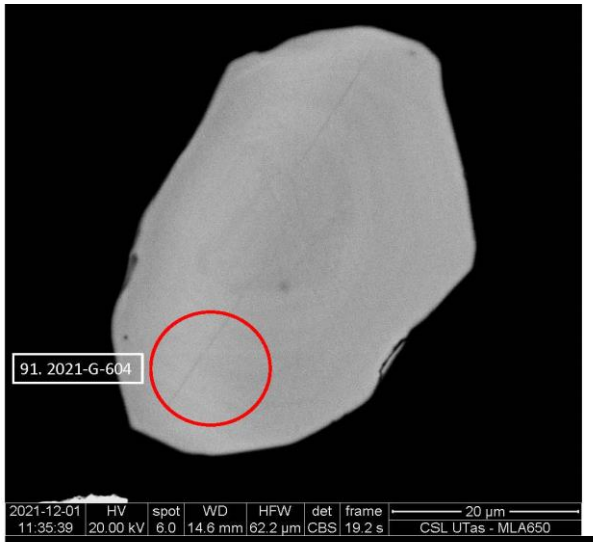

2021-G-605_15
BSE

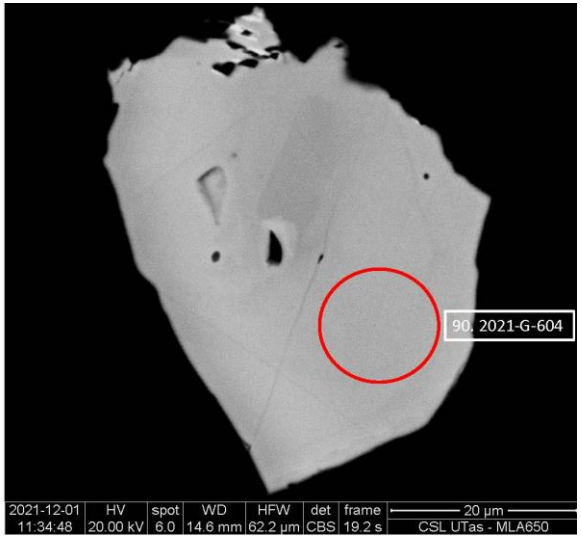

2021-G-605_14
BSE

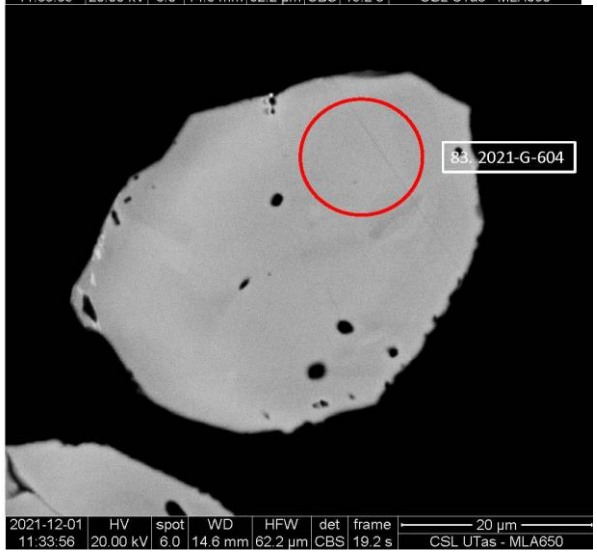

2021-G-605_13
BSE

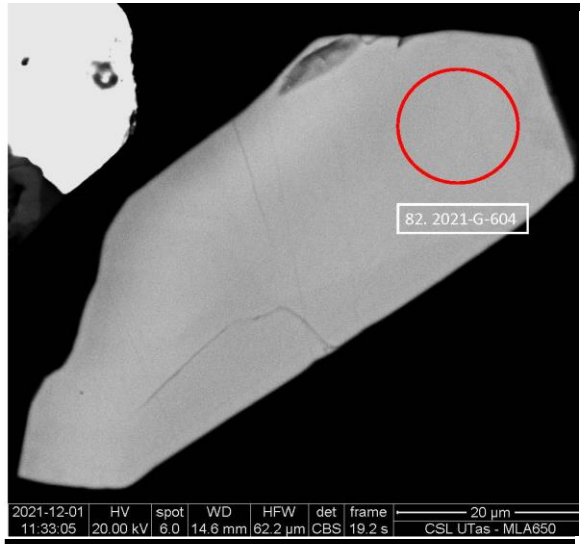

2021-G-605_12
BSE

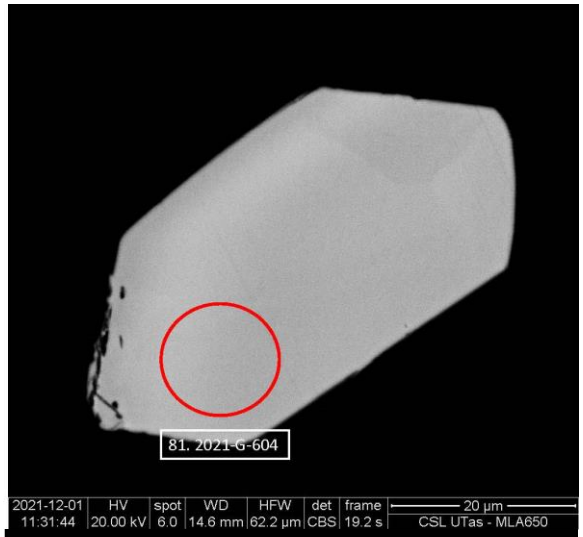

2021-G-605_11
BSE

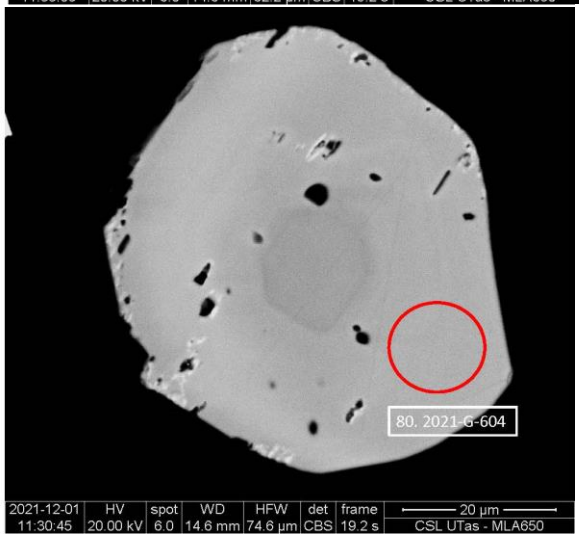

2021-G-605_10
BSE

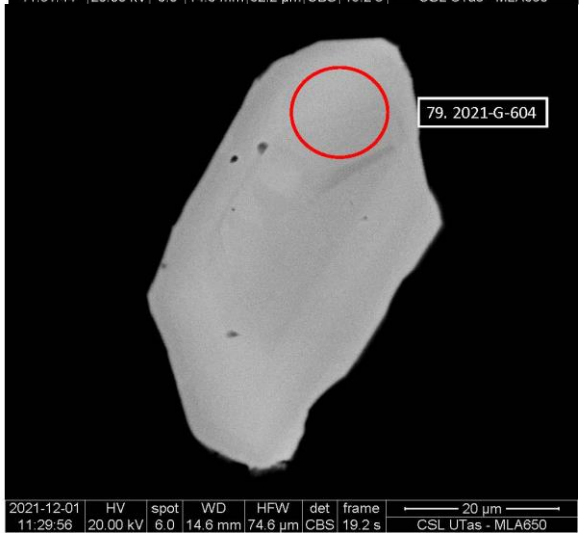

2021-G-605_9
BSE

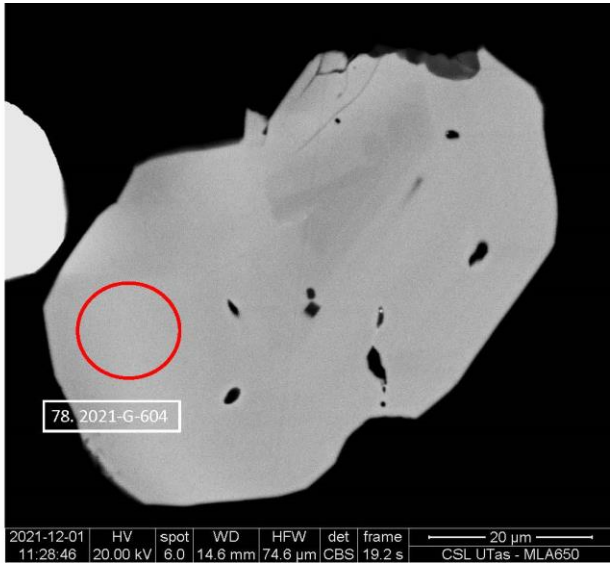

2021-G-605_8
BSE

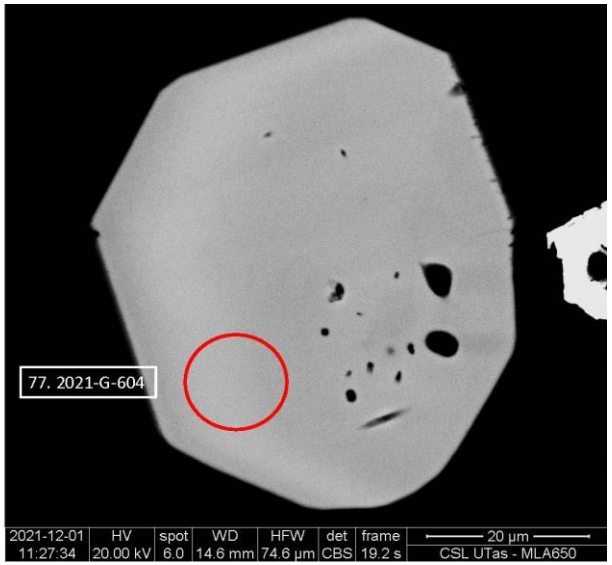

2021-G-605_7
BSE

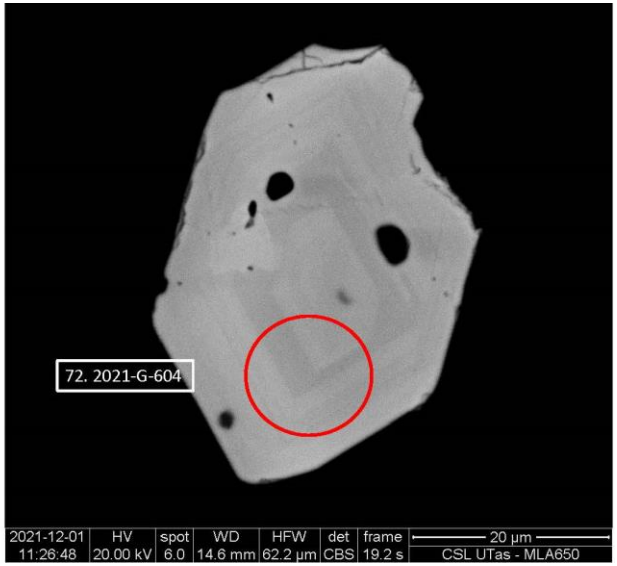

2021-G-605_6
BSE

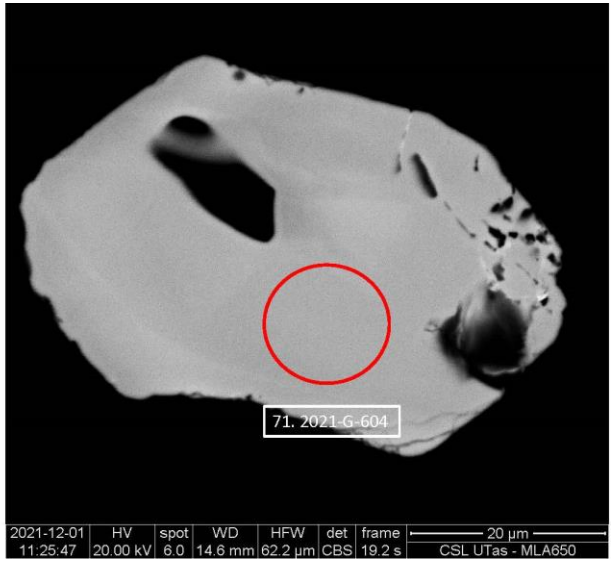

2021-G-605_5
BSE

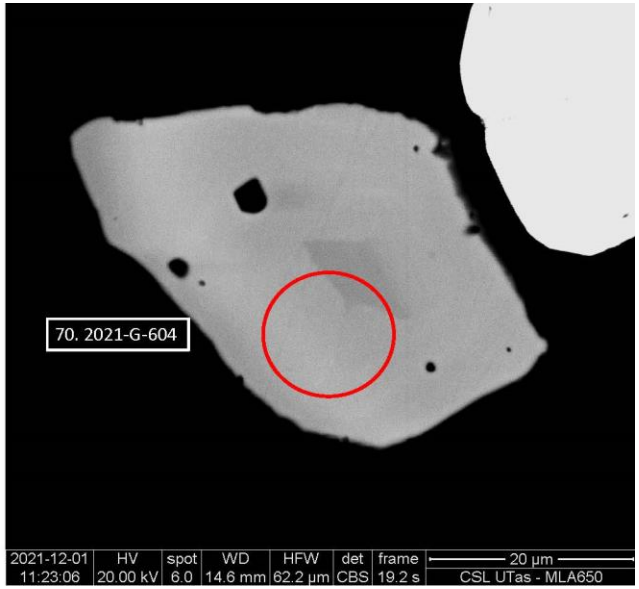

2021-G-605_4
BSE

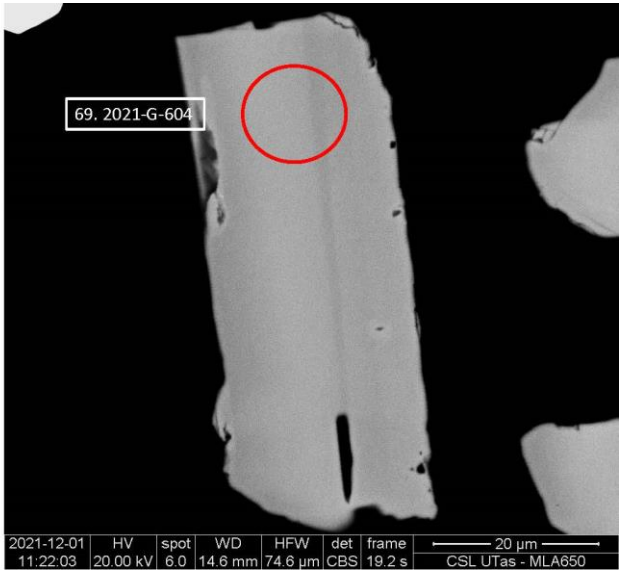

2021-G-605_3
BSE

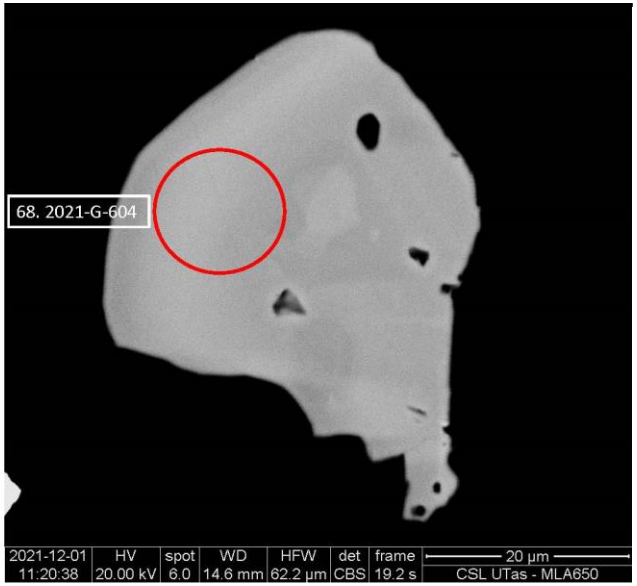

2021-G-605_2
BSE

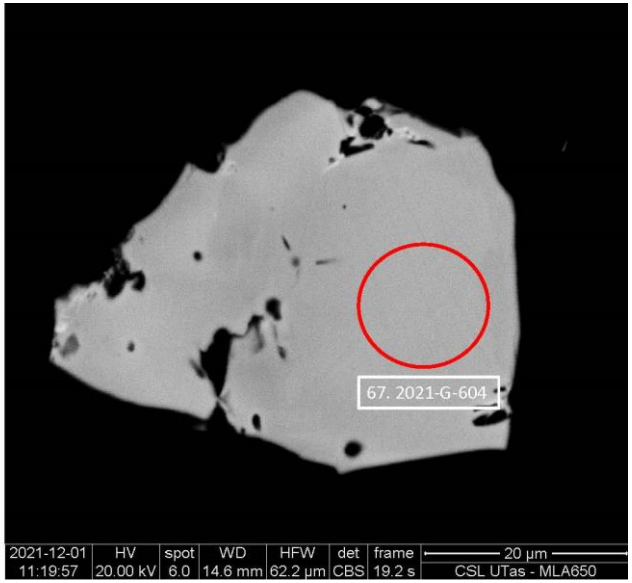

2021-G-605_1
BSE

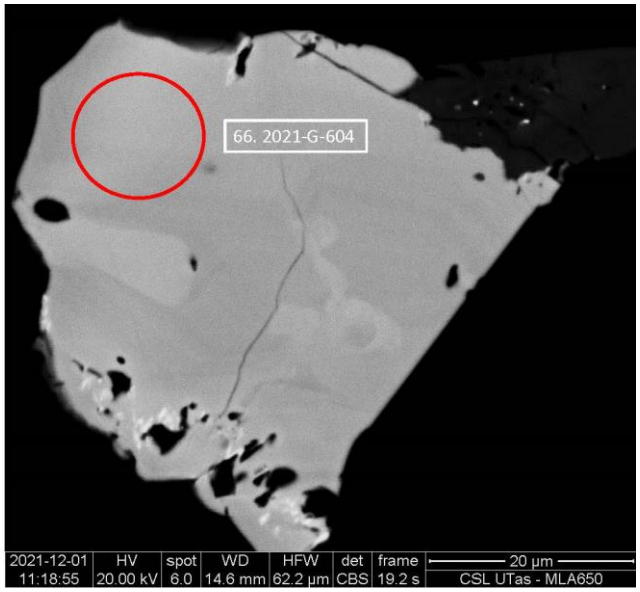

2021-G-604_35
BSE

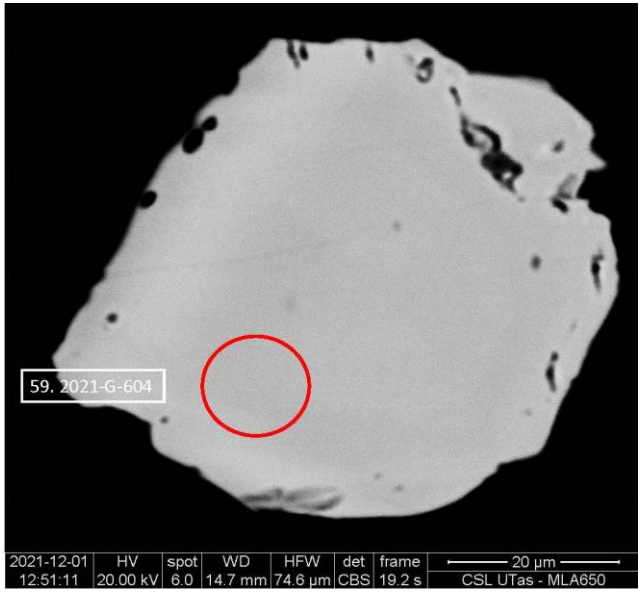

2021-G-604_34
BSE

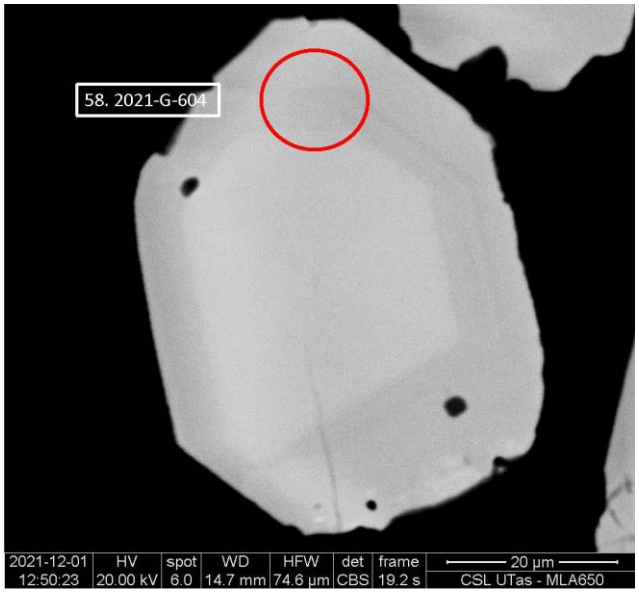

2021-G-604_33
BSE

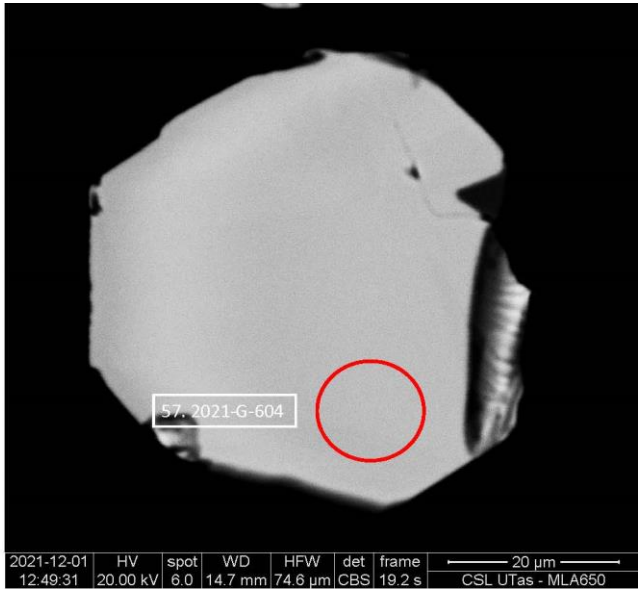

2021-G-604_32
BSE

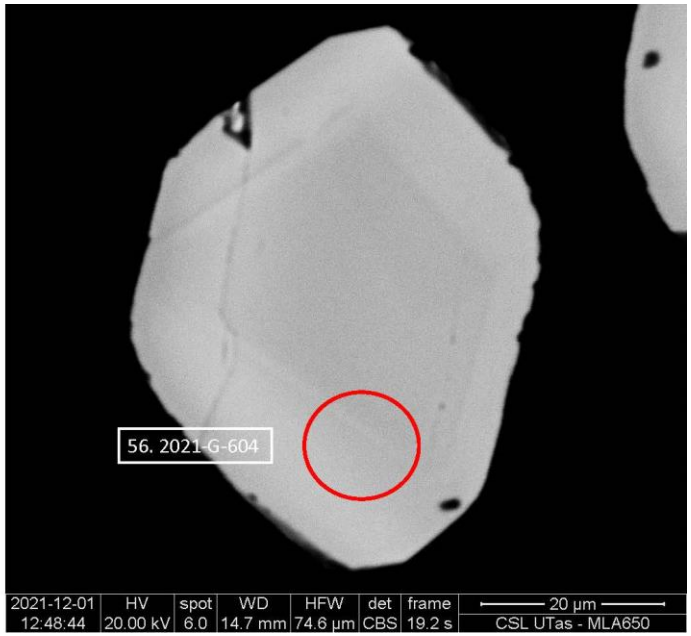

2021-G-604_31
BSE

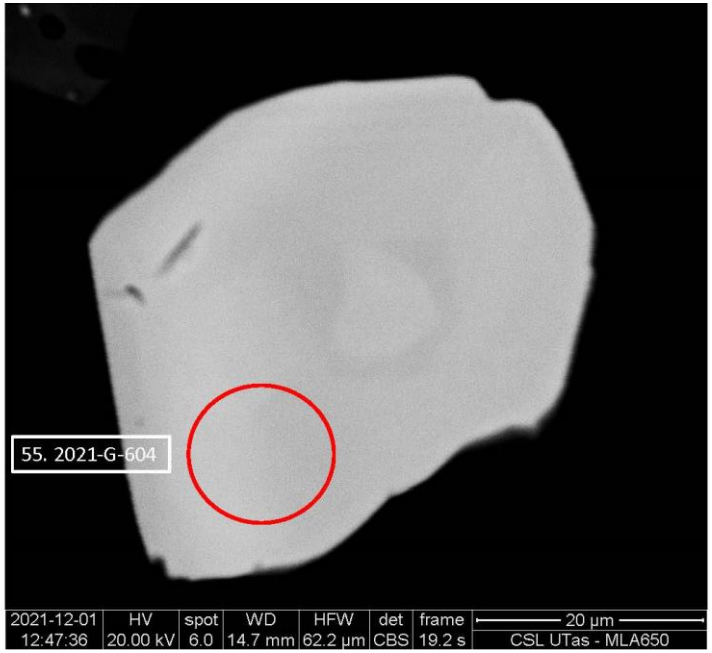

2021-G-604_30
BSE

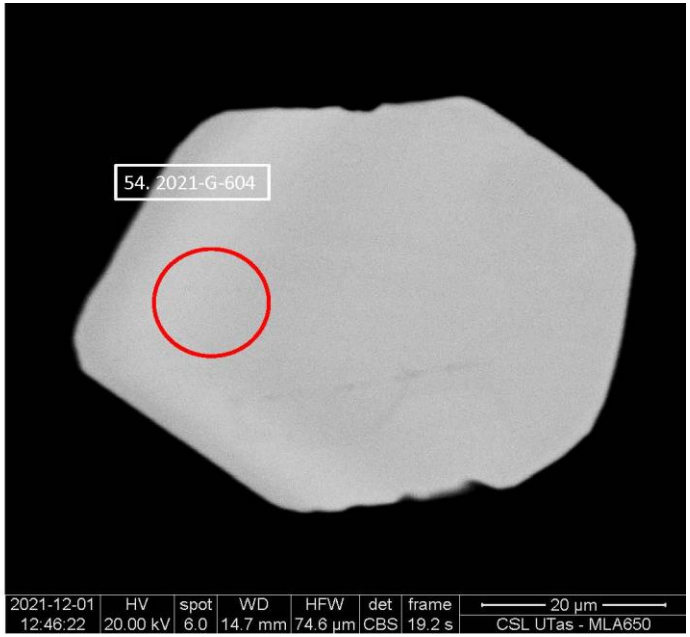

2021-G-604_29
BSE

2021-G-604_28
BSE

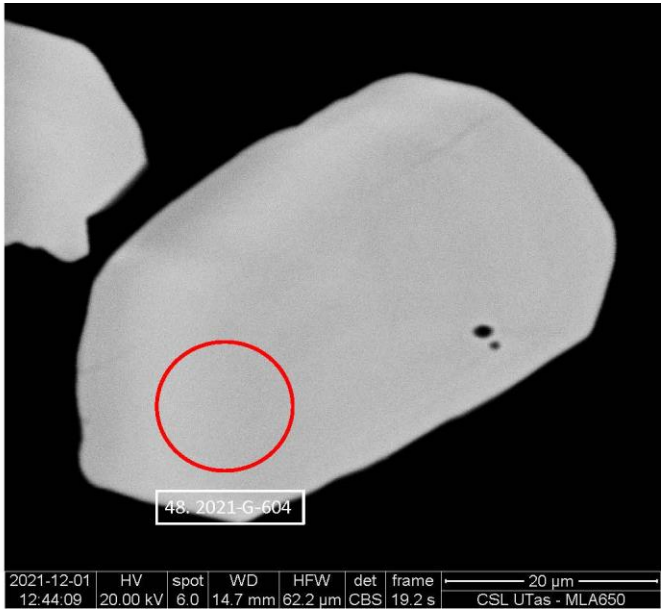

2021-G-604_27
BSE

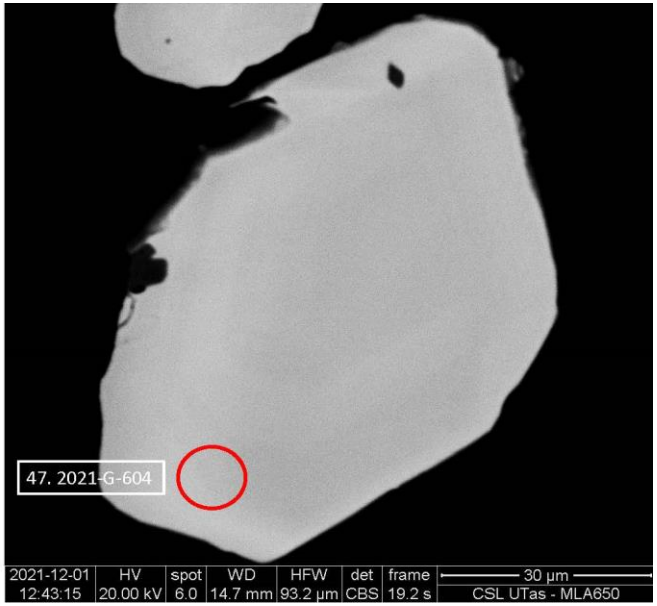

2021-G-604_26
BSE

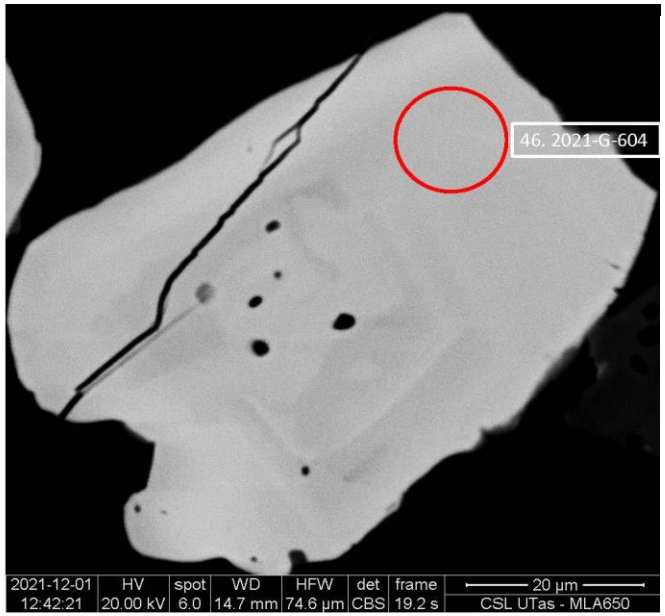

2021-G-604_25
BSE

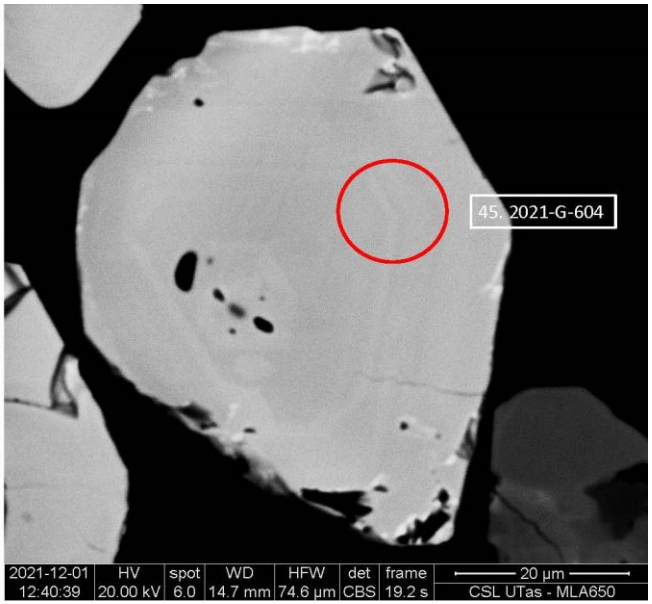

2021-G-604_24
BSE

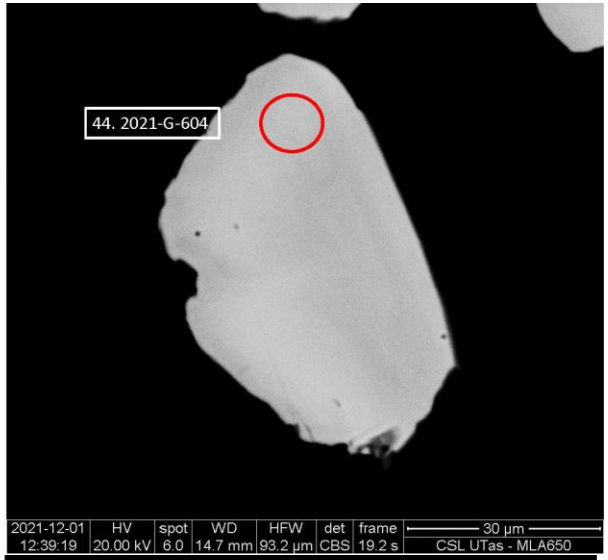

2021-G-604_23
BSE

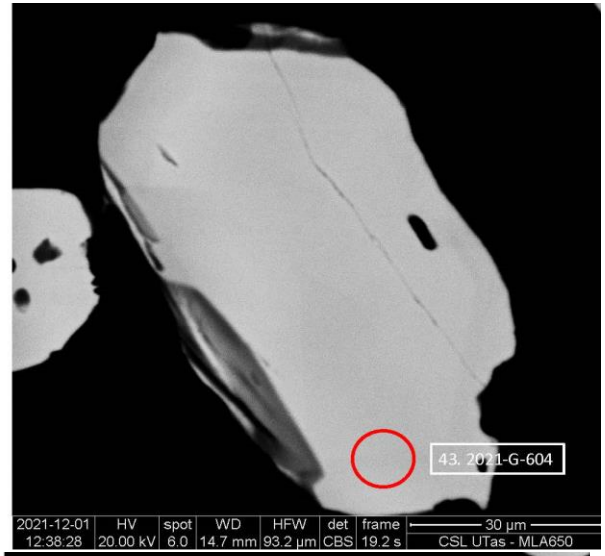

2021-G-604_22
BSE

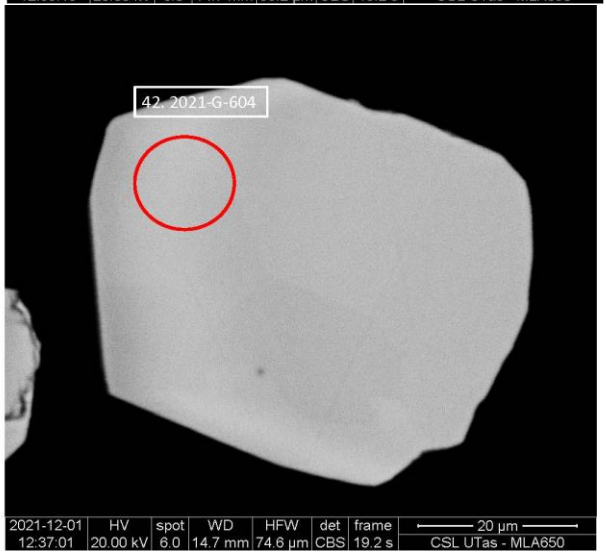

2021-G-604_21
BSE

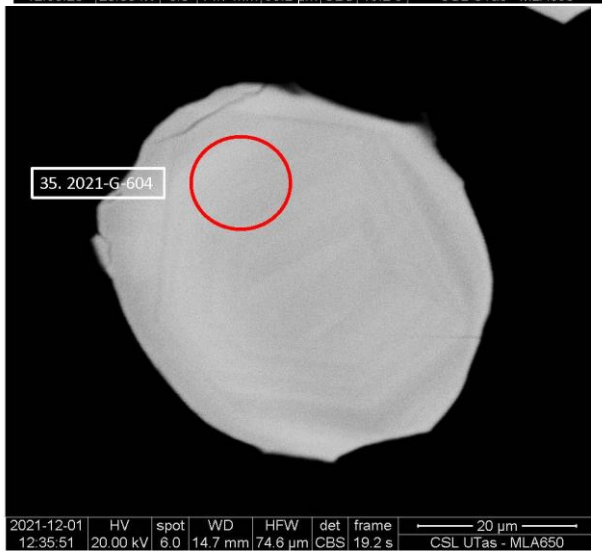

2021-G-604_20
BSE

2021-G-604_19
BSE

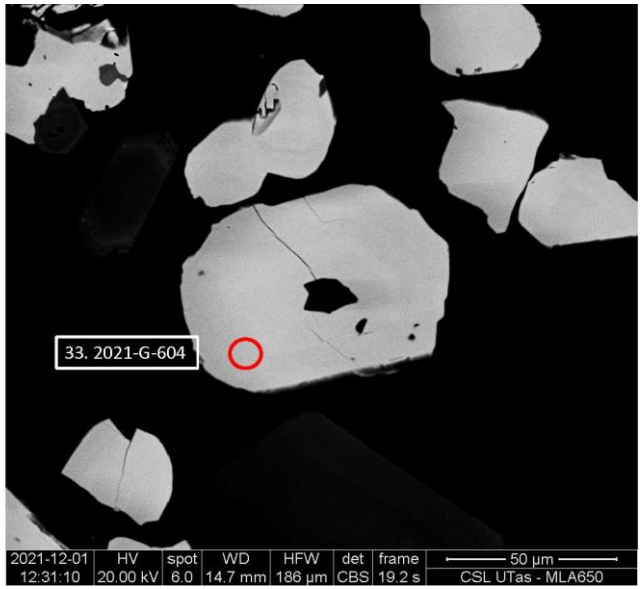

2021-G-604_18
BSE

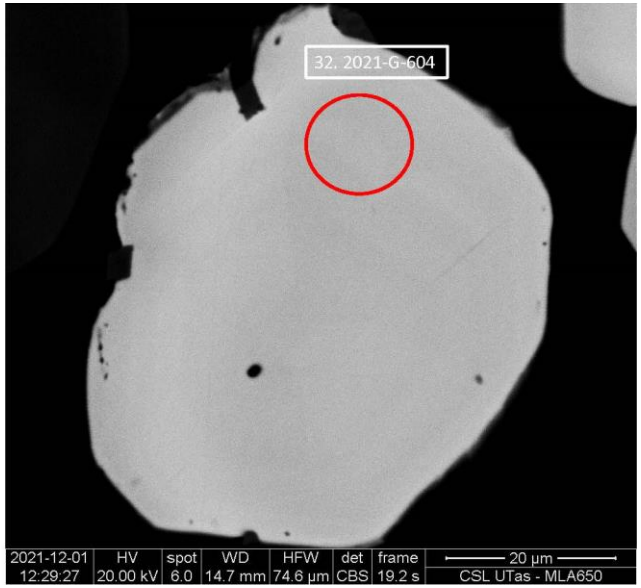

2021-G-604_17
BSE

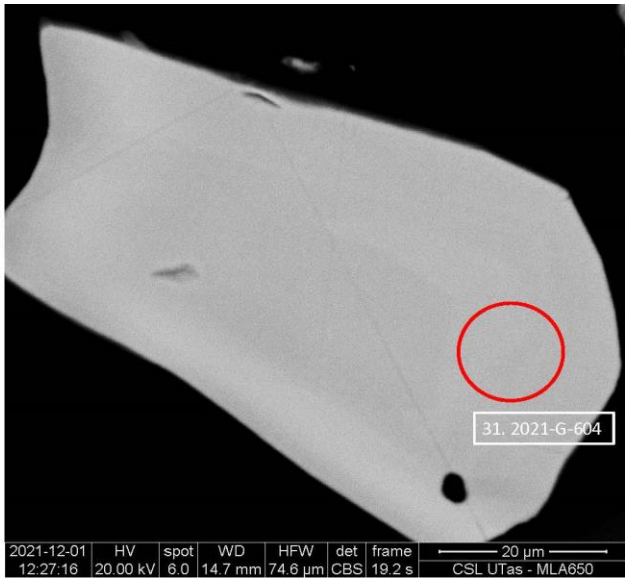

2021-G-604_16
BSE

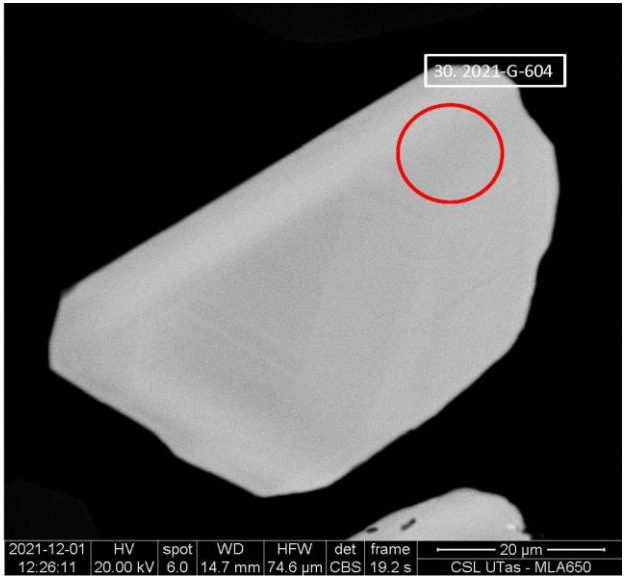

2021-G-604_15
BSE

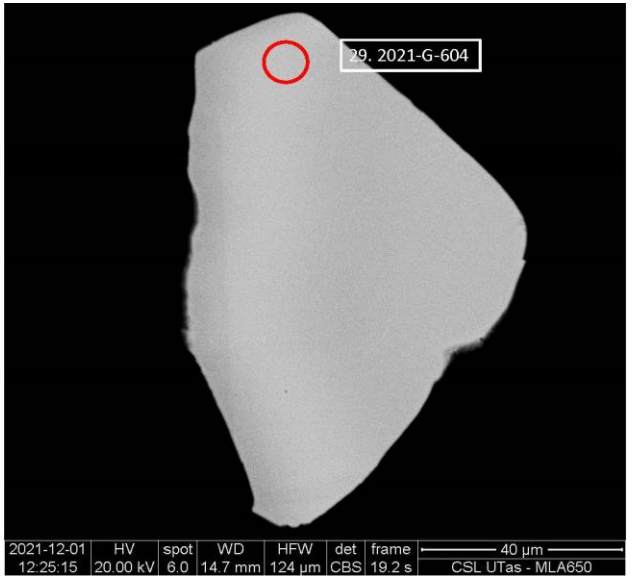

2021-G-604_14
BSE

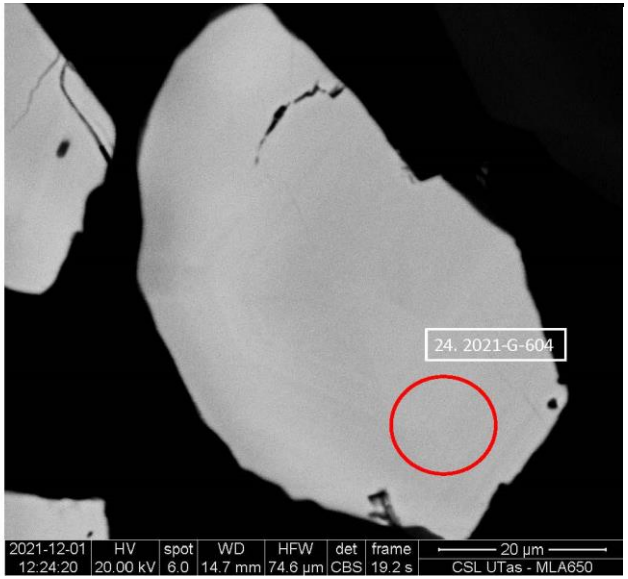

2021-G-604_13
BSE

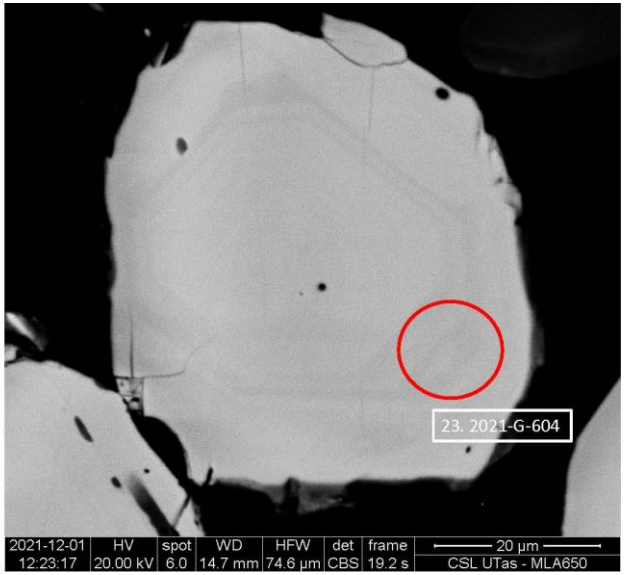

2021-G-604_12
BSE

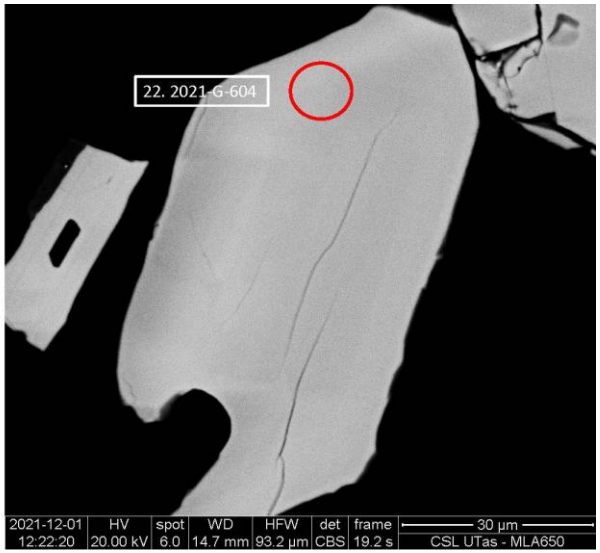

2021-G-604_11
BSE

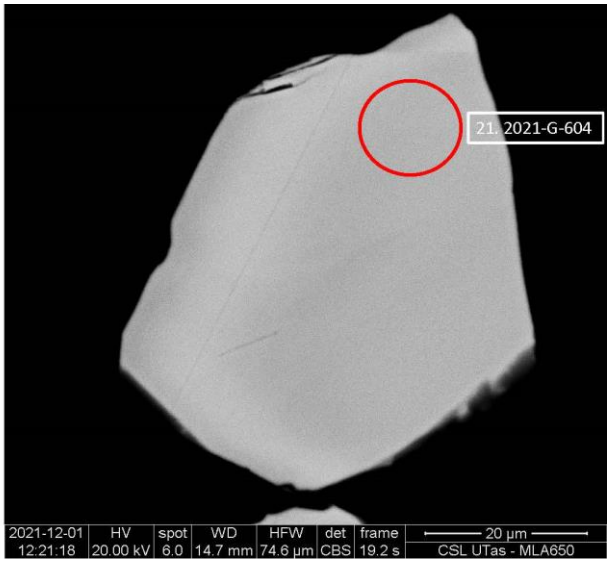

2021-G-604_10
BSE

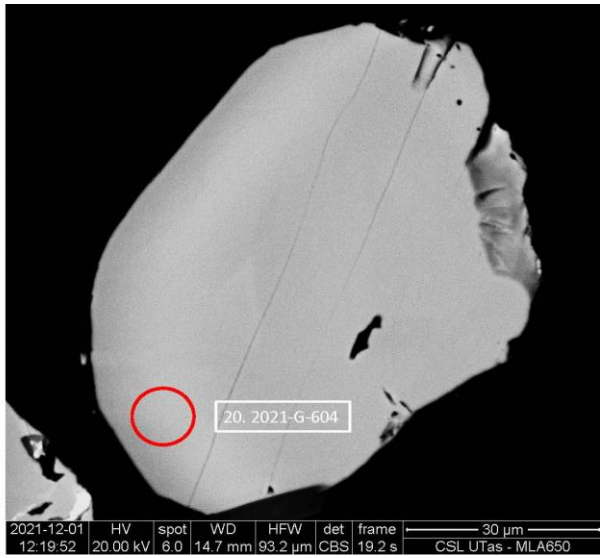

2021-G-604_9
BSE

2021-G-604_8
BSE

2021-G-604_7
BSE

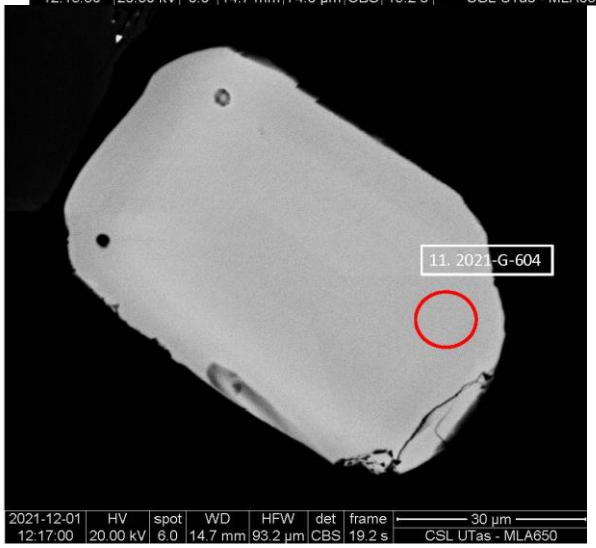

2021-G-604_5
BSE

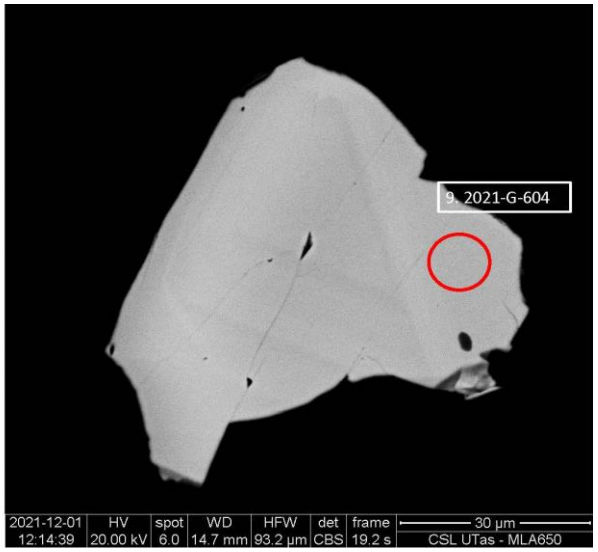

2021-G-604_4
BSE

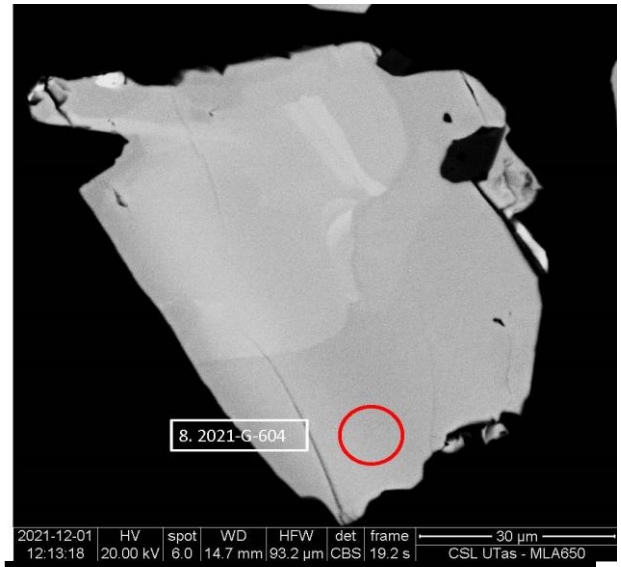

2021-G-604_3
BSE

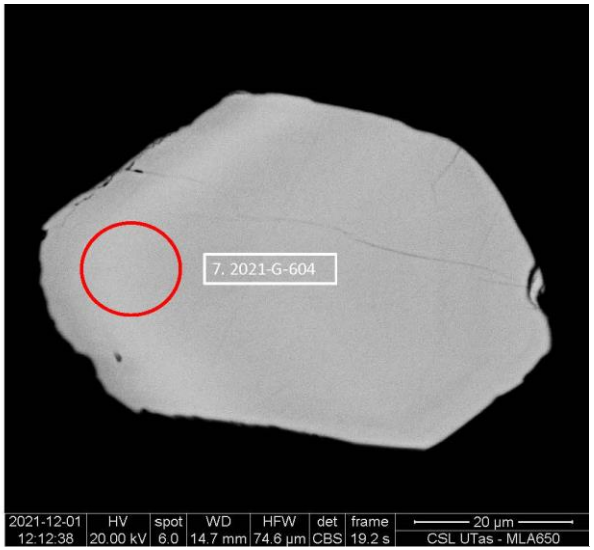

2021-G-604_2
BSE

2021-G-604_1
BSE

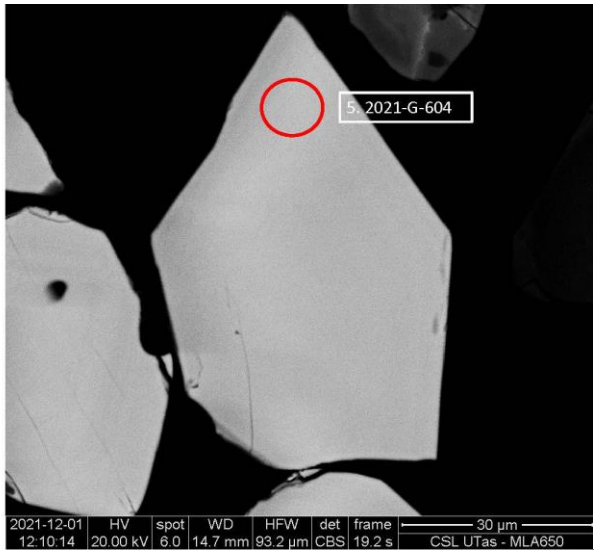

2021-G-605_35
BSE

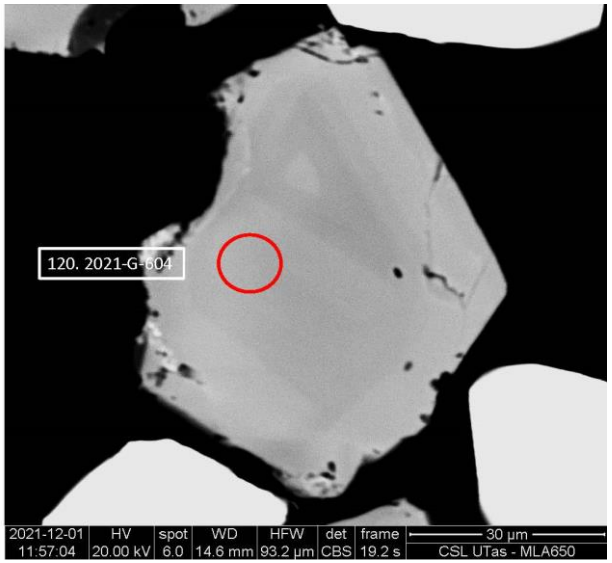

2021-G-605_34
BSE

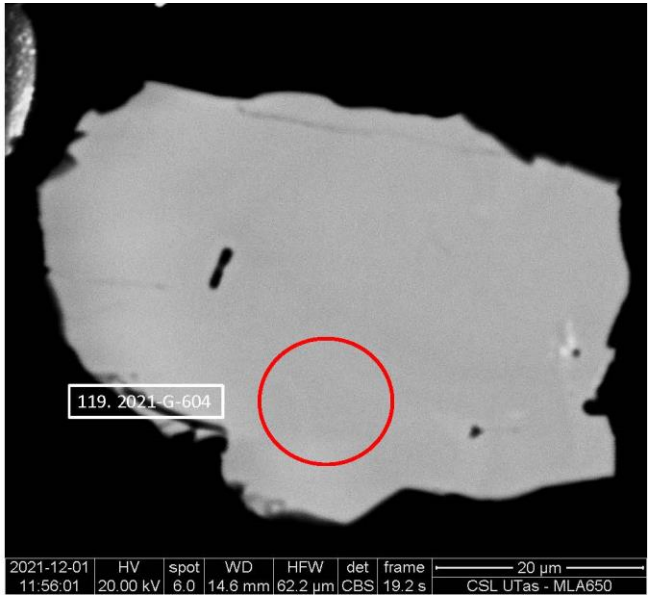

2021-G-605_33
BSE

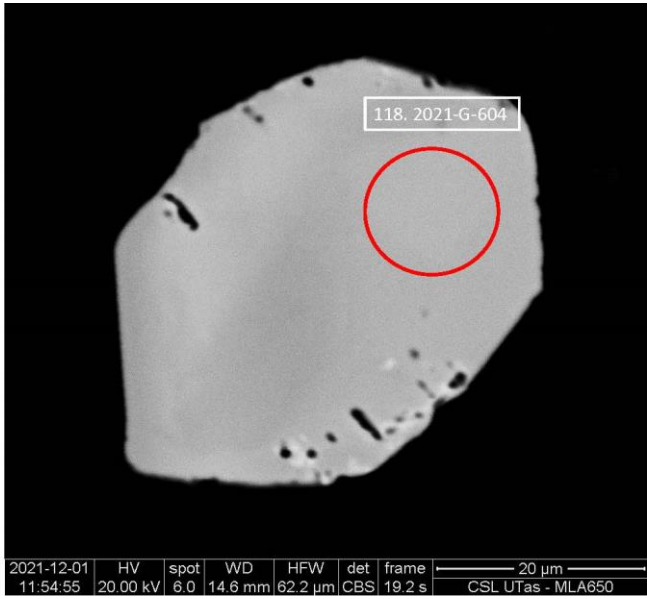

2021-G-605_32
BSE

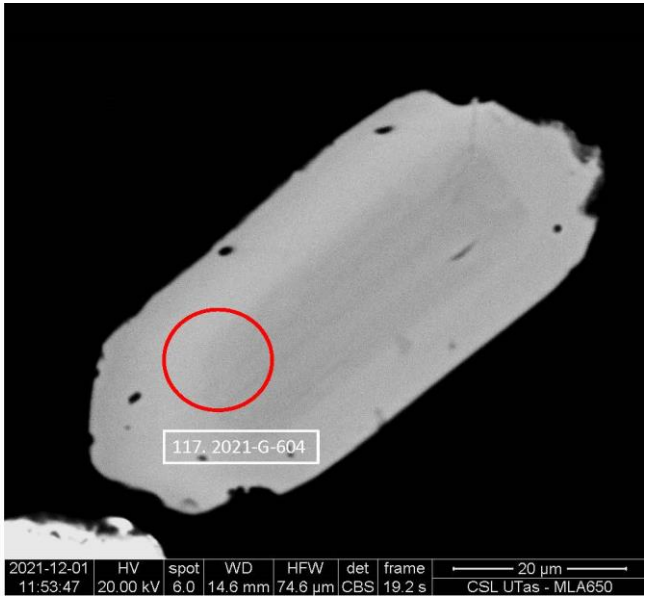

2021-G-605_31
BSE

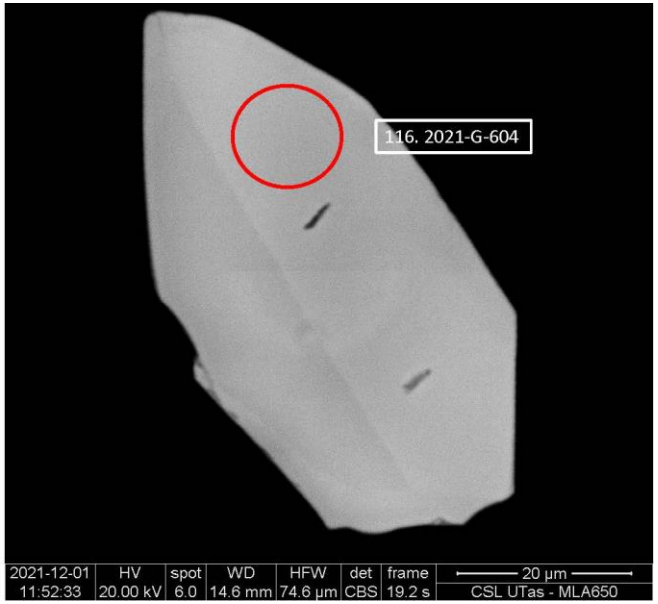

2021-G-605_30
BSE

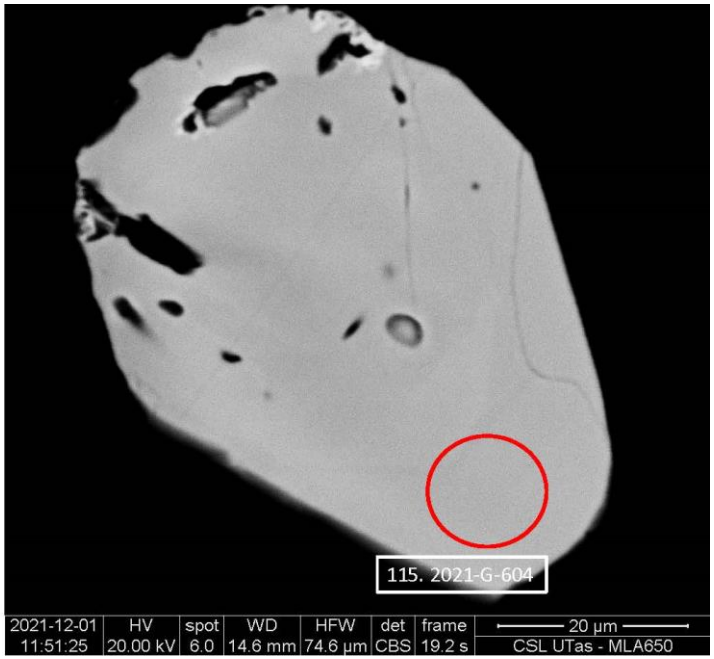

Appendix D: 1.1 Sr-Nd whole rock isotope geochemistry

Sample	$^{143}Nd/^{144}Nd$	2 SD	$^{87}Sr/^{86}Sr$	2 SD	Sm	Nd	Rb	Sr	$^{147}Sm/^{144}Nd$	$^{87}Rb/^{86}Sr$	Two stage age Ma	T CHUR Ma	143 Nd/ 144 Nd CHUR at time T CHUR	E Nd at T CHUR	TSr Ma
ZY-LG-3b	0.51179	0.000023	0.781782	0.000024	5.87	26.7	206	221	0.1328885	2.7174296	2087.74275	2021.743449	0.512378	-14.91	2032.477
ZY-LG-3b, r.2	0.511807	0.000021	0.781729	0.000023	5.87	26.7	206	221	0.132889	2.7174156	2061.840169	1981.491145	0.512383	-14.61	2031.11
ZY-LGT-1	0.511789	0.000021	0.775981	0.000022	1.71	4.79	301	24	0.2157849	37.004684	2089.1116	-6920.881658	0.513526	-14.85	135.834
Y-G-1b	0.511919	0.000023	0.777262	0.000017	2.11	7.49	258	65	0.1702842	11.53094	1891.079944	4121.627694	0.512107	-12.65	445.0373
Y-TG-2	0.512029	0.000016	0.765379	0.000018	3.01	10.6	281	79	0.1716508	10.300934	1723.18132	3687.52302	0.512163	-10.71	417.0474
ZY-LG-2	0.511777	0.000017	0.785197	0.000024	4.46	19.6	304	120	0.1375429	7.3878784	2107.547793	2213.126678	0.512353	-15.14	771.9953
LG-4-(I)	0.511736	0.000021	0.804997	0.00002	3.98	16.9	261	112	0.142348	6.8090126	2169.992771	2521.318321	0.512314	-15.86	1042.682
LG-4-(I), r.2	0.511762	0.000021	0.805036	0.000026	3.98	16.9	261	112	0.1423489	6.8090384	2130.396584	2449.259745	0.512323	-15.40	1043.081
Z-LG-6	0.511757	0.000019	0.784987	0.000022	7.45	37.8	208	271	0.1191302	2.2382706	2138.011354	1729.050396	0.512416	-15.48	2578.011
Z-LG-7	0.511781	0.000018	0.785369	0.000023	7.5	36.9	213	259	0.1228555	2.3983607	2101.45384	1766.696814	0.512411	-15.06	2413.852
Z-2	0.511827	0.000018	0.788204	0.000035	6.99	34.9	237	257	0.1210643	2.6901062	2031.360629	1632.938608	0.512428	-14.25	2221.899
LG-3(I)	0.511678	0.00002	0.813604	0.000026	4.38	17.9	271	96	0.1479007	8.2550909	2258.286039	2984.866387	0.512254	-16.88	932.5026
ZY-G-1	0.511821	0.000002	0.746813	0.000003	9.9	52.2	254	269	0.114638	2.7433864	2040.504907	1516.617245	0.512443	-14.36	1106.859
ZY-G-2	0.511962	0.000011	0.801866	0.000022	7.18	30.3	313	114	0.1432386	8.0199069	1825.467267	1924.886657	0.51239	-11.88	857.1139
Y-G-1	0.512093	0.000024	0.754728	0.000008	8.19	37.2	222	141	0.1330861	4.5779848	1625.408169	1306.450886	0.51247	-9.58	779.7998
LG-2(IV)	0.511958	0.000023	0.752695	0.000011	7.75	40.7	197	158	0.1151026	3.6246295	1831.571133	1270.520854	0.512475	-11.95	948.4665
LG-2(IV), r.2	0.511954	0.000013	0.752725	0.000017	7.75	40.7	197	158	0.1151025	3.6246401	1837.675437	1277.961665	0.512474	-12.02	949.0525